Pharmacometric approaches to assess antibiotic dosing in special patient populations: Towards therapeutic decision support

Inaugural-Dissertation
to obtain the academic degree
Doctor rerum naturalium (Dr. rer. nat.)

submitted to the Department of Biology, Chemistry and Pharmacy
of Freie Universität Berlin

by
Lisa Ehmann

2019

The present thesis was conducted from 2015 to 2019 under the supervision of Prof. Dr. Charlotte Kloft at the Institute of Pharmacy, Freie Universität Berlin.

1. Reviewer: Prof. Dr. Charlotte Kloft

2. Reviewer: Prof. Dr. Gerd Mikus

Date of disputation: 26.11.2019

Dedicated to the memory of Niklas Werner

Abstract

Almost one century has passed since the discovery of the first antibiotic drug, yet bacterial infections remain a major threat to public health. Two alarming trends have been observed in the last decades: While no truly novel antibiotic drugs were developed, the emergence and spread of antimicrobial resistance dramatically increased. Therefore, a rational use of the existing antibiotic drugs is crucial. One key pillar of rational antibiotic treatment is the choice of an appropriate dosing regimen resulting in adequate antibiotic exposure at the site of infection. In special patient populations, such as critically ill patients or morbidly obese patients, appropriate dosing is particularly challenging since these patients commonly show certain patient-specific characteristics altering antibiotic exposure.

The objective of the present thesis was to leverage pharmacometric modelling and simulation approaches in order to (i) enhance the understanding of the pharmacokinetics of antibiotic drugs in special patient populations, but also of the variability in the microdialysis technique – as the method of choice to determine drug exposure at target site, (ii) to evaluate and optimise antibiotic dosing regimens via adequate antibiotic exposure, and (iii) to translate the research results into the clinics supporting future therapeutic decisions. The thesis focused on the two antibiotic drugs 'linezolid' (Project I, II) and 'meropenem' (Project III, IV) in the selected special populations of 'obese surgical patients' and 'critically ill patients', respectively.

Project I characterised the pharmacokinetics (PK) of linezolid in plasma as well as at the target site (interstitial space fluid of s.c. adipose tissue, representing a common location of infections) in obese compared to nonobese surgical patients: The distribution of linezolid to the target site was delayed and exposure was reduced compared to plasma. The body size descriptor 'lean body weight' together with the obesity status of the patient were identified as factors which had an impact on linezolid PK. Both factors led to lower exposure in obese patients compared to nonobese patients, with a particularly pronounced difference at the target site. Interestingly, also anaesthesia and the related haemodynamic changes were found to impact linezolid PK, which resulted in reduced linezolid tissue fluid distribution and excretion. In addition to the PK-related findings, Project I characterised the variability in the microdialysis technique by integrating all available microdialysis data into the pharmacometric model and by dissecting and quantifying various levels of variability (interpatient, intercatheter, intracatheter). While the interpatient variability was almost fully explained by the obesity status of the patient, the quantified inter- and intracatheter variability highlighted the importance of special care in the performance of microdialysis (calibration of catheter, placement of catheter etc.).

Project II, a simulation analysis, applied the developed pharmacometric model of linezolid to assess standard linezolid dosing regarding the attainment of effective linezolid exposure (i.e. attainment of a predefined PK/Pharmacodynamic target). In the setting of perioperative infection prophylaxis, single standard linezolid dosing only resulted in effective target site exposure for susceptible pathogens and/or for surgical procedures of short durations. Overall, an increase in the risk of ineffective exposure was observed with increasing body size. In the setting of acute therapy, standard linezolid dosing was related to high risk of ineffective linezolid exposure at the target site, partly even for susceptible pathogens and/or in plasma. Increasing the daily dose (from 1200 mg to 2400 mg) clearly reduced the risk of ineffective exposure. In general, also prolongation of the infusion duration (from 30 min to 4 h) or shortening of the dosing interval (from 12 h to 8 h) reduced the risk of ineffective exposure, yet, less pronounced than the intensification of the daily dose. For resistant pathogens, none of the investigated dosing alterations resulted in effective linezolid exposure, neither in obese nor in nonobese patients.

Project III and IV characterised the PK of meropenem in a heterogenous critically ill patient population with severe infections. A large PK variability was observed between patients, which was to a large extent explained by the wide disparity in the patient characteristics: creatinine clearance (according to Cockcroft and Gault, $CLCR_{CG}$), body weight and serum albumin concentration. Of these three characteristics, $CLCR_{CG}$ showed by far the strongest impact on the (non)-attainment of effective meropenem exposure. Patients with normal or augmented renal function were at highest risk of ineffective exposure. Increasing the daily dose of meropenem, but particularly increasing the infusion duration (from 30-min to 3-h prolonged and/or continuous infusion regimens) reduced the risk of ineffective exposure.

In order to translate the findings into the clinics, two easy-to-use tools – the 'MeroRisk Calculator' and the '3-level dosing algorithm' – were developed. By providing a simple and intuitive interface, both tools enable the application of the pharmacometric modelling and simulation results by health care professionals. The MeroRisk calculator is an Excel® tool, which allows assessing the risk of ineffective exposure when administering standard meropenem dosing, by considering a patient's $CLCR_{CG}$ and the susceptibility of the identified/suspected pathogen. The 3-level dosing algorithm provides an intuitive dosing overview, which recommends dosing regimens likely to result in effective exposure. The algorithm is based on a patient's $CLCR_{CG}$, considers four different levels of knowledge about the infecting pathogen and for the first time the uncertainty in the underlying pharmacometric model for selection of meropenem dosing regimens.

To conclude, the present thesis contributed to a better understanding of the PK of clinically relevant antibiotic drugs in special patient populations and identified patient- and surgery-specific influencing factors altering antibiotic exposure in plasma and at the target site. By assessing the adequacy of standard and alternative antibiotic dosing regimens and translating the results into easy-to-use tools for clinical application, the present thesis has taken substantial steps towards therapeutic decision support to combat bacterial infections in the context of model-informed precision dosing. Future clinical studies are required to evaluate the tools with respect to clinical efficacy and safety before widespread application of the tools in clinical practice.

Zusammenfassung

Seit der Entdeckung des ersten Antibiotikums ist fast ein Jahrhundert vergangen, dennoch stellen bakterielle Infektionen weiterhin eine ernsthafte Bedrohung für die öffentliche Gesundheit dar. In den letzten Jahrzehnten wurden zwei alarmierende Trends beobachtet: Während keine neuartigen Antibiotika entwickelt wurden, nahm das Auftreten und die Verbreitung von Antibiotikaresistenzen dramatisch zu. Daher ist eine rationale Anwendung der aktuell vorhandenen Antibiotika von entscheidender Bedeutung. Eine wichtige Säule in der rationale Antibiotikatherapie ist die Wahl eines geeigneten Dosierungsschematas, welches in einer adäquaten Antibiotikaexposition am Infektionsort resultiert. In speziellen Patientenpopulationen wie Intensiv- oder krankhaft adipösen Patienten ist eine geeignete Dosierung besonders herausfordernd, da diese Patienten häufig bestimmte patientenspezifische Merkmale aufweisen, welche die Antibiotikaexposition verändern.

Ziel der vorliegenden Arbeit war es, pharmakometrische Modellierungs- und Simulationsansätze zu nutzen, um (i) das Verständnis der Pharmakokinetik von Antibiotika in speziellen Patientenpopulationen, aber auch der Variabilität in der Mikrodialysetechnik - als Methode der Wahl zur Bestimmung der Arzneistoffexposition am Wirkort – zu verbessern, (ii) die Antibiotikadosierung im Hinblick auf eine adäquate Antibiotikaexposition zu evaluieren und zu optimieren und (iii) die Forschungsergebnisse in die Klinik zu übertragen, um zukünftige klinische Dosierungsentscheidungen zu unterstützen. Die Arbeit konzentrierte sich auf die zwei Antibiotika ‚Linezolid' (Projekt I, II) und ‚Meropenem' (Projekt III, IV) in den speziellen Populationen der ‚adipösen chirurgischen Patienten' bzw. der ‚Intensivpatienten'.

In Projekt I wurde die Pharmakokinetik (PK) von Linezolid im Plasma sowie am Wirkort (Interstitialflüssigkeit des s.c. Fettgewebes, welche einen häufigen Infektionsort darstellt) in adipösen im Vergleich zu nicht-adipösen chirurgischen Patienten charakterisiert: Die Verteilung von Linezolid zum Wirkort war verzögert und die Exposition im Vergleich zum Plasma verringert. Die Körpermassenkennzahl ‚Lean Body Weight' wurde zusammen mit dem Adipositasstatus des Patienten als Einflussfaktoren für die PK von Linezolid identifiziert. Beide Faktoren führten in adipösen Patienten zu einer geringeren Linezolidexposition verglichen mit nicht-adipösen Patienten, wobei der Unterschied am Wirkort besonders ausgeprägt war. Interessanterweise zeigten auch die Anästhesie und die damit verbundenen hämodynamischen Veränderungen einen Einfluss auf die PK von Linezolid, was zu einer verminderten Gewebsverteilung und Ausscheidung von Linezolid führte. Neben den Ergebnissen zur Pharmakokinetik charakterisierte Projekt I zusätzlich die Variabilität in der Mikrodialysetechnik, indem alle verfügbaren Mikrodialysedaten in das pharmakometrische Modell integriert und verschiedene Variabilitätsniveaus (Inter-Patienten,

Inter-Katheter, Intra-Katheter) separiert und quantifiziert wurden. Während die Inter-Patienten Variabilität fast vollständig furch den Adipositasstatus des Patienten erklärt wurde, betonte die quantifizierte Inter- und Intra-Katheter Variabilität die Wichtigkeit einer besonderen Sorgfalt bei der Durchführung der Mikrodialyse (Kalibrierung des Katheters, Platzierung des Katheters usw.).

Projekt II, eine Simulationsstudie, nutzte das entwickelte pharmakometrische Linezolidmodell um die Standarddosierung von Linezolid hinsichtlich des Erreichens einer effektiver Linezolid Exposition (d.h., Erreichen eines vordefinierten PK/Pharmakodynamischen Zielwertes) zu evaluieren. In der perioperativen Infektionsprophylaxe führte die einmalige Standarddosierung von Linezolid nur im Falle von empfindlichen Krankheitserregern und/oder chirurgischen Eingriffen von kurzer Dauer mit hoher Wahrscheinlichkeit zu einer effektiven Exposition am Wirkort. Insgesamt wurde ein höheres Risiko für ineffektive Exposition mit zunehmender Körpermasse beobachtet. In der Akuttherapie war die Standarddosierung von Linezolid mit einem hohen Risiko für ineffektiven Linezolidexposition am Wirkort verbunden, teilweise sogar für empfindliche Krankheitserreger und/oder im Plasma. Die Erhöhung der Tagesdosis von Linezolid (von 1200 mg auf 2400 mg), verringerte das Risiko einer ineffektiven Exposition deutlich. Im Allgemeinen verringerten auch eine Verlängerung der Infusionsdauer (von 30 min auf 4 h) oder eine Verkürzung des Dosierungsintervalls (von 12 h auf 8 h) das Risiko einer ineffektiven Exposition, jedoch weniger ausgeprägt als die Intensivierung der Tagesdosis. Bei resistenten Erregern führte keine der untersuchten Dosierungsänderungen zu effektiver Linezolid Exposition, weder bei adipösen noch bei nicht-adipösen Patienten.

Projekt III und IV charakterisierten die PK von Meropenem in einer heterogenen Population von Intensivpatienten mit schweren Infektionen. Es wurde eine hohe PK-Variabilität zwischen den Patienten beobachtet, die sich zu einem Großteil durch starke Unterschiede in Patienteneigenschaften erklären ließ: Kreatinin-Clearance (gemäß Cockcroft und Gault, $CLCR_{CG}$), Körpergewicht und Serumalbumin-Konzentration. Von diesen drei Charakteristika zeigte die $CLCR_{CG}$ bei weitem den stärksten Einfluss auf das (Nicht-)Erreichen einer effektiven Meropenemexposition. Patienten mit normaler oder erhöhter Nierenfunktion zeigten das höchste Risiko einer ineffektiven Exposition. Die Erhöhung der Tagesdosis von Meropenem, insbesondere aber die Verlängerung der Infusionsdauer (von 30-min auf 3-h prolongierte und/oder kontinuierliche Infusionsschemata) verringerten das Risiko einer ineffektiven Exposition.
Um die Ergebnisse in die Klinik zu übertragen, wurden zwei einfach zu bedienende Tools entwickelt - der ‚MeroRisk Calculator' und der ‚3-stufige Dosierungsalgorithmus'. Durch eine simple und intuitive Benutzeroberfläche ermöglichen beide Tools die Anwendung der pharmakometrischen Modellierungs- und Simulationsergebnisse durch Fachpersonal im Gesundheitswesen. Der MeroRisk Calculator ist ein Excel®-Tool, mit welchem das Risiko einer ineffektiven Exposition bei Verabreichung einer Standarddosierung von Meropenem beurteilt

werden kann, indem die $CLCR_{CG}$ des Patienten und die Empfindlichkeit des identifizierten/vermuteten Erregers berücksichtigt werden. Der 3-stufige Dosierungsalgorithmus bietet eine intuitive Dosierungsübersicht, welche Dosierungsschemata empfiehlt, die mit hoher Wahrscheinlichkeit zu einer effektiven Exposition führen. Der Algorithmus basiert auf der $CLCR_{CG}$ des Patienten, berücksichtigt vier verschiedene Wissensniveaus über den infektiösen Erreger, sowie erstmals die Unsicherheit in dem zugrunde liegenden pharmakometrischen Modell für die Auswahl von Dosierungsschemata.

Zusammenfassend hat die vorliegende Arbeit zu einem besseren Verständnis der PK von zwei klinisch relevanten Antibiotika in speziellen Patientenpopulationen beigetragen und patienten- und operationsspezifische Einflussfaktoren identifiziert, welche die Antibiotikaexposition im Plasma und am Wirkort verändern. Durch die Beurteilung der Angemessenheit von Standard- und alternativen Antibiotika-Dosierungsschemata und der Translation der Ergebnisse in einfach zu nutzende Tools für die klinische Anwendung hat die vorliegende Arbeit wesentliche Schritte in Richtung einer therapeutischen Entscheidungshilfe zur Bekämpfung bakterieller Infektionen, im Kontext von modellgestützte Präzisionsdosierung, unternommen. Zukünftige klinische Studien sind erforderlich, um die Tools im Hinblick auf die klinische Wirksamkeit und Sicherheit zu bewerten, bevor sie in der klinischen Praxis eingesetzt werden.

Acknowledgments

I would like to express my sincere gratitude to:

- first and foremost, my *supervisor Prof. Charlotte Kloft* for all the scientific and non-scientific discussions and exchange we had, for your enthusiasm, valuable advice, ideas, feedback and support for my research projects and beyond – particularly also for your support in sad times which I greatly appreciate;
- the *Graduate Research Training Program PharMetrX* (Pharmacometrics and Computational Disease Modelling) for an excellent introduction into the research field of pharmacometrics during academic and industry modules and various PharMetrX and research group meetings, for providing a network of peers to exchange with, for a transdisciplinary co-/supervision as well as mentoring by an industry mentor, for providing exciting clinical collaborations and for financial support during my doctoral studies;
- my *co-supervisor Prof. Wilhelm Huisinga* for your curiosity, for your input from the mathematical perspective and for sharing your expertise during inspiring scientific discussions;
- my collaboration partners *Prof. Hermann Wrigge*, *Dr. Philipp Simon*, *Dr. David Petroff* from the Department of Anaesthesiology and Intensive Care Medicine and the Clinical Trial Centre Leipzig, University of Leipzig, *Prof. Frida Kees*, *Dr. Christoph Dorn* from the Institute of Pharmacy, University of Regensburg, and particularly *Dr. Michael Zoller*, *Dr. Johannes Zander* from the Department of Anaesthesiology and the Institute of Laboratory Medicine, University Hospital, LMU Munich, for sharing exiting clinical data, for various fruitful discussions on our joint research projects as well as for providing clinical insight and constructive feedback;
- my *industry mentor Dr. Diether Rüppel* for taking the time to discuss my projects during our telephone conferences and visits in Frankfurt or Berlin, for your valuable input and advice, as well as for giving me an insight into the use of pharmacometrics in industry;
- *Prof. Gerd Mikus* for your interest in my research projects, reviewing the present thesis and being a member of the doctoral committee,
- all present and past *companions* in the working group and the PharMetrX program for scientific exchange, mutual support and the good teamwork - I very much enjoyed the last 3 ½ years together with you. A big thank you to *Dr. Iris Minichmayr* for your support during my PhD time as academic mentor: for the inspiring scientific but also non-scientific discussions we had at the institute and via phone/skype, for having an open ear and for being the best reviewer for scientific publications I know. A particular thanks also to *Jane Knöchel* for providing mathematical advice whenever needed and for the several scientific discussions we had in the afternoons of the PharMetrX and research group meetings and beyond. Thank you also to

Dr. Lena Klopp-Schulze for our lunch and after-lunch discussions – I always enjoyed your enthusiasm for research, to *Dr. Niklas Hartung* and *Dr. Maximilian Schmitt* for our exciting and successful collaboration on the 'MeroRisk Calculator', to *Stefanie Hennig, PhD* for the valuable project discussions we had when you were joining our group as visiting scientist but also via phone when you were back in Australia, to *Dr. Andrea Henrich*, *Dr. Christine Weiser* and *Dr. Eva Göbgen* for your support especially in the beginning of my doctoral studies, to *Dr. Robin Michelet* for your support in the late stage of my doctoral studies, and to *David Busse* for your support with the linezolid modelling & simulation manuscript. Thanks to all office members in 130A, especially, *Ana-Marija Grišić*, *Franziska Kluwe* and *Dr. Johanna Melin* for the great time we spent together, including our regular yoga breaks, all additional scientific and non-scientific breaks, for always supporting each other and the positive office atmosphere.

A special thanks also goes to the PharMetrX year 2015, *Imke Ortland*, *Kathrin Volz*, *Miro Eigenmann, PhD*, *Dr. Mohamed Omari*, *Niklas Werner* and *Dr. Sulav Duwal*, for the great time we spent together during the PharMetrX modules during which true friendships have evolved.

I also want to thank all who reviewed parts of my PhD thesis: *Ana-Marija Grišić*, *David Busse*, *Ferdinand Weinelt*, *Francis Ojara*, *Franziska Kluwe*, *Dr. Iris Minichmayr*, *Jane Knöchel, Johanna Seeger*, *Dr. Lena Klopp-Schulze, Dr. Maximilian Schmitt* and *Victoria Stachanow*.

Thank you also *René Marrek* for the great time we spent together during the 6 month of your diploma project – I very much enjoyed being your mentor during this time. Further, I thank all my *elective students* Cynthia Vossen, Dorothea Heil, Laura Nessler, Natalie Probst for performing literature research and clinical surveys within the scope of my research projects.

- *Alison Thomson, PhD* for inviting me to visit you and your colleagues in Glasgow, for giving me an insight into the responsibilities of clinical pharmacists in the UK and into how therapeutic decisions-making can be supported by using PK/PD expertise. The valuable impressions I got during my stay in Glasgow stimulated me to translate the results of my PK/PD analyses into practical application by developing easy-to-use tools and have thus shaped my research projects.
- my *family, friends* and particularly *Max* for your support and encouragement, for your love and for always being there for me.
- *Niklas Werner* for spending and enjoying the first 6 month of our doctoral studies together, jointly mastering the first steps as PhD students and for the great time we also spent outside the institute. It was far too early that you passed away – I miss you! You will always have a place in my heart.

Table of contents

Abbreviations

A	Amount
ABW	Adjusted body weight
ALB	Serum albumin concentration (NONMEM® data item label)
AMG	German medicines law (‘Arzneimittelgesetz’)
AMT	Amount (NONMEM® data item label)
ANAE	Anaesthesia status (NONMEM® data item label)
ANAE_TF	Covariate effect of ANAE on TF
APACHE	Acute physiology and chronic health evaluation [1]
APE	Absolute prediction error
ARDS	Acute respiratory distress syndrome
ASHP	American Society of Health-System Pharmacists
AUC	Area under the curve
AUC/MIC	Area under the total drug concentration-time curve divided by MIC
AUC_{24}/MIC	Area under the total drug concentration-time curve over 24 h divided by MIC
BfArM	Federal Institute for Drugs and Medical Devices of Germany (‘Bundesinstitut für Arzneimittel und Medizinprodukte’)
C	Concentration
C(t)	Drug concentration over time
C_u	Unbound concentration
$C_{\mu D}$	Microdialysate concentration
$C_{8h,\ obs}$	Observed concentration 8 h after start of infusion
$C_{8h,\ pred}$	Model-predicted concentration 8 h after start of infusion
CAT	Categories/categorical OR Catheter
C_{crea_serum}	Serum creatinine concentration
C_{crea_urine}	Urine creatinine concentration
CD64	Cluster of Differentiation 64
cdd	Case deletion diagnostics
CFR	Cumulative fraction of response
CI	Confidence interval OR Continuous infusion
CIN	Retroperfusate concentration (NONMEM® data item label)
C_{ISF}	Interstitial space fluid concentration
CL	Clearance
CLCR	Creatinine clearance

$CLCR_{CG}$	Creatinine clearance estimated according to Cockcroft and Gault [2]
$CLCR_{CG}$_INF	$CLCR_{CG}$ value serving as inflection point for meropenem CL in $CLCR_{CG}$-CL relationship
$CLCR_{UC}$	Creatinine clearance measured using urine collection
CL_{Tot}	Total CL, i.e. linear + nonlinear CL
CL_u	Unbound CL, i.e. CL of unbound drug
C_{max}	Maximum concentration
C_{min}	Minimum concentration
C_{min_max}	Maximum of C_{min} values
C_{min_min}	Minimum of C_{min} values
CMT	Compartment (NONMEM® data item label)
CO	Cardiac output
CO_{LZ}	Cardiac output estimated according to Liljestrand and Zander [3]
CONT	Continuous
C_{P_tot}	Total plasma concentrations
C_{P_u}	Unbound plasma concentration
C_{RD}	Retrodialysate concentration
CREA	Serum creatinine concentration (NONMEM® data item label)
C_{RP}	Retroperfusate concentration
CRP	C-reactive protein
CRRT	Continuous renal replacement therapy
CVS	Cardiovascular system
CVVH	Continuous venovenous haemofiltration
CVVHD	Continuous venovenous haemodialysis
CVVHDF	Continuous venovenous haemodiafiltration
CWRES	Conditional weighted residuals
C_{Xh}	Concentration X h after start of infusion (e.g. C_{8h}: Concentration 8 h after start of infusion)
CYP	Cytochrome P450
D	Dose
DD	Daily dose
dop	Dopamine
DV	Dependent variable (NONMEM® data item label)
E.	*Escherichia* OR *Enterobacter*
EBE	Empirical Bayes estimate
ECMO	Extracorporeal membrane oxygenation

EGDA	Exploratory graphical data analysis
ESDA	Exploratory statistical data analysis
EMA	European Medicines Agency
epi	Epinephrine
EUCAST	European Committee on Antimicrobial Susceptibility Testing
EudraCT	European Union Drug Regulating Authorities Clinical Trials
EVID	Event identification (NONMEM® data item label)
f	Unbound ('free') OR fraction
fAUC/MIC	Area under the unbound drug concentration-time curve divided by MIC
fAUC$_{24}$/MIC	Area under the unbound drug concentration-time curve over 24 h divided by MIC
FDA	Food and Drug Administration
f_{fat}	Fraction of fat mass
$fT_{>MIC}$	Time period that unbound drug concentration exceeds the MIC
f_u	Fraction unbound
GOF	Goodness-of-fit
HT	Body height (NONMEM® data item label)
I category	Category 'susceptible at increased exposure' [4]
i.v.	Intravenous
IBW	Ideal body weight
ID	Individual identifier (NONMEM® data item label)
IIV	Interindividual variability
IIV_{Var}	Interindividual variability on variance scale
IL-6	Interleukin 6
INF	Infusion duration
IOV	Interoccasion variability
ISF	Interstitial space fluid
K.	*Klebsiella*
K_m	Michaelis-Menten constant
$K_{m,u}$	'Unbound' K_m, i.e. K_m of unbound drug
LBW	Lean body weight
LMU	Ludwig-Maximilians-Universität
llp	Log-likelihood profiling
log	Natural logarithm (=ln)
log10	Decadic logarithm
LR	Likelihood ratio

MAP	Mean arterial pressure
MAP_CL_{Tot}	Covariate effect of MAP on CL_{Tot}
max.	Maximum
MC	Monte Carlo
MDV	Missing dependent variable (NONMEM® data item label)
med.	Medium
MIC	Minimum inhibitory concentration
min.	Minimum
MRSA	Methicillin-resistant *Staphylococcus aureus*
MSSA	Methicillin-susceptible *Staphylococcus aureus*
n	Number
NFM	Normalised fat mass
NLME	Nonlinear mixed-effects
nor	Norepinephrine
n_p	Number of parameters
OBE	Obesity status (NONMEM® data item label)
ODE	Ordinary differential equation
$P_{0.025}$	2.5th percentile
$P_{0.05}$	5th percentile
$P_{0.5}$	50th percentile (=median)
$P_{0.95}$	95th percentile
$P_{0.975}$	97.5th percentile
P.	*Pseudomonas*
PaO_2/FiO_2	Ratio of partial pressure arterial oxygen and fraction of inspired oxygen
PBPK	Physiologically based pharmacokinetic(s)
P_{bs}	Median of parameter estimates obtained from the bootstrap replicates
PD	Pharmacodynamic(s)
PE	Prediction error
PI	Prediction interval OR prolonged infusion
PK	Pharmacokinetic(s)
P_{orig}	Parameter estimate obtained with original dataset
PPV	Population parameter variability
PPV_{Var}	Population parameter variability on variance scale
PsN	Pearl speaks NONMEM
PTA	Probability of target attainment
Q	Intercompartmental clearance between CMT 1 and 2

Q_2	Intercompartmental clearance between CMT 1 and 3
Q_u	Unbound Q, i.e. Q of unbound drug
qXh	Every X hours (e.g. q8h: every 8 h)
R breakpoint	MIC breakpoint separating I and R category [5]
R category	Category ‘resistant’ [4]
r^2	Coefficient of determination
RAPE	Relative absolute prediction error
RATE	Infusion rate (NONMEM® data item label)
RD	Retrodialysate
RF	Renal function
RP	Retroperfusate
RPE	Relative prediction error
RR	Relative recovery
RR_{IDX}	RR for ID_X (e.g. RR_{ID1}: RR for ID 1)
RR_{IDX_CAT1}	RR_{IDX} for catheter 1
$RR_{IDX\_CAT1\_RD1}$	RR_{IDX_CAT1} determined during first retrodialysis
$RR_{IDX\_CAT1\_RD2}$	RR_{IDX_CAT1} determined during second retrodialysis
RR_{IDX_CAT2}	RR_{IDX} for catheter 2
$RR_{IDX\_CAT2\_RD1}$	RR_{IDX_CAT2} determined during first retrodialysis
$RR_{IDX\_CAT2\_RD2}$	RR_{IDX_CAT2} determined during second retrodialysis
RR_{NOBE}	RR for nonobese patients
RR_{OBE}	RR for obese patients
RR_{pop}	Typical RR (‘population RR’)
RRT	Renal replacement therapy
RSE	Relative standard error
RSE_{Var}	Relative standard error on variance scale
RUV	Residual unexplained variability
S breakpoint	MIC breakpoint separating S and I category [5]
S category	Category ‘susceptible at normal dosing’ [4]
S.	*Staphylococcus* OR *Streptococcus*
s.c.	Subcutaneous
scm	Stepwise covariate model-building
SD	Standard deviation
SE	Standard error
SI	Short-term infusion
SOFA	Sepsis-related organ failure assessment [6]

spp.	*Species pluralis*
sse	Stochastic simulation and estimation
t	Time
$T_{>4xMIC}$	Time period that total drug concentration exceeds four times the MIC
$T_{>MIC}$	Time period that total drug concentration exceeds the MIC
t_{ANAE}	Time since anaesthesia start
t_{ANAE_STOP}	Time of anaesthesia end
TDM	Therapeutic drug monitoring
TF	Tissue factor
TF_{NOBE}	TF for nonobese patients
TF_{OBE}	TF for obese patients
TINT	Time interval (NONMEM® data item label)
T_{int}	Time interval
TIVA	Total intravenous anaesthesia
t_{max}	Time of C_{max}
V	Volume of distribution
V_1	Volume of distribution of central compartment
$V_{1,u}$	Unbound V_1, i.e. V_1 of unbound drug
V_2	Volume of distribution of peripheral compartment
$V_{2,u}$	Unbound V_2, i.e. V_2 of unbound drug
V_3	Volume of distribution of deep peripheral compartment
V_{max}	Maximum elimination rate
$V_{max,u}$	Unbound V_{max}, i.e. V_{max} of unbound drug
VPC	Visual predictive check
VRE	Vancomycin-resistant *Enterococcus*
V_{urine}	Urine volume
w	With
w/o	Without
WT	Total body weight (NONMEM® data item label)

Symbols

α	Level of significance
df	Degree of freedom
Δ	Difference
N	Normal (Gaussian) distribution
f	Function
F	Cumulative distribution function
P	Probability
τ	Dosing interval
θ	Fixed-effects parameter: Typical parameter in population
Θ	Vector of fixed-effects parameters
θ_k	Typical parameter value of k^{th} parameter
$\theta_{k,EBE}$	Individual parameter value of the k^{th} parameter
$\theta_{k,pop}$	Population parameter value of the k^{th} parameter
θ_{ik}	Typical parameter value for the i^{th} individual and the k^{th} parameter
θ_{INF}	Typical parameter describing the inflection point of a piecewise-linear covariate-parameter relationship
θ_Z	Typical parameter describing the effect of the Z^{th} covariate
ϕ_i	Structural model parameters for the i^{th} individual
ϕ_{ik}	Structural model parameter for the i^{th} individual and the k^{th} parameter
ϕ_{ikq}	Structural model parameter of the i^{th} individual, at the q^{th} occasion and the k^{th} parameter
η	Random-effects parameter: Interindividual variability
η_k	Interindividual variability parameter values for the k^{th} parameter
η_{ik}	Interindividual variability parameter value for the i^{th} individual and the k^{th} parameter
η_Z	Interindividual variability parameter value for the Z^{th} covariate
ω_k^2	Variance of η_k
$\omega_{1,1}^2$	Diagonal element (variance) of the first element of Ω
$\omega_{1,2}$	Off-diagonal element (covariance) of the first and second element of Ω
Ω	Omega matrix: Variance-covariance matrix of η
κ	Random-effects parameter: Interoccasion variability

κ_k	Interoccasion variability parameter values for the k^{th} parameter
κ_{ikq}	Interoccasion variability parameter value for the i^{th} individual, at the q^{th} occasion and the k^{th} parameter
π_k^2	Variance of κ_k
ε	Random-effects parameter: Residual unexplained variability
ε_{ij}	Residual variability parameter value for the i^{th} individual at the j^{th} observation
ε_{add}	Additive ε
ε_{prop}	Proportional ε
σ	Standard deviation of ε
σ^2	Variance of ε
${\sigma_{add}}^2$	Variance of ε_{add}
${\sigma_{prop}}^2$	Variance of ε_{prop}
$\hat{\sigma}^2$	Variance of prediction variability
$\hat{\sigma}_{reg}^2$	Variance of regression variability
$\hat{\sigma}_{\varepsilon}^2$	Variance of residual variability
Σ	Sigma matrix: Variance-covariance matrix of ε
OFV	Objective function value
OFV_{Bayes}	Bayes objective function value
Z_i	Observed covariate value(s) of the i^{th} individual
BZ_i	Observed baseline covariate value(s) of the i^{th} individual
Z_{median}	Median covariate value(s)
BZ_{median}	Median baseline covariate value(s)
Y	Matrix of observations
Y_i	Vector of observations of the i^{th} individual
Y_{ij}	j^{th} observation of the i^{th} individual
$\widehat{Y_{ij}}$	j^{th} prediction of the i^{th} individual
$\mathcal{L}$	Likelihood
$\mathcal{L}_i$	Contribution of the i^{th} individual to the likelihood
$\mathcal{LL}$	Log-likelihood
χ^2	Chi-square distribution
x_{ij}	Design variable of the i^{th} individual at the j^{th} observation

Relevant publications

Parts of the present thesis have been published or are in the process of being published in the following original articles:

- **Project I/II:**

  L. Ehmann*, P. Simon*, D. Busse, C. Dorn, W. Huisinga, A. Dietrich, M. Zeitlinger, H. Wrigge, C. Kloft. Risk of target non-attainment in obese compared to non-obese patients in calculated linezolid therapy.
  Clin. Microbiol. Infect. (2019) [in revision]. (*equal contribution)

  P. Simon, D. Petroff, C. Dorn, L. Ehmann, C. Kloft, C. Prettin, A. Dietrich, M. Zeitlinger, F. Kees, H. Wrigge. Measurement of soft tissue drug concentrations in morbidly obese and nonobese patients – a controlled clinical trial.
  Contemp. Clin. Trials Commun. 15: 100375 (2019).
  https://doi.org/10.1016/j.conctc.2019.100375

- **Project III**:

  L. Ehmann*, M. Zoller*, I.K. Minichmayr, C. Scharf, B. Maier, M.V. Schmitt, N. Hartung, W. Huisinga, M. Vogeser, L. Frey, J. Zander[#], C. Kloft[#]. Role of renal function in risk assessment of target non-attainment after standard dosing of meropenem in critically ill patients: A prospective observational study.
  Crit. Care. 21: 263 (2017). (*equal contribution, [#]shared senior authorship)
  https://doi.org/10.1186/s13054-017-1829-4

- **Project IV**:

  L. Ehmann*, M. Zoller*, I.K. Minichmayr, C. Scharf, W. Huisinga, J. Zander[#], C. Kloft[#]. Development of a dosing algorithm for meropenem in critically ill patients based on a population pharmacokinetic/pharmacodynamic analysis.
  Int. J. Antimicrob. Agents. 54: 309-317 (2019). (*equal contribution, [#]shared senior authorship)
  https://doi.org/10.1016/j.ijantimicag.2019.06.016

Further three original articles as well as additional publications (e.g. posters, oral presentations) are presented in Chapter 8.

1

Introduction

Almost one century has passed since the discovery of the first antibiotic drug, and yet bacterial infections remain a major threat to public health [7]. As reported by the World Health Organisation (WHO), worldwide 3 million deaths were caused by lower respiratory infections in 2016 [8]. Certain subgroups of patient populations ('special patient populations') are particular vulnerable to infections: For instance, critically ill patients frequently suffer from severe infections (e.g. sepsis or septic shock), which are related to high mortality rates up to 60% [9–17]. The 'golden age' of antibiotic drug discovery lasted from 1940 to 1962; in the last three decades, however, no truly novel antibiotics have been developed [18–20]. Beyond that, the emergence and spread of antimicrobial resistance has been increasing, a natural process which, however, can be accelerated by inappropriate use of antibiotic drugs [21–24]. Fortunately, global awareness of the threat of infectious diseases is greater than ever and different national and internal action plans have been proposed. These stress not only the need of reinvigorating the antibiotic value change, but also highlight the importance of a more rational use of existing antibiotic drugs [19,25–28].

1.1 Key pillars of rational antibiotic treatment

Apart from developing novel antibiotic compounds, a rational use of the currently available antibiotic drugs is of vital importance to optimise the therapeutic outcome of the patients, to reduce the emergence of antimicrobial resistance and to preserve the antibiotics for future use [29]. Rational antibiotic treatment in human health comprises four key pillars (Figure 1.1 A) which will be outlined hereinafter.

(1) The first pillar is the appropriate indication [30,31]. As highlighted by the WHO and the Antimicrobial Stewardship Working Groups of the International Society of Chemotherapy, evidence-based prescribing of antibiotics should be the standard of care, i.e. the prescription of antibiotic drugs should be based on clear suspicion or evidence of a bacterial infection [29,31]. Unnecessary use of antibiotics, e.g. for the treatment of viral infections, should be avoided.

(2) The second pillar is the appropriate choice of the antibiotic, i.e. choosing an antibiotic drug which shows antibacterial efficacy against the causative pathogen based on the antibiotic's spectrum of antibacterial activity. Microbiological diagnostics based on appropriate

microbiological samples before administration of the antibiotic can support an appropriate choice [31]. Yet, especially for vulnerable populations, such as critically ill patients, a prompt initial empirical antibiotic treatment is indicated [31,32]. The selection of the empirical treatment should be guided by e.g. local epidemiological data on microbiology and susceptibility patterns and a single patient's medical history (e.g. previous infections, recent administration of antibiotics) [31,32]. Once the causative pathogen is identified based on microbiological diagnostics the antibiotic treatment should be adapted to target the pathogen most effectively [33].

(**3**) The third pillar is the appropriate timing of the antibiotic therapy. For critically ill patients, studies revealed an association between each hour delay in the initiation of an appropriate antibiotic treatment and an increase in the mortality in presence of sepsis or septic shock [34–36]. Thus, appropriate antibiotic treatment is required as early as possible. The 'International Guidelines for Management of Sepsis and Septic Shock' by the Surviving Sepsis Campaign recommends the initiation of antibiotic therapy within the first hour after the diagnosis of sepsis or septic shock [37].

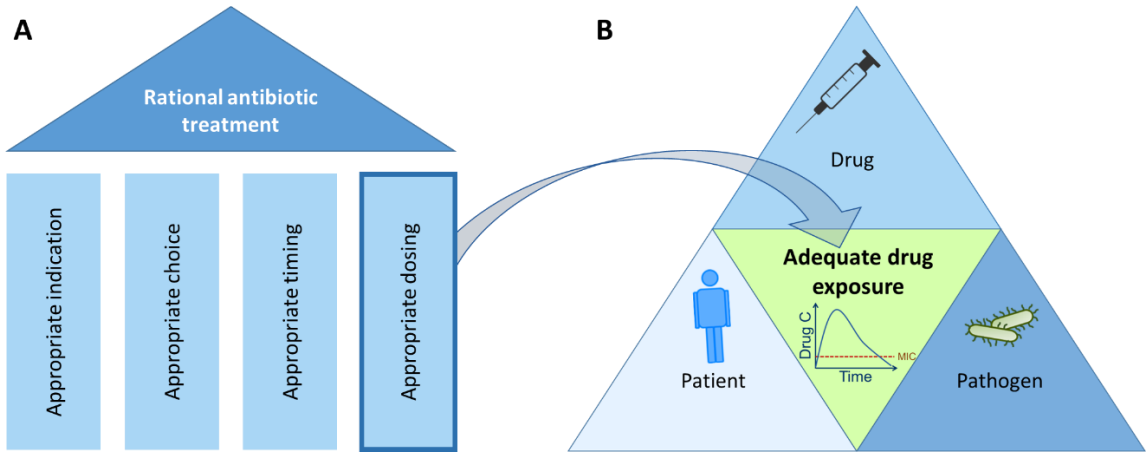

Figure 1.1: Four key pillars of rational antibiotic treatment (A) and the three determinants of adequate drug exposure (B).
Abbreviations: *C*: Concentration; *MIC*: Minimum inhibitory concentration.

(**4**) The fourth pillar is the appropriate dosing of the antibiotic drug resulting in adequate exposure at the site of infection where the pathogen is located [31,33]. Even if the infection is caused by a pathogen which is susceptible against the selected antibiotic drug (first and second pillar) and the treatment is initiated promptly (third pillar) antibiotic therapy might fail due to an inappropriately selected selected dosing regimen resulting in ineffective drug exposure. Previous studies have linked adequate antibiotic exposure to an improved clinical success [38–40]. Furthermore, appropriate dosing is also essential for prevention of emergence and spread of antimicrobial resistance in treated an future patients [41,42]. As illustrated in Figure 1.1 B, adequate antibiotic exposure depends on the triangular relationship between the antibiotic drug, the pathogen and the patient. In the following sections different aspects of the four key pillars for a rational antibiotic treatment will be further elucidated.

1.2 Target site pharmacokinetics utilising the microdialysis technique

As already indicated in section 1.1, the attainment of adequate antibiotic exposure at the site of infection where the pathogen is located (i.e. the 'target site') is crucial for antibacterial efficacy [43,44]. Thus, reliable characterisation of the antibiotic target site pharmacokinetics (PK) is essential. In that regard, three key aspects need to be considered:

(1) Several studies indicated substantial differences between tissue and plasma antibiotic PK, regarding exposure but also regarding kinetics (i.e. the shape of the drug concentration-time profile), both representing important determinants of the antibacterial effect [45–51]. The target site PK is determined by the distribution of the drug from the plasma to the respective tissue, which in turn may depend on both drug-specific and patient-specific characteristics [52]. While drug-specific characteristics include physicochemical properties (e.g. lipophilicity), molecular size and plasma protein binding, patient-specific characteristics include alterations in blood flow/perfusion, capillary density, fluid shifts etc. The PK differences between tissue and plasma PK, as well as the fact that pathogens are mostly located in the extravascular space, i.e. outside the blood [53,54], highlight the value of characterising antibiotic exposure in the respective tissue of interest.

(2) It is important to note that tissue is not a uniform matrix but consists of cells (intracellular space) and the interstitial space fluid (ISF) surrounding the cells (extracellular space). The vast majority of pathogens is localised in extracellular body fluids, only very few pathogens reside intracellularly [40,44]. Furthermore, intra- and extracellular antibiotic concentrations within one tissue may vary considerably: For instance, betalactam antibiotics exclusively distribute into the ISF [55], while quinolones show intracellular accumulation [56]. To reliably determine the antibiotic exposure at the target site, a quantification of the drug concentration in the respective tissue compartment is of interest, rather than in the homogenate of the tissue.

(3) It is well known that only the unbound drug concentration is the driver of the pharmacological effect of a drug [57–59]. Thus, the focus should lie on characterising unbound, not total drug concentrations at the target site.

One method that combines the three aforementioned key aspects is the microdialysis, a minimally invasive sampling technique which can be used to determine antibiotic drug concentrations directly at the target site.

Historical aspects of microdialysis. The microdialysis methodology has its origin in the early mid-1980s. While in the first years the focus was on studying neurotransmitter release in the brain, from 1990 on, microdialysis was increasingly used to characterise tissue fluid distribution of drugs in various therapeutic areas (e.g. neurology, dermatology, oncology and infectiology [60]) but also of endogenous compounds (e.g. cytokines [61]). Particularly in the field of infectiology, several clinical microdialysis studies have been performed to assess the distribution of the antibiotics into the ISF of the tissue of interest (e.g. subcutaneous (s.c.) adipose, muscle, skin, lung, brain, liver,

kidney, bone, eye [62]). Today, microdialysis has been recognised by regulatory agencies as a suitable method to determine drug concentrations in non-homogenate tissues (European Medicines Agency (EMA): 'Guideline on the use of Pharmacokinetics and Pharmacodynamics in the Development of Antibacterial Medicinal Products' [63]).

Microdialysis technique. The microdialysis employs the principle of dialysis, e.g. the passive diffusion of water and small solutes across a semipermeable membrane [64] and is graphically illustrated in Figure 1.2 A.

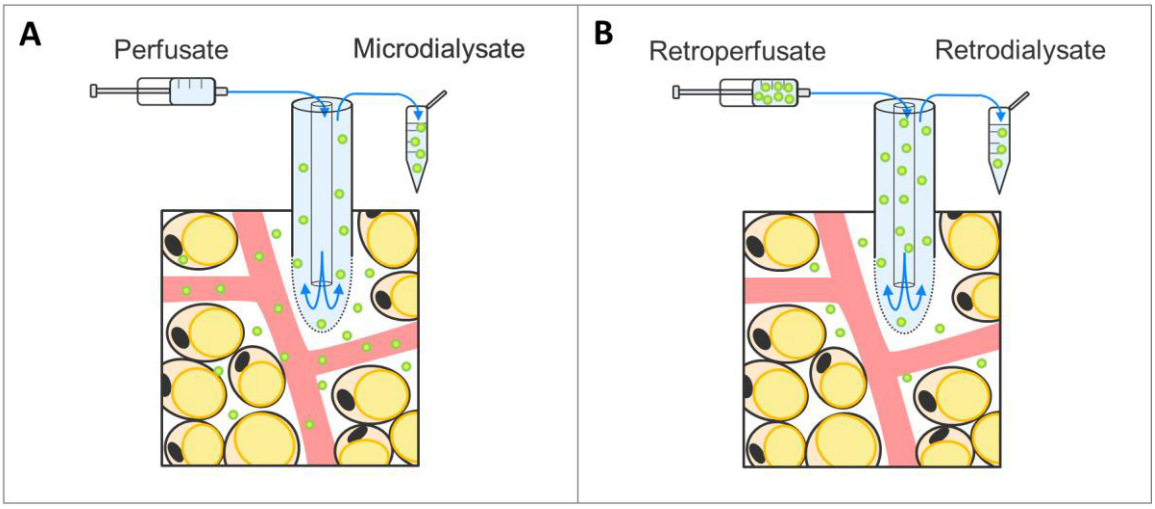

Figure 1.2: Illustration of microdialysis (A) and retrodialysis (B), exemplified for the ISF of s.c. adipose tissue.
Adipose tissue: consists of adipocytes (yellow), blood vessel (red) and ISF (white); *Microdialysis system*: consist of syringe/pump, catheter with semipermeable membrane and microvial; *Green circles*: Drug molecules; *Blue arrows*: Direction of perfusion flow.
Abbreviations: *ISF*: Interstitial space fluid; *s.c.*: subcutaneous.

For microdialysis sampling, a microdialysis catheter is inserted into the tissue fluid of interest (e.g. ISF, used as example in the subsequent text of this section) and constantly perfused with a drug-free physiological solution, the so-called 'perfusate' [60]. If drug molecules become available in the ISF of the tissue, they will diffuse through the semipermeable membrane at the tip of the catheter along the concentration gradient into the drug-free perfusion fluid in the catheter. Due to the molar mass cut-off of the semipermeable membrane, which typically ranges from 6 to 100 kDa (typical: 20 kDa), only unbound drug molecules will diffuse via the membrane [65]. The drug-containing fluid, the so-called 'microdialysate', is collected for a defined collection time interval in the microvial and its drug concentration is subsequently quantified. As the catheter is constantly perfused with the perfusate, an equilibrium at the semipermeable membrane will never be achieved. Consequently, the drug concentration in the microdialysate ($C_{Microdialysate}$), only represents a fraction of the actual ISF drug concentration (C_{ISF}), termed 'relative recovery'(RR) (Eq. 1.1).

$$RR = \frac{C_{Microdialysate}}{C_{ISF}} \qquad \text{(Eq. 1.1)}$$

In order to determine the relative recovery, which can be used to transform the measured microdialysate drug concentrations into the actual ISF drug concentrations, an *in vivo* calibration of every single catheter is required. Different methods have been proposed to estimate the relative recovery, yet the most widely accepted calibration approach is the so-called 'retrodialysis' also known as 'reverse dialysis of the drug' or 'delivery' [66].

Retrodialysis technique. In contrast to the microdialysis setting, during retrodialysis, the catheter is perfused with a solution containing a defined concentration of the drug of interest, the so-called 'retroperfusate' (Figure 1.2 B). The drug molecules will diffuse through the semipermeable membrane along the concentration gradient into the ISF of the tissue. The fluid leaving the catheter, the so-called 'retrodialysate' will be collected in the microvial and the remaining drug concentration quantified. By knowing the drug concentration that enters (retroperfusate, $C_{Retroperfusate}$) and leaves the catheter (retrodialysate, $C_{Retrodialysate}$), the loss via the membrane, also referred to as 'relative delivery' (RD), can be computed (Eq. 1.2).

$$RD = \frac{C_{Retroperfusate} - C_{Retrodialysate}}{C_{Retroperfusate}} \quad \text{(Eq. 1.2)}$$

This calibration method relies on the assumption that the loss (i.e. RD) during retrodialysis equals the gain (i.e. RR) during microdialysis sampling (Eq. 1.3). Hence, the experimentally determined relative delivery for a given catheter is equal to its unknown relative recovery and can be used to convert the microdialysate concentration into the actual ISF concentrations (C_{ISF}) (Eq. 1.4, i.e. rearranging Eq. 1.1.

$$RD = RR \quad \text{(Eq. 1.3)}$$

$$C_{ISF} = \frac{C_{Microdialysate}}{RR} \quad \text{(Eq. 1.4)}$$

In the following of the thesis, solely the term 'relative recovery' will be used to describe the loss during retrodialysis and the gain during microdialysis.

Parameters impacting relative recovery. The relative recovery is dependent on several parameters, including system-specific parameters, such as flow rate, temperature and composition of perfusate, molar mass cut-off and surface of the semipermeable membrane, but also drug-specific parameters, such as molar mass or adsorbing characteristics of the drug to the material of the catheter or the tubing material [66,67]. Hence, *in vitro* investigations prior to the clinical study are recommended to determine optimal conditions for the *in vivo* micro- and retrodialysis [60]. In addition, also patient-specific parameters have been described to influence the relative recovery. First of all, it is well known that the *in vitro* relative recovery is typically higher than the *in vivo* relative recovery, which is why *in vivo* retrodialysis is required for catheter calibration [65]. This

has been explained by different movement rates of the molecules in the ISF of the tissue *in vivo*, compared to the *in vitro* situation in which a buffer solution is used to mimic the ISF [60]: While in the buffer solution the molecules can freely move, in the ISF of the tissue, tortuosity caused by cellular structures in the extracellular matrix and connectivity of the spaces, results in a longer diffusion path of the molecules to reach the semipermeable membrane [60,65]. Furthermore, different relative recovery values have been described for the same drug for different tissues, presumably related to physiological characteristics of each tissue [68]. Furthermore, intracerebral microdialysis studies identified the clearance of an analyte from the site of measurement, by cellular uptake, to impact the relative recovery [69–71].

1.3 Special patient populations

Whether an antibiotic dosing regimen will result in adequate drug exposure also depends on the patient who is treated with the antibiotic drug (Figure 1.1 B). Patient-specific characteristics such as physiological factors (e.g. age), pathophysiological factors (e.g. renal impairment), or genetic factors (e.g. genotype), but also comedications, comorbidities or environmental factors may impact the PK of the antibiotic drug and hence influence drug exposure. In the following, the two special patient populations 'obese surgical patients' and 'critically ill patients' will be introduced as the key populations of the present thesis. The focus is set on the clinical relevance of antibiotic treatment in these patient groups and on special characteristics which might impact drug PK.

1.3.1 Obese surgical patients

Worldwide, the number of obese patients, i.e. patients characterised with an excessive accumulation of fat that may impair their health (according to WHO: BMI>30 kg/m^2 [72]), has dramatically increased in the recent decades [73]. According to WHO, from 1975 to 2016, the prevalence of obesity has almost tripled, with 13% of the adult population worldwide being obese in 2016 [72].

Clinical relevance of antibiotic treatment. Emerging data indicate an association between obesity and the risk and outcome of infections [74,75]. In particular for surgical interventions, various prospective and retrospective studies have demonstrated an increased risk of postoperative wound infections and associated morbidity and mortality in obese patients compared to nonobese patients [76–81]. One type of surgery increasingly used in the obese population is the bariatric surgery, or 'weight loss surgery', which is suggested for obese patients not responding to non-surgical treatments and showing a BMI of ≥40 kg/m^2 or ≥35 kg/m^2, the latter in combination with one or more obesity-associated serious diseases [81–83]. In addition to a significant and sustainable weight loss, bariatric surgery has been associated with an improvement of obesity-related

comorbidities and a reduction in mortality [84–88]. Given the increased risk of surgical site infections and associated morbidity and mortality in the obese population, perioperative antibiotic infection prophylaxis has been recommended for bariatric surgery [81]. Yet, the selection of an appropriate dosing regimen remains challenging, considering that a variety of (patho-)physiological changes related to obesity and/or the performed surgery might impact the antibiotic PK and thus drug exposure.

Special characteristics. In an obese person, both fat mass (FM) and lean body weight (LBW) are increased compared to a nonobese person, with LBW accounting for 20%-40% of the excess of body weight [89,90]. The increase in body size has been linked to an increased volume of distribution for various lipophilic and hydrophilic drugs; yet, different body size descriptors (e.g. total body weight, adjusted body weight) have been identified as determinant [90,91]. Furthermore, cardiac output has been shown to be increased in obese patients resulting in an increased blood flow to the organs; however, the blood flow into the adipose tissue has been described to be reduced [91–93]. The increase in blood flow to eliminating organs (e.g. kidney, liver) together with the increase in organ size, might result in an increased drug clearance [90,93]. Yet, obese patients frequently suffer from obesity-related comorbidities (e.g. diabetic nephropathy, hepatic dysfunctions), which on the other hand might impair the excretion capacity of the eliminating organs [90]. Furthermore, obesity has been suggested to impact the activity of different cytochrome P450 (CYP) enzymes, yet the direction of impact appears to be isozyme-specific [94–96].

In obese patients undergoing a surgical intervention, also surgery-related factors might impact the drug PK, however, limited information is available to date. Anaesthesia has been discussed to alter the blood flow to eliminating organs or to impact enzyme activities, which in turn potentially alter drug elimination [97,98]. In addition, post-surgical pathophysiological changes have been described, e.g. the occurrence of renal impairment, which might impact the clearance of renally excreted drugs [99].

1.3.2 Critically ill patients

The special patient population of critically ill patients is a highly vulnerable patient population, characterised by severe or life-threatening illness that is associated with profound pathophysiological changes requiring an intensive and specialised care, aggressive medical interventions and intensive monitoring [100,101].

Clinical relevance of antibiotic treatment. Infections in critically ill patients remain a major concern, due to high prevalence (~50% [17]) and high mortality rates: For instance, for severe infections such as sepsis or septic shock, mortality rates in intensive care units (ICU) reach up to 60%. [9–17]. There are two major challenges in the antibiotic treatment of critically ill patients. Firstly, infections are typically caused by less susceptible pathogens compared to infections in non-

critically ill patients on general wards [101]. For instance, in Germany, for the carbapenem antibiotic meropenem, considerably higher minimum inhibitory concentration (MIC; Section 1.4.1.1) values were overserved for pathogens detected in patients on the ICU compared to non-ICU patients: The MIC_{90} values (i.e. MIC value required to inhibit the growth of 90% of isolates) for all pathogens combined, were 8 mg/L and 1 mg/L, respectively [102]. The second major challenge is related to the high heterogeneity of patient-specific characteristics observed in ICU patients, which might result in high PK variability, making the selection of an appropriate dosing regimen more difficult.

Special characteristics. Critically ill patients are commonly characterised by a combination of diverse pathophysiological alterations. Haemodynamic changes, towards hyperdynamic circulation, are frequently observed in critically ill patients [103]. This characteristic has been discussed to be related to the systemic inflammatory response syndrome, which is observed in various clinical conditions, e.g. sepsis, burns, major surgeries [104,105]. The systemic inflammation might lead to decreased vascular resistance and increased cardiac output, which together with treatment interventions (e.g. fluid resuscitation, vasopressors), might cause the hyperdynamic state [101,106]. The related increase in blood flow to the eliminating organs, might result in increased drug clearance. In terms of kidney, this phenomenon is called 'augmented renal clearance', which has been described to be related to the clearance of renally excreted drugs [101,106]. Apart from the haemodynamic changes, critically ill patients might show altered fluid balance as a result of various factors. The systemic inflammatory response syndrome can lead to endothelial cell damage and increased vascular permeability, resulting in the so-called 'third spacing', an extravasation of fluid into the interstitial space of the tissues [101,107]. To avoid hypotension, fluid resuscitation is typically administered in the clinics, which might lead to further fluid shift into the interstitial space. This altered fluid balance might impact the drug distribution, particularly of hydrophilic drugs [101,108,109]. The increased vascular permeability might not only result in an extravasation of fluid, but also in a leakage of albumin into the ISF, which is discussed as the main cause of hypoalbuminemia, a frequently observed characteristic of critically ill patients [110,111]. The reduced serum albumin concentrations might result in a higher fraction of unbound drug in plasma, thereby increasing drug distribution and/or clearance, particularly of highly protein-bound drugs [112]. Furthermore, organ dysfunction(s) of one or multiple organs are frequently observed in critically ill patients and are one of the major causes of mortality in the critically ill patient group [113,114]. Especially when drug eliminating organs such as kidney or liver are affected (i.e. renal or hepatic impairment), the drug clearance may be reduced [101]. In the presence of organ failure, critically ill patients might require extracorporeal organ support: e.g. renal replacement therapy (RRT) for kidney support or extracorporeal membrane oxygenation (ECMO) for lung support [101,115]. RRT has been described to potentially impact the drug clearance; however, the impact seems to be highly variable and depend on various factors, such as

RRT-related characteristics (e.g. mode, filter type, blood flow rate) as well as drug-related physicochemical and PK characteristics (e.g. lipophilicity, protein binding) [101,116–119]. ECMO is a relatively new organ support procedure, which seems to have a less pronounced impact on the PK when compared to the influence of the critically illness itself [120]. Yet, clinical and nonclinical investigations are currently ongoing to better characterise the impact of ECMO on drug PK [121,122].

1.4 Antibiotic pharmacokinetics/pharmacodynamics and key antibiotic drugs

As described before, the adequacy of antibiotic drug exposure depends on the antibiotic drug itself (Figure 1.1): While on the one hand the PK characteristics of the drug and the patient-specific characteristics (Section 1.3) determine the achieved drug exposure, the pharmacokinetic/ pharmacodynamic (PK/PD) relationship of the antibiotic drug and the susceptibility of the pathogen, defines the adequacy of antibiotic exposure with respect to the antibacterial efficacy. This chapter provides an introduction in the general concepts of PK/PD relationships of antibiotics (Section 1.4.1), followed by an introduction in the key antibiotic drugs of the present thesis (Section 1.4.2).

1.4.1 Pharmacokinetics/pharmacodynamics of antibiotic drugs

The PK/PD relationship of an antibiotic agent represents the key determinant of antibacterial efficacy and is characterised by the triangular relationship between the antibiotic drug exposure (i.e. PK), the *in vitro* antibacterial activity of the antibiotic (i.e. MIC) and the effect of the antibiotic (e.g. clinical cure) [117,123]. This relationship is typically described by so-called ‘PK/PD targets’. Before elucidating PK/PD targets in more detail, the minimum inhibitory concentration and the PK/PD indices will be introduced.

1.4.1.1 Minimum inhibitory concentration and breakpoints

A well-established standard measure to describe antibacterial activity of an antimicrobial agent against a pathogen is the MIC, which can be determined *in vitro* by susceptibility testing methods (discussed in detail elsewhere [124–126]). The MIC is defined as the concentration of an antibiotic drug that prevents visible growth of the bacterium under defined conditions [127,128]. Hence, it provides valuable information on the susceptibility of a pathogen against the antibiotic drug: The higher the MIC value, the less susceptible the pathogen against the antibiotic agent. In contrast to other *in vitro* PD models (e.g. static/dynamic time-kill curve experiments [129]), the MIC has the advantage of a relatively simple determination, only requiring a single measurement after a defined

time point. Accordingly, the MIC reflects a snapshot of antimicrobial activity at one single time point, however, does not provide information on the growth-kill behaviour of the pathogen over time [129,130]. Despite the relatively simple determination, a routine determination of the MIC in the clinics is still rare – even in the vulnerable ICU setting [131]. Beyond that, susceptibility categories (see below) are frequently reported instead of MIC values [131].

The European Committee on Antimicrobial Susceptibility Testing (EUCAST) reports MIC distributions of microorganisms based on MIC data originating from worldwide sources [132] and classifies isolates depending on their MIC values for a given antimicrobial agent into three categories 'susceptible at normal dosing' (S category), 'susceptible at increased exposure' (I category) and 'resistant' (R category) in order to provide information about the likelihood of therapeutic success [4]. To that end, species-specific MIC breakpoints are defined for an antimicrobial agent, separating the three abovementioned categories for a specific microorganism: 'S breakpoint' (separates isolates of the S and I category), 'R breakpoint' (separates isolates of the I and R category) [5,133]. In case species-specific MIC breakpoints do not exist for a given microorganism, non-species related PK/PD breakpoints (likewise: S and R breakpoints) of the antimicrobial agents are provided [5,134]. Although the MIC breakpoints represent a simple way of assessing the potential likelihood of therapeutic success in the clinics, the individual PK of a patient is not considered in the evaluation, which may be of particular importance for special patient populations that are oftentimes characterised by highly altered pharmacokinetics (Section 1.3).

1.4.1.2 PK/PD indices and targets

In contrast to the MIC breakpoints, which only consider the susceptibility of the pathogen for assessment of dosing adequacy, so-called 'PK/PD indices' and their 'PK/PD targets' additionally consider the pharmacokinetics of a patient. For antibiotic agents, different patterns of antibacterial activity have been observed: Concertation-/ or time-dependent antibacterial activity with or without prolonged persistent effects [129,135]. Depending on the pattern of antibacterial activity of antibiotic agents, three major PK/PD indices have been described which best relate to antibacterial activity (Figure 1.3): (i) C_{max}/MIC, i.e. the ratio of the maximum drug concentration and the MIC, (ii) AUC/MIC, i.e. ratio of the area under the drug concentration-time profile and the MIC, (iii) $T_{>MIC}$, i.e. the time period that the drug concentration exceeds the MIC [129,135]. These PK/PD indices are typically determined using dose fractionation studies in *in vitro* or *in vivo* animal models [136] and are usually related to 24-h treatment period and derived for the unbound – also referred to as free – drug concentration (i.e.

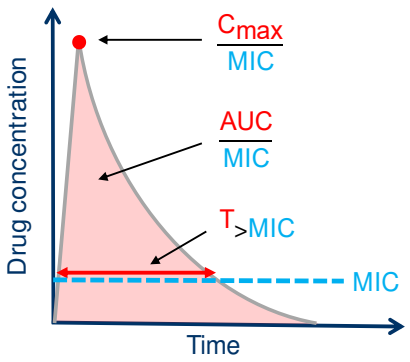

Figure 1.3: Graphical illustration of antibiotic PK/PD indices.
Abbreviations: *AUC*: Area under the curve; *C_{max}*: Maximum concentration; *MIC*: Minimum inhibitory concentration; *$T_{>MIC}$*: Time period that drug concentration exceeds the MIC.

*f*AUC/MIC, *f*C_{max}/MIC, *f*$T_{>MIC}$; *f* indicates *f*ree drug concentration).

While the PK/PD indices describe the relationship between a PK measure (e.g. AUC, C_{max}) and a PD measure (MIC) which is driving the efficacy, the PK/PD target provides information of the magnitude of the PK/PD index required for the desired efficacy of the antibiotic drug, which could for instance be the reduction in bacterial load, bacterial eradication, clinical cure or survival [129]. PK/PD targets can be derived from *in vitro* models or in *in vivo* studies both in animals or in patients, which have been shown to be overall in good agreement [135]. Today, PK/PD targets present a valuable tool to support the identification of an appropriate dosing regimen for newly developed antibiotic drugs in drug discovery and development in pharmaceutical industry, but particularly also for the dosing selection of already approved antibiotic drugs for the treatment of special patient populations in clinical practice [129,137]. How PK/PD targets can be utilised to identify appropriate dosing regimens is introduced in section 2.4.3.

1.4.2 Key antibiotic drugs

In the following, the key antibiotic drugs of the present thesis, linezolid and meropenem, will be introduced with respect to spectrum of activity, indication, dosing, PK, PK/PD targets and safety.

1.4.2.1 Linezolid

Spectrum of activity, indications and dosing regimens. Linezolid is the first representative of the class of oxazolidinone antibiotics and was approved for clinical use in 2000 [129,138]. Linezolid interferes with the protein biosynthesis of the pathogens by targeting the bacterial ribosomes. In contrast to other antibiotics interfering with the protein biosynthesis, linezolid inhibits the initiation of the bacterial translation in a very early step by blocking the formation of 70S initiation complex [139]. This unique mechanism of action avoids cross-resistances with most of the other commonly used antibiotic groups [138]. Linezolid displays antibacterial activity against the vast majority of clinically relevant gram-positive pathogens, including multidrug resistant strains such as Methicillin-resistant *Staphylococcus aureus* (MRSA) or Vancomycin-resistant *Enterococcus* (VRE) [138,140]. In light of this favourable spectrum of activity, linezolid treatment plays an important role in the ICU setting, given the high prevalence of infections caused by multidrug resistant gram-positive pathogens and the high mortality rates following severe infections [10]. Linezolid is approved for the treatment of nosocomial and community-acquired pneumonia and skin and soft tissue infections [139]. The approved standard dosing regimen for adults includes 600 mg linezolid administered either orally or as short-term intravenous (i.v.) infusion, twice daily (q12h) up to 28 days [139].

Pharmacokinetics. Linezolid is a small molecule (molar mass: 337 mg/L [141]) with slight lipophilic character ($logD_{pH7.4}$=0.64 [142]). The bioavailability of linezolid is nearly 100% and is not significantly affected by food intake, thus oral and i.v. formulations are considered equivalent [45,139,143]. Linezolid shows a relatively low plasma protein binding (~10-30%, concentration-independent) and has been shown to distribute into different tissues (e.g. epithelial lining fluid of the lung [129,138,139,144]). The volume of distribution of linezolid approximates to total body water (~40-50 L [139,145,146]). Linezolid clearance comprises both renal and nonrenal clearance [144]. The renal clearance of linezolid is relatively low (average 40 mL/min), which indicates tubular reabsorption [144,145]. The nonrenal clearance accounts for 65% of the total linezolid clearance and includes metabolism of the morpholine ring by oxidation. Linezolid is metabolised to two major inactive (i.e. without significant antibacterial activity) metabolites: The aminoethoxyacetic acid metabolite (metabolite A) and the hydroxyethyl glycine metabolite (metabolite B), the latter being the predominant metabolite in humans [139,144,147]. Yet, the metabolic pathways are not fully understood. For metabolite B, *in vitro* studies indicated that the formation is mediated by a chemical oxidation mechanism rather than by enzymatic oxidation [144,148]. Based on the presumed non-enzymatic metabolism *in vitro*, it is hypothesised that the oxidation *in vivo* may proceed throughout the entire body [147]. As for the parent substance, the two main metabolites are primarily excreted via the urine (proportion of dose under steady-state conditions: 30%, 10% and 40% as parent substance, metabolite A and B, respectively) and additionally to a small extent in faeces (3% and 6% as metabolite A and B, respectively [144]).

PK/PD targets. Previous *in vitro* investigations as well as *in vivo* studies in animals and in patients have been performed to define a PK/PD index that best correlates with the antimicrobial efficacy of linezolid [149–152]. The investigations revealed two relevant PK/PD indices for linezolid, AUC/MIC and $T_{>MIC}$. For instance, Andes et al. demonstrated in an *in vivo* neutropenic mice model with thigh infections, for an AUC_{24}/MIC ratio of 82.9 (mean, SD=57.3), bacteriostatic activity against *Staphylococcus (S.) aureus* [150]. Sanberg et al., who investigated the activity of linezolid against *S. aureus in vitro* and *in vivo* in a mice peritonitis model, associated $fAUC_{24}$/MIC of 100 together with $fT_{>MIC}$ of 100% with an improved infection outcome [149]. In an *in vivo* rat model with *Streptococcus (S.) pneumoniae*, Gentry-Nielson et al. related the two PK/PD targets $fAUC_{24}$/MIC>147 and $fT_{>MIC}$>39% to favourable outcomes [151]. Rayner et al. investigated clinical linezolid PK/PD data originating from critically ill patients, regarding a correlation with clinical success (bacterial eradication and clinical cure) [153]. According to the data, an increased clinical success was observed for $T_{>MIC}$ of around 85% in patients with bacteraemia as well as for AUC_{24}/MIC values of 80-120 in patients with bacteraemia, skin and soft tissue infections and lower respiratory tract infections.

Safety. The most common adverse drug reactions associated with linezolid treatment are diarrhoea, headache and nausea [144]. However, especially after long-term linezolid treatment, rare but

serious adverse drug reactions have been described, that include thrombocytopenia, peripheral and optic neuropathy, and lactic acidosis [129,154,155].

1.4.2.2 Meropenem

Spectrum of activity, indications and dosing regimens. Meropenem is a broad-spectrum carbapenem betalactam antibiotic, which exhibits bactericidal activity by inhibiting the synthesis of the bacterial cell wall via binding to and inactivation of the penicillin-binding protein [156]. Meropenem is active against both gram-negative and gram-positive pathogens, including less susceptible pathogens, e.g. *Pseudomonas (P.) aeruginosa, Acinetobacter* spp., as well as extended-spectrum β-lactamase and AmpC-producing Enterobacteriaceae [157]. It is therefore frequently used to treat severe bacterial infections in critically ill patients [158]. Meropenem is approved for the treatment of e.g. complicated skin and soft tissue infections, complicated intra-abdominal infections, severe pneumonia or complicated urinary tract infections [33]. For these indications, the approved standard dosing regimens for adults (intact renal function) include 500 mg or 1000 mg administered as short-term infusions every 8 h (q8h); for other indications (e.g. meningitis), doses up to 2000 mg are recommended [157]. For patients with creatinine clearance (CLCR) ≤50 mL/min, dose adjustment is suggested, e.g. for patients with CLCR of 10–25 mL/min, half of the indicated dose every 12 h (q12h) is recommended [157].

Pharmacokinetics. Meropenem is a hydrophilic molecule ($logD_{pH7.4}$=-4.36 [157]) with low molar mass (383 g/mol [159]) and with a very low plasma protein binding of 2% [160]. It is excreted primarily via the kidneys (98%, 2% via faeces [157]), predominantly by glomerular filtration, but also by active tubular secretion via organic anion transporters (OAT) (namely OAT1 and OAT3 [161,162]). While the major proportion of the dose is excreted as parent substance (~70%), the remaining proportion is nearly completely excreted renally as inactive beta-lactam ring-opened metabolite (28%), which is likely to be formed by the renal dehydropeptidase-1 [157,158]. Meropenem has been shown to be readily dialysable and effectively removed by RRT [157].

PK/PD target. As a β-lactam antibiotic, meropenem shows time-dependent activity; i.e. its antimicrobial efficacy is linked to the time that meropenem concentrations exceed the MIC value of a pathogen ($T_{>MIC}$) [163]. Various investigations focused on the identification of a respective PK/PD target value. For instance, Craig (results reported by Drusano [164]) and Ong et al. [165], who investigated the activity of meropenem against *Escherichia (E.) coli* and *P. aeruginosa* in a mouse thigh infection model, associated $fT_{>MIC}$ of 40% with a maximum bacterial kill activity. In a clinical study by Crandon et al., clinical success and survival in patients with *P. aeruginosa* ventilator-associated pneumonia were linked to $fT_{>MIC}$ of 19.2% and 47.9%, respectively [166]. Furthermore, Li et al. associated the attainment of the target $fT_{>MIC}$ of 54% to microbiological response in patients with lower respiratory tract infections [167]. For febrile neutropenic patients with bacteraemia, Ariano et al. demonstrated an increased clinical response rate of 80% when

$fT_{>MIC}$ was 76–100% [168]. Furthermore, McKinnon et al. demonstrated a significantly increased clinical cure and bacteriological eradication for the target $T_{>MIC}$ of 100%, in patients with serious bacterial infections treated with betalactam antibiotics [169].

Additional *in vitro* [42,170] and *in vivo* investigations [167,169] for meropenem and other betalactam antibiotics suggested an improved antibiotic efficacy for drug concentrations that achieved ~5 (range: 4-6.3) times the MIC value during the dosing interval.

Safety. Overall, meropenem shows a relatively good safety profile [171]. Most commonly occurring adverse events include diarrhoea, rash and nausea/vomiting [157]. For high meropenem exposure, an increased risk of developing neuro- and nephrotoxicity has been described (minimum concentrations>64.2 mg/L and 44.5 mg/L, respectively [172]).

1.5 Pharmacometrics and its application towards therapeutic decision support in infectious diseases

First introduced in the 1970s, the science of pharmacometrics constitutes a research area, combining disciplines such as pharmacology, medicine, clinical pharmacy, mathematics, statistics and computational methods (Figure 1.4).

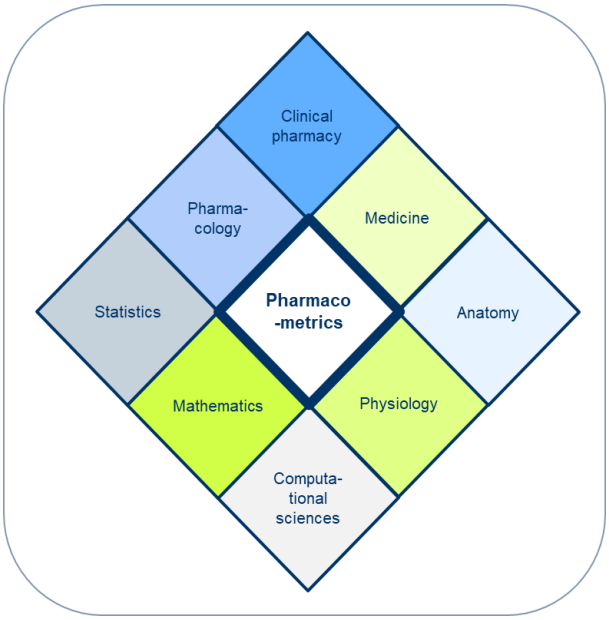

Figure 1.4: Multidisciplinarity of pharmacometrics.

Pharmacometrics develops and applies quantitative mathematical and statistical modelling and simulation approaches with the overall aim to better understand and characterise a system (e.g. a patient) and to identify, describe, quantify and predict the relationships between the system, a drug and/or a disease [173,174]. Thereby, the focus is on elucidating the interactions between the dosing schedule of the drug, the drug concentration-time profile (pharmacokinetics, 'what the body does to the drug'), the drug effect-time profile (pharmacodynamics, 'what the drug does to the body') and the therapeutic outcome or disease progression [173], by means of pharmacometric models (overview on pharmacometric modelling concepts: Section 2.1).

In pharmaceutical industry, 'model-informed drug discovery and development' has become an increasingly important field, which supports an accelerated, efficient and cost-effective development of safe and effective drugs [173,175–179]. The application of pharmacometric

modelling and simulation approaches spans across all stages of pharmaceutical drug development, ranging from drug discovery over pre-clinical and clinical drug development to life cycle management [176,177] and is encouraged by regulatory agencies, such as the EMA or US Food and Drug Administration (FDA) [180,181]. While in the past, dosing regimens in the drug label focused mostly on the average patient, today, regulatory agencies started to adjust the labelled dosing for certain patient subpopulations, based on pharmacometric analyses, when a supportive database is available [180,182]. Yet, in phase III studies, the enrolment of patients is typically restricted by patient-specific characteristics (i.e. inclusion/exclusion criteria [183]). Thus, the collected data is likely to not fully reflect the diversity of the 'real-world' patient population, which will use the approved drug in clinical practice. Special patient subgroups might show patient-specific characteristics outside the eligibility criteria of phase III studies, which could however alter the PK and/or PD and therefore demand dose adjustment [184].

A commonly used strategy to select an appropriate dosing regimen after therapy initiation in clinical practice is therapeutic drug monitoring (TDM), which is based on collected PK blood samples [185]. TDM is applied since the early 1970s and was historically employed to reduce toxicity rather than to improve efficacy, for drugs with a narrow therapeutic range (e.g. aminoglycosides) [186]. However, in light of the emergence of antimicrobial resistance, TDM is more frequently used also for the rarely toxic betalactam antibiotics, with the primary aim to improve efficacy by attaining adequate antibiotic exposure [186,187]. In the critically ill patient group, TDM of betalactam antibiotics is of particular importance [186,187], as the patients exhibit highly altered PK, tend to be infected with less susceptible pathogens, and show high mortality rates up to 60% related to severe infections (Section 1.3.2; [9–15,101,102,186,187]).

Beyond that, in the recent years pharmacometric modelling and simulation has gained increasing attention in clinical practice with respect to dosing individualisation: The new and promising concept of 'model-informed precision dosing', aims to apply pharmacometric models, mostly so-called 'nonlinear mixed-effects' (NLME) models (Section 2.3), in order to individualise drug dosing based on patient-specific characteristics [182,188,189]. Model-informed precision dosing can also be applied in situations in which no PK blood sample is available as the pharmacometric model together with patient-specific characteristics can be used to predict the PK of a patient. Thus, it enables individualised dosing recommendations already prior to the initiation of drug therapy. In the field of antiinfectives, the 'probability of target attainment' (PTA) analysis has proven to be a powerful concept to assess the adequacy of antiinfective dosing regimens and to ultimately support the selection of appropriate dosing regimens (for further details on PTA see Section 2.4.3; [129,190]). The PTA analysis, which has also been recommended by EMA [63], allows to assess various dosing regimens (e.g. altering dose, infusion duration, dosing frequencies etc.) with respect to the attainment of existing PK/PD targets (Section 1.4.1.2) for a given patient-pathogen combination and, based on the results, to select the most appropriate dosing regimen. Thereby,

pharmacometric modelling and simulation provides an important tool for model-informed precision dosing at bedside with the ultimate potential to support therapeutic decisions.

1.6 Objectives

To date, the identification of appropriate antibiotic dosing regimens remains a major challenge in our health care system. An appropriate antibiotic dosing regimen resulting in adequate antibiotic exposure at the site of infection (i.e. the target site) is an essential prerequisite for antibacterial efficacy and related therapeutic outcome in the patients as well as prevention of emergence and spread of antimicrobial resistance. A sampling technique to determine the drug exposure directly at the target site is the microdialysis, a rather new method which still requires basic research to be better characterised. Adequate antibiotic exposure depends on the antibiotic drug as well as on the susceptibility of the pathogen causing the infection. In addition, patient-specific characteristics may impact antibiotic exposure, which is of particular importance for special patient populations (e.g. critically ill or obese patients), who exhibit altered patient-specific characteristics (e.g. impaired organ function or altered body composition). Consequently, an adjustment of the antibiotic dosing regimen for special patient populations might be required to attain adequate antibiotic exposure. Today, even for routinely used antibiotic drugs the relation between patient, pathogen and antibiotic drug as well as the implications on the dosing regimens have not yet fully been assessed and the translation of the results into clinical application is lacking.

The central objective of the present thesis was to leverage pharmacometric approaches in order to:

- enhance the understanding of the PK of antibiotic drugs in special patient populations, but also of the variability in the microdialysis sampling technique,
- evaluate and, if needed, optimise antibiotic dosing regimens in special patient populations via an adequate antibiotic exposure, and to
- translate the research results back into the clinical practice to ultimately support future therapeutic decisions.

Thereby, the present thesis covered objectives within the research categories ‘basic research’, ‘applied research’ and ‘translational research’ as depicted in Figure 1.5.

In the following, a detailed description of the project-specific objectives is provided. For each objective the respective research category is stated as well as the motivation/research question (‘*Why*’) and the approach/strategy (‘*How*’).

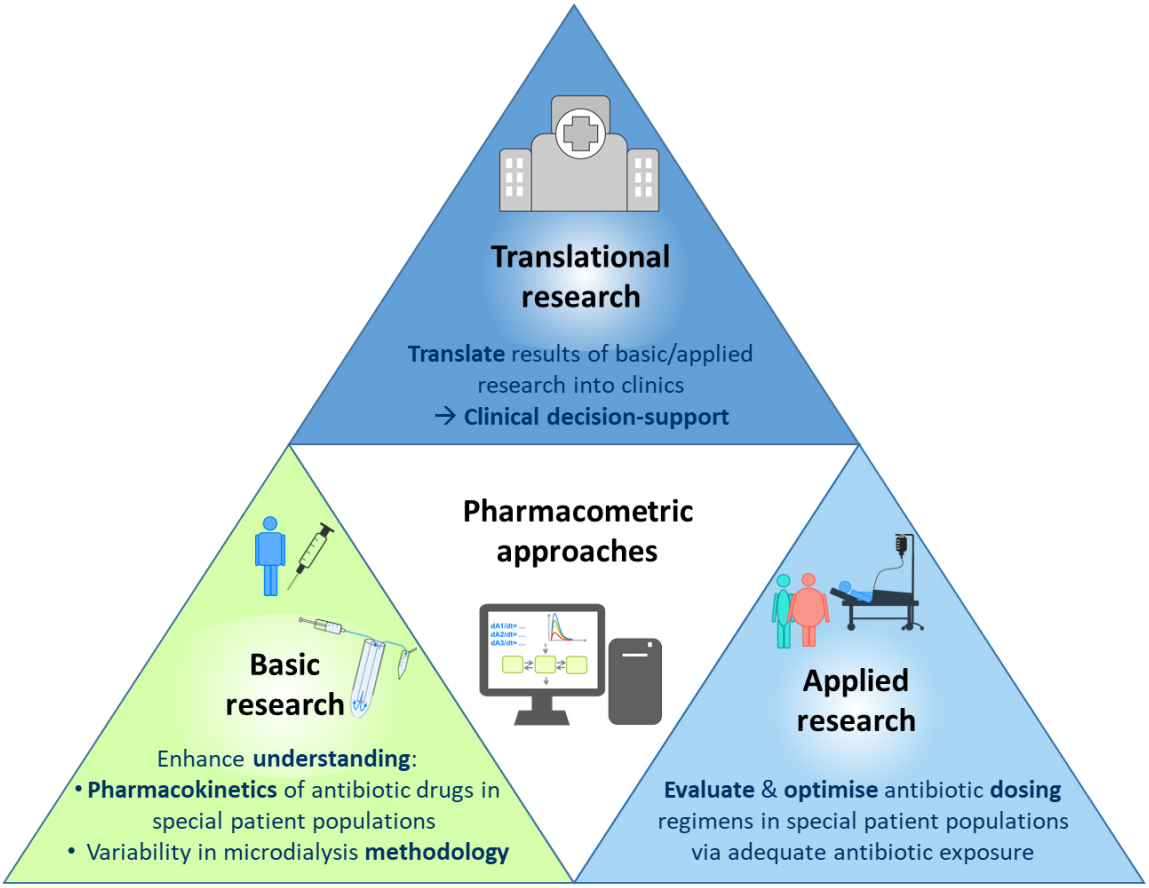

Figure 1.5: Graphical overview of the central objectives of the present thesis and their research categories. The three coloured outer triangles summarise the objectives (dark blue font) and respective research categories (black font, i.e. basic, applied and translational research) of the present thesis; the inner white triangle depicts the approach employed to achieve these objectives.

Project I: Characterisation of linezolid plasma and target site exposure in obese and nonobese surgical patients, including the evaluation of the microdialysis methodology.

Research category: Basic research

- *Why*? The objective of the project was to (i) better characterise the PK of total and unbound linezolid in plasma and of unbound linezolid at the site at risk of wound infection (i.e., target site: interstitial space fluid of subcutaneous adipose tissue) and to (ii) identify and quantify the impact of patient- and/or surgery-specific factors on the PK of linezolid. In addition, this project focused on (iii) the evaluation of variabilities in the microdialysis technique as the method of choice to determine target site exposure.
- *How*? The project employed the NLME modelling and approach to develop a joint model which simultaneously describes PK- and methodology-related aspects, plasma and target site PK and includes patient- and surgery-specific characteristics impacting the PK of linezolid. The project further aimed to apply this model by performing deterministic and stochastic simulations to explore the PK of linezolid in plasma

compared to target site and for patients with varying patient- and surgery-specific characteristics.

Project II: Evaluation and optimisation of linezolid dosing regimens for infection prophylaxis and acute therapy in obese and nonobese surgical patients.

Research category: Applied research

- *Why*? This project aimed to evaluate the adequacy of standard linezolid dosing in the setting of infection prophylaxis and acute infection therapy. For acute therapy, this project further sought to assess alternative linezolid dosing regimens in order to optimise linezolid dosing.
- *How*? The project utilised the NLME PK model (developed in Project I) for stochastic Monte Carlo (MC) simulations, in order to evaluate the probability of PK/PD target attainment in plasma and at the target site for standard and alternative linezolid dosing regimens.

Project III: Development of a risk assessment tool to evaluate standard meropenem dosing in critically ill patients with respect to ineffective meropenem exposure.

Research category: Basic research

- *Why*? The first objective of this project was to assess the impact of renal function on meropenem exposure.
- *How*? The project developed a regression model to quantify the relationship between renal function and meropenem exposure.

Research category: Applied research

- *Why*? The second objective of this project was to evaluate the adequacy of standard meropenem dosing for critically ill patients with respect to renal function.
- *How*? The project used stochastic MC simulations to assess the probability of PK/PD target attainment in dependence of renal function.

Research category: Translational research

- *Why*? The third objective of this project was to develop a tool to assess the risk of ineffective meropenem exposure after standard meropenem dosing for an individual patient.
- *How*? The project translated the results from the regression model and the risk computation into an easy-to-use Excel® tool.

Project IV: Development of a dosing algorithm to identify effective meropenem dosing regimens for critically ill patients.

Research category: Basic research

- *Why*? First, this project aimed to better characterise meropenem exposure in critically ill patients, to identify clinical determinants of PK and to assess and quantify their impact on meropenem exposure.
- *How*? The project employed the NLME modelling approach including a systematic analysis of various patient-specific factors as potential determinants of PK variability and applied the developed NLME PK model by performing deterministic simulations of meropenem exposure.

Research category: Applied research

- *Why*? Second, this project sought to evaluate the adequacy of standard meropenem dosing, to identify major clinical determinants of in-/effective exposure and to assess alternative meropenem dosing regimens in order to optimise meropenem treatment.
- *How*? The project employed stochastic MC simulations including the uncertainty in the parameters of the NLME PK model, in order to evaluate the probability of PK/PD target attainment and the cumulative fraction of response following standard and alternative meropenem dosing regimens.

Research category: Translational research

- *What*? Third, this project aimed to develop a dosing algorithm suggesting improved meropenem dosing regimens for the critically ill patient population already at start of treatment based on the level of knowledge about the pathogen.
- *How*? The project translated the results of probability of the PK/PD target attainment and the cumulative fraction of response analyses into an intuitive dosing overview.

2 Methods

2.1 Pharmacometric modelling and simulation concepts

Pharmacometrics, which was introduced in section 1.5 comprises different concepts, which can be categorised into bottom-up and top-down approaches (Figure 2.1). While bottom-up approaches are typically built upon prior knowledge of the system, i.e. the patient (e.g. anatomy, patho-/physiology) and the drug (e.g. physicochemical properties), top-down approaches are based on (non-)clinical data. In the PK setting, for instance, these clinical data can be drug concentrations determined over time in plasma, tissue or other matrices. Top-down approaches are further classified as (i) non-compartmental or compartmental approaches and (ii) individual or population approaches.

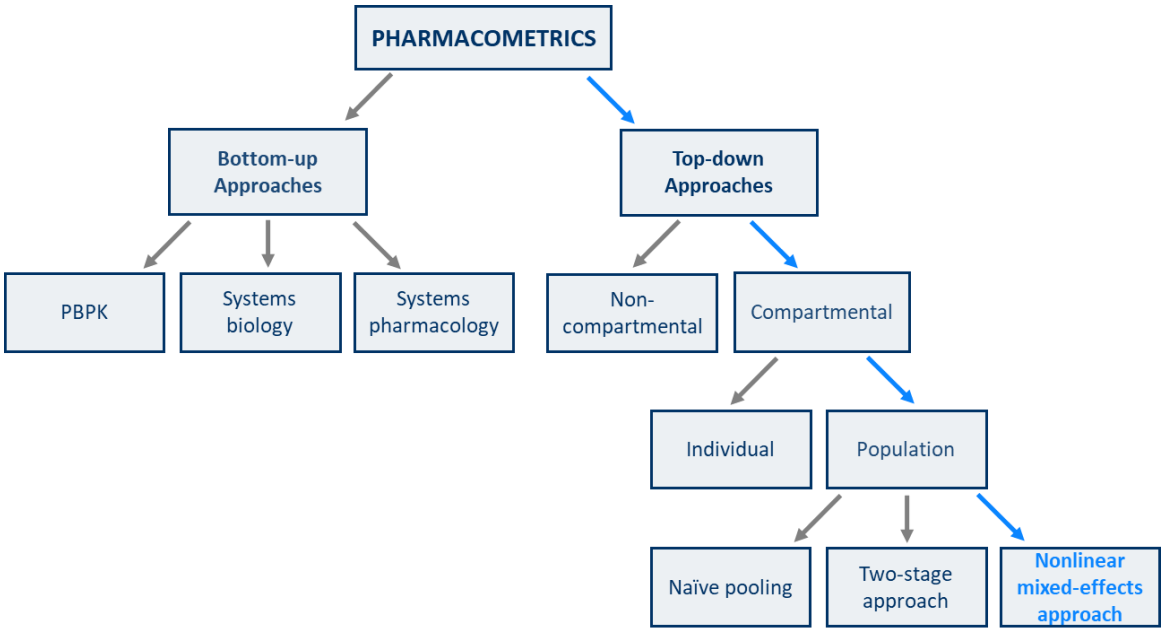

Figure 2.1: Overview of different pharmacometric approaches.
The blue coloured text and arrows highlight the nonlinear mixed-effects approach and its categorisation into the pharmacometric approaches, as the most relevant pharmacometric approach of the present thesis.
Abbreviations: *PBPK*: Physiologically based pharmacokinetic(s).

For the analysis of PK data, compartmental approaches are typically applied, in which the body is assumed to consist of 'compartments' representing kinetically homogeneous regions of the body

to which the drug can distribute [173,191]. In a one-compartment model the body is assumed to behave like a single kinetically homogeneous compartment, whereas in a two-compartment model the body is assumed to comprise two kinetically heterogeneous compartments which drug molecules reach: The central compartment (typically comprising blood and highly perfused regions of the body, e.g. kidneys) and the peripheral compartment (typically comprising less perfused regions of the body, e.g. adipose tissue).

As implied by the name, individual approaches focus on the analysis of available data on the level of the individual, whereas the focus of population approaches is on analysing data of more than one individual on the level of the population of individuals [192]. In order to describe the data of a population, the naïve pooling approach can be used, which jointly analyses the data of all individuals, without considering which data belongs to which individual; hence, this approach results in loss of information on the variability between the patients. In contrast, by using the two-stage approach, the data of each individual are analysed separately (stage 1) and afterwards descriptive summary statistics are computed to describe the central tendency in the population as well as the variabilities between the patients (stage 2; Appendix 7.3.1). This method requires a rich and balanced data situation in each patient, which is often limited in clinical studies. Furthermore, this approach has been shown to overestimate the variability between the patients, as only one level of variability is considered [192]. The population method of choice, which overcomes the drawbacks discussed above, is the nonlinear mixed-effects (NLME) modelling approach. In contrast to the two-stage approach, NLME modelling is also applicable in case of a limited and unbalanced data situation (e.g. few patients with rich and few patients with sparse data), as it simultaneously analyses the data of all individuals and thereby allows to 'borrow' information from the other individuals in the population to 'fill gaps' in the sampling schedule of single individuals [191]. This method allows to describe the central tendency in the population as well as to dissect and quantify different levels of variability (e.g. between the patients or residual variability), which represents a major strength of this approach. Furthermore, NLME modelling aims at identifying patient-specific characteristics (so-called 'covariates'), which explain the observed variability and form the basis for e.g. dose individualisation, to ultimately support therapeutic decisions [191]. The NLME approach was primarily used in this work and is described in more detail in section 2.3.

The pharmacometric modelling and simulation analysis starts from data which can be of different nature (e.g. PK, PD, additional patient-specific data) and can originate from different sources (e.g. pre-clinical experiments, clinical studies). The general steps of a typical pharmacometric modelling and simulation workflow for the nonlinear mixed-effects approach are illustrated in Figure 2.2 and will be further elucidated in the first part of the method chapter (Sections 2.2-2.4). Additional project-specific methodological details and clinical data will be described in the second part (Sections 2.6-2.9).

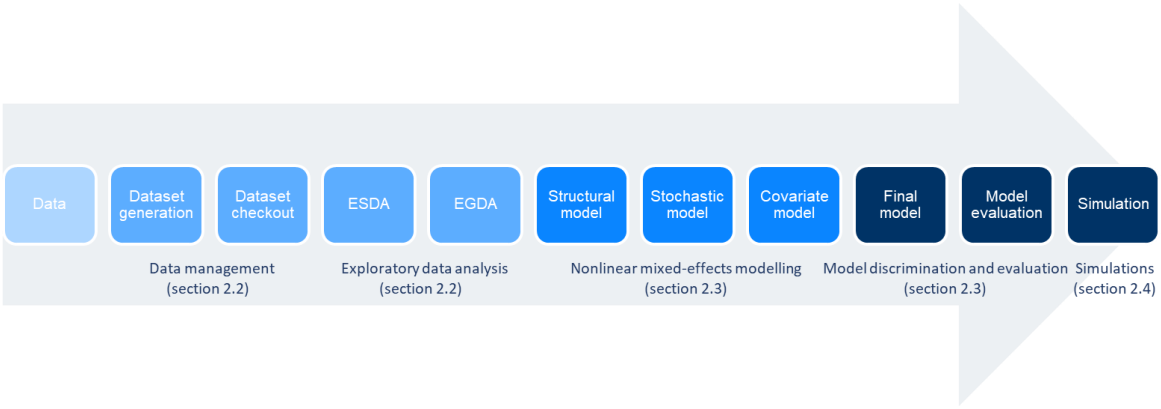

Figure 2.2: Typical pharmacometric modelling and simulation workflow, illustrated for the nonlinear mixed-effects modelling approach.
Abbreviations: *ESDA*: Exploratory statistical data analysis; *EGDA*: Exploratory graphical data analysis.

2.2 Data management and exploratory data analysis

Data management (i.e. dataset generation and checkout) and exploratory statistical and graphical data analyses are crucial steps for the subsequent modelling and simulation analyses.

2.2.1 Dataset generation

To analyse the data in the respective pharmacometric modelling and simulation software, a specific dataset structure is required. In the following, the focus will be on NONMEM®, the main software used for modelling and simulation analyses in the present thesis. All data to be used in the analysis need to be combined into one dataset with numerical data records only [193,194]. This can be, for instance, information on drug dosing history (e.g. dose and dosing time point), PK and PD sampling (e.g. measurement and sampling time point) or patient-specific information (e.g. demographics or clinical chemistry data). Data originating from a single individual need to be contiguous and arranged chronologically. NONMEM®-specific (required and optional) data items are to be specified dependent on the data situation (e.g. required: ID=individual identifier; DV=dependent variable; optional: MDV=missing dependent variable; CMT=compartment [193,194]). Apart from bringing the data in a software-specific dataset structure, dataset generation also comprises handling of missing data or data below the lower limit of quantification for e.g. drug concentration or covariate measurements. Different strategies exist [195–198], of which the ones applied in the projects are discussed in the respective sections (Project I: Section 2.6.3.1, Project IV: Section 2.9.2.1). Note that in the following, the term ‘imputation’ is defined as the replacement of a missing planned observation, whereas the term ‘interpolation’ is defined as the derivation of a new value within two planned observations.
Using programming software combined with version control allows to document and track all changes made to the original dataset (Section 2.5).

2.2.2 Dataset checkout

In order to evaluate the dataset for plausibility and completeness, as well as to detect implausible or erroneous values, different dataset checkout procedures are typically performed and documented [193]. 'Cross column checks' are applied to evaluate whether the combination of dataset items is plausible. 'Index plots' graphically display each data item versus ID and are hence useful to evaluate completeness, implausible values etc. but also give the first impression of special characteristics of the datasets and the value ranges between and within individuals. Project-specific dataset checkout procedures are described in the respective sections (Project I: Section 2.6.3.2, Project IV: Section 2.9.2.2)

2.2.3 Exploratory data analysis

Prior to the actual model development, an extensive exploratory data analysis is typically performed, comprising both statistical and graphical data analysis [193]. Statistical analyses aim at revealing characteristics (e.g. distributional) of the data and discovering possible trends and relationships. For this purpose, different numerical and graphical statistical outputs are generated, such as descriptive summary statistics (Appendix 7.3.1) in a tabular format, graphical illustration of frequency distributions (histograms) or bivariate scatter plots.

The aim of the graphical analyses is to detect potential trends in the relationship between dependent variable (e.g. drug concentration, drug effect) and independent variable (e.g. time, covariate), which will be analysed in the modelling step. In addition, it aims at exploring potential model structures that might be suitable to describe the data (e.g. number of disposition phases, delay etc.). For these purposes, diverse plots of dependent variable versus independent variable are generated: (i) for all patients, stratified by individual or for the typical patient (e.g. geometric mean of drug concentration vs. time), (ii) stratified by covariates, sampling matrix, dosing etc., (iii) on linear, semilogarithmic or logarithmic scale.

2.3 Nonlinear mixed-effects modelling

As described previously (Section 2.1), a nonlinear mixed-effects model is a hierarchical mathematical framework that allows to analyse the data of all individuals of a population simultaneously [199]. The term 'nonlinear' implies that the dependent variable (e.g. drug concentration) is related via a nonlinear function to the model parameters (e.g. clearance) and independent variables (e.g. time, dose). The term 'mixed-effects' refers to the parameterisation of the model, which consists of fixed and random-effects parameters, estimated simultaneously during the modelling procedure. Fixed-effects parameters are assumed to be constant in a population, while random-effects vary among individuals. The following sections provide further information

on the components (Section 2.3.1), parameter estimation (Section 2.3.2) and selection and evaluation (Section 2.3.3) of nonlinear mixed-effects models.

2.3.1 Model components

NLME models comprise three major components (Figure 2.3 A; [193]): (i) the structural submodel, (ii) the statistical submodel, and (iii) the covariate submodel. The structural and statistical submodel form the base model, which completes together with the covariate model the full NLME model. This section aims to provide a general and mathematical overview of the submodels; a detailed description of the model building strategy is provided for the different projects that applied NLME modelling, in the respective chapters (Project I: Section 2.6.4.2, Project IV: Section 2.9.3).

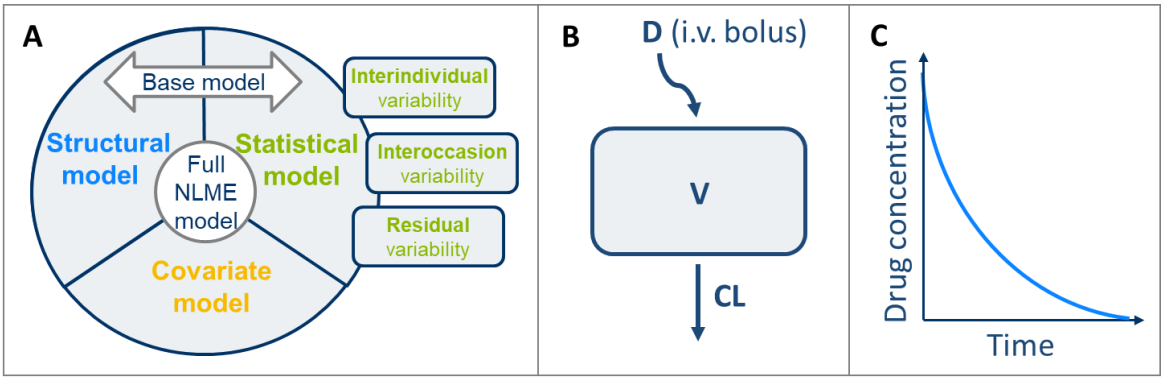

Figure 2.3: Components of nonlinear mixed-effects models (A), sketch of structural one-compartment model (B), and typical drug concentration-time profile (C) for i.v. bolus administration.
Abbreviations: *CL*: Clearance; *D*: Dose; *i.v.*: Intravenous; *NLME*: Nonlinear mixed-effects; *V*: Volume of distribution.

2.3.1.1 Structural submodel

The structural submodel describes the typical behaviour ('central tendency') of the dependent variable versus the independent variable. In case of PK data this could be the typical drug concentration-time profile in plasma of the population and for PD data the typical concentration of an inflammation marker changing over time of the population.

As discussed previously (Section 2.1), for PK models on which this work focused, compartment models are typically used to describe the drug concentration over time [191,199]. Exemplified for the simplest case of a compartment model – a one-compartment model (single i.v. bolus input, first-order elimination, Figure 2.3 B) – the typical drug concentration-time profile C(t) can be described by the following exponential equation Eq. 2.1 and is exemplarily depicted in Figure 2.3 C.

$$C(t) = \frac{D}{V} \cdot e^{-\frac{\theta_{CL}}{\theta_V} \cdot t} \qquad \text{(Eq. 2.1)}$$

In Eq. 2.1, the drug concentration (C) is a function of the administered dose (D), time (t) and the two fixed-effects PK parameters clearance (θ_{CL}) and volume of distribution (θ_V). The structural

submodel is typically described by a system of ordinary differential equations (ODEs) [200]. The concentration-time profile in Eq. 2.1 is the solution of the following ODE (Eq. 2.2) taking into account that the amount (A) over time (t) is $A(t) = C(t) \cdot V$:

$$\frac{dA}{dt} = -\frac{CL}{V} \cdot A \qquad \text{(Eq. 2.2)}$$

A more general mathematical representation of the structural model based on i individuals and j observations can be expressed as depicted in Eq. 2.3, assuming that there is no discrepancy between observations and model predictions (i.e. no residual unexplained variability: Section 2.3.1.2; [201,202]).

$$Y_{ij} = f(\phi_i, x_{ij}) \qquad \text{(Eq. 2.3)}$$

In Eq. 2.3, Y_{ij} is the dependent variable of the i^{th} individual corresponding to the j^{th} observation. The nonlinear function (f) represents the structural model and is dependent on the vector of structural model parameters of the i^{th} individual ϕ_i (e.g. clearance) and the known study design variables x_{ij} (e.g. dose, sampling time).

Note that the fixed-effects-parameters can be used to describe different processes, e.g. PK-related, PD-related and dependent on the type of model also system-related processes (e.g. a microdialysis system integrated in the NLME model, Section 2.6.4.1).

2.3.1.2 Statistical submodel

In addition to the typical behaviour, which is captured by the structural submodel, the statistical submodel describes and quantifies different levels of variability observed in the data. Hence, it allows to describe the individual behaviour of the dependent variable versus the independent variable. The statistical submodel comprises different levels of variability, depending on the available data (Figure 2.3 A): Interindividual and interoccasion variability in the model parameters on individual level (e.g. clearance) as well as residual unexplained variability in the dependent variable on observation level (e.g. drug concentration [193]).

Interindividual variability

The interindividual variability (IIV) quantifies unexplained deviations of the individual parameter value (Empirical Bayes estimate, EBE) from the typical model parameter. For PK models, IIV is typically implemented on the model parameters using an exponential relationship (Eq. 2.4) [199]. Hence, the model parameters are assumed to follow a log-normal distribution which prevents them from taking negative and thus physiologically implausible values.

$$\phi_{ik} = \theta_k \cdot e^{\eta_{ik}} \qquad \eta_k \sim N(0, \omega_k^2) \tag{Eq. 2.4}$$

In Eq. 2.4, the structural model parameter of the i^{th} individual and the k^{th} parameter (ϕ_{ik}) is defined by the typical value of the k^{th} parameter in the population (θ_k) and the individual impact of the patient ($e^{\eta_{ik}}$). The random-effects parameters η_{ik} of all individuals i (η_k) are assumed to follow a normal distribution with a mean of zero and a variance of the estimated random-effects parameter ω_k^2.

The variance and covariance estimates are provided in the omega matrix Ω [202]. In Eq. 2.5, the omega matrix is depicted in lower triangular form for an example with three IIV parameters.

$$\Omega = \begin{pmatrix} \omega_{1,1}^2 & & \\ \omega_{1,2} & \omega_{2,2}^2 & \\ \omega_{1,3} & \omega_{2,3} & \omega_{3,3}^2 \end{pmatrix} \tag{Eq. 2.5}$$

In the omega matrix (Ω), the diagonal elements (highlighted in blue) represent the variances (ω_k^2) of the parameters k=1,2,3; the off-diagonal elements represent the covariances between the corresponding variances, e.g. $\omega_{1,2} = cov(\omega_{1,1}^2, \omega_{2,2}^2)$. In the NONMEM® software, off-diagonal elements are assumed to be zero, unless explicitly defined and estimated using the so-called 'omega block' statement [193].

When reporting random-effects parameters, the variance ω_k^2 is typically converted to the coefficient of variation (CV) for easier interpretation. For log-normally distributed parameters the CV can be computed as follows [199,203] (Eq. 2.6):

$$CV, \% = \sqrt{e^{\omega_k^2} - 1} \cdot 100 \tag{Eq. 2.6}$$

Covariances are typically reported as correlation coefficient ρ which can be derived as follows Eq. 2.7:

$$\rho_{1,2}, \% = \frac{cov(\omega_{1,1}^2, \omega_{2,2}^2)}{\sqrt{\omega_{1,1}^2} \cdot \sqrt{\omega_{2,2}^2}} \cdot 100 = \frac{\omega_{1,2}}{\sqrt{\omega_{1,1}^2} \cdot \sqrt{\omega_{2,2}^2}} \cdot 100 \tag{Eq. 2.7}$$

Interoccasion variability

In case of multiple observations of the dependent variable on more than one occasion, an additional level of variability, the interoccasion variability (IOV), can be quantified. IOV accounts for unexplained deviations of the individual parameter value at each occasion from the typical individual model parameter. Similar to IIV, IOV is typically implemented on the model parameters using an exponential model (Eq. 2.8):

$$\phi_{ikq} = \theta_k \cdot e^{\eta_{ik}+\kappa_{ikq}} \qquad \eta_k \sim N(0, \omega_k^2) \qquad \kappa_k \sim N(0, \pi_k^2) \qquad \text{(Eq. 2.8)}$$

In Eq. 2.8, the structural model parameter of the i^{th} individual, the q^{th} occasion and the k^{th} parameter (ϕ_{ikq}) is defined by the typical value of the k^{th} parameter for the population (θ_k), the impact of the individual ($e^{\eta_{ik}}$) and the impact of the occasion ($e^{\kappa_{ikq}}$). The random-effects parameters η_{ik} of all individuals i (η_k) as well as the random-effects parameters κ_{ikq} of all individuals i at all occasions q (κ_k) are assumed to follow a normal distribution with a mean of zero and a variance of ω_k^2 and π_k^2, respectively. Similar to IIV, IOV is typically reported as CV and π_k^2 can be converted using Eq. 2.6.

Both levels of variability (IIV and IOV) can be implemented on any fixed-effects parameter in the model (e.g. PK-related, PD-related, but also system-related parameters as exemplified in Project I for the 'Relative Recovery' parameter: Section 3.1.2.2).

Residual unexplained variability

In addition to the variability in the PK parameters (IIV and IOV) residual unexplained variability (RUV) can be quantified on the level of the dependent variable. RUV might originate from different sources of variability, such as (i) imprecision of the bioanalytical assay used to measure the dependent variable, (ii) erroneous documentation of the independent variable (e.g. dosing or sampling time points) or (iii) model misspecification. RUV describes the deviation of the observed dependent variable from the model predicted concentration (Eq. 2.9):

$$Y_{ij} = f\left(\phi_i, x_{ij}\right) + \varepsilon_{ij} \qquad \varepsilon \sim N(0, \sigma^2) \qquad \text{(Eq. 2.9)}$$

In Eq. 2.9, ε_{ij} describes the discrepancy between the observation of the i^{th} individual at the j^{th} observation (Y_{ij}) and the model prediction $\left(f\left(\phi_i, x_{ij}\right)\right)$. The random-effects parameters ε_{ij} of all individuals i and all observations j (ε) are assumed to be normally distributed with a mean of zero and a variance of the estimated random-effects parameter σ^2. The variance and covariance estimates of RUV are provided in the sigma matrix Σ [202].

RUV can be implemented into the NLME model using different models, e.g. an additive, proportional or combined RUV model [193]. The example provided above (Eq. 2.9) illustrates an additive RUV model, in which the variance is assumed to be constant over the full range of model predictions. In contrast, the proportional RUV model (Eq. 2.10) assumes a variance that is proportional to the magnitude of the model prediction, i.e. for low model predictions the variance is relatively small, while for higher model predictions the variance increases. The two RUV models can be combined in the 'combined RUV model' (Eq. 2.11), capturing both an additive component

that dominates at lower model predictions and a proportional component that dominates at higher model predictions.

$$Y_{ij} = f(\phi_i, x_{ij}) \cdot (1 + \varepsilon_{ij}) \qquad \varepsilon_{ij} \sim N(0, \sigma^2) \tag{Eq. 2.10}$$

$$Y_{ij} = f(\phi_i, x_{ij}) \cdot (1 + \varepsilon_{prop,ij}) + \varepsilon_{add.ij} \tag{Eq. 2.11}$$

$$\varepsilon_{prop,ij} \sim N(0, {\sigma_{prop}}^2)$$

$$\varepsilon_{add,ij} \sim N(0, {\sigma_{add}}^2)$$

When reporting the RUV, for the additive RUV component oftentimes the standard deviation is chosen, which has the same unit as the dependent variable; for the proportional RUV component the dimensionless CV is typically derived (Eq. 2.6).
In case of data collected from different 'sources' e.g. different studies, different matrices or different sampling techniques, separate RUV models can be implemented (Section 3.1.2.2).

2.3.1.3 Covariate submodel

The implementation of covariates into the model is one of the key objectives of pharmacometric modelling and is typically performed after the development of the base model.
When implementing the covariates into a NLME model, the vector of the fixed-effects model parameters of the i^{th} individual (ϕ_i) is described by the following equation (Eq. 2.12):

$$\phi_i = g(\Theta, \mathrm{Z}_i) \tag{Eq. 2.12}$$

In Eq. 2.12, ϕ_i is defined by the covariate function g, which described the relationship between the vector of the fixed-effects parameters (Θ) and the vector of the observed covariate values (Z_i) of the i^{th} individual.

Covariates can be categorised into continuous covariates (e.g. creatinine clearance) and categorical covariates (e.g. sex). Dependent on the number of categories, categorical covariates can be further classified in dichotomous covariates (i.e. two categories: e.g. sex) and multiple categorical covariates. Multiple categorical covariates in turn can be categorised into ordered (e.g. renal function categories: severely impaired, moderately impaired, mildly impaired, normal, augmented) or not ordered covariates (e.g. sepsis cause: pneumonia, peritonitis, urosepsis, soft tissue infection). Dependent on the number of values recorded during the observation period, covariates can be further classified into single-measured (one value available per individual) or longitudinally measured covariates (multiple values available per individual), in the latter case one also speaks of time-varying covariates. Dependent on the type of covariate, different ways of implementing

covariate-parameter relationships into the NLME model exist.

In the following, examples for the covariate function g (Eq. 2.12) are provided that can be used to implement **continuous covariates** on a structural model parameter θ_k [193]: Linear, piecewise linear and power relationships, as well as a linear relationships in case of time-varying continuous covariates. For reasons of simplicity, all examples are provided under the assumption that only one covariate impacts the PK of the structural parameter θ_k (i.e. Z vector contains only one element). Furthermore, in the examples the covariate effects are centred to the median covariate value in the population (Z_{median}) [193].

Given a **linear covariate-parameter relationship** (Eq. 2.13), the structural model parameter linearly increases or decreases over the full range of observed covariate values.

$$g(\theta_{ik}, Z_i) = \theta_k \cdot (1 + \theta_Z \cdot (Z_i - Z_{median})) \quad \text{(Eq. 2.13)}$$

Eq. 2.13 provides an example for a linear form of function g. The k^{th} fixed-effects parameter of the i^{th} individual with a specific covariate value Z_i (θ_{ik}) is defined by the k^{th} fixed-effects parameter for the median covariate value Z_{median} in the population (θ_k) and the covariate effect (θ_z), which describes the fractional change of θ_k per unit deviation of the covariate value Z_i from the median covariate value Z_{median}.

In a **piecewise linear covariate-parameter relationship** (Eq. 2.14), for different ranges of a covariate ('pieces') different linear covariate-parameter relationships (i.e. with different slopes) are observed. In the following equation (Eq. 2.14), a two-spline relationship (also referred to as hockey-stick relationship) is provided: For this specific example, the model parameter increases linearly up to a specific estimated covariate value (inflection point, θ_{INF}) and is constant for covariate values greater than this value:

$$\begin{aligned} &\text{If } Z_i < \theta_{INF}\text{: } g(\theta_{ik}, Z_i) = \theta_k \cdot (1 + \theta_Z \cdot (Z_i - Z_{median})) \\ &\text{If } Z_i \geq \theta_{INF}\text{: } g(\theta_{ik}, Z_i) = \theta_k \cdot (1 + \theta_Z \cdot (\theta_{INF} - Z_{median})) \end{aligned} \quad \text{(Eq. 2.14)}$$

In addition to linear covariate-parameter relationships, nonlinear relationships, such as the **power covariate-parameter relationship** (Eq. 2.15), can be used. This type of relationship allows high flexibility as it can describe a variety of different relationships, depending on the estimated coefficient parameter (θ_z).

$$g(\theta_{ik}, Z_i) = \theta_k \cdot \left(\frac{Z_i}{Z_{median}}\right)^{\theta_Z} \quad \text{(Eq. 2.15)}$$

Alternatively, for body size descriptors the principle of allometry [204] can be applied in which

the coefficient parameter in Eq. 2.15 is set to 0.75 for clearance parameters and to 1 for volumes of distribution parameters.

In case of **time-varying continuous covariates** two extended **linear relationships** have been proposed by Wählby et al. [205]. 'Extended Wählby model 1' defines separate covariate-parameter relationships between and within individuals (Eq. 2.16). 'Extended Wählby model 2' includes an additional interindividual random-effects parameter on the covariate effect and thus allows the covariate effect to differ between individuals (Eq. 2.17).

$$g(\theta_{ik}, Z_i) = \theta_k \cdot (1 + \theta_{BZ} \cdot (BZ_i - BZ_{median}) + \theta_{DZ} \cdot (Z_i - BZ_i)) \quad \text{(Eq. 2.16)}$$

$$g(\theta_{ik}, Z_i) = \theta_k \cdot (1 + \theta_Z \cdot e^{\eta_Z} \cdot (Z_i - Z_{median})) \quad \text{(Eq. 2.17)}$$

In Eq. 2.16, Z_i, BZ_i and BZ_{median} represent a value of the covariate Z for the individual i, the individuals baseline value and the median baseline value in the population, respectively. θ_{BZ} and θ_{DZ} are the estimated interindividual and intraindividual covariate-parameter relationships.
In Eq. 2.17, η_Z is the estimated interindividual random-effects parameter on the covariate-parameter relationship θ_Z.

As described above, in addition to continuous covariates, **categorical covariates** exist that can be implemented into the NLME model by e.g. estimating separate parameters for each category or by using a **fractional change model**. The latter is demonstrated for an example of a covariate with two potential categories (CAT=1, 2) in the following equation (Eq. 2.18):

$$\text{If CAT=1: } \theta_{k,CAT=1} = \theta_k \quad \text{(Eq. 2.18)}$$

$$\text{If CAT=2: } \theta_{k,CAT=2} = \theta_k \cdot (1 + \theta_Z)$$

In Eq. 2.18, θ_k is the fixed-effects parameter in case of the first covariate category (CAT=1), which is usually the category with the higher number of observations in the dataset. θ_Z defines the fractional change of θ_k, in case of the second covariate category (CAT=2).

The **covariate model building strategies** typically start with the pre-selection of potential covariate candidates based on different criteria, e.g. graphical evaluation (by assessment of the relationship between a covariate and the individual structural and random-effects PK parameters), prior knowledge from publications or clinical interest. Afterwards the pre-selected candidates are investigated within the NLME model. Here, different approaches exist which can be selected based on the question of the analysis and data situation (e.g. stepwise covariate model building, full covariate modelling, LASSO, mechanistic implementation), which have been described in detail

elsewhere [204,206–210]. The covariate model building strategies applied in this work are in more detail described in the respective sections (Project I: Section 2.6.4.2, Project IV: Section 2.9.3.2).

Combining the three submodels as described above, results in the following general mathematical equation for NLME models (Eq. 2.19):

$$Y_{ij} = f((g(\Theta_i, Z_i), \eta_i, \kappa_i), x_{ij}), \varepsilon_{ij} \quad \text{(Eq. 2.19)}$$

2.3.2 Parameter estimation

NLME modelling aims at identifying parameter estimates that best match the observed data, both on population and on individual level. Parameter estimation is typically carried out using the maximum likelihood estimation approach, in order to find the set of parameters which maximises the likelihood of observing the data given the model (Eq. 2.20). These parameters are referred to as maximum likelihood estimates.

$$\mathcal{L}_i(\theta, \omega^2, \sigma^2 \,|Y_i) = p(Y_i|\theta, \omega^2, \sigma^2) = \prod_{j=1}^{n} \mathcal{L}(\,\theta, \omega^2, \sigma^2|Y_{ij}) \quad \text{(Eq. 2.20)}$$

In Eq. 2.20, $\mathcal{L}_i$ denotes the individual contributions to the likelihood of observing the data Y_i of every i^{th} individual given the model parameters $\theta, \omega^2, \sigma^2$. The variable p represents the corresponding probability density function.

In NONMEM® the so-called 'objective function value' (OFV) is used which is defined as minus twice the natural logarithm of the likelihood (Eq. 2.21) and hence minimised during parameter search (best fit = maximum likelihood = minimum OFV) [199].

$$OFV = -2\mathcal{LL} = -2 \cdot \log\big(\mathcal{L}(\theta, \omega^2, \sigma^2 \,|Y)\big) = \sum_{i=1}^{n} -2 \cdot \log\big(\mathcal{L}_i(\theta, \omega^2, \sigma^2 \,|Y_i)\big) \quad \text{(Eq. 2.21)}$$

Computation of the likelihood for nonlinear mixed-effect models is challenging and cannot be solved analytically [211]. That is why the OFV has to be approximated numerically, for which a variety of different estimation methods exist [211,212]. In the present work, the first-order conditional expectation (FOCE) method including the interaction option in NONMEM® was applied. The FOCE method is a gradient-based linearisation algorithm that approximates the likelihood by applying Laplace transformation and Taylor series expansion. The additional use of the interaction option allows for interaction between the interindividual random-effects (η) and residual random-effects (ε) parameters. The FOCE method uses an iterative procedure to determine the likelihood. First the likelihood is evaluated for the set of initial parameter estimates. Then, in the second iteration, the parameters are updated in the direction in which the likelihood increases,

i.e. the OFV decreases. This is repeated until convergence criteria are met and the maximum likelihood, i.e. the minimum OFV is found [211,213].

While the estimation method returns the population parameters, the individual parameter estimates (Empirical Bayes estimates, EBEs) are typically obtained in second *post-hoc* estimation step (also referred to as Bayes or conditional estimation step) [199,214]. In the FOCE method, this *post-hoc* estimation step is performed after each iteration step. The Bayes objective function is used to derive the EBSs for each individual by balancing the posterior and prior term (Eq. 2.22; [199,215]):

$$OFV_{Bayes} = Prior + Posterior = \sum_{k=1}^{m} \frac{\left(\theta_{k,EBE} - \theta_{k,pop}\right)^2}{\omega_k^2} + \sum_{j=1}^{n} \frac{(Y_{ij} - \widehat{Y_{ij}})^2}{\sigma^2} \qquad \text{(Eq. 2.22)}$$

In Eq. 2.22, the prior term is described as the sum of the squared deviation of the k^{th} individual parameter ($\theta_{k,EBE}$) from the k^{th} population parameter ($\theta_{k,pop}$), weighted by the respective k^{th} interindividual random-effects parameter (ω_k^2). The posterior term is defined as the sum of the squared deviation of the observed data for the i^{th} individual and j^{th} observation (Y_{ij}) from the predicted data for the i^{th} individual and j^{th} observation ($\widehat{Y_{ij}}$), weighted by the residual random-effects parameter (σ^2).

2.3.3 Model evaluation and discrimination

A crucial part of the model development process is the evaluation and assessment of the appropriateness of a developed model given a dataset, with the aim to evaluate the model ('model evaluation') and select the most appropriate model from a collection of models under consideration ('model discrimination') [216]. Depending on the dataset used for the evaluation of the model, evaluation methods can be classified in 'internal' and 'external'. While for the internal methods the evaluation is based on the dataset that has already been used for the development of the model, for external methods a dataset from another source (e.g. experiment or clinical study) is used. Additional common classifications comprise (1) 'basic' and 'advanced' according to the complexity of the method (e.g. computational time), (2) 'numerical' and 'graphical' according to the representation of the technique, and (3) 'data-based' and 'simulation-based' according to the basis of the evaluation. Important model evaluation techniques will be discussed in detail in the following, highlighting the allocation to the aforementioned classifications.

2.3.3.1 Goodness-of-fit plots

Classification of technique: 'internal', 'basic', 'graphical', 'data-based'

Goodness-of-fit (GOF) plots represent commonly used basic evaluation plots that are visually assessed to evaluate an NLME model with a special focus on the structural and residual variability

submodel. These plots are typically based on the observed dependent variable (observations), the predicted dependent variable (predictions) both for the population and the individual as well as on the differences between observations and predictions (residuals). Also, individual-/occasion-specific random-effects parameters and empirical Bayes estimates are assessed. The most important GOF plots are introduced in the following.

Observations versus predictions

Observations are plotted against both the population predictions (PRED) and the individual predictions (IPRED) and the scattering around the line of identity (intercept=0, slope=1) is evaluated. In case of an appropriate goodness-of-fit, data points show a symmetric scattering, without any systematic deviations that would suggest a model misspecification. In addition, the magnitude of spread of the data points around the line of identity is assessed. Considering the interindividual differences in the model parameters, observations versus PRED is expected to show a spread around the line of identity. For IPRED, however, the data points should be narrowly distributed around the line of identity. These plots are evaluated for the full population, for population subgroups and on an individual level.

Residuals

As the residuals depend on the absolute magnitude of the observations/predictions, the residuals are commonly weighted in order to use them for model evaluation [199]. The weighing of the residuals is dependent on the estimation algorithm used. In case of the FOCE algorithm in the NONMEM® software, which was applied in the present thesis, conditional weighted residuals are recommended which have been shown to adequately reflect model adequacy [193,217].
The distribution of conditional weighted residuals (CWRES) versus the independent variable and PRED is typically assessed (i.e. in case of PK: time and drug concentration, respectively). The plots are evaluated with respect to occurrence of a systematic trend as well as the magnitude of spread around the reference line (intercept=0, slope=0), for the full population and stratified by individual patients and patient subgroups.

Individual predictions

Per individual, the observations (i.e. in case of PK: drug concentrations) are graphically displayed against the independent variable (i.e. in case of PK: time) and overlaid with the respective PRED and IPRED ('individual predictions'). While PRED should display the central tendency in the population, IPRED should be as close as possible to the observations.

Distribution of random-effects and Empirical Bayes estimate

Distribution of individual-/occasion-specific random-effects (i.e. IIV: η or IOV: κ) and EBEs are

evaluated by histograms. Individual-/occasion-specific random-effects should approximate a normal distribution with a mean not significantly different from zero. A binormal distribution, for instance, might indicate a dichotomous covariate which is not yet implemented in the model, but is dividing the population into two distinct patient subgroups. The width of the distribution indicates the unexplained variability and should be rather small.
The distribution of the EBEs is dependent on the model used for implementation of the random-effects into the NLME model; in case of an exponential model structure (Eq. 2.4), EBEs are log-normally distributed.

2.3.3.2 Parameter precision

Classification of technique: 'internal', 'basic', 'numerical', 'data-based'

Within the NONMEM® software, estimates of the precision of the model parameters can be requested ($COVARIANCE). In this case, after the minimisation routine is complete, NONMEM® is postprocessing the output from the estimation step (Section 2.3.2) and providing as additional output the complete variance-covariance matrix of the estimates [193,194]. The standard errors (SE) of the model parameters can be derived by taking the square root of the diagonal elements of the matrix. For the sake of an easier interpretation of the parameter precision, SE are usually reported as relative standard errors (RSE, Eq. 2.23, Eq. 2.24). When reporting random-effects parameters as %CV instead of the estimated variance – which is typically the case (Section 2.3.1.2) – the RSE can be transformed into the approximate standard deviation scale (Eq. 2.25, [193]). In the following equations the computation of the RSE for fixed-effects parameters θ, Eq. 2.2) and the random-effects parameters (exemplarily represented for ω^2: Eq. 2.24, Eq. 2.25) are provided. For other levels of random-effects parameters (e.g. IOV: π^2, RUV: σ^2) complementary formulas are used. Of note, in this thesis RSE of random-effects parameters were reported on standard deviation scale unless stated otherwise.

$$RSE_{\theta},\% = \frac{SE_{\theta}}{\theta} \cdot 100 \quad \text{(Eq. 2.23)}$$

$$RSE_{\omega^2_{variance\ scale}},\% = \frac{SE_{\omega^2}}{\omega^2} \cdot 100 \quad \text{(Eq. 2.24)}$$

$$RSE_{\omega^2_{standard\ deviation\ scale}},\% = \frac{SE_{\omega^2}}{2 \cdot \omega^2} \cdot 100 \quad \text{(Eq. 2.25)}$$

Assuming a normal distribution of the parameters, 95% CI can be derived as exemplarily shown for the kth fixed-effects parameters θ in the following equation (Eq. 2.26):

$$Lower\ limit\ of\ 95\%CI = \theta_k - (SE \cdot 1.96) \quad \text{(Eq. 2.26)}$$

$$Upper\ limit\ of\ 95\%CI = \theta_k + (SE \cdot 1.96)$$

1.96 corresponds to the 97.5th percentile of the normal distribution and can thus be used to derive the lower limit (2.5th percentile) and the upper limit (97.5th percentile) of the 95% CI.

In addition to the parameter precision derived by NONMEM®, more advanced evaluation techniques exist which allow to derive confidence intervals for the model parameters of interest, without assuming a distribution of the parameter (e.g. bootstrap: Section 2.3.3.5, log-likelihood profiling: Section 2.3.3.4, [218]).

2.3.3.3 Shrinkage

Classification of technique: 'internal', 'basic', 'numerical', 'data-based'

If little and less informative individual information is available in the model building dataset, the individual parameters (i.e. EBEs) tend to shrink towards the typical fixed-effects parameter values, i.e. the variance in the EBEs decreases. This phenomenon is illustrated in Eq. 2.22, in which in case of sparse individual data situations, the posterior term of the formula gets smaller compared to the prior term and hence the population parameter values are given more weight than the data of the individual. This phenomenon is termed η-shrinkage and is described with the following equation (Eq. 2.27; [219]):

$$\eta - shrinkage = 1 - \frac{SD_{EBE_\eta}}{\sqrt{\omega^2}} \cdot 100 \quad \text{(Eq. 2.27)}$$

In Eq. 2.27, SD_{EBE_η} is the standard deviation of the individual values of the EBEs of η, ω^2 is the estimated variance of η. Of note, shrinkage values ≥20%-30%, can impact diagnostic plots based on EBEs (e.g. EBE versus covariates plots) and can thus result in a misinterpretation of the plots and unreliable conclusions.

Similarly to η-shrinkage, in case of sparse data, the distribution of the individual weighted residuals (IWRES, Eq. 2.28) distribution shrinks towards zero as well; this is called ε-shrinkage (Eq. 2.29, [219]).

$$IWRES = \frac{(Y_{ij} - \hat{Y}_{ij})}{\sqrt{\sigma^2}} \quad \text{(Eq. 2.28)}$$

$$\varepsilon - shrinkage = 1 - SD_{IWRES} \quad \text{(Eq. 2.29)}$$

Here, Y_{ij} is the observed dependent variable of the i^{th} individual at each time point j, $\hat{Y}_{ij}$ is the

respective model predicted dependent variable, σ^2 is the estimated variance of ε, and SD_{IWRES} is the standard deviation of the IWRES.

2.3.3.4 Log-Likelihood profiling

Classification of technique: 'internal', 'advanced', 'graphical', 'data-based'

Log-likelihood profiling (also called OFV profiling, objective function mapping or sensitivity analysis) is a technique which can be used to evaluate the precision and identifiability of model parameters. The parameter of interest is fixed to different values close to the final estimate and the remaining parameters are re-estimated. By computing the difference in the OFV between the original model and the re-estimated models, a log-likelihood (OFV) profile is generated which is typically graphically evaluated. Differences in the OFV equal to 3.84 represent the 95% confidence limits, assuming that the difference of the likelihood is approximately x^2 distributed. In addition, the log-likelihood profile of the parameter of interest can be investigated for global and local minima.

2.3.3.5 Bootstrap

Classification of technique: 'internal', 'advanced', 'numerical', 'data-based'

Bootstrap is a technique which can be applied to evaluate the precision and accuracy of the model parameters as well as the model robustness. This section will focus on the non-parametric bootstrap, which was applied in this thesis. By repeated random sampling with replacement from the original dataset on individual level, replicate datasets are created, each with the same size as the original dataset. The number of bootstrap replicates is dependent on the purpose of the bootstrap; e.g. to derive the CI, ≥1000 samples are recommended [220]. Using the re-sampled datasets, the model parameters are then re-estimated. The median of the new parameter estimates is compared with the estimate obtained with the original dataset, in order to assess the accuracy (bias; Eq. 2.30); by computing the 95% CI of the new parameter estimates the parameter precision can be evaluated.

$$Relative\ bias, \% = \frac{P_{orig,k} - P_{bs,k}}{P_{orig,k}} \cdot 100 \qquad \text{(Eq. 2.30)}$$

Here, $P_{orig,k}$ is the original estimate of the kth model parameter and P_{bs} the median of the respective parameters in the bootstrap replicates.

A measure for model robustness is the convergence rate, which is calculated as the percentage of models in the bootstrap replicates that converged during the parameter estimation process.

2.3.3.6 Case deletion diagnostics

Classification of technique: 'internal', 'advanced', 'graphical', 'data-based'

Case deletion diagnostics (also called jackknife, leave-one-out technique or leverage analysis) is a technique which aims at detecting individuals, groups of individuals or observations that show a substantial influence on the parameter estimates and thus also evaluates the model robustness and stability of the parameter estimates. In the following, the procedure is exemplified for case deletion diagnostic on the individual level. Each individual is deleted one-by-one from the dataset and the model parameters re-estimated based on the reduced datasets. The new parameter estimates are graphically compared with the original estimates and their 95% CIs. If the parameter lies outside the 95% CI of the original estimate the individual is considered influential. It is recommended to further investigate whether the individual shows distinctive characteristics which might explain the differences to the rest of the population.

2.3.3.7 Visual predictive checks

Classification of technique: 'internal', 'advanced', 'graphical', 'simulation-based'

The visual predictive check (VPC) is an important simulation-based evaluation technique which aims to assess the predictive performance of the NLME model. More concretely, by comparing percentiles derived from the distribution of observations with percentiles derived from the distribution of stochastic simulations (Section 2.4.2), the model's capability to reproduce the central tendency as well as the variability in the observed data is assessed. Typically, a large number of stochastic simulations (n=1000 replicates in this thesis) is performed and the 5^{th}, 50^{th} and 95^{th} percentiles of the observations and of each simulation replicate (i.e. median and 90% prediction interval) are derived. The percentiles of the observations are graphically compared with the median and the 95% CI of the percentiles of the simulations. A stratification of the VPC by e.g. patient subgroups or sampling matrices (e.g. plasma and microdialysate) can be used to evaluate the predictive model performance with respect to the stratification variables. For assessment of the covariate submodel, the VPC can be displayed using the covariate as independent variable, which allows to evaluate the predictive performance of the model across the full covariate range.

2.3.3.8 Prediction errors

Classification of technique: 'internal/external', 'advanced', 'numerical', 'simulation-based'

Another way of assessing the predictive performance of the model is to compare the observed dependent variable with the model predicted dependent variable by calculating prediction errors. Prediction errors allow evaluating both accuracy (e.g. prediction error (PE); Eq. 2.31) and precision (e.g. absolute prediction error (APE); Eq. 2.32) of the model and can be assessed either as absolute

value (unit of dependent variable; Eq. 2.31-Eq. 2.32: left) or as relative value (in percent; Eq. 2.31-Eq. 2.32: right).

$$PE_{ij} = \hat{Y}_{ij} - Y_{ij} \qquad RPE_{ij} = \frac{\hat{Y}_{ij} - Y_{ij}}{Y_{ij}} \cdot 100 \qquad \text{(Eq. 2.31)}$$

$$APE_{ij} = \left|PE_{ij}\right| \qquad RAPE_{ij} = \left|RPE_{ij}\right| \qquad \text{(Eq. 2.32)}$$

In Eq. 2.31, Y_{ij} is the observed dependent variable of the i^{th} individual at each time point j, $\hat{Y}_{ij}$ is the respective model predicted dependent variable.

To provide an overall measure of precision and accuracy, the mean or median of the prediction errors over all predictions can be reported. Computation for a subset of predictions only, allows to evaluate the predictive performance of the model for this specific subset (e.g. a specific phase of a drug concentration-time profile).

2.3.3.9 Objective function value and Akaike information criterion

Classification of technique: 'internal', 'basic', 'numerical', 'data-based'

As introduced in section 2.3.2 the objective function value (OFV) is defined as twice the natural logarithm of the likelihood. The likelihood ratio test is a statistical test which is commonly used to compare the OFV of two nested models. Two models are termed 'nested' if the parameters of one model (M_1) represent a subset of the parameters of the other model (M_2), i.e. M_1 can be obtained by setting one or more parameter(s) of M_2 to the null hypothesis values(s) [193,199]. For instance, the more complex model M_2 could be a covariate model and M_1 the respective base model. Since the OFV of a model is defined as minus twice the logarithm of the likelihood (Section 2.3.2), the likelihood ratio test can be used to evaluate the difference between the two OFV values of the two nested models (likelihood ratio, LR; Eq. 2.33):

$$LR = OFV_{M2} - OFV_{M1} \qquad LR \sim X^2(df = \Delta n_p) \qquad \text{(Eq. 2.33)}$$

The LR is assumed to be x^2 distributed; the degrees of freedom (df) are defined as the difference in the number parameters between the more complex model M_2 and the model M_1 (Δn_p). The LR is compared to the defined test statistic, which is dependent on the specified significance level α and the df. If the LR is larger than the statistics, the M_2 model results in a statistically significant improved description of the analysed data. Table 2.1 summarises

Table 2.1: Values of the x^2 distribution, for selected significant levels (α values) and degrees of freedom (df).

df	x^2 value (=test statistic)			
	α=0.1	α=0.05	α=0.01	α=0.001
1	2.71	3.84	6.64	10.8
2	4.60	5.99	9.21	13.8
3	6.25	7.82	11.3	16.3

test statistics selected dependent on the model development step (e.g. covariate forward inclusion: α=0.05, df=1, x^2 value=3.84).

For comparison of 'non-nested' models the Akaike information criterion (AIC) can be employed which is computed as follows (Eq. 2.34):

$$AIC = -2LL + 2 \cdot n_p \quad \text{(Eq. 2.34)}$$

In Eq. 2.34, $-2LL$ refers to the OFV of the model and n_p to the total number of parameters in the model, which can be considered as penalising term for larger models. When comparing two models, the model with the lower AIC value is deemed to provide the better description of the data and is thus selected [202].

2.4 Simulations

Simulations constitute a vital and powerful tool during the NLME model development process (for simulation-based model evaluation and discrimination, Section 2.3.3), but even more importantly after the model development. Simulations, as application of the NLME model, can be utilised to explore and better understand the system and relationship between patient, disease and drug, to assess 'what-if' scenarios, e.g. '*Which drug exposure is attained in a patient if the dose is increased by 2-fold?*' or '*Which dosing regimen results in adequate PK/PD target attainment for a critically ill patient with severe renal impairment?*' and to ultimately support therapeutic decisions [173,221]. Simulations can be classified into deterministic (non-stochastic) and stochastic simulations, which are selected depending on the research question [173]. The following section discusses the two types of simulations and introduces the 'probability of target attainment' analysis, a simulation-based approach commonly used to assess the adequacy of antibiotic dosing [63,163].

2.4.1 Deterministic simulations

Deterministic simulations are used to visualise the typical behaviour of the dependent variable over the independent variable considering the design variables. In case of simulations of PK, which will be focused on in this section, this could be the typical drug concentration-time profile for a given dosing regimen and covariate combination. Deterministic simulations are based on the fixed-effects parameters only and do not consider random-effects parameters [173]. This type of simulation represents a valuable tool to gain a better understanding of e.g. the interactions between the drug and the patient, by evaluating the typical drug exposure for specific covariate combinations but also the typical drug exposure resulting from a specific dosing regimen.

2.4.2 Stochastic simulations

Stochastic simulations, or Monte Carlo (MC) simulations, are used to visualise the behaviour in a population of individuals. In contrast to deterministic simulations not only fixed-effects but also random-effects parameters are considered in these simulations [173]. Depending on the research question, different levels of model variability can be considered in the simulations (i.e. PK variabilities IIV and IOV, but additionally also RUV, Eq. 2.19). For a defined set of design variables, a large population (typically n=1000 individuals) is generated by randomly sampling from the respective variability distributions. This type of simulation can be utilised to assess the variability of the drug exposure for a defined set of design variables. Moreover, in the field of antiinfective therapy, MCs form the basis for the probability of target attainment analysis, which is discussed in the following (Section 2.4.3).

2.4.3 Probability of target attainment and cumulative fraction of response analysis

As described before (Section 1.5), the probability of target attainment analysis (PTA) has become a powerful concept to assess the adequacy of antiinfective dosing regimens and to ultimately support dosing regimen selection [129,190]. In this type of analysis, the drug concentration-time profiles of a population of individuals (typically n=1000 patients), generated via stochastic MC simulations applying a NLME PK model (Figure 2.4 top), are evaluated with respect to the attainment of a predefined PK/PD target (e.g. 50%$fT_{>MIC}$). The PTA is derived by computing the percentage of simulated patients achieving the respective target (Figure 2.4 bottom). A PTA of 90%, i.e. 900 of 1000 patients attaining the target, is considered as adequate therapy [63]. Typically, the PTA is derived over a range of MIC values of interest but can also be assessed dependent on e.g. covariates implemented in the model. A PTA analysis can be used to e.g. identify patients at risk for ineffective exposure when administering the standard dosing regimen, but also to identify superior dosing regimens by evaluating alternative dosing regimens.

Based on the results of the PTA analysis, the cumulative fraction of response (CFR) can be derived, which additionally considers the MIC distribution of the bacteria of interest. Hence, the CFR can be applied when aiming to evaluate the probability of target attainment for a given pathogen without knowledge on the specific MIC value in a patient or a patient population. The CFR can be computed according to the following equation (Eq. 2.35):

$$CFR = \sum_{i=1}^{n} PTA_i \cdot f_i \qquad \text{(Eq. 2.35)}$$

in which i represents the index of MIC values ranked from lowest to highest MIC value of a population of pathogens, PTA_i the PTA of each MIC value and f_i the fraction of the respective

MIC value of the MIC distribution [222]. Information on the MIC distribution is collected in databases such as the EUCAST database [4].

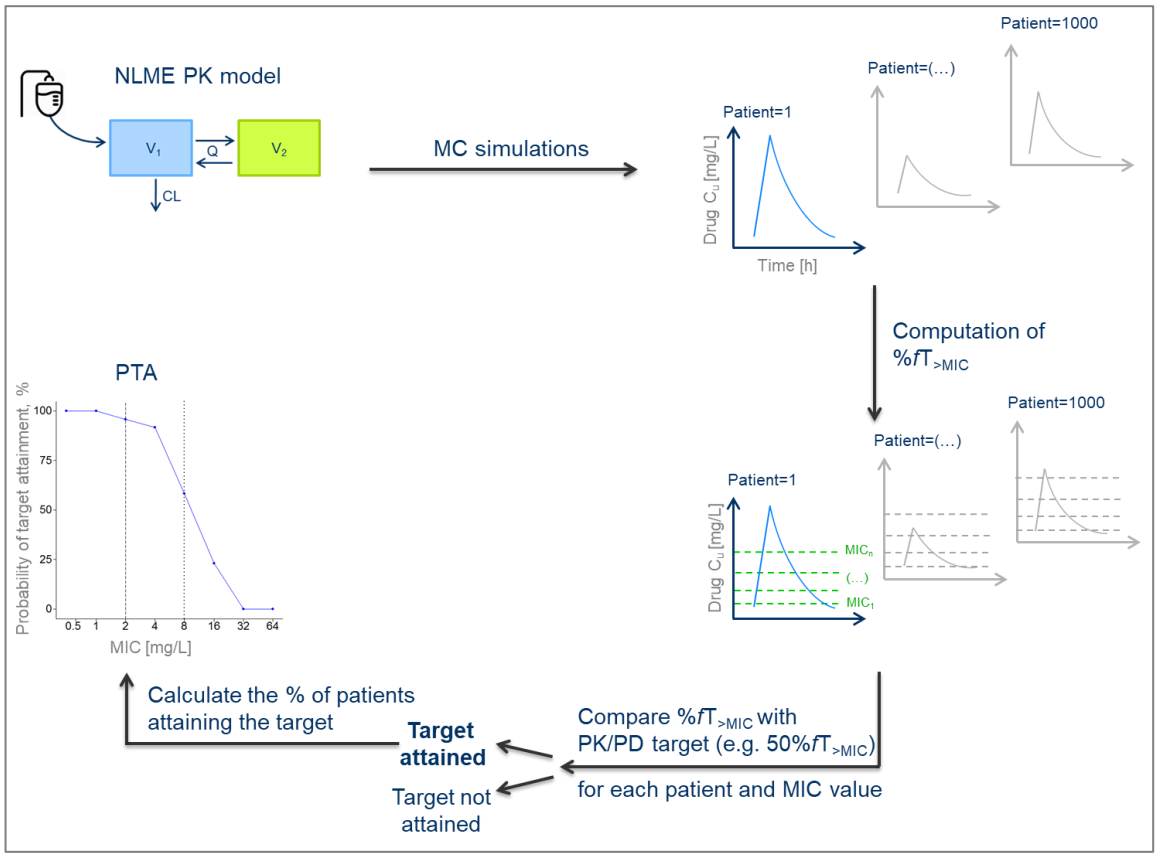

Figure 2.4: Graphical illustration of a typical PTA workflow.
Exemplified for drug administration via i.v. infusion, a two-compartment PK model, the PK/PD index $T_{>MIC}$ and PTA across different MIC values.
Abbreviations: *CL*: Clearance; *MC:* Monte Carlo; *MIC*: Minimum inhibitory concentration; *PK/PD*: Pharmacokinetic/ Pharmacodynamic; *PTA*: Probability of target attainment; *Q:* Intercompartmental clearance; V_1*:* Central volume of distribution; V_2: Peripheral volume of distribution; $\%T_{>MIC}$: Percentage of time that drug concentration exceeds the MIC value.

2.5 Software

This section summarises the software used in the present work (Table 2.2) as well as key functionalities and packages applied in the respective software (Table 2.3).

Table 2.2: Software used in the present thesis.

Software	Version	Reference	Used in projects:
NONMEM®	7.3	Icon Development Solutions, Ellicott City, MD, USA. (www.iconplc.com/innovation/nonmem)	I, II, IV
PsN	4.4.0-4.6.0	Uppsala University, Uppsala, Sweden. (uupharmacometrics.github.io/PsN) [223]	I, II, IV
Pirana	2.8.1-2.9.6	Pirana Software & Consulting BV (www.pirana-software.com) [224]	I, II, IV
R	3.1.2-3.5.0	The project for statistical computing. Vienna, Austria. (www.CRAN.R-project.org)	I, II, III, IV
R Studio	0.98.1091-1.1.447	Integrated development environment for R, Boston, MA. (www.rstudio.org)	I, II, III, IV
Microsoft® Office Excel®	2016	Microsoft Corporation, Redmond, Washington, USA.	III

Abbreviations: *PsN:* Pearl speaks NONMEM.

Table 2.3: Key functionalities and packages used in the respective software (Table 2.2).

Software	Functionalities, packages	Used in projects:
PsN	*vpc* functionality	I, IV
	bootstrap functionality	I, IV
	llp functionality	I, IV
	cdd functionality	I, IV
	sse functionality	IV
	scm functionality	I, IV
R	*ggplot2* package	I, II, III, IV
	xpose4 package	I, IV
	Git version control	I, II
Microsoft® Office Excel®	Visual basics for application	III

Abbreviations: *vpc*: Visual predictive check; *llp:* Log-likelihood profiling; *cdd:* Case deletion diagnostics; *sse:* Stochastic simulation and estimation; *scm*: Stepwise covariate model-building.

Computationally intensive modelling and simulation activities were partly performed on the high-performance computing cluster ‘Soroban’ by the Freie Universitaet Berlin [225].

2.6 Project I: Characterisation of linezolid plasma and target site exposure in obese and nonobese surgical patients, including the evaluation of the microdialysis methodology

2.6.1 Clinical study design

A prospective, open-label, parallel group, controlled single-centre clinical trial was conducted at the University Hospital of Leipzig, Germany, with the aim to assess the antibiotic treatment with four antibiotic drug combinations in obese and nonobese surgical patients (treatment group 1: linezolid and meropenem; 2: tigecycline; 3: cephazolin and metronidazole; 4: fosfomycin and piperacillin/tazobactam) [226]. The clinical study was approved by the ethics committee of Leipzig University, Germany (121/13-ff) and the Federal Institute for Drugs and Medical Devices of Germany (BfArM) and was registered in the European Clinical Trials Database (EudraCT number: 2012-004383-22).

In total, 120 obese and nonobese patients were to be enrolled in the clinical study, i.e. 30 patients per treatment group, each comprising 15 obese (=index group) and 15 nonobese patients (=control group). The current work focused on treatment group 1, more specifically, the treatment with the antibiotic linezolid. Criteria for inclusion comprised an age ≥18 years, an abdominal surgical intervention with a need of antibiotic prophylaxis, written informed consent and a BMI of ≥35 kg/m² and <30 kg/m² in the index group and the control group, respectively. Exclusion criteria included treatment with study medication ≤72 h before surgery, known allergic reactions against one of the study drugs, pregnancy or breastfeeding (for detailed information on inclusion and exclusion criteria see Appendix Table S1). Obese and nonobese patients were matched according to sex and age (maximum accepted age difference: ±5 years).

Anaesthesia was performed according to local clinical standards either by balanced anaesthesia with propofol and sufentanil or remifentanil followed by desflurane/isoflurane/sevoflurane, or by total intravenous anaesthesia (TIVA). All patients received a single standard dose of the antibiotic linezolid (600 mg as 30-min i.v. infusion), 30 min to 1 h before the surgical incision (Figure 2.5). Concurrently, all patients received meropenem as well as an analgesic drug (half of the patients: acetaminophen, the remaining half: metamizole).

The PK of linezolid was monitored over 8 h, i.e., depending on the duration of the surgery, PK samples could be collected during anaesthesia (intra-anaesthetic, anaesthesia status='ON') or after anaesthesia (post-anaesthetic, anaesthesia status='OFF'). The planned blood sampling time points were as follows: 30 min, 1 h, 2 h, 3 h, 4 h, 5 h, 6 h and 8 h after start of the linezolid infusion (Figure 2.5) and were collected via an arterial line which is often used during surgery to monitor blood pressure and analyse arterial blood gasses [227]. In addition, microdialysate samples were collected in the ISF of the s.c. adipose tissue. For this purpose, per patient, two microdialysis

catheters, identical in construction (CMA 63 microdialysis probe, membrane length 30 mm, cut-off 20,000 Da, CMA, Kista, Sweden), were inserted into the s.c. adipose tissue of each upper arm, 90 min before start of linezolid dosing. The catheters were perfused with 0.9% NaCl solution using a flow rate of 2 µL/min. After this 90-min equilibration period, microdialysis samples were collected during the following planned sampling intervals: 0-30 min, 30 min-1 h, 1-1.5 h, 1.5-2 h, 2-3 h, 3-4 h, 4-5 h, 5-6 h, 6-7 h, 7-8 h after start of the linezolid infusion (Figure 2.5). Subsequently, after flushing and equilibration for 5 min, the catheters were calibrated using the retrodialysis technique (Section 1.2). For this purpose, the catheter was perfused with the retroperfusate (planned linezolid concentration of 150 mg/L) and up to two retrodialysate samples were collected per catheter. While for the first 14 enrolled patients one retrodialysis period over 30 min was scheduled, for the following 16 patients a double retrodialysis was performed (with collection intervals à 15 min) – following the suggestions from a concurrently performed *in vitro* investigation [228]. The exact sampling time points and collection intervals were recorded by the medical staff.

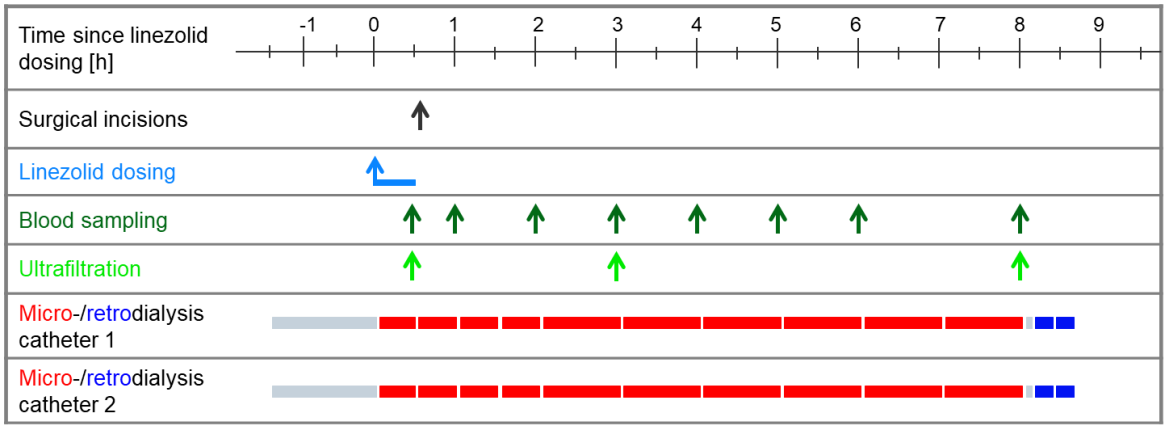

Figure 2.5: Clinical study design and PK sampling schedule (modified from [226]).
Black arrow: Surgical incision; *Blue arrow/bar*: Start/duration of 30-min linezolid infusion; *Dark green arrows*: Blood sampling time points; *Light green arrows*: Blood samples in which unbound linezolid concentrations were determined via ultrafiltration; *Grey bars*: Catheter equilibration/flushing periods; *Red bars*: Microdialysis collection intervals; *Blue bars*: Retrodialysis collection intervals.

In addition to the PK samples, patient- and surgery-specific information were recorded (Section 2.6.4.2: Covariate model development): After obtaining the written informed consent to participate, baseline characteristics, such as sex, age, body height, total body weight and laboratory data were collected. On the day of surgery, information on e.g. the surgery (e.g. indication, type, duration), anaesthesia and intubation were recorded. Furthermore, perioperative arterial blood pressure and heart rate were routinely monitored and reported longitudinally for each patient during the PK monitoring period.

2.6.2 Bioanalytical quantification

PK samples were analysed at the Department of Pharmacology, University of Regensburg, Regensburg, Germany. For 3 of the 8 blood samples per patient, ultrafiltration was performed to characterise the protein binding of linezolid. The 3 blood samples were selected around 30 min, 3 h and 8 h, i.e. at high (30 min=C_{max}), medium (3 h) and low (8 h) drug concentrations, with the aim to assess a potential concentration-dependency in protein binding. Linezolid concentrations in all matrices (plasma, ultrafiltrate, microdialysate, retroperfusate, retrodialysate) were quantified using HPLC methods coupled with spectrometric detection [228].

2.6.3 Data management and exploratory data analysis

All steps of data management and exploratory data analysis were encoded in R in a generalisable way, allowing to use the scripts as a basis for the analysis of other study drugs of all different treatment groups (Section 2.6.1; [226]).

2.6.3.1 Dataset generation

A NONMEM® compatible dataset was generated as outlined in section 2.2.1. Given the variety of the available PK data (plasma, ultrafiltrate, microdialysate, retrodialysate, retroperfusate; Section 2.6.1), additional data items (e.g. FLAG: to specify the PK sampling matrix; CMT: to specify the compartment for the respective matrix; CIN: to specify the retroperfusate concentration; TIN: to specify the length of the dialysate collection interval) were added. Furthermore, additional events (rows) were added to modify the status of a microdialysate compartment, utilised to integrate microdialysate concentrations as part of an advanced integrated dialysate-based modelling approach (Section 2.6.4.1; [229]). At the start of each collection interval, the respective compartment (example: µD compartment represents compartment 3) was ‘turned on’ (EVID=2, CMT=3), thereby initiating the integration over the microdialysate (µD) concentration-time profile. At the end of the collection interval, the compartment was ‘switched off’ and ‘reset’ (EVID=2, CMT=-3). Depending on the desired structure of the NLME model, the dataset was adjusted accordingly. In addition, different body size descriptors (BMI; LBW: lean body weight; FM: fat mass; IBW: ideal body weight; ABW: adjusted body weight) and haemodynamic markers (MAP: mean arterial pressure, CO_{LZ}: cardiac output according to Liljestrand and Zander [3]) were added to the dataset, which were computed as described in Appendix 7.3.2 and Appendix 7.3.4, respectively.

The full final dataset for the 30 patients consisted of 110 columns and 2607 rows. For illustration an exemplary subset of the dataset used for the final NLME model, is provided for a generic patient in Appendix 7.4.1.

Handling of missing data: Imputation

In case of available microdialysis data, but missing catheter calibration data via retrodialysis (i.e. missing RR estimates to the transform microdialysate into ISF concentrations), imputation of retrodialysis data was performed based on identified impact factors on the RR value (Section 3.1.1.2). More specifically, considering the need of raw retrodialysate and -perfusate concentrations in the dataset underlying the dialysate-based integral modelling, not the RR value itself was imputed, but the respective retrodialysate and -perfusate concentrations. As retroperfusate concentration, the originally planned concentration (i.e. 150 mg/L; Section 2.6.1) was imputed. The associated retrodialysate concentration was derived on the basis of the RR value (determined based on the quantified impact factors; Section 3.1.1.2) and the originally planned retroperfusate concentration (Eq. 1.2).

2.6.3.2 Dataset checkout

In addition to the performed cross column checks and index plots (Section 2.2.2.), newly developed individual graphical evaluation plots were generated to assess the sampling schedule of micro- and retrodialysis with respect to plausibility (Appendix Figure S1).

2.6.3.3 Exploratory data analysis

Prior to NLME modelling, available PK and additional patient-specific data were analysed according to the exploratory statistical and graphical data analysis procedures described in section 2.2.3. The current project focused on the evaluation of the different types of PK data with respect to exposure. For this purpose, different PK matrices (e.g. plasma versus ISF), different patients (e.g. obese versus nonobese) and microdialysate data collected with different catheters (i.e. catheter 1 versus catheter 2) were analysed. Apart from exposure evaluation, the PK data were analysed with regard to choosing a potential PK model (e.g. number of disposition phases, nonlinearity, tissue fluid distribution). Furthermore, patient- and surgery-specific characteristics such as body size (e.g. BMI, LBW, FM, IBW, ABW) and anaesthesia status and haemodynamic markers (e.g. MAP, CO_{LZ}) were assessed (e.g. their distribution; section 2.2.3).

2.6.4 Nonlinear mixed-effects modelling

2.6.4.1 Integrated dialysate-based modelling approach for microdialysis data

Two NLME different modelling approaches for analysing data obtained from microdialysis experiments have been described which differ in the complexity, the underlying assumptions and the output of the data analysis: The ‘mid-time approach’ and the ‘integrated dialysate-based modelling approach’ [229–231]. The mid-time approach represents a simple stepwise analysis approach that requires data transformation prior to modelling. More concretely, microdialysate

concentrations are converted into ISF concentrations based on the relative recovery values obtained from the retrodialysis calibration. As the name of this approach implies, the derived ISF concentrations are assigned to the mid-time point of the collection interval for modelling purposes. Hence, this method makes assumptions regarding the time point of the microdialysate observation and assumes an error-free relative recovery.

The integrated dialysate-based modelling approach was first proposed by Tunblad et al. for animal data [229] and Minichmayr and Schaeftlein et al. at our department for humans [45,230] and was applied in the present thesis. In contrast to the mid-time approach, this more advanced modelling approach analyses all available PK data including the untransformed micro- and retrodialysate data ('dialysate-based') simultaneously. Consequently, this approach does not require any data transformation prior to modelling. The relative recovery factor is estimated based on the retroperfusate and retrodialysate concentrations according to Eq. 1.2 and is used to transform microdialysate concentrations into ISF concentrations (Figure 2.6 A).

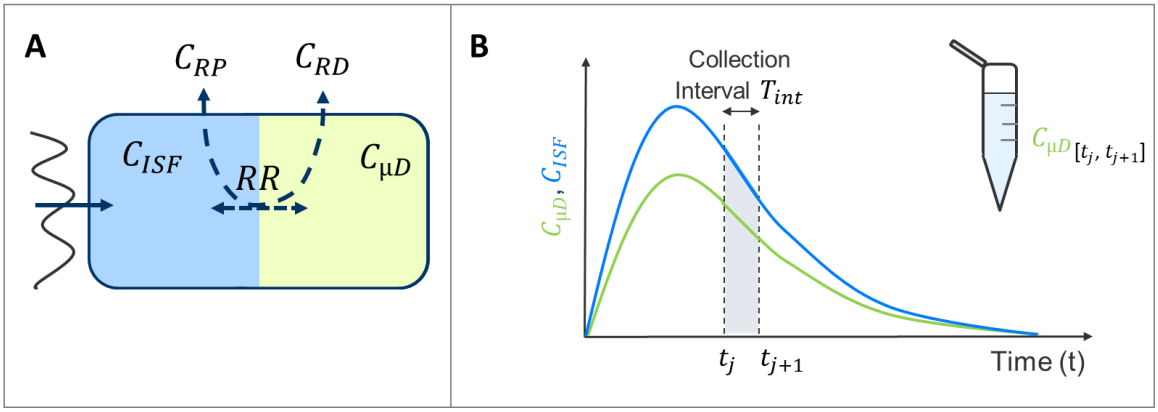

Figure 2.6: Illustration of the integrated dialysate-based modelling approach.
A: Snapshot of full structural NLME model, which illustrates the use of all available PK data ($C_{\mu D}$, C_{RP}, C_{RD}) and the estimation of the RR value within the model, which converts $C_{\mu D}$ into C_{ISF}. *Solid/Dashed arrows*: Indicate mass transfer/no mass transfer.
B: Microdialysate and ISF concentration-time profiles, which illustrate the integration over the profile for a defined collection interval T_{int}.
Abbreviations: C_{ISF}: ISF concentration; $C_{\mu D}$: Microdialysate concentration; C_{RD}: Retrodialysate concentration; C_{RP}: Retroperfusate concentration; *ISF*: Interstitial space fluid; *PK*: Pharmacokinetic; *RR*: Relative recovery; *t*: Time; T_{int}: Time interval.

This is done within the model, by integrating the linezolid concentration-time profile over the collection interval using the underlying PK model (Eq. 2.3; Figure 2.6 B), thus not requiring any assumptions regarding the sampling time points.

$$C_{\mu D_{[t_j, t_{j+1}]}} = \int_{t_j}^{t_{j+1}} C_{ISF}(t) \cdot RR \, dt \, / (t_{j+1} - t_j) \qquad \text{(Eq. 2.36)}$$

In Eq. 2.36, the microdialysate concentration $\left(C_{\mu D_{[t_j, t_{j+1}]}},\ j \in \{1, \dots, n-1\}\right)$ is defined by the integral of the ISF concentration-time profile $\left(C_{ISF}(t)\right)$ multiplied by the relative recovery value (RR) over the collection interval $\left(T_{int} = [t_j, t_{j+1}]\right)$, which is then divided by the duration of the

microdialysate collection ($t_{j+1} - t_j$). To realise this computation in NONMEM®, concentrations are 'accumulated' (i.e. 'integrated') in a separate compartment, as commonly used for e.g. AUC calculations (Appendix 7.4.2).

2.6.4.2 Model development strategy

Given the PK data collected in different matrices, the NLME model was developed in a stepwise sequential procedure (Figure 2.7). In brief, a base model was developed based on the total plasma concentrations (step 1), which was extended by the unbound plasma concentrations determined via ultrafiltration (step 2). The microdialysate concentrations together with the respective retroperfusate and dialysate concentration data of one of the catheters were then added (step 3) and subsequently the data of both catheters (step 4). Finally, a covariate analysis was performed with a special focus on body size descriptors and surgery-specific characteristics (step 5). Further details are provided in the following sections.

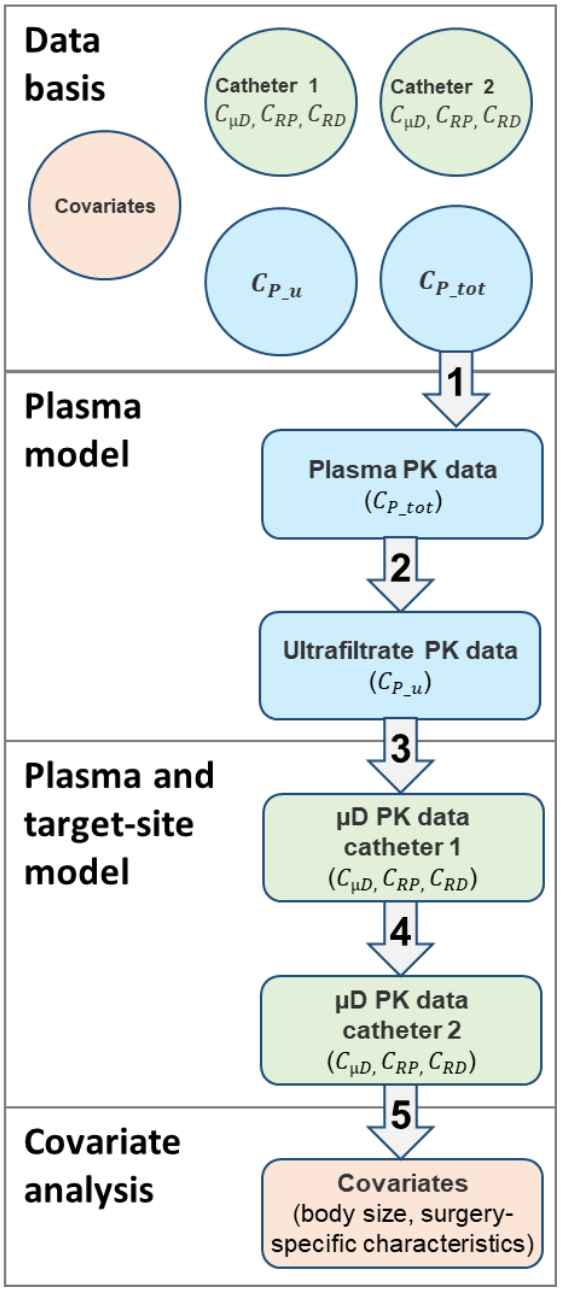

Figure 2.7: Model development strategy. The numbered arrows represent the steps of the model development procedure (for further information see text, section 2.6.4.2).
Abbreviations: C_{P_tot}: Total plasma concentrations; C_{P_u}: Unbound plasma concentrations; C_{RD}: Retrodialysate concentration; C_{RP}: Retroperfusate concentration; $C_{\mu D}$: Microdialysate concentration; µD: Microdialysate.

Base model development: Plasma (steps 1-2)

Base model development started from investigating total plasma concentrations and aimed to characterise the plasma PK of linezolid (**step 1**). Based on the results of the exploratory analysis and prior knowledge from previously published literature, different structural linezolid disposition models (one-, two-compartment) were investigated. IIV was implemented using the 'full approach', i.e. the diagonal random-effects parameters were implemented on all PK parameters simultaneously using an exponential model (Eq. 2.4). IIV parameters were assessed and removed in a stepwise backward deletion procedure until none of the remaining IIV parameters met any of the following exclusion

criteria: Precision (≥50% RSE), η-shrinkage (≥30%) and magnitude of IIV (≤10%CV). Additional covariance between the IIV parameters was assessed using the OMEGA BLOCK functionality in NONMEM® (Section 2.3.1.2) and was implemented if correlation coefficient $\rho \geq 75\%$ (Eq. 2.7). RUV was investigated using additive (Eq. 2.9), proportional (Eq. 2.10) and combined (Eq. 2.11) variability models.

Next, to characterise the protein binding of linezolid, unbound plasma concentrations were integrated in the model and an additional 'fraction unbound' (f_u) parameter was estimated, which linearly scaled total to unbound linezolid concentrations (**step 2**). An additional IIV parameter on the estimated f_u parameter as well as separate RUV for the unbound plasma concentrations were evaluated. In the resulting plasma model for total and unbound linezolid concentrations, different clearance (CL) models were assessed on the basis of the results of the exploratory data analysis and prior knowledge from previously published literature:

- Linear CL
- Concentration-dependent clearance:
    - Nonlinear Michaelis-Menten CL
    - Parallel linear and nonlinear Michaelis-Menten CL
    - Nonlinear CL using an empirical inhibition compartment [45,146]
- Time-varying CL dependent on surgery-specific characteristics:
    - Anaesthesia status
    - Intubation status
    - Haemodynamic markers

Base model development: Plasma and target site (steps 3-4)

The successfully developed plasma base model was extended by the PK data of one of the microdialysis catheters (i.e. its microdialysate, retroperfusate and retrodialysate concentrations) using the integrated dialysate-based modelling approach (Section 2.6.4.1), in order to evaluate the kinetics of tissue fluid distribution (**step 3**). Different structural models, assuming different distribution kinetics, were assessed:

- Model A: Rapid negligible distribution of linezolid from plasma to ISF (i.e. target site), i.e. rapid equilibrium between plasma and ISF:
  Assignment of ISF to the central compartment of the plasma base model and estimation of an additional tissue scaling factor
- Model B: Delayed distribution of linezolid from plasma to the target site, with ISF data showing similar kinetics of linezolid transfer as the peripheral compartment of the plasma base model:
  Assignment of ISF to the already existing peripheral compartment of the plasma base

model and estimation of an additional tissue scaling factor

- Model C: Delayed distribution of linezolid from plasma to the target site; with ISF data showing different kinetics of linezolid transfer than the peripheral compartment of the plasma base model:
  Assignment of ISF to a second separate peripheral compartment and estimation of two additional PK parameters of this compartment (intercompartmental clearance and the volume of distribution)

Apart from the exploratory graphical data analysis, the appropriateness of distribution model A was assessed by evaluating the applicability of an already existing pooled NLME PK model for linezolid, which had ISF assigned to the central compartment [45]. For this purpose, concentration-time profiles of obese and nonobese patients were predicted using the final PK parameters estimated in the pooled population PK model [45] based on an overweight diabetic (BMI_{median}=31 kg/m^2) and a healthy population (BMI_{median}=23 kg/m^2), respectively. Final model parameter estimates and individual data were used for Bayesian estimation of individual PK parameters (Section 2.3.2; MAXEVAL=0 functionality in NONMEM®). Model adequacy was assessed by goodness-of-fit plots (Section 2.3.3.1), visual predictive checks (Section 2.3.3.7) and calculation of prediction errors (Section 2.3.3.8).
For the three structural models (A-C), IIV was investigated on the additional PK- and methodology-related parameters and separate RUV parameters assessed for the micro- and retrodialysate concentrations. Furthermore, the links of the unbound ISF concentrations with the total or the unbound plasma concentrations were investigated, respectively.

After identification of an appropriate structural model, the data of the second catheter was integrated instead of the first catheter and subsequently in addition to the first catheter, with the aim of identifying different levels of catheter variability in the microdialysis technique (**step 4**). After replacing the data of catheter 1 by the data of catheter 2, all model parameters were re-estimated and compared to the parameters of the previous model based on data from catheter 1. Thereafter, the data of both catheters were simultaneously analysed and different levels of variability in the microdialysis technique dissected and quantified: Intercatheter variability (based on 2 catheters/patient) and intracatheter variability (based on 1-2 retrodialysis assessments /catheter).

Covariate model development (step 5)

The covariate model development aimed to identify covariates that explained microdialysis methodology- and PK-related variability between the patients. For the PK-related variability, the analysis focused on the investigation of body size descriptors and surgery-specific characteristics. Body size was pre-investigated using the following three approaches:

- Approach 1: Analysis of the categorical covariate 'obesity' using the automated stepwise covariate model building procedure *scm* in PsN [223].
- Approach 2: Analysis of continuous body size descriptors (total body weight (WT), BMI, ABW, IBW, LBW) and additional pre-selected covariate candidates (sex; ASAT: aspartate aminotransferase; ALAT: alanine aminotransferase; GGT: gamma-glutamyl-transferase; bilirubin; $CLCR_{CG\_LBW}$: Creatinine clearance estimated according to Cockcroft and Gault using LBW [2]) using the automated stepwise covariate model building procedure *scm* in PsN [223]. Preselection was performed based on graphical evaluation and prior knowledge from publications (Section 2.3.1.3).
- Approach 3: Analysis of body size using a mechanistic implementation according to Huisinga et al. [210] and Holford et al. [204].

Approach 3 aimed to more mechanistically implement body size into the NLME model by separating total body weight into LBW and FM, which are jointly used as covariates on the PK parameters. The respective proportional impact of LBW and FM on the PK parameters are estimated in the models and are specific for the drug and the PK parameter. In case of a hydrophilic drug, LBW might be an appropriate covariate to describe volume of distribution or clearance, while for lipophilic drugs, an additional impact of FM is likely [204]. Both models (i.e. Huisinga et al. (Eq. 2.37) and Holford et al. (Eq. 2.38)) use the same approach, but different parameterisations.

$$\theta_{ik} = \theta_{k,ref} \cdot \left((1 - R) \cdot \frac{LBW_i}{LBW_{ref}} + R \cdot \frac{FM_i}{FM_{ref}} \right) \quad \text{(Eq. 2.37)}$$

$$NFM_i = LBW_i + f_{fat} \cdot FM_i \quad \text{(Eq. 2.38)}$$

$$NFM_{ref} = LBW_{ref} + f_{fat} \cdot FM_{ref}$$

$$\theta_{ik} = \theta_{k,ref} \cdot \frac{NFM_i}{NFM_{ref}}$$

In both models, θ_{ik} represents the typical k^{th} PK parameter for the i^{th} individual LBW_i-FM_i combination; $\theta_{k,ref}$ represents the typical k^{th} PK parameter for the reference LBW_{ref}-FM_{ref} combination. In the model by Huisinga et al. (Eq. 2.37), the estimated parameter R defines the proportional impact of LBW and FM on θ_k, if e.g. R=0.5, doubling the FM would have the same impact on θ_k as doubling LBW. The individual LBW and FM (LBW_i, FM_i) are centred around the reference values (LBW_{ref}, FM_{ref}). In the model by Holford et al. (Eq. 2.38), a new body size descriptor 'normalised fat mass' (NFM) is introduced, which is defined by the estimated parameter f_{fat} representing the fraction of FM which is added to LBW. Similar to the model by Huisinga et al., the individual NFM (NFM_i) is centred around the reference NFM (NFM_{ref}).

Based on the results of the three covariate pre-investigations performed, a stepwise covariate analysis strategy was developed in order to identify the final covariate model for body size (Appendix Table S5). For evaluation of the surgery-specific impact on the PK of linezolid, the categorical covariate 'anaesthesia status' and the continuous haemodynamic markers were assessed (heart rate, MAP, CO) using fractional change (Eq. 2.18) and linear (Eq. 2.13) covariate-parameter relationships, respectively.

After having included all identified covariates into the model, the final model refinement step focused on the reassessment of the RUV model structures for the different sampling matrices and the centring of the covariate effects around typical covariate values.

2.6.4.3 Model evaluation and discrimination

A combination of evaluation approaches (goodness-of-fit plots, VPCs (n=1000 simulations, stratified by sampling matrix and/or obesity status of the patient)), assessment of parameter plausibility and precision) was used for model evaluation. In case of competing models, OFV values were compared using the likelihood ratio test or AIC values. In addition, for the final model, the following advanced evaluation techniques were used:

- Non-parametric bootstrap (n=1000 replicate datasets) to assess accuracy and precision of the parameter estimates as well as model robustness (evaluating the convergence rate)
- Case-deletion diagnostics (on patient level) to evaluate model robustness and the presence of influential individuals

Details on the abovementioned evaluation techniques are summarised in section 2.3.3.

2.6.5 Simulations: Exploration of linezolid exposure

To further explore the PK of linezolid after standard dosing, the final NLME PK model was applied by simulating linezolid concentration-time profiles in different body fluids and for different patient characteristics. With regard to body fluids, the analysis focused on the comparison of the total and the unbound linezolid concentrations in plasma with ISF concentrations in the s.c. adipose tissue. Patient characteristics were selected according to the covariates identified in the final NLME PK model.

The first analysis aimed at analysing specific plausible covariate combinations, representing typical patients of the study population (Table 2.4 A). Deterministic and stochastic simulations were performed (n=1000 patients; Sections 2.4.1-2.4.2). In the second analysis, the impact of body size on linezolid exposure was further evaluated. More precisely, the body size descriptor(s) identified in the NLME PK model, were varied over a broad range with the remaining covariates set to the representative values in the population, and the resulting linezolid concentration-time profiles were assessed using deterministic simulations (Table 2.4 B). In both analyses, simulations were

performed for standard linezolid i.v. dosing (600 mg as 30-min infusion) administered as single dose, but also as multiple doses (q12h) for the first 24 h of treatment.

Table 2.4: Patients used for exposure simulations.

A: Typical obese and nonobese patients during and after anaesthesia (used for simulation analysis 1)

Characteristics	**Typical patients**			
	obese and intra-anaesthetic	**nonobese and intra-anaesthetic**	**obese and post-anaesthetic**	**nonobese and post-anaesthetic**
Sex[1]	female	female	female	female
Body weight[2] [kg]	119	65	119	65
Body height[2] [m]	1.65	1.67	1.65	1.67
MAP[2] [mmHg]	71.7	66.7	91.7	83.3
Anaesthesia status[3]	ON	ON	OFF	OFF
BMI[4] [kg/m^2]	43.7	23.3	43.7	23.3
LBW[4] [kg]	56.7	41.7	56.7	41.7

B: Patients with varying LBW[6] during surgery (used for simulation analysis 2).

Characteristics	**Patients with LBW[6] [kg] of:**									
	35	**40**	**45**	**50**	**55**	**60**	**65**	**70**	**75**	**80[8]**
Sex[1]	|—— female ——|									
Anaesthesia status[3]	|—— ON ——|									
Body height[2] [m]	|—— 1.65 ——|									
MAP[2] [mmHg]	|—— 69.2 ——|									
Body weight[5] [kg]	50.1	61.8	75.4	91.7	111	135	166	205	258	334
BMI[5] [kg/m2]	18.4	22.7	27.7	33.7	40.8	49.6	61.0	75.3	94.8	122
Obesity status[7]	0	0	0	1	1	1	1	1	1	1

Symbols '|—— xxx ——|': indicate that same value of a characteristic was used for all patients.
Grey shading: indicates which characteristics were derived or back-calculated from observed characteristics (i.e. characteristics not shaded in grey).
[1]Assigned to most frequently observed sex in the population (i.e. female; Section 3.1.1.1).
[2]Assigned to median of the respective female patient population.
[3]Indicates whether patient is under anaesthesia (intra-anaesthetic, 'ON') or thereafter (post-anaesthetic, 'OFF').
[4]Derived based on the observed characteristics not shaded in grey.
[5]For illustration back-calculated from LBW (Eq. 7.11) and the observed characteristics not shaded in grey.
[6]LBW as the body size descriptor(s) identified in the NLME PK model (Section 3.1.2.2).
[7]For illustration derived from BMI (0: nonobese, i.e. BMI<30 kg/m^2; 1: obese, i.e. BMI≥30 kg/m^2).
[8]Extraploated for female patient population (i.e. LBW of 80 kg was not observed); but observed for male patient population.
Abbreviations: *BMI*: Body mass index; *LBW*: Lean body weight; *MAP*: Mean arterial pressure.

2.7 Project II: Evaluation and optimisation of linezolid dosing regimens for infection prophylaxis and acute therapy in obese and nonobese surgical patients

The NLME PK model which was developed in Project I was applied to assess the adequacy of linezolid dosing regimens in the setting of infection prophylaxis and acute infection therapy for patients with different clinical characteristics and pathogen susceptibilities.

In this paragraph a general description of the analysis approach is provided, while in the following two subsections 2.7.1 and 2.7.2, a more detailed description is provided for the setting of infection prophylaxis and acute infection therapy, respectively. In general, to assess the adequacy of linezolid dosing regimens, for each specific covariate combination and dosing regimen, linezolid concentration-time profiles were simulated for 1000 patients using stochastic MC simulations (Section 2.4.2) considering IIV in the PK parameters. To assess the attainment of 'effective exposure', the PTA (Section 2.4.3, technical details are described in more detail below) was evaluated for the PK/PD target of 95%$fT_{>MIC}$ (considering non-achievability of 100%$fT_{>MIC}$ due to single dose treatment and the delayed distribution of linezolid into ISF). PTA was evaluated for the MIC values 0.5 , 1 , 2 , 4 mg/L (the latter two, representing non-species related as well as species related EUCAST S and R breakpoints of relevant pathogens, e.g. *S. aureus*, *Enterococcus* spp. and α-haemolytic *Streptococcus* spp. [5]). A PTA of ≥90% (i.e., 900 of 1000 patients achieving the PK/PD target [63]) was considered adequate.

2.7.1 Simulations: Evaluation of standard linezolid dosing for infection prophylaxis

In order to evaluate standard linezolid dosing for the setting of infection prophylaxis during surgery, PTA was assessed for three different incision-suture durations, i.e. times between incision and suture (2 h, 4 h, 6 h), based on unbound linezolid concentrations in the ISF of the s.c. adipose tissue (as a potential site of infection) following a single standard linezolid dose (600 mg, as 30-min i.v. infusion, 30 min before incision). As the analysis focused on assessing different incision-suture durations, the analysis was performed for the typical 'intra-anaesthetic' obese and nonobese patient of the study population (Table 2.4 A) as well as for varying values of body size descriptor(s) identified in the NLME PK model (Table 2.4 B).

2.7.2 Simulations: Evaluation and optimisation of linezolid dosing for acute therapy

In order to evaluate and, if needed, optimise linezolid dosing regimens for the setting of acute infection therapy, PTA was assessed for the first 24 h of treatment based on unbound linezolid

concentrations in the ISF of the s.c. adipose tissue as well as in plasma following standard but also alternative linezolid dosing regimens. Compared to standard linezolid dosing, the seven alternatives comprised dosing regimens with an intensified daily dose and/or a prolonged infusion duration and/or a shortened dosing interval (Table 2.5),. Throughout this project an informative code 'XY_Z' was used to indicate the dosing regimens: In this code X represents the type of infusion, Y the administered daily dose in gram and Z the dosing interval in hours (e.g. for the standard linezolid dosing regimen: $SI1.2_{12}$; here, SI indicates the **s**hort-term **i**nfusion of a **1.2** g daily dose which is divided into two 0.6 g doses administered every **12** h).

Table 2.5: Evaluated i.v. dosing regimens of linezolid.

Daily dose [mg]	Short-term infusion (SI) over 30 min	Prolonged infusion (PI) over 4 h
1200	**$SI1.2_{12}$**: 600 mg q12h (=standard dosing regimen)	**$PI1.2_{12}$**: 600 mg q12h
1800	**$SI1.8_{12}$**: 900 mg q12h	**$PI1.8_{12}$**: 900 mg q12h
1800	**$SI1.8_{8}$**: 600 mg q8h	**$PI1.8_{8}$**: 600 mg q8h
2400	**$SI2.4_{12}$**: 1200 mg q12h	**$PI2.4_{12}$**: 1200 mg q12h

Abbreviations: *PI*: Prolonged infusion; *SI*: Short-term infusion, *q8h*: Every 8 hours; *q12h*: Every 12 hours.

The PTA analyses were performed for the eight investigated dosing regimens (Table 2.5), for different typical patients (Table 2.4 A) as well as for varying values of body size descriptor(s) identified in the NLME PK model (Table 2.4 B). Based on these analyses, the impact of dosing alterations (1. intensification of the daily dose, 2. prolongation of the infusion duration, 3. shortening of the dosing interval) on the PTA was assessed, both the actual magnitude of PTA as well as the attainment of adequate PTA (i.e. PTA≥90%).

To evaluate the general impact of the dosing alteration, the investigated dosing regimens were grouped together and compared with respect to the overall frequency of attaining adequate PTA: Grouping was based on the dosing characteristics of interest, e.g. in case of the dosing alteration 'intensification of daily dose', the regimens with the same daily dose were grouped together. In order to allow the assessment of the univariate impact of the dosing alteration of interest, grouping was performed for dosing regimens for which corresponding dosing regimens existed, i.e. dosing regimens which varied in the dosing characteristics of interest (e.g. varying daily dose), but were comparable with respect to the two remaining characteristics (e.g. same infusion duration and dosing interval). To give an example, to assess the general impact of the dosing alteration 'intensification of daily dose' on the attainment of adequate PTA, the two dosing regimens with the daily dose of 1200 mg ($SI1.2_{12}$, $PI1.2_{12}$) were compared to the two corresponding 1800 mg regimens ($SI1.8_{12}$, $PI1.8_{12}$) and the two corresponding 2400 mg regimens ($SI2.4_{12}$, $PI2.4_{12}$). The two regimens with the shortened dosing interval ($SI1.8_8$ and $PI1.8_8$) were not included in the comparison, as no corresponding regimens with the daily dose of 1200 mg and 2400 mg were

investigated (Table 2.5). In addition to the assessment of the general impact of dosing alteration, the impact was further elucidated for selected types of dosing regimens or in selected matrices (i.e. plasma or ISF). For example, in case of the dosing alteration 'intensification of daily dose', the impact was separately assessed for short-term ($SI1.2_{12}$ vs. $SI1.8_{12}$ vs. $SI2.4_{12}$) and prolonged infusion regimens ($PI1.2_{12}$ vs. $PI1.8_{12}$ vs. $PI2.4_{12}$) as well as separately in plasma an in ISF. A detailed overview of all investigated scenarios is provided in the Appendix, Table S9.
In addition to the impact of dosing regimen alteration on the PTA, the impact of the identified body size descriptor(s) on the PTA was elucidated. Lastly, a dosing overview was created, summarising the short-term and prolonged dosing regimens resulting in adequate PTA either in plasma only or both in plasma and in the ISF of the s.c. adipose tissue, for varying values of body size descriptor(s) and the four investigated MIC values.

2.8 Project III: Development of a risk assessment tool to evaluate standard meropenem dosing in critically ill patients with respect to ineffective meropenem exposure

2.8.1 Clinical study design

This prospective observational study was conducted at three intensive care units within the Department of Anaesthesiology, University Hospital, Ludwig-Maximilians-Universitaet (LMU) Munich, Germany. The study protocol (ClinicalTrials.gov Identifier: NCT01793012) was approved by the Institutional Review Board of the Medical Faculty of the LMU Munich, Germany. Criteria for inclusion comprised the presence of severe infection (confirmed or suspected by clinical assessment), an age ≥18 years and treatment with meropenem (including possible de-escalation; clinical assessment independent from the study). Patients were excluded in case of a planned hospitalisation <4 days or meropenem administration >48 h prior to study start. Written informed consent to participate was obtained from all patients or their legal representatives.
All patients received standard doses of meropenem as 30-min i.v. infusions every 8 h (Figure 2.8). Multiple blood samples were collected for the quantification of meropenem concentrations over a study period of 4 days via an arterial line which is commonly used in critically ill patients to monitor blood pressure and analyse arterial blood gasses [227,232]. Intensive sample collection was performed during all three dosing intervals of study day 1 and during the first dosing interval of study days 2–4. An additional single meropenem minimum concentration (C_{min}) sample before the next dose was collected for the third dosing interval of days 2 and 3. The planned sampling time points per intensively monitored dosing interval were as follows: 15 min, 30 min, 1.5 h, 4 h, and 8 h (immediately prior to next dose; C_{min}) after the start of infusion (Figure 2.8).

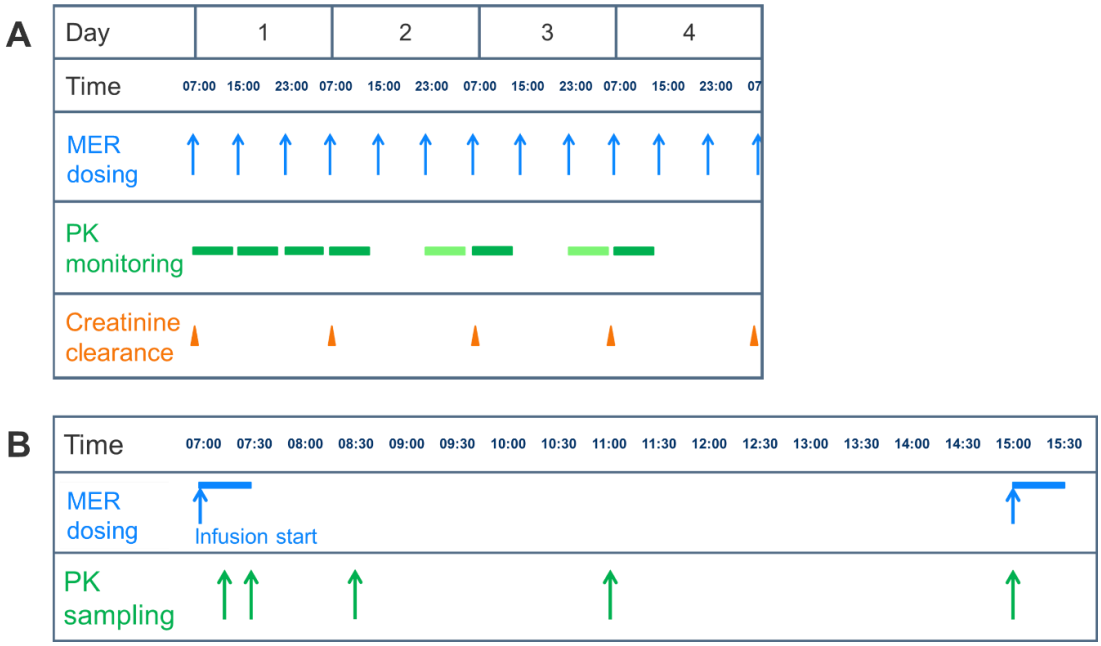

Figure 2.8 Clinical study design (A) and sampling schedule of intensively monitored meropenem (MER) dosing intervals (B) (modified from [233]).
A: *Blue arrows*: Start of 30-min meropenem infusions; *Dark green bars*: Intensively monitored meropenem dosing intervals; *Light green bars*: Monitored meropenem dosing interval with minimum concentration sample only; *Orange triangles*: Determinations of serum creatinine for the estimation of creatinine clearance
B: *Blue arrows/bars*: Start/duration of 30-min meropenem infusion; *Green arrows:* Sampling times (0.25, 0.5, 1.5, 4, 8 h after start of infusion).
Abbreviations: *MER*: Meropenem; *PK:* Pharmacokinetic.

The exact sampling time points were recorded by the medical staff. In addition to the PK samples, patient-specific data such as diagnosis, demographics, disease scores and laboratory data (e.g., serum creatinine) were recorded during the study period (Table S2). Furthermore, pathogens identified in specimens collected from the patients (between 3 days before and 3 days after the study period) were recorded.

2.8.2 Bioanalytical quantification

Blood samples were immediately sent to the Institute of Laboratory Medicine, University Hospital, LMU Munich, Germany and centrifuged. Serum samples were stored at −80°C until total meropenem serum concentration was quantified by using a validated liquid chromatography-tandem mass spectrometry method described previously [234]. Briefly, six-fold deuterated meropenem was used as an internal standard, and validation revealed good analytical performance, with an inaccuracy of less than or equal to ±4% relative error and imprecision ≤6%CV.

2.8.3 Exploratory data analysis

PK and additional patient-specific data were analysed using exploratory statistical and graphical methods as outlined in section 2.2.3. This project further focused on the evaluation of the

variability of meropenem concentrations as described in the following.

To quantify inter- and intraindividual variability of meropenem serum concentrations, measured C_{min} values at the end of the dosing interval were first analysed as observed, irrespective of the actual heterogeneous sampling time points or administered doses. Interindividual variability was evaluated by an exploratory statistical summary analysis of all available C_{min} values; for description of intraindividual variability, the ratios of the maximum (max.) and minimum (min.) C_{min} values $\left(\frac{C_{\min\_max}}{C_{\min\_min}}\right)$ of all dosing intervals monitored within a patient were statistically summarised. Summary statistics included median, range, 95% CI and %CV.

Second, in order to exclude a potential impact of dose- and sampling time point-related variability on meropenem C_{min}, dose-normalised meropenem concentrations (to a dose of 1000 mg, assuming linear PK) at two specific time points (4 h (C_{4h}) and 8 h (C_{8h}) after start of infusion) were calculated and the variability evaluated as described above. C_{4h} and C_{8h} values were determined by linear regression (if ≥3 available data points) or linear interpolation (if 2 available data points) of the logarithmised meropenem concentrations in the declining phase of each concentration-time profile. In case of a coefficient of determination (r^2) of <0.9, being associated with two distinct phases in the declining part of the concentration-time profile, a separate linear interpolation/regression was performed for each of these phases.

2.8.4 Pharmacokinetic/Pharmacodynamic analysis

On the PK side, this analysis focused on a regression model to quantify the impact of renal function on meropenem exposure (Section 2.8.4.1). PK was then linked to PD, by performing a PTA analysis, in order to assess the probability of achieving effective meropenem exposure after standard meropenem dosing and to evaluate the impact of renal function on this probability (Section 2.8.4.2).

2.8.4.1 Regression model: Impact of renal function on meropenem exposure

To investigate the impact of renal function on meropenem exposure, creatinine clearance estimated according to Cockcroft and Gault ($CLCR_{CG}$ [2]) was related to C_{4h} and C_{8h} values. This was done (i) at patient level by using the median individual $CLCR_{CG}$ of a patient and (ii) at sample level by using all single observed $CLCR_{CG}$ values of all patients. For all patients not undergoing CRRT (continuous renal replacement therapy), the relation between $CLCR_{CG}$ and C_{8h} values $\left(C_{8h}=\alpha\cdot\frac{1}{CLCR_{CG}{}^{\beta}}\right)$ was quantified by weighted linear least squares regression in double logarithmic scale (Eq. 2.39), i.e.:

$$\log\left(C_{8h,\,obs}\right) = a + b \cdot \log(CLCR_{CG}) + \varepsilon, \qquad \text{(Eq. 2.39)}$$

in which $a = \log(\alpha)$, $b = -\beta$ (for further details see Section 2.8.5.1). The residual variability ε represented the difference between the logarithmised observed $C_{8h,\,obs}$ values and the logarithmised model-predicted typical $C_{8h,\,pred}$ values and was assumed to be normally distributed with variance $\hat{\sigma}_{\varepsilon}^{2}$ proportional to $CLCR_{CG}$.

2.8.4.2 PK/PD target attainment analysis: Evaluation of standard meropenem dosing

To evaluate the achievement of effective meropenem serum concentrations, PK/PD target attainment was assessed for a broad MIC range from 0.25 mg/L to 8 mg/L, with a special focus on MIC=2 mg/L and MIC=8 mg/L as EUCAST MIC S and R breakpoints for relevant bacteria, such as Enterobacteriaceae, *Pseudomonas* spp. or *Acinetobacter* spp. [5]. Due to the negligible protein binding of meropenem (2%), total meropenem serum concentrations were used for all analyses [63,160]. The PK/PD target $100\%T_{>MIC}$ (i.e. meropenem concentrations exceeding 1x the MIC for the entire dosing interval) was selected [235,236]. In accordance with other studies, $50\%T_{>4xMIC}$ (i.e. meropenem concentration exceeding 4 x the MIC value for half of the dosing interval) was chosen as a second target [237–239]. To evaluate the attainment of the PK/PD targets $100\%T_{>MIC}$, the predicted C_{8h} values of each dosing interval were evaluated regarding the achievement of 1 x MIC breakpoints for all patients not undergoing CRRT (non-CRRT). Similarly, for the target $50\%T_{>4xMIC}$, the predicted C_{4h} values of each dosing interval were evaluated regarding the attainment of 4 x the MIC breakpoints for all non-CRRT patients. Dosing was considered adequate if the PK/PD target was attained in ≥90% of the monitored dosing intervals [41].

To assess the impact of renal function, target attainment at sample level was stratified by the following classes of renal function (RF) based on $CLCR_{CG}$ [104,240,241]: Severely impaired RF: 15-29 mL/min; moderately impaired RF: 30-59 mL/min; mildly impaired RF: 60-89 mL/min; normal RF: 90-129 mL/min; augmented RF: ≥130 mL/min.

2.8.5 Risk assessment tool

A Microsoft Excel® tool for the risk assessment of PK/PD target non-attainment based on the renal function was developed for the PK/PD target $100\%T_{>MIC}$. The quantified $CLCR_{CG}$-C_{8h} relationship for non-CRRT patients (Section 2.8.4.1) was implemented in order to derive the typical meropenem C_{8h} value for a specific $CLCR_{CG}$. In addition, to determine the range of probable C_{8h} values for a patient cohort with a specific $CLCR_{CG}$, the 95% prediction interval (PI) around this relationship was provided [242]. Furthermore, the computation of the risk of target non-attainment for given $CLCR_{CG}$ and MIC values was implemented in the Microsoft Excel® tool.

2.8.5.1 Mathematical basis

The model-predicted typical value was denoted by $\log(C_{8h,\,pred}) = \hat{a} + \hat{b} \cdot \log(CLCR_{CG})$ (â, b̂ are estimated regression model parameters). The regression variability parameter $\hat{\sigma}^2_{reg}$ was determined from $\hat{a}, \hat{b}$ and due to heteroscedasticity varying with the value of $CLCR_{CG}$. The prediction variability $\hat{\sigma}^2$ around the typical $C_{8h,\,pred}$ value consisted of the sum of two components: The regression variability $\hat{\sigma}^2_{reg}$ and the residual variability $\hat{\sigma}^2_{\varepsilon}$. To obtain prediction intervals and the risk of target non-attainment from the prediction variability $\hat{\sigma}^2$, standardised residuals were utilised (part of the classic theory of linear models [242]). The standardised residuals $\frac{\log(C_{8h,\,obs}) - \log(C_{8h,\,pred})}{\hat{\sigma}^2}$ are t-distributed with $n-2$ degrees of freedom, with n being the number of data points used in the regression analysis.

The 95% PI and risk of PK/PD target non-attainment $P(C_{8h,\,pred} \leq \text{MIC})$ were then derived from quantiles $q_{\alpha}^{t_{n-2}}$ and the cumulative distribution function $F^{t_{n-2}}$ of the t-distribution (Eq. 2.40, Eq. 2.41), i.e.

$$95\%\ PI = \left[C_{8h,\,pred} \cdot exp\left(\hat{\sigma} \cdot q_{0.025}^{t_{n-2}}\right);\ C_{8h,\,pred} \cdot exp\left(\hat{\sigma} \cdot q_{0.975}^{t_{n-2}}\right)\right] \qquad \text{(Eq. 2.40)}$$

and

$$P\left(C_{8h,\,pred} \leq MIC\right) = F^{t_{n-2}}\left(\frac{ln(MIC) - ln(C_{8h,\,pred})}{\hat{\sigma}}\right). \qquad \text{(Eq. 2.41)}$$

2.9 Project IV: Development of a dosing algorithm to identify effective meropenem dosing for critically ill patients

2.9.1 Clinical study design

Project IV was based on data from the same clinical study as Project III. For further details on the design of the clinical study as well as the bioanalytical quantification refer to section 2.8.1 and section 2.8.2 respectively.

2.9.2 Data management and exploratory data analysis

2.9.2.1 Dataset generation

The NONMEM® compatible dataset was generated as outlined in section 2.2.1. Based on the observed patient-specific characteristics, further covariates were computed, e.g. creatinine clearance was estimated according to the Cockcroft and Gault equation ($CLCR_{CG}$ [2]; Appendix

7.3.3) on the basis of daily measured serum creatinine (Jaffé assay) as well as measurements from urine collected over 24 h ($CLCR_{UC}$; Appendix 7.3.3). For the patient-specific characteristics additional columns were added to the dataset, indicating missing planned observations, and imputed or interpolated values. The final full dataset for the 48 patients consisted of 394 columns and 3052 rows.

Handling of missing covariate data: Imputation and interpolation

Overall only 3.07% of the planned covariate observations were missing. For each characteristic (e.g. body weight), observations were available in at least 80.5% of the planned observation time points (Appendix Table S2). Missing information of longitudinally measured continuous covariates were imputed at planned observation time points using two **imputation** strategies, i.e. stepwise (*Strategy A*) and a linear strategy (*Strategy B*; Formula: Appendix 7.3.5).

- For missing covariate values between two available covariate values of an individual:
  Strategy A: Imputation of the last available covariate value of the respective individual ('last observation carried forward')
  Strategy B: Imputation of the covariate value derived from linear interpolation between the two covariate values of the respective individual
- For missing values without a following covariate value measured at a later time point within an individual:
  Strategy A/B: Imputation of the last available covariate value of the respective individual ('last observation carried forward')
- For missing values without a preceding covariate value measured at an earlier time point within an individual:
  Strategy A/B: Imputation of the first available covariate value of the respective individual ('next observation carried backward')

The same strategies were used for **interpolation** of additional time points in the dataset in between the observation time points. A graphical illustration of the imputation and interpolation strategies is provided in the Appendix Figure S2.

2.9.2.2 Dataset checkout

The dataset checkout was performed using index plots and cross column checks as outlined in section 2.2.1. To the basic index plots of all covariates, reference ranges as well as the median in the population were added (Appendix Figure S3). In addition, the data subset of three randomly selected patients was evaluated manually for correctness and completeness by comparison with the originally received raw data. For the longitudinally measured covariates, the imputation and/or interpolation was graphically assessed based on individual plots displaying the covariate over time.

2.9.2.3 Exploratory data analysis

In addition to the exploratory data analysis described for Project III in section 2.8.3, this project further focused on the evaluation of the PK data with respect to choosing a potential NLME PK model (e.g. number of disposition phases).

2.9.3 Nonlinear mixed-effects pharmacokinetic modelling

2.9.3.1 Base model development strategy

Based on the results of the exploratory data analysis and prior knowledge from previously published literature, different structural PK disposition models (one-, two-, three-compartment) with zero-order input and first-order elimination were investigated, parameterised in terms of clearance and volume of distribution parameters. Random-effects parameters IIV and IOV were implemented in the model following the 'stepwise approach' i.e. the random-effects parameters were implemented successively/one at a time on a PK parameter. This implementation continued until no further random-effects parameter fulfilled the following three inclusion criteria: precision (<50% RSE), shrinkage (<30%) and magnitude of IIV (>10%CV). IIV and IOV were implemented using exponential models and hence assuming log-normal distribution of individual PK parameters per occasion (Eq. 2.8). The implementation of IOV was assessed by defining as occasion: (i) study day (i.e. ≤4 occasions/patient), or (ii) intensively monitored dosing interval (including also the additional single C_{min} values prior to the intensively monitored interval; i.e. ≤6 occasions/patient). The random-effects parameter RUV was investigated using additive (Eq. 2.9), proportional (Eq. 2.10) and combined (Eq. 2.11) variability models.

2.9.3.2 Covariate model development strategy

Prior to covariate model development, a pre-analysis was performed based on the model covariate $CLCR_{CG}$ to compare and to select one of the two imputation/interpolation strategies (Section 2.9.2.1). The selected imputation/interpolation strategy was used in the actual covariate model development as default strategy for all longitudinally measured continuous covariates and reassessed in a refinement step at the end of the covariate model development (see below: step 6). For covariate model development a systematic semi-automated stepwise strategy was used (Figure 2.9). In **step 1**, the 41 non-CRRT patients were selected as database for the covariate model development and the parameters of the base model re-estimated for this subset. In **step 2**, covariate candidates were preselected from 58 available patient-specific criteria (Appendix Table S2) based on (i) graphical evaluation, assessing the relationship between a covariate at study start and the individual structural and random-effects PK parameters, (ii) prior knowledge from publications and (iii) clinical interest. In **step 3**, a systematic semi-automated stepwise forward-inclusion procedure was used to develop the full covariate model. For the forward-inclusion steps, the *scm*

functionality in PsN [223] was used and preselected covariates were implemented on all PK parameters for which IIV had been included in the base model. For continuous covariates (e.g. $CLCR_{CG}$), linear (Eq. 2.13) and power covariate-parameter relationships (Eq. 2.15) were investigated, and for categorical covariates (e.g. sex), a fractional change in the respective parameter was estimated (Eq. 2.18). Ordered categorical covariates with ≥9 categories (e.g. heart rate extracted from the APACHE II score [1]) were handled as continuous covariates. After each step, the five covariate-parameter relationships leading to the statistically most significant improvement of the model (i.e. leading to the highest drop in the objective function value, OFV) were identified. The respective covariates were further evaluated regarding reduction of unexplained variability (if not stated otherwise, given as relative value on variance scale), precision of the estimate quantifying the covariate effect, clinical relevance (evaluated by the magnitude of change of the respective structural PK parameter across the 90% CI of the respective covariate values of the first study day) and biological plausibility. The covariate best fulfilling these criteria was included in the model, followed by the next step of the forward-inclusion procedure. This process was repeated until no additional significant covariate (ΔOFV≥3.84, α=0.05, df=1) was identified, leading to the full covariate model. In **step 4**, this full covariate model was further refined: Alternative covariates describing similar clinical characteristics (e.g. $CLCR_{CG}$ versus $CLCR_{UC}$, total versus lean body weight) and alternative covariate classifications (e.g. for multiple ordered covariates) were investigated.

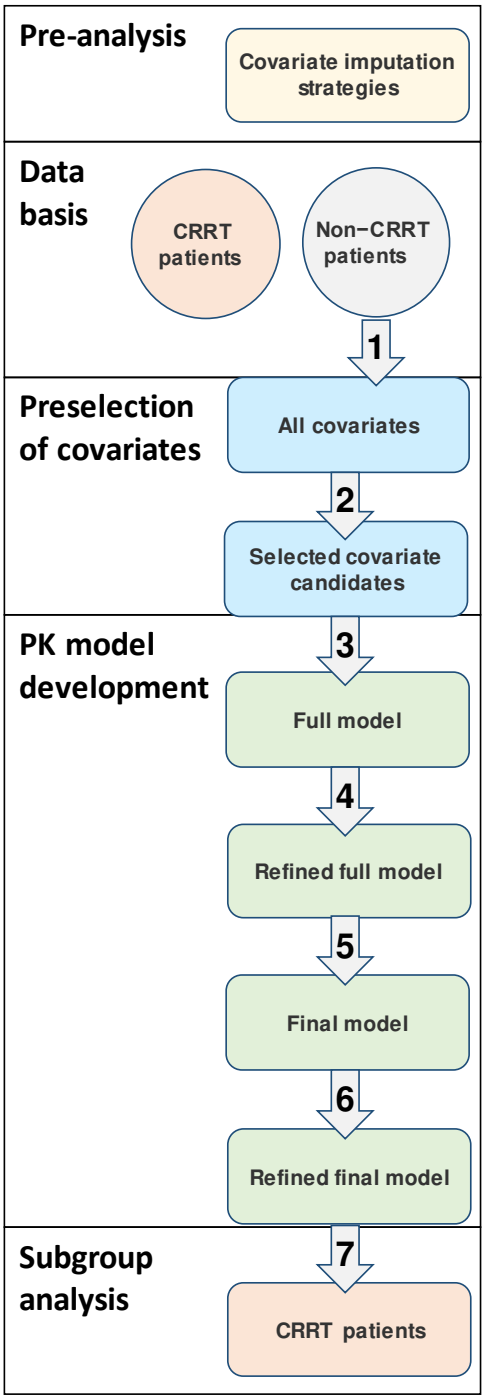

Figure 2.9: Covariate model development strategy. The numbers in the arrows represent the steps of the model development procedure (for further information see text, section 2.9.3.2) (modified from [243]).
Abbreviations: *CRRT*: Continuous renal replacement therapy; *PK*: Pharmacokinetics.

Furthermore, an additional inclusion of interoccasion variability (IOV) was assessed, leading to the refined full covariate model which comprised all quantifiable levels of variability, a prerequisite for the subsequent backward deletion. In **step 5**, i.e. the backward deletion step, all covariates were excluded that reduced ≤5% of the unexplained variability associated with the respective population

parameter, i.e. the population parameter variability (PPV, computed as sum of variances of IIV and IOV [191]). This was accomplished by individual exclusion of the covariates from the full covariate model and assessment of the increase in PPV. Subsequently, a stepwise deletion of covariates was performed based on the precision of the parameter quantifying the covariate effect and – if similar magnitudes of precision – statistical significance. This backward deletion procedure was performed until all covariates fulfilled the prerequisites of precision (RSE<50%) and statistical significance ($\Delta OFV \geq 6.64$, $\alpha=0.01$, df=1), leading to the final covariate model. In **step 6** the final covariate model was refined by defining the centring of covariate relationships as well as evaluating the interpolation strategy of longitudinally measured continuous covariates, by comparing (i) linear with stepwise interpolation in the dataset (Section 2.9.2.1) and (ii) linear interpolation in the dataset with and additional linear interpolation between observations of covariates also within the NONMEM® script. Besides, alternative functional covariate-parameter relationships for continuous covariates (e.g. piecewise linear relationship; Eq. 2.14), the 'extended Wählby model 1' for continuous time-varying covariates (Eq. 2.16) and the statistical submodel were reinvestigated, leading to the refined final covariate model. In **step 7**, the applicability of the covariate-parameter relationships for the CRRT subpopulation (n=7) was evaluated: Model parameters were estimated based on the data of CRRT patients and compared with the parameter estimates of the non-CRRT patients.

2.9.3.3 Model evaluation and discrimination

For model evaluation and discrimination, a similar procedure was used as described for Project I (Section 2.6.4.3). In brief, a combination of graphical and numerical basic evaluation techniques was used for model evaluation and discrimination. For the final NLME PK model, additional advanced techniques were applied: VPC (n=1000 simulations, with time or covariates as independent variables), non-parametric bootstrap (n=1000 replicate datasets) and case-deletion diagnostics (on patient level). Details on the evaluation techniques are summarised in section 2.3.3.

2.9.4 Simulations: Evaluation and optimisation of meropenem exposure and dosing regimens

The developed NLME PK model was used for deterministic simulations to explore and better understand meropenem exposure after standard meropenem dosing (Section 2.4.1). Furthermore, stochastic simulations were performed to assess the adequacy of meropenem exposure after standard meropenem dosing and alternative dosing regimens (Section 2.9.4.2), to evaluate and if needed optimise meropenem dosing regimens.

2.9.4.1 Evaluation of meropenem exposure

To evaluate the plasma pharmacokinetics of meropenem after standard meropenem dosing, deterministic exposure simulations were performed for varying patient characteristics. The patient characteristics were selected according to the covariates identified in the final NLME PK model and were univariately varied to assess their impact on the meropenem concentration-time profile (Table 2.6).

Table 2.6: Patient characteristics used for deterministic exposure simulations

Assess impact of	Identifier	Patient characteristics*		
		$CLCR_{CG}$ [mL/min]	**WT [kg]**	**ALB [g/dL]**
$CLCR_{CG}$	1	**min: 24.8**	med: 70	med: 2.8
	2	**med: 80.8**	med: 70	med: 2.8
	3	**max[1]: 154**	med: 70	med: 2.8
WT	4	med: 80.8	**min: 44**	med: 2.8
	5	med: 80.8	**med: 70**	med: 2.8
	6	med: 80.8	**max: 140**	med: 2.8
ALB	7	med: 80.8	med: 70	**min: 1.7**
	8	med: 80.8	med: 70	**med: 2.8**
	9	med: 80.8	med: 70	**max: 3.8**

*Univariately varied patient characteristic values are highlighted in bold. [1]Inflection point of $CLCR_{CG}$-CL relationship (=154 mL/min) is displayed instead of maximum $CLCR_{CG}$, given the constant meropenem CL for higher $CLCR_{CG}$ values (Appendix Figure S30).
Abbreviation: *ALB*: Serum albumin concentration; *CL*: Clearance; *$CLCR_{CG}$*: Creatinine clearance estimated according to Cockcroft and Gault [2]; *max*: Maximum; *med*: Medium; *min*: Minimum, *WT*: Total body weight.

2.9.4.2 Evaluation and optimisation of meropenem dosing regimens

This section provides a general description of the analysis approach; more detailed information is provided in the subsequent subsections. In order to evaluate the adequacy of standard meropenem dosing, PTA and CFR (Section 2.4.3, technical details described in more detail below) were evaluated for patients with different clinical characteristics and levels of available pathogen information. The impact of single covariates on the PTA was investigated by varying one covariate while fixing the remaining ones to the median value in the population (univariate covariate variation). Considering the available covariate ranges in the critically ill population, additionally 'worst'- and 'best-case' covariate combinations were assessed for standard meropenem dosing (multivariate covariate variation). Based on the results of the uni- and multivariate covariate variation, vital determinants for PTA/CFR were determined.

In a second step, PTA and CFR analyses were performed for seven alternative dosing regimens for varying values of the identified vital covariates. Compared to standard linezolid dosing, the alternative dosing regimens consisted of an intensified or reduced daily dose and/or a prolonged or continuous infusion duration (Table 2.7).

Table 2.7: Evaluated i.v. dosing regimens of meropenem (modified from [243]).

Daily dose [mg]	Short-term infusion (SI) over 30 min	Prolonged infusion (PI) over 3 h	Continuous infusion (CI) over 24 h
2000	**SI2$_{12}$**: 1000 mg q12h	**PI2$_{12}$**: 1000 mg q12h	--
3000 or 3412.5[1]	**SI3$_8$**: 1000 mg q8h (=standard dosing regimen)	**PI3$_8$**: 1000 mg q8h	**CI3**[2]: 3000 mg q24h following an initial loading dose of 500 mg over 30 min
6000 or 6875[1]	**SI6$_8$**: 2000 mg q8h	**PI6$_8$**: 2000 mg q8h	**CI6**[2]: 6000 mg q24h following an initial loading dose of 1000 mg over 30 min

[1]For CI treatment at day 1, the initial loading dose is included; [2]Consider to renew the infusion solution dependent on the drug concentration twice or thrice daily (see supplement of article [244]) to ensure the stability of meropenem
Abbreviations: *CI*: Continuous infusion; *PI*: Prolonged infusion; *SI*: Short-term infusion, *q8h*: Every 8 hours; *q12h*: Every 12 hours; *q24h*: Every 24 hours.

Throughout this project an informative code 'XY_Z' was used to indicate the different dosing regimens: In this code, X represents the type of infusion, Y the administered daily dose in gram and Z the dosing interval in hours (e.g. for the standard meropenem dosing regimen: $SI3_8$; here, SI indicates the **s**hort-term **i**nfusion of a **3** g daily dose which is divided into three 1 g doses administered every **8** h). For continuous infusion regimens the simplified dosing code 'XY' was used. A detailed description on the applied PK/PD target and the PTA and CFR analyses is provided below.

PK/PD target

The PK/PD target $100\%fT_{>MIC}$ (i.e., unbound meropenem serum concentrations exceeding the MIC for 100% of the 24-h period) has been suggested in literature for betalactam treatment in critically ill patients [235,236]. In the present work, total meropenem concentrations ($T_{>MIC}$) were evaluated due to the negligibly low protein binding of meropenem (2%, [63,160]). Furthermore, given the non-achievability of $100\%T_{>MIC}$ when starting the i.v. infusion on the first day of therapy the attainment of $98\%T_{>MIC}$ was assessed, i.e. allowing for a 2% period within 24 h (=30 min), for the increasing part of the concentration-time profile, to reach the MIC concentration. For the evaluation of continuous-infusion regimens a stricter target $98\%T_{>4xMIC}$ was selected [42]. The attainment of the predefined PK/PD target was defined as 'effective exposure'.

Probability of target attainment analysis

For each specific covariate combination and dosing regimen (i.e. standard and alternative dosing regimens), meropenem plasma concentration-time profiles were simulated for 500 patients over four treatment days using stochastic MC simulations (Section 2.4.2) considering IIV and IOV in the PK parameters. The PTA (Section 2.4.3) was computed for treatment day 1 (i.e. start of therapy) and treatment day 4 (i.e. presumably at steady-state) across the full MIC range from 0.002 to 512 mg/L [132]. A PTA of ≥90% (i.e., 450 of 500 patients achieving the PK/PD target [63]) was

considered adequate. To incorporate PK model parameter uncertainty, each MC simulation was repeated 1000 times using the PK parameter sets obtained from a non-parametric bootstrap and the respective PTA values derived (*sse* functionality in PsN [223,245]). A PTA of ≥90% for the 5th percentile of the 1000 computed PTA values was considered a dosing regimen 'reliably' attaining 'effective exposure'.

Cumulative fraction of response

Based on the PTA results, the CFR (Section 2.4.3) was derived for five pathogens commonly encountered in ICUs (*P. aeruginosa, Acinetobacter* spp.*, E. coli, Enterobacter (E.) cloacae, Klebsiella (K.) pneumonia* [246]). For the two least susceptible pathogens, *P. aeruginosa* and *Acinetobacter spp.*, the CFR was separately calculated for the MIC distribution of the isolates belonging to the S category (MIC≤2 mg/L) and of the isolates belonging to the I category (MIC>2 and ≤8 mg/L). A dosing regimen achieving a CFR of ≥90% [63] for the 5th percentile of the 1000 computed CFR values was considered a dosing regimen 'reliably' attaining 'effective exposure'.

2.9.5 Development of a dosing algorithm

Based on the results of the PTA and CFR analyses (Section 2.9.4.2; PK/PD target for SI and PI: 98%$T_{>MIC}$, for CI: 98%$T_{>4xMIC}$), a tabular dosing overview was generated in the R software, considering $CLCR_{CG}$ of the patient (10-154 mL/min) and the level (L) of knowledge about the pathogen:

- 'Level 1' (L1): pathogen unknown,
- 'Level 2' (L2): pathogen known,
- 'Level $3_{(-MIC)}$' ($L3_{(-MIC)}$): pathogen and susceptibility category known,
- 'Level $3_{(+MIC)}$' ($L3_{(+MIC)}$): MIC value known.

L1 and $L3_{(+MIC)}$ were based on the PTA results for the predefined non-species-related EUCAST PK/PD breakpoints for meropenem (S: 2 mg/L, R: 8 mg/L [5]) and a broad MIC range (0.004-16 mg/L), respectively. L2 and $L3_{(-MIC)}$ were based on the results of the CFR analyses for the full MIC distribution and the MIC distribution of the isolates belonging to the S and I category of the pathogens, respectively. Per $CLCR_{CG}$-pathogen/susceptibility combination, the lowest effective SI, PI, and CI dosing regimen was selected (i.e. PTA/CFR>90% for 5th percentile of 1000 MCs).

3 Results

3.1 Project I: Characterisation of linezolid plasma and target site exposure in obese and nonobese surgical patients, including the evaluation of the microdialysis methodology

3.1.1 Exploratory data analysis

3.1.1.1 Patient characteristics

As specified in the study protocol, 30 patients - 15 obese and 15 nonobese - were enrolled (Table 3.1). Considering the matching criteria sex and age, the two subgroups were highly comparable, with 87% females, a median age of 52 and 50 years and a median body height of 1.65 and 1.69 m for the obese and nonobese population, respectively. In contrast and as expected, body size was very diverse, with median BMI values of 45 and 24 kg/m^2 for the obese and nonobese patients, respectively. Overall, the 30 patients covered a large range of body size, from normal weight up to severe obesity (i.e. obesity class III, [247]), indicated by BMI values ranging from 20.5-81.5 kg/m^2 and LBW values from 34.9-84.8 kg (Figure 3.1 A, B; frequency distribution of additional body size descriptors: Appendix Figure S4).

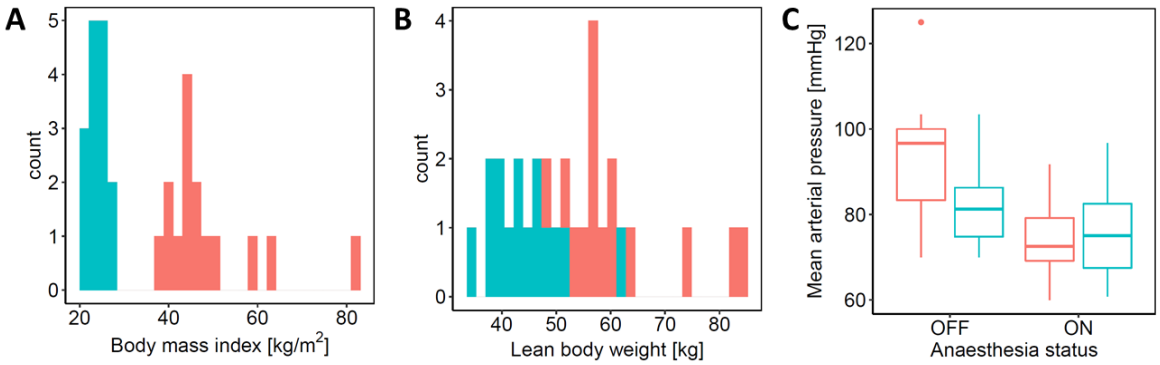

Figure 3.1: Frequency distributions of body size descriptors (A: BMI; B: LBW) and a haemodynamic marker (C: MAP) of obese (red) and nonobese (green) patients.
C: Summary statistics based on individual median observed intra-anaesthetic data and post-anaesthetic data, respectively.
Colour coding: *Red:* Obese patients; *Green*: Nonobese patients.
Abbreviations: *BMI:* Body mass index; *LBW:* Lean body weight; *MAP*: Mean arterial pressure.

Table 3.1: Patient-specific and surgery-specific characteristics of (obese and nonobese) patients.

Characteristics	**Full population (n=30)**		**Obese population (n=15)**		**Nonobese population (n=15)**	
Continuous	**Median**	**$P_{0.05}$-$P_{0.95}$**	**Median**	**$P_{0.05}$-$P_{0.95}$**	**Median**	**$P_{0.05}$-$P_{0.95}$**
Age [years]	51.5	32.4-63.1	52.0	35.6-62.9	50.0	33.1-62.6
Body height [m]	1.66	1.57-1.78	1.65	1.53-1.80	1.69	1.59-1.78
Total body weight [kg]	101	60.0-170	121	104-196	65.0	57.6-81.2
BMI [kg/m^2]	32.6	21-60.6	44.7	39.3-68.3	23.6	20.6-26.8
LBW [kg]	51.9	34.9-61.2	56.7	50.3-83.6	43.7	38.5-79.2
FM [kg]	41.0	17.9-93.3	64.6	51.9-115	22.5	15.5-30.9
$CLCR_{CG\_LBW}$ [mL/min]	63.4	38.0-105	72.3	36.0-113	55.8	41.2-81.5
Incision-suture duration [h]	2.81	2.38-3.57	2.78	2.35-3.55	2.90	2.55-4.32
Anaesthesia duration [h]	4.22	2.55-7.94	4.08	3.39-5.52	4.78	2.49-8.27
Intubation duration [h]	4.08	2.37-7.52	3.88	2.94-5.33	4.43	2.40-7.90
Heart rate[1] [min^{-1}]	71.2	56.6-87.3	71.5	60.0-86.9	71.0	57.1-84.8
• Intra-anaesthetic	65.2	53.9-84.1	65.0	57.2-83.0	65.5	53.8-85.3
• Post-anaesthetic	80.0	61.0-99.5	79.0	61.5-97.4	81.5	61.0-99.0
MAP[1] [mmHg]	75.4	65.8-91.1	76.7	69.5-102	72.5	64.5-85.4
• Intra-anaesthetic	72.7	62.0-91.7	72.5	62.3-85.8	75.0	62.6-93.2
• Post-anaesthetic	85.0	70.7-103	96.7	77.0-110	81.2	71.1-93.6
CO_{LZ}[1] [L/min]	20.9	15.7-29.2	23.7	15.6-30.7	20.6	16.1-23.9
• Intra-anaesthetic	19.6	13.8-26.6	20.2	13.1-27.3	19.3	15.1-26.3
• Post-anaesthetic	26.2	18.3-39.8	26.2	19.8-39.6	24.9	18.4-33.0
Categorical	**Number**	**(%)**	**Number**	**(%)**	**Number**	**(%)**
Sex, female	26	(86.7)	13	(86.7)	13	(86.7)
Type of anaesthesia						
• Balanced	27	(90.0)	13	(86.7)	14	(93.3)
• TIVA	3	(10.0)	2	(13.3)	1	(6.67)

[1]Time-varying characteristics: Summary statistics based on individual median of observed intra-anaesthetic data and post-anaesthetic data, respectively.
Abbreviations: *BMI*: Body mass index; *$CLCR_{CG\_LBW}$:* Creatinine clearance estimated according to Cockcroft and Gault [2] using LBW; *CO_{LZ}*: Cardiac output estimated according to Liljestrand and Zander (unadjusted) [3]; *FM*: Fat mass; *LBW*: Lean body weight; *MAP*: Mean arterial pressure; $P_{0.05}$-$P_{0.95}$: 5th percentile - 95th percentile; *TIVA*: Total intravenous anaesthesia.

All patients underwent abdominal surgery: While the obese population underwent bariatric surgery (i.e. obesity was the indication), the main surgery indication for the nonobese group was cancer (75%, e.g. cervical carcinoma). The median duration of surgery (i.e. time from incision to suture) was 2.8 h, while the median duration for anaesthesia was 50% longer (median duration: 4.2 h). Most of the patients received balanced anaesthesia (90% of patients, Table 3.1). As expected, the routinely monitored time-varying markers HR, MAP and CO_{LZ} indicated reduced haemodynamics during anaesthesia compared to the post-anaesthetic period, e.g. HR increased from 65 to 80 min^{-1} and MAP from 73 to 85 mmHg (Table 3.1 C; Appendix Figure S4). In general, haemodynamic markers were higher in obese compared to nonobese patients.

3.1.1.2 Linezolid dosing and sampling

A single linezolid dose (600 mg as 30-min i.v. infusion) was administered 30 min before surgical incision (=median; 5^{th}-95^{th} percentile: 11.5-46.2 min). In total, 1009 linezolid measurements were available for subsequent NLME modelling, comprising total plasma concentrations (n=239), unbound plasma concentrations (n=90), microdialysate concentrations collected with the two catheters in the s.c. adipose tissue (n=296+295), as well as retrodialysate concentrations (n=43+46). Thus, only very few of the planned linezolid measurements (~1.4%) were missing (Section 2.6.1). Only for one catheter in one obese patient, the retrodialysis and hence the RR value was missing completely, which required imputation in order to make use of the available microdialysate data of the respective catheter (Section 2.6.3.1: Handling of missing data). A strong impact of the obesity status on the RR was detected, which was used for imputation (i.e. median RR of the obese patients was imputed, Appendix Figure S5 B).

3.1.1.3 Linezolid concentrations

The evaluation of the exposure of linezolid in different PK matrices revealed highest exposure for total plasma concentrations, followed by unbound plasma concentrations and ISF concentrations in s.c. adipose tissue (Figure 3.2 A.1, A.2). Unbound plasma concentrations were approximately 15% lower than the total plasma concentrations, indicating a fraction unbound of ~85%. This magnitude was observed and consistent over the full investigated concentration range, independent from the obesity status and seemed to show only low variability between the patients (Appendix Figure S6, r^2=0.994). When comparing the kinetics of linezolid in the different body fluids, a slight time delay in the C_{max} value was observed for ISF compared to plasma (Figure 3.2 A.1; t_{max}: 1.25 h vs. 0.5 h for ISF (mid time of microdialysis collection interval) and plasma, respectively).

Stratification of the concentration-time profiles by obesity status showed lower drug concentrations for obese than nonobese patients especially in the initial phase, both for plasma (Figure 3.2 B.1, B.2) and ISF (Figure 3.2 C.1). The comparison of the individual ISF concentration-time profiles determined concurrently using the two microdialysis catheters, showed very similar exposure for some patients, but larger differences for others (Appendix Figure S7). Yet, these differences showed no systematic pattern but seemed to randomly occur between patients and catheters. Overall, the two catheters demonstrated very similar typical ISF concentration-time profiles (Figure 3.2 C.2).

The linezolid concentration-time profiles also gave first insights into the NLME PK model structure. Firstly, the biphasic disposition in the semilogarithmic plasma concentration-time profile of most patients suggested a two-compartment disposition model (Figure 3.2 B.2). Secondly, an additional third phase was detected in the terminal elimination phase, which showed – opposite to the expectations from a three-compartment model – a steeper decline than the previous phase.

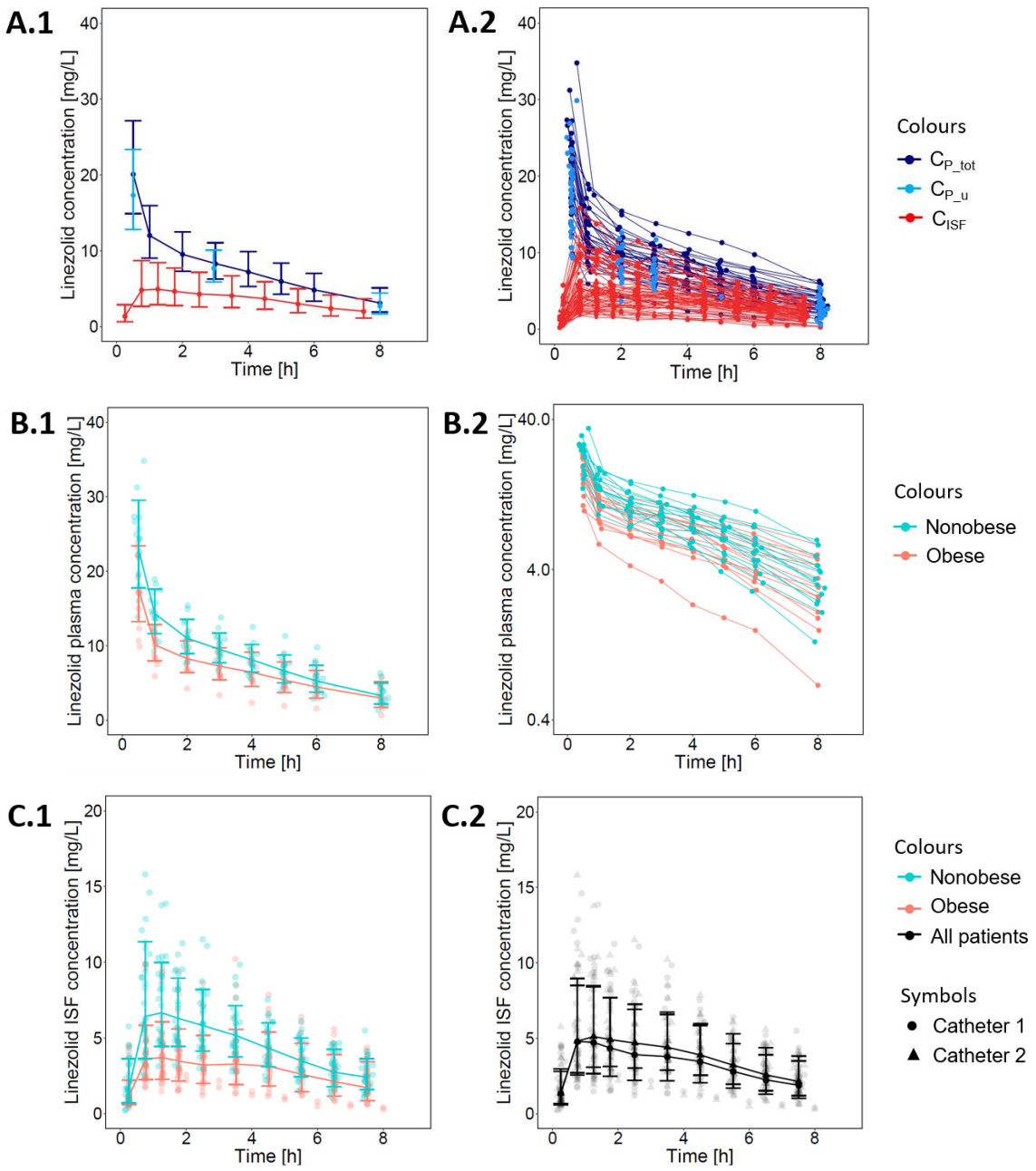

Figure 3.2: Linezolid concentration-time profiles stratified by sampling matrix (A.1, A.2), obesity status (B.1, B.2, C.1) and microdialysis catheter (C.2).
A: Individual (A.1; $n_{profiles}$=106) and typical concentration-time profiles (A.2) for total (dark blue; $n_{profiles}$=30) and unbound linezolid in plasma (light blue; $n_{profiles}$=30) and unbound linezolid in ISF of the s.c. adipose tissue (red; $n_{profiles}$=46).
B: Typical (B.1) and individual (B.2) total linezolid plasma concentration-time profiles for obese (red; $n_{profiles}$=15) and nonobese patients (green) on linear (B.1) and semilogarithmic scale (B.2; $n_{profiles}$=15).
C: Typical linezolid ISF concentration-time profiles for obese ($n_{patients}$=15) and nonobese ($n_{patients}$=15) patients (C.1: red and green, respectively) and catheter 1 and catheter 2 (C.2: circle and triangle, respectively). ISF concentrations are displayed at the mid time of the respective collection intervals.
Typical profiles: Geometric mean concentrations including geometric standard deviation (error bars) are depicted at median sampling time point.
Abbreviations: *ISF:* Interstitial space fluid; *s.c.:* Subcutaneous.

This finding indicated nonlinearity in the PK, more precisely a terminal increase in clearance parameter. The occurrence of nonlinearity was observed at linezolid concentrations of ~2-10 mg/L and at the end of anaesthesia in approximately half of the patients (Appendix Figure S8). Thirdly,

the delayed C_{max} values in ISF compared to plasma indicated that ISF concentrations should rather be allocated to a peripheral delayed compartment than the central compartment.

3.1.2 Nonlinear mixed-effects model

This section focuses on the applied stepwise NLME model development (3.1.2.1), followed by a description of the developed final NLME model (3.1.2.2) and the results of the model evaluation (3.1.2.3).

3.1.2.1 Model development

An overview of the single steps of the model development is illustrated in form of a workflow in Figure 3.3. The models selected in the single steps are highlighted with a green frame. In the following, this comprehensive workflow is described in more detail.

Base model development: Plasma (steps 1-2)

In **step 1**, a base model was developed for the observed total linezolid plasma concentrations. A two-compartment disposition model parameterised in terms of clearance (CL), volumes of distribution (central, peripheral: V_1, V_2) and intercompartmental clearance (Q) was selected as the structural model, as it adequately described the trajectory of the total plasma concentrations. The one-compartment model was inferior to the two-compartment model, as indicated by the apparent misspecifications in the basic goodness-of-fit plots (Appendix Figure S9) and the significantly higher OFV value (ΔOFV:+71.9, df=2, α<0.001). For instance, the graphical assessment of CWRES versus population predictions demonstrated a U-shape (e.g. underprediction for low and high population predicted values), indicating the need of an additional compartment to adequately describe the data (Appendix Figure S9 A.2).

IIV was quantifiable for all PK parameters. The IIV parameters were relatively precisely estimated (≤26.1% RSE) and indicated moderate to higher variability between the patients (≤68.9%CV). The exclusion of IIV on Q – as the parameter with the highest RSE – was tested but resulted in reduced model predictivity. Hence, the selected statistical IIV submodel included variability on all four PK parameters. Covariance between the IIV parameters was found to be ρ≤74.4% and was thus not included in the model. The graphical evaluation of residuals versus population predictions illustrated a fan-shaped pattern, which indicated the need of a RUV model in which the variance is proportional to the magnitude of the model prediction (Appendix Figure S10 A). This was confirmed when implementing and investigating the different RUV models: The solely additive RUV model was markedly inferior compared to the proportional and combined model (ΔOFV≥13.9). The proportional and combined model both adequately described the data. With respect to OFV, the combined model was slightly superior over the proportional model

(ΔOFV=9.1). Considering the moderate precision of the estimated additive term (36% RSE) and the comparably good results in the goodness-of-fit evaluations (Appendix Figure S10), the proportional RUV was finally selected as the statistical RUV submodel in this step, which is in line with the principle of parsimony. Even though most model evaluation techniques revealed adequate model performance, the 'CWRES versus time' plot showed an undulating pattern, indicating a potential model misspecification (Appendix Figure S10 C). An additional evaluation suggested a relation between the occurrence of the undulating pattern and the observed nonlinearity in the concentration-time profiles, which was not yet considered in the structural model of the total plasma data only (Appendix Figure S11).

In **step 2**, the available unbound plasma concentrations were integrated into the model by assigning them to the central compartment and estimating an additional f_u parameter. IIV on f_u was assessed within the model and was found to be negligibly small (0.3%CV), confirming the results from the exploratory analysis (Section 3.1.1.3). Thus, for parsimony reasons, IIV on f_u was not included in the NLME plasma model. Additionally, a separate proportional RUV was estimated for the unbound plasma concentrations.

Within the developed NLME model for total and unbound linezolid plasma concentrations the observed nonlinearity in the terminal phase of the linezolid concentration-time profiles (Figure 3.2 B.2) was investigated by implementation of different nonlinear clearance models, assuming either a concentration dependence of the clearance parameter or a time variation based on surgery-specific characteristics. In contrast to linear clearance, all investigated nonlinear clearance models showed an improved model performance, which is discussed in more detail in the following. Six 'anaesthesia models' were assessed, assuming different patterns of linezolid clearance over time after the end of the anaesthesia (Figure 3.3, model equations: Appendix Figure S12). The model, which described a time-dependent increase of clearance according to an ordinary E_{max} model (Figure 3.3 Step 1, 'Time-varying CL': top row, middle panel; Appendix Figure S12 C), was selected as the most adequate anaesthesia model based on the reduction of the observed pattern of the 'CWRES versus time' plot, the precise and plausible parameter estimates as well as the plausible assumption of a functional change of clearance (Appendix Figure S13 C, Table S3 Model B). The six nonlinear anaesthesia models were reassessed using the end of intubation instead of the end of anaesthesia as the starting time point for the change in clearance. The results were very similar given the high correlation between the two time points (r^2=0.997). The 'anaesthesia model' was chosen over the 'intubation model' due to slightly better parameter precision. In addition to the anaesthesia and intubation status, the continuous time-varying haemodynamic marker heart rate was assessed as an impact factor for clearance. Within the NONMEM® script, heart rate was linearly interpolated between the available observations and a linear relationship with clearance was defined.

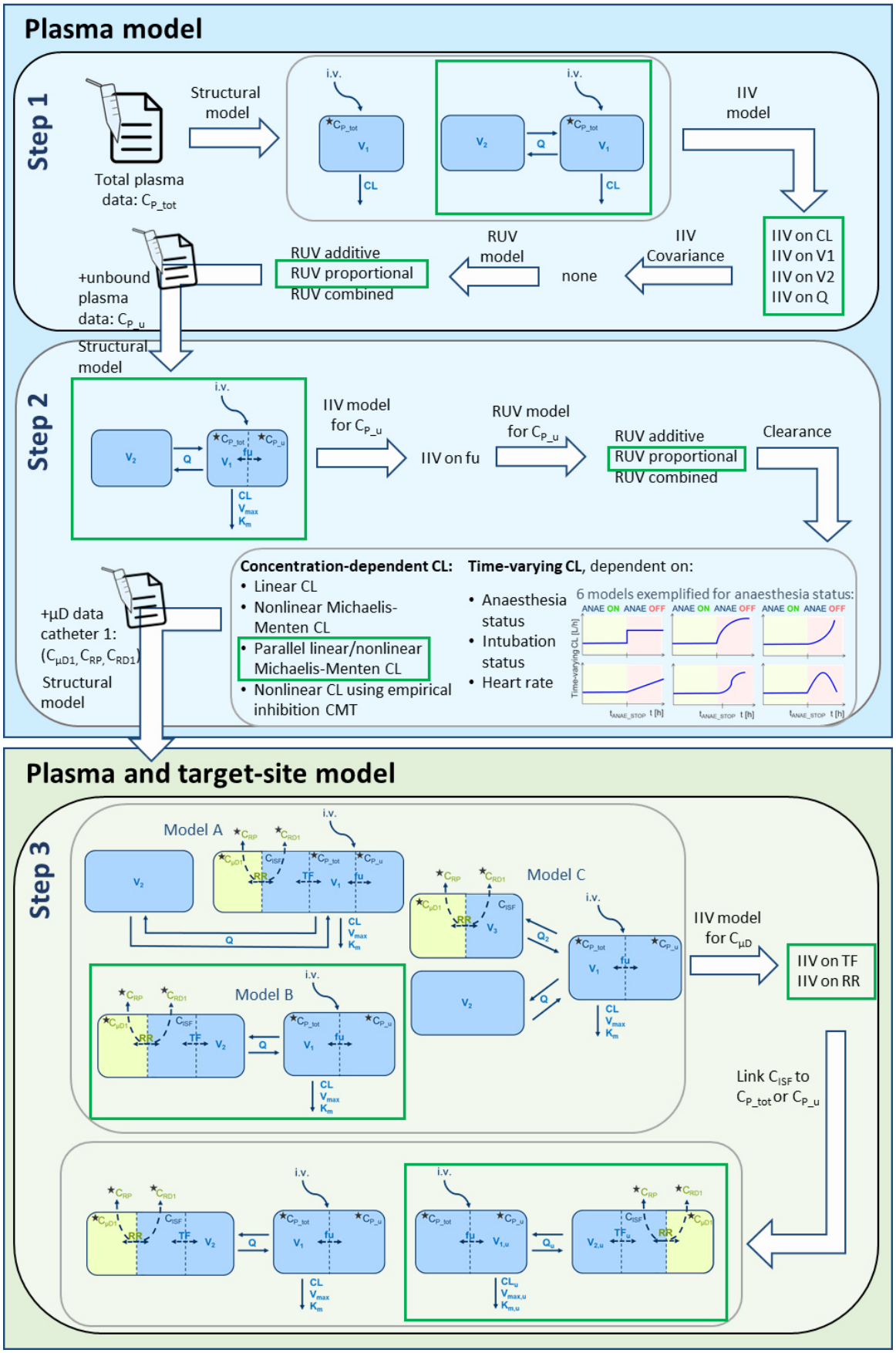

Figure 3.3: Results of model development: steps 1-3 (based on model development strategy, section 2.6.4.2) [continued on next page].

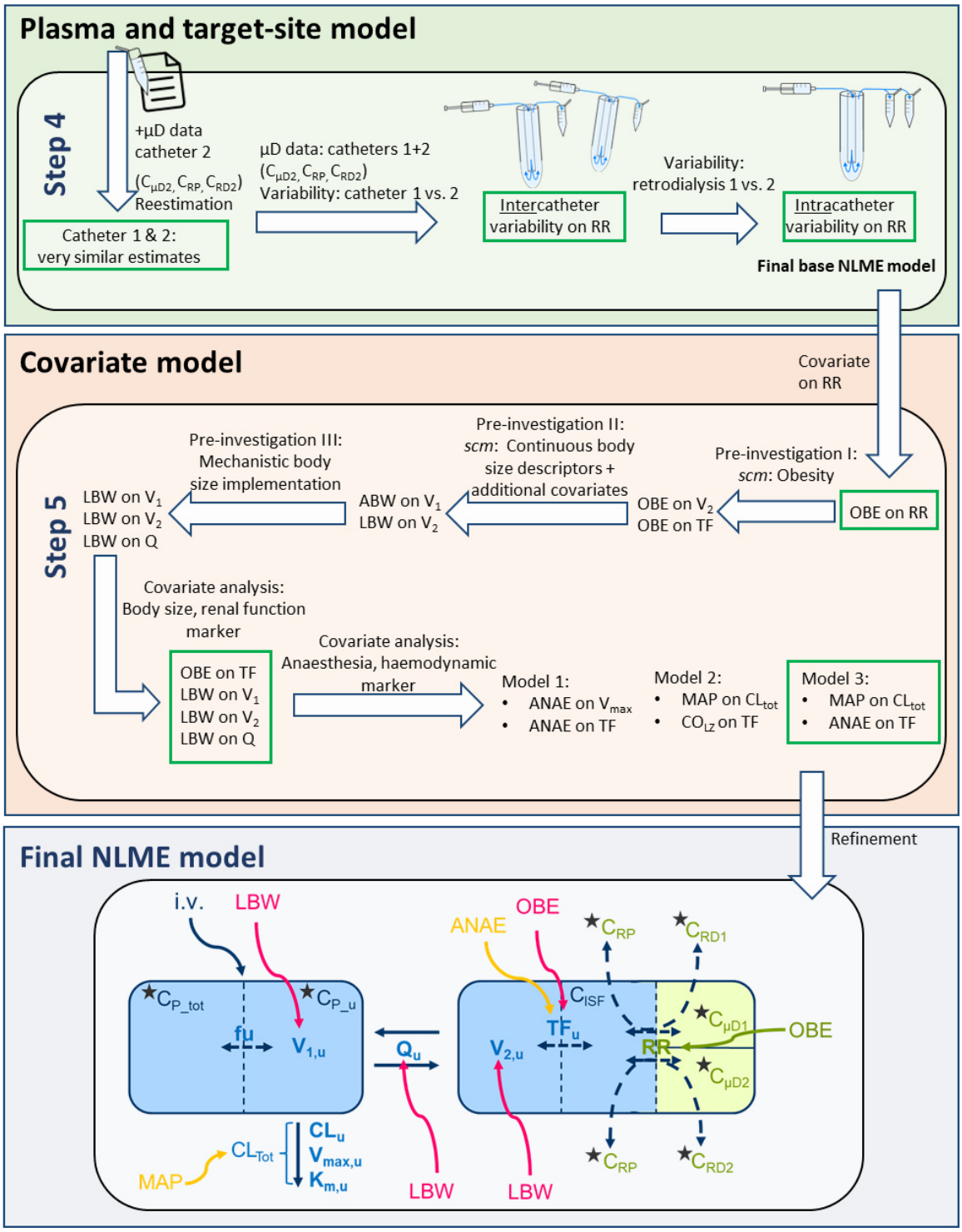

Figure 3.3 [continued]: Results of model development: steps 4-5 and final NLME PK model.
Colour coding in model sketches: *Blue*: PK-related; *Green*: Microdialysis methodology-related; *Pink*: Body size descriptors; *Orange*: Anaesthesia/MAP. ***Symbols in model sketches***: *Solid/Dashed arrows*: Indicate mass transfer/no mass transfer.
Abbreviations: *ABW*: Adjusted body weight; *ANAE*: Anaesthesia; *CL*: Clearance; CL_u: CL of unbound linezolid; *CMT*: Compartment; C_{P_tot}: Total plasma concentrations; C_{P_u}: Unbound plasma concentrations; C_{RD}: Retrodialysate concentration; C_{RP}: Retroperfusate concentration; $C_{\mu D}$: Microdialysate concentration; CO_{LZ}: Cardiac output estimated according to Liljestrand and Zander [3]; f_u: Fraction unbound; *IIV*: Interindividual variability; *i.v.*: Intravenous; K_m: Michaelis-Menten constant; $K_{m,u}$: K_m of unbound linezolid; *LBW*: Lean body weight; *MAP*: Mean arterial pressure; *NLME*: Nonlinear mixed-effects; *OBE*: Obesity; Q, Q_2: Intercompartmental clearance parameters between CMT 1 and 2, and between CMT 1 and 3, respectively; Q_u: Q of unbound linezolid; *RR*: Relative recovery; *RUV*: Residual unexplained variability; t_{ANAE_STOP}: Time of anaesthesia end; *scm*: Stepwise covariate model-building; *TF*: Tissue factor; V_1, V_2, V_3: Volume of distribution parameters of central and two peripheral CMTs; $V_{1,u}$, $V_{2,u}$: V_1, V_2 of unbound linezolid; V_{max}: Maximum elimination rate; $V_{max,u}$: V_{max} of unbound linezolid.

Compared to the sole linear clearance model, the 'heart rate model' was superior (ΔOFV=-28.2, df=1, α<0.001); however, it only led to a slight reduction of the undulating pattern in the 'CWRES versus time' plot (Appendix Figure S13 B, Table S3 D). Hence, the 'anaesthesia model' was still considered as the most adequate time-varying nonlinearity model.

In addition to time-varying clearance models, concentration-dependent clearance models were assessed: Comparing the concentration-dependent nonlinear Michaelis-Menten model with the combined linear and nonlinear Michaelis-Menten model, the latter demonstrated better model performance as indicated by the significantly lower OFV value (ΔOFV=-276, df=1, α<0.001). The implementation of an empirical inhibition compartment (describing a time- and concentration-dependent clearance; Appendix Figure S14) was not supported by the data, as indicated by the rate transfer parameter into the empirical inhibition compartment, which was estimated to be close to 0, as well as the increase in the AIC value compared to the linear clearance model (ΔAIC=+8.06). Consequently, the parallel linear and nonlinear Michalis-Menten model was considered as the most adequate concentration-dependent model (Appendix Figure S13 D, Table S3 C).

The two most adequate nonlinearity models (time-varying anaesthesia model and concentration-dependent parallel linear/nonlinear Michaelis-Menten model) were compared by evaluating GOF plots, VPCs, individual clearance estimates versus time and deterministic simulations. Both models illustrated good model predictivity and performance given the observed data, however, resulted in different predictions when extrapolating to altered linezolid dosing regimens (Appendix Figure S15). At this stage, the Michaelis-Menten model was included in the plasma base model, as this type of clearance model had been identified for linezolid before [248]. Yet, a reassessment of the time-varying impact of the surgery-specific characteristics was performed during the covariate analysis, after having all available PK information (also target site exposure) included into the model (Section 3.1.2.1: Covariate model development (step 5)).

Base model development: Plasma and target site (steps 3-4)

In **step 3**, the PK data collected with one of the microdialysis catheters was integrated into the model by three different distribution kinetics models (Figure 3.3 Step 3: Model A-C). Model A, which was investigated by external evaluation of an already existing NLME PK model [45], did not satisfactorily capture the distribution process from plasma into ISF in the obese/nonobese population. Evaluation of goodness-of-fit plots, VPCs and high relative prediction errors revealed that the initial concentrations were less well captured than those measured in the elimination phase (Appendix Figure S16). While an overprediction was observed for the initial microdialysate concentrations, an underprediction was apparent for the plasma concentrations. This confirmed the results of the exploratory analysis, which already indicated a delayed distribution of linezolid (Section 3.1.1.3).

A graphical comparison of the deterministic simulations of the individual linezolid concentration-

time profiles in the peripheral compartment of the plasma model showed similar kinetics as the observed microdialysis data and hence suggested that Model B might be suitable to describe the tissue fluid distribution (Appendix Figure S17). This was confirmed when investigating both delayed distribution models (Model B and C) in the NLME model. Model C was not supported by the data as demonstrated by its poor predictivity for the retrodialysate concentrations (Appendix Figure S18 B.4.a, B.4.b), the imprecisely estimated parameters of the additional peripheral compartment (V_3: 49.3, Q_2: 49.1% RSE), and the low values of the parameters (V_3: 1.59 L, Q_2: 2.16 L/h). With Model B, however, plausible and precisely estimated parameters were obtained with an adequate predictivity for all matrices (Appendix Figure S18 A). Thus, Model B, assigning the ISF concentrations of the s.c. adipose tissue to the peripheral compartment and estimating an additional scaling factor ('tissue factor', TF), was integrated in the joint NLME model, which enabled the description of target site exposure. The statistical submodel was extended by additional IIV parameters for the TF and the RR. Unbound ISF concentrations were linked to the unbound concentrations in the peripheral compartment of the model to allow a better physiological interpretation of the TF.

In **step 4**, re-estimation of all parameter estimates based on the PK data of the second catheter resulted in very similar parameter estimates, justifying the joint modelling of the data of both catheters. For the joint model including data from both catheters, a second microdialysate compartment was added describing the concentrations determined with the second microdialysis catheter. Both microdialysate compartments were linked via the RR parameter to the ISF concentrations. The RR parameter allowed to implement and hence to dissect 'intercatheter variability' which was estimated based on the PK data of the two catheters, and 'intracatheter variability' which was estimated based on the PK data of the two retrodialysis assessments performed for half of the catheters (Section 2.6.1). In NONMEM®, this was achieved by encoding the inter- and intracatheter variability parameters as additional hierarchical levels of random-effects parameters (like 'interoccasion variability' (Eq. 2.8)). Overall, the final base NLME model adequately described the data, however, for the 'CWRES versus time' plot, a remaining undulating pattern in the microdialysate data was observed (Appendix Figure S19 A.1).

Covariate model development (step 5)

The difference in the RR values of obese and nonobese patients, which had already been observed in the exploratory analysis (Appendix Figure S5 B), was assessed within the model by investigating the obesity status (i.e. obese/non-obese) and continuous body size descriptors (e.g. body weight) as covariates on the RR parameter. Obesity was found to be by far the best predictor of RR, almost completely explaining the interindividual variability on the RR (reduction of unexplained IIV on RR from 14.8%CV to 0.3%CV). Hence, obesity was implemented in the NLME base model by estimating a separate typical RR value for obese and nonobese patients, and IIV on RR was

removed (Appendix Table S4).

The three pre-investigations performed to assess the impact of body size (+ additional pre-selected covariates) on the PK of linezolid, identified a potential influence of body size on the PK parameters V_1, V_2, Q and TF (Section 2.6.4.2: Covariate model development (step 5)). This was further investigated and confirmed in a comprehensive stepwise covariate analysis, for which the strategy was developed based on the results of the pre-investigations (Appendix Table S5). In brief body size was first investigated (i) as categorical (i.e. obesity) and continuous covariates (according to Holford et al. [204]: total body weight, LBW and NFM; Eq. 2.38), (ii) with and without allometric scaling and (iii) with combinedly and separately estimated NFM for the volume and clearance parameters, respectively. A following step assessed renal function markers (serum creatinine, $CLCR_{CG\_LBW}$) on the clearance parameters. Furthermore, following a one-by-one backward deletion of the selected covariates, the need of obesity as an additional impact factor for PK parameters was evaluated in addition to the impact of body size. The stepwise comprehensive evaluation identified the obesity status as a predictor of TF and LBW as an adequate predictor for V_1 and V_2 and Q (allometric implementation). No body size descriptor was identified as a covariate on the linezolid clearance parameters (Appendix Table S6). Detailed information on the results of the stepwise covariate analysis are summarised in the Appendix, Table S7.

The investigation of the surgery-specific characteristics as predictors of linezolid clearance and tissue fluid distribution resulted in the three following models, which were further compared (Appendix Table S8):

- Model 1: Including the anaesthesia status on the clearance parameter V_{max} and on TF
- Model 2: Including the two haemodynamic markers MAP and CO_{LZ} as continuous time-varying covariates on total clearance (i.e. sum of linear and nonlinear clearance) and on TF, respectively
- Model 3: Including the anaesthesia status on TF and MAP on total clearance

Model 3 was superior to the two other models with respect to reduction in unexplained IIV and/or the precision of the parameter estimates (Appendix Table S8). Furthermore, this model almost fully explained the undulating pattern in the ‘CWRES versus time’ plot of the microdialysate data (Appendix Figure S19 B.1) and was hence implemented in the NLME model.

In a final refinement step, proportional RUV models were selected for all measurement matrices. In addition, all implemented covariate effects of continuous covariates were centred to the median value of the investigated population.

3.1.2.2 Final joint nonlinear mixed-effects model

A sketch of the final joint NLME model of linezolid is provided at the bottom of Figure 3.3 and captures the following aspects: (i) total (i.e. bound + unbound) and unbound linezolid plasma and

unbound linezolid target site PK, (ii) PK in patients with varying body size/obesity status (highlighted in pink), (iii) intra-anaesthetic and post-anaesthetic PK (orange), as well as (iv) PK-related and microdialysis methodology-related aspects (blue and green, respectively). The NONMEM® model script of the joint NLME model is provided in Appendix 7.4.2 and the respective PK parameters are summarised in Table 3.2, using the same colour coding as in the model sketch.

In summary, the final model was a two-compartment model with an unbound volume of distribution of 50 L and parallel linear and nonlinear Michaelis-Menten clearance (average unbound CL over monitored time period of 8 h: 8.92 L/h). The ISF of the s.c. adipose tissue was identified to be part of the peripheral compartment and an additional TF was estimated to scale the concentrations in the peripheral compartment to the ISF concentrations. The TF was lower for the obese patients (54%) than for the nonobese patients (69%), thus resulting in lower target site exposure in the obese population. The obesity status of the patient was additionally found to impact RR, with a lower value for obese than nonobese patients (37.5% vs. 57.5%). The continuous body size descriptor LBW was identified as an impact factor for volume of distribution parameters (V_1, V_2) and Q according to allometric principles [204]: The volume of distribution parameters linearly scaled with LBW (allometric exponent: 1), i.e. increasing the LBW by 50% (e.g. 50 kg vs. 75 kg) also increased the volume of distribution of unbound linezolid by 50% (e.g. 48.5 L vs. 72.8 L). The parameter Q scaled with body weight to the power of 0.75 (=allometric exponent), i.e. increasing the LBW by 50% (e.g. 50 kg vs. 75 kg) increased the unbound Q of linezolid by 35.5% (e.g. 60.7 L/h vs. 82.2 L/h). In addition, the anaesthesia status of the patients and the haemodynamic marker MAP were found to impact the TF and the total (i.e. linear + nonlinear) CL of unbound linezolid, respectively. During anaesthesia, the TF was 13.6% lower than after anaesthesia; an increase of MAP of 10 mmHg led to an increase in total CL by 8%. The inclusion of the aforementioned covariates considerably decreased the unexplained interindividual and method-related variability compared to the base model (IIV on variance scale (IIV_{Var}) V_2: -68.6%, IIV_{Var} TF: -55.0%, IIV_{Var} CL: -50.5%, IIV_{Var} V_1: -40.1%, IIV_{Var} K_m: -38.9%; IIV_{Var} Q: -20.5%, IIV_{Var} RR: -99.95%; Table 3.2 and Table S4).

The dissected variabilities in the microdialysis technique, i.e. intercatheter- and intracatheter variability on the RR parameter, showed similar magnitudes with 26%CV and 27%CV, respectively. Residual unexplained variability was estimated separately for the matrices plasma (total plasma concentrations), ultrafiltrate (unbound plasma concentrations) and microdialysate. For the retrodialysate concentrations, RUV was fixed to the bioanalytical assay imprecision (1.9%CV [249]), to facilitate a separation of intracatheter variability and RUV. Total and unbound plasma concentrations showed similar magnitudes of RUV (total: 4.76%CV; unbound: 4.56%CV), while RUV for microdialysate was approximately twice as high as RUV for plasma (13.3%CV).

Table 3.2: Parameter estimates of final joint NLME model of linezolid in obese and nonobese surgical patients. PK parameter estimates for unbound linezolid and derived parameters for total linezolid, microdialysis methodology-related parameter estimates, as well as bootstrap results are displayed.

Parameter [unit]	**Final model**		**Bootstrap[3]**	
	'Unbound' estimate (RSE[1], %)	**Computed 'total' parameter[2]**	**Median**	**95% CI**
OFV	-247.45	--	-285.61	[-676.94, 116.23]
Fixed-effects parameters				
θ CL_u [L/h]	3.32 (30.7)	2.84	3.47	[1.56, 5.61]
θ $V_{max,u}$ [mg/h]	45.9 (21.8)	39.3	45.2	[20.6, 65.6]
θ $K_{m,u}$ [mg/L]	2.93 (23.8)	2.51	2.68	[0.464, 5.57]
θ MAP_CL_{Tot}[4], %	0.805 (41.0)	--	0.793	[0. 251, 1.49]
θ $V_{1,u}$ [L][5]	17.0 (8.20)	14.6	17.0	[14.5, 20.3]
θ Q_u [L/h][5]	62.4 (9.00)	53.4	62.1	[51.4, 74.8]
θ $V_{2,u}$ [L][5]	33.4 (4.60)	28.6	33.4	[29.8, 36.1]
θ f_u, %	85.6 (0.700)	--	85.6	[84.5, 86.9]
θ $TF_{OBE,u}$, %	54.1 (7.30)	--	54.3	[47.1, 63.4]
θ $TF_{NOBE,u}$, %	69.0 (5.70)	--	69.0	[61.2, 76.8]
θ ANAE_TF[7], %	-13.6 (19.5)	--	-13.7	[-19.0, -8.86]
θ RR_{OBE}, %	37.5 (7.80)	--	37.4	[32.1, 43.6]
θ RR_{NOBE}, %	57.5 (4.70)	--	57.6	[52.2, 63.4]
Interindividual and method variability parameters, %CV				
ω CL_u	66.7 (32.3)	--	63.1	[32.9, 128]
ω $K_{m,u}$	74.4 (48.8)	--	74.4	[31.6, 2520]
ω $V_{1,u}$	42.1 (11.6)	--	41.3	[32.6, 50.3]
ω Q_u	46.8 (17.7)	--	44.6	[31.1, 60.3]
ω $V_{2,u}$	16.7 (23.6)	--	15.8	[8.64, 23.0]
ω TF_u	14.8 (22.9)	--	13.5	[7.32, 18.8]
ω ANAE_TF	82.2 (22.3)	--	78.0	[49.3, 127]
$\omega_{Intercatheter}$ RR	26.1 (19.5)	--	25.1	[16.7, 33.8]
$\omega_{Intracatheter}$ RR	27.2 (10.4)	--	27.0	[21.8, 32.0]
Residual variability parameters, %CV				
σ_{prop} C_{P_tot}	4.76 (12.9)	--	4.67	[3.59, 5.89]
σ_{prop} C_{P_u}	4.56 (12.7)	--	4.49	[3.22, 5.62]
σ_{prop} $C_{\mu D}$	13.3 (6.50)	--	13.3	[11.6, 15.0]
σ_{prop} C_{RD}	1.9 FIX[8]	--	1.9 FIX[8]	--

[1]RSE of random-effects parameter estimates ω and σ are reported on approximate standard deviation scale; [2]Total parameter = Unbound parameter estimate · fu; [3]Convergence rate of non-parametric bootstrap (n=1000): 92%;[4]Change of clearance per mmHg deviation of MAP from 75 mmHg (linear MAP-$CL_{Tot,u}$ relationship); [5]Allometrically scaled with LBW (exponent of 1 and 0.75 for V_1/V_2 and Q, respectively) and centred to median in overall population (51.9 kg); [6]Post-anaesthetic TF_u; [7]Intra-anaesthetic change of TF; [8]Fixed to interassay variability [228].
Colour coding: Refers to the colours used in the model sketch (Figure 3.3); *Blue*: PK-related parameters; *Green*: microdialysis-methodology-related parameters; *Pink*: Body size impact; *Orange*: Anaesthesia/MAP impact.
Abbreviations: *ANAE_TF$_u$:* Anaesthesia effect on TF_u; *CI*: Confidence interval; *CL$_u$*: CL of unbound linezolid; *$CL_{Tot,u}$*: Total clearance of unbound linezolid; *CMT*: Compartment; C_{P_tot}: Total plasma concentrations; C_{P_u}: Unbound plasma concentrations; C_{RD}: Retrodialysate concentration; C_{RP}: Retroperfusate concentration; $C_{\mu D}$: Microdialysate concentration; *CV*: Coefficient of variation (calculated for random-effects parameters according to Eq. 2.6); *f_u*: Fraction unbound; *$K_{m,u}$*: Michaelis-Menten constant of unbound linezolid; *LBW*: Lean body weight; *MAP*: Mean arterial pressure; *MAP_$CL_{Tot,u}$*: Effect of MAP on *$CL_{Tot,u}$*; *NLME*: Nonlinear mixed-effects; *OBE*: Obesity; *Q_u*: Intercompartmental clearance of unbound linezolid; *RSE*: Relative standard error; *RR_{OBE}, RR_{NOBE}*: Relative recovery for obese and nonobese patients; *$TF_{OBE,u}$, $TF_{NOBE,u}$:* Tissue factor of unbound linezolid for obese and nonobese patients; *$V_{1,u}$, $V_{2,u}$:* Volume of distribution parameters of central and peripheral CMTs of unbound linezolid; *$V_{max,u}$:* Maximum elimination rate of unbound linezolid; θ: Fixed-effects parameter; ω: Random-effects parameter: Interindividual variability; σ: Random-effects parameter: Residual unexplained variability.

3.1.2.3 Model evaluation

Standard goodness-of-fit plots indicated adequate model predictions as shown by the symmetric and narrow distribution of observed versus predicted linezolid concentrations around the line of identity (Figure 3.4 A, B) and CWRES around the 0 reference line (Figure 3.4 C, D). The undulating pattern in the CWRES versus time plot, which had been observed for the base model without covariates and linear clearance was almost not present anymore, both for plasma and microdialysate data (Figure 3.4 D.1, D.2). The non-parametric bootstrap confirmed model robustness (convergence rate=92%) and accurately estimated parameter as indicated by the median of the bootstrap replicates, which were overall very similar to the estimates of the developed model. The 95% confidence intervals derived from the bootstrap replicates included the point estimates of the parameters, did not include 0, and were overall narrow which indicated statistical significance and precisely estimated parameters. Only the random-effect parameter IIV on the Michaelis-Menten constant K_m showed a comparably high upper limit of the confidence interval. A log-likelihood profiling of this parameter indicated a steep increase in OFV for parameter values lower than the one resulting in the observed OFV minimum, whereas for higher parameter values the change in OFV was rather flat (95% CI: 33.4-320%CV, Appendix Figure S20). The visual predictive checks indicated good predictive model performance for the three different matrices (Figure 3.4 E). Case deletion diagnostics on individual level revealed that none of the newly obtained parameter estimates fell outside the 95% confidence intervals of the final model parameter estimates, which indicated no influential individuals.

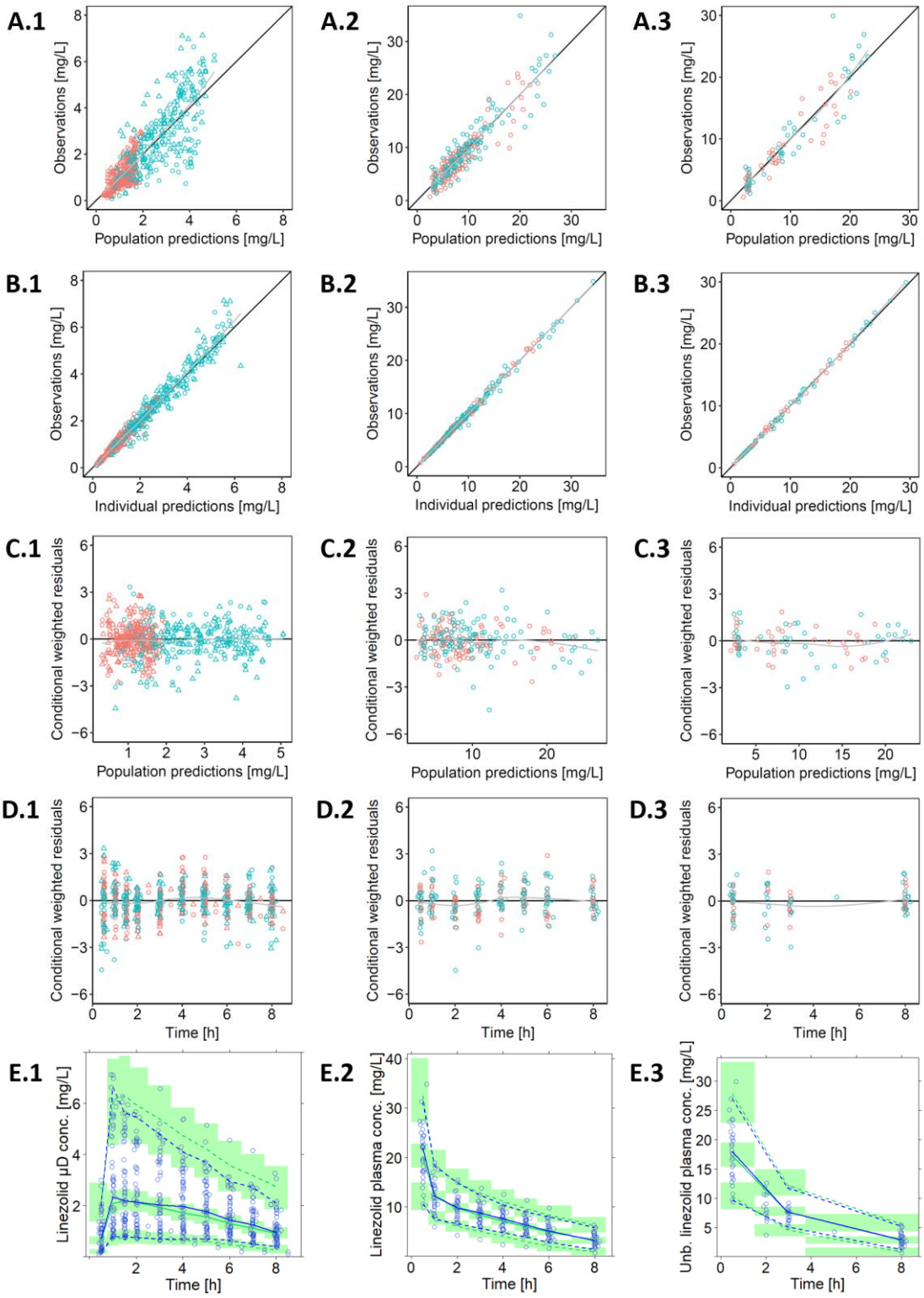

Figure 3.4: Basic goodness-of-fit plots (A-D) and VPC (n=1000 simulations, E) for the final NLME PK model for microdialysate concentrations (left panel; 1), total plasma concentrations (middle panel; 2), unbound plasma concentrations (right panel; 3).

A, B: *Circles*: Observed vs. population predicted (A) and individual predicted linezolid concentrations (B) for obese (red) and nonobese patients (green); *Triangles*: Microdialysate concentrations of the second catheter. *Black line*: Line of identity; *Grey line*: Loess smoother [250].

C, D: *Circles*: Conditional weighted residuals vs. population predicted linezolid concentrations (C) and time (D) for obese (red) and nonobese patients (green); *Triangles*: Microdialysate concentrations of the second catheter. *Lines*: Reference lines at y=0; *Grey lines*: Loess smoothers [250].

E: *Circles*: Observed linezolid concentrations; *Lines*: 5th, 95th percentile (dashed), 50th percentile (solid) of the observed (blue) and simulated (green) data. *Green shaded areas*: 95% confidence interval around 5th, 50th and 95th percentile of simulated data.

3.1.3 Simulations: Exploration of linezolid exposure

Deterministic and stochastic exposure simulations for standard linezolid dosing illustrated substantially lower linezolid drug concentrations in ISF of the s.c. adipose tissue than in plasma (especially around C_{max}) as well as a delayed distribution into the tissue fluid, as indicated by the C_{max} value, which was reached later in ISF than in plasma (Figure 3.5 A). The difference in the concentrations between the two matrices was most pronounced in obese patients (Figure 3.5 A: red, orange), resulting from the reduced tissue fluid penetration in the obese patient population (Table 3.2). Furthermore, a strong impact of body size on linezolid exposure was observed. Obese patients (Figure 3.5 B: red) showed markedly lower linezolid exposure compared to nonobese patients (Figure 3.5 B: green). This difference was detected both in plasma and in ISF and was particularly high in ISF and around the C_{max} value.

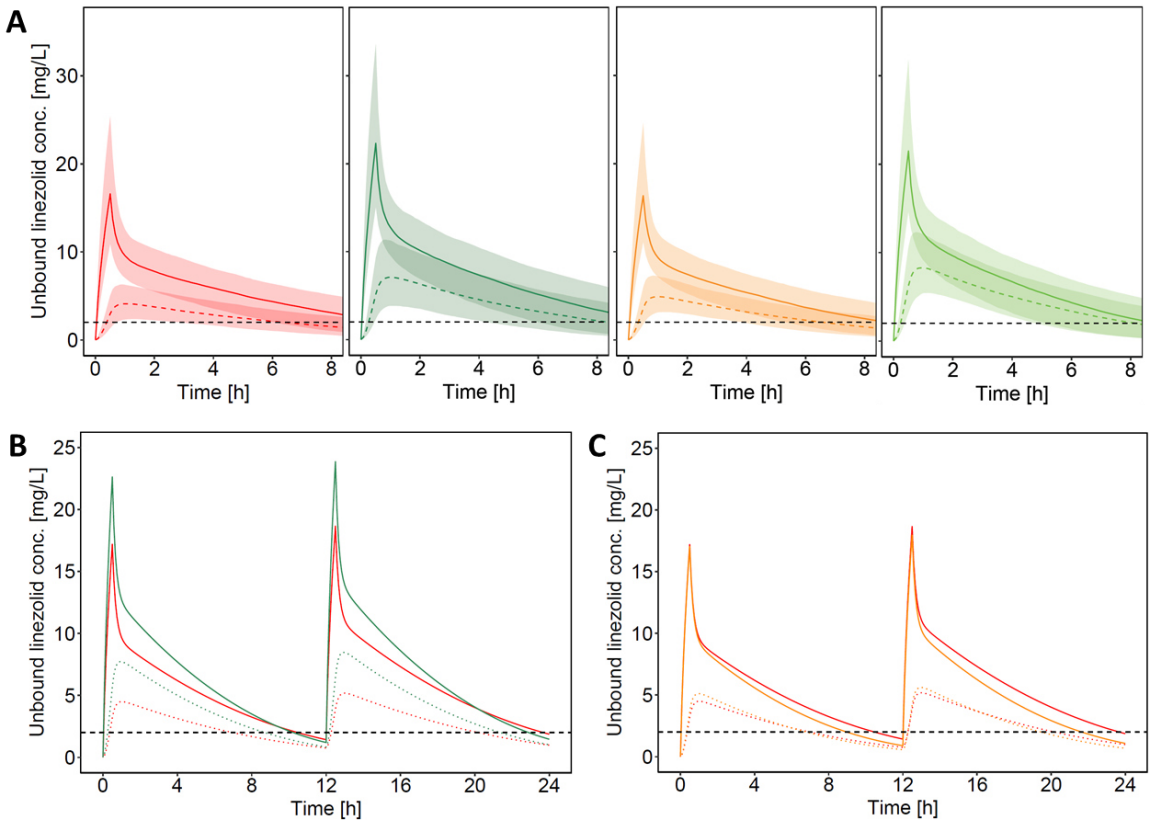

Figure 3.5: Simulated unbound linezolid concentration-time profiles for selected typical patients following standard linezolid dosing (600 mg, 30-min i.v. infusion, q12h).
A: Median (line), 5th and 95th percentile (shaded areas) of stochastic simulations (n=1000) of the unbound linezolid concentration-time profiles in plasma (solid) and ISF of the s.c. adipose tissue (dashed) for 4 typical patients over the first 8 h.
B: Typical linezolid concentration-time profile (i.e. deterministic simulation) of an exemplary obese and nonobese intra-anaesthetic patient over 24 h.
C: Typical linezolid concentration-time profile (i.e. deterministic simulation) of an exemplary intra-anaesthetic and post-anaesthetic obese patient over 24 h.
Dashed horizontal line: Exemplary MIC value of 2 mg/L(non-species-related EUCAST PK/PD S breakpoint [251]).
Colour coding: *Red*: Obese and intra-anaesthetic patient; *Dark green*: Nonobese and intra-anaesthetic patient; *Orange*: Obese and post-anaesthetic patient; *Light green*: Nonobese and post-anaesthetic patient (for detailed information on patient characteristics see Table 2.4 A).
Abbreviations: *EUCAST*: European Committee on Antimicrobial Susceptibility Testing; *ISF*: Interstitial space fluid; *i.v.:* Intravenous; *q12h:* Every 12 h; *MIC*: Minimum inhibitory concentration; *PK/PD*: Pharmacokinetic/Pharmacodynamic; *s.c.:* Subcutaneous.

An additional influence of the anaesthesia status and the MAP on the linezolid concentrations was observed, yet less pronounced than for body size. An intra-anaesthetic patient with a lower MAP value (Figure 3.5 C: red) showed slightly higher plasma concentrations in the terminal phase of the concentration-time profile than a post-anaesthetic patient with a higher MAP value (Figure 3.5 C: orange), reflecting the impact of MAP on linezolid clearance. For ISF, however, exposure was lower for the intra-anaesthetic patients, resulting from the reduced tissue factor during anaesthesia. Univariate deterministic exposure simulations for varying LBW showed a strong impact of body size on the linezolid concentration-time profile, which was particularly pronounced for the maximum concentrations and the concentrations in the early declining part of the profile (Figure 3.6). Maximum linezolid plasma concentrations for a typical patient with a low LBW value of 35 kg (i.e. body weight of 50.1 kg for a 1.65 m tall female patient) were ~2-fold higher than for a patient with a very high LBW of 80 kg (i.e. body weight of 334 kg for a 1.65 m tall female patient) (26.3 and 12.7 mg/L for first dose, respectively; Figure 3.6 A). In the later phase of the dosing interval (>8 h), an inverse trend was observed, with the high-LBW patient (80 kg) reaching ~2-fold higher linezolid plasma concentrations at 12 h after start of infusion, compared to the low-LBW patient (35 kg) (1.74 and 0.826 mg/L for first dose, respectively; Figure 3.6 A).

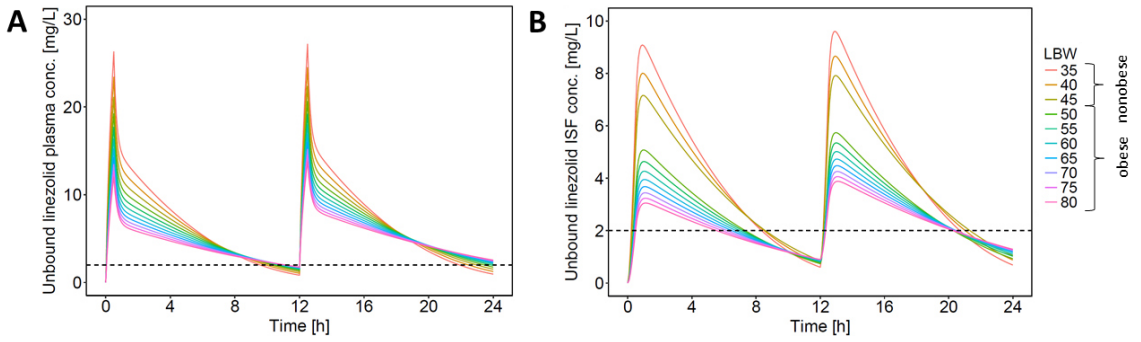

Figure 3.6: Simulated unbound linezolid concentration-time profiles in plasma (A) and ISF of the s.c. adipose tissue (B) for patients with varying LBW, following standard linezolid dosing (600 mg, 30-min i.v. infusion, q12h).
All other covariates in the NLME PK model were set to median values of the patient population (for detailed information on patient characteristics see Table 2.4 B).
Dashed horizontal line: Exemplary MIC value of 2 mg/L (non-species-related EUCAST PK/PD S breakpoint [251]).
Abbreviations: *LBW*: Lean body weight; Further abbreviation see Figure 3.5.

Similar trends were also observed for ISF (Figure 3.6 B). Here, the differences in the maximum linezolid concentrations of obese and nonobese patients was even more marked than for plasma, resulting from the reduced tissue factor in obese patients (in this example, LBW ≥50 kg – i.e. body weight ≥91.7 kg and BMI=33.7 kg/m^2 for a 1.65 m tall female patient – was defined as obese patients due to BMI ≥30 kg/m^2; Table 2.4 B). Maximum ISF linezolid concentrations were ~2.5-fold lower for the high-LBW (80 kg) patient compared to the low-LBW patient (35 kg) (9.08 and 3.23 mg/L for first dose, respectively), while linezolid ISF concentrations at 12 h after the start of infusion were ~1.5-fold higher (0.892 and 0.602 mg/L for first dose, respectively; Figure 3.6 B).

3.2 Project II: Evaluation and optimisation of linezolid dosing regimens for infection prophylaxis and acute therapy in obese and nonobese surgical patients

3.2.1 Simulations: Evaluation of standard linezolid dosing for infection prophylaxis

For the prophylactic setting of linezolid dosing (600 mg, as 30-min i.v. infusion, 30 min before incision), the results of the PTA analysis (PK/PD taget 95%$fT_{>MIC}$, assessed for incision-suture duration) for the site of a potential wound infection (i.e. ISF of the s.c. adipose tissue) are summarised in Table 3.3 for the typical obese (BMI=43.7 kg/m^2) and nonobese (BMI=23.3 kg/m^2) intra-anaesthetic patient. For illustration, the underlying stochastic exposure simulations for these two patients are depicted in Figure 3.7.

Table 3.3: Probability of target (95%$fT_{>MIC}$) attainment for different typical patients for infection prophylaxis.
PTA is given for ISF of the s.c. adipose tissue following a single standard linezolid dose (600 mg, 30-min i.v. infusion) in a typical obese and non-obese intra-anaesthetic patient for selected MIC values and incision-suture durations.

MIC [mg/L]	Incision-suture duration [h]	Probability of target attainment, %	
		"obese & intra-anaesthetic"[1]	"non-obese & intra-anaesthetic"[1]
0.5	2	99.6	99.8
	4	99.3	99.7
	6	98.7	98.7
1	2	98.8	99.5
	4	98	99
	6	92.8	96.4
2	2	90.1	97.9
	4	80.6	95.8
	6	51.8	81
4	2	25.5	83.1
	4	9.1	59.6
	6	1	25

[1]Detailed information on patient characteristics: Table 2.4 A.
Colour coding: *Green*: PTA≥90%, *Yellow*: PTA 80-<90%, *Orange*: PTA>50-<80%, *Red*: PTA≤50%
Abbreviations: *$fT_{>MIC}$:* Time period that unbound drug concentration exceeds the MIC; *ISF*: Interstitial space fluid; *s.c.:* Subcutaneous.

Overall, the following three trends were observed: (i) PTA increased with decreasing MIC value, (ii) PTA increased with decreasing incision-suture duration and (iii) PTA was higher for nonobese than for obese patients. More precisely, standard linezolid dosing resulted in adequate target attainment (i.e. PTA ≥90%) for both the typical obese and nonobese patient for MIC values ≤1 mg/L and incision-suture durations up to 6 h. For MIC=2 mg/L, however, PTA was adequate

only for the incision-suture duration of 2 h for the obese patient and 4 h for the nonobese patient. In case of even higher MIC values (≥4 mg/L), standard dosing did not result in adequate PTA for any of the investiagated incision-suture durations and patients.

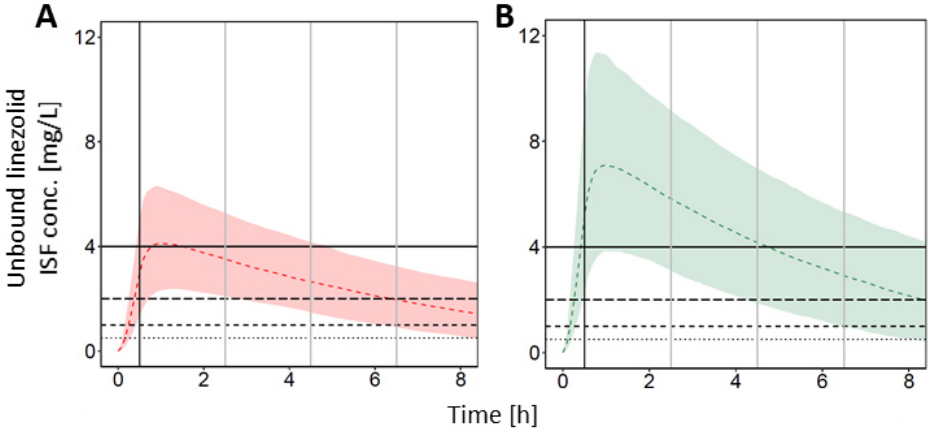

Figure 3.7: Stochastic simulations (n=1000) of the unbound linezolid concentration-time profiles in the ISF of the s.c. adipose tissue for the typical obese (A) and nonobese (B) intra-anaesthetic patient following a single standard dose of linezolid (600 mg, 30-min. i.v. infusion).
Lines: *Horizontal solid*: MIC=4 mg/L; *Horizontal long dashed*: MIC=2 mg/L; *Horizontal short-dashed*: MIC=1 mg/L; *Horizontal dotted*=0.5 mg/L; *Vertical black*: Incision time; *Vertical grey*: Incision-suture duration of 2 h, 4 h, 6 h.
Colour coding: *Red*: Obese and intra-anaesthetic patient; *Green*: Nonobese and intra-anaesthetic patient (for detailed information on patient characteristics see Table 2.4 A)
Abbreviations: *ISF*: Interstitial space fluid; *i.v.*: Intravenous; *MIC*: Minimum inhibitory concentration; *PK/PD*: Pharmacokinetic/Pharmacodynamic; *R*: Resistant.

Similar trends were observed when evaluating the PTA over a broad range of LBW values for an intra-anaesthetic patient (Figure 3.8). While for MIC ≤1 mg/L, adequate PTA was reached for the full investigated LBW range (35-80 kg; i.e. body weight of 50.1-334 kg for a 1.65 m tall female patient), for MIC=2 mg/L, PTA was only adequate for incision-suture durations of 2 and 4 h in the lower investigated LBW range (LBW ≤50 and ≤45 kg, respectively; i.e. body weight ≤111 kg and ≤75.4 kg, respectively, for a 1.65 m tall female patient; Figure 3.8). For MIC=4 mg/L, none of the LBW values reached adequate PTA: While PTA was yet relatively high for the incision-suture duration of 2 h and low LBW (e.g. 88.3% for LBW=35 kg, i.e. body weight of 46.7 kg for a 1.65 m tall female patient), for high LBW values PTA declined markedly (e.g. 4.5%, for LBW=80 kg; Figure 3.8).

3.2.2 Simulations: Evaluation and optimisation of linezolid dosing for acute therapy

For linezolid standard dosing in the setting of acute infection therapy (SI1.2$_{12}$: 600 mg, as 30-min i.v. infusion, q12h), the results of the PTA analysis (PK/PD taget 95%$fT_{>MIC}$) for the initial phase of treatment (i.e first 24 h) are summarised in Figure 3.9 A.1-A.2 for varying LBW values, both for unbound linezolid concentrations in plasma and in ISF of the s.c. adipose tissue

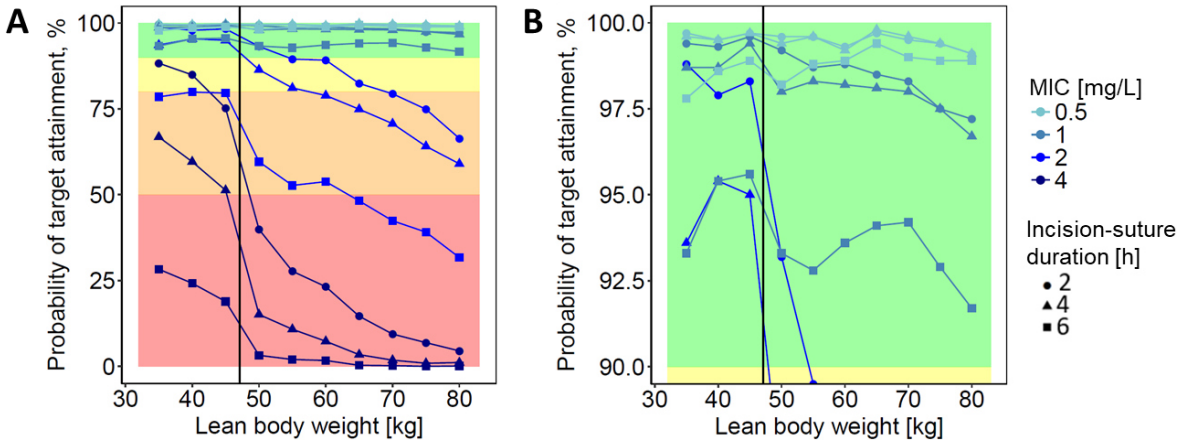

Figure 3.8: Probability of target (PTA; 95%$fT_{>MIC}$) attainment versus LBW depicted for full PTA range (A: 0-100%) and selected PTA range (B: 90-100%).
PTA evaluated in ISF of the s.c. adipose tissue following a single standard linezolid dose (600 mg, 30-min i.v. infusion) for infection prophylaxis. PTA is provided for varying LBW values, for selected MIC values, and incision-suture durations. All other covariates in the NLME PK model were set to median values of the patient population (for detailed information on patient characteristics see Table 2.4 B).
Vertical line: LBW obesity threshold of 47.1 kg (translating into the BMI obesity threshold of 30 kg/m^2 for a 1.65 m tall female patient).
Colour coding (shaded areas): *Green*: PTA≥90%, *Yellow*: PTA 80-<90%, *Orange*: PTA>50-<80%, *Red*: PTA≤50%.
Abbreviations: *$fT_{>MIC}$:* Time period that unbound drug concentration exceeds the MIC; *ISF*: Interstitial space fluid; *LBW*: Lean body weight; *MIC*: Minimal inhibitory concentration; *PTA*: Probability of target attainment; *s.c.:* Subcutaneous.

This analysis revealed adequate PTA (i.e. PTA ≥90%) after 24 h of standard linezolid treatment, only in plasma for the lowest investigated MIC value (0.5 mg/L) and the upper range of LBW (LBW ≥60 kg, i.e. body weight of ≥135 kg for a 1.65 m tall female patient; Figure 3.9 A.1). In ISF, none of the investigated combinations of MIC value (0.5, 1, 2, 4 mg/L) and LBW value (35-80 kg) reached adequate PTA (Figure 3.9 A.2).

In the following the impact of the of dosing regimen alterations (intensification of the daily dose: Section 3.2.2.1, prolongation of the infusion duration: Section 3.2.2.2, shortening of the dosing interval: Section 3.2.2.3) and LBW on the PTA (Section 3.2.2.4) is elucidated as well as an overview of adequate dosing regimens (Section 3.2.2.5) is provided. The underlying raw results of the PTA analyses are provided in the Appendix chapter (Appendix Figure S21 and Table S10); additionally, deterministic simulations of the linezolid concentration-time profiles resulting from the different dosing regimens are provided for graphical illustration (Appendix Figure S22).

3.2.2.1 Impact of intensification of daily dose on the PTA

The intensification of the total daily dose (DD) overall clearly improved the attainment of adequate PTA (i.e. PTA ≥90%). Increasing the daily dose for the q12h infusion regimens by 50% (i.e. from 1200 mg to 1800 mg) enhanced the attainment of adequate PTA by 3.56-fold. Doubling the daily dose (i.e. from 1200 mg to 2400 mg) even increased the achievement of adequate PTA by 5.43-fold. More precisely, the impact of the daily dose on the attainment of adequate PTA was more pronounced for short-term than prolonged infusion regimens as well as for ISF compared to plasma. Raw results are provided in the Appendix, Table S12.

Comparing the actual magnitude of the PTA, also revealed a clear increase in PTA with intensification of the daily dose (Figure 3.9).

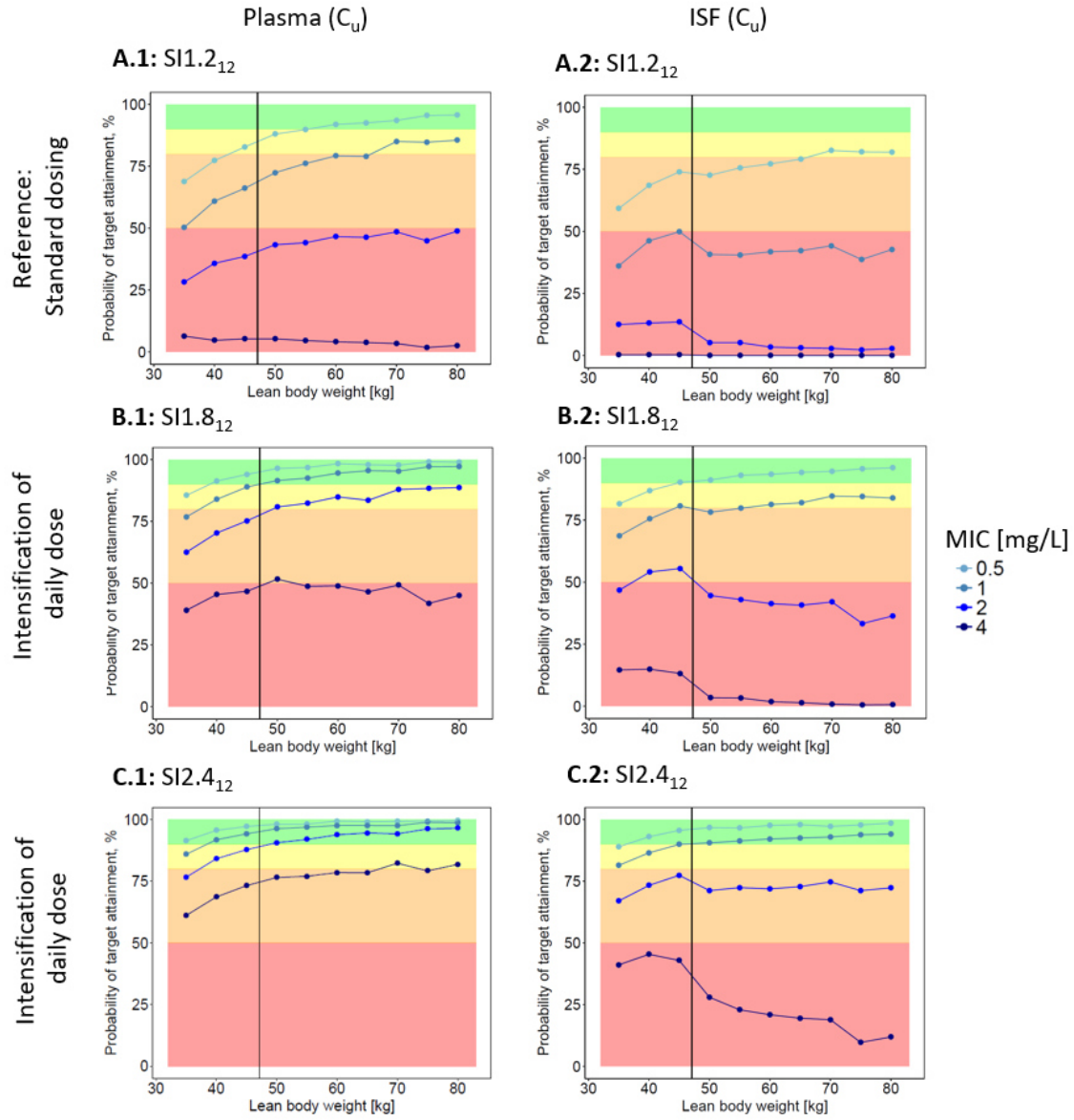

Figure 3.9: Probability of target (95%$fT_{>MIC}$) attainment vs. LBW in plasma (1) and ISF of the s.c. adipose tissue (2), for standard linezolid dosing SI1.2$_{12}$ (A) and the two alternative dosing regimens with intensified daily dose SI1.8$_{12}$ (B) and SI2.4$_{12}$ (C).

All other covariates in the NLME PK model were set to median values of the patient population (for detailed information on patient characteristics see Table 2.4 B). PTA results of all eight investigated dosing regimens: Appendix Figure S21. Deterministic simulations of unbound linezolid concentration-time profiles in plasma and ISF for the eight different dosing regimens: Appendix Figure S22.

Vertical line: LBW obesity threshold of 47.1 kg (translating into the BMI obesity threshold of 30 kg/m^2 for a 1.65 m tall female patient).

Dosing regimens: *SI1.2$_{12}$*: 600 mg 30-min i.v. infusion, q12h; *SI1.8$_{12}$*: 900 mg 30-min i.v. infusion, q12h; *SI2.4$_{12}$*: 1200 mg 30-min i.v. infusion, q12h.

Colour coding (shaded areas): *Green*: PTA≥90%, *Yellow*: PTA 80-<90%, *Orange*: PTA>50-<80%, *Red*: PTA≤50%.

Abbreviations: *$fT_{>MIC}$:* Time period that unbound drug concentration exceeds the MIC; *ISF*: Interstitial space fluid; *LBW*: Lean body weight; *q8h*: Every 8 h; *q12h*: Every 12 h; *MIC*: Minimum inhibitory concentration; *s.c.:* Subcutaneous.

While, for instance, for the short-term dosing regimen with standard daily dose of 1200 mg ($SI1.2_{12}$), PTA in plasma was only 43.3% ('red' area; Figure 3.9 A.1) for LBW of 50 kg and a MIC value of 2 mg/L, PTA increase to 80.8% ('yellow' area; Figure 3.9 B.1) for the daily dose of 1800 mg and even up to 90.6% ('green' area, Figure 3.9 C.1) for a daily dose of 2400 mg.

3.2.2.2 Impact of prolongation of infusion duration on the PTA

Prolongation of the infusion duration (INF) overall improved the attainment of adequate PTA (i.e. PTA ≥90%). The investigated prolonged infusion regimens (INF=4 h) resulted 16.5% more often in adequate PTA compared to the investigated short-term infusion regimens (INF=30 min). More precisely, the superiority of the prolonged over the short-term infusion regimens was more pronounced for standard than intensified daily doses: While for standard daily dose (1200 mg) the prolongation of the infusion interval led to a 3.20-fold improvement in the attainment of adequate PTA, for the intensified daily doses of 1800 mg and 2400 mg, a 1.38-fold and 1.07-fold improvement was reached, respectively. In addition, the impact of the prolongation of infusion duration on the attainment of adequate PTA differed between q12h and q8h dosing regimens: For the q12h dosing regimens (τ=12 h), the prolongation of the dosing interval clearly improved the attainment of adequate PTA by 32.4% compared to short-term regimens. However, for the q8h dosing regimens (τ=8 h) the prolongation of the infusion duration showed no impact on the attainment of adequate PTA. Furthermore, the impact of the prolongation of infusion duration on the attainment of adequate PTA also differed between plasma and ISF: While, in plasma prolonged infusion regimens resulted 24.3% more often in adequate PTA than short-term regimens; in ISF, the attainment of adequate PTA was comparable between prolonged and short-term infusion regimens. Raw results are provided in the Appendix, Table S13.

Assessing the impact of the prolongation of the infusion duration on the actual magnitude of PTA, overall showed an improvement in PTA (Figure 3.10). For some investigated combinations an inverse impact was observed with prolongation of the infusion duration resulting in reduced PTA compared to the corresponding short-term infusion regimens (Figure 3.10; Appendix Figure S21). This was in general the case for higher MIC values and/or high LBW values and was particularly pronounced in ISF. While, for example, the PTA in ISF for the prolonged regimen $PI1.2_{12}$ and the low MIC value of 0.5 mg/L was superior to the standard dosing ($SI1.2_{12}$) up to LBW values of 70 kg, it was inferior for higher LBW values (LBW ≥75 kg; Figure 3.10). For the higher MIC value of 1 mg/L, however, the prolonged infusion regimen was already inferior at LBW values ≥50 kg.

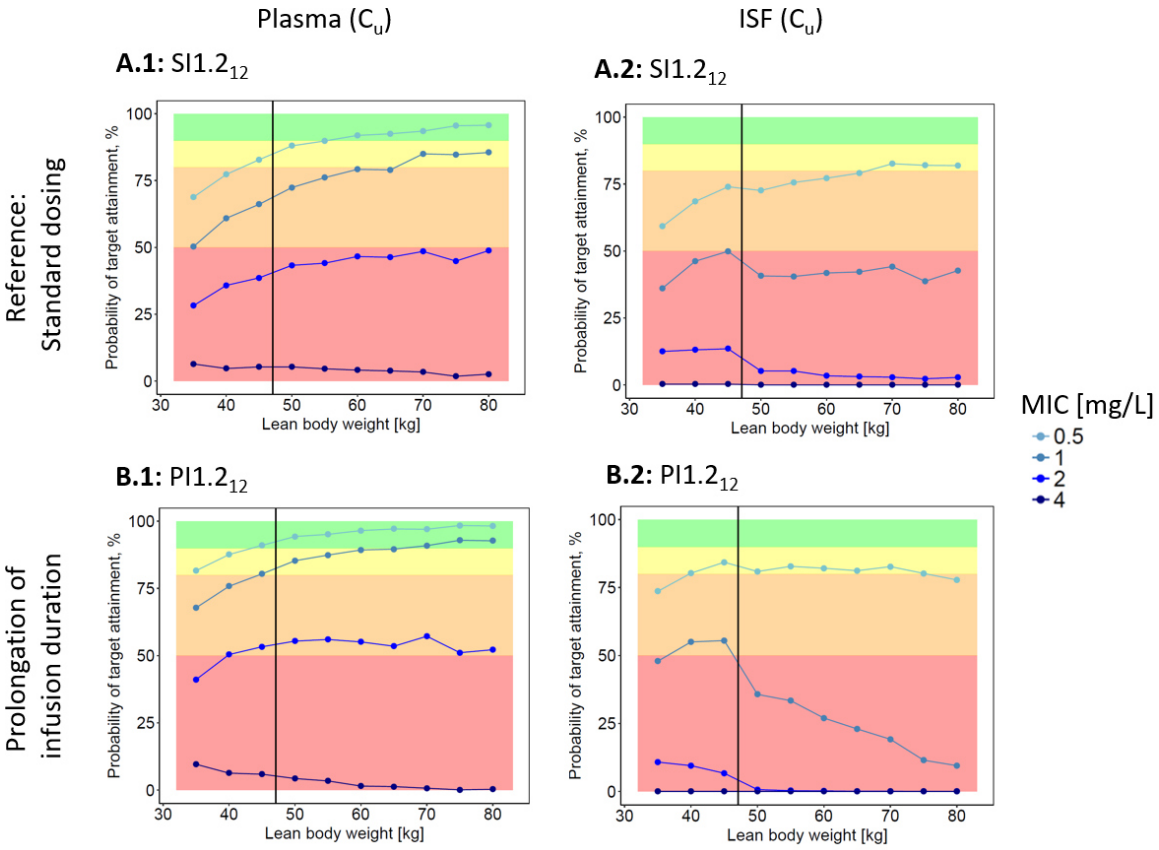

Figure 3.10: Probability of target (95%$fT_{>MIC}$) attainment vs. LBW in plasma (1) and ISF of the s.c. adipose tissue (2), for standard linezolid dosing $SI1.2_{12}$ (A) and one selected alternative dosing regimen with prolonged infusion duration $PI1.8_{12}$ (B).
Dosing regimens: *$SI1.2_{12}$*: 600 mg 30-min i.v. infusion, q12h; *$PI1.2_{12}$*: 600 mg 4-h i.v. infusion, q12h.
For further information and abbreviations see Figure 3.9.

3.2.2.3 Impact of shortening of dosing interval on the PTA

Shortening the dosing interval (τ) overall improved the attainment of adequate PTA (i.e. PTA ≥90%). The investigated q8h infusion regimens (τ=8 h) resulted 33.3% more often in adequate PTA compared to the investigated corresponding q12h infusion regimens (τ=12 h). In general, the superiority was more pronounced for short-term than for prolonged infusion regimens: While for short-term infusions, the shortening of the dosing interval increased the attainment of adequate PTA by ~1.58-fold, for prolonged infusions the increase was ~1.15-fold. In addition, the impact of shortening the dosing interval on the attainment of adequate PTA was stronger in plasma than in ISF, with a ~1.38-fold and ~1.24-fold improvement, respectively. Raw results are provided in the Appendix, Table S14.

Assessing the impact of shortening the dosing interval on the actual magnitude of PTA, an overall improvement in PTA was observed (Figure 3.11); yet, for some MIC-LBW combinations an inverse impact was observed with shortening of dosing intervals (τ=8 h) resulting in a reduction of PTA compared to standard dosing intervals (τ=12 h) (Figure 3.11; Appendix Figure S21).

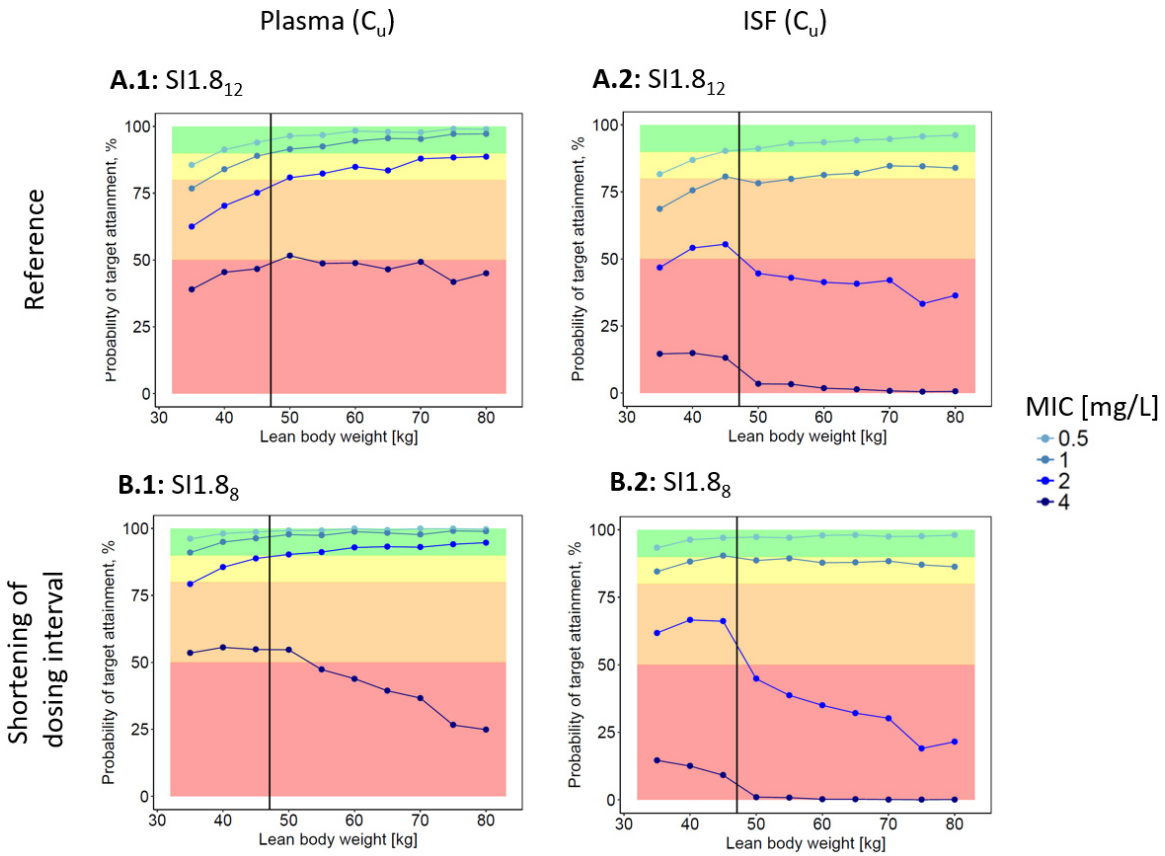

Figure 3.11: Probability of target (95%$fT_{>MIC}$) attainment vs. LBW in plasma (1) and ISF of the s.c. adipose tissue (2), for standard linezolid dosing SI1.2$_{12}$ (A) and one selected alternative dosing regimen with prolonged infusion duration PI1.8$_{12}$ (B).
Dosing regimens: *SI1.2$_{12}$*: 600 mg 30-min i.v. infusion, q12h; *SI1.8$_8$: 600 mg 30-min i.v. infusion, q8h.*
For further information and abbreviations see Figure 3.9.

In general, this impact was observed for higher MIC values and/or high LBW values and was particularly pronounced in ISF. For example, the PTA in ISF for the q8h infusion regimen SI1.8$_8$ and the MIC value of 1 mg/L was higher compared to the q12h infusion regimen SI1.8$_{12}$ over the full investigated LBW range (i.e. 35-80 kg; Figure 3.11). For the higher MIC value of 2 mg/L, however, the q8h infusion regimen showed a higher magnitude of PTA values compared to the q12h infusion regimens up to LBW values of 50 kg, while for higher LBW values (≥55 kg) an inverse relation was observed.

3.2.2.4 Impact of lean body weight on the PTA

As indicated in the previous sections, the relationship between LBW and PTA was influenced by the MIC value and various determinants of linezolid exposure (Appendix Figure S22), namely, the LBW value, the matrix of interest (i.e. plasma, ISF) and the type of dosing regimen (daily dose, infusion duration, dosing interval).

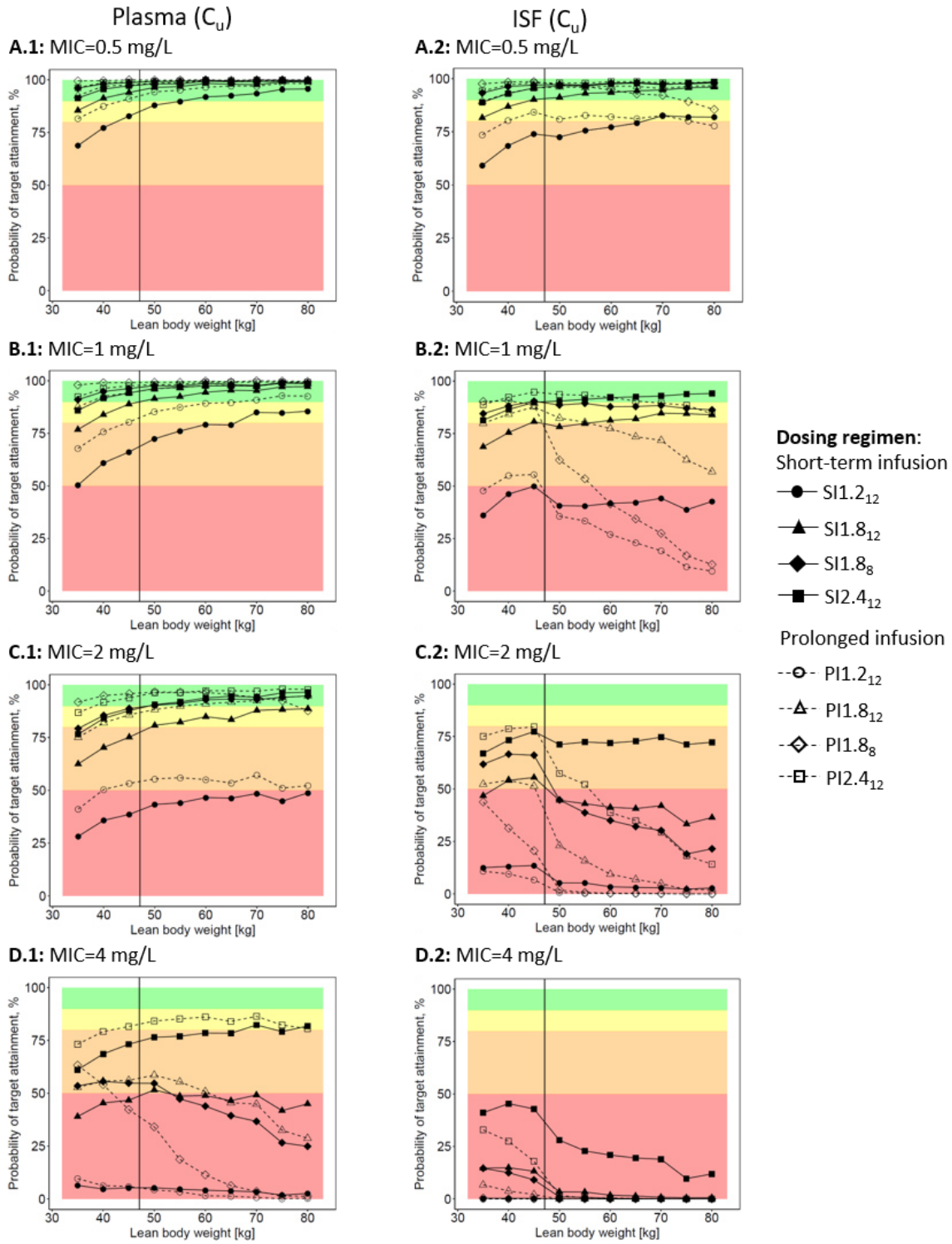

Figure 3.12: Probability of target (95%$fT_{>MIC}$) attainment vs. LBW in plasma (1) and ISF of the s.c. adipose tissue (2), for four different MIC values (A-D) and eight different linezolid dosing regimens.
Dosing regimens: *SI1.2$_{12}$*: 600 mg 30-min i.v. infusion, q12h; *SI1.8$_{12}$*: 900 mg 30-min i.v. infusion, q12h; *SI1.8$_{8}$*: 600 mg 30-min i.v. infusion, q8h; *SI2.4$_{12}$*: 1200 mg 30-min i.v. infusion, q12h; *PI1.2$_{12}$*: 600 mg 4-h i.v. infusion, q12h; *PI1.8$_{12}$*: 900 mg 4-h i.v. infusion, q12h; *PI1.8$_{8}$*: 600 mg 4-h i.v. infusion, q8h; *PI2.4$_{12}$*: 1200 mg 4-h i.v. infusion, q12h.
For further information and abbreviations see Figure 3.9.

Jointly assessing all investigated combinations (Figure 3.12) indicated the following general tendencies:

i. for lower MIC values and/or lower LBW values a positive LBW-PTA relationship was detected, i.e. an increase in LBW improved the PTA,
ii. for higher MIC values and/or higher LBW values a negative LBW-PTA relationship was observed, i.e. an increase in LBW reduced the PTA,
iii. the change from a positive to a negative LBW-PTA relationship occurred earlier (i.e. at lower MIC and/or LBW values)
    a. in ISF compared to plasma,
    b. for lower compared to the corresponding higher daily doses,
    c. for prolonged compared to the corresponding short-term infusion regimens, and
    d. for q8h compared to the corresponding q12h infusion regimens.

These tendencies will be elucidated by selected examples in the following. *Tendency i-ii:* While, for instance, for a low MIC value of 0.5 mg/L the PTA in plasma increased with increasing LBW (Figure 3.12 A.1), for a higher MIC value of 4 mg/L, the PTA decreased for some dosing regimens (e.g. $SI1.8_8$; Figure 3.12 D.1). In addition, at lower LBW values ≤50 kg, the PTA in plasma increased for the dosing regimen $SI1.8_{12}$, while the PTA decreased for higher LBW values ≥55 kg (Figure 3.12 D.1). *Tendency iiia:* While in plasma only at a MIC value of 4 mg/L a clear decline in PTA with increasing LBW was observed for some of the dosing intervals (e.g. $SI1.8_8$; Figure 3.12 D.1), in ISF already at a MIC value of 1 mg/L a clear negative LBW-PTA relationships was observed (e.g. $SI1.8_8$; Figure 3.12 B.2). In addition, in plasma a positive PTA-LBW relationship was revealed up to LBW values of 70 kg for the dosing regimen $SI2.4_{12}$ and MIC value of 4 mg/L (Figure 3.12 D.1), whereas in ISF a positive relationship was only detected up to a LBW value of 40 kg (Figure 3.12 D.2). *Tendency iiib:* While for the low-dose regimen $SI1.2_{12}$ a positive LBW-PTA relationship was only observed up to MIC values of 1 mg/L in plasma, for the high-dose regimen $SI2.4_{12}$ the positive LBW-PTA relationship was detected up to MIC values of 2 mg/L. Furthermore, for the dosing regimen $SI1.8_{12}$ a positive PTA-LBW relationship was revealed up to LBW values of 59 kg for a MIC of 4 mg/L in plasma, whereas the high-dose regimen $SI2.4_{12}$ demonstrated a positive relationship up to a LBW value of 70 kg. *Tendency iiic:* While the PTA for the standard short-term infusion regimen $SI1.2_{12}$ increased up to a LBW value of 70 kg in plasma and for a MIC value of 4 mg/L, the PTA of the corresponding prolonged infusion regimen $PI1.2_{12}$ only increased up to a LBW value of 55 kg. *Tendency iiid:* The PTA for the q12h infusion regimen $PI1.8_{12}$ increased up to a LBW value of 50 kg and decreased for LBW values ≥55kg; the PTA of the corresponding q8h regimen $PI1.8_8$, however, declined over the full investigated LBW range (i.e. 35-80 kg).

3.2.2.5 Dosing overview

A tabular overview of dosing regimens resulting in adequate PTA (i.e. PTA ≥90%) is provided in Table 3.4 and shall be explained in the following (*example provided in parenthesis for illustration*): Given the information on sex (*female*) and total body weight (*110 kg*) of a patient, the corresponding LBW (*~55 kg*) can be computed (Appendix Section 7.3.2: Eq. 7.11). In addition to the patient-specific LBW the pathogen-specific MIC value is required (*1 mg/L*). In a next step it needs to be defined whether adequate PTA is aimed for in plasma only or both in plasma and ISF of the s.c. adipose tissue (*plasma&ISF*). Based on this information short-term and/or prolonged dosing regimens can be identified resulting in adequate PTA ($SI2.4_{12}$, $PI2.4_{12}$).

Table 3.4: Overview of adequacy of different dosing regimens to attain PK/PD target (95%$fT_{>MIC}$) for varying LBW in plasma (A) or both in plasma and ISF (B) [continued on next page].
Results given for selected short-term and prolonged dosing regimens, selected MIC values and varying LBW values. Dosing regimens resulting in adequate PTA for plasma (A) or plasma and ISF (B) are highlighted with ✓.

MIC [mg/L]	LBW [kg][1]	Dosing regimens[3]															
		A: …resulting in adequate PTA[2] in plasma								B: …resulting in adequate PTA[2] in plasma and ISF							
		Short-term infusion				Prolonged infusion				Short-term infusion				Prolonged infusion			
		$SI1.2_{12}$	$SI1.8_{12}$	$SI1.8_{8}$	$SI2.4_{12}$	$PI1.2_{12}$	$PI1.8_{12}$	$PI1.8_{8}$	$PI2.4_{12}$	$SI1.2_{12}$	$SI1.8_{12}$	$SI1.8_{8}$	$SI2.4_{12}$	$PI1.2_{12}$	$PI1.8_{12}$	$PI1.8_{8}$	$PI2.4_{12}$
0.5	35			✓	✓		✓	✓	✓			✓				✓	✓
	40		✓	✓	✓		✓	✓	✓			✓	✓		✓	✓	✓
	45		✓	✓	✓	✓	✓	✓	✓		✓	✓	✓		✓	✓	✓
	50		✓	✓	✓	✓	✓	✓	✓		✓	✓	✓		✓	✓	✓
	55		✓	✓	✓	✓	✓	✓	✓		✓	✓	✓		✓	✓	✓
	60	✓	✓	✓	✓	✓	✓	✓	✓		✓	✓	✓		✓	✓	✓
	65	✓	✓	✓	✓	✓	✓	✓	✓		✓	✓	✓		✓	✓	✓
	70	✓	✓	✓	✓	✓	✓	✓	✓		✓	✓	✓		✓	✓	✓
	75	✓	✓	✓	✓	✓	✓	✓	✓		✓	✓	✓		✓		✓
	80	✓	✓	✓	✓	✓	✓	✓	✓		✓	✓	✓		✓		✓
1	35			✓				✓	✓		none					✓	
	40			✓	✓		✓	✓	✓		none					✓	✓
	45			✓	✓		✓	✓	✓			✓					✓
	50		✓	✓	✓		✓	✓	✓				✓				✓
	55		✓	✓	✓		✓	✓	✓				✓				✓
	60		✓	✓	✓		✓	✓	✓				✓				✓
	65		✓	✓	✓		✓	✓	✓				✓				✓
	70		✓	✓	✓	✓	✓	✓	✓				✓		none		
	75		✓	✓	✓	✓	✓	✓	✓				✓		none		
	80		✓	✓	✓	✓	✓	✓	✓				✓		none		

Table 3.4 [continued].

MIC [mg/L]	LBW [kg][1]	Dosing regimens[3]															
		A: …resulting in adequate PTA[2] in plasma								B: …resulting in adequate PTA[2] in plasma and ISF							
		Short-term infusion				Prolonged infusion				Short-term infusion				Prolonged infusion			
		SI1.2$_{12}$	SI1.8$_{12}$	SI1.8$_{8}$	SI2.4$_{12}$	PI1.2$_{12}$	PI1.8$_{12}$	PI1.8$_{8}$	PI2.4$_{12}$	SI1.2$_{12}$	SI1.8$_{12}$	SI1.8$_{8}$	SI2.4$_{12}$	PI1.2$_{12}$	PI1.8$_{12}$	PI1.8$_{8}$	PI2.4$_{12}$
2	35	none						✓		none				none			
	40	none						✓	✓	none				none			
	45	none						✓	✓	none				none			
	50			✓	✓			✓	✓	none				none			
	55			✓	✓			✓	✓	none				none			
	60			✓	✓		✓	✓	✓	none				none			
	65			✓	✓		✓	✓	✓	none				none			
	70			✓	✓		✓	✓	✓	none				none			
	75			✓	✓		✓		✓	none				none			
	80			✓	✓		✓		✓	none				none			
4	35	none				none				none				none			
	(…)	none				none				none				none			
	80	none				none				none				none			

[1]All other covariates in the NLME PK model were set to median values of the patient population (for detailed information on patient characteristics see Table 2.4 B). [2]Adequate PTA is defined as PTA ≥90%, for the PK/PD target 95%$fT_{>MIC}$ (for detailed information on PTA see Table S10); [3]Dosing regimens: *SI1.2$_{12}$*: 600 mg 30-min i.v. infusion, q12h; *SI1.8$_{12}$*: 900 mg 30-min i.v. infusion, q12h; *SI1.8$_{8}$*: 600 mg 30-min i.v. infusion, q8h; *SI2.4$_{12}$*: 1200 mg 30-min i.v. infusion, q12h; *PI1.2$_{12}$*: 600 mg 4-h i.v. infusion, q12h; *PI1.8$_{12}$*: 900 mg 4-h i.v. infusion, q12h; *PI1.8$_{8}$*: 600 mg 4-h i.v. infusion, q8h; *PI2.4$_{12}$*: 1200 mg 4-h i.v. infusion, q12h.

Horizontal dashed line: Separates obese from nonobese patients according to LBW obesity threshold of 47.1 kg (translating into the BMI obesity threshold of 30 kg/m^2 for a 1.65 m tall female patient).

Abbreviations: *$fT_{>MIC}$:* Time period that unbound drug concentration exceeds the MIC; *ISF*: Interstitial space fluid; *LBW*: Lean body weight; *PL*: Plasma; *PTA*: Probability of target attainment; *s.c.:* Subcutaneous.

Overall, in contrast to standard dosing, at least one of the alternative dosing regimens resulted in adequate PTA for the full LBW range up to a MIC value of 2 mg/L and 1 mg/L for plasma and plasma & ISF, respectively. Of note, for a MIC value of 4 mg/L, none of the eight investigated dosing regimens reached adequate PTA.

Similar results were observed for the investigated typical patients (PTA: Table S11, Table S15; deterministic simulations of linezolid concentration-time profiles: Appendix Figure S23).

3.3 Project III: Development of a risk assessment tool to evaluate standard meropenem dosing in critically ill patients with respect to ineffective meropenem exposure

3.3.1 Exploratory data analysis

3.3.1.1 Patient characteristics

A total of 48 patients (27 male, 21 female) were included in the study (Table 3.5). 83% of the patients suffered from sepsis, which was most frequently caused by pneumonia or peritonitis (75% or 20% of the sepsis patients, respectively). Pathogens detected in the patients comprised bacteria such as Enterobactericeae, non-fermenters (e.g. *Pseudomonas* spp.), *Staphylococcus* spp., *Streptococcus* spp., *Enterococcus* spp., *Bacillus* spp., *Clostridium* spp., *Bacteroides* spp., *Mycoplasma* spp. and fungi (*Candida* spp. and *Aspergillus* spp.). The patient group covered a broad range of age (24-84 years), BMI (16-49 kg/m^2) and severity of illness (APACHE II score: 11-42). Renal function determined by $CLCR_{CG}$ was highly variable, ranging from severely impaired up to augmented renal function (e.g. first study day: 24.8-191 mL/min). Seven patients received CRRT and six patients underwent extracorporeal membrane oxygenation (ECMO). 28 patients were post-lung- or post-liver-transplant recipients.

3.3.1.2 Meropenem dosing and sampling

Meropenem treatment was initiated in median 22.0 h before start of the study (i.e. drawing of first PK serum sample; Appendix Figure S24). During the study period, patients were treated with 1000 mg ($n_{patients}$=47) or 2000 mg ($n_{patients}$=1) of meropenem administered as 30-min infusions approximately every 8 h (median 8 h, $P_{0.025}$-$P_{0.975}$: 6.94-9.19 h). A total of 1376 blood samples (median per patient: 31) were taken during 349 dosing intervals (per patient: median 8, range 4-8). 23.5% (n=324) of the measurements were C_{min} samples, which were collected 7.92 h (median) after infusion start ($P_{0.025}$-$P_{0.975}$: 6.85-9.08 h). Very few serum concentrations (0.36% of data) revealed an implausible increase in the terminal part of the concentration-time profiles and were therefore excluded from the data analyses (Appendix Figure S25: red data points).

3.3.1.3 Meropenem concentrations

Large interindividual variability was observed for both the observed C_{min} values (Figure 3.13) and the calculated concentrations C_{8h} and C_{4h} (Table 3.6). While interindividual variability in C_{min} and C_{8h} was particularly large, varying in both concentrations by up to a factor of approximately 1000 between the patients, C_{4h} values were slightly less variable (C_{min}: range 0.03-30.0 mg/L, 104 %CV; C_{8h}: range 0.0426-30.0 mg/L, 110 %CV; C_{4h}: range 0.933-43.3 mg/L, 69.9 %CV).

Table 3.5: Patient characteristics of critically ill population at first study day (modified from [233]).

Diagnosis (multiple possible)	**Number of patients**	**Percentage of patients, %**
Sepsis	40	83.3
• Origin: Pneumonia	30	75.0[1]
- Hospital-acquired pneumonia	18	60.0[2]
- Community-acquired pneumonia	12	40.0[2]
• Origin: Peritonitis	8	20.0[1]
• Origin: Urosepsis	1	2.50[1]
• Origin: Soft tissue infection	1[3]	2.50[1]
ARDS	7	14.6
Others	6	12.5
Continuous patient characteristics [unit]	**Median**	**$P_{0.05}$-$P_{0.95}$**
APACHE II score [-]	27	13-38
SOFA score [-]	12	4-18
IL-6 serum concentration [pg/mL]	94.2	24.5-7330
CRP serum concentration [mg/dL]	9.75	2.10-31.8
Albumin serum concentration [g/dL]	2.80	2.20-3.56
$CLCR_{CG}$ [mL/min]	70.8	34.8-160
• $CLCR_{CG}$ of patients without CRRT [mL/min]	80.8	24.8-191
• $CLCR_{CG}$ of patients with CRRT [mL/min]	54.1	26.5-72.9
Age [years]	55.5	32.0-69.9
Total body weight [kg]	70.5	47.4-121
BMI [kg/m^2]	24.0	18.4-39.6
Categorical patient characteristics	**Number of patients**	**Percentage of patients, %**
Sex (male)	27	56.3
CRRT	7	14.6
• CVVH	1	14.3[4]
• CVVHD	3	42.9[4]
• CVVHDF	3	42.9[4]
Lung transplantation[5]	19	39.6
Liver transplantation[5]	9	18.8
ECMO	6	12.5

[1]In relation to total number of sepsis patients; [2]In relation to total number of pneumonia patients; [3]Abdominal wall abscess; [4]In relation to total number of CRRT patients; [5]Transplantation within last 28 days.

Abbreviations: *APACHE II*: Acute Physiology And Chronic Health Evaluation II [1]; *ARDS*: Acute respiratory distress syndrome; *BMI*: Body mass index; $CLCR_{CG}$: Creatinine clearance estimated according to Cockcroft and Gault [2]; *CRP*: C-reactive protein; *CRRT*: Continuous renal replacement therapy; *CVVH*: Continuous venovenous haemofiltration; *CVVHD*: Continuous venovenous haemodialysis; *CVVHDF*: Continuous venovenous haemodiafiltration; *ECMO*: Extracorporeal membrane oxygenation; *IL-6*: Interleukin 6; $P_{0.05}$: 5th percentile; $P_{0.95}$: 95th percentile; *SOFA*: Sepsis-related Organ Failure Assessment [6].

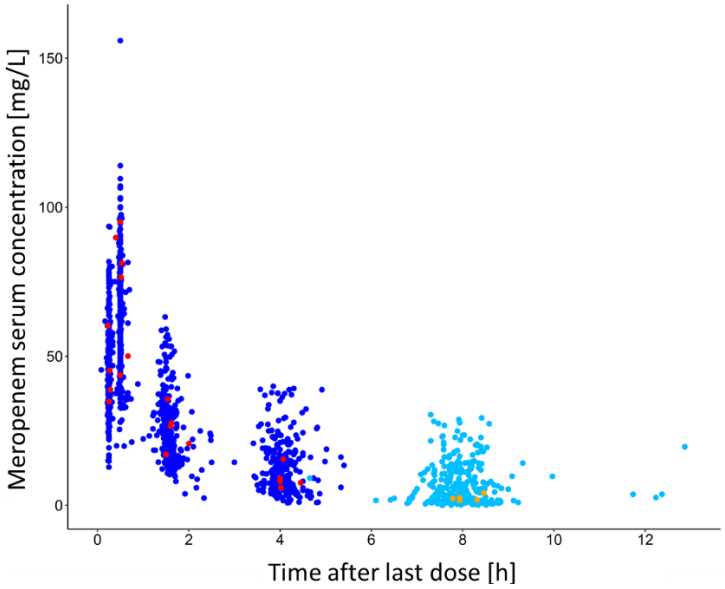

Figure 3.13: Meropenem serum concentrations versus time after last meropenem dose (n=48 patients; modified from [233]).
Dark blue/red circles: Concentrations of patients treated with 1000 mg/2000 mg meropenem; *Light blue/orange circles*: C_{min} values of patients treated with 1000 mg/2000 mg meropenem at the end of the actual dosing interval.
***Abbreviations**: C_{min}*: Minimum concentration.

Apart from interindividual variability, large intraindividual variability was identified (Table 3.6). Particularly C_{min} (Appendix Figure S25) and calculated C_{8h} values showed large variability, with concentrations varying in median 2-fold, up to more than 10-fold within a patient (range of ratio $\frac{C_{min\_max}}{C_{min\_min}}$: 1.3-10.9, range of ratio $\frac{C_{8h\_max}}{C_{8h\_min}}$: 1.22-11.4). Intraindividual variability in C_{4h} values was slightly lower but the C_{4h} values within a patient still varied up to more than 5-fold (range of ratio $\frac{C_{4h\_max}}{C_{4h\_min}}$: 1.10-5.47).

Table 3.6: Inter- and intraindividual variability of meropenem concentrations at specific time points (C_X) (modified from [233]).

Variability level	**C_X (N)**	**Median**	**$P_{0.025}$-$P_{0.975}$**
Inter-individual	*N=Number of C_X values*	*Meropenem concentration (C_X) [mg/L]*	
	C_{min} (320)	3.74	0.348-25.0
	C_{8h} (265)	3.41	0.133-24.1
	C_{4h} (265)	11.1	2.08- 39.3
Intra-individual	*N=Number of C_X ratios*	*Meropenem $\left(\frac{C_{X\_max}}{C_{X\_min}}\right)$ ratio in individual patient*	
	C_{min} (48)	2.00	1.35-7.87
	C_{8h} (48)	2.17	1.29-7.22
	C_{4h} (48)	1.60	1.17 -3.70

Abbreviations: *C_{min}*: Minimum concentrations (here: measured meropenem serum concentration at end of actual dosing interval); *C_X*: Concentration at specific time point X of concentration-time profile (here: calculated meropenem serum concentrations); $P_{0.025}$: 2.5th percentile; $P_{0.975}$: 97.5th percentile.

3.3.2 Pharmacokinetic/Pharmacodynamic analysis

3.3.2.1 Regression model: Impact of renal function on meropenem exposure

In addition to the large inter- and intrapatient variability in meropenem exposure, i.e. C_{4h} values (Figure 3.14 A, y-axis) and C_{8h} values (Figure 3.14 B, y-axis), large variability was also observed for renal function, with representatives in all renal function classes from severe renal impairment up to augmented renal function (Figure 3.14, x-axes). In addition to the 41 non-CRRT patients, 7 CRRT patients were investigated. Whereas within the monitored study period for half of the patients (n=24), renal function was stable (i.e. constant renal function class), renal function of the other half changed between two ($n_{patients}$=21) or even three ($n_{patients}$=3) classes of renal function.

Already at the patient level, a strong dependency between median individual $CLCR_{CG}$ and C_{4h} (Figure 3.14 A1) and C_{8h} (Figure 3.14 B1) of the patients was found, interestingly also for the CRRT patients (Figure 3.14 A2, B2). Also of note, in patients undergoing ECMO, meropenem concentrations were comparable to the meropenem concentrations in non-ECMO patients with similar median individual $CLCR_{CG}$ values (bold x-axis tick mark label Figure 3.14 A, B). Moreover, within most of the individuals with changing renal function, the same tendency of higher meropenem concentrations for decreased renal function was observed: E.g. patient 34 revealed worsening of renal function and at the same time increasing meropenem exposure across the four study days (grey tick mark label Figure 3.14 A1, B1).

At the sample level, i.e. when relating all single $CLCR_{CG}$ values as a continuous variable to meropenem exposure (C_{8h}), a distinct relation was found, which was described by the hyperbolic function $C_{8h} = 40363 \cdot \frac{1}{(CLCR_{CG})^{2.27}}$ (Figure 3.14 C) and quantified using a regression model in logarithmic scale (Figure 3.14 C; Appendix Figure S26). In this model, four C_{8h} values of one patient (ID 36) were excluded from the regression since being considerably larger than those of the remaining patients with similar renal function; when including the four values of this patient, the predicted C_{8h} values in the investigated $CLCR_{CG}$ range changed only negligibly for all metrics: Quantified $CLCR_{CG}$-meropenem exposure relationship, 95% confidence interval, 95% prediction interval (Appendix Figure S27).

3.3.2.2 PK/PD target attainment analysis: Evaluation of standard meropenem dosing

For infections in non-CRRT patients with pathogens of MIC=2 mg/L, both investigated targets were attained in approximately half of the dosing intervals monitored, with slightly higher attainment for the $50\%T_{>4xMIC}$ (56%) than the $100\%T_{>MIC}$ target (48%; Table 3.7). Given a MIC of 8 mg/L, the target $100\%T_{>MIC}$ was attained only in about one fifth of the monitored meropenem dosing intervals; attainment of the target $50\%T_{>4xMIC}$ was very low (7%; Table 3.7). Target attainment for the full MIC range (0.25-8 mg/L) is summarised in the Appendix Table S16.

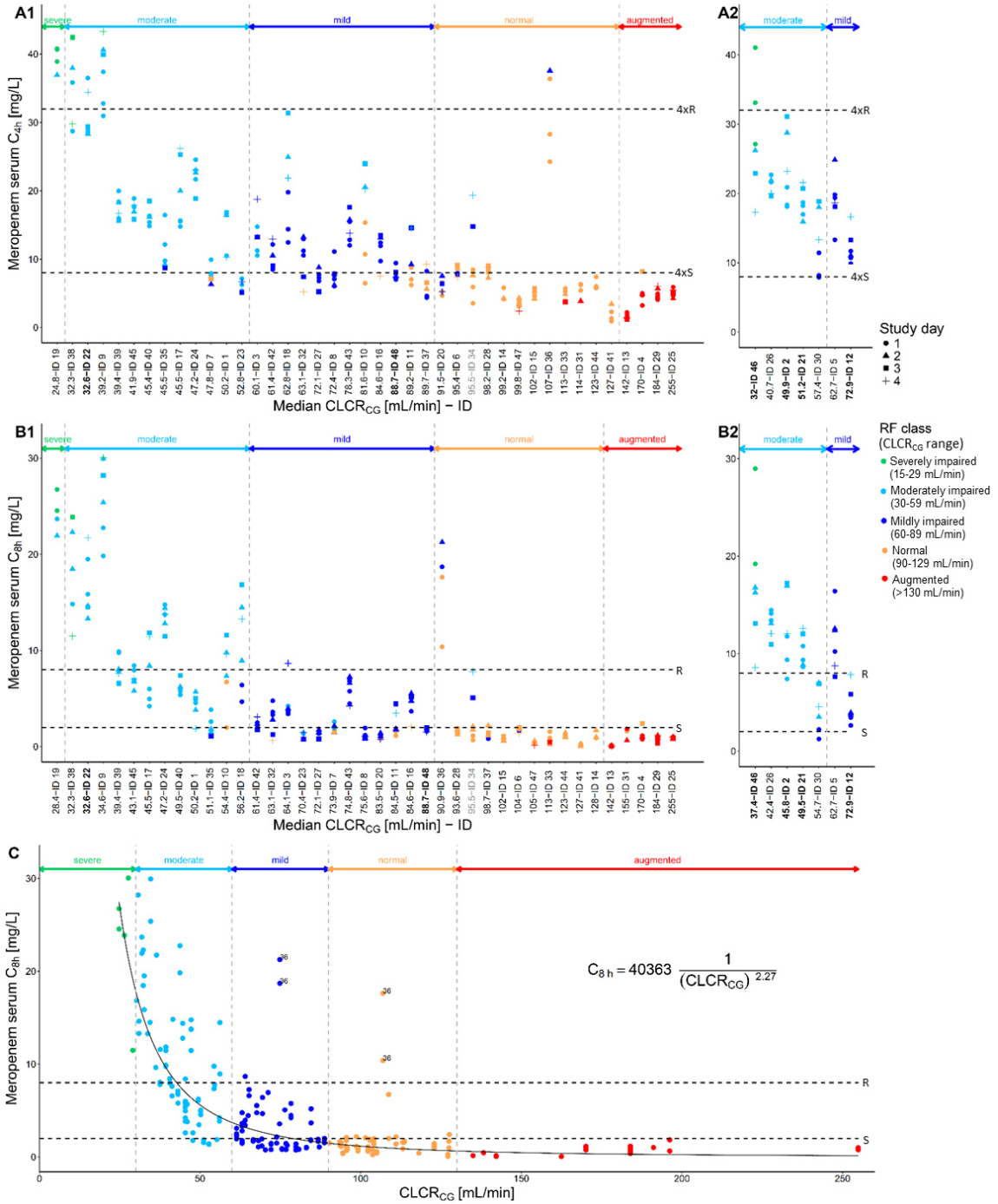

Figure 3.14: Relationship between meropenem serum concentration and creatinine clearance (modified from [233]).

Meropenem serum concentrations at 4 h, C_{4h} (A1, A2), and at 8 h, C_{8h} (B1, B2, C) after start of infusion in non-CRRT (A1, B1, C) and CRRT (A2, B2) patients vs. median individual $CLCR_{CG}$ ('patient level': A, B) or vs. all single $CLCR_{CG}$ ('sample level': C) of the patients.

Tick mark of x-axis (A, B)*:* Median individual $CLCR_{CG}$ at time of determined meropenem C_{4h} or C_{8h} value; *Bold tick mark labels* (A, B): ECMO patients; *Grey tick mark labels* (A1, B1): Patient example mentioned in the text of section 3.3.2.1; *Colour of symbols* (A-C): Renal function class of a patient at time of determined meropenem C_{4h} or C_{8h} value; *Shape of symbol* (A, B): Study day on which meropenem C_{4h} or C_{8h} value was determined; *Dashed vertical lines/horizontal arrows* (A-C): Separation of renal function classes; *Dashed horizontal lines* (A-C): EUCAST MIC breakpoints for Enterobacteriaceae, *Pseudomonas* spp. or *Acinetobacter* spp. (S breakpoint: 2 mg/L, R breakpoint: 8 mg/L [5]); *Data points labelled with 36* (C): Four meropenem C_{8h} values of patient 36; *Black curve* (C)*:* Quantified hyperbolic relationship between $CLCR_{CG}$ and meropenem C_{8h} values, excluding data of patient 36.

Abbreviations: *$CLCR_{CG}$*: Creatinine clearance estimated according to Cockcroft and Gault [2]; *CRRT*: Continuous renal replacement therapy; *C_{4h}*: Concentration at 4 h after start of infusion; *C_{8h}*: Concentration at 8 h after start of infusion; *ECMO*: Extracorporeal membrane oxygenation; *EUCAST*: European Committee on Antimicrobial Susceptibility Testing; *ID*: Patient identifier; *MIC*: Minimum inhibitory concentration; *RF*: Renal function; *R*: R breakpoint; *S*: S breakpoint.

Stratification of target attainment by the renal function classes in non-CRRT patients, identified augmented renal function to mild renal impairment ($CLCR_{CG}$ >130-60 mL/min) as a risk factor for non-attainment of both targets (target attainment: 0-46.2% for $100\%T_{>MIC}$, 0-59.7% for $50\%T_{>4xMIC}$; Table 3.7) for infections with pathogens of MIC=2 mg/L. Given a MIC of 8 mg/L, meropenem treatment reliable target attainment was only achieved in presence of severe renal impairment ($CLCR_{CG}$: 15-29 mL/min); thus, already moderate renal impairment ($CLCR_{CG}$: 30-59 mL/min) was identified as a risk factor for target non-attainment (target attainment for moderate renal impairment: 51.4% for $100\%T_{>MIC}$, 12.5% for $50\%T_{>4xMIC}$; Table 3.7).

Table 3.7: Pharmacokinetic/pharmacodynamic (PK/PD) target attainment for all non-CRRT patients and stratified by renal function class (modified from [233]).

Target	**Renal function class**	**$N_{Patients}$[1]**	**$N_{C_x\ samples}$**	**PK/PD target attainment for**	
				MIC=2 mg/L	**MIC=8 mg/L**
$50\%T_{>4xMIC}$			*$C_X=C_{4h}$*	*C_{4h} ≥ 4x2 mg/L, % ($N_{C_{4h}\ samples}$)*	*C_{4h} ≥ 4x8 mg/L, % ($N_{C_{4h}\ samples}$)*
	All	41	223	56.1 (125)	7.17 (16)
	Severely impaired	1	5	100 (5)	100 (5)
	Moderately impaired	12	72	93.1 (67)	12.5 (9)
	Mildly impaired	11	62	59.7 (37)	1.61 (1)
	Normal	13	60	26.7 (16)	1.67 (1)
	Augmented	4	24	0 (0)	0 (0)
$100\%T_{>MIC}$			*$C_X=C_{8h}$*	*C_{8h} ≥ 2 mg/L, % ($N_{C_{8h}\ samples}$)*	*C_{8h} ≥ 8 mg/L, % ($N_{C_{8h}\ samples}$)*
	All	41	223	48.4 (108)	20.6 (46)
	Severely impaired	1	4	100 (4)	100 (4)
	Moderately impaired	12	72	91.7 (66)	51.4 (37)
	Mildly impaired	12	65	46.2 (30)	4.62 (3)
	Normal	11	57	14 (8)	3.51 (2)
	Augmented	5	25	0 (0)	0 (0)

[1]Patients were assigned to a renal function class based on their median individual $CLCR_{CG}$ at the time of C_{4h} or C_{8h} determination.

Abbreviations: *$CLCR_{CG}$*: Creatinine clearance estimated according to Cockcroft and Gault [2]; *CRRT*: Continuous renal replacement therapy; *C_X*: Concentration at specific time point X of concentration-time profile (here: calculated meropenem serum concentrations); *PK/PD*: Pharmacokinetic/pharmacodynamic; *RF*: Renal function; *$T_{>MIC}$:* Time period that total drug concentration exceeds the MIC; *$T_{>4xMIC}$:* Time period that total drug concentration exceeds four times the MIC .

3.3.3 Risk assessment tool

Based on the quantified relationship between $CLCR_{CG}$ and meropenem exposure (Section 3.3.2.1), the tool 'MeroRisk Calculator' (short: MR_C) was developed. The MeroRisk Calculator is an easy-to-use, 3-step Excel® spreadsheet (graphical user interface) which can be utilised to assess the risk of target non-attainment of the PK/PD index $100\%T_{>MIC}$ for non-CRRT patients after standard meropenem dosing (Figure 3.15 A). In 'Step 1', the user provides either the $CLCR_{CG}$ of a patient or its determinants (sex, age, total body weight, serum creatinine concentration), which will then be used to calculate $CLCR_{CG}$. In 'Step 2', the user provides the MIC value of a determined or suspected infecting pathogen, which is used as the target meropenem concentration. In cases in which the MIC value is not available, no MIC value needs to be provided (for handling of blank MIC entry see next step). In 'Step 3', the MeroRisk Calculator computes the probability ('risk') of target non-attainment for the given $CLCR_{CG}$ and MIC value; if the MIC entry was left blank, the user has now the option to select a EUCAST MIC breakpoint for relevant bacteria [5]. The calculated risk (rounded to integer) of target non-attainment is displayed with the following 3-colour coding system: green (≤10%), orange (>10%-<50%), red (≥50%) (Figure 3.15 B). In addition, the tool provides a graphical illustration of the quantified $CLCR_{CG}$ - C_{8h} relationship including the 95% prediction interval. Moreover, the tool predicts, based on the provided/calculated $CLCR_{CG}$, the most likely concentration to which meropenem concentrations after multiple dosing will decline before the next dosing (C_{8h}), which is graphically highlighted in the $CLCR_{CG}$ - C_{8h} relationship (Figure 3.15 B).

The developed risk assessment tool MeroRisk Calculator (beta version) is publicly available as additional file in the article Ehmann et al. Critical Care (2017) [233]. The tool is compatible with Windows operating systems and Excel® version 2010 and onwards. When opening the tool, the user might be asked to enable macros, enable content, and add to trusted documents.

3.4 Project IV: Development of a dosing algorithm to identify effective meropenem dosing for critically ill patients

3.4.1 Exploratory data analysis

For the results of the exploratory data analysis of patient-specific characteristics and meropenem dosing, sampling and concentrations refer to section 3.3.1. Further detailed information on patient-specific characteristics are summarised in Appendix Table S17.

With respect to suggestions for a potential NLME PK model, the biphasic meropenem concentration-time profile on a semilogarithmic scale, indicated a two-CMT characteristic disposition (Appendix Figure S28).

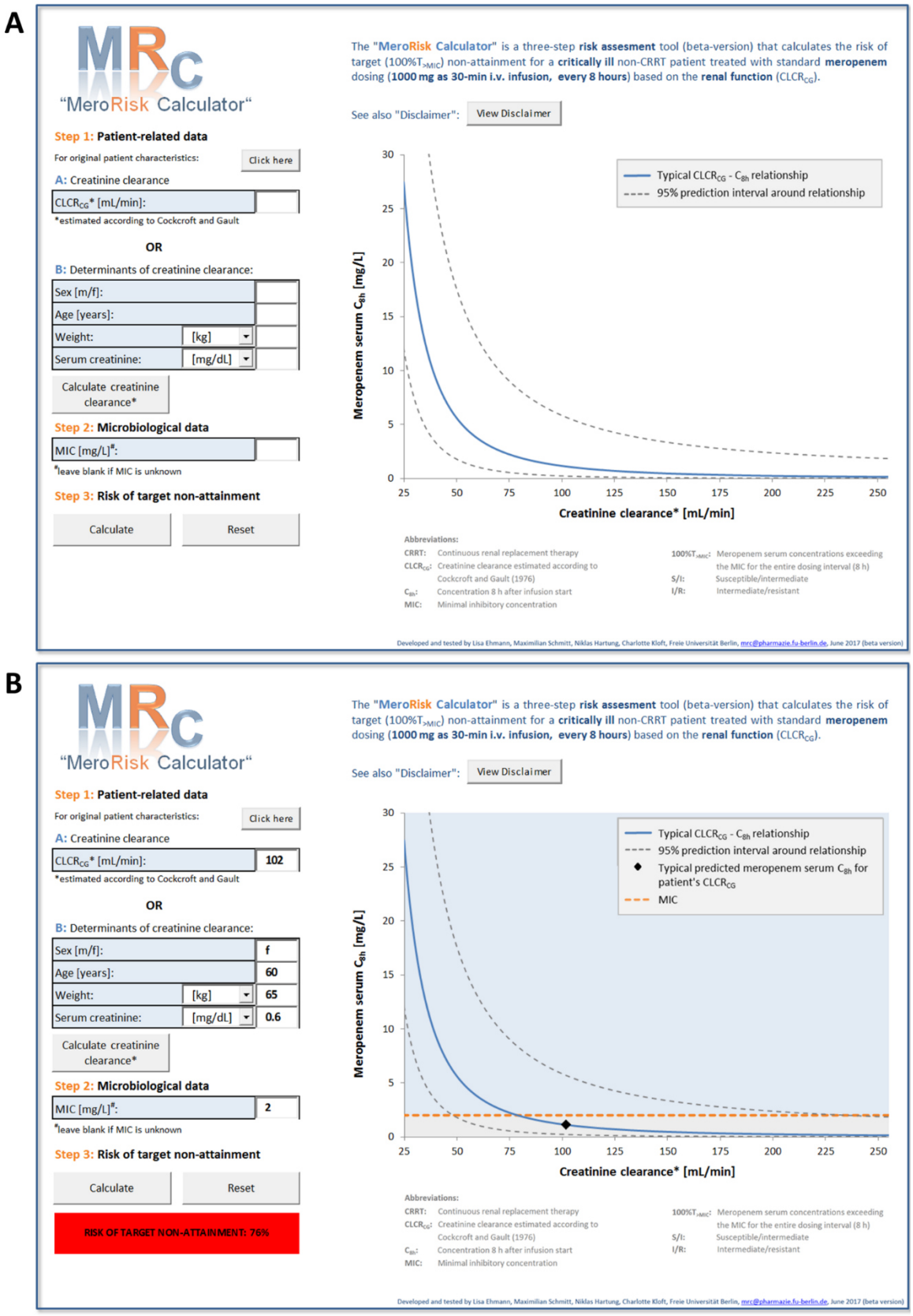

Figure 3.15: Graphical user interface of the MeroRisk Calculator (modified from [233]).
A: Display when opening the tool, i.e. without any entries; **B:** Display after risk calculation for exemplary patient: female, 60 years, 65 kg body weight, 0.6 mg/dL serum creatinine, infected with pathogen of MIC=2 mg/L.
Abbreviations: *$CLCR_{CG}$*: Creatinine clearance estimated according to Cockcroft and Gault [2]; *CRRT*: Continuous renal replacement therapy; *C_{8h}*: Concentration 8 h after start of infusion; *MIC*: Minimum inhibitory concentration.

3.4.2 Nonlinear mixed-effects pharmacokinetic model

In the following, the results of the PK model development are presented, with a focus on covariate analysis (Section 3.4.2.1), the final NLME PK model (Section 3.4.2.3) and the evaluation (Section 3.4.2.4).

3.4.2.1 Base model development

Pursuant to the results of the exploratory data analysis a two-compartment PK disposition model with first-order elimination, parameterised in terms of CL, V_1, V_2 and Q was selected as structural submodel over a one- and three-compartment model, considering the misspecification in the goodness-of-fit plots (Appendix Figure S29) and the imprecisely estimated volume of distribution parameter of the third compartment (RSE=66.1%) for the one- and three-compartment models, respectively. In the stepwise inclusion procedure, IIV was implemented on CL, followed by V_1 and V_2. IIV on Q showed poor precision (RSE=173%) and high η-shrinkage (75%) and was hence not included in the model. The fan-shape pattern of the residuals over population predictions (Appendix Figure S29) clearly indicated the need of a proportional or combined RUV model, which was supported by the considerably higher OFV value when implementing the additive RUV model (ΔOFV≥918). The combined RUV model was selected over the proportional model, as the additive part (i) was found to be important for the low concentrations, (ii) was estimated with adequate precision (RSE=34%), and (iii) led to an improved model performance (ΔOFV=-87.8 compared to proportional RUV). The investigation of IOV demonstrated superiority of approach (ii), i.e. defining as occasion each intensively monitored dosing interval (Section 2.9.3.1, Appendix Table S18). IOV was identifiable on CL and V_1, however, was at this stage not yet included in the model, considering also the high computational demand for the subsequent forward inclusion (e.g. execution of 147 models for forward selection step 1 only).

3.4.2.2 Covariate model development

The pre-analysis of the two imputation/interpolation strategies using $CLCR_{CG}$ on CL as case covariate, revealed clear superiority of the linear interpolation strategy (i.e. strategy B), both in terms of OFV (ΔOFV compared to the base model: strategy A=-234, strategy B=-401) but also reduction of the unexplained IIV compared to base model (IIV_{Var} CL: strategy A=-65%, strategy B=-75%; Appendix Table S19 Subtable A). Hence, the linear interpolation strategy was utilised for time-varying covariates in the subsequent covariate model development, which is illustrated in Figure 3.16.

In **step 1**, the re-estimation of the base model parameters for the non-CRRT patients, revealed similar parameter estimates as for all patients, with slightly higher meropenem clearance (~6%; Appendix Table S19 Subtable B). In **step 2**, of the 58 patient-specific characteristics (Appendix

Table S2), 27 covariate candidates were selected for further analysis (Figure 3.16). Of these, in the forward selection step (**step 3**), 17 covariate-parameter relationships were selected on CL, V_1 and V_2 (Figure 3.16; information on respective covariate-relationships: Appendix Table S17). In the model refinement step (**step 4**), alternatively investigated covariates and covariate classifications did not improve the model; hence, a corresponding adjustment of the full covariate model was not made. Additional IOV was implemented on the CL and V_1 parameters using exponential models and defining each intensively sampled dosing interval as occasion (Section 2.9.3.1), leading to the refined full covariate model. In the first part of the backward deletion step (**step 5**), 9 covariates (Figure 3.16) did not reduce the unexplained population parameter variability by more than 5% and were hence excluded. In the second part of the backward deletion 5 more covariates were excluded successively (in the following order: pH, C-reactive protein, bilirubin, sex, age), based on the exclusion criteria precision and statistical significance (Figure 3.16). The last removed covariate 'age', which showed a negative linear relationship with V_1 (per 10 years increase in age: 8% decrease in V_1), was borderline in terms of precision (RSE=51.9%) and statistical significance (ΔOFV=5.73). The resulting final covariate model included the three covariates $CLCR_{CG}$ on CL (linear model), body weight on V_1 (power model), serum albumin concentration on V_2 (power model) and was undertaken an additional refinement step (**step 6**, Figure 3.16): First, the automatic centring of the covariate relationship, which was implemented by *scm* was updated to the median of the respective covariate values of the non-CRRT patients on the first study day (i.e. $CLCR_{CG}$: 80.8 mL/min, body weight: 70 kg, serum albumin concentration: 2.8 g/dL). Second, the reassessment of the interpolation of the continuous covariates, again confirmed the superiority of the linear interpolation strategy (stepwise compared to linear: ΔOFV=123, up to 67.1% more unexplained variability). An additional linear interpolation between the observations of covariates also within the NONMEM® script, did not further improve the model and was hence not included. Third, a linear covariate model was selected to describe the relationship between serum albumin concentration and V_2, given the highly comparable results for the power model and linear model (ΔOFV=0.498, 1.86% difference in IIV_{Var} on V_2). For $CLCR_{CG}$ a piecewise linear relationship was selected over the linear relationship (Figure S30) as it was found to significantly improve the model prediction (ΔOFV=-10.7, df=1) and reduced the unexplained variability further (e.g. IIV_{Var} on CL: 8% relative deviation between linear and piecewise linear relationship). Fourth, the implementation of the 'extended Wählby model 1', which separated within and between-individual covariate effects, did not significantly improve the model (ΔOFV=-1.47, df=1) and was hence not included. Fifth, the reassessment of the statistical submodel confirmed the need of a combined RUV model (ΔOFV=35.9 for sole proportional model) and resulted in an exclusion of the IOV on V_2, considering the precision of the IOV estimate (RSE_{Var}>50%) and the - with respect to allometric principles [204] - less plausible exponent in the power covariate model (model with IOV: 0.78, model without IOV: 0.95). The final subgroup analysis (**step 7**), demonstrated similar PK model

parameter estimates for CRRT and non-CRRT patients: For instance, meropenem clearance values were highly similar (9.82 and 9.25 L/h, respectively), indicating a similar magnitude of meropenem excretion via the CRRT process as for the typical non-CRRT patient via the kidney.

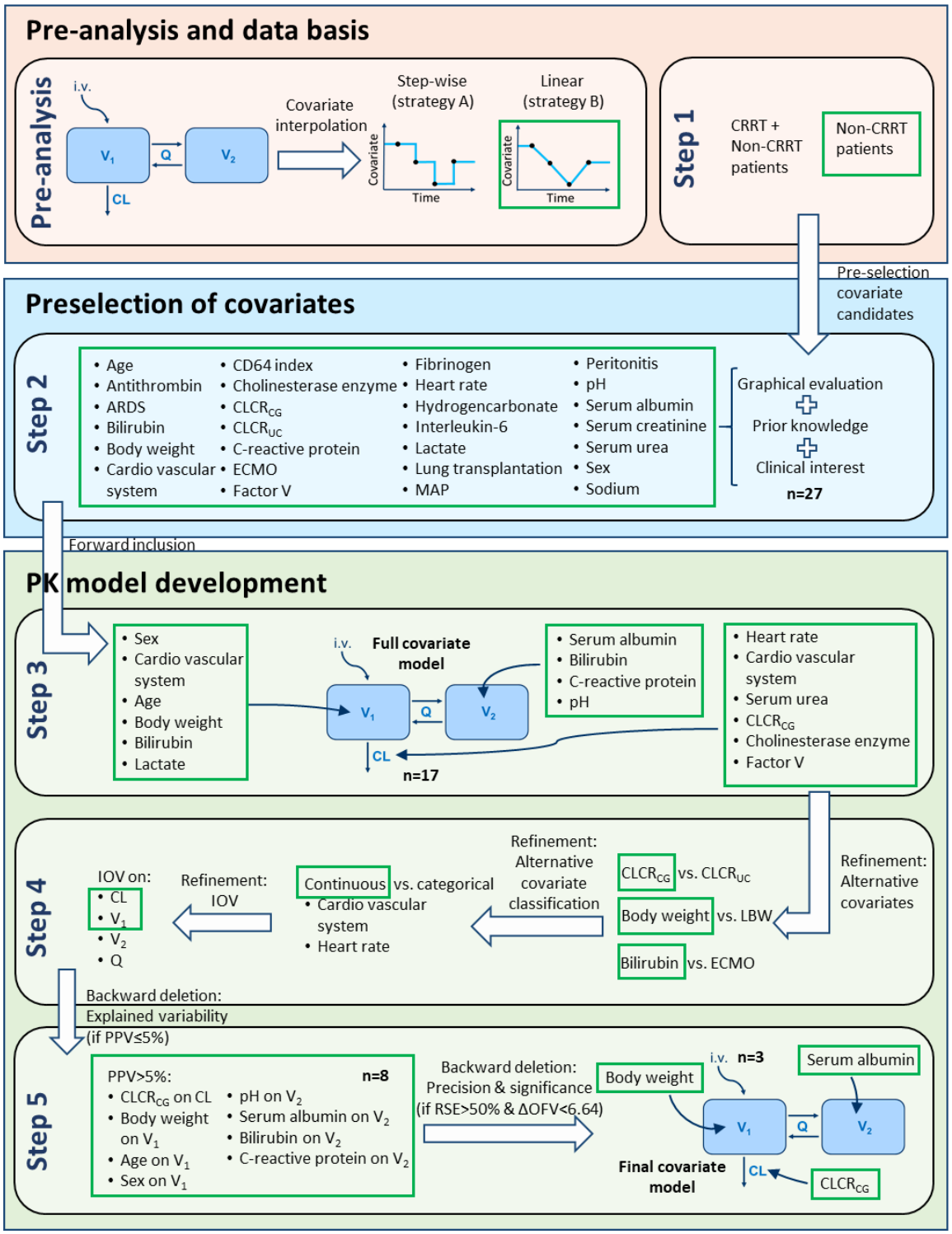

Figure 3.16: Results of covariate model development: preanalysis and steps 1-5 (based on covariate model development strategy, section 2.9.3.2) [continued on next page].

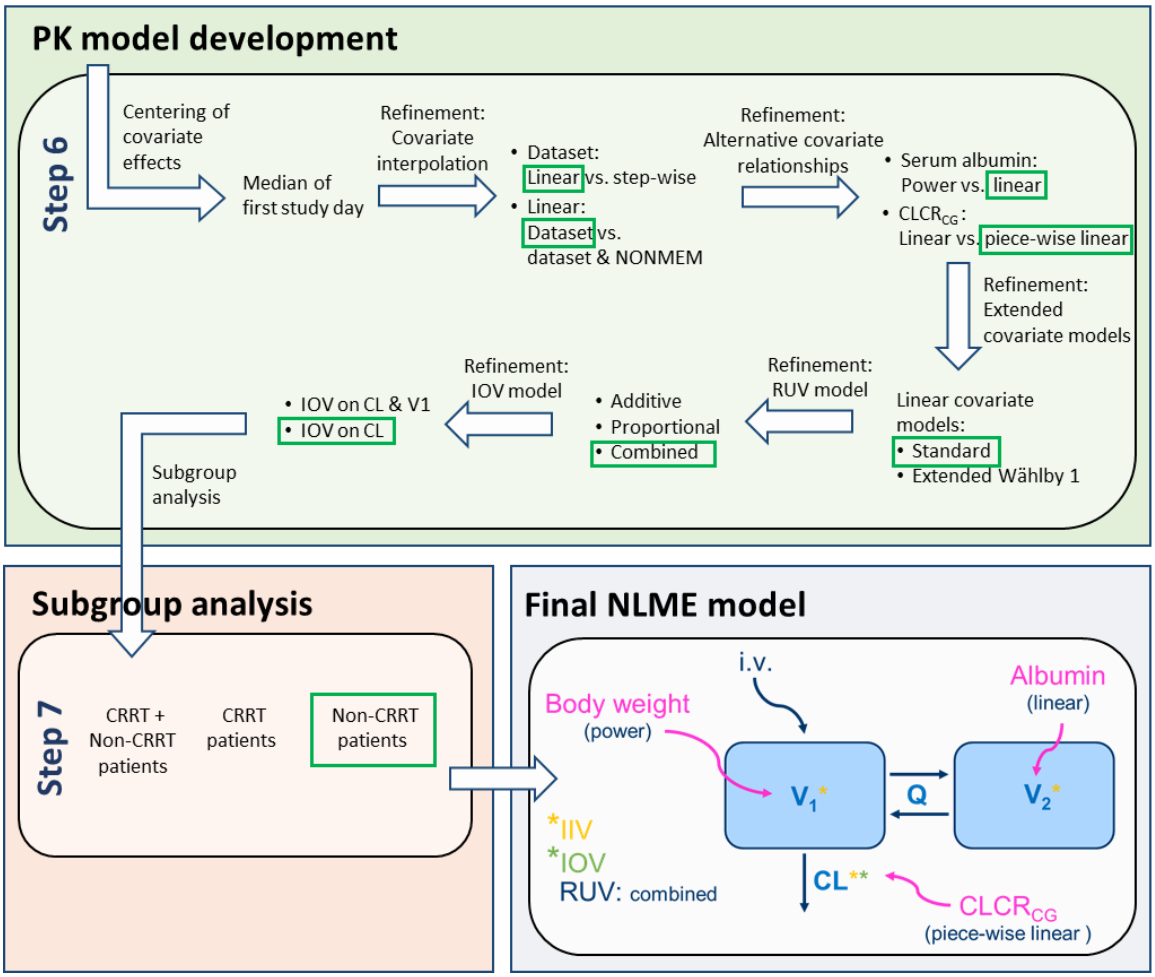

Figure 3.16 [continued]: Results of covariate model development: steps 6-7 and final NLME PK model. ***Abbreviations:*** *CL*: Clearance; *CLCR$_{CG}$*: Creatinine clearance estimated according to Cockcroft and Gault [2]; *CLCR$_{UC}$*: Creatinine clearance measured using urine collection; *CMT*: Compartment; *CRRT*: Continuous renal replacement therapy; *ECMO*: Extracorporeal membrane oxygenation; *IIV*: Interindividual variability; *IOV*: Interoccasion variability; *i.v.*: Intravenous; *LBW*: Lean body weight; *MAP*: Mean arterial pressure; *n*: Number; *NLME*: Nonlinear mixed-effects; *PPV*: Population parameter variability; *Q*: Intercompartmental clearance; *RSE*: Relative standard error; *RUV*: Residual unexplained variability; *V$_1$, V$_2$*: Volume of distribution parameters of central and peripheral CMT.

Interestingly. also the parameter describing the relationship between CLCR$_{CG}$ and meropenem CL (i.e. CLCR$_{CG}$_CL) was similar between CRRT and non-CRRT patients (per 1 mL/min change in CLCR: CL change of 1.29% and 0.977%, respectively; Appendix Table S20), supporting the results of Project III (Section 3.3.2.1). Given the limited number of CCRT patients, overall not all parameters could be reliably estimated and hence the CRRT patients were not included in the final developed NLME PK model.

3.4.2.3 Final nonlinear mixed-effects PK model

The final NLME PK model for meropenem in the critically ill population was a two-compartment PK disposition model (typical CL and V: 9.25 L/h and 24 L, respectively) which included interindividual variability on CL, V_1 and V_2, interoccasion variability on CL, a combined residual variability model and three covariates: total body weight on V_1, serum albumin concentration on

V_2 and $CLCR_{CG}$ on CL. The NONMEM® model script of the final NLME PK model is provided in Appendix 7.4.3, a model sketch can be found in the bottom part of Figure 3.16, and the respective PK parameters are summarised in Table 3.8.

Table 3.8: Parameter estimates including bootstrap results of the final NLME PK model of meropenem in critically ill patients (modified from [243]).

Parameter [unit]	Final model		Bootstrap[3]	
	Estimate (RSE[1], %)	95% CI[2]	Median	95% CI
Fixed-effects parameters				
θ CL[4] [L/h]	9.25 (4.60)	[8.42, 10.1]	9.28	[8.38, 10.1]
θ V_1[5] [L]	7.89 (11.9)	[6.05, 9.73]	7.92	[6.11, 11.5]
θ Q [L/h]	28.4 (16.1)	[19.4, 37.4]	28.4	[11.1, 38.2]
θ V_2[6] [L]	16.1 (7.40)	[13.8, 18.4]	16.1	[11.9, 18.4]
θ $CLCR_{CG}$_CL[7], %	0.977 (9.20)	[0.800, 1.15]	0.987	[0.800, 1.15]
θ $CLCR_{CG}$_INF [mL/min]	154 (6.90)	[133, 175]	155	[111, 178]
θ WT_V_1[8]	0.945 (16.6)	[0.637, 1.25]	0.936	[0.531, 1.32]
θ ALB_V_2[9], %	-20.2 (36.6)	[-34.7, -5.72]	-20.3	[-40.3, -5.21]
Interindividual variability parameters, %CV				
ω CL	27.1 (19.3)	[13.2, 36.5]	26.3	[17.1, 36.7]
ω V_1	31.5 (14.3)	[20.6, 39.8]	30.5	[20.0, 40.2]
ω V_2	16.9 (18.1)	[9.02, 22.2]	16.3	[8.07, 23.2]
Interoccasion variability parameters[10], %CV				
Κ CL	12.5 (12.0)	[9.11, 15.2]	12.4	[9.61, 15.5]
Residual variability parameters				
σ_{prop}, %CV	16.6 (6.60)	[14.5, 18.7]	16.5	[14.5, 18.9]
σ_{add}, SD [mg/L]	0.246 (29.0)	[0.106, 0.386]	0.234	[0.0932, 0.337]

[1]RSE of random-effects parameter estimates ω and σ are reported on approximate standard deviation scale; [2]Limits of 95% confidence intervals are computed as: parameter estimate ± 1.96·SE; [3]Non-parametric bootstrap (n=1000): convergence rate of 89.7%; [4]CL given for median $CLCR_{CG}$ of non-CRRT patients on first study day (80.8 mL/min); [5]V_1 given for median WT of non-CRRT patients (70 kg); [6]V_2 given for median ALB of non-CRRT patients at first study day (2.8 g/dL); [7]Change of clearance per mL/min deviation of $CLCR_{CG}$ from 80.8 mL/min (linear $CLCR_{CG}$-CL relationship); [8]Estimated exponent in power WT-V_1 relationship, centred to median in overall population (70 kg); [9]Change of V_2 per g/dL deviation of ALB from 2.79 g/dL (linear ALB-V_2 relationship); [10]Occasion was defined as intensively monitored dosing interval.
Abbreviations: *ALB*: Serum albumin concentration; *ALB_V2*: ALB effect on V_2; *CI*: Confidence interval; *CL*: Clearance; *$CLCR_{CG}$*: Creatinine clearance estimated according to Cockcroft and Gault [2]; *$CLCR_{CG}$_CL*: $CLCR_{CG}$ effect on CL; *$CLCR_{CG}$_INF*: $CLCR_{CG}$ value serving as inflection point for meropenem CL in $CLCR_{CG}$-CL relationship; CMT: Compartment; *CRRT*: Continuous renal replacement therapy, *CV*: Coefficient of variation (calculated for random-effects parameters according to Eq. 2.6); *IIV*: Interindividual variability; *IOV*: Interoccasion variability; *Q*: Intercompartmental clearance; *RSE*: Relative standard error; *SD*: Standard deviation; *V_1, V_2*: Volume of distribution parameters of central and peripheral CMTs; *WT*: Body weight; *WT_V_1:* WT effect on V_1; *θ:* Fixed-effects parameter; *ω*: Random-effects parameter: Interindividual variability; Κ: Random-effects parameter: Interoccasion variability; *σ*: Random-effects parameter: Residual unexplained variability.

Body weight was implemented on V_1 using a power model with an estimated exponent of ~1, i.e. doubling the body weight (e.g. 50 kg vs. 100 kg) approximately doubled V_1 of meropenem (e.g. 5.74 L vs. 11.1 L). Between serum albumin concentration and V_2, a negative linear relationship was implemented which indicated a 20%-change of V_2 per 1 g/dL deviation of the serum albumin concentration from the median serum albumin concentration (2.8 g/dL). A piecewise linear

relationship was implemented and quantified between $CLCR_{CG}$ and meropenem CL: Per 10 mL/min $CLCR_{CG}$ deviation from the median $CLCR_{CG}$ (80.8 mL/min), meropenem CL changed by ~10% and increased up to a maximum meropenem CL of 15.9 L/h at the precisely estimated $CLCR_{CG}$ inflection point (154 mL/min, RSE=7%; Table 3.8; graphical illustration: Appendix Figure S30 A). The impact of these covariates on the PK parameters is graphically illustrated as forest plot in Appendix Figure S31: Considering the covariate ranges covered in the critically ill study population the impact of extreme $CLCR_{CG}$ values and high body weight was particularly pronounced (e.g. min. $CLCR_{CG}$ (24.8 mL/min): ~0.45 · reference CL; max. WT (140 kg): ~1.93 · reference V_1). The inclusion of the three covariates considerably reduced the unexplained variability on the PK parameters: $CLCR_{CG}$ reduced PPV_{Var} on CL by ~70%, body weight reduced IIV_{Var} on V_1 by ~40%, and serum albumin concentration IIV_{Var} on V_2 by ~30% (Figure 3.17). In the final model, the unexplained variability was ≤31.5%CV, with the variability within a patient (i.e. IOV) being considerably lower than between the patients (i.e. IIV; e.g. on CL: IOV=12.5 %CV vs. IIV=27.1 %CV).

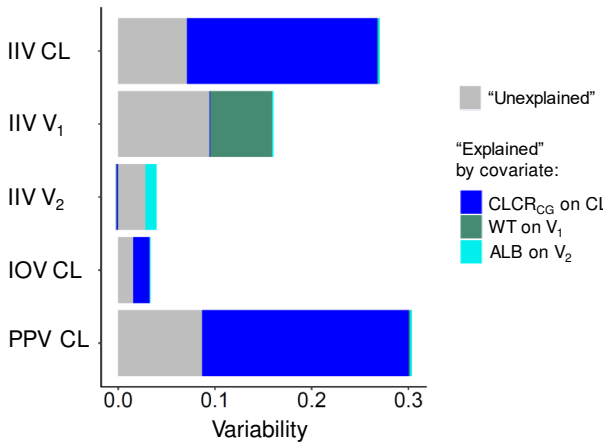

Figure 3.17: Reduction of unexplained variability by covariates in the final NLME model for meropenem.
Absolute variability on variance scale shown. Reduction of unexplained variability was derived by univariate exclusion of covariates from final model, re-estimation of parameters and evaluation of the relative increase in respective variability parameters on variance scale, which was considered "explained variability".
Abbreviations: *ALB*: Serum albumin concentration; *CL*: Clearance; *$CLCR_{CG}$*: Creatinine clearance according to Cockcroft and Gault; *IIV*: Interindividual variability; *IOV*: Interoccasion variability; *PPV*: Population parameter variability (computed as sum of variances of IIV and IOV); *WT*: Total body weight.

3.4.2.4 Model evaluation

Standard goodness-of-fit plots indicated adequate model predictions (Figure 3.18 B-E). The VPC demonstrated good predictive performance both for the typical trend and the variability of the meropenem concentration-time profiles (Figure 3.18 A) as well as across the full $CLCR_{CG}$ range (Appendix Figure S32). A non-parametric bootstrap for the final model (Table 3.8) confirmed model robustness (indicated by convergence rate of ~90%), precision (indicated by the narrow 95% confidence intervals of the bootstrap parameter estimates) and accuracy of the parameter estimates (indicated by low relative bias: Median (min; max) for fixed-effects parameters=-0.358% (-0.945%; 0.928%); random-effects parameters=5.36% (0.658%; 6.25%)).

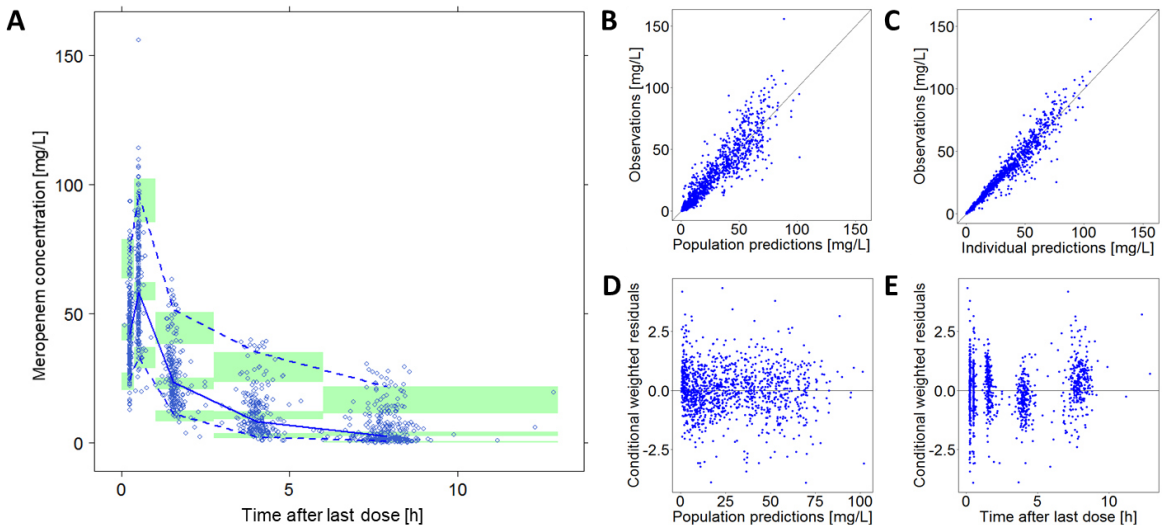

Figure 3.18: Visual predictive check (A, n=1000 simulations) and goodness-of-fit plots (B-E) for the final NLME PK model of meropenem in critically ill patients (modified from [243]).
A: *Circles:* Observed meropenem concentrations; *Lines:* 5th, 95th percentile (dashed), 50th percentile (solid) of the observed data; *Shaded areas:* 95% confidence interval around 5th, 50th and 95th percentile of simulated data.
B, C: *Circles:* Observed vs. population predicted (B) and individual predicted meropenem concentrations (C)*; Lines*: Line of unity.
D, E: *Circles:* Conditional weighted residuals vs. population predicted meropenem concentrations (D) and time after last dose (E); *Horizontal lines*: Reference lines at y=0.

As expected, during case deletion diagnostics, single patients with high $CLCR_{CG}$ values were found to be essential for the estimation of the inflection point of $CLCR_{CG}$ (Appendix Figure S33). Yet, their impact on the estimate of the inflection point was only moderate, with a change of the parameter by ≤17.9% from the original estimate of 154 mL/min.

3.4.3 Simulations: Evaluation and optimisation of meropenem exposure and dosing regimens

3.4.3.1 Evaluation of meropenem exposure

The impact of the three covariates identified in the final NLME PK model (Section 3.4.2.3) on the meropenem concentration-time profiles is illustrated in Figure 3.19 by means of deterministic exposure simulations. $CLCR_{CG}$, which was implemented as a covariate on the meropenem clearance parameter, mainly affected the terminal phase of the concentration-time profile and was hence a strong determinant of meropenem concentrations at the end of the dosing interval, both after first and multiple dosing (Figure 3.19: A.1, A.2). In contrast, body weight (implemented on V_1, Figure 3.19: B.1, B.2) and serum albumin concentration (implemented on V_2, Figure 3.19: C.1, C.2), only showed a minor impact on the terminal concentration-time profile, but as expected rather on maximum concentrations and concentrations in the early declining part of the meropenem concentration-time profile.

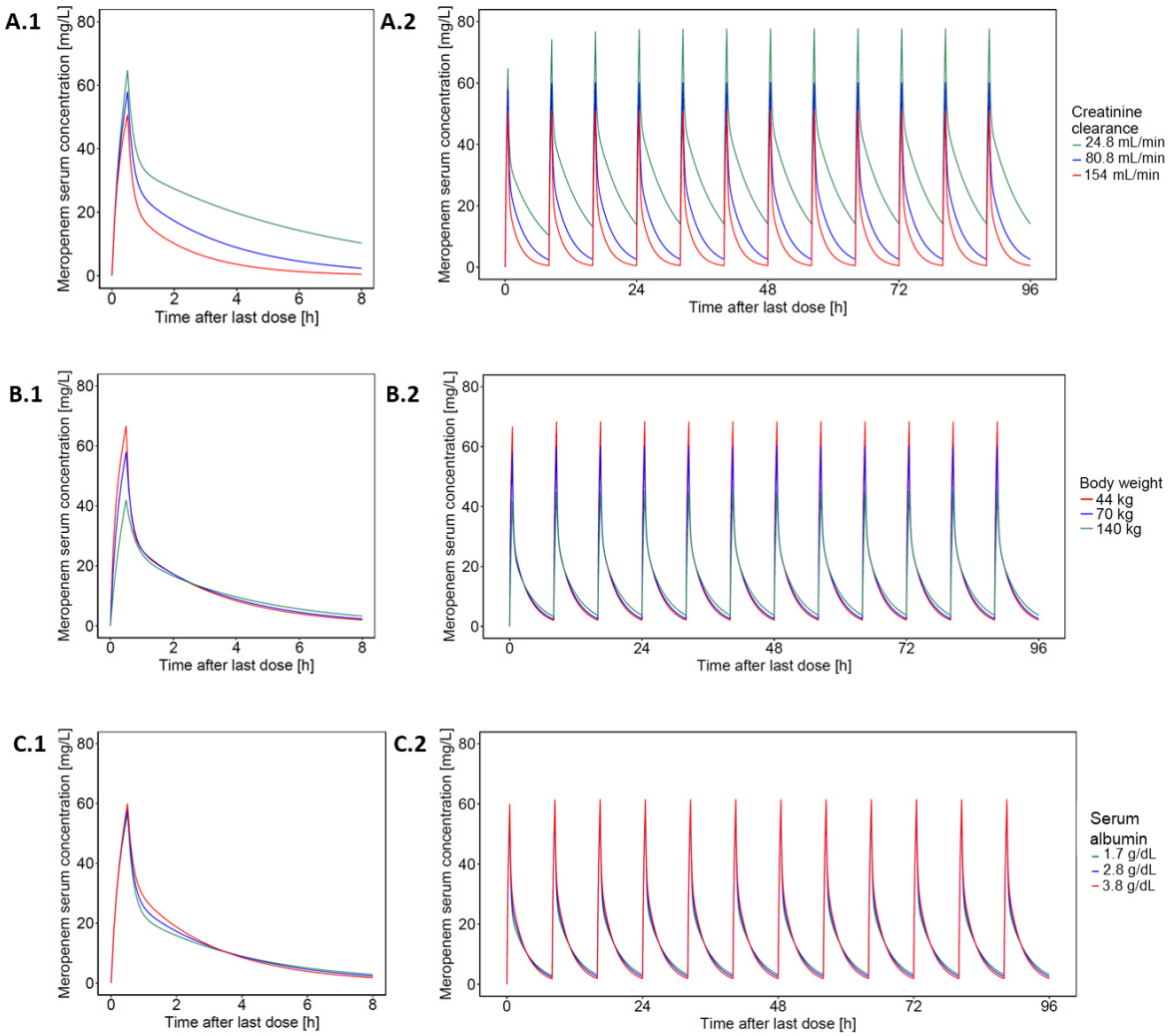

Figure 3.19: Impact of $CLCR_{CG}$ (A), body weight (B) and serum albumin concentrations (C) on the typical simulated meropenem concentration-time profiles (modified from [243]).
For each patient characteristic deterministic simulations were performed for varying covariate values (minimum and maximum value of study period and median value of first study day), resulting from standard meropenem dosing (1000 mg, 30- min i.v. infusion, q8h).
A: Varied $CLCR_{CG}$ (inflection point of $CLCR_{CG}$-CL relationship (=154 mL/min) is displayed instead of maximum $CLCR_{CG}$, given the constant meropenem CL for higher $CLCR_{CG}$ values), body weight and serum albumin set to median of first study day (i.e. 70 kg and 2.8 g/dL).
B: Varied body weight, $CLCR_{CG}$ and albumin set to median of first study day (i.e. 80.8 mL/min and 2.8 g/dL).
C: Varied albumin, $CLCR_{CG}$ and body weight set to median of first study day (i.e. 80.8 mL/min and 70 kg).
Left panel (A.1, B.1, C.1): First dosing interval; ***Right panel*** (A.2, B.2, C2): First 4 treatment days.
Abbreviations: *CL*: Clearance; *$CLCR_{CG}$*: Creatinine clearance estimated according to Cockcroft and Gault [2].

3.4.3.2 Evaluation and optimisation of meropenem dosing regimens

This section summarises the results of the PTA and CFR analyses performed for (i) standard meropenem dosing to identify impact factors and to evaluate the standard dosing, and (ii) alternative meropenem dosing regimens in order to identify optimised meropenem dosing regimens.

Evaluation of standard meropenem dosing

PTA analysis based on the standard meropenem dosing regimen $SI3_8$ ($n_{simulated\ patients}$: 52,500,000 =

105 covariate combinations · 500 patients · 1000 uncertainty simulations) indicated a decreasing PTA (i.e. increasing risk of target non-attainment) for patients with increasing $CLCR_{CG}$ (Figure 3.20 A.1, Table 3.9 Subtable A), decreasing body weight (Figure 3.20 B.1, Appendix Table S21) and increasing serum albumin concentration (Figure 3.20 C.1, Appendix Table S21). Of the three covariates, $CLCR_{CG}$ revealed by far the strongest impact on PTA, given the strong impact of $CLCR_{CG}$ on the meropenem concentrations in the terminal phase of the concentration-time profile (Figure 3.20 A). For a MIC value of 2 mg/L, for example, the PTA ranged from 6% to 100% (Δ ~94%) given the investigated range of $CLCR_{CG}$. For body weight and serum albumin concentration, however, the PTA covered a markedly smaller range (43%-77.8% and 39.8%-73.0%, i.e. Δ ~35% and Δ ~33%, respectively) and PTA values were mainly determined by the $CLCR_{CG}$ value (fixed to 80.8 mL/min; Appendix Table S21). The vast importance of creatinine clearance as a determinant of PTA was also illustrated by the PTA analyses for 'best', 'typical' and 'worst' case scenarios (Appendix Figure S35 A): The PTA values regarding creatinine clearance (i.e. low, medium and high creatinine clearance), were similar to PTA values investigating 'best', 'typical' and 'worst' case scenarios considering all three covariates (e.g. 'best' case: low creatinine clearance, high body weight, low serum albumin concentration; Figure B.4 A). Further evidence for creatinine clearance as main determinant of PTA was provided by the PTA analyses for a broad range of varying body weight (Appendix Figure S35 B) or serum albumin concentration (Appendix Figure S35 C) values given three creatinine clearance values (minimum, median and inflection point of $CLCR_{CG}$-CL relationship). To summarise, the analyses clearly identified creatinine clearance as main determinant of PTA and hence as key factor for the risk assessment of potential therapy failure.

Furthermore, as expected, PTA was dependent on the susceptibility of the pathogen, or more precisely, increased with decreasing susceptibility of the pathogen, i.e. increasing MIC (Figure 3.20 A.1, B.2, C.2). For instance, for a normal renal function ($CLCR_{CG}$: 90 mL/min), standard meropenem dosing reliably resulted in effective meropenem exposure (i.e. 5^{th} percentile of PTA≥90%) for MIC≤0.25 mg/L and declined to 29.2% and even to 0% for MIC=2 mg/L and 8 mg/L, respectively (Table 3.9 Subtable A). Overall, standard meropenem dosing reliably reached effective exposure in highly susceptible pathogens (i.e. MIC≤0.06 mg/L) for the full renal function range. However, already for the upper level of the isolates belonging to the S category (i.e. MIC=2 mg/L) only renal functions ≤40 mL/min reliably attained effective exposure; for the upper level of the isolates belonging to the I category (i.e. MIC=8 mg/L) none of the investigated renal functions did. Of note, when comparing the PTA results between treatment days 1 and 4, the differences were found to be marginal (Appendix Figure S34, Figure S36).

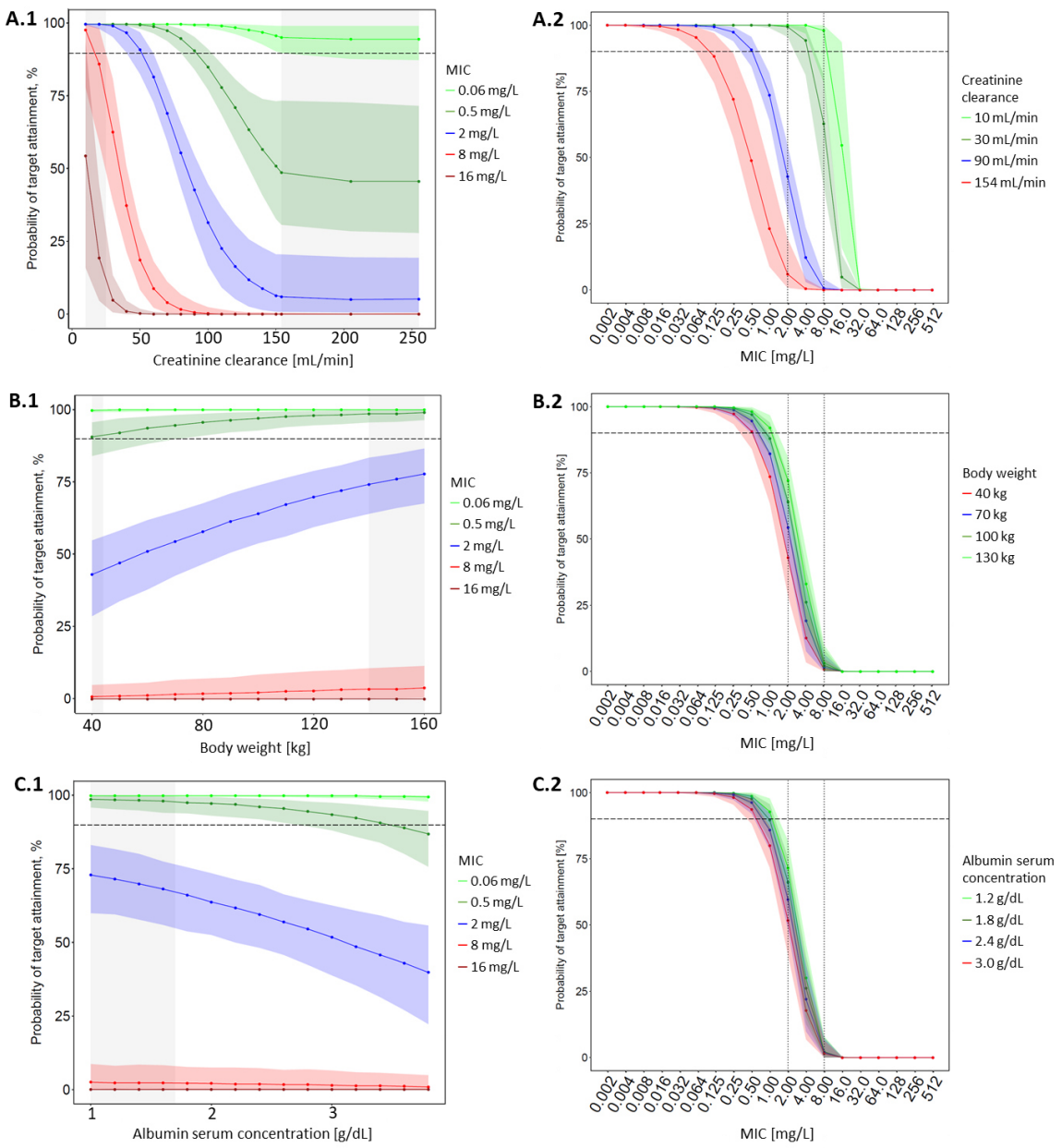

Figure 3.20: Probability of target (98%$T_{>MIC}$) attainment vs. covariates (A.1, B.1, C,1) and vs. MIC (A.2, B.2, C.2) on the first day of standard meropenem treatment (1000 mg, 30-min i.v. infusion, q8h) (modified from [243]).

A: Varied $CLCR_{CG}$, body weight and serum albumin concentration set to median of first study day (i.e. 70 kg, 2.8 g/dL); *B:* Varied body weight, $CLCR_{CG}$ and serum albumin concentration set to median of first study day (i.e. 80.8 mL/min, 2.8 g/dL); *C:* Varied serum albumin concentration, $CLCR_{CG}$ and body weight set to median of first study day (i.e. 80.8 mL/min, 70 kg). *Dashed horizontal line*: PTA of 90%; *Coloured circles and lines + shaded areas*: Median + 90% CI of the 1000 PTA values derived from the 1000 Monte Carlo simulations considering PK parameter uncertainty; Note: Dosing selection was based on 5th percentile (i.e. lower end of coloured shaded area) for dosing algorithm (Table 3.10); *Grey shaded areas:* Extrapolated covariate range not covered by the study population or $CLCR_{CG}$ ≥154 mL/min (=inflection point of $CLCR_{CG}$-CL relationship). ***Abbreviations***: *MIC*: Minimum inhibitory concentration; *CI*: Confidence interval; *$CLCR_{CG}$*: Creatinine clearance estimated according to Cockcroft and Gault [2]; *PTA*: Probability of target attainment; *$T_{>MIC}$:* Time period that total drug concentration exceeds the MIC.

Table 3.9: Probability of target attainment (PTA, **A**) and cumulative fraction of response (CFR, **B**) for the first day of standard meropenem treatment (1000 mg, 30-min i.v. infusion, q8h) evaluated for the PK/PD target 98%$T_{>MIC}$ (modified from [243]).

PTA and CFR are given for varied values of creatinine clearance as well as for selected MIC values and are presented as the median ($P_{0.5}$), 5th ($P_{0.05}$) and 95th percentile ($P_{0.95}$) of the 1000 PTA values derived from the 1000 Monte Carlo simulations considering PK parameter uncertainty.

Subtable A: Probability of target attainment

$CLCR_{CG}$[1] [mL/min]	**Probability of target attainment, %**																													
	MIC [mg/L]																													
	0.06			0.12			0.25			0.5			1			2			4			8			16			32		
	$P_{0.05}$	$P_{0.5}$	$P_{0.95}$	**$P_{0.05}$**	$P_{0.5}$	$P_{0.95}$	**$P_{0.05}$**	$P_{0.5}$	$P_{0.95}$	**$P_{0.05}$**	$P_{0.5}$	$P_{0.95}$	**$P_{0.05}$**	$P_{0.5}$	$P_{0.95}$	**$P_{0.05}$**	$P_{0.5}$	$P_{0.95}$	**$P_{0.05}$**	$P_{0.5}$	$P_{0.95}$	**$P_{0.05}$**	$P_{0.5}$	$P_{0.95}$	**$P_{0.05}$**	$P_{0.5}$	$P_{0.95}$	**$P_{0.05}$**	$P_{0.5}$	$P_{0.95}$
10	**100**	100	100	**100**	100	100	**100**	100	100	**100**	100	100	**100**	100	100	**99.6**	100	100	**96.8**	100	100	**78.2**	98	100	**16**	54.6	93.6	**0**	0	0.8
20	**100**	100	100	**100**	100	100	**100**	100	100	**100**	100	100	**99.6**	100	100	**98.4**	100	100	**90.6**	99	100	**59.2**	86.2	98.6	**4.6**	19.4	44.4	**0**	0	0
30	**100**	100	100	**100**	100	100	**100**	100	100	**99.8**	100	100	**99**	100	100	**95.6**	99.4	100	**81.2**	94.2	99.4	**39**	62.8	81.2	**0.6**	4.8	13.4	**0**	0	0
40	**100**	100	100	**100**	100	100	**99.8**	100	100	**99.4**	100	100	**97.6**	99.6	100	**90.2**	97	99.6	**68.8**	82.6	93.2	**21.6**	37.4	51	**0**	1	4.6	**0**	0	0
50	**100**	100	100	**99.8**	100	100	**99.6**	100	100	**98.4**	99.8	100	**94.6**	98.4	99.8	**82.8**	91.2	97.2	**52.4**	65.6	77	**8.39**	18.7	30.2	**0**	0.2	1.8	**0**	0	0
60	**99.8**	100	100	**99.6**	100	100	**98.8**	99.8	100	**96.8**	99.2	100	**90**	95.6	98.8	**73**	81.8	89.8	**34.8**	47.2	57.8	**2.2**	8.8	18.2	**0**	0	0.8	**0**	0	0
70	**99.8**	100	100	**99.4**	100	100	**98**	99.6	100	**94.2**	97.8	99.6	**84.2**	90.6	96	**59.6**	69.2	78.2	**19.4**	31.8	43.4	**0.4**	4	11.2	**0**	0	0.4	**0**	0	0
80	**99.6**	100	100	**98.8**	99.8	100	**96.4**	98.8	100	**90.2**	95	98.4	**75.4**	83	90	**43.8**	55.6	66.2	**8.19**	19.9	32.2	**0**	1.6	6.8	**0**	0	0.2	**0**	0	0
90	**99.2**	99.8	100	**97.8**	99.4	100	**94**	97.4	99.4	**84.4**	90.8	95.6	**64**	73.6	81.8	**29.2**	42.8	54.8	**3**	12.2	23.6	**0**	0.6	4.2	**0**	0	0	**0**	0	0
100	**98.6**	99.8	100	**96.2**	98.8	100	**90**	95.2	98.4	**77.4**	85.2	91.4	**51.4**	63.2	73.4	**16.8**	31.6	44.8	**1**	7	17.2	**0**	0.2	2.4	**0**	0	0	**0**	0	0
110	**97.8**	99.4	100	**94.4**	97.6	99.4	**85.8**	92	96.6	**68.8**	78.2	86.2	**39.4**	53	65.2	**9.2**	22.7	37	**0.39**	4.1	12.6	**0**	0	1.6	**0**	0	0	**0**	0	0
120	**96.6**	98.8	100	**92**	96.2	98.8	**81**	87.6	94	**59.6**	71.2	81	**28.4**	44.1	58.2	**5.2**	16.4	30.8	**0**	2.4	9.6	**0**	0	1	**0**	0	0	**0**	0	0
130	**95**	98	99.8	**88.6**	94	98	**74.2**	83.4	91.8	**50.4**	63.6	76.8	**19.4**	36	52	**2.6**	11.8	25.8	**0**	1.4	7.2	**0**	0	0.6	**0**	0	0	**0**	0	0
140	**93**	97.2	99.6	**85**	91.8	97.6	**67.8**	78.8	90.4	**41**	56.8	74.2	**14**	29.8	49.2	**1.4**	8.8	23	**0**	0.8	6.2	**0**	0	0.6	**0**	0	0	**0**	0	0
150	**90.6**	96	99.4	**80.2**	89.4	97.2	**60**	74.4	89.4	**32.8**	51	73.4	**9.99**	24.5	46.6	**0.8**	6.4	20.6	**0**	0.6	5	**0**	0	0.4	**0**	0	0	**0**	0	0
≥154	**90**	95.4	99.4	**78.2**	88.2	97.4	**57.4**	72	89.6	**30.8**	48.8	73.6	**8.79**	23.2	47	**0.79**	6	20.6	**0**	0.4	4.6	**0**	0	0.4	**0**	0	0	**0**	0	0

Table 3.9 [continued].

Subtable B: Cumulative fraction of response

$CLCR_{CG}$[1] [mL/min]	Cumulative fraction of response, %																										
	Full MIC distribution[2]															MIC distribution of isolates belonging to the S category[2]						MIC distribution of isolates belonging to the I category[2]					
	Escherichia coli			*Klebsiella pneumonia*			*Enterobacter cloacae*			*Pseudomonas aeruginosa*			*Acinetobacter* spp.			*Pseudomonas aeruginosa*			*Acinetobacter* spp.			*Pseudomonas aeruginosa*			*Acinetobacter* spp.		
	$P_{0.05}$	$P_{0.5}$	$P_{0.95}$	**$P_{0.05}$**	$P_{0.5}$	$P_{0.95}$	**$P_{0.05}$**	$P_{0.5}$	$P_{0.95}$	**$P_{0.05}$**	$P_{0.5}$	$P_{0.95}$	$P_{0.05}$	$P_{0.5}$	$P_{0.95}$	**$P_{0.05}$**	$P_{0.5}$	$P_{0.95}$	**$P_{0.05}$**	$P_{0.5}$	$P_{0.95}$	**$P_{0.05}$**	$P_{0.5}$	$P_{0.95}$	$P_{0.05}$	$P_{0.5}$	$P_{0.95}$
10	**100**	100	100	**99.8**	99.9	100	**99.8**	99.9	100	**91.2**	95.2	98	88.2	94	99.1	**100**	100	100	**99.9**	100	100	**88.2**	99.1	100	89.5	99.2	100
20	**100**	100	100	**99.8**	99.8	99.9	**99.7**	99.8	99.9	**88.8**	92.1	94.6	85.4	89.1	92.8	**99.7**	100	100	**99.6**	100	100	**76.1**	93.1	99.4	78.3	94	99.5
30	**100**	100	100	**99.7**	99.8	99.8	**99.6**	99.7	99.8	**86.4**	89.4	91.4	83	86	88.2	**99.3**	99.9	100	**98.8**	99.9	100	**61.7**	79.7	91	64.7	81.9	92.3
40	**100**	100	100	**99.6**	99.7	99.8	**99.5**	99.6	99.7	**83.7**	86.6	88.7	80.4	83.5	85.5	**98.2**	99.6	100	**97.1**	99.2	99.9	**47**	61.7	73.7	50.4	65	76.7
50	**100**	100	100	**99.5**	99.6	99.7	**99.4**	99.5	99.6	**80.5**	83.7	86	77	80.6	83.1	**96.5**	98.6	99.6	**94.5**	97.7	99.3	**32**	43.9	55.3	35.2	47.3	58.7
60	**99.9**	100	100	**99.2**	99.5	99.6	**99.1**	99.4	99.5	**76.9**	80.4	83.1	72.9	76.9	80	**93.8**	96.8	98.6	**90.8**	94.8	97.5	**19.7**	29.4	39.5	22.1	32.2	42.3
70	**99.9**	99.9	100	**99.1**	99.4	99.5	**98.8**	99.3	99.4	**72.9**	76.9	80.2	68	72.5	76.4	**90.3**	94	96.6	**85.7**	90.5	94.2	**10.6**	18.9	28.5	12	20.9	30.8
80	**99.8**	99.9	100	**98.8**	99.3	99.4	**98.3**	99	99.3	**68.2**	72.9	77	62.1	67.5	72.2	**85.3**	90.1	93.8	**79**	85	89.9	**4.4**	11.4	20.5	4.99	12.8	22.3
90	**99.6**	99.9	99.9	**98.2**	99	99.3	**97.6**	98.6	99.1	**63**	68.5	73.3	55.8	62.2	67.6	**79.2**	85.3	90.1	**71.3**	78.7	84.8	**1.61**	6.83	14.6	1.83	7.67	16
100	**99.4**	99.9	99.9	**97.5**	98.8	99.1	**96.6**	98.2	98.8	**57.4**	63.9	69.5	49.4	56.7	63.1	**72.3**	79.9	86	**63.2**	72.2	79.5	**0.537**	3.85	10.4	0.61	4.35	11.4
110	**99.2**	99.7	99.9	**96.6**	98.2	99	**95.5**	97.4	98.5	**52.1**	59.1	65.7	43.6	51.4	58.8	**65.6**	74.2	81.6	**55.9**	65.6	74.4	**0.21**	2.2	7.51	0.238	2.5	8.31
120	**98.8**	99.6	99.8	**95.4**	97.6	98.8	**94**	96.5	98.1	**46.9**	54.6	62.2	38.4	46.7	55	**59.1**	68.7	77.5	**49.2**	59.6	69.7	**0**	1.29	5.62	0	1.46	6.24
130	**98.2**	99.3	99.8	**93.9**	96.7	98.6	**92.1**	95.4	97.7	**41.6**	50.3	59.2	33.5	42.3	51.7	**52.5**	63.2	74	**42.9**	54	65.7	**0**	0.752	4.15	0	0.853	4.62
140	**97.5**	99.1	99.8	**92.1**	95.9	98.3	**90**	94.3	97.4	**37.1**	46.5	57.6	29.5	38.6	50	**46.7**	58.5	72.1	**37.7**	49.4	63.6	**0**	0.43	3.61	0	0.488	4.01
150	**96.7**	98.8	99.8	**89.9**	94.8	98.2	**87.5**	93	97.1	**32.6**	43.1	56.5	25.7	35.3	48.7	**41.1**	54.2	70.8	**32.9**	45.2	62.1	**0**	0.322	2.87	0	0.366	3.2
≥154	96.2	98.7	99.8	**89.2**	94.3	98.2	**86.7**	92.3	97.2	**31.3**	41.8	56.7	24.6	34.2	48.9	**39.4**	52.6	71	**31.5**	43.8	62.2	**0**	0.215	2.66	0	0.244	2.96

[1]Body weight and serum albumin concentration set to median value of first study day (i.e. 70 kg and 2.8 g/dL); [2]According to EUCAST [132].

Colour coding: *Green*: CFR or PTA≥90%, *Yellow*: CFR or PTA 80-<90%, *Orange*: CFR or PTA>50-<80%, *Red*: CFR or PTA≤50%; *Grey shaded values*: Extrapolated $CLCR_{CG}$ range not covered by the study population or $CLCR_{CG}$≥154 mL/min (=inflection point of $CLCR_{CG}$-CL relationship). ***Bold values***: 5th percentile of the 1000 PTA values (derived from the 1000 Monte Carlo simulations considering PK parameter uncertainty), which was used for dosing selection in the dosing algorithm (Table 3.10).

Abbreviations: *CL:* Clearance*; $CLCR_{CG}$*: Creatinine clearance estimated according to Cockcroft and Gault [2]; *CFR*: Cumulative fraction of response; *$fT_{>MIC}$:* Time period that unbound drug concentration exceeds the MIC; *I category*: Category 'susceptible at increased exposure' [4]; *MIC*: Minimum inhibitory concentration; *$P_{0.05}$*: 5th percentile; *$P_{0.5}$*: 50th percentile = median; *$P_{0.95}$:* 95th percentile; *q8h*: administered every 8 h, *PK*: Pharmacokinetic, *PD*: Pharmacodynamics*; S category*: Category 'susceptible at normal dosing' [4]; *$T_{>MIC}$:* Time period that total drug concentration exceeds the MIC.

For the CFR, similar impact factors and trends were identified as for PTA for meropenem standard dosing ($CLCR_{CG}$: Table 3.9 Subtable B, body weight and serum albumin concentrations: Appendix Table S22). For a normal renal function ($CLCR_{CG}$: 90 mL/min), effective meropenem exposure was reliably attained (i.e. 5th percentile of CFR≥90%) for *E. coli, E. cloacae* and *K. pneumonia* (Table 3.9 Subtable B). For the two least susceptible pathogens *P. aeruginosa* and *Acinetobacter spp.,* however, effective exposure was not reliably reached when evaluating the full MIC distribution (68.5% and 62.2%, respectively). Separate evaluation of the MIC distributions based on the isolates belonging to the S and I categories, showed considerably higher CFR values for isolates of the S category (5th percentile of CFR: *P. aeruginosa*: 85.3% vs. 6.83%; *Acinetobacter* spp.: 78.7% vs. 7.67%).

Evaluation of alternative meropenem dosing regimens

Given the importance of $CLCR_{CG}$ and the similar results for treatment day 1 and 4 (previous section), for alternative dosing regimens (Table 2.7) PTA and CFR analyses were performed for varying $CLCR_{CG}$ values for treatment day 1 ($n_{simulated\ patients}$: 72,000,000 = 18 covariate combinations· 8 dosing regimens · 500 patients · 1000 uncertainty simulations). All results are summarised in tabular format in the Appendix chapter: Table S23 (PTA, short-term infusions), Table S24 (PTA, prolonged infusions), Table S25 (PTA, continuous infusions), Table S26 (CFR, short-term infusions), Table S27 (CFR, prolonged infusions), Table S28 (CFR, continuous infusions). Typical meropenem concentration-time profiles following all investigated dosing regimens are illustrated for varying $CLCR_{CG}$ in Appendix Figure S37.

Overall, the analyses demonstrated that for bacteria of the S category (MIC≤2 mg/L) effective meropenem exposure was reliably attained (i.e. 5th percentile of PTA≥90%) in all investigated patients, with at least one of the 8 investigated dosing regimens: Whereas in patients with augmented renal function (≥130 mL/min) only the most intensified dosing regimen (CI6) reliably resulted in effective exposure: for patients with moderate renal insufficiency ($CLCR_{CG}$=30-<60 mL/min), dosing regimens with a standard daily dose did ($SI3_8$/$PI3_8$/CI3). Bacteria belonging to the I category (MIC≥4 mg/L), however, seemed to only be effectively covered in patients with renal insufficiency (MIC=4 mg/L: $CLCR_{CG}$≤80 mL/min, MIC=8 mg/L: $CLCR_{CG}$≤30 mL/min) using intensified dosing regimens ($SI6_8$/$PI6_8$/CI6). Conversely, for highly susceptible pathogens (e.g. MIC<0.12 mg/L for $CLCR_{CG}$=90 mL/min), even lower than standard dosing reliably resulted in effective meropenem exposure ($SI2_{12}$/$PI2_{12}$).

The analyses demonstrated the following important trends, for MIC≤4 mg/L and day 1 of treatment: Firstly, for a given daily dose, continuous-infusion regimens (Appendix Table S25) were superior to prolonged (Appendix Table S24) and prolonged to short-term dosing regimens (Appendix Table S23). The superiority of continuous over prolonged infusion was more pronounced than of prolonged over short-term infusion. Secondly, the type of infusion (e.g.

continuous vs. prolonged) on the achievement of effective exposure was more relevant than the administered total daily dose (e.g. 3000/3412.5 vs. 6000/6875 mg). For MIC>4 mg/L and *P. aeruginosa* or *Acinetobacter* spp. isolates of the I category, prolonged infusion rather than continuous-infusion regimens was superior.

3.4.4 Dosing algorithm

The developed 3-level dosing algorithm is provided in Table 3.10 and shall be illustrated for different levels of knowledge about the pathogen by the following example: If at start of treatment an infecting pathogen of the S category (L1; non-species-related S breakpoint=2 mg/L) is suspected in patients with $CLCR_{CG}$=50 mL/min, the short-term infusion regimen with an increased daily dose of 6000 mg ($SI6_8$) would be needed to reliably reach effective exposure (i.e. 5th percentile of PTA≥90%); for the prolonged and continuous-infusion regimens lower daily doses ($PI3_8$/CI3, i.e. 3000/3412.5 mg) would be sufficient. For patients with normal renal function, only the highest investigated continuous-infusion regimen (CI6) would reliably reach effective exposure. When for the latter patient information on the type of pathogen becomes available (L2), a regimen with a reduced daily dose ($SI2_{12}$/$SI3_8$/$PI2_{12}$/CI3) could be selected in case of different Enterobacteriaceae, whereas for *P. aeruginosa* or *Acinetobacter* spp., no regimen seemed effective. If additional knowledge of the susceptibility of the pathogen ($L3_{(-MIC)}$) becomes available, e.g. for *P. aeruginosa* of the S category, apart from the intensified short-term infusion ($SI6_8$) an even lower daily dose administered as prolonged infusion ($PI3_8$) or continuous-infusion (CI3) regimen was found to reliably result in adequate PK/PD target attainment; for *Acinetobacter* spp. of the S category: Short-term ($SI6_8$), prolonged ($PI6_8$) or continuous (CI3) infusion regimens. If the actual MIC value is also provided ($L3_{(+MIC)}$) and is ≤0.12 mg/L, irrespective of the pathogen but depending on the particular MIC value the dosing regimen could be kept or reduced even further ($SI2_{12}$/$SI3_8$/$PI2_{12}$/$PI3_8$/CI3).

Table 3.10: Three-level dosing algorithm[1] for the first day of meropenem treatment in critically ill patients (modified from [243]). The proposed eight dosing regimens[2] cover three different durations of infusion: short-term infusion (*SI*: $SI2_{12}$, $SI3_8$, $SI6_8$), prolonged infusion (*PI*: $PI2_{12}$, $PI3_8$, $PI6_8$), continuous infusion (*CI*: CI3, CI6d); and cover three different daily doses: 2000 mg (*light blue:* $SI2_{12}$, $PI2_{12}$), 3000[3] mg (*blue:* $SI3_8$, $PI3_8$, CI3) and 6000[4] mg (*pink:* $SI6_8$, $PI6_8$, CI6). For detailed description of the eight dosing regimens refer to footnote of the table.

Level 1: Pathogen unknown

$CLCR_{CG}$[5] [mL/min]	Non-species related EUCAST PK/PD breakpoint [5]					
	S breakpoint (MIC=2 mg/L)			R breakpoint (MIC=8 mg/L)		
	SI	PI	CI	SI	PI	CI
10	$SI2_{12}$	$PI2_{12}$	CI3	$SI6_8$	$PI6_8$	CI6
20	**$SI3_8$**	$PI3_8$	CI3	$SI6_8$	$PI6_8$	-
30	**$SI3_8$**	$PI3_8$	CI3	-	$PI6_8$	-
40	**$SI3_8$**	$PI3_8$	CI3	-	-	-
50	$SI6_8$	$PI3_8$	CI3	-	-	-
60	$SI6_8$	$PI6_8$	CI3	-	-	-
70	-	$PI6_8$	CI3	-	-	-
80	-	$PI6_8$	CI3	-	-	-
90	-	-	CI6	-	-	-
100	-	-	CI6	-	-	-
110	-	-	CI6	-	-	-
120	-	-	CI6	-	-	-
130	-	-	CI6	-	-	-
140	-	-	CI6	-	-	-
150	-	-	CI6	-	-	-
≥154	-	-	CI6	-	-	-

Level 2: Pathogen known

$CLCR_{CG}$[5] [mL/min]	Full MIC distribution[6]														
	Escherichia coli			*Klebsiella pneumonia*			*Enterobacter cloacae*			*Pseudomonas aeruginosa*			*Acinetobacter* spp.		
	SI	PI	CI	SI	PI	CI	SI	PI	CI	SI	PI	CI	SI	PI	CI
10	$SI2_{12}$	$PI2_{12}$	CI3	$SI2_{12}$	$PI2_{12}$	CI3	$SI2_{12}$	$PI2_{12}$	CI3	**$SI3_8$**	$PI3_8$	CI6	$SI6_8$	$PI6_8$	-
20	$SI2_{12}$	$PI2_{12}$	CI3	$SI2_{12}$	$PI2_{12}$	CI3	$SI2_{12}$	$PI2_{12}$	CI3	$SI6_8$	$PI6_8$	CI6	$SI6_8$	$PI6_8$	-
30	$SI2_{12}$	$PI2_{12}$	CI3	$SI2_{12}$	$PI2_{12}$	CI3	$SI2_{12}$	$PI2_{12}$	CI3	$SI6_8$	$PI6_8$	CI6	$SI6_8$	$PI6_8$	-
40	$SI2_{12}$	$PI2_{12}$	CI3	$SI2_{12}$	$PI2_{12}$	CI3	$SI2_{12}$	$PI2_{12}$	CI3	$SI6_8$	$PI6_8$	-	-	$PI6_8$	-
50	$SI2_{12}$	$PI2_{12}$	CI3	$SI2_{12}$	$PI2_{12}$	CI3	$SI2_{12}$	$PI2_{12}$	CI3	-	$PI6_8$	-	-	-	-
60	$SI2_{12}$	$PI2_{12}$	CI3	$SI2_{12}$	$PI2_{12}$	CI3	$SI2_{12}$	$PI2_{12}$	CI3	-	-	-	-	-	-
70	$SI2_{12}$	$PI2_{12}$	CI3	$SI2_{12}$	$PI2_{12}$	CI3	$SI2_{12}$	$PI2_{12}$	CI3	-	-	-	-	-	-
80	$SI2_{12}$	$PI2_{12}$	CI3	$SI2_{12}$	$PI2_{12}$	CI3	**$SI3_8$**	$PI2_{12}$	CI3	-	-	-	-	-	-
90	$SI2_{12}$	$PI2_{12}$	CI3	**$SI3_8$**	$PI2_{12}$	CI3	**$SI3_8$**	$PI2_{12}$	CI3	-	-	-	-	-	-
100	$SI2_{12}$	$PI2_{12}$	CI3	**$SI3_8$**	$PI3_8$	CI3	**$SI3_8$**	$PI3_8$	CI3	-	-	-	-	-	-
110	**$SI3_8$**	$PI2_{12}$	CI3	**$SI3_8$**	$PI3_8$	CI3	**$SI3_8$**	$PI3_8$	CI3	-	-	-	-	-	-
120	**$SI3_8$**	$PI2_{12}$	CI3	**$SI3_8$**	$PI3_8$	CI3	**$SI3_8$**	$PI3_8$	CI3	-	-	-	-	-	-
130	**$SI3_8$**	$PI3_8$	CI3	**$SI3_8$**	$PI3_8$	CI3	**$SI3_8$**	$PI3_8$	CI3	-	-	-	-	-	-
140	**$SI3_8$**	$PI3_8$	CI3	**$SI3_8$**	$PI3_8$	CI3	**$SI3_8$**	$PI3_8$	CI3	-	-	-	-	-	-
150	**$SI3_8$**	$PI3_8$	CI3	$SI6_8$	$PI3_8$	CI3	$SI6_8$	$PI3_8$	CI3	-	-	-	-	-	-
≥154	**$SI3_8$**	$PI3_8$	CI3	$SI6_8$	$PI3_8$	CI3	$SI6_8$	$PI3_8$	CI3	-	-	-	-	-	-

Level 3$_{(-MIC)}$: Pathogen and susceptibility known

$CLCR_{CG}$[5] [mL/min]	MIC distribution of isolates belonging to S category[6]						MIC distribution of isolates belonging to I category[6]					
	Pseudomonas aeruginosa			*Acinetobacter* spp.			*Pseudomonas aeruginosa*			*Acinetobacter* spp.		
	SI	PI	CI	SI	PI	CI	SI	PI	CI	SI	PI	CI
10	$SI2_{12}$	$PI2_{12}$	CI3	$SI2_{12}$	$PI2_{12}$	CI3	$SI6_8$	$PI3_8$	CI6	$SI6_8$	$PI3_8$	CI6
20	$SI2_{12}$	$PI2_{12}$	CI3	$SI2_{12}$	$PI2_{12}$	CI3	$SI6_8$	$PI6_8$	CI6	$SI6_8$	$PI6_8$	CI6
30	$SI2_{12}$	$PI2_{12}$	CI3	**$SI3_8$**	$PI2_{12}$	CI3	-	$PI6_8$	CI6	$SI6_8$	$PI6_8$	CI6
40	**$SI3_8$**	$PI2_{12}$	CI3	**$SI3_8$**	$PI3_8$	CI3	-	$PI6_8$	-	-	$PI6_8$	-
50	**$SI3_8$**	$PI3_8$	CI3	**$SI3_8$**	$PI3_8$	CI3	-	-	-	-	-	-
60	**$SI3_8$**	$PI3_8$	CI3	**$SI3_8$**	$PI3_8$	CI3	-	-	-	-	-	-
70	**$SI3_8$**	$PI3_8$	CI3	$SI6_8$	$PI3_8$	CI3	-	-	-	-	-	-
80	$SI6_8$	$PI3_8$	CI3	$SI6_8$	$PI3_8$	CI3	-	-	-	-	-	-
90	$SI6_8$	$PI3_8$	CI3	-	$PI6_8$	CI3	-	-	-	-	-	-
100	-	$PI6_8$	CI3	-	$PI6_8$	CI3	-	-	-	-	-	-
110	-	$PI6_8$	CI3	-	$PI6_8$	CI3	-	-	-	-	-	-
120	-	$PI6_8$	CI3	-	-	CI3	-	-	-	-	-	-
130	-	-	CI3	-	-	CI3	-	-	-	-	-	-
140	-	-	CI3	-	-	CI6	-	-	-	-	-	-
150	-	-	CI3	-	-	CI6	-	-	-	-	-	-
≥154	-	-	CI3	-	-	CI6	-	-	-	-	-	-

Table 3.10 [continued].

Level 3$_{(+MIC)}$: MIC value known

CLCR$_{CG}$[5] [mL/min]	MIC [mg/L]																																			
	0.004			0.008			0.015			0.03			0.06			0.12			0.25			0.5			1			2			4			8		
	SI	PI	CI	SI	PI	CI	SI	PI	CI	SI	PI	CI	SI	PI	CI	SI	PI	CI	SI	PI	CI	SI	PI	CI	SI	PI	CI	SI	PI	CI	SI	PI	CI	SI	PI	CI
10	$SI2_{12}$	$PI2_{12}$	CI3	$SI2_{12}$	$PI2_{12}$	CI3	$SI2_{12}$	$PI2_{12}$	CI3	$SI2_{12}$	$PI2_{12}$	CI3	$SI2_{12}$	$PI2_{12}$	CI3	$SI2_{12}$	$PI2_{12}$	CI3	$SI2_{12}$	$PI2_{12}$	CI3	$SI2_{12}$	$PI2_{12}$	CI3	$SI2_{12}$	$PI2_{12}$	CI3	$SI2_{12}$	$PI2_{12}$	CI3	**$SI3_8$**	$PI3_8$	CI3	$SI6_8$	$PI6_8$	CI6
20	$SI2_{12}$	$PI2_{12}$	CI3	$SI2_{12}$	$PI2_{12}$	CI3	$SI2_{12}$	$PI2_{12}$	CI3	$SI2_{12}$	$PI2_{12}$	CI3	$SI2_{12}$	$PI2_{12}$	CI3	$SI2_{12}$	$PI2_{12}$	CI3	$SI2_{12}$	$PI2_{12}$	CI3	$SI2_{12}$	$PI2_{12}$	CI3	$SI2_{12}$	$PI2_{12}$	CI3	**$SI3_8$**	$PI3_8$	CI3	**$SI3_8$**	$PI3_8$	CI6	$SI6_8$	$PI6_8$	-
30	$SI2_{12}$	$PI2_{12}$	CI3	$SI2_{12}$	$PI2_{12}$	CI3	$SI2_{12}$	$PI2_{12}$	CI3	$SI2_{12}$	$PI2_{12}$	CI3	$SI2_{12}$	$PI2_{12}$	CI3	$SI2_{12}$	$PI2_{12}$	CI3	$SI2_{12}$	$PI2_{12}$	CI3	$SI2_{12}$	$PI2_{12}$	CI3	**$SI3_8$**	$PI2_{12}$	CI3	**$SI3_8$**	$PI3_8$	CI3	$SI6_8$	$PI3_8$	CI6	-	$PI6_8$	-
40	$SI2_{12}$	$PI2_{12}$	CI3	$SI2_{12}$	$PI2_{12}$	CI3	$SI2_{12}$	$PI2_{12}$	CI3	$SI2_{12}$	$PI2_{12}$	CI3	$SI2_{12}$	$PI2_{12}$	CI3	$SI2_{12}$	$PI2_{12}$	CI3	$SI2_{12}$	$PI2_{12}$	CI3	$SI2_{12}$	$PI2_{12}$	CI3	**$SI3_8$**	$PI3_8$	CI3	**$SI3_8$**	$PI3_8$	CI3	$SI6_8$	$PI6_8$	CI6	-	-	-
50	$SI2_{12}$	$PI2_{12}$	CI3	$SI2_{12}$	$PI2_{12}$	CI3	$SI2_{12}$	$PI2_{12}$	CI3	$SI2_{12}$	$PI2_{12}$	CI3	$SI2_{12}$	$PI2_{12}$	CI3	$SI2_{12}$	$PI2_{12}$	CI3	$SI2_{12}$	$PI2_{12}$	CI3	**$SI3_8$**	$PI2_{12}$	CI3	**$SI3_8$**	$PI3_8$	CI3	$SI6_8$	$PI3_8$	CI3	-	$PI6_8$	CI6	-	-	-
60	$SI2_{12}$	$PI2_{12}$	CI3	$SI2_{12}$	$PI2_{12}$	CI3	$SI2_{12}$	$PI2_{12}$	CI3	$SI2_{12}$	$PI2_{12}$	CI3	$SI2_{12}$	$PI2_{12}$	CI3	$SI2_{12}$	$PI2_{12}$	CI3	**$SI3_8$**	$PI2_{12}$	CI3	**$SI3_8$**	$PI3_8$	CI3	**$SI3_8$**	$PI3_8$	CI3	$SI6_8$	$PI6_8$	CI3	-	-	CI6	-	-	-
70	$SI2_{12}$	$PI2_{12}$	CI3	$SI2_{12}$	$PI2_{12}$	CI3	$SI2_{12}$	$PI2_{12}$	CI3	$SI2_{12}$	$PI2_{12}$	CI3	$SI2_{12}$	$PI2_{12}$	CI3	**$SI3_8$**	$PI2_{12}$	CI3	**$SI3_8$**	$PI3_8$	CI3	**$SI3_8$**	$PI3_8$	CI3	$SI6_8$	$PI3_8$	CI3	-	$PI6_8$	CI3	-	-	CI6	-	-	-
80	$SI2_{12}$	$PI2_{12}$	CI3	$SI2_{12}$	$PI2_{12}$	CI3	$SI2_{12}$	$PI2_{12}$	CI3	$SI2_{12}$	$PI2_{12}$	CI3	$SI2_{12}$	$PI2_{12}$	CI3	**$SI3_8$**	$PI2_{12}$	CI3	**$SI3_8$**	$PI3_8$	CI3	**$SI3_8$**	$PI3_8$	CI3	$SI6_8$	$PI3_8$	CI3	-	$PI6_8$	CI3	-	-	CI6	-	-	-
90	$SI2_{12}$	$PI2_{12}$	CI3	$SI2_{12}$	$PI2_{12}$	CI3	$SI2_{12}$	$PI2_{12}$	CI3	$SI2_{12}$	$PI2_{12}$	CI3	**$SI3_8$**	$PI2_{12}$	CI3	**$SI3_8$**	$PI3_8$	CI3	**$SI3_8$**	$PI3_8$	CI3	$SI6_8$	$PI3_8$	CI3	-	$PI6_8$	CI3	-	-	CI6	-	-	-	-	-	-
100	$SI2_{12}$	$PI2_{12}$	CI3	$SI2_{12}$	$PI2_{12}$	CI3	$SI2_{12}$	$PI2_{12}$	CI3	**$SI3_8$**	$PI2_{12}$	CI3	**$SI3_8$**	$PI2_{12}$	CI3	**$SI3_8$**	$PI3_8$	CI3	**$SI3_8$**	$PI3_8$	CI3	$SI6_8$	$PI3_8$	CI3	-	$PI6_8$	CI3	-	-	CI6	-	-	-	-	-	-
110	$SI2_{12}$	$PI2_{12}$	CI3	$SI2_{12}$	$PI2_{12}$	CI3	$SI2_{12}$	$PI2_{12}$	CI3	**$SI3_8$**	$PI2_{12}$	CI3	**$SI3_8$**	$PI3_8$	CI3	**$SI3_8$**	$PI3_8$	CI3	$SI6_8$	$PI3_8$	CI3	-	$PI6_8$	CI3	-	-	CI3	-	-	CI6	-	-	-	-	-	-
120	$SI2_{12}$	$PI2_{12}$	CI3	$SI2_{12}$	$PI2_{12}$	CI3	**$SI3_8$**	$PI2_{12}$	CI3	**$SI3_8$**	$PI3_8$	CI3	**$SI3_8$**	$PI3_8$	CI3	**$SI3_8$**	$PI3_8$	CI3	$SI6_8$	$PI3_8$	CI3	-	$PI6_8$	CI3	-	-	CI3	-	-	CI6	-	-	-	-	-	-
130	$SI2_{12}$	$PI2_{12}$	CI3	**$SI3_8$**	$PI2_{12}$	CI3	**$SI3_8$**	$PI2_{12}$	CI3	**$SI3_8$**	$PI3_8$	CI3	**$SI3_8$**	$PI3_8$	CI3	$SI6_8$	$PI3_8$	CI3	-	$PI3_8$	CI3	-	$PI6_8$	CI3	-	-	CI3	-	-	CI6	-	-	-	-	-	-
140	$SI2_{12}$	$PI2_{12}$	CI3	**$SI3_8$**	$PI2_{12}$	CI3	**$SI3_8$**	$PI2_{12}$	CI3	**$SI3_8$**	$PI3_8$	CI3	**$SI3_8$**	$PI3_8$	CI3	$SI6_8$	$PI3_8$	CI3	-	$PI3_8$	CI3	-	$PI6_8$	CI3	-	-	CI3	-	-	CI6	-	-	-	-	-	-
150	**$SI3_8$**	$PI2_{12}$	CI3	**$SI3_8$**	$PI2_{12}$	CI3	**$SI3_8$**	$PI3_8$	CI3	**$SI3_8$**	$PI3_8$	CI3	**$SI3_8$**	$PI3_8$	CI3	$SI6_8$	$PI3_8$	CI3	-	$PI6_8$	CI3	-	-	CI3	-	-	CI3	-	-	CI6	-	-	-	-	-	-
≥154	**$SI3_8$**	$PI2_{12}$	CI3	**$SI3_8$**	$PI2_{12}$	CI3	**$SI3_8$**	$PI3_8$	CI3	**$SI3_8$**	$PI3_8$	CI3	**$SI3_8$**	$PI3_8$	CI3	-	$PI3_8$	CI3	-	$PI6_8$	CI3	-	-	CI3	-	-	CI3	-	-	CI6	-	-	-	-	-	-

[1]The algorithm is currently intended for clinical research and needs further validation in future clinical studies. [2]Lowest possible dosing regimen for which the 5[th] percentile of the 1000 Monte Carlo simulations considering PK parameter uncertainty, achieved CFR≥90% (for Level 2, Level 3$_{(-MIC)}$) or PTA≥90% (for Level 1, Level 3$_{(+MIC)}$). For SI and PI the PK/PD target 98%T$_{>MIC}$ was evaluated, for CI 98%T$_{>4xMIC}$. [3]For first day of treatment: Daily dose of 3412.5 mg incl. loading dose. [4]For first day of treatment: Daily dose of 6875 mg incl. loading dose. [5]Body weight and serum albumin concentration fixed to median of first study day (i.e. 70 kg and 2.8 g/dL). [6]EUCAST MIC distribution [132].

Dosing regimens: *$SI2_{12}$*: 1000 mg, 30-min i.v. infusion, q12h; *$SI3_8$*: 1000 mg, 30-min i.v. infusion, q8h (=standard dosing; highlighted in bold); *$SI6_8$*: 2000 mg, 30-min i.v. infusion, q8h; *$PI2_{12}$*: 1000 mg, 3-h i.v. infusion, q12h; *$PI3_8$*: 1000 mg, 3-h i.v. infusion, q8h; *$PI6_8$*: 2000 mg, 3-h i.v. infusion, q8h; *CI3*: 3000 mg, CI, q24h following 500 mg, 30-min loading dose; *CI6*: 6000 mg, CI, q24h following 1000 mg, 30-min loading dose. For CI regimens (CI3, CI6) consider to renew the infusion solution dependent on the drug concentration twice or thrice daily (see supplement of [380]) to ensure the stability of meropenem.

Abbreviations: *CLCR$_{CG}$*: Creatinine clearance estimated according to Cockcroft and Gault [2]; *CFR*: Cumulative fraction of response; *CI*: Continuous infusion; *EUCAST*: European Committee on Antimicrobial Susceptibility Testing; *h*: Hours; *I category*: Category 'susceptible at increased exposure [4]; *MIC*: Minimum inhibitory concentration; *min*: Minutes; *PI*: Prolonged infusion; *PTA*: Probability of target attainment; *S category*: Category 'susceptible at normal dosing' [4]; *SI*: Short-term infusion; *q8h*: Every 8 hours; *q12h*: Every 12 hours; *q24h*: Every 24 hours; *T$_{>MIC}$:* Time period that total drug concentration exceeds the MIC; *T$_{>4xMIC}$:* Time period that total drug concentration exceeds four times the MIC.

4

Discussion

By employing pharmacometric modelling and simulation approaches, the present thesis provided an enhanced quantitative understanding of the PK of selected antibiotic drugs (linezolid, meropenem) in special patient populations (obese surgical, critically ill). The identification of patient-specific characteristics, influencing the PK and subsequently the attainment of effective drug exposure, enabled the identification of patients at risk for therapy failure with the standard antibiotic dosing regimen and allowed suggestions of optimised dosing regimens for the 'patients at risk'. Translating the results gained from the pharmacometric analyses into easy-to-use tools, this thesis provided a strategy to make the research results applicable in the clinics which shall ultimately support future therapeutic decisions. In addition, the thesis contributed to a better characterisation of the variability in the microdialysis sampling technique, as the method of choice to determine unbound (i.e. pharmacologically active) drug concentrations directly at the target site.

Research questions, research categories and key results of the present thesis are graphically summarised in Figure 4.1 and will be further discussed in the following sections, also in the light of currently available knowledge from scientific literature.

4.1 Leveraging pharmacometric approaches to characterise linezolid plasma and target site exposure in obese and nonobese surgical patients and to evaluate and optimise dosing (Project I, II)

Employing pharmacometric approaches, Project I and II assessed linezolid therapy in obese and nonobese surgical patients. While Project I focused on the characterisation of linezolid PK in plasma (total and unbound) as well as at the target site (unbound) by means of the development of a NLME PK model and the performance of deterministic exposure simulations (research category: basic research; Figure 4.1), Project II utilised probability of target attainment analyses to evaluate, and if needed, optimise the dosing regimens (research category: applied research; Figure 4.1).

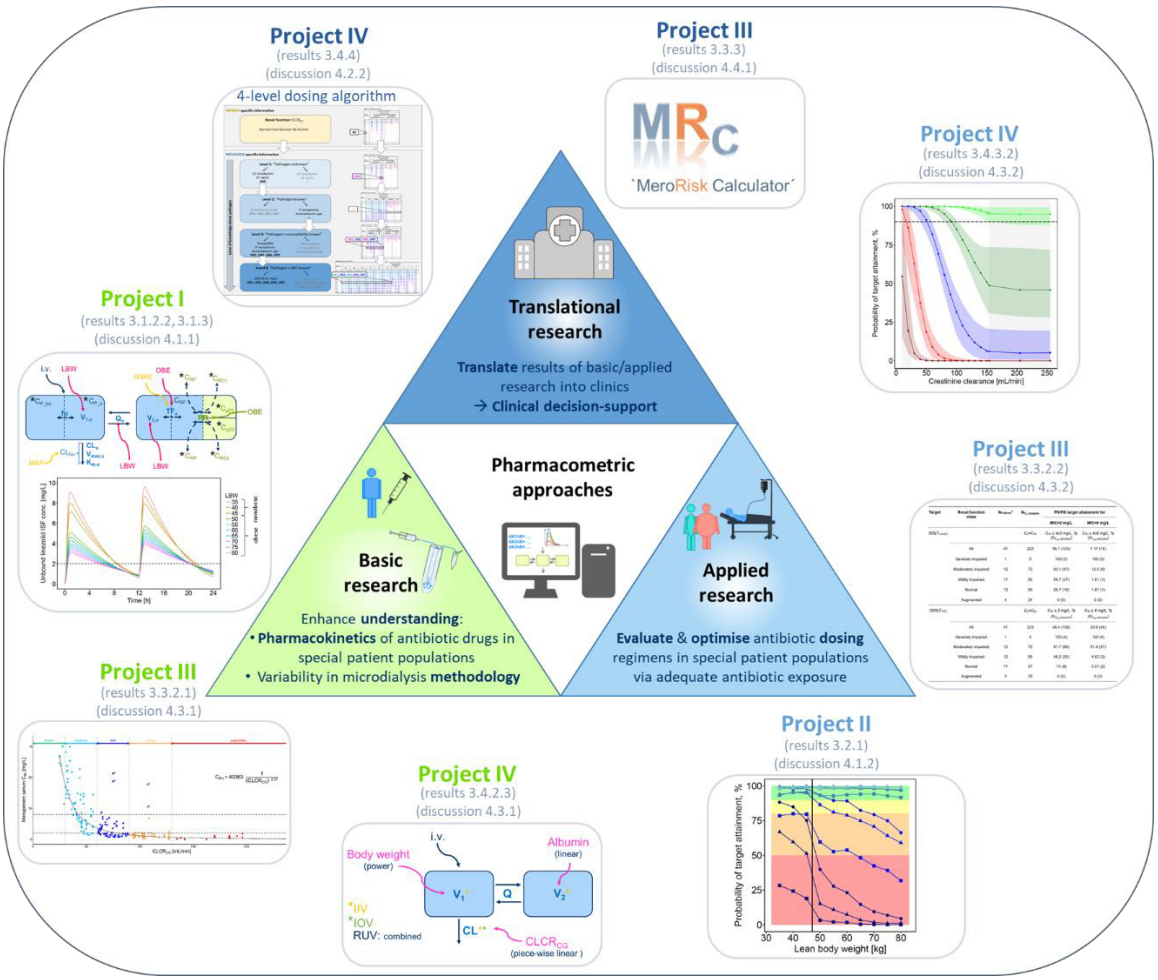

Figure 4.1: Graphical overview of key results, central objectives and research categories of the present thesis. The key results of the four research projects are illustrated in form of the key figures/tables around the illustration of the objectives and research categories (Figure 1.5). Each figure/table is assigned by the colour of the project header, to one of the research categories (green: basic research; light blue: applied research; dark blue: translational research). For each figure/table, the section is provided in which the key results are presented and discussed.

4.1.1 Characterisation of linezolid plasma and target site exposure in obese and nonobese surgical patients (Project I)

Database. The pharmacometric analysis in Project I was based on a solid and unique PK database which allowed to, for the first time, characterise not only plasma PK of total (i.e. bound + unbound) and unbound linezolid but also target site PK of unbound linezolid, both in obese and nonobese patients undergoing abdominal surgery. In contrast to other microdialysis studies that typically included around 10 patients [46,48,50,51,252–254], the present study investigated a relatively large number of patients (n=30). Furthermore, a rich PK database was available ($n_{samples}$>1000), collected in plasma and in the ISF of the s.c. adipose tissue using the microdialysis technique. This enabled the comparison of linezolid exposure in plasma and s.c. adipose tissue and the identification of patient- and surgery-specific clinical determinants. A special characteristic of the dataset was the availability of target site PK data that had been collected via two microdialysis catheters per patient which were identical in construction and inserted in the s.c. adipose tissue.

Since additionally calibration was performed twice per catheter, the quantification of different variability levels in the microdialysis technique was possible, leading to an improved characterisation of the microdialysis sampling technique. The methodology-related aspects will be discussed in section 4.2, while the present section (4.1.1) will mainly focus on PK-related aspects.

NLME modelling approach. In order to provide a better understanding of the results in the following, the underlying NLME modelling approach will be shortly discussed, before focusing on the PK-related findings of the project. In a systematic stepwise manner, a NLME PK model was developed integrating all available PK data, i.e. total plasma concentrations, unbound plasma concentrations as well as microdialysate and retroperfusate/-dialysate concentrations collected with both microdialysis catheters. By jointly assessing all available PK data, separation and quantification of the RUV by sampling matrix and sampling technique was possible, which enabled a comparison of the magnitudes of RUV. Overall, RUV was relatively low, with microdialysate concentrations (13.3%CV) showing higher RUV than total and unbound plasma concentrations (<4.76%CV). This is likely to be related to the complexity in the microdialysis sampling technique (for further discussion on variability in technique see section 4.2). However, in contrast to previous clinical microdialysis studies, the observed magnitude of RUV related to microdialysate concentrations was comparably low (e.g. RUV, %CV: 33.9 [45], 27.0 [45], 20.7 [255], 17.0 [46]). To jointly analyse all available PK data (i.e. plasma, micro- and retrodialysis), the advanced integrated dialysate-based modelling approach (Section 2.6.4.1) was applied, which was originally developed by Tunblad et al. [229], based on animal data and afterwards successfully applied by Minichmayr and Schaeftlein et al. at our department for the analysis of clinical microdialysis PK data [45,230]. This modelling approach – although more complex (also with respect to the required dataset structure; Section 2.6.3.1) and computationally more intensive – was proven superior to the often-used basic mid-time approach in terms of the underlying assumptions, being less biased, and more informative. The use of this modelling approach further facilitated the assessment of variability in the microdialysis technique, as the RR value was estimated within the model and different variability levels were assessable and quantifiable by the inclusion of random-effects parameters. Also, the microdialysate and retroperfusate/-dialysate data were included into the model in a stepwise manner (i.e. in a first step only the data of one catheter per patient were implemented, in a second step data of second catheter were added; Figure 3.3). This enabled to focus on the development of a suitable structural PK model describing linezolid distribution and elimination in the first place, before assessing variability linked to the measurement technique itself, i.e. different levels of variability based on the data of both catheters. Of note, dissecting the variability in the microdialysis methodology-related parameters (i.e. RR) from the variability in the PK parameters (e.g. CL, V_2, TF), allowed to consider only the relevant PK variability in stochastic exposure simulations which served as basis for the dosing evaluation and optimisation in Project II.

Protein binding of linezolid. The availability of both total and unbound plasma concentrations enabled the assessment of the protein binding of linezolid. In contrast to the protein binding reported by the manufacturer (~31% [139]), the protein binding observed in the present clinical study was considerably lower (f_u=85.6%, i.e. protein binding 14.4%; Section 3.1.2.2). This finding supported prior clinical investigations that showed f_u values of similar magnitude (f_u=88.2% [45,256], f_u=85% [253], f_u=83.1% [257], f_u=87.6% [258]). Of note, in all clinical investigations, ultrafiltration was used to determine the unbound concentrations; yet, it remains unclear which method was used by the manufacturer. Future clinical studies are warranted, investigating and substantiating the magnitude of linezolid protein binding, potentially also by comparing different methodologies [259,260]. Reliable knowledge on protein binding is crucial, considering that published f_u values are used to derive unbound linezolid concentrations, in situations in which only total concentrations are available [261]. Using the computed unbound linezolid concentrations for instance for the assessment of PTA might severely impact or bias the resulting clinical implications. The analysis of the unbound linezolid plasma concentrations for low, medium and high drug concentrations, revealed no concentration-dependency of the protein binding, which was in concordance with the manufacturer's information [139]. Moreover, the present analysis demonstrated similar f_u values between obese and nonobese patients, indicating that body size did not impact f_u, which has been reported for other drugs in obese patients as well [262,263]. Note that also on the individual level (i.e. between the 30 investigated patients), the f_u values were consistent as demonstrated by the negligibly small interindividual variability (0.3%CV).

In light of the increasing evidence that the plasma protein binding of linezolid in the clinics is approximately 14% as well as the low interindividual variability in protein binding, this work suggests using a f_u value of 86% for future studies in which protein binding has not been determined.

Plasma versus target site: Tissue fluid distribution of linezolid. NLME modelling has been proven to be an adequate approach to analyse microdialysis data ([229], Section 2.6.4.1). In contrast to exploratory data analyses, NLME modelling facilitates an integration of the microdialysate concentration-time profile over the collection interval and thus allows to analyse the data without making any assumptions regarding the allocation of the measured microdialysate concentration. Accordingly, NLME modelling is a valuable methodology to adequately characterise the kinetic behaviour of the drug at the target site. Of the different distribution kinetics models assessed for linezolid in the present work (assuming a rapid or delayed distribution; Figure 3.3: Target site model), the delayed distribution model was selected, that assigned the s.c. adipose tissue ISF to the peripheral compartment of the plasma model. The model included an additional parameter, the tissue factor TF, scaling the concentration-time profile in the peripheral compartment to the concentration-time profile in the ISF of the s.c. adipose tissue. This model structure is supported from a physiological point of view: As also the central compartment, the

peripheral compartment can be understood as a 'lumped compartment' in which tissues showing similar delayed distribution kinetics (i.e. concentration-time profiles in the tissues show similar 'shapes') are lumped together [210,264]. Huisinga and colleagues, for instance, reduced physiologically based pharmacokinetic (PBPK) models to low-dimensional compartment models by lumping highly perfused tissues such as lung, kidney, liver, spleen to the central compartment and by assigning less perfused adipose, bone, skin, or muscle tissues to peripheral compartment(s) [210,264]. Thus, the concentration-time profile in the peripheral compartment represents the volume-normalised profile of all lumped tissues and the estimated tissue-specific parameter TF scales this concentration-time profile to the actual profile in the ISF of the s.c. adipose tissue. Moreover, taking into consideration that the ISF concentrations of the s.c. adipose tissue determined using the microdialysis method, represent unbound drug concentrations, the remaining structural model was defined on the unbound scale as well. This resulted in an even more physiologically plausible model, considering that only the unbound concentrations can distribute from plasma into tissue [54,265].

For the studied patient population of obese and nonobese patients undergoing an abdominal surgery, the typical TF without stratification was estimated to be 55.6% (Table S4), indicating that the typical unbound linezolid concentrations in the ISF of the s.c. adipose tissue were approximately half of the typical unbound linezolid concentrations in the lumped peripheral compartment. Consequently, interpreting the peripheral compartment as the lumped compartment comprising different tissues with similar kinetic behaviour, other tissues may show comparably higher linezolid concentrations. For muscle tissue, for instance, previous investigations demonstrated a good penetration of linezolid. Schwameis et al. determined an AUC ratio of 0.98 for unbound linezolid concentrations in muscle tissue (determined using microdialysis) to unbound concentrations in plasma, in patients who underwent an elective knee arthroscopy [266]. Similarly, Minichmayr et al. demonstrated high distribution of linezolid into muscle tissue in healthy volunteers and septic patients ($TF_{plasma \rightarrow ISF\ muscle}$: 98.0%; [256]). While this study revealed high tissue penetration also for adipose tissue in the two subpopulations ($TF_{plasma \rightarrow ISF\ adipose}$: 102%), diminished linezolid penetration into adipose tissue for an overweight diabetic population was indicated ($TF_{plasma \rightarrow ISF\ adipose}$: 74.0%). The high proportion of morbidly obese patients in the present study population might explain the reduced linezolid distribution into ISF of s.c. adipose tissue observed in the present study. This is also supported by an investigation by Stein et al., that identified an even lower mean ratio of 51% between linezolid concentrations in plasma and in the s.c. adipose tissue for a diabetic population (mean body weight: 98 kg; [267]). Yet, in that study tissue concentrations were determined in homogenised tissue biopsy samples (i.e. homogenised ISF, adipocytes, blood vessels), which might have lowered the observed linezolid concentrations, given the low accumulation of linezolid in cells [268] i.e. adipocytes.

Overall, in contrast to other antiinfective drugs for which target site exposure has been shown to

be similar to plasma exposure [269,270], linezolid target site exposure in obese and nonobese patients was found to be considerably lower than linezolid exposure in plasma and the distribution of linezolid from plasma to target site was delayed.

Obese versus nonobese: Impact of body size on linezolid PK. The covariate analysis revealed that linezolid tissue fluid distribution was impaired by the obesity status of the patient, with obese patients tending to show lower magnitudes of linezolid concentrations in the ISF of the s.c. adipose tissue than nonobese patients. In the NLME model this was captured by a considerably lower TF for obese patients (~54% vs. 69% for nonobese patients; Table 3.2). This appears plausible, considering that obese patients typically show a reduced peripheral perfusion of the s.c. adipose tissue, as the density of capillary vessels decreases with increasing mass of adipose tissue [90,271]. In line with the findings of previous investigations of linezolid PK in obese patients [257,272], the comprehensive stepwise covariate analysis further demonstrated an impact of body size on both volume of distribution parameters (i.e. V_1 and V_2) as well as on the intercompartmental exchange between the central and the peripheral compartment (i.e. Q). More concretely, LBW was identified as most appropriate predictor, implemented according to the principle of allometry [204]. The adequacy of LBW as size descriptor was verified by a mechanistic implementation of body size into the NLME model proposed by Huisinga et al. [210] and Holford et al. [204] (Eq. 2.37, Eq. 2.38, respectively). This approach aims to define appropriate body size descriptors based on the available information on drug PK and body size of the patient. Concretely, within the NLME model, the body size descriptor impacting a specific PK parameter is defined as a composition of LBW and FM and the proportions of the two measures are estimated. This body size descriptor is drug-specific and also PK parameter-specific, i.e. the physicochemical properties of the drug impact the proportions as well as the type of PK parameter (biological structure parameter (e.g. V) or function parameter (e.g. CL) [204]). In the present analyses, for none of the investigated linezolid PK parameters this estimated body size descriptor was superior to LBW alone, suggesting LBW as an appropriate body size descriptor to scale the PK parameters of linezolid. This was supported by the marked reduction in the interindividual variability of the respective PK parameters, e.g. in the final NLME model interindividual variability in V_2 was reduced by ~70% compared to the base model (Section 3.1.2.2). The magnitude of the volume of distribution (when transformed from the unbound to the total linezolid concentration scale) of 45.7 L (for a typical male subject: WT=70 kg, LBW=55 kg, HT=1.75 m [273]) was in line with prior clinical investigations (e.g. V=46 L/45.4 L after single/multiple i.v. dosing of 625 mg linezolid in healthy adults [274], V=42.6 L after multiple p.o. and i.v. dosing of 600 mg q12h, for WT=69.5 kg [256]). Given the identified LBW-PK parameter relationships, on the exposure level, LBW mainly impacted the maximum linezolid concentrations and the concentrations in the early declining phase of the concentration-time profile in such a way, that higher LBW resulted in lower linezolid concentrations and a steeper initial decline (Figure 3.6). Yet, the impact of LBW on the terminal

concentrations was less pronounced and the relationship inverse, i.e. higher LBW resulted in higher terminal linezolid concentrations. This observation can be explained by the increase in half-life of linezolid resulting from the increase in both volumes of distribution as consequence of the increase in LBW.

Of note, for linezolid clearance no impact of body size was detectable, but rather the opposite was observed: The inclusion of any body size descriptor reduced the model predictivity and increased the variability in linezolid clearance (Appendix Table S6). From the perspective of allometry, an increase in clearance would have been expected for obese patients, when assuming an increase in the size of eliminating organs and an increased renal blood flow associated with obesity [90]. However, comorbidities in the obese patients (e.g. diabetic nephropathy) might have also led to an opposite impact, i.e. resulting in a reduced excretion of linezolid in obese patients [90], which has already been indicated by Minichmayr et al. who detected a lower linezolid clearance in a diabetic subpopulation compared to healthy volunteers and other patient groups (septic patients, cystic fibrosis patients [256]). On the basis of the present dataset, a first analysis assessed a combined impact of LBW according to allometric principles with an empirical counteractive impact of FM on linezolid clearance – an approach which has been suggested by Holford et al. [204,275] (Appendix Table S5: Steps 4I and 4J). This approach assumed a decrease in linezolid clearance with increasing FM; yet, did not improve model predictivity. It needs to be kept in mind that this approach is limited in such a way that it assumes a direct link between FM and the occurrence of comorbidities reducing the excretion of linezolid, which may not necessarily hold true. Future investigations, focusing on the evaluation of comorbidities of the patients, might allow to adequately capture both impact factors and relationships and might help to better understand the impact of obesity on linezolid clearance.

Linezolid clearance. On the basis of clinical linezolid PK data, different empirical clearance models have been described before. The clearance models published, cover linear [261,276–284,266,285,286,257,287–289] and nonlinear clearance models, the latter depending on linezolid concentrations (Michaelis Menten [290,248,291–293]) or on linezolid concentration and additionally on time of treatment (empirical inhibition compartment [45,146,272,294]). The variety of detected clearance models is likely to be explained by the differences in the underlying datasets which might (not) have supported the identification of nonlinearity models (e.g. due to richness of data in terminal phase of the concentration-time profile, data on single/multiple dosing). Additionally, not all authors even investigated nonlinear clearance models and might thus have missed to detect a potential nonlinearity in linezolid elimination. In the present work, the exploratory graphical data analysis already demonstrated an increase in the steepness of the decline in the terminal phase of the linezolid plasma concentration-time profile (Figure 3.2 B), which provided strong evidence for a nonlinearity in linezolid clearance. Considering that this observed nonlinearity tended to occur at similar concentrations in the individual concentration-time profiles

but, at the same time, at the end of the anaesthesia, two possibly adequate clearance models were identified. In line with previously published models for linezolid [290,248,291,292], one of the two models comprised a parallel linear and nonlinear Michaelis Menten implementation of clearance, i.e. one proportion of the clearance was considered constant, the other proportion changed depending on the linezolid concentration. In the second model, linezolid clearance was independent of linezolid concentrations but was impacted by the anaesthesia status of the patient: While a reduced and constant clearance was assumed in the intra-anaesthetic period, an increase of clearance according to an E_{max} model was identified after the end of anaesthesia. Of note, also additional described nonlinearity models for linezolid clearance were assessed based on the plasma data, however, were found to be clearly inferior (Michaelis Menten model) to the two favourite clearance models described above or not supported by the available single dose data (empirical inhibition compartment, Appendix Figure S14, which should be considered for long-term microdialysis data).

Anaesthesia has previously been discussed to impact drug metabolism and excretion by altering the drug transport to eliminating organs or by impacting enzymes involved in drug metabolism [97,98]. More precisely, anaesthesia-related haemodynamic changes such as decrease in cardiac output, heart rate and blood pressure, might lead to a reduced blood flow into the periphery and to vital organs, which again results in a reduced transport of drugs to the eliminating organs (e.g. liver and kidney) and thus a reduced elimination [98]. Furthermore, during anaesthesia the delivery of oxygen to the organs may be reduced, considering the impaired organ blood flow and impaired capacity of the blood to carry oxygen [98,295]. As Phase I enzymes, especially the ones involved in oxidative metabolic processes are susceptible to small changes in oxygen tensions, reduced hepatic oxygen delivery might also hamper drug metabolism [295]. Also, mitochondrial function has been described as susceptible to mild hypoxic changes. Considering these discussions about the impact of anaesthesia on drug metabolism and excretion, and given the improved model predictivity after implementing its impact on model parameters, it seems likely that linezolid elimination was altered by anaesthesia in the present study. Firstly, as linezolid is partly excreted as parent substance via the urine, the relatively low median MAP observed in the present patient population during anaesthesia might have led to a reduced intra-anaesthetic renal excretion of linezolid (median MAP intra-anaesthetic 72.7 mmHg; Table 3.1), [144]. As an example, for cefazolin, an antibiotic drug which is largely excreted via the kidneys, a reduction in clearance by nearly 50% during surgery was demonstrated when compared with pre- and post-surgery clearance [296]. Secondly, it also appears likely that the nonrenal clearance of linezolid via oxidation was reduced by anaesthesia-related changes in metabolism and excretion. Nevertheless, to formulate hypotheses on the potential impact of anaesthesia on the nonrenal pathway of linezolid, future *in vitro* studies are needed to better understand and characterise the metabolism pathways of linezolid. Integrating all available information in the assessment of an adequate nonlinearity model for

linezolid elimination in the present surgical patient population, a combination of the previously described parallel linear and nonlinear Michaelis Menten model including an additional impact of anaesthesia was most suitable. In order to achieve this, the parallel linear and nonlinear Michalis Menten model was implemented in the structural base model and a subsequent covariate analysis in the NLME model allowed to describe and quantify the additional impact of anaesthesia. Besides the anaesthesia status also haemodynamic markers (e.g. heart rate, MAP, estimated CO) were assessed as potential impact factors on linezolid clearance. The final NLME model included in addition to the parallel linear and nonlinear Michaelis Menten clearance, the longitudinally monitored marker MAP as determinant of total linezolid clearance, which – in comparison to the binary marker anaesthesia status – contained time-varying information on the haemodynamic changes. The implementation of MAP on the total linezolid clearance indicated that both the linear and the nonlinear clearance of linezolid were impacted by hamedoynamic changes. Unexplained interindividual variability in the clearance-related parameter (i.e. CL and K_m), considerably reduced in the final NLME model including the covariates compared to the base NLME model (IIV_{Var}: CL -50.5%, K_m: -39.9%; Section 3.1.2.2).

As discussed in the section above, the impact of different body size descriptors on linezolid clearance was comprehensively investigated during covariate model development as well; yet, no relationship was identifiable. Nevertheless, given the MAP-linezolid CL relationship, obese patients tended to show slightly higher CL values, due to their higher MAP values (median MAP: 76.7 vs. 72.5 mmHg for obese and nonobese patient, respectively; Table 3.1). Altered haemodynamics have been described for obese patients in literature before [91]: For instance, a recent study that compared haemodynamic patterns in obese and nonobese patients, demonstrated increased magnitudes of haemodynamic markers in the obese population (normal weight/obesity: mean systolic arterial pressure 133/142 mmHg, mean CO 5.2/6.7 L/min; [93]). Furthermore, in the present analysis no relationship between $CLCR_{CG}$ and linezolid CL was detected, although previous clinical PK studies suggested the renal function marker as determinant of linezolid CL [45,276,278,279,281,248,297]. In this context Minichmayr et al. pointed out, that the clinical PK studies which identified a significant relationship between $CLCR_{CG}$ and linezolid clearance, were almost exclusively based on multiple dosing data [256]. The availability of solely single dose data – as it was the case in the present study - might hinder the detection of the relationship [256]. Moreover, the observed distribution of $CLCR_{CG}$ in the present population (covering moderately impaired up to normal renal function; 90%CI: 38.0-105 mL/min) might have additionally hindered the detection of a significant impact of $CLCR_{CG}$ on clearance.

In the final NLME PK model the unexplained variability in the clearance parameters was considerably reduced compared to the base model (IIV_{Var} CL and K_m: -50.5% and -38.9%, respectively). Despite the relatively high degree of complexity in the linezolid clearance model, jointly describing the concentration dependency in clearance and the impact of the haemodynamic

changes, the respective parameters were still precisely estimated. Only for the random-effects parameter IIV on the Michaelis Menten constant K_m, the bootstrap indicated a high upper limit of the confidence interval. This indicated that in some bootstrap samples, mainly patients with extreme K_m values were sampled, i.e. patients in whom nonlinear clearance was less relevant at clinically observed linezolid concentrations (i.e. patients that showed only two phases in declining phase of the concentration-time profile; Figure 3.2 B2) or patients in whom nonlinear clearance became already relevant at very low linezolid concentrations (i.e. patients with an additional third steeper phase; Figure 3.2 B2). Moreover, this finding is not surprising considering the limited number of patients (i.e. sample size) underlying the non-parametric bootstrap and keeping in mind that the estimation of a Michaelis Menten model purely based on clinical PK data can oftentimes be challenging [298–300]. The inclusion of a higher number of patients would allow to further inform and thus more precisely estimate the variability in the K_m parameter [299].

The average total clearance of linezolid (7.80 L/h) which was derived based on integration of the observed linezolid clearance-time profiles and transformation from the unbound to the total concentration scale, was of similar magnitude as total clearance values previously described for linezolid in overweight/obese populations (e.g. 7.80 L/h [257], 6.11-8.24 L/h [290], 9.98 L/h [285]). In the developed model, the linear linezolid clearance (2.84 L/h on total scale, Table 3.2) accounted for approximately 36% of the total linezolid clearance. It is notable that this percentage corresponds to what is described for renal clearance (35%). This suggests that the linear clearance might reflect the renal clearance pathway of linezolid. Under this assumption, the nonlinear clearance would consequently reflect the nonrenal elimination of linezolid, i.e. the metabolism via oxidation mechanisms. Yet, future *in vitro* investigations should be performed to better characterise the metabolic pathways, to interpret and verify the plausibility of the nonlinear clearance according to the Michaelis Menten, which suggests a saturable process involved in the linezolid elimination.

Intra- versus post-anaesthetic: Impact of anaesthesia on linezolid PK. In addition to the impact of MAP as a marker for anaesthesia-related haemodynamic changes (see section above), the present analysis revealed an influence of anaesthesia on the tissue fluid distribution of linezolid. This was already indicated by the base model including plasma and micro-/retrodialysis data, which tended to overestimate the microdialysate concentrations in the intra-anaesthetic period and to underestimate the microdialysate concentrations in the post-anaesthetic period as depicted by the undulating pattern in the CWRES versus time plot (Appendix Figure S19 A.1). The inclusion of the anaesthesia status as a covariate on the TF parameter considerably improved the model predictivity (Appendix Figure S19 A.1) and reduced the interindividual variability in the TF by more than half. The TF was 13.6% lower in the intra-anaesthetic period compared to the post-anaesthetic period, which indicated a reduced distribution of linezolid into the ISF of the s.c. adipose tissue during anaesthesia. From a physiological point of view this appears plausible, considering the reduced blood flow to the periphery caused by anaesthesia, which was already

discussed in more detail above. Keeping in mind that the tissue distribution has been quantified based on intra- and post-anaesthetic linezolid PK data, future clinical studies are warranted that in addition to the intra- and post-anaesthetic data also determine pre-anaesthetic linezolid PK data in obese and non-obese patients. Similar tissue distribution in the pre- and post-anaesthetic period would even broaden the applicability of the developed NLME model towards translation of the PK to the non-surgical setting.

Conclusion and perspectives. Based on the unique dataset comprising total and unbound plasma linezolid concentration and target site concentration data of linezolid originating from obese and nonobese surgical patients, for the first time a joint NLME model was developed simultaneously describing PK- and microdialysis methodology-related aspects, plasma (total and unbound linezolid concentration) and target site PK as well as the impact of body size and anaesthesia on the PK of linezolid. This novel model improves the understanding of the PK of linezolid in obese and nonobese surgical patients:

- Firstly, target site exposure of linezolid was found to be considerably lower than in plasma and the distribution of linezolid from plasma to target site delayed.
- Secondly, LBW, which was generally higher for obese patients, was identified as a vital determinant for the PK of linezolid. On top of that, an additional effect of obesity on tissue fluid distribution was observed, i.e. an effect not directly linked to body mass, but likely to be a surrogate for other not available covariates. Both impacts resulted in a lower linezolid exposure in obese patients compared to nonobese patients, which was particularly pronounced at the target site.
- Thirdly, an impact of anaesthesia and the related haemodynamic changes on linezolid clearance and tissue fluid distribution was detected and quantified, with reduced linezolid clearance and tissue fluid distribution during the intra-anaesthetic period.

Future studies are warranted that assess whether the observed PK characteristics and influential factors determined in the present non-ICU population also hold true for special patient populations such as critically ill patients, for which linezolid plays a vital role in the treatment of severe infections. In light of the known haemodynamic variations in ICU patients, for instance due to pathophysiological causes (e.g. sepsis [103]), sedation therapy [301]), a reassessment of the finding of the present work may also be of value for the ICU population. Furthermore, the development of similar types of NLME models and/or even combined NLME models based on the PK data available for the additional drugs investigated in the clinical study [226] might help to further characterise the impact of obesity and anaesthesia on the drug PK and to identify drug-specific differences. For this purpose, the proposed NLME model development strategy (Section 2.6.4.2; including the implementation of different levels of microdialysis methodology-related variability, the mechanistic implementation of body size as covariate etc.) forms a versatile basis.

4.1.2 Evaluation and optimisation of linezolid dosing in obese and nonobese surgical patients (Project II)

The NLME PK model of linezolid developed in Project I enabled the evaluation and optimisation of linezolid dosing in obese and nonobese surgical patients by the use of PTA analyses (Project II). A first application of the model focused on the evaluation of the adequacy of standard linezolid dosing for perioperative infection prophylaxis in abdominal surgery, which corresponds to the study design on which the developed NLME PK model was based. In a second step, the model was used to extrapolate to the treatment of an acute infection, i.e. a clinically more frequently observed setting.

Selection of PK/PD target for infection prophylaxis. PK/PD target values for linezolid have been derived based on acute infection therapy [149–152], but no targets exist for infection prophylaxis. Yet, different national and international guidelines on perioperative antibiotic prophylaxis highlight the importance of adequate antibiotic exposure in the surgical area (i.e. the target site) during the period of potential contamination, i.e. from the time of incision until the time of suture [302–304]. The 'Clinical practice guidelines for antimicrobial prophylaxis in surgery' from the American Society of Health-System Pharmacists (ASHP) further specifies that the drug concentrations in serum and tissue should exceed the MIC of a probable pathogen associated with the surgery during the duration of the surgical intervention [303]. According to these recommendations, a strict PK/PD target of 100%$fT_{>MIC}$ for evaluation of antibiotic target site exposure is deemed reasonable in order to assess the adequacy of antibiotic dosing in the setting of perioperative infection prophylaxis. This was deemed reasonable considering that even the available $T_{>MIC}$ targets for linezolid treatment of acute infections, which were notably determined based on plasma PK data, were of similar magnitude (e.g. $fT_{>MIC}$ 100% [149]; Section 1.4.2.1 PK/PD targets). Considering the observed delayed distribution of linezolid to target site (i.e. ISF of the s.c. adipose tissue; Section 3.1.3), the target 95%$fT_{>MIC}$ was selected, in order to allow classifying patients that achieved the target MIC during nearly the full incision-suture duration (e.g. 99.0%) as 'effectively treated' rather than 'ineffectively treated'. Three different incision-suture durations of 2 h, 4 h, and 6 h were selected for PTA evaluation, capturing the time periods observed in the present study ($P_{0.05}$-$P_{0.95}$: 2.38-3.57) as well as typical time periods of bariatric surgery, generally not exceeding 4 h [255,305]. As mentioned above, adequate antibiotic exposure is recommended with respect to MIC values of pathogens which are likely to be associated with the surgery type [303]. The pathogens that are reported to most frequently cause postoperative wound infections in bariatric surgeries are *S. aureus*, *Enterococcus* spp. and α-haemolytic *Streptococcus* spp. [306,307]. Based on the information on the MIC distributions of these pathogens, the MIC values of 4 mg/L and 2 mg/L were selected, representing EUCAST MIC R and S breakpoints of the respective pathogens (R/S [mg/L]: *S. aureus* 4/4, *Enterococcus* spp. 4/4,

Streptococcus spp. 2/4 [5]). For comparison also two more susceptible MIC values were selected (1 mg/L and 0.5 mg/L).

PTA analysis for infection prophylaxis. Although linezolid is not frequently used for infection prophylaxis in clinical routine, the PTA analysis in obese surgical patients was deemed valuable considering the following aspects which are also emphasised in current guidelines on perioperative infection prophylaxis [303]: First, in the setting of preoperative infection prophylaxis, the obese patient population is regarded as a highly vulnerable patient group, considering the increased incidence of postoperative wound infections and at the same time the associated severity of these complications. Secondly, PK information on antibiotic target site exposure is limited for the obese surgical population and the suitability of standard antibiotic dosing remains unclear. The NLME PK model for plasma and target site (Section 3.1.2.2), together with the PK/PD targets elucidated above, enabled the assessment of linezolid exposure directly at the surgical site at risk of potential contamination (i.e. target site) in obese and nonobese patients undergoing abdominal surgery. For the typical obese and nonobese patient of the present patient population, the PTA analysis suggested that a single standard linezolid dose is likely to result in effective target site exposure (i.e. PTA≥90%) for pathogens with MIC up to 1 mg/L for incision-suture durations up to 6 h. However, for pathogens with a MIC value of 2 mg/L only in case of short incision-suture durations (up 2 h and 4 h for typical obese and nonobese typical patient) effective exposure was reached; for a MIC value of 4 mg/L, for none of the incision-suture durations standard linezolid dosing seemed effective (Table 3.3). Given that bariatric surgeries are typically of rather short duration (<4 h [255,305]), for MIC values up to 2 mg/L standard linezolid dosing for infection prophylaxis is relatively likely to result in a sufficient prophylactic effect in a typical obese patient undergoing bariatric surgery. Thus, for *S. aureus* which is reportedly the most frequent pathogen for surgical site infections in bariatric surgeries [303,307], the methicillin-sensitive isolates (MSSA) are likely to be covered, but not the methicillin-resistant isolates (MRSA) (MIC_{90}: 2 mg/L and 4 mg/L, respectively; derived based on EUCAST MIC distributions [132]).

Comparing the PTA for obese and nonobese patients, the typical obese patient was found to show lower PTA values than the typical nonobese patients. It needs to be kept in mind that the simulations focused on the two typical study patients who did not solely differ in body size, but also in their haemodynamic patterns, with the typical obese patient showing slightly higher MAP values than the typical nonobese patient (median $MAP_{intra\text{-}anaesthetic}$: 71.7 vs. 66.7 mmHg, respectively; Table 2.4). Despite the positive relation between MAP and the total clearance of linezolid, the impact of the MAP on the PTA at the target site, however, is likely to be low, considering that the exposure simulations for different MAP values showed only little impact on the declining phase of concentration-time profile at the target site (Figure 3.5 C).

To better characterise the sole impact of body size on the attainment of effective linezolid exposure at the target site, PTA analyses were performed for varying body size (i.e. varying values of the

identified covariate LBW), but constant MAP. The analysis indicated a decline in the PTA with increasing body size of the patient. This can be explained by the implementation of LBW and obesity in the NLME model (Section 3.1.2.2): (i) an increase in LBW resulted in an increase in the volume of distribution which led to decline in linezolid concentrations especially in the maximum and the early declining phase of the linezolid concentration-time; (ii) the presence of obesity further reduced the exposure at the target site by its impact on the TF profile (Figure 3.6 B). Consequently, linezolid target site exposure was lower in obese than in nonobese patients at the time points of interest (2/4/6 h after start of incision, i.e. 2.5/4.5/6.5 h after start of linezolid infusion; Figure 3.7). The overall conclusions with respect to adequacy of standard linezolid dosing in the setting of infection prophylaxis were similar as for the typical obese and nonobese patients: While for susceptible MIC values up to 1 mg/L dosing seemed effective, for a MIC value of 4 mg/L dosing seemed ineffective across the full LBW range. For the MIC value of 2 mg/L, only for the short incision-suture durations and low LBW values, standard dosing was likely to show effective antibiotic exposure.

Conclusion and perspectives for infection prophylaxis. For the study drug linezolid, the present analysis indicated that single standard linezolid dosing for perioperative infection prophylaxis is likely to show effective antibiotic exposure for a prophylactic effect in obese patients undergoing bariatric surgery, in case of infecting susceptible pathogens. Yet, if aiming at prophylactically covering pathogens with reduced susceptibility, intensified dosing might be required to reliably attain effective exposure at the target site.

In line with the recommendations by different national and international guidelines on perioperative antibiotic prophylaxis, the present PTA analysis was based on the PK/PD index $T_{>MIC}$ (target 95%$fT_{>MIC}$). The PK/PD index AUC/MIC, which has been suggested for linezolid before based on data of acute infection therapy, was not deemed adequate for the setting of infection prophylaxis. Future research on target site specific PK/PD targets for infection prophylaxis is highly warranted. In this regard, complementary to clinical investigations, *in silico* investigations – as has been proposed for acute infection therapy by Minichmayr et al [256] – could provide a valuable approach: The developed NLME PK model could be linked to a semi-mechanistic PD model describing the bacterial growth/death of a relevant pathogen (e.g. *S. aureus*) resulting from linezolid target site exposure, which could ultimately be used to simulate dose fractionating studies in order to derive target site specific PK/PD targets [256].

Furthermore, based on the developed NLME PK model a next simulation study could focus on assessing the impact of haemodynamic changes during surgery on the linezolid PK and the respective impact on the PTA at the target site. Additional simulation studies could assess and further optimise the timing of linezolid infusion with respect to the incision time. Deterministic exposure simulations already indicated that linezolid target site concentrations – even though showing a relatively steep initial increase (Figure 3.6 B) – were only reaching the MIC values of

interest after 30 min, i.e. the typical time observed between start of antibiotic infusion and surgical cut in the present study. Considering the PK variability between the patients (Figure 3.7), an earlier initiation of linezolid treatment with respect to incision time might further improve the attainment of the PK/PD target in some patients and thus enhance the PTA. Overall, similar PTA analyses are warranted for the additional antibiotic drugs which were assessed in the clinical study, especially the antibiotics that are more frequently used for perioperative infection prophylaxis (e.g. cefazolin).

PTA analysis for acute therapy. Keeping in mind that linezolid is rarely used for perioperative infection prophylaxis, a second application of the NLME PK model focused on the evaluation of linezolid dosing for the clinically highly relevant treatment of acute infection. For this purpose, the model was used to predict linezolid concentrations in plasma and at the target site following multiple standard linezolid dosing in the initial phase of treatment, i.e. the first 24 h. Because a large amount of PK data underlying the model development was collected during intra-anaesthetic period, all PTA analyses for the acute therapy were performed for intra-anaesthetic patients, which could represent patients in medically induced coma as frequently encountered at the ICU [308]. As for infection prophylaxis, the PK/PD target 95%$fT_{>MIC}$ was selected, which is in line with previously derived $T_{>MIC}$ targets for linezolid treatment (e.g. $fT_{>MIC}$ 100% [149]; Section 1.4.2.1 PK/PD targets). Again, the PTA was assessed for linezolid exposure in the ISF of the s.c. adipose tissue, representing a potential target site of a skin and soft tissue infection [132]. In addition to target site assessment, the PTA was analysed for plasma in order to evaluate the adequacy of linezolid standard dosing to prevent a spread of the pathogen from the site of infection via the blood circulation. Note that in contrast to the infection prophylaxis, in which the attainment of the PK/PD target was assessed for a short time period (i.e. incision-suture duration), in acute infection therapy, target attainment was evaluated over the full 24 h.

Overall, the results of the PTA analysis suggested that standard linezolid dosing is likely to result in ineffective exposure (i.e. PTA<90%) at the target site and even also in plasma for most of the investigated pathogen-patient combinations (Figure 3.9). In plasma, standard linezolid dosing achieved effective exposure (i.e. PTA≥90%) only for the lowest investigated MIC value (0.5 mg/L) in combination with a higher LBW value (>35 kg). Similar results were obtained by Minichmayr et al., who investigated the PTA for standard linezolid dosing in plasma and in the ISF of s.c. adipose tissue for a septic population with varying renal function, yet for the AUC/MIC index in plasma [45,256]: For a $CLCR_{CG}$ value of 63.8 mL/min, which is in line with the median renal function in the present population (Table 3.1), Minichmayr et al. demonstrated adequate PTA only for MIC values ≤0.25 mg/L and ≤1 mg/L in ISF and plasma, respectively. Furthermore, a recent clinical investigation by Cojutti et al. focused on the assessment of linezolid dosing in an overweight/obese population, however, based on plasma PK data only and using the AUC/MIC index [290]: For standard linezolid dosing all investigated patient groups reliably attained the PK/PD target only for a MIC of 0.5 mg/L. Taken together, the findings of the previous

investigations and the present work suggest that standard linezolid dosing is only effective in highly susceptible pathogens, especially when aiming to target pathogens located in the ISF of the s.c. adipose tissue.

In view of these findings, seven alternative dosing regimens with intensified doses and/or prolonged infusion duration and/or shortened dosing interval were assessed (Table 2.5). In particular the increase of the linezolid daily dose by 1.5- to 2-fold was found to enhance the PTA (Section 3.2.2.1). Although assessing intensified linezolid doses which were up to twice as high as the approved linezolid dose (e.g. 2400 mg per day), effective exposure (i.e. PTA≥90%) for the full LBW range was only attained for MIC values up to 2 mg/L or 1 mg/L for plasma and ISF, respectively. It is worth noting that none of the regimens led to effective exposure for MIC=4 mg/L and MIC≥2 mg/L in plasma and ISF, respectively. Minichmayr et al., who assessed two additional alternative dosing regimens (front loading with 1200 mg before standard dosing; 1200 mg q24h following a single dose of 600 mg; [45,256]), similarly described that even for the alternative dosing regimens an achievement of adequate PTA was unlikely for both matrices for MIC>4 mg/L. In general, also the prolongation of the infusion duration from 30 min to 4 h improved the PTA (Section 3.2.2.2) In some scenarios, however, PTA was lower for the prolonged than for the corresponding short-term infusion regimen (e.g. for scenarios with higher MIC values and/or high LBW values and particularly in ISF). In these scenarios the prolongation of the infusion duration resulted in relevant time periods in which linezolid concentrations were lower than the respective MIC value in the initial phase of the concentration-time profile (Appendix Figure S22), which in turn resulted in linezolid concentrations not exceeding the MIC value for the targeted 95% of the 24 h. The findings suggest that a frontloading prior to start of prolonged linezolid dosing, either with an intensified loading dose and/or with a short-term infusion regimen may be beneficial. A future simulation study based on the developed NLME PK model, could assess the impact of different types of frontloading on the PTA for varying MIC values and varying body size. The impact of shorting the dosing interval on the PTA was investigated for the daily dose of 1800 mg, by administering either every 12 h a linezolid dose of 900 mg or every 8 h a linezolid dose of 600 mg. In general, shortening of the dosing interval improved the PTA (Section 3.2.2.3). However, in some scenarios (e.g. for higher MIC values and/or high LBW values and particularly in ISF), the reduced linezolid dose which was administered every 8 h, resulted in relevant time periods in which linezolid concentrations were lower than the respective MIC value. This explains why in some of the investigated scenarios, lower PTA was observed for the q8h regimen than for the corresponding q12h regimen.

Overall, of the three investigated dosing alterations (intensification of daily dose, prolongation of infusion duration and shortening of dosing interval), the increase of the daily dose showed the strongest impact on the attainment of adequate PTA. Furthermore, the increase in daily dose

consistently resulted in an improvement in PTA, while for the prolongation of the infusion duration or the shortening of the dosing interval, in a few investigated scenarios (especially for higher MIC values and/or high LBW values and/or in ISF) the alterations of the dosing resulted in a reduction of the PTA.

The impact of LBW on the PTA (Section 3.2.2.4) was highly dependent on the MIC value and various determinants of linezolid exposure, namely, the LBW value, the matrix of interest (i.e. plasma, ISF) and the type of dosing regimen (daily dose, infusion duration, dosing interval). As discussed above, an increase in LBW led to reduced linezolid concentrations in the maximum and early declining part of the concentration-time profile. At the same time, however, the increase in LBW resulted in a slower decline of the linezolid concentrations at the end of the dosing interval, due the higher volume of distribution and thus the increase in half-life. As a result, in various investigated scenarios, the linezolid concentrations for a high LBW value exceeded the linezolid concentrations for a low LBW value after the intersection of the respective concentration-time profiles (point of intersection) in the terminal phase of the concentration-time profiles (Appendix Figure S22). Depending on the magnitude of the MIC value relative to linezolid concentration at the point of intersection (C_{Int}), the time that linezolid concentrations exceeded the MIC value was higher for a low LBW value (if MIC>C_{Int}) or for a high LBW value (if MIC<C_{Int}). This explains why overall for lower MIC values and/or lower LBW values a positive LBW-PTA relationship was detected (i.e. an increase in LBW improved the PTA), while for higher MIC values and/or higher LBW values a negative LBW-PTA relationship was observed (i.e. an increase in LBW reduced the PTA).

Assumptions, conclusion and perspectives. Some assumptions and limitations have to be acknowledged with respect to the PTA analyses performed for acute infection therapy. Firstly, the NLME PK model which was developed based on the single dose PK data over 8 h, was used to extrapolate to multiple linezolid dosing over 24 h, i.e. the underlying PK of linezolid was assumed to be the same for single and multiple dosing. This assumption seems justified as a previous analysis showed a relevant change of linezolid CL over time only after several days of treatment, while in the present analysis only a short time frame of 24 h was assessed [146,230]. Further PK data originating from similar patients (i.e. obese/nonobese surgical patients) treated with multiple linezolid dosing over a longer time period could confirm this assumption. Secondly, extrapolating to higher doses might be compromised by the fact that a partly nonlinear concentration-dependent CL was observed. The CL model should be confirmed by assessing the predictivity for high-exposure data originating from intensified linezolid dosing regimens. Thirdly, PTA analyses were based on the PK/PD target 95%$fT_{>MIC}$ which has previously been shown to correlate with the efficacy of linezolid in animal models and in clinical investigations [149,153]. Yet, also the PK/PD index AUC/MIC has been identified for linezolid before [150,151,153]. Future PTA analysis should be performed using the developed model for the *f*AUC/MIC target in order to assess whether

similar results are obtained as for the $fT_{>MIC}$ target. Considering that overall similar results were obtained by others [45,290,256] who used AUC/MIC targets for plasma PK data, the general conclusion is expected to stay the same. Nevertheless, the relationship between LBW on the PTA might differ, as a different PK measure (AUC) is evaluated. Fourthly, the PTA analyses for acute infection therapy were performed for intra-anaesthetic patients, i.e. the results are not directly transferable to patients not receiving anaesthesia. The NLME model which is based on intra- and post-anaesthetic linezolid PK data could be expanded by PK data originating from patients without anaesthesia. This would not only allow to perform PTA analysis also for non-anaesthetic patients, but additionally provide further information on the PK differences between a non-anaesthetic and a post-anaesthetic patient, as well as on the impact of anaesthesia on the PK.

Despite the aforementioned assumptions and limitations, the PTA analysis based on the NLME PK model for plasma and target site in obese and nonobese surgical patients, allowed to draw conclusions for the adequacy of linezolid dosing in acute infection treatment. Overall, the results of the analysis suggested that already for susceptible pathogens, standard linezolid dosing is unlikely to result in effective exposure for infections located in the s.c. adipose tissue and also to prevent the spread of pathogens via blood circulation. Dosing intensification might be beneficial; however, for pathogens with reduced susceptibility (e.g. MRSA) very high doses seem to be required, which bare the risk of increased toxicity. As outlined above, future PTA analyses for dosing regimens combining frontloading followed by prolonged infusion, would allow to detect and quantify the impact and added value of the frontloading on the PTA and to potentially suggest appropriate frontloading schemes. Future clinical studies are warranted to simultaneously assess the efficacy and toxicity of intensified linezolid dosing regimens. Given the complex relationships discussed above between PTA and the body size of the patient, which are determined by various influencing factors (MIC, LBW, dosing regimen and matrix of interest), the use of the NLME PK model – after successful clinical evaluation – would be beneficial to determine an appropriate dosing regimen for a given patient. In order to facilitate the application in a clinical setting, the model could be implemented in a dosing software (e.g. TDMx [309]), which could ultimately support therapeutic decisions by health-care professionals.

4.2 Leveraging pharmacometric approaches to characterise variability in the microdialysis sampling technique (Project I)

The present thesis illustrated that pharmacometric modelling and simulation approaches do not only provide a powerful tool to enhance the knowledge on the pharmacokinetics of antibiotic drugs in special patient populations, but can also be successfully employed to evaluate and quantify different types of variability in the microdialysis sampling method based on clinical data collected

using this technique (Project I; research category: basic research; Figure 4.1).

In the last three decades microdialysis has become an important technique to gain a better understanding of unbound drug concentrations in ISF of the target tissue, which represent the actual drivers of the drug effect and thus provide highly valuable information. [60]. To reliably quantify the drug concentrations in the target tissue, *in vivo* calibration of each microdialysis catheter is crucial [65,310]. Today retrodialysis is the most frequently used calibration technique in the clinical setting and was also applied in the clinical study underlying Project I. The retrodialysis calibration provides a RR value, which can be used to convert the drug concentrations quantified using the microdialysis technique, into the ISF concentrations of the target tissue [65,310]. Previous studies have identified multiple factors influencing the RR value (flow rate, semipermeable membrane of catheter, drug characteristics, catheter-surrounding tissue etc. [65,66]); however a model-based systematic *in vivo* investigation of different levels of variability in the RR value is still lacking. To provide a better understanding of the variability in the microdialysis technique an informative unique dataset had been collected in the study underlying Project I, containing information on various levels of variability (Figure 4.2): (i) data originating from the retrodialysis, which was performed twice for a large portion of the catheters, containing information on the variability within one catheter between two consecutive retrodialysis samplings (in the thesis referred to as 'intracatheter variability'; illustrated in Figure 4.2 by two vials), (ii) data originating from two catheters that were identical in construction and were inserted in the same type of tissue of the same patient, containing information on the variability between two inserted catheters (in the thesis referred to as 'intercatheter variability'; illustrated in Figure 4.2 by two microdialysis systems), and (iii) data originating from microdialysis experiments performed in a variety of patients, containing information on the variability between the patients (in the thesis referred to as 'interindividual variability'; illustrated in Figure 4.2 by 30 patients). The NLME modelling approach allowed to dissect and quantify different hierarchical levels of variability by including additional random-effects parameters on the fixed-effects parameter RR, which were estimated within the integrated dialysate-based modelling approach (Figure 4.3).

Intercatheter variability. The analysis revealed moderate intercatheter variability in the RR value (26.1%CV, Figure 4.3). This was expected, considering that firstly, each single catheter – although identical in construction – might show slight variations in membrane surface due to the handmade production process, which might impact the RR value. Secondly, the exact location of the catheter in s.c. adipose tissue might show an additional impact on the resulting RR value. Here, for instance, it might be of relevance whether the semipermeable membrane is inserted close to a capillary vessel, as this might result in a shorter diffusion path of the drug to reach the semipermeable membrane of the microdialysis catheter. *In vivo*, ultrasound can assist positioning the catheter into the tissue of interest [311]. A recent investigation by Burau et al. [249] revealed intercatheter variability in linezolid RR values, although investigated *in vitro* using a standardised microdialysis

system (difference between max. and min. RR values: ≤18.1% RR). Similar findings were also described by other research groups [312,313]. Considering the highly standardised conditions of the *in vitro* experiments, which reduce variability caused by the surrounding medium, the findings from the i*n vitro* investigations illustrated that the catheters themselves are already variable in their determined RR values. Yet, it needs to be kept in mind that the interindividual variability in RR value is not a concern for the resulting ISF drug concentrations, as long as the RR value per catheter is the same during the drug delivery (i.e. retrodialysis setting) and the drug recovery (i.e. microdialysis setting). In other words, variability observed on the level of the RR values might cancel out on the level of ISF drug concentrations, as the ratio of microdialysate concentrations and the RR value of a catheter, determines the resulting ISF exposure. However, this requires an *in vivo* calibration of each single catheter. Nevertheless, dissecting and quantifying the intercatheter variability within the NLME model is crucial, as otherwise the variability will show up on other random-effects parameters and lead to inflated magnitudes of the corresponding variabilities. To further dissect the observed intercatheter variability into variability caused by the catheter itself and variability caused by the exact location of the catheter in the tissue, future *in vitro* investigations could aim at systematically investigating variabilities between the catheters. The results could ultimately inform the NLME model about the magnitude of variability caused by the catheter.

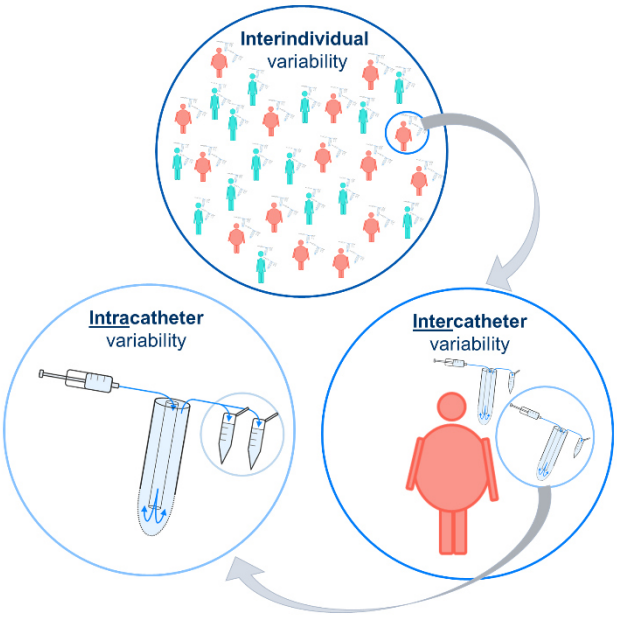

Figure 4.2: Schematic representation of database of the present clinical microdialysis study informing different levels of variability in the microdialysis technique

Intracatheter variability. On the basis of the two successively performed retrodialysis samplings within one catheter (i.e. retroperfusate/retrodialysate concentrations), intracatheter variability in the RR value was quantified, which was found to be of moderate magnitude (27.2%CV; Figure 4.3). Similar findings were observed by others: For instance Bouw et al. [314] reported already for rats a fluctuation of the RR value over time within each probe. Potential impact factors of the retrodialysis setting on the RR value (e.g. flow rate changes, air in the microdialysis system) were recently investigated for linezolid and other antibiotics by Burau et al. at our department. The analysis revealed that flushing of the microdialysis catheter (i.e. using an increased flow rate) before the performance of retrodialysis might lead to erroneously low RR values. In the present study the catheter was flushed only before the first retrodialysis, but not prior to the second one.

As the observed variability in RR values was random and not due to lower RR values observed during the first retrodialysis, this was not considered as explanation for the present finding. Moreover, the analysis demonstrated that air in the microdialysis system increased the variability in the RR value [249]. Since the perfusate was changed before performance of retrodialysis, an unintended inclusion of air in the microdialysis system might have occurred, potentially causing the observed intracatheter variability. This hypothesis was also supported by the fact that the measured microdialysate concentrations showed a relatively 'smooth' profile over time (i.e. without greater fluctuations), which indicated a low variability in the RR value during microdialysis sampling. In the present analysis, all available retrodialysis data were included in the analysis, to minimise a potential impact of the variable RR values on the converted ISF concentrations. It also needs to be kept in mind that a separation of RUV and intracatheter variability is not possible based on the retrodialysate data , since on the basis of the catheter input (i.e. retroperfusate concentration) and the output of the two catheters (i.e. retrodialysate concentrations) only one level of variability is supported. Thus, in the NLME model the RUV was assumed to be as high as the reported assay imprecision (1.9%CV [249]). This was deemed reasonable as most of the typically discussed sources of RUV for *in vivo* PK data (e.g. erroneous documentation of sampling time point or model misspecification; section 2.3.1.2), are of little relevance in the setting of retrodialysis.

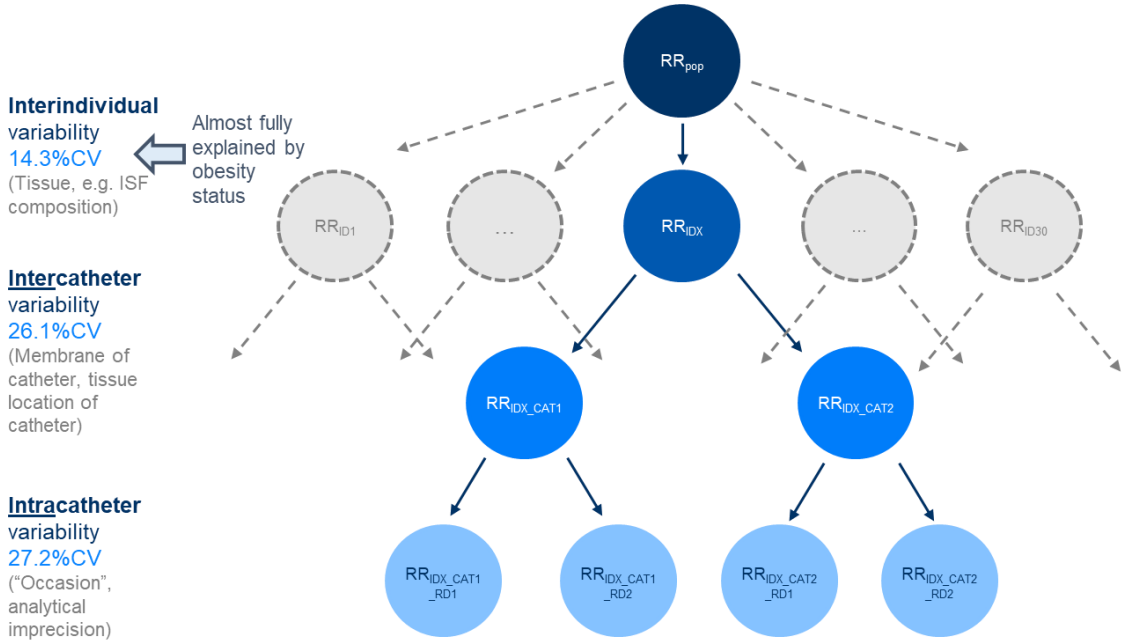

Figure 4.3: Hierarchical structure of three different levels of unexplained variability on the relative recovery parameter.
Level 1: Interpatient variability; *Level 2:* 'Intercatheter' variability; *Level 3:* 'Intracatheter' variability.
Abbreviations: *CAT*: Catheter; *CV*: Coefficient of variation; ID_X: Individual identifier X (e.g. ID_1: Individual identifier 1); *RR*: Relative recovery; RR_{IDX}: RR for ID_X; RR_{IDX_CAT1}: RR_{IDX} for catheter 1; $RR_{IDX\_CAT1\_RD1}$: RR_{IDX_CAT1} determined during first retrodialysis; $RR_{IDX\_CAT1\_RD2}$: RR_{IDX_CAT1} determined during second retrodialysis; RR_{IDX_CAT2}: RR_{IDX} for catheter 2; $RR_{IDX\_CAT2\_RD1}$: RR_{IDX_CAT2} determined during first retrodialysis; $RR_{IDX\_CAT2\_RD2}$: RR_{IDX_CAT2} determined during second retrodialysis; RR_{pop}: Typical RR ('population RR').

In light of the previously discussed hypothesis of air inclusion into the microdialysate system when changing the perfusate, alternative catheter calibration techniques might be assessed. For instance, the so-called 'retrodialysis by calibrator' [60,65,66] - a modified retrodialysis strategy - would not require a change of the perfusate for catheter calibration. Here, a calibrator, ideally the modified study drug (e.g. deuterated drug [315]), is added to the perfusate during the course of the investigations allowing to continuously monitor the RR, which in turn could be implemented in the NLME model. In addition, future analyses shall aim at investigating the variability levels also for the additional drugs measured in this study – considering that for some of the drugs the retrodialysis sampling per catheter was even performed thrice.

Interindividual variability. The use of the NLME approach also allowed to separate and quantify an additional impact of the individual patient on the RR values of the two catheters inserted in the patient which was captured in the interindividual variability parameter and was estimated to be ~14%CV (Figure 4.3) which is relatively low compared to interindividual variability of PK parameters (Table 3.2). Interestingly, when investigating potential factors that explain the observed variability between the patients, the obesity status of the patients was identified as strong impact factor and was found to be superior to continuous body size descriptors such as body weight. The inclusion of the obesity status as dichotomous covariate on the RR parameter almost completely explained the interindividual variability in RR (IIV RR after inclusion of obesity status: 0.3%CV). In obese patients, the typical RR value was considerably lower than in the nonobese population (RR obese vs. nonobese: 37.5% vs. 57.5%). Related supporting findings were described by Lutgers et al. [316] who observed a negative relationship between skinfold thickness of diabetic patients and the RR value of glucose when performing microdialysis in the abdominal adipose tissue. Knowing that the tortuosity of the sampling matrix surrounding the microdialysis catheter influences the RR value [60,65,66], the observed differences in the RR value of obese and nonobese patients might be explained by differences in the structure and/or composition of the s.c. adipose tissue. It is known that the adipocytes in obese patients tend to be hyperplastic (i.e. increased number of cells) and/or hypertrophic (i.e. increased size of the cells) [317]. Moreover, the density of capillary vessels decreases with increasing mass of adipose tissue, which results in a reduced perfusion of the adipose tissue in the obese population [90]. In addition to that, obesity has been found to impair the lymphatic function, more concretely to reduce the interstitial fluid transport as well as the pumping of lymphatic collecting vessels [318–320]. The aforementioned points, together with the 'tighter packed' adipocytes, might cause the reduced RR value in the obese population. Furthermore, differences in the volume and/or composition (e.g. lipids, proteins, electrolytes, pH [321,322]) of the ISF of the s.c. adipose tissue between obese and nonobese patients might be a reason for the observed differences in the RR values, yet, further research is needed. This hypothesis could be addressed by additionally analysing the remaining study drugs [226] with respect to differences in RR between obese and nonobese patients. Beyond that, future

systematic microdialysis *in vitro* investigations in artificial ISF and/or s.c. adipose tissue using a standardised *in vitro* microdialysis system [228,323] could provide valuable knowledge to better understand the clinical finding.

Conclusion and perspectives. Microdialysis is a powerful technique to enhance the understanding of unbound drug concentration-time profiles at the site of therapeutic action; yet, knowledge on variability in the technique *in vivo* has been lacking. The present work systematically investigated and quantified different levels of variability in the RR value based on clinical data using the NLME approach. The quantified inter- and intracatheter variabilities emphasise the importance of individually calibrating every single catheter *in vivo* and the need of special care in placement of the microdialysis catheter (e.g. using ultrasound) and the performance of the micro- and retrodialysis. As a next step, a systematic simulation study, successively including the quantified variability levels in the microdialysis technique, would help to assess their impact on the predicted target site exposure. Furthermore, the proposed approach to dissect and quantify the variability levels using NLME software (e.g. NONMEM®) can be applied for the additional study drugs [226]. This would allow to further evaluate and substantiate the findings for linezolid.

The investigations did not only enhance the understanding of the variabilities in the microdialysis technique but also generated new hypotheses which require future research: For instance, the obesity status of the patient seemed to impact the RR value. To date, differences in adipose tissue, blood flow and lymph function have been described in obese compared to nonobese patients; yet, little is known about the differences in the composition of the ISF in the s.c. adipose tissue. Future *in vitro* investigations should focus on the assessment of these pathophysiological differences and their impact on the RR value to explain the observed impact of obesity on the RR value and/or to derive an even better marker than obesity.

4.3 Leveraging pharmacometric approaches to characterise the pharmacokinetics of meropenem in critically ill patients and to evaluate and optimise dosing (Project III, IV)

By means of pharmacometric approaches, this thesis contributed to a better characterisation of the pharmacokinetics of the betalactam antibiotic meropenem in the vulnerable population of critically ill patients (Project III and IV; research category: basic research; Figure 4.1), identified the patient subgroups at risk for therapy failure when administering standard meropenem dosing (Project III, IV; research category: applied research; Figure 4.1) and suggested optimised dosing regimens (Project IV; research category: applied research; Figure 4.1). The respective results and technical considerations of the modelling and simulation analyses in Project III and IV will jointly be discussed in the following sections.

4.3.1 Characterisation of meropenem pharmacokinetics in critically ill patients (Project III, IV)

The pharmacometric analyses in both projects (Project III: non-compartmental approach; Project IV: compartmental NLME approach) were based on extensively sampled data from a prospective observational study. A large number of patients with highly heterogeneous patient-specific characteristics from different ICUs was included to best represent the diversity in ICU patients [324], though at one single study centre. This clinical study focused on evaluating the PK of the approved and still most frequently used standard meropenem dosing regimens in ICUs (1000 mg administered as 30-min i.v. infusion every 8 h; [325,326]).

Variability in meropenem PK. The analyses demonstrated large interindividual variability in meropenem exposure, in accordance with previous studies in critically ill patients [327,328]. The exploratory analysis in Project III revealed larger variability in concentrations of the late phase compared with the earlier phase of the concentration-time profile (variability in C_{min} and C_{8h} > variability in C_{4h}, Section 3.3.1.3), which suggested that PK variability was due to variability in drug elimination processes rather than in drug distribution. This finding was supported by the NLME PK base model developed in Project IV (Appendix Table S18) as well as previously performed NLME analyses [329,330], that identified larger interindividual variability on the PK parameter clearance compared to variability on volume of distribution. The relatively long observation period of 4 days and the large number of samples collected per patient, additionally enabled the quantification of intraindividual variability in meropenem exposure. Its relatively large value led to the hypothesis that meropenem exposure is influenced by certain time-varying patient-specific factors which was confirmed in the systematic covariate analysis performed in Project IV.

Patient characteristics impacting meropenem PK. To provide further knowledge about patient characteristics (not) impacting the PK of meropenem, in Project IV, a systematic covariate analysis was performed on the basis of 58 available patient characteristics (categorical and continuous, many of them determined longitudinally during study period). In contrast to previous PK studies of meropenem, which typically investigated around 8 covariates (=median, range: 4-15 [327–343]), a high number of pre-selected covariate candidates (n=27) was assessed within the NLME modelling framework. For this purpose, a comprehensive systematic stepwise covariate analysis strategy was set up and applied (Sections 2.9.3.2 and 3.4.2.1). The strategy did not solely base the selection of the covariates on statistically significant improvement of the model (i.e. significant reduction in OFV) but considered additional crucial criteria: Reduction of unexplained variability, precision of the estimate quantifying the covariate effect, clinical relevance and biological plausibility of the covariate effect. Although of importance for reliable covariate selection, today, additional selection criteria are still widely neglected or ignored completely in NLME covariate analyses [207,340,342,344–347]. This is likely to be due to the higher complexity and expenditure

of time for the multi-criteria-based covariate analysis strategy, compared to the OFV-based covariate analysis strategy for which rapid, automated methodologies exist (e.g. *scm* in PsN [209]). The covariate analysis strategy proposed in Project IV may serve as starting point for further NLME analyses; but naturally, requires adjustments depending on the data situation.

Of the 27 preselected patient characteristics, approximately 37% were not selected during forward inclusion of the covariate model building, (e.g. ECMO, lung transplantation, sodium serum concentration etc.; Table S17, Figure 3.16) and were thus considered unlikely to influence the PK of meropenem. At the final step of the analysis, three physiologically plausible covariate-PK parameter relationships fulfilled all covariate selection criteria and were kept in the final NLME PK model ($CLCR_{CG}$ on CL, body weight on V_1, serum albumin concentration on V_2). For the remaining covariates that were included in the NLME PK model during forward inclusion, but excluded during the backward deletion, especially the 'borderline covariates' which were excluded late during the backward deletion (e.g. age, sex, bilirubin, C-reactive protein, pH value of the blood; Table S17, Figure 3.16), a reassessment is recommended when additional clinical data will be available.

Impact of $CLCR_{CG}$ on meropenem CL. As expected from the predominantly renal excretion of meropenem [161] and as described previously [235,329–332,334,335,337,338,341,342,346], $CLCR_{CG}$ was identified as important factor, influencing the CL of meropenem. For instance, for a $CLCR_{CG}$ of 80.8 mL/min (i.e. 4.85 L/h) the typical meropenem CL was 9.25 L/h, indicating both glomerular filtration and active secretion of meropenem in the kidneys. This is in line with the results of interaction studies with probenecid - a drug which blocks active secretion transporters in the proximal tubule of the kidney [160,348]: The studies observed an increase in AUC of meropenem (by 55% [348] and 43% [160]) when administering meropenem concomitantly with probenecid, thus demonstrating that meropenem is partly cleared via active secretion. The magnitude of meropenem CL was in good agreement with previous studies investigating meropenem PK in critically ill patients with similar renal function (e.g. 9.2 L/h for $CLCR_{CG}$=80 mL/min [256]; 7.34 L/h for CLCR=67 mL/min [349]). The broad range of $CLCR_{CG}$ values (25-255 mL/min; i.e. covering the full spectrum of five renal function classes) allowed the identification of a piecewise linear $CLCR_{CG}$-CL relationship, which indicated a linear increase of meropenem CL with increasing $CLCR_{CG}$ up to a maximum constant CL of approximately 16 L/h at a $CLCR_{CG}$ inflection point of 154 mL/min, i.e. for highly augmented renal function, meropenem CL was not further increasing. Comparing the piecewise linear relationship with the a sole linear $CLCR_{CG}$-CL relationship, it was noticeable that the two models were nearly congruent up to the inflection point and differed mainly for augmented renal function (Figure S30). Most previous analyses for meropenem in ICU patients described the $CLCR_{CG}$-CL relationship by using a linear function [271,328–332,334,336,340,350] or power function [337]. Yet, in many of the studies, the range of $CLCR_{CG}$ values covered in the study population was narrower and/or it remained unclear

whether a piecewise linear relationship was investigated. An analysis by Roehr et al., however, demonstrated a similar piecewise linear $CLCR_{CG}$-CL relationship when investigating meropenem PK in patients covering a $CLCR_{CG}$ range similar to the present study [351]. Beyond that, a very recent analysis by Dhaese et al. [344] evaluated the predictive performance of eight published PK models of meropenem in critically ill patients that included mainly linear [327–329,335,336,342,344] or power relationship [343] between renal function and meropenem CL, for an evaluation dataset with a broad range of $CLCR_{CG}$ (13.6-346 mL/min). Five of the models showed an underprediction of meropenem concentrations in the evaluation dataset which might suggest a misspecification of the included relationship between renal function and meropenem clearance: The extrapolation of the linear/power relationships to patients with augmented renal function is likely to have resulted in the extremely high meropenem CL values, which again has caused the observed underprediction in meropenem exposure. Yet, in the article the model predictivity was not stratified by renal function. In light of the findings of the present thesis as well as by Roehr et al. [351] and Dhaese et al. [344], a future evaluation of the functional $CLCR_{CG}$-CL relationship is warranted, as the identified relationship might impact model predictions – especially for augmented renal function - and hence also model-based clinical implication: An external evaluation of the developed NLME PK model based on a rich PK dataset originating from patients with augmented renal function (e.g. the evaluation dataset by Dhaese et al.) would allow to assess and confirm the identified piecewise linear relationship. Future analyses could focus on further refining the meropenem clearance model by assessing alternative $CLCR_{CG}$-CL relationship which allow a less abrupt but more smooth change in CL. Beyond that, even more physiological approaches could be applied which dissect and quantify the two parallel clearance processes, glomerular filtration and active secretion.

Impact of body weight and serum albumin concentration on the volume of distribution of meropenem. In addition, total body weight was identified as predictor for the central volume of distribution of meropenem (Table 3.8), which is in line with others, who already identified body size descriptors to influence the volume of distribution of meropenem [90,336,341,347,352,353]. Within the model, the relationship was quantified using a power model, with an estimated exponent of approximately 1, which is in line with the principle of allometry [204,354]. Thus, the model described a plausible, approximately linear relationship between body weight and V_1: An increase in body weight (e.g. doubling the body weight from 50 kg to 100 kg) resulted in an increase in V_1 (e.g. from 5.4 L to 11.1 L, respectively).

As already indicated by Mattioli et al. [327] and Ramon-Lopez et al. [333], the covariate analysis identified serum albumin concentration to be negatively related with the peripheral volume of distribution of meropenem: A decrease in albumin concentrations by 0.5 g/dL, resulted in 10% increase in V_2. Such a decrease in albumin concentrations is not unusual for the critically ill population, considering the high incidence of hypoalbuminaemia (40-50% [355]). This relation can

potentially be explained by an increased capillary leakage and the resulting fluid shifts from the intravascular space to the interstitial space in tissue which is related to the reduced serum albumin concentrations [110,111]. Contrary to highly protein-bound drugs, for meropenem, an impact of albumin concentration on the protein binding is not expected, considering the low magnitude of protein binding (2% [63,160]). The total volume of distribution of 24 L, for the typical study patient (body weight=70 kg, serum albumin=2.8 g/dL), was in line with previous investigations for meropenem in this special patient group (e.g. 23.7 L [329], 20.6 L [343], 22.7 L [350]).

Reduction in unexplained variability. The inclusion of the three covariates into the population PK model led to a distinct reduction in both inter- and intraindividual unexplained PK variabilities (with $CLCR_{CG}$ causing the strongest reduction of PPV_{Var} on CL by ~70%; Figure 3.17), resulting in – for the special critically ill population – low unexplained variabilities of ≤31.5%CV (Table 3.8; compared with e.g. ≤66.5%CV [327]; ≤48.0%CV [329]; ≤44.7%CV [350]). Yet, the remaining unexplained PK parameter variability of 12.5%CV to 31.5%CV (for IOV on CL and IIV on V_1, respectively; Table 3.8) indicates that further factors, not identified in the NLME PK modelling in Project IV, impact the PK of meropenem. Similarly, Project III identified patients (e.g. ID 36: higher C_{8h} values, Figure 3.14) for whom the $CLCR_{CG}$-meropenem C_{8h} relationship deviated from the remaining patients, suggesting additional impact factors, which have not yet been identified. In light of the high average numbers of administered drugs per critically ill patient (~13 [356–358]), future investigations of PK drug-drug interactions are warranted. Considering the renal active tubular secretion of meropenem via organic anion transporters (OAT) (namely OAT1 and OAT3 [161,162]), comedication impacting the OAT system (e.g. OAT inhibitors such as probenecid but also NSAIDs [359]) should be documented and analysed as potential impact factor for meropenem PK in future NLME analyses. In addition, investigation of comedication influencing the pH of the urine is desirable, as the distribution of microspecies of meropenem and hence the urinary excretion processes might differ at altered pH [360,361], which in turn might have an impact on the renal excretion of meropenem.

Of note, the observed lower magnitude of intraindividual PK variability compared to interindividual variability, provides an essential prerequisite for therapeutic drug monitoring (TDM) of meropenem, if e.g. aiming to individualise the dosing for an individual patient based on the measured meropenem concentration [362,363].

Impact of patient characteristics on meropenem concentration-time profile. The application of the NLME PK model by exposure simulations in Project IV allowed to characterise the phases of the concentration-time profile in which the covariates were most influential. Body weight and serum albumin concentrations were implemented on volume parameters (i.e. V_1, V_2, respectively) and therefore affected the maximum meropenem concentrations and the early declining part, while $CLCR_{CG}$ was implemented on the CL parameter and consequently had a strong impact on the terminal phase. The strong impact of $CLCR_{CG}$ on the terminal concentrations, also explained why

$CLCR_{CG}$ was identified as key determinant during PTA analyses (further discussed in section 4.3.2). The hyperbolic relationship between $CLCR_{CG}$ and meropenem C_{8h} values quantified in Project III, is another consequence of the impact of $CLCR_{CG}$ on the terminal phase of the meropenem concentration-time profile.

Special patient subgroups. The present study also included special patient subgroups such as CRRT and ECMO patients. For CRRT patients, authors of other publications identified measured CLCR determined via 24-h urine collection [330] or residual diuresis [345,353] as influencing factors on meropenem exposure, both requiring time-consuming urine collection. Although the present analysis included a rather small number of CRRT patients, it revealed $CLCR_{CG}$ as a potential determinant of meropenem exposure (Project III: Figure 3.14 A.1, B2; Project IV: Appendix Table S20) which can be assessed more easily and quickly in clinical practise than renal function markers determined via 24-h urine collection. This finding requires further investigation with a larger number of patients under a well-designed study protocol. For the six ECMO patients, the relationship between $CLCR_{CG}$ and meropenem concentrations, quantified in Project III, did not seem different from that of the remaining patients, suggesting that ECMO therapy did not have a strong impact on meropenem serum exposure (Figure 3.14). This was confirmed in Project IV, in which ECMO was not identified as covariate on the PK parameters of meropenem and is in line with findings reported by Donadello et al. showing no significant difference between the PK parameters of ECMO and control non-ECMO ICU patients [364]. Further scientific evidence was provided by a very recent study by Hanberg et al. [346] that investigated meropenem dosing in patients undergoing both ECMO and CRRT and demonstrated comparable PK for the ECMO-CRRT patients, as characterised before for CRRT patients not undergoing ECMO [365]. Note that in these analyses only a limited number of patients was investigated. However, a large clinical study is currently ongoing which may shed more light on the impact of ECMO on the PK of meropenem [122].

Conclusions and perspectives. The PK analyses demonstrated large variability in meropenem pharmacokinetics between the individuals but also within one patient between different occasions. The systematic covariate analysis identified three vital clinical determinants for meropenem PK which reduced the unexplained PK variability considerably: Renal function estimated according to Cockcroft and Gault [2], total body weight and serum albumin concentration. Yet, future analyses are warranted that evaluate and refine the developed models (regression model: Project III, NLME model: Project IV) based on clinical PK data of meropenem in the critically ill population. The inclusion of more patients with heterogeneous patient characteristics and information on administered comedication would allow to even better capture the real-life variability in the PK, to confirm the identified covariate-parameter relationships and to potentially identify further clinical determinants.

4.3.2 Evaluation and optimisation of meropenem dosing in critically ill patients (Project III, IV)

Project III and IV both contributed to the evaluation and optimisation of meropenem dosing in the critically ill population by the performance of PTA analyses which are summarised in Table 4.1 and will be jointly discussed in more detail below.

Evaluation of standard dosing in the study population. The PK/PD analysis in Project III (Table 4.1, Analysis A) demonstrated that standard meropenem dosing did not achieve the desired meropenem PK/PD targets $100\%T_{>MIC}$ and $50\%T_{>4\times MIC}$ in a considerable fraction of patients in the study population (Table 3.7): For pathogens with a MIC of 2 mg/L, which represents the upper MIC limit of the S category for many important bacteria (EUCAST MIC S breakpoint [5]), meropenem exposure was inadequate in every second dosing interval monitored. In line with the present work, Carlier et al. found similar results for the target $100\%T_{>MIC}$ given the same MIC value (target attainment 55% [366]). For infections with less susceptible bacteria of MIC 8 mg/L (EUCAST MIC R breakpoint [5]), which have been shown to commonly occur in ICUs [102,367], target non-attainment was high, with even four out of five dosing intervals resulting in subtherapeutic concentrations (target $100\%T_{>MIC}$).

PK/PD target. The PK/PD target $100\%T_{>MIC}$ (i.e. meropenem concentrations exceeding 1x the MIC for the entire dosing interval) was selected for target attainment analysis, as it has previously been shown to improve clinical cure and bacteriological eradication in patients with serious bacterial infections treated with betalactam antibiotics [235,236]. In Project III, a second target $50\%T_{>4\times MIC}$ (i.e. meropenem concentration exceeding 4xMIC for half of the dosing interval) was evaluated and the results compared to the results for the target $100\%T_{>MIC}$. For this second target clinical evidence is currently lacking, yet it has been selected for PTA analysis in previous clinical studies [237–239]. The target attainment analysis, performed in the present thesis, revealed similar results for the two selected PK/PD targets (Table 3.7), thus providing some first evidence for the use of this PK/PD target. However, future studies are warranted that confirm the validity of the PK/PD target $50\%T_{>4\times MIC}$ in the clinics. Moreover, it needs to be considered that current knowledge on PK/PD targets for meropenem in heterogeneous ICU populations is limited and a PK/PD target for this special patient population has not been derived. In relation to other PK/PD targets determined for meropenem in diverse clinical studies (e.g., $19.2\%T_{>MIC}$ and $47.9\%T_{>MIC}$ [166], $54\%T_{>MIC}$ [167] and $76\text{-}100\%T_{>MIC}$ [235]), the two PK/PD targets selected for the present analysis were at the upper end (i.e., stricter). The selection of the higher targets seemed reasonable, given (i) limited knowledge on an adequate PK/PD target for heterogeneous ICU populations and (ii) the high mortality rates in ICU patients and high severity of illness (median APACHE II first study day: 27), (iii) the high proportion of patients with transplants (~58%) in the evaluated population and (iv) given the relatively good safety profile of meropenem [171].

Table 4.1: Overview of PTA analyses performed in Project III and IV for meropenem dosing in critically ill patients.

Analysis	Project number (cross-reference methods and results section)	Investigated setting			Objective
		Patients	Dosing regimen	PK/PD target	
A	III (Sections 2.8.4.2 and 3.3.2.2)	Study population	Study dosing (i.e. standard dosing: $SI3_8$)	$100\%T_{>MIC}$, $50\%T_{>4xMIC}$	• Evaluation of standard dosing in the study population • Comparison of PK/PD targets
B	III (Sections 2.8.4.2 and 3.3.2.2)	Study population; stratified by renal function class	Study dosing (i.e. standard dosing: $SI3_8$)	$100\%T_{>MIC}$, $50\%T_{>4xMIC}$	• Evaluation of standard dosing in the study population dependent on renal function class
C	IV (Sections 2.9.4.2 and 3.4.3.2)	Virtual population; with varying covariates (CLC_{CG}, body weight, serum albumin concentration)	Standard dosing (i.e. $SI3_8$)	$98\%T_{>MIC}$	• Evaluation of impact of covariates on PTA → identification of vital determinants • Evaluation of standard dosing dependent on $CLCR_{CG}$
D	IV (Sections 2.9.4.2 and 3.4.3.2)	Virtual population; with varying CLC_{CG}	Standard + alternative dosing (i.e. $SI2_{12}$, $SI3_8$, $SI6_8$, $PI2_{12}$, $PI3_8$, $PI6_8$, CI3, CI6)	$98\%T_{>MIC}$	• Evaluation of standard + alternative dosing dependent on $CLCR_{CG}$ → optimisation of dosing

$SI2_{12}$: 1000 mg, 30-min i.v. infusion, q12h; *$SI3_8$*: 1000 mg, 30-min i.v. infusion, q8h (=standard dosing; highlighted in bold); *$SI6_8$*: 2000 mg, 30-min i.v. infusion, q8h; *$PI2_{12}$*: 1000 mg, 3-h i.v. infusion, q12h; *$PI3_8$*: 1000 mg, 3-h i.v. infusion, q8h; *$PI6_8$*: 2000 mg, 3-h i.v. infusion, q8h; *CI3*: 3000 mg, CI, q24h following 500 mg, 30-min loading dose; *CI6*: 6000 mg, CI, q24h following 1000 mg, 30-min loading dose.
Abbreviations: *CI*: Continuous infusion; *$CLCR_{CG}$*: Creatinine clearance estimated according to Cockcroft and Gault [2]; *i.v.*: Intravenous; *PK/PD*: Pharmacokinetic/pharmacodynamic; *PTA*: Probability of target attainment; *qXh*: Every X hours (e.g. q8h: every 8 h); *$\%T_{>MIC}$*: Percentage of time period that total drug concentration exceeds the MIC; *$\%T_{>4xMIC}$*: Percentage of time period that total drug concentration exceeds four times the MIC.

Indeed, the two selected targets have been reported to be commonly used in clinical practise for ICU patients [131] and a recent guideline on the 'Optimisation of the treatment with betalactam antibiotics in critically ill patients' recommends to use strict PK/PD targets in the ICU setting [368]. However, owing to the limited knowledge of PK/PD targets in ICU patients, there is a crucial need to explore which PK/PD target is best related to clinical outcome of critically ill patients in a prospective clinical trial. Further analyses should also be aimed at investigating differences in PK/PD targets between, for example, different patient subgroups (e.g., with vs. without transplants), different states of severity of illness or different types of infecting bacteria (gram-positive vs. gram-negative) in a sufficiently large number.

In the context of the MIC-based PK/PD targets, it needs to be kept in mind that the MIC value is associated with a certain inaccuracy: The susceptibility of the pathogen is provided on a discontinuous scale (usually 2-fold dilution scale), which categorises all values across the 2-fold

intervals (e.g. although a MIC is determined as 2 mg/L, the MIC of the bacterial strain might lie between >1 mg/L and 2 mg/L). Furthermore, MIC values might differ between/within laboratories due to differences in experimental settings (e.g. media, incubation temperature/time) or differences in technical skills and degree of training of the technician [129]. Nonetheless, the MIC value has proven as practical standard susceptibility measure and the assessment of MIC-based PK/PD targets is suggested by regulatory authorities to assess the adequacy of antibiotic dosing [63].

Evaluation of standard dosing dependent on the renal function class. The stratification of the PTA by the renal function class in Project III (Table 4.1, Analysis B), demonstrated a strong impact of renal function on the target attainment (Table 3.7), which was overall in accordance with the results of a recent publication by Isla et al. [369], in which the probability of attaining the target $100\%T_{>MIC}$ was analysed for three specific $CLCR_{CG}$ values: Target attainment was 51% for $CLCR_{CG}$ 35 mL/min (vs. 51% in the present study for $CLCR_{CG}$ range 30–59 mL/min), 3% for $CLCR_{CG}$ 71 mL/min (vs. 4.6%, 60–89 mL/min) and 0% for $CLCR_{CG}$ 100 mL/min (vs. 3.5%, 90–129 mL/min) for a MIC value of 8 mg/L. Because the present study included patients covering the full spectrum of five renal function classes, additional investigation of target attainment in extreme renal function classes (severely impaired, augmented renal function) was possible. For infections caused by bacteria of MIC 2 mg/L, augmented, normal and mildly impaired renal function was identified as a risk factor of target non-attainment; given bacteria of MIC 8 mg/L, moderate renal impairment was an additional risk factor. These findings imply the need for dosing intensification in patients identified to be at risk of target non-attainment, such as by increasing the dose or prolonged up to continuous infusion, which was one objective of Project IV. Continuous infusion – currently a 'hot topic' in antibiotic therapy – is under clinical investigation, owing to the results of previous studies that have associated continuous infusion with improved clinical cure rates [370,371]. In the study population, the only patient group that reliably reached the PK/PD targets was the subgroup with severe renal impairment. It must be kept in mind that these patients also received 1000 mg meropenem every 8 h as 30-min infusions and thus received higher doses than recommended in the summary of product characteristics (half of indicated dose every 12 h for patients with $CLCR_{CG}$ 10–25 mL/min [157]).

Evaluation of standard dosing dependent on the three covariates. In Project IV, the impact of renal function on the PTA following standard meropenem dosing, was further elucidated by assessing the impact not of the categorised but of the continuous renal function marker $CLCR_{CG}$ as well as the impact of the two other covariates body weight and serum albumin concentration, implemented in the NLME PK model (Table 4.1, Analysis C). The PK/PD target $98\%T_{>MIC}$ was used, considering the similar PTA results for the two selected PK/PD targets demonstrated in Project III ($100\%T_{>MIC}$, $50\%T_{>4\times MIC}$) and the available clinical evidence for this target (attainment resulted in improved clinical cure and bacteriological eradication in patients with serious bacterial infections treated with betalactam antibiotics [235,236]). Of the three covariates implemented in

the NLME PK model, $CLCR_{CG}$ revealed by far the strongest impact on PTA (Figure 3.20). While an increase in $CLCR_{CG}$ and serum albumin concentration led to a reduced PTA, an increase in body weight improved (i.e. increased) the PTA (Table 3.9). The observed direction of the impact of body weight and serum albumin concentration on the PTA – systematically investigated and illustrated for meropenem for the first time – can be explained by their impact on the volume of distribution and hence on the half-life of meropenem, slightly influencing the terminal concentrations of the meropenem concentration-time profile. These relationships will be further illustrated in the following using body weight as example: An increase in body weight (e.g. of 50 kg) increases the volume of distribution (e.g. by 71%), which in turn prolongs the half-life of meropenem (e.g. 71%). Thereby, meropenem concentrations in the terminal phase of the concentration-time profile increase and thus also the time that the drug concentration exceeds the MIC value. This explains the observed increase in PTA with increasing body weight. Consequently, according to the observed covariate-PTA relationships, the 'high-risk patient' subpopulation under standard meropenem dosing, was the low-weight critically ill patient with augmented renal function and high serum albumin concentrations. Yet, the impact of body weight and serum albumin concentrations was marginal compared to $CLCR_{CG}$ and consequently $CLCR_{CG}$ was considered as key determinant for risk assessment. Overall, the results of the PTA analysis indicated a relevant risk of ineffective meropenem exposure in many of the patients (i.e. 5th percentile of PTA<90%). Already for susceptible bacteria with a MIC value of 0.5 mg/L for instance, $CLCR_{CG}$ values ≥90 mL/min were identified as risk factors for ineffective meropenem exposure when administering standard meropenem dosing; i.e., only $CLCR_{CG}$ values ≤80 mL/min reliably resulted in effective exposure (5th percentile of PTA≥90%). For the S breakpoint for many relevant bacteria (MIC=2 mg/L [5]), even $CLCR_{CG}$ values ≥50 mL/min were identified as risk factors. For the R breakpoint for many relevant bacteria (MIC=8 mg/L ([5]), even none of the investigated $CLCR_{CG}$ values (i.e. ≥10 mL/min) reliably reached effective meropenem exposure (Table 3.9).

Cumulative fraction of response analysis. In addition to the PTA analysis, which is typically performed when information on the MIC values is available, in Project IV, the CFR was investigated (Section 2.9.4.2). In contrast to the PTA, the full MIC value distribution of a pathogen is considered, i.e. all possible MIC values of the pathogen including their respective frequencies. This allows to assess the probability of therapeutic exposure for a given pathogen when the actual MIC value is unknown – a situation which is still frequently encountered on ICUs [239]. For this purpose, five pathogens, commonly encountered on the ICU, with varying susceptibility against meropenem were selected [372–374]: Three more susceptible pathogens *E. coli, K. pneumonia, E. cloacae* and two rather susceptible pathogens *P. aeruginosa* and *Acinetobacter spp.* (MIC_{90}=0.032, 0.064, 0.125 and 8, 16 mg/L, respectively; derived based on EUCAST MIC distributions [375]). Following standard meropenem dosing, effective meropenem exposure was reliably reached (i.e., 5th percentile of CFR≥90%) for the three susceptible pathogens across all

renal function classes, whereas for *P. aeruginosa* and *Acinetobacter spp.* only in some of the patients with severely impaired renal function standard meropenem dosing seemed sufficient. By considering available knowledge on the MIC distribution of the pathogen, the CFR provides the most likely estimate of the probability of target attainment, in situations in which the infecting pathogen is known, but information on the susceptibility of the pathogen is lacking. Yet, in case of pathogens of the S category, the CFR might overestimate the risk of inadequate exposure, while for pathogens of the I or R category the risk might be underestimated. To further refine the CFR estimate, the present analysis assessed the CFR of meropenem separately for MIC distributions of the pathogens belonging to the S and I category (Section 2.9.4.2). These results provide valuable information in situations in which in addition to the pathogen, the susceptibility category is known (i.e. S, I, R category). In hospitals, the susceptibility category is still frequently used to report pathogen susceptibilities, as alternative to MIC values. This promising novel approach of assessing the CFR in dependence of the available knowledge on the susceptibility category of the pathogen can also be applied for other antibiotic drugs and/or patient groups.

Consideration of PK parameter uncertainty in the simulations. Today, PTA analyses are frequently applied to assess the adequacy of antibiotic dosing based on NLME PK models. However, recently, Colin et al. sounded a note of caution when interpretation the results of PTA analyses [245]. The authors emphasised that, at this point, PTA analyses are based on MC simulations for the typical individual/population only, i.e. uncertainty which is associated with the PK parameters of the NLME PK model is typically ignored completely, not allowing a reliable judgement of PTA results in support of therapeutic decision making. This point of view was also supported by the recently published EMA guideline on the use of PK and PD in the development of antimicrobial medicinal products, which suggested to report a measure of uncertainty (more concretely, the 95% confidence intervals) for the PTA [63]. To the best of found knowledge, the present work for the first time implemented these recommendations for meropenem in the PTA and CFR analyses, by considering PK parameter uncertainty in the underlying MC simulations, providing confidence intervals around the typical PTA/CFR and considering the uncertainty in the dosing selection (Section 3.4.4). Of note, despite the relatively precisely estimated PK parameters in the final population PK model (Table 3.8), a relevant impact on the selection of the dosing regimens was observed when considering PK parameter uncertainty ('novel approach') compared to not considering PK parameter uncertainty ('traditional approach'). With increasing elimination capacity of the kidney (i.e. increasing $CLCR_{CG}$), an intensified dosing regimen was required earlier (i.e. at lower $CLCR_{CG}$ values) when using the novel approach compared to the traditional approach (Table S29): While, for instance, for a patient with 'normal' renal function ($CLCR_{CG}$=90 mL/min) and a pathogen with a MIC of 2 mg/L, only the most intensified continuous dosing regimen (CI6: 6000 mg, q24h following a 1000 mg, 30-min loading dose) was selected using the 'novel approach'; for the 'traditional approach' a less intensified continuous-infusion dosing regimen

(CI3: 3000 mg, q24h following a 500 mg, 30-min loading dose) seemed adequate (Table S29). Of note, the differences between the dosing regimens identified based on the novel versus traditional approach were particularly relevant in less susceptible pathogens (Table S29).

To sum up, it can be noted that the inclusion of parameter uncertainty into PTA/CFR analyses utilised for dosing selection may have clinical implications, even in case of relatively precisely estimated PK parameters. Thus, it is recommended to considered PK parameter uncertainty in future analyses, particularly for vulnerable patient populations such as critically ill patients for which adequate dosing is of crucial importance.

Evaluation and optimisation of meropenem dosing dependent on $CLCR_{CG}$. Due to the pronounced impact of $CLCR_{CG}$ on the PTA, caused by its strong influence on the descending part of the concentration-time profile, the dosing simulations for alternative dosing regimens in Project IV, were performed for varying $CLCR_{CG}$ values (Table 4.1, Analysis D).

Overall, the analyses suggested that for bacteria of the S category (MIC≤2 mg/L), effective concentrations were reliably reached (i.e. 5th percentile of PTA≥90%) in all investigated patients with at least one of the eight investigated dosing regimens, even if displaying augmented renal function, a characteristic which is frequently observed in the ICU setting (Section 3.4.3.2). Bacteria of the I category, however, seemed to only be effectively treated in patients with renal insufficiency (MIC=4 mg/L: $CLCR_{CG}$≤80 mL/min, MIC=8 mg/L: $CLCR_{CG}$≤30 mL/min) using the most intensified dosing regimens ($SI6_8$/$PI6_8$/CI6). Conversely, for highly susceptible pathogens (e.g. MIC<0.12 mg/L for $CLCR_{CG}$=90 mL/min), even lower than standard dosing seemed to be sufficient, however, advantages or disadvantages of such adaptions to lower dosing have to be further evaluated in prospective clinical trials. Yet, this finding demonstrated that reporting MIC values in the clinics, even within the low susceptible range, might be relevant.

The systematic PK/PD analysis demonstrated superiority of prolonged over short-term infusion regimens and of continuous-infusion over prolonged infusion regimens for MIC≤4 mg/L and day 1 of treatment – emphasising that even a stricter PK/PD target was evaluated for continuous infusion compared to the remaining infusion regimens. Previous investigations for meropenem revealed that continuous infusion – despite the reported instability [376–379] – is feasible at 25°C, if renewing the solution depending on the drug concentration twice or thrice daily (see Supplement of article by Minichmayr et al. [380]). For MIC>4 mg/L and *P. aeruginosa* or *Acinetobacter spp*. of the I category, prolonged infusion rather than continuous-infusion regimens was superior. Furthermore, the type of infusion (e.g. continuous vs. prolonged) on the achievement of effective exposure was more relevant than the administered total daily dose (e.g. 3000/3412.5 vs. 6000/6875 mg). Yet, it needs to be kept in mind, that due to the initial loading dose on day 1, for continuous infusion total daily doses were ≤14.6% higher compared to the other regimens. Note, that the above-mentioned findings are based on the evaluation of the selected PK/PD targets (for SI and PI: $98\%T_{>MIC}$, for CI: $98\%T_{>4xMIC}$). The selection of the stricter target of $98\%T_{>4xMIC}$ for

continuous-infusion regimens, was deemed reasonable in light of the increasing spread of resistance [22] and the raised concerns that plateau-like meropenem concentrations achieved at steady state following continuous infusion, may – if close to/below the MIC value – favour the selection of resistant strains [42,381,382]. It needs to be noted that even stricter targets have been suggested: For instance, Tam et al. [42] suggested an target of C_{min} values not only exceeding 4x but 6.2x the MIC value to supress *in vitro* resistance of *Pseudomonas aeruginosa.* Despite the strict target of 98%$T_{>4xMIC}$ the evaluation revealed that continuous-infusion regimens were superior over short-term or prolonged infusion regimens with respect to the PTA/CFR for MIC values ≤4 mg/L. However, trends might differ when evaluating other targets (e.g. 50%$T_{>MIC}$ or 50%$T_{>4xMIC}$) or non-critically ill patient populations.

Conclusions and perspectives. The PK/PD analyses demonstrated that standard meropenem dosing is likely to result in ineffective meropenem exposure in a considerable fraction of critically ill patients, especially when assuming infections caused by less susceptible bacteria commonly encountered in ICU patients. Of the three covariates identified in the NLME PK model, $CLCR_{CG}$ was found to be a vital clinical determinant for PTA and was thus focus of the dosing simulations. While patients with higher $CLCR_{CG}$ and lower pathogen susceptibility required mainly intensified dosing regimens, even lower than standard doses seemed effective for highly susceptible pathogens. Integrating for the first time PK parameter uncertainty in the meropenem dosing simulations, allowed to more reliably judge the PTA results and hence dosing selections. Considering the available knowledge on the pathogen causing the infection and its susceptibility, which varies between hospitals, the comprehensive PK/PD analysis focused on the identification of improved dosing regimens based on the available level (L) of knowledge: L1: not knowing the infecting pathogens, L2: knowing the infecting pathogen, $L3_{(-MIC)}$: knowing the infecting pathogen and susceptibility category and $L3_{(+MIC)}$: knowing the MIC value. The findings of the present work indicate that dosing adjustment is needed, depending on a patient's renal function and the susceptibility of the infecting pathogen. In addition to the assessment of effective exposure, which is certainly most relevant for the vulnerable patient population of ICU patients, future analyses shall aim at investigating dosing regimens with respect to the achievement of exposure linked to high risk of adverse drug reactions and/or occurrence of toxicity. In an analysis by Minichmayr et al. an upper threshold of steady state meropenem concentrations of 32 mg/L was used in a PK analysis of critically ill patients. Nevertheless, as currently available evidence for meropenem toxicity thresholds in critically ill patients is limited, future clinical research is warranted in this field [131,383].

4.4 Translating research results into the clinics: Towards therapeutic decision support (Project III, IV)

In contrast to most analyses performed to evaluate and/or optimise meropenem dosing in special patient populations [335,345,349,365,384], the present thesis went one step further and translated the research results into the clinics. The focus was set on the development of easy-to-use tools which convey the clinically relevant aspects of the pharmacometric modelling and simulation results and are easily applicable and interpretable by non-pharmacometricians (Project III, IV; research category: translational research; Figure 4.1).

4.4.1 Risk assessment tool: MeroRisk Calculator (Project III)

To enable the practical applicability of the quantified relationship between renal function and meropenem exposure and consequently target attainment, in Project III a risk assessment tool, the MeroRisk Calculator, was developed in a commonly available and known software (Microsoft Excel®; Section 3.3.3). The beta version of this tool is publicly and freely accessible as additional file of the open access article by Ehmann et al. Critical Care (2017) [233] and has been accompanied by an dedicated editorial by Abdul-Aziz et al. Critical Care (2017) [385], supporting the translational approach taken in this analysis: ‘investigators are certainly heading in the right direction with their proposed solution’. This easy-to-use tool allows the assessment of the risk of target ($100\%T_{>MIC}$) non-attainment, i.e. ineffective meropenem exposure, for non-CRRT patients displaying renal function within a broad range ($CLCR_{CG}$ 25–255 mL/min) and receiving standard dosing of meropenem (1000 mg every 8 h as 30-min infusions). The PK/PD target $100\%T_{>MIC}$ was selected for the assessment of target attainment as it originates from the results of clinical investigations and as the PTA results in the present work were comparable to the results of the additionally investigated target $50\%T_{>4xMIC}$ (Section 3.3.2.2). The risk of target non-attainment of meropenem was implemented depending on creatinine clearance estimated according to Cockcroft and Gault ($CLCR_{CG}$) rather than creatinine clearance determined by 24-h urine collection ($CLCR_{UC}$), as $CLCR_{CG}$ can be assessed much more easily in clinical practise and as the relationship between $CLCR_{UC}$ and meropenem exposure was not more predictive than between $CLCR_{CG}$ and meropenem exposure (Figure S38).

To tool can be easily applied in three steps: In step 1, the user needs to provide only the $CLCR_{CG}$ or its determinants (i.e., sex, age, total body weight and the routinely determined laboratory value serum creatinine; Figure 3.15). In step 2, the MIC value of a pathogen determined or suspected in the patient needs to be provided. Should MIC values not be available, the user has the option to select an MIC breakpoint for important pathogens from the EUCAST database [4]. In step 3, the tool then calculates the risk of target non-attainment which is displayed with a 3-colour coding

system, indicating low-risk patients in green (probability of target non-attainment: ≤10%), medium-risk patients in orange (>10%-<50%) and high-risk patients in red (≥50%). Because only a limited number of patients with augmented or severely impaired renal function were included in this analysis, the uncertainty of the $CLCR_{CG}$-meropenem exposure relationship implemented in the MeroRisk Calculator is higher for the extremes of the renal function spectrum. Furthermore, the user of the tool needs to keep in mind that in addition to $CLCR_{CG}$, other factors might influence meropenem C_{8h} values. To visualise the prediction uncertainty (i.e., uncertainty in the $CLCR_{CG}$-meropenem C_{8h} relationship combined with the variability in C_{8h} values) of the calculated meropenem C_{8h} value for a patient's $CLCR_{CG}$, the prediction interval around the $CLCR_{CG}$-meropenem exposure relationship is additionally provided in the risk assessment tool. Of particular note, using the MeroRisk calculator does not require the measurement of a meropenem serum concentration of a patient and can thus be used *a priori* to meropenem treatment. In case of available meropenem concentrations in a patient, use of therapeutic drug monitoring is encouraged to aid therapeutic decision making in the course of meropenem treatment.

Conclusion and perspectives. The MeroRisk Calculator, an easy-to-use tool to assess the risk of PK/PD target non-attainment after meropenem standard treatment, has been developed for critically ill patients. The current beta version of the MeroRisk Calculator is intended to be used in the setting of clinical research and training. As also suggested in the editorial by Abdul-Aziz and colleagues [385], as a next step, a comprehensive prospective validation of the risk calculator in clinical research setting is warranted. In a first step, the evaluation of the 'PK-side' of the tool shall be aimed for, i.e. an evaluation of the predictivity for the meropenem C_{8h} values based on the $CLCR_{CG}$ of a patient. In addition, in a second step, clinical studies shall further address the 'PD-side' of the tool, i.e. evaluate whether the risk of target non-attainment correlates with clinical PD data (e.g. change in inflammation makers). Step 1 has already been initiated in collaboration with the University Hospital, LMU Munich, Germany, and PK data collection based on routinely monitored TDM samples is currently ongoing (ClinicalTrials.gov Identifier: NCT03985605). In future, the newly developed risk assessment tool as a graphical user interface might, if all requirements are met, be beneficial in clinical practise for therapeutic decision making. An ICU patient's risk of target non-attainment, given his/her renal function and the MIC value of the infecting pathogen, would already be accessible when no meropenem concentration measurement is available, such as prior to the start of antibiotic treatment.

4.4.2 Three-level dosing algorithm (Project IV)

In the present thesis, a three-level meropenem dosing algorithm (Table 3.10) was generated proposing dosing regimens for meropenem in critically ill patients, aiming to reach effective meropenem exposure by means of a comprehensive NLME pharmacokinetic/pharmacodynamic

modelling analysis. In short, the investigated dosing regimens are provided in an intuitive tabular overview, which only considers creatinine clearance as the crucial patient-specific factor for meropenem target attainment. No additional covariates were needed to be included, as they only showed little impact on the achievement of effective antibiotic exposure. Additionally, the dosing overview considers different levels of pathogen-specific information (L1: pathogen unknown, L2: pathogen known, $L3_{(-MIC)}$: pathogen and susceptibility category known, $L3_{(+MIC)}$: MIC value known) as might be encountered in different clinical settings. Moreover, the reliability of the proposed dosing regimens is deemed high, as the underlying analysis considered also the uncertainty in the estimated PK model parameters.

For the vulnerable population of critically ill patients, TDM has been recommended for individual dose adjustment [327,339,386,387]. However, TDM of antibiotics is still only rarely available in clinical routine, e.g. the recent ADMIN-ICU survey indicated only 2% of the investigated ICUs implementing TDM for carbapenems [325]. As especially at start, but also during meropenem treatment, TDM is mostly not available, reliable dosing recommendations are needed. In contrast to previous suggestions, the present work systematically investigated seven alternative dosing regimens for meropenem given different levels of information about the pathogen and considered PK parameter uncertainty in the underlying simulations [347,350,369,380,388]. To the best of found knowledge, this is the first analysis of meropenem which also considered PK parameter uncertainty in the MC simulations [245] underlying the selection of dosing regimens for the dosing algorithm. Compared to the traditional approach not considering PK parameter uncertainty, the dose selection was more conservative (Table S29) and thus, the results were deemed to be more reliable, which may be important to ensure effective meropenem exposure especially for critically ill patients. The developed three-level dosing algorithm (Table 3.10) summarises improved dosing regimens based on a patient's renal function and the level of knowledge about a pathogen. Hence, the algorithm provides information for different stages of treatment (pathogen and/or antibiogram available or not (yet)) and for different ways of reporting susceptibility in the patient records (S/R classification or MIC value). Choosing the dosing regimen based on the highest level of knowledge about a pathogen could allow to achieve effective exposure with the potential advantage of more probable or faster eradication of the pathogen [38,40,168] and reduced risk of unnecessary high or toxic concentrations and of resistance development and spread.

To give an example, in 'Level 1' (pathogen unknown; based on the non-species related EUCAST PK/PD breakpoints, e.g. S=2 mg/L [246]) for patients with normal renal function (CRCL≥90 mL/min) a very high dosing regimen is proposed (CI6, Figure 4.4). However, if the infecting strain is known ('Level 2') in most cases (for all evaluated Enterobacteriaceae) it is recommended to reduce the dosing. For the bacteria listed in the algorithm, only for infections with *P. aeruginosa* or *Acinetobacter spp*. none of the investigated dosing regimens was sufficient, which can be explained by the higher proportion of pathogens in the I or R category for meropenem [132].

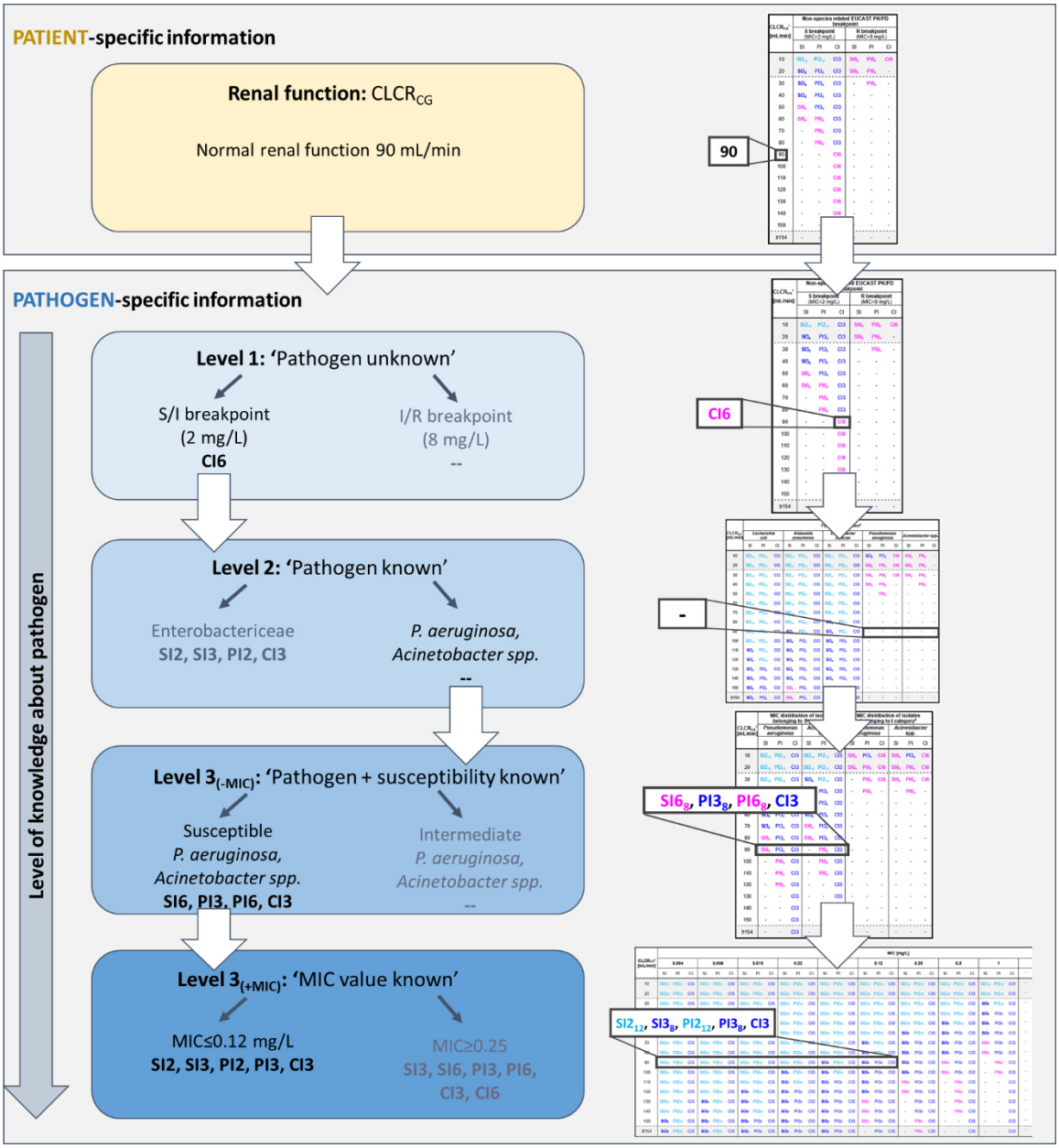

Figure 4.4: Example illustrating the application of the dosing algorithm, which is also described in the result chapter (Section 3.4.4) (modified from [243]).
Left: Flow chart; ***Right***: Snapshot of parts of the dosing algorithm (s. main text, Table 4) relevant for the example given on the left in black font.
Dosing regimens: *SI2*$_{12}$: 1000 mg, 30-min i.v. infusion, q12h; *SI3*$_8$: 1000 mg, 30-min i.v. infusion, q8h (=standard dosing; highlighted in bold); *SI6*$_8$: 2000 mg, 30-min i.v. infusion, q8h; *PI2*$_{12}$: 1000 mg, 3-h i.v. infusion, q12h; *PI3*$_8$: 1000 mg, 3-h i.v. infusion, q8h; *PI6*$_8$: 2000 mg, 3-h i.v. infusion, q8h; *CI3*: 3000 mg, CI, q24h following 500 mg, 30-min loading dose; *CI6*: 6000 mg, CI, q24h following 1000 mg, 30-min loading dose.
For CI regimens (CI3, CI6) consider to renew the infusion solution dependent on the drug concentration twice or thrice daily (see supplement of article [380]) to ensure the stability of meropenem.
Abbreviations: *CI*: Continuous infusion; *CLCR*$_{CG}$: Creatinine clearance estimated according to Cockcroft and Gault [2]; *i.v.:* Intravenous; *MIC*: Minimum inhibitory concentration; *qXh*: Every X hours (e.g. q8h: every 8 h).

In such situations, combination therapy might be an option for critically ill patients, which has been recommended by the most recent International Guideline for Management of Sepsis and Septic Shock [37] for empirical treatment of multidrug-resistant pathogens such as *P. aeruginosa* or *Acinetobacter spp*. However, no clear evidence is yet established that suggests the use of

combination therapies over monotherapy for infections with e.g. *P. aeruginosa* [389]. Thus, future randomised controlled trials, that assess survival and resistance development in large patient cohorts, are warranted. When applying the dosing algorithm, the availability of additional information on the susceptibility of the pathogen (either as S/I/R categorisation, 'Level $3_{(-MIC)}$' or as MIC value, 'Level $3_{(+MIC)}$') would allow to adjust and further specify the dosing for the specific patient-pathogen combination (Figure 4.4 bottom). Of note, the PTA and CFR analyses of treatment day 1 and 4 revealed only little difference, with the results of day 1 being slightly more conservative. This is in line with the short elimination half-life of meropenem (study ICU patient: median=2.27 h, range=0.946-5.64 h) and the therefore limited accumulation of meropenem over time of treatment. In light of the minor difference between the results of days 1 and 4, the dosing algorithm – which is provided for the start of treatment – is considered appropriate also during later meropenem treatment.

Conclusion and perspectives. In conclusion, a three-level meropenem dosing algorithm was developed, suggesting meropenem dosing regimens for critically ill patients based on their renal function as well as different levels of knowledge about the pathogen. Additional independent clinical studies will be necessary to validate the dosing algorithm in order to make it applicable in clinical practise. Apart from evaluating the proposed dosing regimen with respect to improved clinical outcome, the assessment of the occurrence of adverse drug reactions and toxicity and resistance development of the pathogens is warranted. A first prospective clinical investigation has already been initiated in collaboration with the University Hospital Charité – Universitätsmedizin Berlin, Germany.

The meropenem dosing algorithm is provided for a broad range of $CLCR_{CG}$ values, but fixed body weight and albumin concentration, which was deemed reasonable considering the pronounced impact of $CLCR_{CG}$ on the PTA (Section 4.3.2). Particular attention should be paid to the extremes of the renal function spectrum, considering the limited number of patients with severely impaired and augmented renal function that were included in the underlying analyses. If aiming at additionally taking body weight and albumin values into account, the use of the full NLME PK model by means of a dosing software (e.g. TDMx: tdmx.eu [309], InsightRx: insight-rx.com, DoseMeRx: doseme-rx.com, BestDose: lapk.org/bestdose.php) is required, which can ultimately allow to determine an improved dosing regimen for individual patients (with individual $CLCR_{CG}$-weight-albumin combinations). While, e.g. in TDMx the 'Probabilistic Dosing' module would facilitate *a priori* dose suggestion based on the covariates implemented in the model, the 'Bayesian dosing' module would allow *a posterior* dose suggestion considering in addition to the covariate information also TDM information on individual drug concentration by means of Bayesian methods.

5

Overall conclusions and perspectives

The present thesis has taken substantial steps towards therapeutic decision support of antibiotic dosing in special patient populations, leveraging pharmacometric modelling and simulation approaches in basic, applied and translational research.
The thesis focused on the two clinically relevant antibiotic drugs, 'linezolid' and 'meropenem', in the selected special patient populations of 'obese surgical patients' and 'critically ill patients', respectively.

As basic research, the successfully developed pharmacometric models contributed to an advanced quantitative understanding of the antibiotic PK in these special patient populations. Integrating clinical microdialysis data into the pharmacometric model, as done for linezolid, advanced the understanding of the distribution of the antibiotic drug to the potential target site of bacterial infection. This provides valuable information on the antibiotic exposure at the target site, which is the driving factor for antibacterial efficacy. Furthermore, the pharmacometric models allowed to better characterise the PK variabilities between and within patients and importantly also to identify factors causing the observed variabilities. For meropenem, high inter- and intrapatient variability was observed in the critically ill population which could be explained to a large extent by three highly diverse patient-specific characteristics (renal function, body weight and serum albumin concentrations). Besides patient-specific characteristics (LBW, obesity status), the modelling revealed also surgery-specific characteristics (anaesthesia status and haemodynamic changes) influencing the PK of linezolid. The identification of such factors is of crucial importance for individual exposure predictions, which serve as basis for model-based dosing suggestions, as utilised within the applied research part of present thesis.
In addition to the PK-related aspects, the present work contributed to a more detailed characterisation of the variability in the microdialysis sampling technique, the method of choice for determining unbound (i.e. pharmacologically active) drug concentrations directly at the target site. Integrating the data originating from a variety of clinical microdialysis samplings into the pharmacometric model, enabled to (i) discriminate between PK and microdialysis methodology-related variabilities and to (ii) further dissect and quantify different levels of variability in the microdialysis methodology. This illustrates how pharmacometric modelling approaches can be

leveraged to assess data other than PK. Applying the proposed approach to a larger number of microdialysis sampling data, would further inform the variability levels and provide valuable knowledge on the interpretation/reliability of target site concentrations determined by microdialysis. In summary, the present thesis successfully utilised pharmacometric modelling approaches to synthesise knowledge on the antibiotic PK in special patient groups, as well as on the variability in the microdialysis technique.

The application of the developed pharmacometric models enabled the evaluation of standard antibiotic dosing regimens in special patient groups with respect to the attainment of effective antibiotic exposure – crucial for antibacterial efficacy. Overall, the results of the present thesis indicate that standard dosing frequently results in ineffective antibiotic exposure in these special patient populations, partly even for susceptible pathogens. Utilising the pharmacometric models allowed to determine factors associated with ineffective exposure and thus enabled to identify patients at potential risk of therapy failure. For meropenem treatment in critically ill patients, the risk of ineffective exposure was strongly related to the renal function of the patient. The risk was highest for patients with normal or augmented renal function and expectedly for pathogens with low susceptibility. Thus, the present work underlined the need of tailoring the dosing regimen to patient-specific and pathogen-specific characteristics. The application of pharmacometric models to simulate the antibiotic exposure in 'at risk patients' for various alternative dosing regimens (e.g. intensified dose and/or prolonged infusion duration and/or shortened dosing interval), allowed to identify regimens resulting in effective antibiotic exposure. By additionally integrating different levels of knowledge about the pathogen (i.e. pathogen unknown / pathogen known / pathogen + susceptibility category known / MIC value known) into simulations, the present work did not only consider the patient for dosing suggestions, but also the available knowledge about the pathogen.

The present thesis took one step further and translated the model-based dosing suggestions into practical applicability. The focus was set on the critically ill population, a highly vulnerable population which exhibits large infection-related mortality rates. To this end, the present thesis developed easy-to-use tools that convey the clinically relevant aspects of the pharmacometric modelling and simulation results without presenting complex equations or graphics. The risk assessment tool 'MeroRisk Calculator' is provided in a commonly used software (Microsoft Excel®) which is familiar to many health-care professionals. The tool supports the user in identifying 'at-risk patients' for which standard meropenem dosing is likely to result in ineffective exposure and encourages meropenem dosing adjustment in these patients. The newly developed '3-level dosing algorithm' provides an intuitive tabular overview to support dosing selection for individual patients. The algorithm is applicable for different levels of knowledge about the suspected or infecting pathogen and therefore offers a wide range of application. This is particularly helpful in situations in which the MIC value is not (yet) available. The newly developed tools are

easily applicable and interpretable by non-pharmacometricians and therefore have the potential to support a rapid selection of an individualised dosing regimen in the clinics – which is of crucial importance for the critically ill population in which 'speed is life'. In the future, after successful clinical evaluation, such tools could be used directly by the attending physician and/or by other health-care professional (e.g. members of antibiotic steward ship team, clinical pharmacists).

By translating the modelling and simulation results into the clinics, the present thesis took substantial steps towards model-based therapeutic decision support to combat bacterial infections with a rational and patient-centred treatment. To make the tools applicable in clinical practise, a comprehensive evaluation of the tools in clinical research setting is warranted. First clinical studies have already been initiated, e.g. the PK predictivity of the MeroRisk calculator is currently under clinical investigation. Additional clinical studies should evaluate the tools with respect to clinical response (i.e. efficacy/clinical benefit and safety) and emergence of antimicrobial resistance. Collected clinical data could also be used to further refine the underlying pharmacometric models. In light of the increasing availability of electronic health record systems in hospitals, a link between therapeutic decision supporting tools and patient-specific information in the systems, could provide automated warnings for 'at-risk patients' or model-based dosing regimen suggestions. This would further facilitate the shift to a 'model-informed precision dosing'.

6

Bibliography

[1] W.A. Knaus, E.A. Draper, D.P. Wagner, J.E. Zimmerman. APACHE II: a severity of disease classification system. Crit. Care Med., 13: 818–29 (1985).

[2] D.W. Cockcroft, M.H. Gault. Prediction of creatinine clearance from serum creatinine. Nephron, 16: 31–41 (1976).

[3] J. Koenig, L.K. Hill, D.P. Williams, J.F. Thayer. Estimating cardiac output from blood pressure and heart rate: The Liljestrand & Zander formula. Biomed. Sci. Instrum., 51: 85–90 (2015).

[4] http://www.eucast.org (last access 23 Mar 2019).

[5] European Committee on Antimicrobial Susceptibility Testing. Breakpoint tables for interpretation of MICs and zone diameters. Version 9.0. (2019).

[6] J.L. Vincent, R. Moreno, J. Takala, S. Willatts, A. De Mendonca, H. Bruining, C.K. Reinhart, P.M. Suter, L.G. Thijs. The SOFA (Sepsis-related Organ Failure Assessment) score to describe organ dysfunction/failure. Intensive Care Med., 22: 707–710 (1996).

[7] K. Gould. Antibiotics: from prehistory to the present day. J. Antimicrob. Chemother., 71: 572–575 (2016).

[8] https://www.who.int/news-room/fact-sheets/detail/the-top-10-causes-of-death (last access 31 Mar 2019).

[9] Y. Sakr, U. Jaschinski, X. Wittebole, T. Szakmany, J. Lipman, S.A. Ñamendys-Silva, I. Martin-Loeches, M. Leone, M.-N. Lupu, J.-L. Vincent. Sepsis in intensive care unit patients: worldwide data from the intensive care over nations audit. Open Forum Infect. Dis., 5: 1–9 (2018).

[10] J.A. Kempker, G.S. Martin. The changing epidemiology and definitions of sepsis. Clin. Chest Med., 37: 165–179 (2016).

[11] F.B. Mayr, S. Yende, D.C. Angus. Epidemiology of severe sepsis. Virulence, 5: 4–11 (2014).

[12] C. Engel, F.M. Brunkhorst, H.-G. Bone, R. Brunkhorst, H. Gerlach, S. Grond, M. Gruendling, G. Huhle, U. Jaschinski, S. John, K. Mayer, M. Oppert, D. Olthoff, M. Quintel, M. Ragaller, R. Rossaint, F. Stuber, N. Weiler, T. Welte, H. Bogatsch, C. Hartog, M. Loeffler, K. Reinhart. Epidemiology of sepsis in Germany: results from a national prospective multicenter study. Intensive Care Med., 33: 606–618 (2007).

[13] M. Shankar-Hari, D.A. Harrison, G.D. Rubenfeld, K. Rowan. Epidemiology of sepsis and septic shock in critical care units: comparison between sepsis-2 and sepsis-3 populations using a national critical care database. Br. J. Anaesth., 119: 626–636 (2017).

[14] G. Marx. Incidence of severe sepsis and septic shock in german intensive care units - the insep study. Intensive Care Med. Exp., 3: A223 (2015).

[15] D.C. Angus, W.T. Linde-Zwirble, J. Lidicker, G. Clermont, J. Carcillo, M.R. Pinsky. Epidemiology of severe sepsis in the United States: Analysis of incidence, outcome, and associated costs of care. Crit. Care Med., 29: 1303–1310 (2001).

[16] C. Chelazzi, E. Pettini, G. Villa, A.R. De Gaudio. Epidemiology, associated factors and outcomes of ICU-acquired infections caused by Gram-negative bacteria in critically ill patients: an observational, retrospective study. BMC Anesthesiol., 15: 125 (2015).

[17] J. Vincent. International study of the prevalence and outcomes of infection in intensive care units. JAMA, 302: 2323–2329 (2009).

[18] World Health Organization. Antimicrobial resistance: Global report on surveillance. (2014).

[19] Federal Ministry of Health. Follow-up report for the German Guard Initiative: Breaking through the wall - A call for concerted action on antibiotics research and development. (2017).

[20] M.S. Kinch, E. Patridge, M. Plummer, D. Hoyer. An analysis of FDA-approved drugs for infectious disease: antibacterial agents. Drug Discov. Today, 19: 1283–1287 (2014).

[21] M. Nadimpalli, E. Delarocque-Astagneau, D.C. Love, L.B. Price, B.-T. Huynh, J.-M. Collard, K.S. Lay, L. Borand, A. Ndir, T.R. Walsh, D. Guillemot, L. Borand, A. De Lauzanne, A. Kerleguer, A. Tarantola, P. Piola, T. Chon, S. Lach, V. Ngo, S. Touch, Z.Z. Andrianirina, M. Vray, V. Richard, A. Seck, R. Bercion, A.G. Sow, J.B. Diouf, P.S. Dieye, B. Sy, B. Ndao, M. Seguy, L. Watier, A.Y. Abdou. Combating global antibiotic resistance: Emerging one health concerns in lower- and middle-income countries. Clin. Infect. Dis., 66: 963–969 (2018).

[22] S. Bin Zaman, M.A. Hussain, R. Nye, V. Mehta, K.T. Mamun, N. Hossain. A review on antibiotic resistance: Alarm bells are ringing. Cureus, 9: e1403 (2017).

[23] T.F. Schäberle, I.M. Hack. Overcoming the current deadlock in antibiotic research. Trends Microbiol., 22: 165–167 (2014).

[24] B. Li, T.J. Webster. Bacteria antibiotic resistance: New challenges and opportunities for implant-associated orthopedic infections. J. Orthop. Res., 36: 22–32 (2017).

[25] The Federal Government Germany. DART 2020: Fighting antibiotic resistance for the good of both humans and animals. (2015).

[26] Joint programming initiative on antimicrobial resistance: JPIAMR implementation plan 2014 – 2018. (2015).

[27] European Comission. A european one health action plan against antimicrobial resistance (AMR). (2017).

[28] L. Matthiessen, R. Bergström, S. Dustdar, P. Meulien, R. Draghia-Akli. Increased momentum in antimicrobial resistance research. Lancet, 388: 865 (2016).

[29] Wold Health Organisation. Global action plan on antimicrobial resistance. (2015).

[30] K. Lambrini. The rational use of antibiotics medicine. J. Healthc. Commun., 2: 1–4 (2017).

[31] G. Levy Hara, S.S. Kanj, L. Pagani, L. Abbo, A. Endimiani, H.F.L. Wertheim, C. Amábile-Cuevas, P. Tattevin, S. Mehtar, F. Lopes Cardoso, S. Unal, I. Gould. Ten key points for the appropriate use of antibiotics in hospitalised patients: a consensus from the Antimicrobial Stewardship and Resistance Working Groups of the International Society of Chemotherapy. Int. J. Antimicrob. Agents, 48: 239–246 (2016).

[32] J. Cohen, J.-L. Vincent, N.K.J. Adhikari, F.R. Machado, D.C. Angus, T. Calandra, K. Jaton, S. Giulieri, J. Delaloye, S. Opal, K. Tracey, T. van der Poll, E. Pelfrene. Sepsis: a roadmap for future research. Lancet Infect. Dis., 15: 581–614 (2015).

[33] K. de With, F. Allerberger, S. Amann, P. Apfalter, H.-R. Brodt, T. Eckmanns, M. Fellhauer, H.K. Geiss, O. Janata, R. Krause, S. Lemmen, E. Meyer, H. Mittermayer, U. Porsche, E. Presterl, S. Reuter, B. Sinha, R. Strauß, A. Wechsler-Fördös, C. Wenisch, W. V. Kern. Strategies to enhance rational use of antibiotics in hospital: a guideline by the German Society for Infectious Diseases. Infection, 44: 395–439 (2016).

[34] A. Kumar. Early antimicrobial therapy in severe sepsis and septic shock. Curr. Infect. Dis. Rep., 12: 336–344 (2010).

[35] S. Harbarth, J. Garbino, J. Pugin, J.A. Romand, D. Lew, D. Pittet. Inappropriate initial antimicrobial therapy and its effect on survival in a clinical trial of immunomodulating therapy for severe sepsis. Am. J. Med., 115: 529–535 (2003).

[36] R.D. MacArthur, M. Miller, T. Albertson, E. Panacek, D. Johnson, L. Teoh, W. Barchuk. Adequacy of early empiric antibiotic treatment and survival in severe sepsis: experience from the MONARCS trial. Clin. Infect. Dis., 38: 284–288 (2004).

[37] A. Rhodes, L.E. Evans, W. Alhazzani, M.M. Levy, M. Antonelli, R. Ferrer, A. Kumar, J.E. Sevransky, C.L. Sprung, M.E. Nunnally, B. Rochwerg, G.D. Rubenfeld, D.C. Angus, D. Annane, R.J. Beale, G.J. Bellinghan, G.R. Bernard, J.-D. Chiche, C. Coopersmith, D.P. De Backer, C.J. French, S. Fujishima, H. Gerlach, J.L. Hidalgo, S.M. Hollenberg, A.E. Jones, D.R. Karnad, R.M. Kleinpell, Y. Koh, T.C. Lisboa, F.R. Machado, J.J. Marini, J.C. Marshall, J.E. Mazuski, L.A. McIntyre, A.S. McLean, S. Mehta, R.P. Moreno, J. Myburgh, P. Navalesi, O. Nishida, T.M. Osborn, A. Perner, C.M. Plunkett, M. Ranieri, C.A. Schorr, M.A. Seckel, C.W. Seymour, L. Shieh, K.A. Shukri, S.Q. Simpson, M. Singer, B.T. Thompson, S.R. Townsend, T. Van der Poll, J.-L. Vincent, W.J. Wiersinga, J.L. Zimmerman, R.P. Dellinger. Surviving sepsis campaign: international guidelines for management of sepsis and septic shock: 2016. Intensive Care Med., 43: 304–377 (2017).

[38] J.A. Roberts, S.K. Paul, M. Akova, M. Bassetti, J.J. De Waele, G. Dimopoulos, K.-M. Kaukonen, D. Koulenti, C. Martin, P. Montravers, J. Rello, A. Rhodes, T. Starr, S.C. Wallis, J. Lipman, J.A. Roberts, J. Lipman, T. Starr, S.C. Wallis, S.K. Paul, A. Margarit Ribas, J.J. De Waele, L. De Crop, H. Spapen, J. Wauters, T. Dugernier, P. Jorens, I. Dapper, D. De Backer, F.S. Taccone, J. Rello, L. Ruano, E. Afonso, F. Alvarez-Lerma, M.P. Gracia-Arnillas, F. Fernandez, N. Feijoo, N. Bardolet, A. Rovira, P. Garro, D. Colon, C. Castillo, J. Fernado, M.J. Lopez, J.L. Fernandez, A.M. Arribas, J.L. Teja, E. Ots, J. Carlos Montejo, M. Catalan, I. Prieto, G. Gonzalo, B. Galvan, M.A. Blasco, E. Meyer, F. Del Nogal, L. Vidaur, R. Sebastian, P.M. Garde, M. d. M. Martin Velasco, R. Zaragoza Crespo, M. Esperatti, A. Torres, P. Montravers, O. Baldesi, H. Dupont, Y. Mahjoub, S. Lasocki, J.M. Constantin, J.F. Payen, C. Martin, J. Albanese, Y. Malledant, J. Pottecher, J.-Y. Lefrant, S. Jaber, O. Joannes-Boyau, C. Orban, M. Ostermann, C. McKenzie, W. Berry, J. Smith, K. Lei, F. Rubulotta, A. Gordon, S. Brett, M. Stotz, M. Templeton, A. Rhodes, C. Ebm, C. Moran, K.-M. Kaukonen, V. Pettila, G. Dimopoulos, D. Koulenti, A. Xristodoulou, V. Theodorou, G. Kouliatsis, E. Sertaridou, G. Anthopoulos, *et al.* DALI: Defining antibiotic levels in intensive care unit patients: are current β-Lactam antibiotic doses sufficient for critically Ill patients? Clin. Infect. Dis., 58: 1072–1083 (2014).

[39] R.E. Ariano, S.A. Zelenitsky, A. Nyhlén, D.S. Sitar. An evaluation of an optimal sampling strategy for meropenem in febrile neutropenics. J. Clin. Pharmacol., 45: 832–835 (2005).

[40] A.E. Muller, N. Punt, J.W. Moutona. Exposure to ceftobiprole is associated with microbiological eradication and clinical cure in patients with nosocomial pneumonia. Antimicrob. Agents Chemother., 58: 2512–2519 (2014).

[41] J. a Roberts, P. Kruger, D.L. Paterson, J. Lipman. Antibiotic resistance--what's dosing got to do with it? Crit. Care Med., 36: 2433–2440 (2008).

[42] V.H. Tam, A.N. Schilling, S. Neshat, D. a Melnick, E. a Coyle, K. Poole. Optimization of meropenem minimum concentration / MIC ratio to suppress in vitro resistance of Pseudomonas aeruginosa. Antimicrob. Agents Chemother., 49: 4920–4927 (2005).

[43] U. Theuretzbacher. Tissue penetration of antibacterial agents: how should this be incorporated into pharmacodynamic analyses? Curr. Opin. Pharmacol., 7: 498–504 (2007).

[44] M. Muller, A. dela Pena, H. Derendorf. Issues in pharmacokinetics and pharmacodynamics of anti-infective agents: Distribution in tissue. Antimicrob. Agents Chemother., 48: 1441–1453 (2004).

[45] I.K. Minichmayr, A. Schaeftlein, J.L. Kuti, M. Zeitlinger, C. Kloft. Clinical Determinants of target non-attainment of linezolid in plasma and interstitial space fluid: A pooled population pharmacokinetic analysis with focus on critically ill patients. Clin. Pharmacokinet., 56: 617–633 (2017).

[46] M.J.E. Brill, A.P.I. Houwink, S. Schmidt, E.P.A. Van Dongen, E.J. Hazebroek, B. van Ramshorst, V.H. Deneer, J.W. Mouton, C.A.J. Knibbe. Reduced subcutaneous tissue distribution of cefazolin in morbidly obese versus non-obese patients determined using clinical microdialysis. J. Antimicrob. Chemother., 69: 715–723 (2014).

[47] T.A. Riccobene, R. Pushkin, A. Jandourek, W. Knebel, T. Khariton. Penetration of ceftaroline into

the epithelial lining fluid of healthy adult subjects. Antimicrob. Agents Chemother., 60: 5849–5857 (2016).

[48] K.K. Hansen, F. Nielsen, T.B. Stage, U. Jørgensen, O. Skov, L.E. Rasmussen. Microdialysis as a tool to determine the local tissue concentration of dicloxacillin in man. Br. J. Clin. Pharmacol., 84: 533–541 (2018).

[49] A.M. Barbour, S. Schmidt, L. Zhuang, K. Rand, H. Derendorf. Application of pharmacokinetic/pharmacodynamic modelling and simulation for the prediction of target attainment of ceftobiprole against meticillin-resistant Staphylococcus aureus using minimum inhibitory concentration and time–kill curve based approaches. Int. J. Antimicrob. Agents, 43: 60–67 (2014).

[50] A. Barbour, S. Schmidt, W.R. Rout, K. Ben-David, O. Burkhardt, H. Derendorf. Soft tissue penetration of cefuroxime determined by clinical microdialysis in morbidly obese patients undergoing abdominal surgery. Int. J. Antimicrob. Agents, 34: 231–235 (2009).

[51] M.T. Heinrichs, S. Vashakidze, K. Nikolaishvili, I. Sabulua, N. Tukvadze, N. Bablishvili, S. Gogishvili, B.P. Little, A. Bernheim, J. Guarner, C.A. Peloquin, H.M. Blumberg, H. Derendorf, R.R. Kempker. Moxifloxacin target site concentrations in patients with pulmonary TB utilizing microdialysis: a clinical pharmacokinetic study. J. Antimicrob. Chemother., 73: 477–483 (2018).

[52] J. Lin. Tissue distribution and pharmacodynamics: A complicated relationship. Curr. Drug Metab., 7: 39–65 (2006).

[53] D.M. Ryan. Pharmacokinetics of antibiotics in natural and experimental superficial compartments in animals and humans. J. Antimicrob. Chemother., 31: 1–16 (1993).

[54] D. Gonzalez, S. Schmidt, H. Derendorf. Importance of relating efficacy measures to unbound drug concentrations for anti-infective agents. Clin. Microbiol. Rev., 26: 274–288 (2013).

[55] A.T. Y. Deguchi, T. Terasaki, H. Yamada. An application of microdialysis to drug tissue distribution study: In vivo evidence for free-ligand hypothesis and tissue binding of ß-Lactam antibiotics in interstitial fluids. J. Pharmacobiodyn., 15: 79–89 (1992).

[56] M. Müller, O. Haag, T. Burgdorff, A. Georgopoulos, W. Weninger, B. Jansen, G. Stanek, H. Pehamberger, E. Agneter, H.G. Eichler. Characterization of peripheral-compartment kinetics of antibiotics by in vivo microdialysis in humans. Antimicrob. Agents Chemother., 40: 2703–9 (1996).

[57] S. Schmidt, K. Rock, M. Sahre, O. Burkhardt, M. Brunner, M.T. Lobmeyer, H. Derendorf. Effect of protein binding on the pharmacological activity of highly bound antibiotics. Antimicrob. Agents Chemother., 52: 3994–4000 (2008).

[58] R. Wise. The clinical relevance of protein binding and tissue concentrations in antimicrobial therapy. Clin. Pharmacokinet., 11: 470–482 (1986).

[59] W.A. Craig, P.G. Welling. Protein binding of antimicrobials. Clin. Pharmacokinet., 2: 252–268 (1977).

[60] M. Hammarlund-Udenaes. Microdialysis as an important technique in systems pharmacology—a historical and methodological review. AAPS J., 19: 1294–1303 (2017).

[61] C. Kirbs, C. Kloft. In vitro microdialysis recovery and delivery investigation of cytokines as prerequisite for potential biomarker profiling. Eur. J. Pharm. Sci., 57: 48–59 (2014).

[62] A.N. Deitchman, M.T. Heinrichs, V. Khaowroongrueng, S.B. Jadhav, H. Derendorf. Utility of microdialysis in infectious disease drug development and dose optimization. AAPS J., 19: 334–342 (2017).

[63] European Medicines Agency. Guideline on the use of pharmacokinetics and pharmacodynamics in the development of antibacterial medicinal products. (2016).

[64] C.S. Chaurasia. In vivo microdialysis sampling: theory and applications. Biomed. Chromatogr., 13: 317–332 (1999).

[65] N. Plock, C. Kloft. Microdialysis—theoretical background and recent implementation in applied life-sciences. Eur. J. Pharm. Sci., 25: 1–24 (2005).

[66] E.C.M. De Lange. Recovery and calibration techniques: Toward quantitative microdialysis. In: Müller M (Ed.). Microdialysis in Drug Development. Springer, New York: 13–33 (2013).

[67] S. Quist, C. Kirbs, C. Kloft, H. Gollnick. Cytokine and chemokine recovery is increased by colloid perfusates during dermal microdialysis. Materials (Basel)., 11: 682 (2018).

[68] E.S. Zimmermann, J.V. Laureano, C.N. dos Santos, S. Schmidt, C. V. Lagishetty, W.V. de Castro, T. Dalla Costa. Simultaneous semimechanistic population analyses of levofloxacin in plasma, lung, and prostate to describe the influence of efflux transporters on drug distribution following intravenous and intratracheal administration. Antimicrob. Agents Chemother., 60: 946–954 (2016).

[69] A.D. Smith, J.B. Justice. The effect of inhibition of synthesis, release, metabolism and uptake on the microdialysis extraction fraction of dopamine. J. Neurosci. Methods, 54: 75–82 (1994).

[70] R.J.O. Cosford, A.P. Vinson, S. Kukoyi, J.B. Justice. Quantitative microdialysis of serotonin and norepinephrine: Pharmacological influences on in vivo extraction fraction. J. Neurosci. Methods, 68: 39–47 (1996).

[71] E.C.M. De Lange, G. De Bock, A.H. Schinkel, A.G. De Boer, D.D. Breimer. BBB transport and P-glycoprotein functionality using MDR1A (-/-) and wild-type mice. Total brain versus microdialysis concentration profiles of rhodamine-123. Pharm. Res., 15: 1657–1665 (1998).

[72] https://www.who.int/en/news-room/fact-sheets/detail/obesity-and-overweight (last access 10 Mar 2019).

[73] A. Hruby, F.B. Hu. The epidemiology of obesity: A big picture. Pharmacoeconomics, 33: 673–689 (2015).

[74] R. Huttunen, J. Syrjänen. Obesity and the risk and outcome of infection. Int. J. Obes., 37: 333–340 (2013).

[75] M.E. Falagas, M. Kompoti. Obesity and infection. Lancet Infect. Dis., 6: 438–446 (2006).

[76] M.A. Olsen, J. Higham-Kessler, D.S. Yokoe, A.M. Butler, J. Vostok, K.B. Stevenson, Y. Khan, V.J. Fraser. Developing a risk stratification model for surgical site infection after abdominal hysterectomy. Infect. Control Hosp. Epidemiol., 30: 1077–1083 (2009).

[77] G. Beldi, S. Bisch-Knaden, V. Banz, K. Mühlemann, D. Candinas. Impact of intraoperative behavior on surgical site infections. Am. J. Surg., 198: 157–162 (2009).

[78] A. Di Leo, S. Piffer, F. Ricci, A. Manzi, E. Poggi, V. Porretto, P. Fambri, G. Piccini, T. Patrizia, L. Fabbri, R. Busetti. Surgical site infections in an italian surgical ward: A prospective study. Surg. Infect. (Larchmt)., 10: 533–538 (2009).

[79] E. Waisbren, H. Rosen, A.M. Bader, S.R. Lipsitz, S.O. Rogers, E. Eriksson. Percent body fat and prediction of surgical site infection. J. Am. Coll. Surg., 210: 381–389 (2010).

[80] D. Dindo, M.K. Muller, M. Weber, P.-A. Clavien. Obesity in general elective surgery. Lancet, 361: 2032–2035 (2003).

[81] T. Chopra, J.J. Zhao, G. Alangaden, M.H. Wood, K.S. Kaye. Preventing surgical site infections after bariatric surgery: value of perioperative antibiotic regimens. Expert Rev. Pharmacoecon. Outcomes Res., 10: 317–328 (2010).

[82] N. Runkel, M. Colombo-Benkmann, T.P. Hüttl, H. Tigges, O. Mann, R. Flade-Kuthe, E. Shang, M. Susewind, S. Wolff, R. Wunder, A. Wirth, K. Winckler, A. Weimann, M. de Zwaan, S. Sauerland. Evidence-based German guidelines for surgery for obesity. Int. J. Colorectal Dis., 26: 397–404 (2011).

[83] National Insitute of Health. Clinical guidelines on the identification, evaluation, and treatment of overweight and obesity in adults: The evidence report. (1998).

[84] N. V. Christou, J.S. Sampalis, M. Liberman, D. Look, S. Auger, A.P.H. McLean, L.D. MacLean. Surgery decreases long-term mortality, morbidity, and health care use in morbidly obese patients. Ann. Surg., 240: 416–424 (2004).

[85] R. Marsk, E. Näslund, J. Freedman, P. Tynelius, F. Rasmussen. Bariatric surgery reduces mortality in Swedish men. Br. J. Surg., 97: 877–883 (2010).

[86] D. Bradley, F. Magkos, S. Klein. Effects of bariatric surgery on glucose homeostasis and type 2 diabetes. Gastroenterology, 143: 897–912 (2012).

[87] S.-H. Chang, C.R.T. Stoll, J. Song, E. Varela, C.J. Eagon, G. a Colditz. Bariatric surgery: an updated systematic review and meta analysis, 2003–2012. JAMA Surg., 149: 275–287 (2014).

[88] C. Koliaki, S. Liatis, C.W. le Roux, A. Kokkinos. The role of bariatric surgery to treat diabetes: current challenges and perspectives. BMC Endocr. Disord., 17: 50 (2017).

[89] G.B. Forbes, S.L. Welle. Lean body mass in obesity. Int. J. Obes., 7: 99–107 (1983).

[90] A.S. Alobaid, M. Hites, J. Lipman, F.S. Taccone, J.A. Roberts. Effect of obesity on the pharmacokinetics of antimicrobials in critically ill patients: A structured review. Int. J. Antimicrob. Agents, 47: 259–268 (2016).

[91] P. Poirier, T.D. Giles, G.A. Bray, Y. Hong, J.S. Stern, F.X. Pi-Sunyer, R.H. Eckel. Obesity and cardiovascular disease. Arterioscler. Thromb. Vasc. Biol., 26: 968–976 (2006).

[92] G.T. Lesser, S. Deutsch. Measurement of adipose tissue blood flow and perfusion in man by uptake of $^{85}Kr^{1}$. J. Appl. Physiol., 23: 621–630 (1967).

[93] C. Santos, P. Marques da Silva. Hemodynamic patterns in obesity associated hypertension. BMC Obes., 5: 13 (2018).

[94] D. O'Shea, S.N. Davis, R.B. Kim, G.R. Wilkinson. Effect of fasting and obesity in humans on the 6-hydroxylation of chlorzoxazone: a putative probe of CYP2E1 activity. Clin. Pharmacol. Ther., 56: 359–67 (1994).

[95] M. Emery. CYP2E1 activity before and after weight loss in morbidly obese subjects with nonalcoholic fatty liver disease. Hepatology, 38: 428–435 (2003).

[96] M. Kotlyar, S.W. Carson. Effects of obesity on the cytochrome P450 enzyme system. Int. J. Clin. Pharmacol. Ther., 37: 8–19 (1999).

[97] W.S. Nimmo, J.E. Peacock. Effect of anaesthesia and surgery on pharmacokinetics and pharmacodynamics. Br. Med. Bull., 44: 286–301 (1988).

[98] J.M. Kennedy, A.M. Van Riji. Effects of surgery on the pharmacokinetic parameters of drugs. Clin. Pharmacokinet., 35: 293–312 (1998).

[99] J.W. Sear. Kidney dysfunction in the postoperative period. Br. J. Anaesth., 95: 20–32 (2005).

[100] J.C. Marshall, L. Bosco, N.K. Adhikari, B. Connolly, J. V. Diaz, T. Dorman, R.A. Fowler, G. Meyfroidt, S. Nakagawa, P. Pelosi, J.-L. Vincent, K. Vollman, J. Zimmerman. What is an intensive care unit? A report of the task force of the World Federation of Societies of Intensive and Critical Care Medicine. J. Crit. Care, 37: 270–276 (2017).

[101] J.A. Roberts, M.H. Abdul-Aziz, J. Lipman, J.W. Mouton, A.A. Vinks, T.W. Felton, W.W. Hope, A. Farkas, M.N. Neely, J.J. Schentag, G. Drusano, O.R. Frey, U. Theuretzbacher, J.L. Kuti. Individualised antibiotic dosing for patients who are critically ill: challenges and potential solutions. Lancet Infect. Dis., 14: 498–509 (2014).

[102] G. Valenza, H. Seifert, S. Decker-Burgard, J. Laeuffer, I. Morrissey, R. Mutters. Comparative Activity of Carbapenem Testing (COMPACT) study in Germany. Int. J. Antimicrob. Agents, 39: 255–258 (2012).

[103] A. Vieillard-Baron, S. Prin, K. Chergui, O. Dubourg, F. Jardin. Hemodynamic instability in sepsis. Am. J. Respir. Crit. Care Med., 168: 1270–1276 (2003).

[104] A.A. Udy, J.P. Baptista, N.L. Lim, G.M. Joynt, P. Jarrett, L. Wockner, R.J. Boots, J. Lipman. Augmented renal clearance in the ICU. Crit. Care Med., 42: 520–527 (2014).

[105] I. Bilbao-Meseguer, A. Rodríguez-Gascón, H. Barrasa, A. Isla, M.Á. Solinís. Augmented renal

clearance in critically ill patients: A systematic review. Clin. Pharmacokinet., 57: 1107–1121 (2018).

[106] A.A. Udy, J.M. Varghese, M. Altukroni, S. Briscoe, B.C. McWhinney, J.P. Ungerer, J. Lipman, J.A. Roberts. Subtherapeutic initial β-Lactam concentrations in select critically ill patients. Chest, 142: 30–39 (2012).

[107] C.-Y. Yang, P. Xu, Y.-J. Yang, B.-Y. Li, S.-Z. Sun, Q.-Z. Yang, L.-X. Wang. Systemic capillary leak syndrome due to systemic inflammatory response syndrome in infants: a report on 31 patients. Open Med., 9: 477–480 (2014).

[108] E. Frazee, K. Kashani. Fluid management for critically ill patients: A review of the current state of fluid therapy in the intensive care unit. Kidney Dis., 2: 64–71 (2016).

[109] J. Lipman, A.A. Udy, J.A. Roberts. Do we understand the impact of altered physiology, consequent interventions and resultant clinical scenarios in the intensive care unit? The Antibiotic Story. Anaesth. Intensive Care, 39: 999–1000 (2011).

[110] M. Ulldemolins, J.A. Roberts, J. Rello, D.L. Paterson, J. Lipman. The effects of hypoalbuminaemia on optimizing antibacterial dosing in critically ill patients. Clin. Pharmacokinet., 50: 99–110 (2011).

[111] J.P. Nicholson, M.R. Wolmarans, G.R. Park. The role of albumin in critical illness. Br. J. Anaesth., 85: 599–610 (2000).

[112] G.G. Zhanel, C. Johanson, J.M. Embil, A. Noreddin, A. Gin, L. Vercaigne, D.J. Hoban. Ertapenem: review of a new carbapenem. Expert Rev. Anti. Infect. Ther., 3: 23–39 (2005).

[113] Y. Imanaka, T. Umegaki, H. Ikai. The impact of acute organ dysfunction on patients′ mortality with severe sepsis. J. Anaesthesiol. Clin. Pharmacol., 27: 180–184 (2011).

[114] N.I. Lone, T.S. Walsh. Impact of intensive care unit organ failures on mortality during the five years after a critical illness. Am. J. Respir. Crit. Care Med., 186: 640–647 (2012).

[115] F. Husain-Syed, Z. Ricci, D. Brodie, J.-L. Vincent, V.M. Ranieri, A.S. Slutsky, F.S. Taccone, L. Gattinoni, C. Ronco. Extracorporeal organ support (ECOS) in critical illness and acute kidney injury: from native to artificial organ crosstalk. Intensive Care Med., 44: 1447–1459 (2018).

[116] D.M. Roberts, X. Liu, J.A. Roberts, P. Nair, L. Cole, M.S. Roberts, J. Lipman, R. Bellomo. A multicenter study on the effect of continuous hemodiafiltration intensity on antibiotic pharmacokinetics. Crit. Care, 19: 84 (2015).

[117] F.B. Sime, J.A. Roberts. Antibiotic dosing in critically ill patients receiving renal replacement therapy. Expert Rev. Clin. Pharmacol., 9: 497–499 (2016).

[118] A. Isla, J. Maynar, J.Á. Sánchez-Izquierdo, A.R. Gascón, A. Arzuaga, E. Corral, J.L. Pedraz. Meropenem and continuous renal replacement therapy: In vitro permeability of 2 continuous renal replacement therapy membranes and influence of patient renal function on the pharmacokinetics in critically ill patients. J. Clin. Pharmacol., 45: 1294–1304 (2005).

[119] M.G. Vossen, L. Ehmann, S. Pferschy, A. Maier-Salamon, M. Haidinger, C. Weiser, J.M. Wenisch, K. Saria, C. Kajahn, S. Jilch, R. Lemmerer, M. Bécède, M. Zeitlinger, C. Kloft, W. Jäger, F. Thalhammer. Elimination of doripenem during dialysis and pharmacokinetic evaluation of posthemodialysis dosing for patients undergoing intermittent renal replacement therapy. Antimicrob. Agents Chemother., 62: e02430-17 (2018).

[120] V. Cheng, M.-H. Abdul-Aziz, J.A. Roberts, K. Shekar. Optimising drug dosing in patients receiving extracorporeal membrane oxygenation. J. Thorac. Dis., 10: S629–S641 (2018).

[121] K. Shekar, J.A. Roberts, M.T. Smith, Y.L. Fung, J.F. Fraser. The ECMO PK Project: an incremental research approach to advance understanding of the pharmacokinetic alterations and improve patient outcomes during extracorporeal membrane oxygenation. BMC Anesthesiol., 13: 7 (2013).

[122] K. Shekar, J.A. Roberts, S. Welch, H. Buscher, S. Rudham, F. Burrows, S. Ghassabian, S.C. Wallis, B. Levkovich, V. Pellegrino, S. McGuinness, R. Parke, E. Gilder, A.G. Barnett, J. Walsham, D. V Mullany, Y.L. Fung, M.T. Smith, J.F. Fraser. ASAP ECMO: Antibiotic, sedative and analgesic pharmacokinetics during extracorporeal membrane oxygenation: a multi-centre study to optimise

drug therapy during ECMO. BMC Anesthesiol., 12: 29 (2012).

[123] J.W. Mouton, P.G. Ambrose, R. Canton, G.L. Drusano, S. Harbarth, A. MacGowan, U. Theuretzbacher, J. Turnidge. Conserving antibiotics for the future: New ways to use old and new drugs from a pharmacokinetic and pharmacodynamic perspective. Drug Resist. Updat., 14: 107–117 (2011).

[124] J.H. Jorgensen, M.J. Ferraro. Antimicrobial susceptibility testing: A review of general principles and contemporary practices. Clin. Infect. Dis., 49: 1749–1755 (2009).

[125] K. Syal, M. Mo, H. Yu, R. Iriya, W. Jing, S. Guodong, S. Wang, T.E. Grys, S.E. Haydel, N. Tao. Current and emerging techniques for antibiotic susceptibility tests. Theranostics, 7: 1795–1805 (2017).

[126] S. Puttaswamy, S.K. Gupta, H. Regunath, L.P. Smith, S. Sengupta. A comprehensive review of the present and future antibiotic susceptibility testing (AST) systems. Arch. Clin. Microbiol., 9: 1–9 (2018).

[127] M. Balouiri, M. Sadiki, S.K. Ibnsouda. Methods for in vitro evaluating antimicrobial activity: A review. J. Pharm. Anal., 6: 71–79 (2016).

[128] Clinical and Laboratory Standards Institute. Methods for dilution antimicrobial susceptibility tests for bacteria that grow aerobically: M07. Wayne, PA, 11th ed. (2018).

[129] A.A. Vinks, J.W. Mouton, H. Derendorf. Fundamentals of Antimicrobial Pharmacokinetics and Pharmacodynamics. Springer, New York (2014).

[130] J.B. Bulitta, W.W. Hope, A.E. Eakin, T. Guina, V.H. Tam, A. Louie, G.L. Drusano, J.L. Hoover. Generating robust and informative nonclinical in vitro and in vivo bacterial infection model efficacy data to support translation to humans. Antimicrob. Agents Chemother., 63: e02307-18 (2019).

[131] G. Wong, A. Brinkman, R.J. Benefield, M. Carlier, J.J. De Waele, N. El Helali, O. Frey, S. Harbarth, A. Huttner, B. McWhinney, B. Misset, F. Pea, J. Preisenberger, M.S. Roberts, T.A. Robertson, A. Roehr, F.B. Sime, F.S. Taccone, J.P.J. Ungerer, J. Lipman, J.A. Roberts. An international, multicentre survey of -lactam antibiotic therapeutic drug monitoring practice in intensive care units. J. Antimicrob. Chemother., 69: 1416–1423 (2014).

[132] EUCAST database: Antimicrobial wild type distributions of microorganisms. https://mic.eucast.org (last access 23 Mar 2019).

[133] The European Committee on Antimicrobial Susceptibility Testing. Standard Operating Procedure Harmonization of breakpoints for existing antimicrobial agents, SOP 2.2. http//www.eucast.org (last access 17 Aug 2019).

[134] J. Turnidge, D.L. Paterson. Setting and revising antibacterial susceptibility breakpoints. Clin. Microbiol. Rev., 20: 391–408 (2007).

[135] P.G. Ambrose, S.M. Bhavnani, C.M. Rubino, A. Louie, T. Gumbo, A. Forrest, G.L. Drusano. Antimicrobial resistance: Pharmacokinetics-pharmacodynamics of antimicrobial therapy: It's not just for mice anymore. Clin. Infect. Dis., 44: 79–86 (2007).

[136] T. Velkov, P.J. Bergen, J. Lora-Tamayo, C.B. Landersdorfer, J. Li. PK/PD models in antibacterial development. Curr. Opin. Microbiol., 16: 573–579 (2013).

[137] T. Tuntland, B. Ethell, T. Kosaka, F. Blasco, R.X. Zang, M. Jain, T. Gould, K. Hoffmaster. Implementation of pharmacokinetic and pharmacodynamic strategies in early research phases of drug discovery and development at Novartis Institute of Biomedical Research. Front. Pharmacol., 5: 1–16 (2014).

[138] A. Zahedi Bialvaei, M. Rahbar, M. Yousefi, M. Asgharzadeh, H. Samadi Kafil. Linezolid: a promising option in the treatment of Gram-positives. J. Antimicrob. Chemother., 72: 354–364 (2017).

[139] Pfizer. Zyvox 2 mg/ml Solution for Infusion, Summary of Product Characteristics (2017). https://www.medicines.org.uk/emc/product/2931/smpc (last access 17 Aug 2019).

[140] A. Di Paolo, P. Malacarne, E. Guidotti, R. Danesi, M. Del Tacca. Pharmacological issues of linezolid. Clin. Pharmacokinet., 49: 439–447 (2010).

[141] https://www.drugbank.ca/drugs/DB00601 (last access 04 Mar 2019).

[142] ChemAxon for Linezolid. https://chemicalize.com/ (last access 27 Jul 2019).

[143] S.M. Hashemian, T. Farhadi, M. Ganjparvar. Linezolid: a review of its properties, function, and use in critical care. Drug Des. Devel. Ther., 12: 1759–1767 (2018).

[144] Pfizer. Zyvox injection, tablets, for oral suspension, Summary of Product Characteristics (2011). https://www.accessdata.fda.gov/drugsatfda_docs/label/2012/021130s028lbl.pdf (last access 17 Aug 2019). (2011).

[145] D.J. Stalker, G.L. Jungbluth. Clinical pharmacokinetics of linezolid, a novel oxazolidinone antibacterial. Clin. Pharmacokinet., 42: 1129–1140 (2003).

[146] N. Plock, C. Buerger, C. Joukhadar, S. Kljucar, C. Kloft. Does linezolid inhibit its own metabolism? Population pharmacokinetics as a tool to explain the observed nonlinearity in both healthy volunteers and septic patients. Drug Metab. Dispos., 35: 1816–1823 (2007).

[147] J.G. Slatter, D.J. Stalker, K.L. Feenstra, I.R. Welshman, J.B. Bruss, J.P. Sams, M.G. Johnson, P.E. Sanders, M.J. Hauer, P.E. Fagerness, R.P. Stryd, G.W. Peng, E.M. Shobe. Pharmacokinetics, metabolism, and excretion of linezolid following an oral dose of [^{14}C]linezolid to healthy human subjects. Drug Metab. Dispos., 29: 1136–45 (2001).

[148] M.A. Wynalda, M.J. Hauer, L.C. Wienkers. Oxidation of the novel oxazolidinone antibiotic linezolid in human liver microsomes. Drug Metab. Dispos., 28: 1014–1017 (2000).

[149] A. Sandberg, K.S. Jensen, P. Baudoux, F. van Bambeke, P.M. Tulkens, N. Frimodt-Møller. Intra- and extracellular activity of linezolid against Staphylococcus aureus in vivo and in vitro. J. Antimicrob. Chemother., 65: 962–973 (2010).

[150] D. Andes, M.L. Van Ogtrop, J. Peng, W.A. Craig. In vivo pharmacodynamics of a new oxazolidinone (linezolid). Antimicrob. Agents Chemother., 46: 3484–3489 (2002).

[151] M.J. Gentry-Nielsen, K.M. Olsen, L.C. Preheim. Pharmacodynamic activity and efficacy of linezolid in a rat model of pneumococcal pneumonia. Antimicrob. Agents Chemother., 46: 1345–1351 (2002).

[152] C. Jacqueline, E. Batard, L. Perez, D. Boutoille, A. Hamel, J. Caillon, M.-F. Kergueris, G. Potel, D. Bugnon. In vivo efficacy of continuous infusion versus intermittent dosing of linezolid compared to vancomycin in a methicillin-resistant staphylococcus aureus rabbit endocarditis model. Antimicrob. Agents Chemother., 46: 3706–3711 (2002).

[153] C.R. Rayner, A. Forrest, A.K. Meagher, M.C. Birmingham, J.J. Schentag. Clinical pharmacodynamics of linezolid in seriously ill patients treated in a compassionate use programme. Clin. Pharmacokinet., 42: 1411–23 (2003).

[154] M. Narita, B.T. Tsuji, V.L. Yu. Linezolid-associated peripheral and optic neuropathy, lactic acidosis, and serotonin syndrome. Pharmacotherapy, 27: 1189–1197 (2007).

[155] H. Jang, S. Kim, K.H. Kim, C.J. Kim, S. Lee, K. Song, J.H. Jeon, W.B. Park, H. Bin Kim, S. Park, N.J. Kim, E. Kim, M. Oh, K.W. Choe. Salvage treatment for persistent methicillin-resistant staphylococcus aureus bacteremia: Efficacy of linezolid with or without carbapenem. Clin. Infect. Dis., 49: 395–401 (2009).

[156] G.G. Zhanel, R. Wiebe, L. Dilay, K. Thomson, E. Rubinstein, D.J. Hoban, A.M. Noreddin, J.A. Karlowsky. Comparative Review of the Carbapenems. 67: 1027–1052 (2007).

[157] Pfizer. Meronem IV 500mg, Summary of Product Characteristics (2019), https://www.medicines.org.uk/emc/product/6731/smpc (last access 17 Aug 2019).

[158] C.M. Baldwin, K.A. Lyseng-Williamson, S.J. Keam. Meropenem - A Review of its Use in the Treatment of Serious Bacterial Infections. Drugs, 68: 803–838 (2008).

[159] https://www.drugbank.ca/drugs/DB00760 (last access 04 Mar 2019).

[160] W.A. Craig. The pharmacology of meropenem, a new carbapenem antibiotic. Clin. Infect. Dis., 24: S266–S275 (1997).

[161] T. Shibayama, D. Sugiyama, E. Kamiyama, T. Tokui, T. Hirota, T. Ikeda. Characterization of CS-023 (RO4908463), a novel parenteral carbapenem antibiotic, and meropenem as substrates of human renal transporters. Drug Metab. Pharmacokinet., 22: 41–47 (2007).

[162] Y. Hagos, N.A. Wolff. Assessment of the role of renal organic anion transporters in drug-induced nephrotoxicity. Toxins (Basel)., 2: 2055–2082 (2010).

[163] F. de Velde, J.W. Mouton, B.C.M. de Winter, T. van Gelder, B.C.P. Koch. Clinical applications of population pharmacokinetic models of antibiotics: Challenges and perspectives. Pharmacol. Res., 134: 280–288 (2018).

[164] G.L. Drusano. Prevention of resistance: a goal for dose selection for antimicrobial agents. Clin. Infect. Dis., 36: S42–S50 (2003).

[165] C.T. Ong, P.R. Tessier, C. Li, C.H. Nightingale, D.P. Nicolau. Comparative in vivo efficacy of meropenem, imipenem, and cefepime against Pseudomonas aeruginosa expressing MexA-MexB-OprM efflux pumps. Diagn. Microbiol. Infect. Dis., 57: 153–161 (2007).

[166] J.L. Crandon, C. Luyt, A. Aubry, J. Chastre, D.P. Nicolau. Pharmacodynamics of carbapenems for the treatment of Pseudomonas aeruginosa ventilator-associated pneumonia : associations with clinical outcome and recurrence. J. Antimicrob. Chemother., 71: 1534–2537 (2016).

[167] C. Li, X. Du, J.L. Kuti, D.P. Nicolau. Clinical pharmacodynamics of meropenem in patients with lower respiratory tract infections. Antimicrob. Agents Chemother., 51: 1725–1730 (2007).

[168] R.E. Ariano, S.A. Zelenitsky, A.N. MD, D.S. Sitar. An evaluation of an optimal sampling strategy for meropenem in febrile neutropenics. J. Clin. Pharmacol., 45: 832–835 (2005).

[169] V.H. Tam, P.S. McKinnon, R.L. Akins, M.J. Rybak, G.L. Drusano. Pharmacodynamics of cefepime in patients with Gram-negative infections. J. Antimicrob. Chemother., 50: 425–428 (2002).

[170] J.W. Mouton, J.G. Den Hollander. Killing of Pseudomonas aeruginosa during continuous and intermittent infusion of ceftazidime in an in vitro pharmacokinetic model. Antimicrob. Agents Chemother., 38: 931–936 (1994).

[171] P. Linden. Safety profile of meropenem. Drug Saf., 30: 657–668 (2007).

[172] S. Imani, H. Buscher, D. Marriott, S. Gentili, I. Sandaradura. Too much of a good thing: a retrospective study of β-lactam concentration–toxicity relationships. J. Antimicrob. Chemother., 72: 2891–2897 (2017).

[173] D.R. Mould, R.N. Upton. Basic concepts in population modeling, simulation, and model-based drug development. CPT Pharmacometrics Syst. Pharmacol., 1: e6 (2012).

[174] J.S. Barrett, M.J. Fossler, K.D. Cadieu, M.R. Gastonguay. Pharmacometrics: A multidisciplinary field to facilitate critical thinking in drug development and translational research settings. J. Clin. Pharmacol., 48: 632–649 (2008).

[175] S. Marshall, R. Madabushi, E. Manolis, K. Krudys, A. Staab, K. Dykstra, S.A.G. Visser. Model-informed drug discovery and development: Current industry good practice and regulatory expectations and future perspectives. CPT Pharmacometrics Syst. Pharmacol., 8: 87–96 (2019).

[176] T.H. Kim, S. Shin, B.S. Shin. Model-based drug development: application of modeling and simulation in drug development. J. Pharm. Investig., 48: 431–441 (2018).

[177] S. Marshall, R. Burghaus, V. Cosson, S. Cheung, M. Chenel, O. DellaPasqua, N. Frey, B. Hamrén, L. Harnisch, F. Ivanow, T. Kerbusch, J. Lippert, P. Milligan, S. Rohou, A. Staab, J. Steimer, C. Tornøe, S. Visser. Good practices in model-informed drug discovery and development (MID3): Practice, application and documentation. CPT Pharmacometrics Syst. Pharmacol., 5: 93–122 (2016).

[178] P. a Milligan, M.J. Brown, B. Marchant, S.W. Martin, P.H. van der Graaf, N. Benson, G. Nucci, D.J. Nichols, R. a Boyd, J.W. Mandema, S. Krishnaswami, S. Zwillich, D. Gruben, R.J. Anziano, T.C. Stock, R.L. Lalonde. Model-based drug development: A rational approach to efficiently accelerate

drug development. Clin. Pharmacol. Ther., 93: 502–514 (2013).

[179] G.R. Davies, W. Hope, S. Khoo. Opinion: The pharmacometrics of infectious disease. CPT Pharmacometrics Syst. Pharmacol., 2: e70 (2013).

[180] J.Y. Lee, C.E. Garnett, J.V.S. Gobburu, V.A. Bhattaram, S. Brar, J.C. Earp, P.R. Jadhav, K. Krudys, L.J. Lesko, F. Li, J. Liu, R. Madabushi, A. Marathe, N. Mehrotra, C. Tornoe, Y. Wang, H. Zhu. Impact of pharmacometric analyses on new drug approval and labelling decisions. Clin. Pharmacokinet., 50: 627–635 (2011).

[181] European Medicines Agency. 2014 Activity report of the modelling and simulation working group (MSWG). (2015).

[182] D. Gonzalez, G.G. Rao, S.C. Bailey, K.L.R. Brouwer, Y. Cao, D.J. Crona, A.D.M. Kashuba, C.R. Lee, K. Morbitzer, J.H. Patterson, T. Wiltshire, J. Easter, S.W. Savage, J.R. Powell. Precision dosing: Public health need, proposed framework, and anticipated impact. Clin. Transl. Sci.,: 443–454 (2017).

[183] Food and Drug Administration. Evaluating inclusion and exclusion criteria in clinical trials: Workshop report. (2018).

[184] I.R. Younis, J. Robert Powell, A. Rostami-Hodjegan, B. Corrigan, N. Stockbridge, V. Sinha, P. Zhao, P. Jadhav, B. Flamion, J. Cook. Utility of model-based approaches for informing dosing recommendations in specific populations: Report from the public AAPS Workshop. J. Clin. Pharmacol., (2016).

[185] D.J. Touw, C. Neef, A.H. Thomson, A.A. Vinks. Cost-effectiveness of therapeutic drug monitoring. Ther. Drug Monit., 27: 10–17 (2005).

[186] A.E. Muller, B. Huttner, A. Huttner. Therapeutic drug monitoring of beta-lactams and other antibiotics in the intensive care unit: Which agents, which patients and which infections? Drugs, 78: 439–451 (2018).

[187] I. Balakrishnan, R.J. Shorten. Therapeutic drug monitoring of antimicrobials. Ann. Clin. Biochem., 53: 333–346 (2016).

[188] R.J. Keizer, R. ter Heine, A. Frymoyer, L.J. Lesko, R. Mangat, S. Goswami. Model-informed precision dosing at the bedside: Scientific challenges and opportunities. CPT Pharmacometrics Syst. Pharmacol., 7: 785–787 (2018).

[189] D. Chan, V. Ivaturi, J. Long-Boyle. The time is now: model-based dosing to optimize drug therapy. Int. J. Pharmacokinet, 2: 213–215 (2017).

[190] J.W. Mouton, D.F.J. Brown, P. Apfalter, R. Cantón, C.G. Giske, M. Ivanova, A.P. MacGowan, A. Rodloff, C.-J. Soussy, M. Steinbakk, G. Kahlmeter. The role of pharmacokinetics/pharmacodynamics in setting clinical MIC breakpoints: the EUCAST approach. Clin. Microbiol. Infect., 18: E37–E45 (2012).

[191] S.B. Duffull, D.F.B. Wright, H.R. Winter. Interpreting population pharmacokinetic-pharmacodynamic analyses - a clinical viewpoint. Br. J. Clin. Pharmacol., 71: 807–814 (2011).

[192] H. Derendorf. Populationspharmakokinetik. In: Derendorf H, Gramatté T, Günter Schäfer H, Staab A (Eds.). Pharmakokinetik kompakt. Wissenschaftliche Verlagsgesellschaft, Stuttgart, 3rd ed.: 295–312 (2010).

[193] J. Owen, J. Fiedler-Kelly. Introduction to population pharmacokinetic/pharmacodynamic analysis with nonlinear mixed effects models. John Wiley & Sons, Hoboken, New Jersey (2014).

[194] S. Beal, L. Sheiner, A. Boeckmann, R. Bauer. Beal, S., Sheiner, L.B., Boeckmann, A., & Bauer, R.J., NONMEM User's Guide I. (1989-2013), Icon Development Solutions, Ellicott City, MD, USA (2013).

[195] Å.M. Johansson. Methodology for Handling Missing Data in Nonlinear Mixed Effects Modelling. (2014).

[196] A. Gelman, J. Hill. Missing-data imputation. In: Gelman A, Hill J (Eds.). Data analysis using regression and multilevel/hierarchical models. Cambridge University Press: 529–544 (2007).

[197] M. Bergstrand, M.O. Karlsson. Handling data below the limit of quantification in mixed effect models. AAPS J., 11: 371–380 (2009).

[198] S.L. Beal. Ways to fit a PK model with some data below the quantification limit. J. Pharmacokinet. Pharmacodyn., 28: 481–504 (2001).

[199] D.R. Mould, R.N. Upton. Basic concepts in population modeling, simulation, and model-based drug development—Part 2: Introduction to pharmacokinetic modeling methods. CPT Pharmacometrics Syst. Pharmacol., 2: e38 (2013).

[200] P.L. Bonate. Pharmacokinetic-pharmacodynamic modeling and simulation. Springer, New York Dordrecht Heidelberg London, 2nd ed. (2011).

[201] E.L. Plan, A. Maloney, F. Mentré, M.O. Karlsson, J. Bertrand. Performance comparison of various maximum likelihood nonlinear mixed-effects estimation methods for dose–response models. AAPS J., 14: 420–432 (2012).

[202] Beal, S., Sheiner, L.B., Boeckmann, A., & Bauer, R.J., NONMEM User's Guide V. (1989-2011), Icon Development Solutions, Ellicott City, MD, USA (2011).

[203] J. Elassaiss-schaap, S.H. Heisterkamp. Variability as constant coefficient of variation: Can we right two decades in error? Population Approach Group Europe (PAGE), St. Petersburg, Russia, 23-26 June 2009. [www.page-meeting.org/?abstract=1508], 2009.

[204] N.H.G. Holford, B.J. Anderson. Allometric size: The scientific theory and extension to normal fat mass. Eur. J. Pharm. Sci., 109: S59–S64 (2017).

[205] U. Wählby, A.H. Thomson, P.A. Milligan, M.O. Karlsson. Models for time-varying covariates in population pharmacokinetic-pharmacodynamic analysis. Br. J. Clin. Pharmacol., 58: 367–377 (2004).

[206] M.M. Hutmacher, K.G. Kowalski. Covariate selection in pharmacometric analyses: A review of methods. Br. J. Clin. Pharmacol., 79: 132–147 (2015).

[207] J. Ribbing. Covariate Model Building in Nonlinear Mixed Effects Models. (2007).

[208] X.S. Xu, M. Yuan, H. Zhu, Y. Yang, H. Wang, H. Zhou, J. Xu, L. Zhang, J. Pinheiro. Full covariate modelling approach in population pharmacokinetics: understanding the underlying hypothesis tests and implications of multiplicity. Br. J. Clin. Pharmacol., 84: 1525–1534 (2018).

[209] SCM user guide, PsN 4.4.8. [https://uupharmacometrics.github.io/PsN/docs.html], 2015.

[210] W. Huisinga, A. Solms, L. Fronton, S. Pilari. Modeling interindividual variability in physiologically based pharmacokinetics and its link to mechanistic covariate modeling. CPT pharmacometrics Syst. Pharmacol., 1: e4 (2012).

[211] L. Gibiansky, E. Gibiansky, R. Bauer. Comparison of Nonmem 7.2 estimation methods and parallel processing efficiency on a target-mediated drug disposition model. J. Pharmacokinet. Pharmacodyn., 39: 17–35 (2012).

[212] X. Liu, Y. Wang. Comparing the performance of FOCE and different expectation-maximization methods in handling complex population physiologically-based pharmacokinetic models. J. Pharmacokinet. Pharmacodyn., 43: 359–370 (2016).

[213] E.L. Plan, A. Maloney, F. Mentré, M.O. Karlsson, J. Bertrand. Performance comparison of various maximum likelihood nonlinear mixed-effects estimation methods for dose–response models. AAPS J., 14: 420–32 (2012).

[214] Beal, S., Sheiner, L.B., Boeckmann, A., & Bauer, R.J., NONMEM User's Guide VII. (1989-2013), Icon Development Solutions, Ellicott City, MD, USA (2013).

[215] R.E. Port. Populations-Pharmakokinetik und individuelle Dosisanpassung. In: Zeller WJ, Zur Hausen H (Eds.). Onkologie. ecomed-Storck GmbH, Berlin, Heidelberg, 16th ed.: 1–14 (2003).

[216] A.E. Gelfand. Model determination using sampling based methods. In: Gilks WR, Richardson S, Spiegelhalter D (Eds.). Markov Chain Monte Carlo in practice. Chapman and Hall, 1st ed.: 145–161

(1996).

[217] A.C. Hooker, C.E. Staatz, M.O. Karlsson. Conditional weighted residuals (CWRES): A model diagnostic for the FOCE method. Pharm. Res., 24: 2187–2197 (2007).

[218] LLP user guide, PsN 4.4.8. [https://uupharmacometrics.github.io/PsN/docs.html], 2015.

[219] R.M. Savic, M.O. Karlsson. Importance of Shrinkage in Empirical Bayes Estimates for Diagnostics: Problems and Solutions. AAPS J., 11: 558–569 (2009).

[220] A. Yafune, M. Ishiguro. Bootstrap approach for constructing confidence intervals for population pharmacokinetic parameters. I: A use of bootstrap standard error. Stat. Med., 18: 581–99 (1999).

[221] N. Holford, S.C. Ma, B.A. Ploeger. Clinical trial simulation: A review. Clin. Pharmacol. Ther., 88: 166–182 (2010).

[222] J.W. Mouton, M.N. Dudley, O. Cars, H. Derendorf, G.L. Drusano. Standardization of pharmacokinetic/pharmacodynamic (PK/PD) terminology for anti-infective drugs: an update. J. Antimicrob. Chemother., 55: 601–607 (2005).

[223] L. Lindbom, P. Pihlgren, N. Jonsson. PsN-Toolkit - A collection of computer intensive statistical methods for non-linear mixed effect modeling using NONMEM. Comput. Methods Programs Biomed., 79: 241–257 (2005).

[224] R.J. Keizer, M. van Benten, J.H. Beijnen, J.H.M. Schellens, A.D.R. Huitema. Piraña and PCluster: A modeling environment and cluster infrastructure for NONMEM. Comput. Methods Programs Biomed., 101: 72–79 (2011).

[225] https://www.zedat.fu-berlin.de/HPC/Soroban (last access 17 Aug 2019).

[226] P. Simon, D. Petroff, C. Dorn, L. Ehmann, C. Kloft, C. Prettin, A. Dietrich, M. Zeitlinger, F. Kees, H. Wrigge. Measurement of soft tissue drug concentrations in morbidly obese and non-obese patients – A prospective, parallel group, open-labeled, controlled, phase IV, single center clinical trial. Contemp. Clin. Trials Commun., doi: 10.1016/j.conctc.2019.100375 (2019).

[227] B. Gupta. Invasive blood pressure monitoring. Updat. Anaesth., 21: 37–42 (2007).

[228] D. Burau, D. Petroff, P. Simon, L. Ehmann, C. Weiser, C. Dorn, A. Kratzer, H. Wrigge, C. Kloft. Drug combinations and impact of experimental conditions on relative recovery in in vitro microdialysis investigations. Eur. J. Pharm. Sci., 127: 252–260 (2019).

[229] K. Tunblad, M. Hammarlund-Udenaes, E.N. Jonsson. An integrated model for the analysis of pharmacokinetic data from microdialysis experiments. Pharm. Res., 21: 1698–1707 (2004).

[230] A. Schäftlein. Neue Wege in der Modellierung von Mikrodialysatdaten im Menschen: Charakterisierung der klinischen ADMER-Prozesse von Moxifloxacin, Levofloxacin und Linezolid in Gesunden und Hochrisikopopulationen. (2013).

[231] A. Schaeftlein, I.K. Minichmayr, C. Kloft. Population pharmacokinetics meets microdialysis: Benefits, pitfalls and necessities of new analysis approaches for human microdialysis data. Eur. J. Pharm. Sci., 57: 68–73 (2014).

[232] J. Huygh, Y. Peeters, J. Bernards, M.L.N.G. Malbrain. Hemodynamic monitoring in the critically ill: an overview of current cardiac output monitoring methods. F1000Research, 5: 2855 (2016).

[233] L. Ehmann, M. Zoller, I.K. Minichmayr, C. Scharf, B. Maier, M. V. Schmitt, N. Hartung, W. Huisinga, M. Vogeser, L. Frey, J. Zander, C. Kloft. Role of renal function in risk assessment of target non-attainment after standard dosing of meropenem in critically ill patients: a prospective observational study. Crit. Care, 21: 263 (2017).

[234] J. Zander, B. Maier, M. Zoller, D. Teupser, M. Vogeser. Quantification of linezolid in serum by LC-MS/MS using semi-automated sample preparation and isotope dilution internal standardization. Clin. Chem. Lab. Med., 52: 381–389 (2014).

[235] R.E. Ariano, A. Nyhlén, J.P. Donnelly, D.S. Sitar, G.K. Harding, S.A. Zelenitsky. Pharmacokinetics and pharmacodynamics of meropenem in febrile neutropenic patients with bacteremia. Ann.

Pharmacother., 39: 32–38 (2005).

[236] P.S. McKinnon, J.A. Paladino, J.J. Schentag. Evaluation of area under the inhibitory curve (AUIC) and time above the minimum inhibitory concentration (T>MIC) as predictors of outcome for cefepime and ceftazidime in serious bacterial infections. Int. J. Antimicrob. Agents, 31: 345–351 (2008).

[237] F.S. Taccone, P.F. Laterre, T. Dugernier, H. Spapen, I. Delattre, X. Wittebole, D. De Backer, B. Layeux, P. Wallemacq, J.L. Vincent, F. Jacobs. Insufficient beta-lactam concentrations in the early phase of severe sepsis and septic shock. Crit. Care, 14: R126 (2010).

[238] J.A. Jamal, M.B. Mat-Nor, F.S. Mohamad-Nor, A.A. Udy, S.C. Wallis, J. Lipman, J.A. Roberts. Pharmacokinetics of meropenem in critically ill patients receiving continuous venovenous haemofiltration: A randomised controlled trial of continuous infusion versus intermittent bolus administration. Int. J. Antimicrob. Agents, 45: 41–45 (2015).

[239] G. Wong, A. Brinkman, R.J. Benefield, M. Carlier, J.J. De Waele, N. El Helali, O. Frey, S. Harbarth, A. Huttner, B. McWhinney, B. Misset, F. Pea, J. Preisenberger, M.S. Roberts, T.A. Robertson, A. Roehr, F.B. Sime, F.S. Taccone, J.P.J. Ungerer, J. Lipman, J.A. Roberts. An international, multicentre survey of β-lactam antibiotic therapeutic drug monitoring practice in intensive care units. J. Antimicrob. Chemother., 69: 1416–1423 (2014).

[240] European Medicines Agency. Guideline on the evaluation of the pharmacokinetics of medicinal products in patients with decreased renal function. (2015).

[241] Food and Drug Administration. Guidance for Industry Pharmacokinetics in Patients with Impaired Renal Function — Study Design , Data Analysis , and Impact on Dosing and Labeling: Draft guidance. (2010).

[242] V.G. Montgomery DC, Peck EA. Introduction to linear regression analysis. Wiley, New York, 5th ed. (2012).

[243] L. Ehmann, M. Zoller, I.K. Minichmayr, C. Scharf, W. Huisinga, J. Zander, C. Kloft. Development of a dosing algorithm for meropenem in critically ill patients based on a population pharmacokinetic/pharmacodynamic analysis. Int. J. Antimicrob. Agents, doi: 10.1016/j.ijantimicag.2019.06.016 (2019).

[244] I.K. Minichmayr, J.A. Roberts, O.R. Frey, A.C. Roehr, C. Kloft, A. Brinkmann. Development of a dosing nomogram for continuous-infusion meropenem in critically ill patients based on a validated population pharmacokinetic model. J. Antimicrob. Chemother., 73: 1330–1339 (2018).

[245] P. Colin, D.J. Eleveld, S. Jonckheere, J. Van Bocxlaer, J. De Waele, A. Vermeulen. What about confidence intervals? A word of caution when interpreting PTA simulations. J. Antimicrob. Chemother., 71: 2502–2508 (2016).

[246] T.E.C. on A.S. Testing, Breakpoint. Breakpoint tables for interpretation of MICs and zone diameters, version 8.1. http://www.eucast.org. (last access 17 Aug 2019).

[247] https://www.who.int/dietphysicalactivity/childhood_what/en/ (last access 17 Aug 2019).

[248] A.K. Meagher, A. Forrest, C.R. Rayner, M.C. Birmingham, J.J. Schentag. Population pharmacokinetics of linezolid in patients treated in a compassionate-use program. Antimicrob. Agents Chemother., 47: 548–553 (2003).

[249] D. Burau, D. Petroff, P. Simon, L. Ehmann, C. Weiser, C. Dorn, A. Kratzer, C. Kloft. Drug combinations and impact of experimental conditions on relative recovery in in vitro microdialysis investigations. Eur. J. Pharm. Sci., (2018).

[250] https://www.rdocumentation.org/packages/stats/versions/3.5.1/topics/loess (last access 21 Nov 2018).

[251] European Committee on Antimicrobial Susceptibility Testing. Linezolid: Rationale for the clinical breakpoints, version 1.0. (2005). http//www.eucast.org (last access 17 Aug 2019).

[252] S.M. Stainton, M.L. Monogue, A. Baummer-Carr, A.K. Shepard, J.F. Nugent, J.L. Kuti, D.P.

Nicolau. Comparative assessment of tedizolid pharmacokinetics and tissue penetration between Diabetic Patients with wound infections and healthy volunteers via in vivo microdialysis. Antimicrob. Agents Chemother., 62: AAC.01880-17 (2017).

[253] D.E. Wiskirchen, A. Shepard, J.L. Kuti, D.P. Nicolau. Determination of tissue penetration and pharmacokinetics of linezolid in patients with diabetic foot infections using in vivo microdialysis. Antimicrob. Agents Chemother., 55: 4170–4175 (2011).

[254] M. Wittau, S. Paschke, M. Kurlbaum, J. Scheele, N.S. Ly, E. Hemper, M. Kornmann, D. Henne-Bruns, J.B. Bulitta. Population Pharmacokinetics and Target Attainment of Ertapenem in Plasma and Tissue Assessed via Microdialysis in Morbidly Obese Patients after Laparoscopic Visceral Surgery. Antimicrob. Agents Chemother., 61: e00952-16 (2017).

[255] E.C. Palma, N.G. Meinhardt, A.T. Stein, I. Heineck, M.I. Fischer, B. de Araújo, T. Dalla Costa. Efficacious cefazolin prophylactic dose for morbidly obese women undergoing bariatric surgery based on evidence from subcutaneous microdialysis and populational pharmacokinetic modeling. Pharm. Res., 35: 116 (2018).

[256] I.K. Minichmayr. Pharmacometrics-based evaluation of antibiotic target-site exposure to improve dosing regimens in special populations. (2017).

[257] F. Xie, K. Mantzarlis, P. Malliotakis, V. Koulouras, S. Degroote, D. Koulenti, S. Blot, K. Boussery, J. Van Bocxlaer, P. Colin, E. Zakynthinos, D. Georgopoulos, A. Papathanasiou, K. Arvaniti, D. Matamis, A. Spring, V. Bekos, A. Komnos, T. Zafeiridis, D. Vogelaers. Pharmacokinetic evaluation of linezolid administered intravenously in obese patients with pneumonia. J. Antimicrob. Chemother., 74: 667–674 (2019).

[258] P. Dehghanyar, C. Bu, M. Zeitlinger, F. Islinger, F. Kovar, M. Mu, C. Kloft, C. Joukhadar. Penetration of linezolid into soft tissues of healthy volunteers after single and multiple doses. 49: 2367–2371 (2005).

[259] N. Dow. Determination of compound binding to plasma proteins. Curr. Protoc. Pharmacol., 34: 7.5.1-7.5.15 (2006).

[260] J. Barre, J.M. Chamouard, G. Houin, J.P. Tillement. Equilibrium dialysis, ultrafiltration, and ultracentrifugation compared for determining the plasma-protein-binding characteristics of valproic acid. Clin. Chem., 31: 60–64 (1985).

[261] C. Adembri, S. Fallani, M.I. Cassetta, S. Arrigucci, A. Ottaviano, P. Pecile, T. Mazzei, R. De Gaudio, A. Novelli. Linezolid pharmacokinetic/pharmacodynamic profile in critically ill septic patients: intermittent versus continuous infusion. Int. J. Antimicrob. Agents, 31: 122–129 (2008).

[262] M.J. Hanley, D.R. Abernethy, D.J. Greenblatt. Effect of obesity on the pharmacokinetics of drugs in humans. Clin. Pharmacokinet., 49: 71–87 (2010).

[263] G. Cheymol. Drug pharmacokinetics in the obese. Fundam. Clin. Pharmacol., 2: 239–256 (1988).

[264] S. Pilari, W. Huisinga. Lumping of physiologically-based pharmacokinetic models and a mechanistic derivation of classical compartmental models. J. Pharmacokinet. Pharmacodyn., 37: 365–405 (2010).

[265] M. a. Zeitlinger, H. Derendorf, J.W. Mouton, O. Cars, W. a. Craig, D. Andes, U. Theuretzbacher. Protein binding: Do we ever learn? Antimicrob. Agents Chemother., 55: 3067–3074 (2011).

[266] R. Schwameis, S. Syré, K. Sarahrudi, A. Appelt, D. Marhofer, D. Burau, C. Kloft, M. Zeitlinger. Penetration of linezolid into synovial fluid and muscle tissue after elective arthroscopy. J. Antimicrob. Chemother., 72: 2817–2822 (2017).

[267] G.E. Stein, S. Schooley, C.A. Peloquin, A. Missavage, D.H. Havlichek. Linezolid tissue penetration and serum activity against strains of methicillin-resistant Staphylococcus aureus with reduced vancomycin susceptibility in diabetic patients with foot infections. J. Antimicrob. Chemother., 60: 819–823 (2007).

[268] S. Lemaire, F. Van Bambeke, P.C. Appelbaum, P.M. Tulkens. Cellular pharmacokinetics and intracellular activity of torezolid (TR-700): studies with human macrophage (THP-1) and endothelial (HUVEC) cell lines. J. Antimicrob. Chemother., 64: 1035–1043 (2009).

[269] R. Schwameis, S. Syré, D. Marhofer, A. Appelt, D. Burau, K. Sarahrudi, C. Kloft, M. Zeitlinger. Pharmacokinetics of cefuroxime in synovial fluid. Antimicrob. Agents Chemother., 61: 1–7 (2017).

[270] C. Kirbs, F. Kluwe, F. Drescher, E. Lackner, P. Matzneller, J. Weiss, M. Zeitlinger, C. Kloft. High voriconazole target-site exposure after approved sequence dosing due to nonlinear pharmacokinetics assessed by long-term microdialysis. Eur. J. Pharm. Sci., 131: 218–229 (2019).

[271] A.S. Alobaid, S.C. Wallis, P. Jarrett, T. Starr, J. Stuart, M. Lassig-Smith, J.L. Ordóñez Mejia, M.S. Roberts, J. Lipman, J.A. Roberts. Effect of obesity on the population pharmacokinetics of meropenem in critically ill patients. Antimicrob. Agents Chemother., 60: 4577–4584 (2016).

[272] A.A. Bhalodi, P.K. Papasavas, D.S. Tishler, D.P. Nicolau, J.L. Kuti. Pharmacokinetics of intravenous linezolid in moderately to morbidly obese adults. Antimicrob. Agents Chemother., 57: 1144–1149 (2013).

[273] S. McLeay, G. Morrish, C. Kirkpatrick, B. Green. The relationship between drug clearance and body size: Systematic review and meta-analysis of the literature published from 2000 to 2007. Clin. Pharmacokinet., 51: 319–330 (2012).

[274] D.J. Stalker, G.L. Jungbluth, N.K. Hopkins, D.H. Batts. Pharmacokinetics and tolerance of single- and multiple-dose oral and intravenous linezolid, an oxazolidinone antibiotic, in healthy volunteers. J. Antimicrob. Chemother., 51: 1239–1246 (2003).

[275] L.I. Cortínez, B.J. Anderson, N.H.G. Holford, V. Puga, N. De La Fuente, H. Auad, S. Solari, F.A. Allende, M. Ibacache. Dexmedetomidine pharmacokinetics in the obese. Eur. J. Clin. Pharmacol., 71: 1501–1508 (2015).

[276] K. Matsumoto, A. Shigemi, A. Takeshita, E. Watanabe, Y. Yokoyama, K. Ikawa, N. Morikawa, Y. Takeda. Analysis of thrombocytopenic effects and population pharmacokinetics of linezolid: a dosage strategy according to the trough concentration target and renal function in adult patients. Int. J. Antimicrob. Agents, 44: 242–247 (2014).

[277] C. Töpper, C.L. Steinbach, C. Dorn, A. Kratzer, S.G. Wicha, M. Schleibinger, U. Liebchen, F. Kees, B. Salzberger, M.G. Kees. Variable linezolid exposure in intensive care unit patients-possible role of drug-drug interactions. Ther. Drug Monit., 38: 573–8 (2016).

[278] L.M. Boak, C.R. Rayner, M.L. Grayson, D.L. Paterson, D. Spelman, S. Khumra, B. Capitano, A. Forrest, J. Li, R.L. Nation, J.B. Bulitta. Clinical population pharmacokinetics and toxicodynamics of linezolid. Antimicrob. Agents Chemother., 58: 2334–2343 (2014).

[279] T. Sasaki, H. Takane, K. Ogawa, S. Isagawa, T. Hirota, S. Higuchi, T. Horii, K. Otsubo, I. Ieiri. Population pharmacokinetic and pharmacodynamic analysis of linezolid and a hematologic side effect, thrombocytopenia, in Japanese patients. Antimicrob. Agents Chemother., 55: 1867–1873 (2011).

[280] T. Whitehouse, J.A. Cepeda, R. Shulman, L. Aarons, R. Nalda-Molina, C. Tobin, A. MacGowan, S. Shaw, C. Kibbler, M. Singer, A.P.R. Wilson. Pharmacokinetic studies of linezolid and teicoplanin in the critically ill. J. Antimicrob. Chemother., 55: 333–340 (2005).

[281] Y. Tsuji, N.H.G. Holford, H. Kasai, C. Ogami, Y.-A. Heo, Y. Higashi, A. Mizoguchi, H. To, Y. Yamamoto. Population pharmacokinetics and pharmacodynamics of linezolid-induced thrombocytopenia in hospitalized patients. Br. J. Clin. Pharmacol., 83: 1758–1772 (2017).

[282] M. Zoller, B. Maier, C. Hornuss, C. Neugebauer, G. Döbbeler, D. Nagel, L.-M. Holdt, M. Bruegel, T. Weig, B. Grabein, L. Frey, D. Teupser, M. Vogeser, J. Zander. Variability of linezolid concentrations after standard dosing in critically ill patients: a prospective observational study. Crit. Care, 18: R148 (2014).

[283] M. Taubert, J. Zander, S. Frechen, C. Scharf, L. Frey, M. Vogeser, U. Fuhr, M. Zoller. Optimization of linezolid therapy in the critically ill: The effect of adjusted infusion regimens. J. Antimicrob. Chemother., 72: 2304–2310 (2017).

[284] S. Abe, K. Chiba, B. Cirincione, T.H. Grasela, K. Ito, T. Suwa. Population pharmacokinetic analysis of linezolid in patients with infectious disease: Application to lower body weight and elderly patients. J. Clin. Pharmacol., 49: 1071–1078 (2009).

[285] R. Hamilton, X.C. Thai, D. Ameri, M.P. Pai. Oral bioavailability of linezolid before and after Roux-en-Y gastric bypass surgery: Is dose modification necessary in obese subjects? J. Antimicrob. Chemother., 68: 666–673 (2013).

[286] C. Bürger. Pharmakokinetik von Linezolid in der Biophase bei gesunden Probanden und Intensivpatienten. (2006).

[287] T. Ide, Y. Takesue, K. Ikawa, N. Morikawa, T. Ueda, Y. Takahashi, K. Nakajima, K. Takeda, S. Nishi. Population pharmacokinetics/pharmacodynamics of linezolid in sepsis patients with and without continuous renal replacement therapy. Int. J. Antimicrob. Agents, 51: 745–751 (2018).

[288] S. Swoboda, M.C. Ober, C. Lichtenstern, S. Saleh, V. Schwenger, H.G. Sonntag, W.E. Haefeli, G. Hempel, T. Hoppe-Tichy, M.A. Weigand. Pharmacokinetics of linezolid in septic patients with and without extended dialysis. Eur. J. Clin. Pharmacol., 66: 291–298 (2010).

[289] T.T. Nguyen, L. Massias, G. Defrance, N. Bourgeois-Nicolaos, X. Duval, F. Mentré, A. Andremont. Population pharmacokinetic of linezolid in inpatients. Population Approach Group Europe (PAGE), Berlin, Germany, 08-11 June 2010. [www.page-meeting.org/?abstract=1742], 2010.

[290] P. Cojutti, M.P. Pai, F. Pea. Population pharmacokinetics and dosing considerations for the use of linezolid in overweight and obese adult patients. Clin. Pharmacokinet., 57: 989–1000 (2018).

[291] P.F. Smith, M.C. Birmingham, G.A. Noskin, A.K. Meagher, A. Forrest, C.R. Rayner, J.J. Schentag. Safety, efficacy and pharmacokinetics of linezolid for treatment of resistant Gram-positive infections in cancer patients with neutropenia. Ann. Oncol., 14: 795–801 (2003).

[292] E. Antal, T. Grasela, T. Bergstrom, J. Bruss, E. Wong. The role of population PK/PD analysis during the implementation of a bridging strategy for linezolid, Drug Information Association, Hong Kong, China, November 2000. [www.simulations-plus.com/assets/103_poster05_tgrasel2.pdf], 2000.

[293] P. Beringer, M. Nguyen, N. Hoem, S. Louie, M. Gill, M. Gurevitch, A. Wong-Beringer. Absolute bioavailability and pharmacokinetics of linezolid in hospitalized patients given enteral feedings. Antimicrob. Agents Chemother., 49: 3676–3681 (2005).

[294] R.A. Keel, A. Schaeftlein, C. Kloft, J.S. Pope, R.F. Knauft, M. Muhlebach, D.P. Nicolau, J.L. Kuti. Pharmacokinetics of intravenous and oral linezolid in adults with cystic fibrosis. Antimicrob. Agents Chemother., 55: 3393–3398 (2011).

[295] D.P. Jones, T.Y. Aw, X. Shan. Drug metabolism and toxicity during hypoxia. Drug Metab. Rev., 20: 247–260 (1989).

[296] K. Miller, H. McCoy, K. Chan, R. Fischer, W. Lindsay, R. Seifert, D. Zaske. Effect of cardiopulmonary bypass on cefazolin disposition. Clin. Pharmacol. Ther., 27: 550–556 (1980).

[297] S.G. Wicha, O.R. Frey, A.C. Roehr, J. Pratschke, M. Stockmann, R. Alraish, T. Wuensch, M. Kaffarnik. Linezolid in liver failure: exploring the value of the maximal liver function capacity (LiMAx) test in a pharmacokinetic pilot study. Int. J. Antimicrob. Agents, 50: 557–563 (2017).

[298] D.J. Currie. Estimating michaelis-menten parameters: Bias, variance and experimental design. Biometrics, 38: 907–919 (1982).

[299] T.C. Hesterberg. What teachers should know about the bootstrap: Resampling in the undergraduate statistics curriculum. Am. Stat., 69: 371–386 (2015).

[300] D. Fisher, S. Shafer. Fisher/Shafer NONMEM workshop pharmacokinetic and pharmacodynamic analysis with NONMEM and PLT tools basic concepts. Het Pand, Ghent, Belgium (2007).

[301] S. McGrane, P.P. Pandharipande. Sedation in the intensive care unit. Minerva Anestesiol., 78: 369–380 (2012).

[302] Arbeitskreis „Krankenhaus- und Praxishygiene“ der AWMF. Perioperative Antibiotikaprophylaxe (PAP). (2012).

[303] D.W. Bratzler, E.P. Dellinger, K.M. Olsen, T.M. Perl, P.G. Auwaerter, M.K. Bolon, D.N. Fish, L.M. Napolitano, R.G. Sawyer, D. Slain, J.P. Steinberg, R.A. Weinstein. Clinical practice guidelines for antimicrobial prophylaxis in surgery. Am. J. Heal. Pharm., 70: 195–283 (2013).

[304] D.W. Bratzler, E.P. Dellinger, K.M. Olsen, T.M. Perl, P.G. Auwaerter, M.K. Bolon, D.N. Fish, L.M. Napolitano, R.G. Sawyer, D. Slain, J.P. Steinberg, R. a. Weinstein, 'European Centre for Disease Prevention and Control'. Systematic review and evidence- based guidance on perioperative antibiotic prophylaxis. (2013).

[305] C.S. Inaba, C. Koh, S. Sujatha-Bhaskar, S. Gallagher, Y. Chen, N.T. Nguyen. Operative time as a marker of quality in bariatric surgery. J. Am. Coll. Surg., 225: S16–S17 (2017).

[306] S. Monkhouse, J. Morgan, S. Norton. Complications of bariatric surgery: Presentation and emergency management – a review. Ann. R. Coll. Surg. Engl., 91: 280–286 (2009).

[307] N. V. Christou, J. Jarand, J.L. Sylvestre, A.P.H. McLean. Analysis of the incidence and risk factors for wound infections in open bariatric surgery. Obes. Surg., 14: 16–22 (2004).

[308] J.W. Devlin, G.L. Fraser, R.R. Riker. Drug-induced coma and delirium. In: Papadopoulos J, Cooper B, Kane-Gill S, Mallow Corbett S, Barletta JF (Eds.). Drug-induced complications in the critically ill patient: A guide for recognition and treatment. Society of Critical Care Medicine, Mount Prospect, IL: 107–116 (2012).

[309] S.G. Wicha, M.G. Kees, A. Solms, I.K. Minichmayr, A. Kratzer, C. Kloft. TDMx: A novel web-based open-access support tool for optimising antimicrobial dosing regimens in clinical routine. Int. J. Antimicrob. Agents, 45: 442–444 (2015).

[310] S. Marchand, A. Chauzy, C. Dahyot-Fizelier, W. Couet. Microdialysis as a way to measure antibiotics concentration in tissues. Pharmacol. Res., 111: 201–207 (2016).

[311] B. Homapour, J.E. Bowen, E.J. Want, K. O'Neill, V. Apostolopoulos, D. Nandi, J.R. Van Dellen, F. Roncaroli. Intra-operative, real-time, three-dimensional ultrasound assisted positioning of catheters in the microdialysis of glial tumours. J. Clin. Neurosci., 17: 506–510 (2010).

[312] J.P. Galea, P.J. Tyrrell, H.P. Patel, A. Vail, A.T. King, S.J. Hopkins. Pitfalls in microdialysis methodology: an in vitro analysis of temperature, pressure and catheter use. Physiol. Meas., 35: N21–N28 (2014).

[313] R. Clément, J.M. Malinovsky, G. Dollo, P. Le Corre, F. Chevanne, R. Le Verge. In vitro and in vivo microdialysis calibration using retrodialysis for the study of the cerebrospinal distribution of bupivacaine. J. Pharm. Biomed. Anal., 17: 665–670 (1998).

[314] M.R. Bouw, M. Hammarlund-Udenaes. Methodological aspects of the use of a calibrator in in vivo microdialysis-further development of the retrodialysis method. Pharm. Res., 15: 1673–9 (1998).

[315] J. Bengtsson, E. Boström, M. Hammarlund-Udenaes. The Use of a Deuterated Calibrator for In Vivo Recovery Estimations in Microdialysis Studies. J. Pharm. Sci., 97: 3433–3441 (2008).

[316] H.L. Lutgers, L.M. Hullegie, K. Hoogenberg, W.J. Sluiter, R.P.F. Dullaart, K.J. Wientjes, A.J.M. Schoonen. Microdialysis measurement of glucose in subcutaneous adipose tissue up to three weeks in Type 1 diabetic patients. Neth. J. Med., 57: 7–12 (2000).

[317] L.B. Salans, S.W. Cushman, R.E. Weismann. Studies of Human Adipose Tissue. Adipose cell size and number in nonobese and obese patients. J. Clin. Invest., 52: 929–941 (1973).

[318] I.L. Savetsky, N.J. Albano, D.A. Cuzzone, J.C. Gardenier, J.S. Torrisi, G.D. García Nores, M.D. Nitti, G.E. Hespe, T.S. Nelson, R.P. Kataru, J.B. Dixon, B.J. Mehrara. Lymphatic function regulates contact hypersensitivity dermatitis in obesity. J. Invest. Dermatol., 135: 2742–2752 (2015).

[319] E.S. Weitman, S.Z. Aschen, G. Farias-Eisner, N. Albano, D.A. Cuzzone, S. Ghanta, J.C. Zampell, D. Thorek, B.J. Mehrara. Obesity Impairs Lymphatic Fluid Transport and Dendritic Cell Migration to Lymph Nodes. PLoS One, 8: e70703 (2013).

[320] G.D. García Nores, D.A. Cuzzone, N.J. Albano, G.E. Hespe, R.P. Kataru, J.S. Torrisi, J.C. Gardenier, I.L. Savetsky, S.Z. Aschen, M.D. Nitti, B.J. Mehrara. Obesity but not high-fat diet impairs lymphatic function. Int. J. Obes., 40: 1582–1590 (2016).

[321] L. Santambrogio. Lymph formation and composition. In: Lee B-B, Rockson SG, Bergan J (Eds.). Lymphedema. Springer, Cham, 2nd ed.: 139–152 (2018).

[322] K.C. Hansen, A. D'Alessandro, C.C. Clement, L. Santambrogio. Lymph formation, composition and circulation: a proteomics perspective. Int. Immunol., 27: 219–227 (2015).

[323] F. Simmel. Development , optimisation and application of in vitro and in vivo microdialysis methods contributing to characterise drug disposition processes. (2010).

[324] The Lancet Respiratory Medicine. Critical care guidelines—more science less art? Lancet Respir. Med., 4: 925 (2016).

[325] A. Tabah, J. de Waele, J. Lipman, J.R. Zahar, M.O. Cotta, G. Barton, J.F. Timsit, J.A. Roberts. The ADMIN-ICU survey: A survey on antimicrobial dosing and monitoring in ICUs. J. Antimicrob. Chemother., 70: 2671–2677 (2015).

[326] M. Iv. Meronem IV 500mg & 1g. Pfizer, (2018).

[327] F. Mattioli, C. Fucile, & Valerio, D. Bono, V. Marini, A. Parisini, A. Molin, M.L. Zuccoli, G. Milano, R. Danesi, A. Marchese, M. Polillo, C. Viscoli, P. Pelosi, A. Martelli, & Antonello, D. Paolo. Population pharmacokinetics and probability of target attainment of meropenem in critically ill patients. Eur. J. Clin. Pharmacol., 72: 839–848 (2016).

[328] D. Tsai, P. Stewart, R. Goud, S. Gourley, S. Hewagama, S. Krishnaswamy, S.C. Wallis, J. Lipman, J.A. Roberts. Optimising meropenem dosing in critically ill Australian Indigenous patients with severe sepsis. Int. J. Antimicrob. Agents, 48: 542–546 (2016).

[329] S. Jaruratanasirikul, S. Thengyai, W. Wongpoowarak, T. Wattanavijitkul, K. Tangkitwanitjaroen, W. Sukarnjanaset, M. Jullangkoon, M. Samaeng. Population pharmacokinetics and Monte Carlo dosing simulations of meropenem during the early phase of severe sepsis and septic shock in critically ill patients in intensive care units. Antimicrob. Agents Chemother., 59: 2995–3001 (2015).

[330] A. Isla. Population pharmacokinetics of meropenem in critically ill patients undergoing continous renal replacement therapy. Clin. Pharmacokinet., 47: 173–180 (2008).

[331] M.G. Kees, I.K. Minichmayr, S. Moritz, S. Beck, S.G. Wicha, F. Kees, C. Kloft, T. Steinke. Population pharmacokinetics of meropenem during continuous infusion in surgical ICU patients. J. Clin. Pharmacol., 56: 307–315 (2016).

[332] K. Doh, H. Woo, J. Hur, H. Yim, J. Kim, H. Chae, S. Han, D.S. Yim. Population pharmacokinetics of meropenem in burn patients. J. Antimicrob. Chemother., 65: 2428–2435 (2010).

[333] A. Ramon-Lopez, J.M. Allen, a. H. Thomson, B.S. Dheansa, S.E. James, G.W. Hanlon, B. Stewart, J.G. Davies. Dosing regimen of meropenem for adults with severe burns: a population pharmacokinetic study with Monte Carlo simulations. J. Antimicrob. Chemother., 70: 882–890 (2015).

[334] Q. Zhou, B. He, C. Zhang, S. Zhai, Z. Liu, J. Zhang. Pharmacokinetics and pharmacodynamics of meropenem in elderly chinese with lower respiratory tract infections: population pharmacokinetics analysis using nonlinear mixed-effects modelling and clinical pharmacodynamics study. Drugs Aging, 28: 903–12 (2011).

[335] J.A. Roberts, C.M.J. Kirkpatrick, M.S. Roberts, T.A. Robertson, A.J. Dalley, J. Lipman. Meropenem dosing in critically ill patients with sepsis and without renal dysfunction: intermittent bolus versus continuous administration? Monte Carlo dosing simulations and subcutaneous tissue distribution. J. Antimicrob. Chemother., 64: 142–150 (2009).

[336] J.L. Crandon, R.E. Ariano, S.A. Zelenitsky, A.M. Nicasio, J.L. Kuti, D.P. Nicolau. Optimization of meropenem dosage in the critically ill population based on renal function. Intensive Care Med., 37: 632–638 (2011).

[337] D.G. Lee, S.M. Choi, W.S. Shin, H.O. Lah, D.S. Yim. Population pharmacokinetics of meropenem in febrile neutropenic patients in Korea. Int. J. Antimicrob. Agents, 28: 333–339 (2006).

[338] K. Shekar, J.F. Fraser, F.S. Taccone, S. Welch, S.C. Wallis, D. V Mullany, J. Lipman, J. a Roberts. The combined effects of extracorporeal membrane oxygenation and renal replacement therapy on meropenem pharmacokinetics: a matched cohort study. Crit. Care, 18: 565 (2014).

[339] F. Sjövall, A.S. Alobaid, S.C. Wallis, A. Perner, J. Lipman, J.A. Roberts. Maximally effective dosing regimens of meropenem in patients with septic shock. J. Antimicrob. Chemother., 73: 191–198 (2018).

[340] X. Li, S. Sun, Q. Wang, Z. Zhao. Population pharmacokinetics of combined intravenous and local intrathecal administration of meropenem in aneurysm patients with suspected intracranial infections after craniotomy. Eur. J. Drug Metab. Pharmacokinet., 43: 45–53 (2018).

[341] C. Li, J.L. Kuti, C.H. Nightingale, D.P. Nicolau. Population pharmacokinetic analysis and dosing regimen optimization of meropenem in adult patients. J. Clin. Pharmacol., 46: 1171–1178 (2006).

[342] A.S. Alobaid, S.C. Wallis, P. Jarrett, T. Starr, J. Stuart, M. Lassig-Smith, J. Lisette, O. Mejia, M.S. Roberts, J. Lipman, A. Roberts. Effect of obesity on the population pharmacokinetics of meropenem in critically ill patients. Antimicrob. Agent Chemother., 60: 4577–4584 (2016).

[343] S.K. Mathew, B.S. Mathew, M.N. Neely, G.S. Naik, R. Prabha, G.G. Jacob, K. Subramani, D.H. Fleming. A nonparametric pharmacokinetic approach to determine the optimal dosing regimen for 30-minute and 3-hour meropenem infusions in critically ill patients. Ther. Drug Monit., 38: 593–599 (2016).

[344] S.A.M. Dhaese, A. Farkas, P. Colin, J. Lipman, V. Stove, A.G. Verstraete, J.A. Roberts, J.J. De Waele. Population pharmacokinetics and evaluation of the predictive performance of pharmacokinetic models in critically ill patients receiving continuous infusion meropenem: a comparison of eight pharmacokinetic models. J. Antimicrob. Chemother., 74: 432–441 (2019).

[345] S. Braune, C. König, J.A. Roberts, A. Nierhaus, O. Steinmetz, M. Baehr, S. Kluge, C. Langebrake. Pharmacokinetics of meropenem in septic patients on sustained low-efficiency dialysis: a population pharmacokinetic study. Crit. Care, 22: 25 (2018).

[346] P. Hanberg, K. Öbrink-Hansen, A. Thorsted, M. Bue, M. Tøttrup, L.E. Friberg, T.F. Hardlei, K. Søballe, J. Gjedsted. Population pharmacokinetics of meropenem in plasma and subcutis from patients on extracorporeal membrane oxygenation treatment. Antimicrob. Agents Chemother., 62: 1–13 (2018).

[347] D. Tsai, P. Stewart, R. Goud, S. Gourley, S. Hewagama, S. Krishnaswamy, S.C. Wallis, J. Lipman, J.A. Roberts. Optimising meropenem dosing in critically ill Australian Indigenous patients with severe sepsis. Int. J. Antimicrob. Agents, 48: 542–546 (2016).

[348] R.P. Bax, W. Bastain, A. Featherstone, D.M. Wilkinson, M. Hutchison. The pharmacokinetics of meropenem in volunteers. J. Antimicrob. Chemother., 24: 311–320 (1989).

[349] F. Sjövall, A.S. Alobaid, S.C. Wallis, A. Perner, J. Lipman, J.A. Roberts. Maximally effective dosing regimens of meropenem in patients with septic shock. J. Antimicrob. Chemother., 73: 191–198 (2018).

[350] J.A. Roberts, C.M.J. Kirkpatrick, M.S. Roberts, T.A. Robertson, A.J. Dalley, J. Lipman. Meropenem dosing in critically ill patients with sepsis and without renal dysfunction: Intermittent bolus versus continuous administration? Monte Carlo dosing simulations and subcutaneous tissue distribution. J. Antimicrob. Chemother., 64: 142–150 (2009).

[351] A.C. Roehr, O.R. Frey, A. Köberer, T. Fuchs, S. Helbig, A. Brinkmann, J.W. Mouton. Creatinine-clearance as predictor for meropenem clearance. European Congress on Clinical Microbiology and Infectious Diseases (ECCMID), Copenhagen, Denmark, 25-38 April 2015. [www.escmid.org/escmid_publications/escmid_elibrary/material/?mid=25641], 2015.

[352] R.E. Ariano, S.A. Zelenitsky, A.N. MD, D.S. Sitar. An evaluation of an optimal sampling strategy for meropenem in febrile neutropenics. J. Clin. Pharmacol., 45: 832–835 (2005).

[353] M. Ulldemolins, D. Soy, M. Llaurado-Serra, S. Vaquer, P. Castro, A.H. Rodríguez, C. Pontes, G. Calvo, A. Torres, I. Martín-Loeches. Meropenem population pharmacokinetics in critically ill patients with septic shock and continuous renal replacement therapy: Influence of residual diuresis on dose requirements. Antimicrob. Agents Chemother., 59: 5520–5528 (2015).

[354] B.J. Anderson, N.H.G. Holford. Mechanism-based concepts of size and maturity in pharmacokinetics. Annu. Rev. Pharmacol. Toxicol., 48: 303–332 (2008).

[355] R. Bellomo, S. McEvoy, S. Kai Lo, J. Myburgh, B. Neal, R. Norton, J. French, S. Finfer, G. Doig, M. Hayek, S. O'Donnell, A. Bell, N. Boyce, D. Blythe, J. Cade, M. Chapman, L. Cole, J. Cooper, A. Davies, C. French, C. Joyce, C. McArthur, S. MacMahon, J. Presneill, P. Saul, I. Seppelt, D. Stephens, A. Turner, A. Williams, C. Woolfe, P. Sandercock, C. Sprung, J. Duncan Young, S. Sivarajasingham, L. Francis, M. Woodward, J. Charlton, C. Harry, L. Higgins, K. Moulden, S. Vallance, J. Chadderton, L. Newby, S. Bates, D. Goldsmith, A. Voss, A. Palermo, K. Jayne, M. Merai, S. Pandey, M. Schmidt, R. Carroll, B. McFadyen, J. Clarke, C. Powell, J. Tai, I. Hynesova, L. Weisbrodt, L. Bradley, T. Kelly, A. Limpus, R. Moore, S. Creed, S. Kaplan, J. Rivett, J. Thomas, K. Marsden, C. Boyce, B. Howe, M. Robertson, A. O'Connor, J. Potter, N. Ramakrishnan, D. Rajbhandari, K. Girling, M. Hodgetts, A. Jovanovska, L. Little. Effect of baseline serum albumin concentration on outcome of resuscitation with albumin or saline in patients in intensive care units: analysis of data from the saline versus albumin fluid evaluation (SAFE) study. BMJ, 333: 1044 (2006).

[356] S. Acharya, A.S. Ragam, R. Holla, A.R.A. Bhat Y. Prevalence of potential drug-drug interactions in the intensive care unit of a tertiary care hospital: A cross-sectional study. J. Young Pharm., 11: 197–201 (2019).

[357] P. Pichala, B. Kumar, S. Zachariah, D. Thomas, L. Saunchaz, G. Alvarez-Uria. An interventional study on intensive care unit drug therapy assessment in a rural district hospital in India. J. Basic Clin. Pharm., 4: 64–67 (2013).

[358] E. Moyen, E. Camiré, H.T. Stelfox. Clinical review: Medication errors in critical care. Crit. Care, 12: 1–7 (2008).

[359] G. Burckhardt. Drug transport by organic anion transporters (OATs). Pharmacol. Ther., 136: 106–130 (2012).

[360] S. Freudenthaler. Influence of urine pH and flow rate on the renal excretion of chlorpheniramine in man. Br. J. Clin. Pharmacol., 46: 541–546 (1998).

[361] P.L. Madan. Effect of urinary pH on renal excretion of drugs. JAMA, 238: 210 (1977).

[362] M.O. Karlsson, L.B. Sheiner. The importance of modeling interoccasion variability in population pharmacokinetic analyses. J. Pharmacokinet. Biopharm., 21: 735–750 (1993).

[363] E. Chatelut, R. Bruno, M.J. Ratain. Intraindividual pharmacokinetic variability: Focus on small-molecule kinase inhibitors. Clin. Pharmacol. Ther., 103: 956–958 (2017).

[364] K. Donadello, E. Antonucci, S. Cristallini, J.A. Roberts, M. Beumier, S. Scolletta, F. Jacobs, B. Rondelet, D. De Backer, J.L. Vincent, F.S. Taccone. ß-Lactam pharmacokinetics during extracorporeal membrane oxygenation therapy: A case-control study. Int. J. Antimicrob. Agents, 45: 278–282 (2015).

[365] M. Usman, O.R. Frey, G. Hempel. Population pharmacokinetics of meropenem in elderly patients: dosing simulations based on renal function. Eur. J. Clin. Pharmacol., 73: 333–342 (2017).

[366] M. Carlier, S. Carrette, J. a Roberts, V. Stove, A. Verstraete, E. Hoste, P. Depuydt, J. Decruyenaere, J. Lipman, S.C. Wallis, J.J. De Waele. Meropenem and piperacillin/tazobactam prescribing in critically ill patients: does augmented renal clearance affect pharmacokinetic/pharmacodynamic target attainment when extended infusions are used? Crit. care, 17: R84 (2013).

[367] J. Cohen. Confronting the threat of multidrug-resistant Gram-negative bacteria in critically ill patients. J. Antimicrob. Chemother., 68: 490–491 (2013).

[368] R. Guilhaumou, S. Benaboud, Y. Bennis, C. Dahyot-Fizelier, E. Dailly, P. Gandia, S. Goutelle, S. Lefeuvre, N. Mongardon, C. Roger, J. Scala-Bertola, F. Lemaitre, M. Garnier. Optimization of the treatment with beta-lactam antibiotics in critically ill patients—guidelines from the French Society of Pharmacology and Therapeutics (Société Française de Pharmacologie et Thérapeutique—SFPT) and the French Society of Anaesthesia and . Crit. Care, 23: 104 (2019).

[369] A. Isla, A. Canut, J. Arribas, E. Asín-Prieto, A. Rodríguez-Gascón. Meropenem dosing requirements against Enterobacteriaceae in critically ill patients: influence of renal function, geographical area and presence of extended-spectrum β-lactamases. Eur. J. Clin. Microbiol. Infect. Dis., 35: 511–519

(2016).

[370] M.H. Abdul-Aziz, H. Sulaiman, M.B. Mat-Nor, V. Rai, K.K. Wong, M.S. Hasan, A.N. Abd Rahman, J.A. Jamal, S.C. Wallis, J. Lipman, C.E. Staatz, J.A. Roberts. Beta-lactam infusion in severe sepsis (BLISS): a prospective, two-centre, open-labelled randomised controlled trial of continuous versus intermittent beta-lactam infusion in critically ill patients with severe sepsis. Intensive Care Med., 42: 1535–1545 (2016).

[371] J.M. Dulhunty, J.A. Roberts, J.S. Davis, S.A.R. Webb, R. Bellomo, C. Gomersall, C. Shirwadkar, G.M. Eastwood, J. Myburgh, D.L. Paterson, J. Lipman. Continuous infusion of beta-lactam antibiotics in severe sepsis: A multicenter double-blind, randomized controlled trial. Clin. Infect. Dis., 56: 236–244 (2013).

[372] F. Yetkin, Y. Yakupogullari, C. Kuzucu, Y. Ersoy, B. Otlu, C. Colak, N. Parmaksiz. Pathogens of intensive care unit-acquired infections and their antimicrobial resistance: A 9-year analysis of data from a university hospital. Jundishapur J. Microbiol., doi: 10.5812/jjm.67716 (2018).

[373] R. Venkataraman, J. DIvatia, N. Ramakrishnan, R. Chawla, P. Amin, P. Gopal, D. Chaudhry, K. Zirpe, B. Abraham. Multicenter observational study to evaluate epidemiology and resistance patterns of common intensive care unit-infections. Indian J. Crit. Care Med., 22: 20–26 (2018).

[374] R.D. Savage, R.A. Fowler, A.H. Rishu, S.M. Bagshaw, D. Cook, P. Dodek, R. Hall, A. Kumar, F. Lamontagne, F. Lauzier, J. Marshall, C.M. Martin, L. McIntyre, J. Muscedere, S. Reynolds, H.T. Stelfox, N. Daneman. Pathogens and antimicrobial susceptibility profiles in critically ill patients with bloodstream infections: a descriptive study. C. Open, 4: E569–E577 (2016).

[375] EUCAST database: Antimicrobial wild type distributions of microorganisms. https://mic.eucast.org (last access 30 Nov 2018).

[376] L. Franceschi, P. Cojutti, M. Baraldo, F. Pea. Stability of generic meropenem solutions for administration by continuous infusion at normal and elevated temperatures. Ther. Drug Monit., 36: 674–676 (2014).

[377] M. Carlier, V. Stove, A.G. Verstraete, J.J. De Waele. Stability of generic brands of meropenem reconstituted in isotonic saline. Minerva Med., 81: 283–287 (2015).

[378] K. Berthoin, C.S. Le Duff, J. Marchand-Brynaert, S. Carryn, P.M. Tulkens. Stability of meropenem and doripenem solutions for administration by continuous infusion. J. Antimicrob. Chemother., 65: 1073–1075 (2010).

[379] S.G. Wicha, C. Kloft. Simultaneous determination and stability studies of linezolid, meropenem and vancomycin in bacterial growth medium by high-performance liquid chromatography. J. Chromatogr. B, 1028: 242–248 (2016).

[380] I.K. Minichmayr, J.A. Roberts, O.R. Frey, A.C. Roehr, C. Kloft, A. Brinkmann. Development of a dosing nomogram for continuous-infusion meropenem in critically ill patients based on a validated population pharmacokinetic model. J. Antimicrob. Chemother., 73: 1330–1339 (2018).

[381] L.M. Boak, J. Li, C.R. Rayner, R.L. Nation. Pharmacokinetic/pharmacodynamic factors influencing emergence of resistance to linezolid in an in vitro model. Antimicrob. Agents Chemother., 51: 1287–1292 (2007).

[382] T.W. Felton, J. Goodwin, L. O'Connor, A. Sharp, L. Gregson, J. Livermore, S.J. Howard, M.N. Neely, W.W. Hope. Impact of bolus dosing versus continuous infusion of piperacillin and tazobactam on the development of antimicrobial resistance in Pseudomonas aeruginosa. Antimicrob. Agents Chemother., 57: 5811–5819 (2013).

[383] M. Beumier, G.S. Casu, M. Hites, F. Wolff, J. Vincent, F. Jacobs, F.S. Taccone. Elevated ß-lactam concentrations are associated with neurological deterioration in ICU septic patients. 81: 497–506 (2015).

[384] D.-H. Lee, Y.K. Kim, K. Jin, M.J. Kang, Y.-D. Joo, Y.W. Kim, Y.S. Moon, J.-G. Shin, S. Kiem. Population pharmacokinetic analysis of doripenem after intravenous infusion in Korean patients with acute infections. Antimicrob Agents Chemother, 24: 1–12 (2017).

[385] M.H. Abdul-Aziz, J. Lipman, J.A. Roberts. Identifying “at-risk” patients for sub-optimal beta-lactam exposure in critically ill patients with severe infections. Crit. Care, 21: 283 (2017).

[386] J.A. Roberts, M. Ulldemolins, M.S. Roberts, B. McWhinney, J. Ungerer, D.L. Paterson, J. Lipman. Therapeutic drug monitoring of β-lactams in critically ill patients: Proof of concept. Int. J. Antimicrob. Agents, 36: 332–339 (2010).

[387] T.W. Felton, W.W. Hope, J.A. Roberts. How severe is antibiotic pharmacokinetic variability in critically ill patients and what can be done about it? Diagn. Microbiol. Infect. Dis., 79: 441–447 (2014).

[388] F. Pea, P. Viale, P. Cojutti, M. Furlanut. Dosing nomograms for attaining optimum concentrations of meropenem by continuous infusion in critically ill patients with severe gram-negative infections: A pharmacokinetics/pharmacodynamics-based approach. Antimicrob. Agents Chemother., 56: 6343–6348 (2012).

[389] M. Paul, L. Leibovici. Combination therapy for Pseudomonas aeruginosa bacteremia: Where do we stand? 57: 217–220 (2013).

[390] EUCAST database: Antimicrobial wild type distributions of microorganisms. https://mic.eucast.org, (last access 02. Apr 2018).

[391] F.Q. Nuttall. Body mass index. Obesity, BMI and heath: A critical review. Nutr. Today, 50: 117–128 (2015).

[392] G.B. Janmahasatian S, Duffull SB, Ash S, Ward LC, Byrne NM. Quantification of lean body weight. Clin Pharmacokinet, 44: 1051–1065 (2005).

[393] B.J. Devine. Gentamycin Therapy. Drug Intell. Clin. Pharm., 8: 650–655 (1974).

7

Appendix

7.1 Supplementary tables

Table S1 (Project I) Inclusion and exclusion criteria.

Inclusion criteria	Exclusion criteria
Index group: • Age ≥18 years • Abdominal surgical intervention with a need of an antibiotic prophylaxis • Written informed consent • BMI of ≥35 kg/m² (= at least class II obesity[1]) **Control group:** • Age ≥18 years • Abdominal surgical intervention with a need of an antibiotic prophylaxis • Written informed consent • BMI of <30 kg/m² (= up to max. overweight[1])	• Treatment with the study medication within 72 h before surgery • Known allergic reactions, hypersensitivity or contraindications against one of the drugs • Severe liver insufficiency • Bone-marrow function disorders (e.g. after cytostatic treatment) or diseases of the haematopoietic system • Genetically caused Glucose-6-phosphate dehydrogenase deficiency • Acute hepatic porphyria • Hypotension • Phenylketonuria or hereditary fructose intolerance • Treatment with drugs that inhibit monoamine oxidases A or B, within the last 2 weeks • Pregnancy or breastfeeding • Participation of additional interventional therapy studies according to the German medicines law (AMG)

[1]Classification according to WHO.
Abbreviations: *AMG:* German medicines law ('Arzneimittelgesetz'); *BMI*: Body mass index; *WHO*: World health organisation

Table S2 (Project IV) Overview of patient-specific characteristics recorded during study period. Pre-selected patient-specific characteristics for covariate analysis are highlighted in blue.

Measured once during study period			**Measured longitudinally during study period**		
A: categorical		**B: continuous**	**A: categorical**		**B: continuous**
A.1: dichotomous	**A.2: multiple**		**A.1: dichotomous**	**A.2: multiple ordered**	
• Sex • RRT • ECMO • Sepsis • 28-day mortality • Liver transpl. • Lung transpl. • ARDS • Peritonitis[4]	• Cause of sepsis	• Age • Body height • Body weight • BMI[4]	• Anuria[2,4]	Disease score items[1]: • Body temperature[2] • Mean arterial pressure[2] • Heart rate[2] • Respiratory rate[2] • Respiratory rate[2] • PaO_2/FiO_2 ratio[2] • Cardio vascular system[2] • Glasgow coma score[2]	• Urine volume[2] • Fluid balance[2] • Urine creatinine[2] • Urine albumin[2] • Serum creatinine[2] • Serum albumin[2] • Serum urea[2] • $CLCR_{CG}$[2,4] • $CLCR_{UC}$[2,4] • Erythrocytes[2] • Haemoglobin[2] • Haematocrit[2] • Thrombocytes[2] • Prothrombin time[2] • Partial thrombo-plastin time[2] • Fibrinogen[2] • Antithrombin[2]	• Bilirubin[2] • Aspartate Aminotransferase[2] • Alanine Aminotransferase[2] • Cholinesterase enzyme[2] • Factor V[2] • Interleukin-6[3] • C-reactive protein[3] • CD64 Index[2] • Leukocytes[2] • Sodium[2] • Potassium[2] • Glucose[2] • Inorganic phosphate[2] • pH value in blood[2] • Lactate[2] • Hydrogencarbonate[2] • APACHE II Score • SOFA Score

[1]Extracted from APACHE II or SOFA score; [2]Determined once every study day; [3]Determined once every study day and the two days before and after the study period; [4]Derived/Computed from determined/measured patient-specific characteristics.

Abbreviations: *APACHE*: Acute Physiology And Chronic Health Evaluation [1]; *ARDS*: Acute respiratory distress syndrome; *BMI*: Body mass index; *CD64*: Cluster of Differentiation 64; $CLCR_{CG}$: Creatinine clearance estimated according to Cockcroft and Gault [2]; $CLCR_{UC}$: Creatinine clearance measured using urine collection; *ECMO*: Extracorporeal membrane oxygenation; PaO_2/FiO_2: Ratio of partial pressure arterial oxygen and fraction of inspired oxygen; *RRT*: Renal replacement therapy; transpl: Transplantation; *SOFA*: Sepsis-related Organ Failure Assessment [6].

Table S3: (Project I) Parameter estimates of plasma NLME base models for linezolid with different clearance (CL) models.
Model A: Linear CL; *Model B:* Heart rate as covariate on CL; *Model C:* Time-varying CL according to an E_{max} model after end of anaesthesia; *Model D:* Concentration-dependent parallel linear and nonlinear Michaelis-Menten clearance.

Parameter [unit]	**Estimate (RSE[1], %)**			
	Model A: 'Linear clearance model'	**Model B: 'Favourite time-varying anaesthesia model'**	**Model C: 'Favourite concentration-dependent model'**	**Model D: 'Heart rate model'**
OFV	189.775	64.618	70.173	161.586
Fixed-effects parameters				
θ CL [L/h]	7.34 (6.20)	5.81[2] (8.80)	2.06[3] (22.3)	7.42[4] (6.20)
θ $CL_{Time\text{-}varying\_max}$ [L/h]	--	6.83 (18.0)	--	--
θ t_{50} [h]	--	1.53 (25.6)	--	--
θ V_{max} [mg/h]	--	--	45.9 (8.10)	--
θ K_m [mg/L]	--	--	1.82 (21.3)	--
θ HR_CL, %	--	--	--	1.37[5] (27.1)
θ V_1 [L]	12.3 (12.6)	15.7 (9.70)	15.5 (10.3)	12.3 (12.0)
θ Q [L/h]	65.5 (12.0)	47.2 (12.8)	49.9 (12.0)	65.7 (14.1)
θ V_2 [L]	25.2 (7.50)	27.4 (6.10)	28.4 (6.80)	26.2 (7.60)
θ f_u, %	83.6 (0.60)	85.5 (0.70)	85.6 (0.70)	83.9 (0.60)
Interindividual variability parameters, %CV				
ω CL	35.1 (17.3)	49.7 (19.2)	94.4 (18.6)	35.9 (15.5)
ω V_1	60.3 (13.5)	49.1 (14.0)	45.9 (13.9)	57.7 (14.9)
ω Q	57.4 (21.6)	61.5 (18.8)	60.2 (22.3)	61.3 (20.1)
ω V_2	30.1 (17.2)	30.7 (14.5)	28.5 (17.1)	29.0 (16.9)
ω $CL_{Time\text{-}varying\_max}$		41.5 (17.5)	--	--
Residual variability parameters, %CV				
σ_{prop} C_{P_tot}	6.7 (8.40)	4.21 (13.9)	4.59 (8.10)	6.17 (9.20)
σ_{prop} C_{P_u}	3.4 (17.2)	3.71 (14.3)	3.95 (13.6)	3.53 (19.5)

[1]RSE of random-effects parameter estimates ω and σ are reported on approximate standard deviation scale; [2]Linear clearance during anaesthesia; [3]Linear clearance of parallel linear/nonlinear clearance model; [4]For median heart rate of 71 min^{-1}; [5]Change in clearance per min^{-1} deviation from median heart rate of 71 min^{-1} (i.e. indicates 13.7% change in clearance per 10 min^{-1} heart rate deviation from median; linear HR-CL relationship).
Abbreviations: *CL*: Clearance; $CL_{Timevarying\_max}$: Maximum time-varying clearance; C_{P_tot}: Total plasma concentrations; C_{P_u}: Unbound plasma concentrations; *CV*: Coefficient of variation (calculated for random-effects parameters according to Eq. 2.6); f_u: Fraction unbound; K_m: Michaelis-Menten constant; *HR_CL*: Effect of heart rate on CL; *NLME*: Nonlinear mixed-effects; *Q*: Intercompartmental clearance; *RSE*: Relative standard error; t_{50} : Time to reach half-maximum of time-varying clearance; V_1, V_2: Volume of distribution parameters of central and peripheral CMTs; V_{max}: Maximum elimination rate; θ: Fixed-effects parameter; ω: Random-effects parameter: Interindividual variability; σ: Random-effects parameter: Residual unexplained variability.

Table S4: (Project I) Parameter estimates (PK parameters of unbound linezolid and microdialysis methodology-related parameters) of the base NLME model of linezolid in obese and nonobese surgical patients, already including obesity status as covariate on methodology-related parameter RR. For final joint NLME model including all covariates on PK parameters see Table 3.2.

Parameter [unit]	**Final model**	
	'Unbound' estimate (RSE[1], %)	**Computed 'total' parameter[2]**
OFV	-50.032	--
Fixed-effects parameters		
θ CL_u[4] [L/h]	1.95 (31.5)	1.68
θ $V_{max,u}$ [mg/h]	45.3 (9.80)	38.9
θ $K_{m,u}$ [mg/L]	0.977 (35.9)	0.839
θ $V_{1,u}$ [L][5]	17.5 (9.50)	15.0
θ Q_u [L/h][5]	56.8 (9.70)	48.8
θ $V_{2,u}$ [L][5]	34.2 (6.30)	29.4
θ f_u, %	85.9 (0.80)	--
θ TF_u, %	55.6 (5.60)	--
θ RR_{OBE}, %	35.7 (7.10)	--
θ RR_{NOBE}, %	59.5 (5.00)	--
Interindividual and method variability parameters, %CV		
ω CL_u	105 (25.2)	--
ω $K_{m,u}$	102.9 (33.4)	--
ω $V_{1,u}$	55.9 (11.4)	--
ω Q_u	53.2 (15.7)	--
ω $V_{2,u}$	30.3 (16.1)	--
ω TF_u	22.3 (15.7)	--
$\omega_{Intercatheter}$ RR	26.2 (18.7)	--
$\omega_{Intracatheter}$ RR	26.9 (10.6)	--
Residual variability parameters, %CV		
σ_{prop} C_{P_tot}	5.02 (14.4)	--
σ_{prop} C_{P_u}	4.82 (14.7)	--
σ_{prop} $C_{\mu D}$	15.3 (6.00)	--
σ_{prop} C_{RD}	1.9 FIX[3]	--

[1]RSE of random-effects parameter estimates ω and σ are reported on approximate standard deviation scale; [2]'Total' parameter='Unbound' parameter estimate·fu; [3]Fixed to interassay variability [228].

Abbreviations: CL_u: Clearance of unbound linezolid; $CL_{Tot,u}$: Total clearance of unbound linezolid; *CMT*: Compartment; C_{P_tot}: Total plasma concentrations; C_{P_u}: Unbound plasma concentrations; C_{RD}: Retrodialysate concentration; C_{RP}: Retroperfusate concentration; $C_{\mu D}$: Microdialysate concentration; *CV*: Coefficient of variation (calculated for random-effects parameters according to Eq. 2.6); f_u: Fraction unbound; $K_{m,u}$: Michaelis-Menten constant of unbound linezolid; *NLME*: Nonlinear mixed-effects; Q_u: Intercompartmental clearance of unbound linezolid; *RSE*: Relative standard error; RR_{OBE}, RR_{NOBE}: Relative recovery for obese and nonobese patients; TF_u: Tissue factor of unbound linezolid; $V_{1,u}$, $V_{2,u}$: Volume of distribution parameters of central and peripheral CMTs of unbound linezolid; $V_{max,u}$: Maximum elimination rate of unbound linezolid; θ: Fixed-effects parameter; ω: Random-effects parameter: Interindividual variability; σ: Random-effects parameter: Residual unexplained variability.

Table S5: (Project I) Strategy of the stepwise covariate analysis to identify the impact of body size and renal function markers on the PK of linezolid. [continued on next page]

Step		PK parameter	Body size descriptor	Additional information
Step 1: Body size on TF				
1	A	TF	OBE	--
1	B	TF	WT	--
1	C	TF	LBW	--
1	D	TF	FM	--
1	E	TF	NFM	--
Step 2: Body size on V_1 and V_2				
2	A	V_1, V_2	WT	--
2	B	V_1, V_2	LBW	--
2	C	V_1, V_2	Same NFM	--
2	D	V_1, V_2	Separate NFM	--
2	E	V_1	NFM	--
2	F	V_2	NFM	--
2	G	V_1, V_2	NFM, LBW, respectively	--
2	H	V_1, V_2	LBW, NFM, respectively	--
Step 3: Body size on Q				
3	A	Q	TBW	w and w/o allometric scaling
3	B	Q	LBW	w and w/o allometric scaling
3	C	Q	NFM	w and w/o allometric scaling
Step 4[1]: Body size on CL and V_{max}				
4	A	CL, V_{max}	TBW	w and w/o allometric scaling
4	B	CL, V_{max}	LBW	w and w/o allometric scaling
4	C	CL, V_{max}	Same NFM	w and w/o allometric scaling
4	D	CL, V_{max}	Separate NFM	w and w/o allometric scaling
4	E	CL	NFM	w and w/o allometric scaling
4	F	V_{max}	NFM	w and w/o allometric scaling
4	G	CL, V_{max}	NFM, LBW, respectively	w and w/o allometric scaling
4	H	CL, V_{max}	LBW, NFM, respectively	w and w/o allometric scaling
4	I	CL, V_{max}	LBW	w allometric scaling
			+ Same FM	see table footnote[3]
4	J	CL, V_{max}	LBW	w allometric scaling
			+ Separate FM	see table footnote[4]
Step 5: Renal function marker on CL				
5	A	CL	CREA	--
5	B	CL, V_{max}	CREA	--
5	C	CL	$CLCR_{CG\_LBW}$	--
5	D	CL, V_{max}	$CLCR_{CG\_LBW}$	--
Step 6: 1-by-1 backward deletion[2]				
Step 7: Additional impact of OBE				

Step		PK parameter	Body size descriptor	Additional information
7	A	CL	OBE	--
7	B	V_{max}	OBE	--
7	C	V_1	OBE	--
7	D	V_2	OBE	--
7	E	Q	OBE	--
Step 8: Reinvestigate OBE on TF				
8	A	V_2	OBE	Instead of OBE on TF
8	B	Q	OBE	Instead of OBE on TF

[1]Based on base model with IIV on V_{max}; [2]Backward deletion: for df=1 ΔOFV≥6.64 (α=0.01).

[3]Step 4I: $TVCL_{LBW,FM} = \theta_{CL} \cdot \left(\frac{LBW}{LBW_{ref}}\right)^{0.75} \cdot e^{\theta_{FM} \cdot (FM - FM_{ref})}$, $TVVmax_{LBW,FM} = \theta_{V_{max}} \cdot \left(\frac{LBW}{LBW_{ref}}\right)^{0.75} \cdot e^{\theta_{FM} \cdot (FM - FM_{ref})}$

[4]Step 4J: $TVCL_{LBW,FM} = \theta_{CL} \cdot \left(\frac{LBW}{LBW_{ref}}\right)^{0.75} \cdot e^{\theta_{FM\_CL} \cdot (FM - FM_{ref})}$, $TVVmax_{LBW,FM} = \theta_{V_{max}} \cdot \left(\frac{LBW}{LBW_{ref}}\right)^{0.75} \cdot e^{\theta_{FM\_V_{max}} \cdot (FM - FM_{ref})}$

Abbreviations: *CL*: Clearance; *CMT*: Compartment; $CLCR_{CG\_LBW}$: Creatinine clearance according to Cockcroft and Gault using LBW; *CREA*: Serum creatinine concentration: *FM*: Fat mass; FM_{ref}: Reference FM value; *LBW*: Lean body weight; LBW_{ref}: Reference LBW value; *NFM*: Normalised fat mass; *OBE*: Obesity status; *PK*: Pharmacokinetics; *Q*: Intercompartmental clearance; *TF*: Tissue factor; $TVCL_{LBW,FM}$: Typical value of CL for a given LBW and FM value; *WT*: Total body weight; V_1, V_2: Volume of distribution parameters of central and peripheral CMTs; V_{max}: Maximum elimination rate; $TVVmax_{LBW,FM}$: Typical value of V_{max} for a given LBW and FM value; *w*: With; *w/o*: Without; θ_{CL}: Typical value of CL for LBW_{ref} and FM_{ref}; $\theta_{V_{max}}$: Typical value of V_{max} for LBW_{ref} and FM_{ref}; θ_{FM}: Impact of FM on CL and V_{max}; θ_{FM_CL}: Impact of FM on CL; $\theta_{FM\_V_{max}}$: Impact of FM on V_{max}.

Table S6: (Project I) Parameter estimates of NLME model of linezolid in obese and nonobese surgical patients including body size as covariate on linezolid clearance parameters.
Selected models of step 4 (allometrically scaled: 4 A – 4 D) of the covariate analysis (Table S5) are presented for illustration. Reference model: Selected covariate model of step 3 of the covariate analysis (i.e. OBE on TF, LBW on V_1 and V_2 with allometric exponent of 1, LBW on Q with allometric exponent of 0.75).

Parameter [unit]	**Estimate (RSE[1], %)**				
	Reference model (Step 3)	**Step 4 A:** TBW on CL, V_{max}	**Step 4 B:** LBW on CL, V_{max}	**Step 4 C:** Same NFM on CL, V_{max}	**Step 4 D:** Separate NFM on CL, V_{max}
OFV	-82.309	-50.184	-67.508	-68.556	-68.584
Fixed-effects parameters					
θ CL_u [L/h]	2.00 (29.8)	1.49 (49.6)	1.88 (34.8)	2.09 (32.2)	2.03 (36.0)
θ $V_{max,u}$ [mg/h]	44.2 (9.00)	39.4 (28.7)	52.7 (8.40)	55.0 (9.20)	55.5 (7.00)
θ $K_{m,u}$ [mg/L]	0.89 (37.5)	1.53 (66.0)	1.41 (27.1)	1.31 (26.6)	1.34 (26.7)
θ $V_{1,u}$ [L]	19.3 (7.80)	19.5 (7.90)	19.4 (7.70)	19.4 (7.70)	19.4 (7.70)
θ Q_u [L/h]	61.0 (8.80)	60.3 (9.00)	60.8 (8.80)	60.8 (8.80)	60.8 (8.80)
θ $V_{2,u}$ [L]	37.4 (4.30)	36.8 (4.60)	37. (4.40)	37.2 (4.40)	37.2 (4.40)
θ f_u, %	85.8 (0.80)	85.6 (0.80)	85.7 (0.80)	85.7 (0.80)	85.7 (0.80)
θ $TF_{OBE,u}$, %	47.4 (8.10)	38.7 (7.60)	38.7 (7.60)	38.7 (7.60)	38.7 (7.60)
θ $TF_{NOBE,u}$, %	64.4 (6.50)	64.6 (6.50)	64.5 (6.50)	64.5 (6.50)	64.5 (6.50)
θ RR_{OBE}, %	38.7 (7.60)	38.7 (7.60)	38.7 (7.60)	38.7 (7.60)	38.7 (7.60)
θ RR_{NOBE}, %	55.5 (7.00)	55.5 (7.00)	55.5 (7.00)	55.5 (7.00)	55.5 (7.00)
Interindividual and method variability parameters, %CV					
ω CL_u	107 (24.0)	153 (24.9)	130 (23.2)	124 (23.0)	127 (21.1)
ω $K_{m,u}$	127 (32.2)	125 (20.9)	113 (17.9)	122 (19.1)	120 (18.5)
ω $V_{1,u}$	40.7 (12.1)	40.4 (12.1)	40.4 (12.1)	40.4 (12.0)	40.5 (12.0)
ω Q_u	46.3 (17.3)	46.9 (17.1)	46.7 (17.2)	46.5 (17.3)	46.5 (17.3)
ω $V_{2,u}$	15.9 (28.0)	17.0 (26.1)	16.4 (26.6)	16.3 (27.0)	16.3 (27.0)
ω TF_u	18.2 (25.4)	18.2 (25.5)	18.2 (25.5)	18.2 (25.5)	18.2 (25.5)
$\omega_{Intercatheter}$ RR	27.2 (23.8)	27.2 (23.9)	27.2 (23.8)	27.2 (23.9)	27.2 (23.9)
Residual variability parameters, %CV					
σ_{prop} C_{P_tot}	5.04 (14.5)	5.14 (14.4)	5.08 (14.7)	5.07 (14.6)	5.06 (14.6)
σ_{prop} C_{P_u}	4.95 (14.6)	4.96 (15.0)	4.97 (14.8)	4.97 (14.7)	4.97 (14.8)
σ_{prop} $C_{\mu D}$	15.3 (6.10)	15.3 (6.30)	15.3 (6.20)	15.3 (6.10)	15.3 (6.20)
σ_{prop} C_{RD}	27.4 (12.0)	27.4 (12.0)	27.4 (12.0)	27.4 (12.0)	27.4 (12.0)

[1]RSE of random-effects parameter estimates ω and σ are reported on approximate standard deviation scale.
Abbreviations: CL_u: Clearance of unbound linezolid; *CMT*: Compartment; C_{P_tot}: Total plasma concentrations; C_{P_u}: Unbound plasma concentrations; C_{RD}: Retrodialysate concentration; C_{RP}: Retroperfusate concentration; $C_{\mu D}$: Microdialysate concentration; *CV*: Coefficient of variation (calculated for random-effects parameters according to Eq. 2.6); f_u: Fraction unbound; $K_{m,u}$: Michaelis-Menten constant of unbound linezolid; *LBW*: Lean body weight; *NLME*: Nonlinear mixed-effects; *OBE*: Obesity; Q_u: Intercompartmental clearance of unbound linezolid; *RSE*: Relative standard error; RR_{OBE}, RR_{NOBE}: Relative recovery for obese and nonobese patients; $TF_{OBE,u}$, $TF_{NOBE,u}$: Tissue factor of unbound linezolid for obese and nonobese patients; $V_{1,u}$, $V_{2,u}$: Volume of distribution parameters of central and peripheral CMTs of unbound linezolid; $V_{max,u}$: Maximum elimination rate of unbound linezolid; θ: Fixed-effects parameter; ω: Random-effects parameter: Interindividual variability; σ: Random-effects parameter: Residual unexplained variability.

Table S7: (Project I) Results of stepwise covariate analysis to identify the impact of body size and renal function markers on the PK of linezolid (Table S5).

Step	**Identified covariate-parameter relationship**		
	Covariate	**PK parameter**	**Functional relationship**
Step 1: Body size on TF	OBE	TF	Fractional change
Step 2: Body size on V_1 and V_2	LBW	V_1 and V_2	Power (with fixed allometric exponent of 1)
Step 3: Body size on Q	LBW	Q	Power (with fixed allometric exponent of 0.75)
Step 4: Body size on CL and V_{max}	-	-	-
Step 5: Renal function marker on CL	-	-	-
Step 6: 1-by-1 backward deletion[2]	Note: No covariate removed during backward deletion		
Step 7: Additional impact of OBE	-	-	-
Step 8: Reinvestigate OBE on TF	-	-	-

Abbreviations: *CL*: Clearance; *CMT*: Compartment; *LBW*: Lean body weight; *OBE*: Obesity status; *PK*: Pharmacokinetics; *Q*: Intercompartmental clearance; *TF*: Tissue factor; V_1, V_2: Volume of distribution parameters of central and peripheral CMTs; V_{max}: Maximum elimination rate.

Table S8: (Project I) Parameter estimates of NLME models for linezolid considering the impact of different surgery-specific characteristics. [continued on next page]
Model 0: No surgery-specific characteristics implemented; *Model 1*: Anaesthesia impact implemented on V_{max} and TF; *Model 2*: Cardiac output and MAP implemented on TF and CL_{Tot}, respectively; *Model 3*: Anaesthesia impact and MAP implemented on TF and CL_{Tot}, respectively.

Parameter [unit]	**Estimate (RSE[1], %)**			
	Model 0: 'No impact of surgery-specific characteristics'	**Model 1: 'Anaesthesia model'**	**Model 2: 'Haemodynamic marker model'**	**Model 3: 'Anaesthesia and MAP model'**
OFV	-82.309	-100.679	-143.318	-194.060
Fixed-effects parameters				
θ CL_u [L/h]	2.00 (29.8)	4.67 (36.4)	2.80 (32.3)	3.47 (27.0)
θ $V_{max,u}$ [mg/h]	44.2 (9.00)	23.3[2] (82.0)	44.1 (17.8)	42.0 (22.0)
θ $K_{m,u}$ [mg/L]	0.89 (37.5)	3.14 (114)	2.02 (27.2)	2.53 (28.9)
θ ANAE_$V_{max,u}$[3], %	--	88.8 (59.2)	--	--
θ MAP_$CL_{Tot,u}$[4], %	--	--	0.782 (43.5)	0.836 (41.3)
θ $V_{1,u}$[5] [L]	19.3 (7.80)	20.0 (16.4)	18.8 (7.90)	18.5 (8.20)
θ Q_u[5] [L/h]	61.0 (8.80)	75.2 (25.9)	63.7 (8.80)	66.0 (9.00)
θ $V_{2,u}$[5] [L]	37.4 (4.30)	36.4 (8.70)	36.9 (4.80)	36.1 (4.70)
θ f_u, %	85.8 (0.800)	85.6 (1.60)	85.7 (0.700)	85.6 (0.700)
θ $TF_{OBE,u}$, %	47.4 (8.10)	43.8[6] (15.3)	45.8 (7.80)	51.6[8] (7.90)
θ $TF_{NOBE,u}$, %	64.4 (6.50)	60.7[6] (13.3)	63.4 (6.60)	71.3[8] (5.70)
θ ANAE_TF_u, %	--	17.5[7] (12.9)	--	-15.4[9] (15.9)
θ CO_{LZ}_TF_u[10], %	--	--	0.819 (21.2)	--
θ RR_{OBE}, %	38.7 (7.60)	38.7 (19.4)	38.8 (7.70)	38.6 (7.70)
θ RR_{NOBE}, %	55.5 (7.00)	55.5 (13.3)	55.4 (7.00)	55.6 (6.80)
Interindividual and method variability parameters, %CV				
ω CL_u	107 (24.0)	56.8 (24.5)	81.3 (31.5)	69.4 (30.0)
ω $K_{m,u}$	127 (32.2)	152 (77.1)	106 (46.4)	120 (47.8)
ω $V_{1,u}$	40.7 (12.1)	43.6 (28.4)	41.1 (11.9)	41.8 (12.0)
ω Q_u	46.3 (17.3)	59.5 (21.9)	45.9 (16.2)	49.0 (18.4)
ω $V_{2,u}$	15.9 (28.0)	15.9 (43.8)	16.4 (25.9)	16.6 (24.5)
ω TF_u	18.2 (25.4)	17.5 (40.9)	17.6 (25.5)	17.8 (22.5)
$\omega_{Intercatheter}$ RR	27.2 (23.8)	27.4 (19.6)	27.2 (23.5)	27.4 (23.5)
Residual variability parameters, %CV				
σ_{prop} C_{P_tot}	5.04 (14.5)	6.19 (1.10)	4.82 (13.0)	4.87 (12.8)
σ_{prop} C_{P_u}	4.95 (14.6)	4.82 (16.2)	4.71 (12.6)	4.61 (12.9)
σ_{prop} $C_{\mu D}$	15.3 (6.10)	13.6 (3.20)	14.7 (6.30)	13.8 (6.20)
σ_{prop} C_{RD}	27.4 (12.0)	27.6 (11.7)	27.4 (11.8)	27.5 (11.9)

[1]RSE of random-effects parameter estimates ω and σ are reported on approximate standard deviation scale; [2]Intra-anaesthetic $V_{max,u}$; [3]Post-anaesthetic change of $V_{max,u}$; [4]Change of clearance per mmHg deviation of MAP from 75 mmHg (linear MAP-CL relationship); [5]Allometrically scaled with LBW (exponent of 1 and 0.75 for V_1/V_2 and Q, respectively) and centred to reference LBW of 70 kg; [6]Intra-anaesthetic TF_u; [7]Post-anaesthetic change of TF_u; [8]Post-anaesthetic TF_u; [9]Intra-anaesthetic change of TF_u; [10]Change of TF_u per L/min deviation of CO_{LZ} from 20 L/min (linear CO_{LZ}-TF_u relationship).
Abbreviations: *ANAE_TF$_u$*: Anaesthesia effect on *TF$_u$*: ANAE_$V_{max,u}$: Anaesthesia effect on $V_{max,u}$;*CL$_u$*: Clearance of unbound linezolid; *CL$_{Tot,u}$*: Total clearance of unbound linezolid; *CMT*: Compartment; *CO$_{LZ}$*: Cardiac output estimated according to Liljestrand and Zander (unadjusted) [3]; *CO$_{LZ}$_TF$_u$*: Effect of CO_{LZ} on TF_u; C_{P_tot}: Total plasma concentrations; C_{P_u}: Unbound plasma concentrations; C_{RD}: Retrodialysate concentration; C_{RP}: Retroperfusate concentration; C_{uD}: Microdialysate concentration; *CV*: Coefficient of variation (calculated for random-effects parameters according to Eq. 2.6); *f$_u$*: Fraction unbound; *K$_{m,u}$*: Michaelis-Menten constant of unbound linezolid; *LBW*: Lean body weight; *MAP*: Mean arterial blood pressure; *MAP_CL$_{Tot,u}$*: Effect of MAP on $CL_{Tot,u}$; *NLME*: Nonlinear mixed-effects; *Q$_u$*: Intercompartmental clearance of unbound linezolid; *RSE*: Relative standard error; *RR$_{OBE}$, RR$_{NOBE}$*: Relative recovery for obese and nonobese patients; *TF$_{OBE,u}$, TF$_{NOBE,u}$*: Tissue factor for obese and nonobese patients of unbound linezolid; *V$_{1,u}$, V$_{2,u}$*: Volume of distribution parameters of central and peripheral CMTs of unbound linezolid; *V$_{max,u}$*: Maximum elimination rate of unbound linezolid; θ: Fixed-effects parameter; ω: Random-effects parameter: Interindividual variability; σ: Random-effects parameter: Residual unexplained variability.

Table S9: (Project II) Scenarios investigated to assess the impact dosing alteration on the frequency of the attainment of adequate PTA (i.e. PTA≥90%). Dosing alteration comprised intensification of the daily dose (DD), prolongation of the infusion duration (INF) and shortening of the dosing interval (τ)). [continued on next page]

Dosing alteration	**Scenario identifier (details)**	**Setting of scenarios**		
		Details on investigated combinations of LBW, MIC, dosing regimen and matrix LBW (n_{LBW}=10: 35-80 kg in steps of 5 kg) MIC (n_{MIC}=4: 0.5, 1, 2, 4 mg/L)		**Number of investigated combinations** (n_{comb})[1]
		Dosing regimens	Matrix	
DD	A1 (all)	$n_{regimen}$=2 per DD: • *DD=1200 mg* ($SI1.2_{12}$ & $PI1.2_{12}$) • *DD=1800 mg* ($SI1.8_{12}$ & $PI1.8_{12}$) • *DD=2400 mg* ($SI2.4_{12}$ & $PI2.4_{12}$)	n_{matrix}=2 Plasma, ISF	n_{comb}=160 per DD
DD	B1 (INF=30 min)	$n_{regimen}$=1 per DD: • *DD=1200 mg* ($SI1.2_{12}$) • *DD=1800 mg* ($SI1.8_{12}$) • *DD=2400 mg* ($SI2.4_{12}$)	n_{matrix}=2 Plasma, ISF	n_{comb} =80 per DD
DD	C1 (INF=4 h)	$n_{regimen}$=1 per DD: • *DD=1200 mg* ($PI1.2_{12}$) • *DD=1800 mg* ($PI1.8_{12}$) • *DD=2400 mg* ($PI2.4_{12}$)	n_{matrix}=2 Plasma, ISF	n_{comb}=80 per DD
DD	D1 (plasma)	$n_{regimen}$=2 per DD: • *DD=1200 mg* ($SI1.2_{12}$ & $PI1.2_{12}$) • *DD=1800 mg* ($SI1.8_{12}$ & $PI1.8_{12}$) • *DD=2400 mg* ($SI2.4_{12}$ & $PI2.4_{12}$)	n_{matrix}=1 Plasma	n_{comb}=80 per DD
DD	E1 (ISF)	$n_{regimen}$=2 per DD: • *DD=1200 mg* ($SI1.2_{12}$, $PI1.2_{12}$) • *DD=1800 mg* ($SI1.8_{12}$, $PI1.8_{12}$) • *DD=2400 mg* ($SI2.4_{12}$, $PI2.4_{12}$)	n_{matrix}=1 ISF	n_{comb}=80 per DD
INF	A2 (all)	$n_{regimen}$=4 per INF: • *INF=30 min* ($SI1.2_{12}$ & $SI1.8_{12}$ & $SI1.8_{8}$ & $SI2.4_{12}$) • *INF=4 h* ($PI1.2_{12}$ & $PI1.8_{12}$ & $PI1.8_{8}$ & $PI2.4_{12}$)	n_{matrix}=2 Plasma, ISF	n_{comb}=320 per INF
INF	B2 (DD=1200 mg)	$n_{regimen}$=1 per DD: • *INF=30 min* ($SI1.2_{12}$) • *INF=4 h* ($PI1.2_{12}$)	n_{matrix}=2 Plasma, ISF	n_{comb} =80 per INF

Dosing alteration	Scenario identifier (details)	Setting of scenarios: Details on investigated combinations of LBW, MIC, dosing regimen and matrix LBW (n_{LBW}=10: 35-80 kg in steps of 5 kg) MIC (n_{MIC}=4: 0.5, 1, 2, 4 mg/L) Dosing regimens	Matrix	Number of investigated combinations (n_{comb})[1]
INF	C2 (DD=1800 mg)	$n_{regimen}$=2 per DD: • *INF=30 min* ($SI1.8_{12}$ & $SI1.8_{8}$) • *INF=4 h* ($PI1.8_{12}$ & $PI1.8_{8}$)	n_{matrix}=2 Plasma, ISF	n_{comb} =160 per INF
INF	D2 (DD=2400 mg)	$n_{regimen}$=1 per DD: • *INF=30 min* ($SI2.4_{12}$) • *INF=4 h* ($PI2.4_{12}$)	n_{matrix}=2 Plasma, ISF	n_{comb} =80 per INF
INF	E2 (τ=12h)	$n_{regimen}$=3 per INF: • *INF=30 min* ($SI1.2_{12}$ & $SI1.8_{12}$ & $SI2.4_{12}$) • *INF=4 h* ($PI1.2_{12}$ & $PI1.8_{12}$ & $PI2.4_{12}$)	n_{matrix}=2 Plasma, ISF	n_{comb}=240 per INF
INF	F2 (τ=8h)	$n_{regimen}$=1 per DD: • *INF=30 min* ($SI1.8_{8}$) • *INF=4 h* ($PI1.8_{8}$)	n_{matrix}=2 Plasma, ISF	n_{comb}=80 per INF
INF	G2 (plasma)	$n_{regimen}$=4 per INF: • *INF=30 min* ($SI1.2_{12}$ & $SI1.8_{12}$ & $SI1.8_{8}$ & $SI2.4_{12}$) • *INF=4 h* ($PI1.2_{12}$ & $PI1.8_{12}$ & $PI1.8_{8}$ & $PI2.4_{12}$)	n_{matrix}=1 Plasma	n_{comb}=160 per INF
INF	H2 (ISF)	$n_{regimen}$=4 per INF: • *INF=30 min* ($SI1.2_{12}$ & $SI1.8_{12}$ & $SI1.8_{8}$ & $SI2.4_{12}$) • *INF=4 h* ($PI1.2_{12}$ & $PI1.8_{12}$ & $PI1.8_{8}$ & $PI2.4_{12}$)	n_{matrix}=1 Plasma	n_{comb}=160 per INF
τ	A3 (all)	$n_{regimen}$=2 per τ: • *τ=12 h* ($SI1.8_{12}$ & $PI1.8_{12}$) • *τ=8 h* ($SI1.8_{8}$ & $PI1.8_{8}$)	n_{matrix}=2 Plasma, ISF	n_{comb}=160 per τ
τ	B3 (INF=30 min)	$n_{regimen}$=1 per τ: • *τ=12 h* ($SI1.8_{12}$) • *τ=8 h* ($SI1.8_{8}$)	n_{matrix}=2 Plasma, ISF	n_{comb}=80 per τ
τ	C3 (INF=4 h)	$n_{regimen}$=1 per τ: • *τ=12 h* ($PI1.8_{12}$) • *τ=8 h* ($PI1.8_{8}$)	n_{matrix}=2 Plasma, ISF	n_{comb}=80 per τ
τ	D3 (plasma)	$n_{regimen}$=2 per τ: • *τ=12 h* ($SI1.8_{12}$ & $PI1.8_{12}$) • *τ=8 h:* ($SI1.8_{8}$ & $PI1.8_{8}$)	n_{matrix}=1 Plasma	n_{comb}=80 per τ
τ	E3 (ISF)	$n_{regimen}$=2 per τ: • *τ=12 h* ($SI1.8_{12}$ & $PI1.8_{12}$) • *τ=8 h* ($SI1.8_{8}$ & $PI1.8_{8}$)	n_{matrix}=1 ISF	n_{comb}=80 per τ

[1] $n_{comb} = n_{regimen} \cdot n_{matrix} \cdot n_{LBW} \cdot n_{MIC}$.

Dosing regimens: *$SI1.2_{12}$*: 600 mg 30-min i.v. infusion, q12h; *$SI1.8_{12}$*: 900 mg 30-min i.v. infusion, q12h; *$SI1.8_{8}$*: 600 mg 30-min i.v. infusion, q8h; *$SI2.4_{12}$*: 1200 mg 30-min i.v. infusion, q12h; *$PI1.2_{12}$*: 600 mg 4-h i.v. infusion, q12h; *$PI1.8_{12}$*: 900 mg 4-h i.v. infusion, q12h; *$PI1.8_{8}$*: 600 mg 4-h i.v. infusion, q8h; *$PI2.4_{12}$*: 1200 mg 4-h i.v. infusion, q12h. .

Abbreviations: *DD*: Daily dose; *INF*: Infusion duration; *ISF*: Interstitial space fluid; *LBW*: Lean body weight; n_{comb}: number of investigated combinations of dosing regimen, matrix, LBW and MIC; n_{LBW}: Number of investigated LBW values; n_{MIC}: Number of investigated MIC values; *PI*: Prolonged infusion; *PTA*: Probability of target attainment; *SI*: Short-term infusion; τ: Dosing interval.

Table S10: (Project II) Probability of target (95%$fT_{>MIC}$) attainment for varying LBW [continued on next page].
PTA given for plasma and ISF of the s.c. adipose tissue for selected short-term and prolonged linezolid dosing regimens, for selected MIC values and varying LBW values (35-80 kg).

MIC [mg/L]	LBW[1] [kg]	Probability of target attainment, %															
		Short-term infusion regimens[2]								Prolonged infusion regimens[2]							
		SI1.2$_{12}$		SI1.8$_{12}$		SI1.8$_{8}$		SI2.4$_{12}$		PI1.2$_{12}$		PI1.8$_{12}$		PI1.8$_{8}$		PI2.4$_{12}$	
		Plasma	ISF	Plasma	ISF	Plasma	ISF	Plasma	ISF	Plasma	ISF	Plasma	ISF	Plasma	ISF	Plasma	ISF
0.5	35	68.8	59.2	85.5	81.6	96.1	93.3	91.4	88.9	81.6	73.6	92.5	89.3	99.5	97.6	96.3	94.2
	40	77.3	68.5	91.3	86.9	98.1	96.3	95.6	93	87.6	80.3	97	93.2	99.6	98.4	98.7	97.1
	45	82.8	74	94	90.2	98.7	97	97.2	95.6	91	84.3	97.6	95.6	100	98.6	98.9	98
	50	88	72.6	96.4	91.2	99.2	97.3	98.1	96.7	94.3	80.9	98.4	96.1	99.9	97	99.4	98
	55	89.8	75.6	96.8	93.1	99.3	97	98.1	96.6	95.1	82.8	98.6	95.8	99.9	96.3	99.5	97.9
	60	91.9	77.2	98.3	93.5	99.9	97.9	99.4	97.6	96.5	82.1	99.7	96.6	100	94.7	99.9	98.6
	65	92.5	79.1	97.9	94.3	99.4	98.1	99.1	97.9	97.1	81.2	99.2	96.4	99.8	92.8	99.6	98.6
	70	93.5	82.6	97.7	94.7	99.9	97.5	99.2	97.2	97	82.7	99.7	95.3	100	92.2	100	98.1
	75	95.5	82	99.1	95.7	99.9	97.6	99.4	97.8	98.4	80.2	99.6	96.5	100	89.2	100	98.1
	80	95.7	81.9	98.9	96.1	99.7	98	99.5	98.5	98.2	77.8	99.6	96.7	100	85.5	99.8	98.5
1	35	50.3	36.1	76.8	68.7	91	84.5	85.9	81.4	67.8	47.9	87.6	79.9	98	90.3	92.4	88.8
	40	60.9	46.2	83.9	75.5	94.9	88.2	91.8	86.5	75.8	55	92.6	84.3	99.1	90.6	96.4	92.3
	45	66.1	49.9	88.9	80.7	96.3	90.4	94.2	89.9	80.4	55.5	94.3	87.7	99.1	88.6	97.6	94.8
	50	72.4	40.7	91.5	78.2	97.7	88.6	96.3	90.5	85.3	35.7	96.2	82.4	99.3	62.4	98.2	93.6
	55	76.1	40.5	92.5	79.8	97.4	89.4	96.9	91.3	87.4	33.4	96.8	80.4	99.3	53.5	98.2	93.3
	60	79.2	41.8	94.5	81.3	98.8	87.8	97.6	92.1	89.3	27	97.7	77.4	99.9	41.5	99.4	92.3
	65	79	42.2	95.5	82	98.3	87.9	97.6	92.5	89.6	23	97.8	73.5	99.5	34.4	99.2	90.5
	70	85	44.2	95.3	84.7	97.7	88.4	97.5	92.9	90.9	19.2	97.4	71.8	100	27.5	99.4	89.5
	75	84.7	38.7	97.1	84.5	99.1	87	98.9	93.8	92.9	11.5	98.9	62.5	99.9	16.9	99.4	88.5
	80	85.5	42.7	97.2	83.9	98.9	86.3	98.7	94.1	92.7	9.5	98.7	56.9	99.7	12.7	99.4	84.4

Table S10 [continued]

MIC [mg/L]	LBW[1] [kg]	Probability of target attainment, %															
		Short-term infusion regimens[2]								Prolonged infusion regimens[2]							
		$SI1.2_{12}$		$SI1.8_{12}$		$SI1.8_{8}$		$SI2.4_{12}$		$PI1.2_{12}$		$PI1.8_{12}$		$PI1.8_{8}$		$PI2.4_{12}$	
		Plasma	ISF	Plasma	ISF	Plasma	ISF	Plasma	ISF	Plasma	ISF	Plasma	ISF	Plasma	ISF	Plasma	ISF
2	35	28.2	12.5	62.5	46.8	79.3	61.8	76.6	67	41.1	10.8	75.1	52.3	91.8	43.8	86.8	75.1
	40	35.8	13.1	70.3	54.1	85.5	66.6	84.1	73.3	50.4	9.5	82	54.2	94.9	31.3	91.7	78.7
	45	38.6	13.5	75.2	55.5	88.8	66.1	87.8	77.4	53.3	6.7	85.8	51.4	95.8	20.6	93.8	79.6
	50	43.3	5.2	80.8	44.6	90.3	44.8	90.6	71.2	55.4	0.7	88.3	23	96.6	1.8	96.3	57.4
	55	44.1	5.2	82.3	43	91.2	38.7	91.9	72.4	56	0.3	89.9	15.8	96.5	0.7	96.3	52.2
	60	46.6	3.4	84.9	41.3	92.9	35	93.8	71.9	55.1	0.2	91	9.4	96.4	0.3	97.2	38.8
	65	46.3	3.1	83.5	40.7	93.2	32.1	94.6	72.8	53.5	0.1	91.8	6.9	95.4	0.3	97.2	34.9
	70	48.5	2.9	87.9	42	93	30.2	94.2	74.7	57.2	0.1	92.5	4.9	94	0.1	97	29.4
	75	44.9	2.3	88.3	33.3	94.1	19	96.2	71.2	51.1	0	94.1	2	92.4	0	98.1	18.2
	80	48.8	2.8	88.7	36.4	94.7	21.5	96.5	72.3	52.2	0	94.7	2.1	87.7	0	97.8	14.1
4	35	6.4	0.3	39	14.6	53.5	14.6	61.1	41.1	9.6	0	52.8	6.7	63.3	0.4	73.2	32.9
	40	4.7	0.3	45.4	14.9	55.6	12.5	68.6	45.4	6.3	0	55.7	3.8	54.1	0.1	79.2	27.5
	45	5.3	0.3	46.7	13.2	54.8	9.1	73.2	42.9	5.9	0	56.1	2.1	42.3	0.1	81.6	17.9
	50	5.3	0	51.6	3.4	54.7	1	76.5	28	4.3	0	58.6	0	34.1	0	84.2	1.7
	55	4.6	0	48.7	3.3	47.3	0.8	77	22.9	3.4	0	55.4	0	18.7	0	85.2	0.5
	60	4.1	0	48.9	1.8	43.9	0.2	78.5	20.9	1.5	0	50.8	0.1	11.4	0	86.1	0.5
	65	3.8	0	46.5	1.4	39.4	0.2	78.4	19.5	1.3	0	45.5	0	6.3	0	84	0.2
	70	3.4	0	49.2	0.8	36.7	0.1	82.3	18.9	0.7	0	44.9	0	3.6	0	86.4	0.1
	75	1.8	0	41.8	0.5	26.6	0	79.2	9.7	0.1	0	32.5	0	1.4	0	82.3	0
	80	2.6	0	45	0.6	24.9	0.1	81.8	11.9	0.3	0	28.7	0	1.3	0	80.6	0

[1]All other covariates in the NLME model were set to median values of the patient population (for detailed information on patient characteristics see Table 2.4 B). [2]Dosing regimens: $SI1.2_{12}$: 600 mg 30-min i.v. infusion, q12h; $SI1.8_{12}$: 900 mg 30-min i.v. infusion, q12h; $SI1.8_{8}$: 600 mg 30-min i.v. infusion, q8h; $SI1.2_{12}$: 1200 mg 30-min i.v. infusion, q12h; $PI1.2_{12}$: 600 mg 4-h i.v. infusion, q12h; $PI1.8_{12}$: 900 mg 4-h i.v. infusion, q12h; $PI1.8_{8}$: 600 mg 4-h i.v. infusion, q8h; $PI2.4_{12}$: 1200 mg 4-h i.v. infusion, q12h.
Horizontal dashed line: Separates obese from nonobese patients according to LBW obesity threshold of 47.1 kg (translating into the BMI obesity threshold of 30 kg/m^2 for a 1.65 m tall female patient).

Colour coding: *Green*: PTA≥90%, *Yellow*: PTA 80-<90%, *Orange*: PTA>50-<80%, *Red*: PTA≤50%
Abbreviations: $fT_{>MIC}$: Time period that unbound drug concentration exceeds the MIC; *ISF*: Interstitial space fluid; *LBW*: Lean body weight; *MIC*: Minimum inhibitory concentration; *PTA*: Probability of target attainment; *s.c.*: Subcutaneous.

Table S11: (Project II) Probability of target (95%$fT_{>MIC}$) attainment for typical patients.

PTA given for plasma and ISF of the s.c. adipose tissue for selected short-term and prolonged linezolid dosing regimen and selected MIC values for the typical obese and non-obese patient[1], during (intra-anaesthetic) and after anaesthesia (post-anaesthetic).

Typical patient[1]	MIC [mg/L]	Probability of target attainment, %															
		Short-term infusion regimens[2]								Prolonged infusion regimens[2]							
		SI1.2$_{12}$		SI1.8$_{12}$		SI1.8$_{8}$		SI2.4$_{12}$		PI1.2$_{12}$		PI1.8$_{12}$		PI1.2$_{8}$		PI2.4$_{12}$	
		Plasma	ISF	Plasma	ISF	Plasma	ISF	Plasma	ISF	Plasma	ISF	Plasma	ISF	Plasma	ISF	Plasma	ISF
"obese & intra-anaesthetic"	0.5	88.6	73.4	96.9	90.7	99.4	97.1	98.6	96.2	95.7	79.6	98.9	95	100	95.1	99.6	98.1
	1	74	39.3	92.2	77.6	97.2	85.9	96.7	89.5	85.5	29.1	96.8	75.8	99.5	47.7	98.8	91
	2	42.4	3.8	79.8	39.2	89.5	36.7	90.7	69.6	52.6	0.2	88.5	12.3	95.8	0.7	95.4	44.9
	4	3.5	0	46.7	2.4	45.1	0.5	74.8	22.5	2.3	0	51.1	0	13.6	0	81.5	0.9
"non-obese & intra-anaesthetic"	0.5	78.2	70.5	91.8	87.5	97.9	96.4	96.2	94	88.5	81.3	97.1	94.4	99.5	98.4	98.2	96.7
	1	63.2	47.7	84.2	77.3	95.2	89.1	91.9	86.5	76.7	55.6	92.3	84.6	98.2	90.3	96.8	93.5
	2	37.7	14.4	71.7	53.7	85.2	66.4	83.9	74.7	51	9.4	81.7	53.5	95.1	27.6	92.4	78.3
	4	6.4	0.1	45.1	15.1	54.8	11.5	69.5	43.2	8.1	0	54.9	3.2	50.6	0	78.8	25.1
"obese & post-anaesthetic"	0.5	75.9	62.2	92.4	88.7	97.4	96.7	96.7	95.7	87.4	74.6	97.1	94.2	99.6	98.6	98.2	97.4
	1	51.3	32.3	83.4	73.1	93.9	86.6	92.9	86.9	68.2	29.2	92.1	79.3	98.1	69.5	97.1	93.5
	2	23.4	2.8	65	35.8	80.3	37.1	83.4	67.6	31.4	0.4	77.5	18.5	90.6	1.7	91.2	59.7
	4	1.6	0	26.6	1.8	23.7	0.5	60.8	21.7	0.6	0	30.6	0	8.3	0	70.3	2
"non-obese & post-anaesthetic"	0.5	64.7	60.4	85.2	83.8	96.3	96	92.7	91.9	79.7	77.5	93.5	92.5	99.6	99.5	97.5	96.7
	1	44.4	38.5	75.8	71.9	89.7	88.1	85.4	83.5	60.7	49.9	86.1	82.3	98	95.2	93.7	92.2
	2	19	10.7	56.2	46.7	76.3	65.5	76	70.1	31.4	9.2	72.4	55.2	90.3	44.8	86.1	79.4
	4	2	0.1	27.9	11.7	36.5	10.9	54.8	42	3.2	0	37.7	4.9	37.5	0.1	68.1	33.8

[1]Detailed information on patient characteristics: Table 2.4 A. [2]Dosing regimens: *SI1.2$_{12}$*: 600 mg 30-min i.v. infusion, q12h; *SI1.8$_{12}$*: 900 mg 30-min i.v. infusion, q12h; *SI1.8$_{8}$*: 600 mg 30-min i.v. infusion, q8h; *SI1.2$_{12}$*: 1200 mg 30-min i.v. infusion, q12h; *PI1.2$_{12}$*: 600 mg 4-h i.v. infusion, q12h; *PI1.8$_{12}$*: 900 mg 4-h i.v. infusion, q12h; *PI1.8$_{8}$*: 600 mg 4-h i.v. infusion, q8h; *PI2.4$_{12}$*: 1200 mg 4-h i.v. infusion, q12h.

Colour coding: *Green*: PTA≥90%, *Yellow*: PTA 80-<90%, *Orange*: PTA>50-<80%, *Red*: PTA≤50%

Abbreviations: *$fT_{>MIC}$:* Time period that unbound drug concentration exceeds the MIC; *ISF*: Interstitial space fluid; *MIC*: Minimum inhibitory concentration; *PTA*: Probability of target attainment; *s.c.:* Subcutaneous.

Table S12: (Project II) Impact of intensification of daily dose (DD) on the attainment of adequate PTA (i.e. PTA ≥90%).
For details on comparison scenarios see Table S9.

Comparison scenario (details)	Number of investigated combinations[1] per DD (n_{comb})	Number (%) of investigated combinations attaining PTA ≥90% per DD		
		DD=1200 mg	DD=1800 mg	DD=2400 mg
A1 (all)	160	16 (10)	57 (35.6)	87 (54.4)
B1 (INF=30 min)	80	5 (6.25)	24 (30.0)	42 (52.5)
C1 (INF=4 h)	80	11 (13.8)	33 (41.3)	45 (56.3)
D1 (plasma)	80	16 (20)	40 (50.0)	55 (68.8)
E1 (ISF)	80	0 (0.00)	17 (21.3)	32 (40)

[1]Combinations of investigated dosing regimen, matrix (i.e. plasma, ISF), LBW, MIC (see Table S9).
Abbreviations: *DD*: Daily dose; *INF*: Infusion duration; *ISF*: Interstitial space fluid; n_{comb}: number of investigated combinations of dosing regimen, matrix, LBW and MIC; *PTA*: Probability of target attainment.

Table S13: (Project II) Impact of prolongation of infusion duration (INF) on the attainment of adequate PTA (i.e. PTA ≥90%).
For details on comparison scenarios see Table S9.

Comparison scenario (details)	Number of investigated combinations per INF (n_{comb})	Number (%) of investigated combinations attaining PTA ≥90% per DD	
		INF=30 min	INF=4 h
A2 (all)	320	109 (34.1)	127 (39.7)
B2 (DD=1200 mg)	80	5 (6.25)	16 (20.0)
C2 (DD=1800 mg)	160	24 (15.0)	33 (20.6)
D2 (DD=2400 mg)	80	42 (52.5)	45 (56.3)
E2 (τ=12h)	240	71 (29.6)	94 (39.2)
F2 (τ=8h)	80	38 (47.5)	38 (47.5)
G2 (plasma)	160	74 (46.3)	92 (57.5)
H2 (ISF)	160	35 (21.9)	35 (21.9)

[1]Combinations of investigated dosing regimen, matrix (i.e. plasma, ISF), LBW, MIC (see Table S9).
Abbreviations: *DD*: Daily dose; *INF*: Infusion duration; *ISF*: Interstitial space fluid; n_{comb}: number of investigated combinations of dosing regimen, matrix, LBW and MIC; *PTA*: Probability of target attainment; τ: Dosing interval.

Table S14: (Project II) Impact of shortening of the dosing interval (τ) on the attainment of adequate PTA (i.e. PTA≥90%).
For details on comparison scenarios see Table S9.

Comparison scenario (details)	Number of investigated combinations per τ (n_{comb})	Number of (%) investigated combinations attaining PTA≥90% per τ	
		τ=12 h	τ=8 h
A3 (all)	160	57 (35.6)	76 (47.5)
B3 (INF=30 min)	80	24 (30)	38 (47.5)
C3 (INF=4 h)	80	33 (41.3)	38 (47.5)
D3 (plasma)	80	40 (50)	55 (68.5)
E3 (ISF)	80	17 (21.3)	21 (26.3)

[1]Combinations of investigated dosing regimen, matrix (i.e. plasma, ISF), LBW, MIC (see Table S9).
Abbreviations: *DD*: Daily dose; *INF*: Infusion duration; *ISF*: Interstitial space fluid; n_{comb}: number of investigated combinations of dosing regimen, matrix, LBW and MIC; *PTA*: Probability of target attainment; τ: Dosing interval.

Table S15: (Project II) Overview of adequacy of different dosing regimens to attain PK/PD target (95%fT$_{>MIC}$) in plasma (A) or both in plasma and ISF (B) for typical patients.

Results given for selected short-term and prolonged dosing regimens, selected MIC values and varying LBW values. Dosing regimens resulting in adequate PTA for plasma (A) or plasma and ISF (B) are highlighted with ✓.

Typical patient[1]	MIC [mg/L]	Dosing regimens[3]															
		A: …resulting in adequate PTA[2] in plasma								B: …resulting in adequate PTA[2] in plasma and ISF							
		Short-term infusion				Prolonged infusion				Short-term infusion				Prolonged infusion			
		SI1.2$_{1\ 2}$	SI1.8$_{1\ 2}$	SI1.8$_{8}$	SI2.4$_{1\ 2}$	PI1.2$_{1\ 2}$	PI1.8$_{1\ 2}$	PI1.8$_{8}$	PI2.4$_{1\ 2}$	SI1.2$_{1\ 2}$	SI1.8$_{1\ 2}$	SI1.8$_{8}$	SI2.4$_{1\ 2}$	PI1.2$_{1\ 2}$	PI1.8$_{1\ 2}$	PI1.8$_{8}$	PI2.4$_{1\ 2}$
obese and intra-anaesthetic	0.5		✓	✓	✓	✓	✓	✓	✓		✓	✓	✓		✓	✓	✓
	1		✓	✓	✓		✓	✓	✓		none						✓
	2				✓			✓	✓		none				none		
	4		none				none				none				none		
nonobese and intra-anaesthetic	0.5		✓	✓	✓		✓	✓	✓			✓	✓		✓	✓	✓
	1			✓	✓		✓	✓	✓		none					✓	✓
	2		none					✓	✓		none				none		
	4		none				none				none				none		
obese and post-anaesthetic	0.5		✓	✓	✓		✓	✓	✓			✓	✓		✓	✓	✓
	1			✓	✓		✓	✓	✓		none						✓
	2		none					✓	✓		none				none		
	4		none				none				none				none		
nonobese and post-anaesthetic	0.5			✓	✓		✓	✓	✓			✓	✓		✓	✓	✓
	1		none					✓	✓		none					✓	✓
	2		none					✓			none				none		
	4		none				none				none				none		

[1]All other covariates in the NLME PK model were set to median values of the patient population (for detailed information on patient characteristics see Table 2.4 A). [2]Adequate PTA is defined as PTA≥90%, for the PK/PD target 95%fT$_{>MIC}$ (for detailed information on PTA see Table S11); [3]Dosing regimens: $SI1.2_{12}$: 600 mg 30-min i.v. infusion, q12h; $SI1.8_{12}$: 900 mg 30-min i.v. infusion, q12h; $SI1.8_{8}$: 600 mg 30-min i.v. infusion, q8h; $SI2.4_{12}$: 1200 mg 30-min i.v. infusion, q12h; $PI1.2_{12}$: 600 mg 4-h i.v. infusion, q12h; $PI1.8_{12}$: 900 mg 4-h i.v. infusion, q12h; $PI1.8_{8}$: 600 mg 4-h i.v. infusion, q8h; $PI2.4_{12}$: 1200 mg 4-h i.v. infusion, q12h.

Horizontal dashed line: Separates obese from nonobese patients according to LBW obesity threshold of 47.1 kg (translating into the BMI obesity threshold of 30 kg/m^2 for a 1.65 m tall female patient).

Abbreviations: *fT$_{>MIC}$:* Time period that unbound drug concentration exceeds the MIC*; ISF*: Interstitial space fluid; *LBW*: Lean body weight; *PL*: Plasma; *PTA*: Probability of target attainment; *s.c.:* Subcutaneous.

Table S16: (Project III) PK/PD target attainment for all non-CRRT patients after standard meropenem dosing (1000 mg, i.v. 30 min, every 8 h) for different MIC values (modified from [233]).

MIC [mg/L]	**PK/PD target attainment, %**	
	$50\%T_{>4xMIC}$ $C_{4h} \geq 4xMIC$	$100\%T_{>MIC}$ $C_{4h} \geq MIC$
0.25	99.6	95.5
0.5	96.9	91.9
1	91.0	78.0
2	56.1	48.4
4	27.4	38.1
8	7.17	20.6

Colour coding: Target attainment ≥90% (green), 80-<90% (yellow), >50-<80% (orange), ≤50 (red)
Abbreviations: C_X: Concentration at specific time point X of concentration-time profile (here: calculated meropenem serum concentrations); *MIC*: Minimum inhibitory concentration; *PK/PD*: Pharmacokinetic/pharmacodynamic; $T_{>MIC}$: Time period that total drug concentration exceeds the MIC; $T_{>4xMIC}$: Time period that unbound drug concentration exceeds four times the MIC.

Table S17: (Project IV) Summary of preselected covariates[1] (n=27) of non-CRRT patients (n=41) and results of covariate modelling. [continued on next pages]

Covariate	Classification			Summary statistics on first study day				Included in model (+) or not (-)		
	CAT or CONT, $N_{categories}$	For CAT: ordered (+) or not (-)	$N_{observations\_planned}$[2]/ patient	For CAT: % For CONT: median	For CONT: 5th percentile	For CONT: 95th percentile	Missing data, %[3]	Full model	Final model	PK parameter (direction of effect[4])
Sex, male	CAT, 2	-	1	58.5			0	+	-	V_1 (male> female)
ECMO	CAT, 2	-	1	4.88			0	-	-	
Lung transplantation	CAT, 2	-	1	40			0	-	-	
ARDS	CAT, 2	-	1	9.76			0	-	-	
Peritonitis	CAT, 2	-	1	12.2			0	-	-	
Mean arterial pressure[5]	CAT, 9	+	4	CAT=1: 7.32 CAT=2: n.a. CAT=3: 46.3 CAT=4: n.a. CAT=5: 9.76 CAT=6: n.a. CAT=7: 26.8 CAT=8: 4.88 CAT=9: 4.88			0	-	-	
Heart rate[6]	CAT, 9	+	4	CAT=1: 2.44 CAT=2: 24.4 CAT=3: 2.44 CAT=4: n.a. CAT=5: 58.5 CAT=6: n.a. CAT=7: 58.5 CAT=8: 12.2 CAT=9: 0.00			0	+	-	CL (↑)

Table S17 [continued]

Covariate	Classification			Summary statistics on first study day				Included in model (+) or not (-)		
	CAT or CONT, $N_{categories}$	For CAT: ordered (+) or not (-)	$N_{observations\_planned}$[2]/ patient	For CAT: % For CONT: median	For CONT: 5th percentile	For CONT: 95th percentile	Missing data, %[3]	Full model	Final model	PK parameter (direction of effect[4])
Cardio vascular system[7]	CAT, 5	-	4	CAT=1: 14.6 CAT=2: 0.00 CAT=3: 2.44 CAT=4: 0.00 CAT=5: 82.9			0	+	-	V_1 (↓), CL (↓)
Age [years]	CONT		1	56	32	70	0	+	-	V_1 (↓)
Body weight [kg]	CONT		1	70	47	121	0	+	+	V_1 (↑)
Serum creatinine [mg/dL]	CONT		4	1.0	0.6	1.9	0	-	-	
Serum albumin [g/L]	CONT		4	2.8	2.2	3.6	0	+	+	V_2 (↓)
Serum urea [mg/dL]	CONT		4	41	20	92	0	+	-	CL (↓)
$CLCR_{UC}$ [mL/min]	CONT		4	81	19	171	4.88	-	-	
$CLCR_{CG}$ [mL/min]	CONT		4	80.8	39.4	170	0	+	+	CL (↑)
Fibrinogen [mg/dL]	CONT		4	340	187	647	0	-	-	
Antithrombin, %	CONT		4	74	49	94	0	-	+	
Bilirubin [mg/dL]	CONT		4	0.8	0.3	7.4	0	+	-	V_2 (↓), V_1 (↑)
Cholinesterase [kU/L]	CONT		4	3.99	2.11	6.63	0	+	-	CL (↑)
Factor V, %	CONT		4	107	49	150	0	+	-	CL (↓)

Table S17 [continued]

Covariate	Classification			Summary statistics on first study day				Included in model (+) or not (-)		
	CAT or CONT, $N_{categories}$	For CAT: ordered (+) or not (-)	$N_{observations\_planned}$[2]/ patient	For CAT: % For CONT: median	For CONT: 5th percentile	For CONT: 95th percentile	Missing data, %[3]	Full model	Final model	PK parameter (direction of effect[4])
Interleukin-6 [pg/mL]	CONT		8	88.3	24.0	1460	0		-	
C-reactive protein [mg/dL]	CONT		8	8.9	2.1	32.	0	+	-	V_2 (↑)
CD64 index	CONT		4	1.23	0.53	3.73	19.5	-	-	
Sodium [mmol/L]	CONT		4	143	138	149	0	-	-	
pH	CONT		4	7.41	7.30	7.51	0	+	-	V_2 (↓)
Lactate [mmol/L]	CONT		4	1.51	0.680	3.64	0	+	-	V_1 (↓)
Hydrogencarbo-nate [mmol/L]	CONT		4	27.4	20.5	37.0	0	+	-	CL (↓)

[1]58 patient-specific characteristics: 27 preselected covariates (Table S17) + body height, body mass index, urine volume, fluid balance, urine creatinine, urine albumin, anuria, erythrocytes, haemoglobin, haematocrit, thrombocytes, prothrombin time, partial thromboplastin time, aspartate aminotransferase, alanine aminotransferase, cholinesterase enzyme, factor V, leucocytes, potassium, glucose, inorganic phosphate, sepsis, cause of sepsis, liver transplantation, 28-day mortality, APACHE II score, SOFA score, Glasgow coma score, body temperature (extracted from APACHE II score), respiratory rate (extracted from APACHE II score), PaO_2/FiO_2 ratio (extracted from APACHE II score).

[2]Number of covariate observations planned per patient within the study period of 4 days.

[3]Related to total number of observations planned (i.e. $N_{observations\_planned}$/patient 41 patients).

[4]Direction of covariate-parameter relationship; for CONT covariates: the higher the covariate value, the higher (↑) or the lower (↓) the PK parameter; for ordered CAT covariates: the higher the category class of the covariate, the higher (↑) or the lower (↓) the PK parameter; for dichotomous CAT covariates: specification for which covariate class PK parameter is higher)

[5]Extracted from APACHE II score (blood pressure [mmHg]: CAT=1 ≤49, CAT=2: n.a., CAT=3: 50-69, CAT=4: n.a., CAT=5: 70-109, CAT=6: n.a., CAT=7: 110-129, CAT=8 130-159, CAT=9: ≥160).

[6]Extracted from APACHE II score (heart rate [1/min]: CAT=1: ≤39, CAT=2: 40-54, CAT=3: 55-69, CAT=4: n.a., CAT=5: 70-109, CAT=6: n.a., CAT=7: 110-139, CAT=8: 140-179, CAT=9: ≥180).

[7]Extracted from SOFA score (CVS: CAT=1 no hypotension, CAT=2: MAP < 70 mmHg, CAT=3: dop <= 5 or dob (any dose), CAT=4: dop > 5 OR epi <= 0.1 OR nor <= 0.1, CAT=5: dop > 15 OR epi > 0.1 OR nor > 0.1).

***Abbreviations*:** *APACHE:* Acute Physiology And Chronic Health Evaluation [1]; *ARDS*: Acute respiratory distress syndrome; *CAT*: Categorical; *CONT:* Continuous; $CLCR_{CG}$*:* Creatinine clearance estimated according to Cockcroft and Gault [2]; *CRRT*: Continuous renal replacement therapy; *dop*: Dopamine; *CVS*: Cardiovascular system; *ECMO*: Extracorporeal membrane oxygenation; *epi*: Epinephrine, *MAP*: Mean arterial pressure; *nor*: Norepinephrine; *SOFA*: Sepsis-related Organ Failure Assessment [6].

Table S18: (Project IV) Comparison of NLME base model including interoccasion variability, when defining an occasion as study day or intensively monitored dosing interval.

Parameter [unit]	**Estimate (RSE[1], %)**		
	'Base model'	**Base model + IOV (occasion=study day)**	**Base model + IOV (occasion=intensively monitored dosing interval)**
OFV	6090.465	5653.12	5517.641
ΔOFV	--	-437.345	-572.824
Fixed-effects parameters			
θ CL [L/h]	8.31 (7.30)	8.21 (7.30)	8.31 (7.30)
θ V_1 [L]	8.62 (10.9)	8.54 (8.30)	9.04 (8.40)
θ Q [L/h]	30.6 (13.7)	28.8 (10.8)	25.8 (12.9)
θ V_2 [L]	18.7 (6.70)	16.9 (5.80)	16.3 (6.40)
Interindividual variability parameters, %CV			
ω CL	54.1 (7.80)	53.3 (8.10)	53.4 (8.40)
ω V_1	43.2 (11.7)	41.7 (10.3)	39.8 (10.20)
ω V_2	25.4 (16.0)	22.7 (13.9)	24.4 (13.8)
Interoccasion variability parameters, %CV			
Κ CL	--	16.0 (9.90)	17.6 (10.2)
Κ V_1	--	13.9 (34.0)	16.1 (28.6)
Residual variability parameters, %CV			
σ_{prop}, %CV	24.8 (6.60)	18.9 (5.40)	16.1 (8.20)
σ_{add}, SD [mg/L]	0.378 (34.0)	0.308 (19.7)	0.273 (31.8)

[1]RSE of random-effects parameter estimates ω and σ are reported on approximate standard deviation scale.
Abbreviations: *CL*: Clearance; *CMT*: Compartment; *CRRT*: Continuous renal replacement therapy; *CV*: Coefficient of variation (calculated for random-effects parameters according to Eq. 2.6); *NLME*: Nonlinear mixed-effects; *Q*: Intercompartmental clearance; *RSE*: Relative standard error; *SD*: Standard deviation; V_1, V_2: Volume of distribution parameters of central and peripheral CMTs; *θ:* Fixed-effects parameter; *ω*: Random-effects parameter: Interindividual variability; Κ*:* Random-effects parameter: Interoccasion variability; *σ*: Random-effects parameter: Residual unexplained variability.

Table S19: (Project IV) Comparison of imputation/interpolation strategies for $CLCR_{CG}$ (Subtable A) and comparison of NLME base model for all patients and non-CRRT patients (Subtable B).
Subtable A: Parameter estimates of NLME base model and NLME model including stepwise imputed/interpolated $CLCR_{CG}$ (strategy A) and linear imputed/interpolated $CLCR_{CG}$ (strategy B) as covariate on meropenem clearance.
Subtable B: Parameter estimates of NLME base model based on all patients (n=48) and based on non-CRRT patients only (n=41).

Parameter [unit]	**Estimate (RSE[1], %)**				
	Subtable A			**Subtable B**	
	Base model'	**Base model + $CLCR_{CG}$ strategy A**	**Base model + $CLCR_{CG}$ strategy B**	**Base model, all patients**	**Base model, non-CRRT patients**
OFV	6090.465	5856.377	5689.452	6090.465	4913.332
Fixed-effects parameters					
θ CL^2 [L/h]	8.31 (7.30)	8.85 (4.50)	9.14 (3.90)	8.31 (7.30)	8.82 (8.00)
θ V_1 [L]	8.62 (10.9)	7.94 (9.40	8.31 (9.50)	8.62 (10.9)	8.41 (12.1)
θ Q [L/h]	30.6 (13.7)	31.7 (11.1)	30.4 (10.6)	30.6 (13.7)	30.9 (15.7)
θ V_2 [L]	18.7 (6.70)	17.0 (6.40)	17.6 (5.30)	18.7 (6.70)	17.8 (7.80)
θ $CLCR_{CG}$_CL^2, %	--	0.856 (11.9)	1.05 (6.50)	--	--
Interindividual variability parameters, %CV					
ω CL	54.1 (7.80)	30.5 (15.4)	25.7 (16.5)	54.1 (7.80)	55 (9.00)
ω V_1	43.2 (11.7)	46.4 (10.3)	45.1 (10.5)	43.2 (11.7)	41.5 (13.3)
ω V_2	25.4 (16.0)	25.2 (18.1)	24.8 (15.5)	25.4 (16.0)	21.6 (14.3)
Residual variability parameters, %CV					
σ_{prop}, %CV	24.8 (6.60)	19.0 (9.80)	20.8 (10.0)	24.8 (6.60)	24.1 (27.9)
σ_{add}, SD [mg/L]	0.378 (34.0)	1.11 (39.3)	0.534 (71.5)	0.378 (34.0)	0.367 (27.9)

[1]RSE of random-effects parameter estimates ω and σ are reported on approximate standard deviation scale, [2]Given for a $CLCR_{CG}$ value of 80.8 mL/min; [2]Change of clearance per mL/min deviation of $CLCR_{CG}$ from 80.8 mL/min.
Abbreviations: *CL*: Clearance; *$CLCR_{CG}$*: Creatinine clearance estimated according to Cockcroft and Gault [2]; *$CLCR_{CG}$_CL*: Effect of $CLCR_{CG}$ on CL; *CMT*: Compartment; *CRRT*: Continuous renal replacement therapy; *CV*: Coefficient of variation (calculated for random-effects parameters according to Eq. 2.6); *NLME*: Nonlinear mixed-effects; *Q*: Intercompartmental clearance; *RSE*: Relative standard error; *SD*: Standard deviation; *V_1, V_2*: Volume of distribution parameters of central and peripheral CMTs; *θ*: Fixed-effects parameter; *ω*: Random-effects parameter: Interindividual variability; *σ*: Random-effects parameter: Residual unexplained variability.

Table S20: (Project IV) Parameter estimates of NLME model of meropenem in critically ill non-CRRT (n=41) vs. CRRT (n=7) patients (modified from [243]).

Parameter [unit]	Parameter estimate (RSE[1], %)	
	Non-CRRT patients	CRRT patients
Fixed-effects parameters		
θ CL^2 [L/h]	9.25 (4.60)	9.82 (9.90)
θ V_1[3] [L]	7.89 (11.9)	8.09 (16.8)
θ Q [L/h]	28.4 (16.1)	27.4 (10.9)
θ V_2[4] [L]	16.1 (7.40)	19.1 (16.2)
θ $CLCR_{CG}$_CL^5, %	0.977 (9.20)	1.29 (8.00)
θ $CLCR_{CG}$_INF [mL/min]	154 (6.90)	154*
θ WT_V_1[6]	0.945 (16.6)	1*
θ ALB_V_2[7]	-0.202 (36.6)	-0.211 (122.3)
Interindividual variability parameters, %CV		
ω CL	27.1 (19.3)	18.8 (32.7)
ω V_1	31.5 (14.3)	62.7 (16.1)
ω V_2	16.9 (18.1)	30.9 (37.8)
Interoccasion variability parameters[8], %CV		
Κ CL	12.5 (12.0)	16.4 (13.8)
Residual variability parameters		
σ_{prop}, %CV	16.6 (6.60)	11.4 (10.8)
σ_{add}, SD [mg/L]	0.246 (29.0)	1.75 (10.6)

[1]RSE of random-effects parameter estimates ω and σ are reported on approximate standard deviation scale; [2]CL given for median $CLCR_{CG}$ of non-CRRT patients on first study day (80.8 mL/min); [3]V_1 given for median WT of non-CRRT patients (70 kg); [4]V_2 given for median ALB of non-CRRT patients at first study day (2.8 g/dL); [5]Change of clearance per mL/min deviation of $CLCR_{CG}$ from 80.8 mL/min ; [6]Estimated exponent in power WT-V_1 relationship, centred to median in overall population (70 kg); [7]Change of V_2 per g/dL deviation of ALB from 2.79 g/dL; [8]Occasion was defined as intensively monitored dosing interval. *Fixed parameters: $CLCR_{CG}$_INF fixed to inflection point of non-CRRT patients, as no information on high $CLCR_{CG}$ values available in CRRT patients; WT_V_1 fixed to allometry exponent of 1, as implausible estimate below 0, probably due to the low number of patients.

Abbreviations: *ALB*: Serum albumin concentration; *ALB_V_2*: ALB effect on V_2; *CI*: Confidence interval; *CL*: Clearance; *$CLCR_{CG}$*: Creatinine clearance estimated according to Cockcroft and Gault [2]; *$CLCR_{CG}$_CL*: $CLCR_{CG}$ effect on CL; *$CLCR_{CG}$_INF*: $CLCR_{CG}$ value serving as inflection point for meropenem CL (Figure S30); *CMT*: Compartment; *CRRT*: Continuous renal replacement therapy, *CV*: Coefficient of variation (calculated for random-effects parameters according to Eq. 2.6); *IIV*: Interindividual variability; *IOV*: Interoccasion variability; *Q*: Intercompartmental clearance; *RSE*: Relative standard error; *SD*: Standard deviation; *V_1, V_2*: Volume of distribution parameters of central and peripheral CMTs; *WT*: Body weight; *WT_V_1*: WT effect on V_1; *θ*: Fixed-effects parameter; *ω*: Random-effects parameter: Interindividual variability; Κ: Random-effects parameter: Interoccasion variability; *σ*: Random-effects parameter: Residual unexplained variability.

Table S21: (Project IV): Probability of target (98%$T_{>MIC}$) attainment on the first day of standard meropenem treatment (1000 mg, 30-min i.v. infusion, q8h) (modified from [243]). PTA is given for varied values of one covariate and for selected MIC values and is presented as the median ($P_{0.5}$), 5th ($P_{0.05}$) and 95th percentile ($P_{0.95}$) of the 1000 PTA values derived from the 1000 Monte Carlo simulations considering PK parameter uncertainty.

CLCR$_{CG}$ [mL/min]	Body weight [kg]	Albumin [g/dL]	Probability of target attainment, %																													
			MIC [mg/L]																													
			0.06			0.12			0.25			0.5			1			2			4			8			16			32		
			$P_{0.05}$	$P_{0.5}$	$P_{0.95}$	$P_{0.05}$	$P_{0.5}$	$P_{0.95}$	$P_{0.05}$	$P_{0.5}$	$P_{0.95}$	$P_{0.05}$	$P_{0.5}$	$P_{0.95}$	$P_{0.05}$	$P_{0.5}$	$P_{0.95}$	$P_{0.05}$	$P_{0.5}$	$P_{0.95}$	$P_{0.05}$	$P_{0.5}$	$P_{0.95}$	$P_{0.05}$	$P_{0.5}$	$P_{0.95}$	$P_{0.05}$	$P_{0.5}$	$P_{0.95}$	$P_{0.05}$	$P_{0.5}$	$P_{0.95}$
10	70	2.8	100	100	100	100	100	100	100	100	100	100	100	100	100	100	100	99.6	100	100	96.8	100	100	78.2	98	100	16	54.6	93.6	0	0	0.8
20	70	2.8	100	100	100	100	100	100	100	100	100	100	100	100	99.6	100	100	98.4	100	100	90.6	99	100	59.2	86.2	98.6	4.6	19.4	44.4	0	0	0
30	70	2.8	100	100	100	100	100	100	100	100	100	99.8	100	100	99	100	100	95.6	99.4	100	81.2	94.2	99.4	39	62.8	81.2	0.6	4.8	13.4	0	0	0
40	70	2.8	100	100	100	100	100	100	99.8	100	100	99.4	100	100	97.6	99.6	100	90.2	97	99.6	68.8	82.6	93.2	21.6	37.4	51	0	1	4.6	0	0	0
50	70	2.8	100	100	100	99.8	100	100	99.6	100	100	98.4	99.8	100	94.6	98.4	99.8	82.8	91.2	97.2	52.4	65.6	77	8.39	18.7	30.2	0	0.2	1.8	0	0	0
60	70	2.8	99.8	100	100	99.6	100	100	98.8	99.8	100	96.8	99.2	100	90	95.6	98.8	73	81.8	89.8	34.8	47.2	57.8	2.2	8.8	18.2	0	0	0.8	0	0	0
70	70	2.8	99.8	100	100	99.4	100	100	98	99.6	100	94.2	97.8	99.6	84.2	90.6	96	59.6	69.2	78.2	19.4	31.8	43.4	0.4	4	11.2	0	0	0.4	0	0	0
80	***70***	***2.8***	***99.6***	***100***	***100***	***98.8***	***99.8***	***100***	***96.4***	***98.8***	***100***	***90.2***	***95***	***98.4***	***75.4***	***83***	***90***	***43.8***	***55.6***	***66.2***	***8.19***	***19.9***	***32.2***	***0***	***1.6***	***6.8***	***0***	***0***	***0.2***	***0***	***0***	***0***
90	70	2.8	99.2	99.8	100	97.8	99.4	100	94	97.4	99.4	84.4	90.8	95.6	64	73.6	81.8	29.2	42.8	54.8	3	12.2	23.6	0	0.6	4.2	0	0	0	0	0	0
100	70	2.8	98.6	99.8	100	96.2	98.8	100	90	95.2	98.4	77.4	85.2	91.4	51.4	63.2	73.4	16.8	31.6	44.8	1	7	17.2	0	0.2	2.4	0	0	0	0	0	0
110	70	2.8	97.8	99.4	100	94.4	97.6	99.4	85.8	92	96.6	68.8	78.2	86.2	39.4	53	65.2	9.2	22.7	37	0.39	4.1	12.6	0	0	1.6	0	0	0	0	0	0
120	70	2.8	96.6	98.8	100	92	96.2	98.8	81	87.6	94	59.6	71.2	81	28.4	44.1	58.2	5.2	16.4	30.8	0	2.4	9.6	0	0	1	0	0	0	0	0	0
130	70	2.8	95	98	99.8	88.6	94	98	74.2	83.4	91.8	50.4	63.6	76.8	19.4	36	52	2.6	11.8	25.8	0	1.4	7.2	0	0	0.6	0	0	0	0	0	0
140	70	2.8	93	97.2	99.6	85	91.8	97.6	67.8	78.8	90.4	41	56.8	74.2	14	29.8	49.2	1.4	8.8	23	0	0.8	6.2	0	0	0.6	0	0	0	0	0	0
150	70	2.8	90.6	96	99.4	80.2	89.4	97.2	60	74.4	89.4	32.8	51	73.4	9.99	24.5	46.6	0.8	6.4	20.6	0	0.6	5	0	0	0.4	0	0	0	0	0	0
≥154	70	2.8	90	95.4	99.4	78.2	88.2	97.4	57.4	72	89.6	30.8	48.8	73.6	8.79	23.2	47	0.79	6	20.6	0	0.4	4.6	0	0	0.4	0	0	0	0	0	0
80.8	**40**	2.8	99.2	99.8	100	97.6	99.4	100	93.4	97.2	99.4	84	90.6	95.6	63.4	73.6	82.2	28.6	43	54.8	3.4	12.6	24.2	0	0.8	4.8	0	0	0.2	0	0	0
80.8	**50**	2.8	99.2	100	100	98	99.6	100	94.6	97.8	99.6	86.2	92	97	67.2	76.8	85	33.8	47	58.2	4.8	14.8	26.4	0	1	5.2	0	0	0.2	0	0	0
80.8	**60**	2.8	99.4	100	100	98.4	99.6	100	95.4	98.4	99.8	88.2	93.6	97.6	71.4	79.8	87	37.8	51	61.8	6.2	17	29	0	1.2	5.6	0	0	0.2	0	0	0
80.8	***70***	***2.8***	***99.6***	***100***	***100***	***98.8***	***99.8***	***100***	***96.2***	***98.8***	***99.8***	***89.8***	***94.6***	***98.2***	***74.6***	***82.2***	***89.2***	***42.6***	***54.4***	***64.6***	***7.59***	***19.2***	***31.4***	***0***	***1.6***	***6.6***	***0***	***0***	***0.2***	***0***	***0***	***0***
80.8	**80**	2.8	99.6	100	100	98.8	99.8	100	96.6	99	100	91	95.6	98.6	77.4	84.6	90.8	46.6	57.8	67.6	9.39	21.3	33.6	0	1.8	7	0	0	0.2	0	0	0
80.8	**90**	2.8	99.6	100	100	99.2	99.8	100	97.4	99.2	100	92.2	96.4	99	79.4	86.4	92.4	50.6	61.4	71	11.4	23.8	36	0	2	7.4	0	0	0.2	0	0	0
80.8	**100**	2.8	99.6	100	100	99.2	100	100	97.6	99.4	100	92.8	97	99.2	81.2	88	94	53.8	64	73.8	13.2	26.2	38.6	0	2.2	8.4	0	0	0.2	0	0	0
80.8	**110**	2.8	99.8	100	100	99.4	100	100	97.8	99.5	100	94	97.6	99.4	83	89.6	94.6	56.2	67.2	76.4	15.4	28.3	40.8	0.2	2.6	9	0	0	0.2	0	0	0
80.8	**120**	2.8	99.8	100	100	99.4	100	100	98.2	99.6	100	94.6	98	99.6	84.2	91	95.6	59.4	69.8	78.8	17.2	30.6	43.4	0.2	2.8	9.6	0	0	0.2	0	0	0
80.8	**130**	2.8	99.8	100	100	99.4	100	100	98.4	99.6	100	95	98.2	99.8	85.8	92	96.8	61.8	72	80.8	18.6	33	45.6	0.2	3.2	10	0	0	0.2	0	0	0
80.8	**140**	2.8	99.8	100	100	99.6	100	100	98.4	99.8	100	95.6	98.6	99.8	87	93	97.2	64	74.2	83.4	21	35.2	48.6	0.2	3.4	10.6	0	0	0.2	0	0	0
80.8	**150**	2.8	99.8	100	100	99.6	100	100	98.8	99.8	100	95.8	98.6	99.8	87.6	93.8	97.8	66	76	84.8	22	36.8	50.8	0.2	3.4	11	0	0	0	0	0	0
80.8	**160**	2.8	99.8	100	100	99.6	100	100	98.8	99.8	100	96.4	99	100	88.8	94.4	98.2	67.6	77.8	86.6	24	39	52.6	0.39	3.8	11.4	0	0	0	0	0	0
80.8	70	**1**	100	100	100	99.6	100	100	98.8	99.8	100	96	98.8	100	86.4	93.6	98	60	73	83.2	15.8	31.4	44	0	2.4	8.61	0	0	0	0	0	0
80.8	70	**1.2**	99.8	100	100	99.6	100	100	98.8	99.8	100	95.4	98.6	100	85.4	92.8	97.8	59.6	71.6	81.8	15.2	30	42.8	0	2.2	8	0	0	0.2	0	0	0
80.8	70	**1.4**	99.8	100	100	99.6	100	100	98.4	99.8	100	95	98.4	99.8	84.4	92.1	97.4	57.8	70	80.2	14.4	28.6	41.8	0	2.2	8.4	0	0	0	0	0	0
80.8	70	**1.6**	99.8	100	100	99.6	100	100	98.4	99.8	100	94.2	98.2	99.8	83.2	90.8	96.4	56	68.2	77.6	13.4	27.2	40.4	0	2.2	8.2	0	0	0.2	0	0	0
80.8	70	**1.8**	99.8	100	100	99.4	100	100	98	99.6	100	94	97.6	99.6	82	89.6	95.6	53.8	66.2	75.6	12.6	26.2	38.4	0	2.1	7.6	0	0	0.2	0	0	0
80.8	70	**2**	99.8	100	100	99.4	100	100	97.8	99.4	100	93.2	97.4	99.6	81.2	88.8	94.6	52.6	63.8	73.6	11.4	24.6	36.8	0	2	7.41	0	0	0.2	0	0	0
80.8	70	**2.2**	99.8	100	100	99.2	100	100	97.6	99.4	100	92.6	97	99.2	79.6	87.6	93.4	50	61.8	71.4	11.2	23.6	36.2	0	1.8	7.4	0	0	0.2	0	0	0
80.8	70	**2.4**	99.6	100	100	99	99.8	100	97.2	99.2	100	92	96.2	99	78.4	85.8	92.2	48.2	59.6	69.6	9.8	22	35	0	1.8	7.2	0	0	0.2	0	0	0
80.8	70	**2.6**	99.6	100	100	99	99.8	100	96.6	99	100	90.8	95.6	98.6	76	84.2	90.6	45.8	57	66.4	9	20.4	33.2	0	1.6	6.6	0	0	0.2	0	0	0
80.8	***70***	***2.8***	***99.4***	***100***	***100***	***98.8***	***99.8***	***100***	***96.2***	***98.6***	***99.8***	***89.6***	***94.6***	***98***	***74.2***	***82.2***	***89.2***	***42.4***	***54.6***	***64.4***	***7.79***	***19***	***31.2***	***0***	***1.6***	***6.8***	***0***	***0***	***0.2***	***0***	***0***	***0***
80.8	70	**3**	99.2	100	100	98.4	99.6	100	95.4	98.2	99.8	88.2	93.6	97.6	71.6	80	87.2	38.8	51.8	62.6	6.8	17.8	29.8	0	1.4	6.4	0	0	0.2	0	0	0
80.8	70	**3.2**	99.2	100	100	98	99.6	100	94.4	97.8	99.6	86	92.4	97	68.4	77.5	86.2	35.4	48.6	60.8	5.79	16.2	28.8	0	1.2	5.8	0	0	0.2	0	0	0
80.8	70	**3.4**	98.8	99.8	100	97.4	99.4	100	93	97.2	99.4	84	90.8	96.2	64.2	74.8	84.6	31.4	45.8	59.2	4.6	14.8	27.2	0	1.2	5.6	0	0	0.2	0	0	0
80.8	70	**3.6**	98.6	99.8	100	96.4	99	100	91.4	96.4	99.2	80.2	89	95.6	59.2	72	83.2	27	43	57	3.8	13.2	26.2	0	1	5.2	0	0	0.2	0	0	0
80.8	70	**3.8**	98	99.6	100	95.2	98.8	100	88.6	95.4	99	75.8	87	94.8	53.2	68.8	82	22.2	39.8	55.8	3	12	25	0	0.8	4.8	0	0	0.2	0	0	0

Italic values: Highlight rows based on comparable covariate values of CLCR$_{CG}$, body weight and serum albumin concentration.
Colour coding: *Green*: PTA≥90%, *Yellow*: PTA 80-<90%, *Orange*: PTA>50-<80%, *Red*: PTA≤50%; *Grey shaded values*: Extrapolated covariate range not covered by the study population or CLCR$_{CG}$ ≥154 mL/min (=inflection point of CLCR$_{CG}$-CL relationship).
Abbreviations: *CL*: Clearance; *CLCR$_{CG}$*: Creatinine clearance estimated according to Cockcroft and Gault [2]; *MIC*: Minimum inhibitory concentration; $P_{0.05}$: 5th percentile; $P_{0.5}$: 50th percentile = median; $P_{0.95}$: 95th percentile, *q8h*: Every 8 hours; $T_{>MIC}$: Time period that total drug concentration exceeds the MIC.

Table S22: (Project IV) Cumulative fraction of response (98%$T_{>MIC}$) for the first day of standard meropenem treatment (1000 mg, 30-min i.v. infusion, q8h) (modified from [243]). CFR is given for varied values of one covariate and for selected MIC values and is presented as the median ($P_{0.5}$), 5th ($P_{0.05}$) and 95th percentile ($P_{0.95}$) of the 1000 PTA values derived from the 1000 Monte Carlo simulations considering PK parameter uncertainty.

$CLCR_{CG}$ [mL/min]	Body weight [kg]	Albu-min [g/dL]	Cumulative fraction of response %																							
			Full MIC distribution[1]														MIC distribution of isolates belonging to the S category[1]						MIC distribution of isolates belonging to the I category[1]			
			Escherichia coli			*Klebsiella pneumonia*			*Enterobacter cloacae*			*Pseudomonas aeruginosa*			*Acinetobacter* spp.			*Pseudomonas aeruginosa*			*Acinetobacter* spp.			*Pseudomonas aeruginosa*			*Acinetobacter* spp.		
			$P_{0.05}$	$P_{0.5}$	$P_{0.95}$	$P_{0.05}$	$P_{0.5}$	$P_{0.95}$	$P_{0.05}$	$P_{0.5}$	$P_{0.95}$	$P_{0.05}$	$P_{0.5}$	$P_{0.95}$	$P_{0.05}$	$P_{0.5}$	$P_{0.95}$	$P_{0.05}$	$P_{0.5}$	$P_{0.95}$	$P_{0.05}$	$P_{0.5}$	$P_{0.95}$	$P_{0.05}$	$P_{0.5}$	$P_{0.95}$	$P_{0.05}$	$P_{0.5}$	$P_{0.95}$
10	70	2.8	100	100	100	99.8	99.9	100	99.8	99.9	100	91.2	95.2	98	88.2	94	99.1	100	100	100	99.9	100	100	88.2	99.1	100	89.5	99.2	100
20	70	2.8	100	100	100	99.8	99.8	99.9	99.7	99.8	99.9	88.8	92.1	94.6	85.4	89.1	92.8	99.7	100	100	99.6	100	100	76.1	93.1	99.4	78.3	94	99.5
30	70	2.8	100	100	100	99.7	99.8	99.8	99.6	99.7	99.8	86.4	89.4	91.4	83	86	88.2	99.3	99.9	100	98.8	99.9	100	61.7	79.7	91	64.7	81.9	92.3
40	70	2.8	100	100	100	99.6	99.7	99.8	99.5	99.6	99.7	83.7	86.6	88.7	80.4	83.5	85.5	98.2	99.6	100	97.1	99.2	99.9	47	61.7	73.7	50.4	65	76.7
50	70	2.8	100	100	100	99.5	99.6	99.7	99.4	99.5	99.6	80.5	83.7	86	77	80.6	83.1	96.5	98.6	99.6	94.5	97.7	99.3	32	43.9	55.3	35.2	47.3	58.7
60	70	2.8	99.9	100	100	99.2	99.5	99.6	99.1	99.4	99.5	76.9	80.4	83.1	72.9	76.9	80	93.8	96.8	98.6	90.8	94.8	97.5	19.7	29.4	39.5	22.1	32.2	42.3
70	70	2.8	99.9	99.9	100	99.1	99.4	99.5	98.8	99.3	99.4	72.9	76.9	80.2	68	72.5	76.4	90.3	94	96.6	85.7	90.5	94.2	10.6	18.9	28.5	12	20.9	30.8
80	***70***	***2.8***	***99.8***	***99.9***	***100***	***98.8***	***99.3***	***99.4***	***98.3***	***99***	***99.3***	***68.2***	***72.9***	***77***	***62.1***	***67.5***	***72.2***	***85.3***	***90.1***	***93.8***	***79***	***85***	***89.9***	***4.4***	***11.4***	***20.5***	***4.99***	***12.8***	***22.3***
90	70	2.8	99.6	99.9	99.9	98.2	99	99.3	97.6	98.6	99.1	63	68.5	73.3	55.8	62.2	67.6	79.2	85.3	90.1	71.3	78.7	84.8	1.61	6.83	14.6	1.83	7.67	16
100	70	2.8	99.4	99.9	99.9	97.5	98.8	99.1	96.6	98.2	98.8	57.4	63.9	69.5	49.4	56.7	63.1	72.3	79.9	86	63.2	72.2	79.5	0.537	3.85	10.4	0.61	4.35	11.4
110	70	2.8	99.2	99.7	99.9	96.6	98.2	99	95.5	97.4	98.5	52.1	59.1	65.7	43.6	51.4	58.8	65.6	74.2	81.6	55.9	65.6	74.4	0.21	2.2	7.51	0.238	2.5	8.31
120	70	2.8	98.8	99.6	99.8	95.4	97.6	98.8	94	96.5	98.1	46.9	54.6	62.2	38.4	46.7	55	59.1	68.7	77.5	49.2	59.6	69.7	0	1.29	5.62	0	1.46	6.24
130	70	2.8	98.2	99.3	99.8	93.9	96.7	98.6	92.1	95.4	97.7	41.6	50.3	59.2	33.5	42.3	51.7	52.5	63.2	74	42.9	54	65.7	0	0.752	4.15	0	0.853	4.62
140	70	2.8	97.5	99.1	99.8	92.1	95.9	98.3	90	94.3	97.4	37.1	46.5	57.6	29.5	38.6	50	46.7	58.5	72.1	37.7	49.4	63.6	0	0.43	3.61	0	0.488	4.01
150	70	2.8	96.7	98.8	99.8	89.9	94.8	98.2	87.5	93	97.1	32.6	43.1	56.5	25.7	35.3	48.7	41.1	54.2	70.8	32.9	45.2	62.1	0	0.322	2.87	0	0.366	3.2
≥154	70	2.8	96.2	98.7	99.8	89.2	94.3	98.2	86.7	92.3	97.2	31.3	41.8	56.7	24.6	34.2	48.9	39.4	52.6	71	31.5	43.8	62.2	0	0.215	2.66	0	0.244	2.96
80.8	**40**	2.8	99.6	99.9	99.9	98.2	99	99.3	97.5	98.6	99.1	62.7	68.5	73.4	70.8	78.7	84.9	78.7	85.2	90.1	55.5	62.2	67.8	1.83	7.14	15.2	2.07	7.99	16.6
80.8	**50**	2.8	99.7	99.9	99.9	98.3	99.1	99.3	97.8	98.8	99.1	64.5	69.9	74.6	73.6	80.8	86.6	80.9	86.8	91.5	57.7	63.9	69.3	2.58	8.41	16.6	2.93	9.41	18.1
80.8	**60**	2.8	99.7	99.9	99.9	98.5	99.2	99.4	98	98.9	99.2	66.3	71.4	75.6	76.1	82.8	88	83	88.4	92.5	59.7	65.6	70.5	3.33	9.69	18.2	3.78	10.8	19.9
80.8	***70***	***2.8***	***99.8***	***99.9***	***99.9***	***98.7***	***99.2***	***99.4***	***98.3***	***99***	***99.2***	***67.8***	***72.5***	***76.5***	***78.4***	***84.4***	***89.3***	***84.8***	***89.7***	***93.4***	***61.6***	***67***	***71.7***	***4.08***	***11.1***	***19.9***	***4.63***	***12.3***	***21.7***
80.8	**80**	2.8	99.8	99.9	100	98.8	99.3	99.4	98.4	99.1	99.3	69	73.6	77.4	80.3	86	90.4	86.2	90.8	94.2	63.2	68.4	72.7	5.04	12.3	21.3	5.72	13.7	23.2
80.8	**90**	2.8	99.8	99.9	100	98.8	99.3	99.4	98.5	99.1	99.3	70.3	74.5	78.2	82.1	87.4	91.6	87.6	91.8	95	64.7	69.6	73.8	6.12	13.7	22.8	6.94	15.3	24.8
80.8	**100**	2.8	99.8	99.9	100	98.9	99.4	99.5	98.6	99.2	99.4	71.1	75.4	78.9	83.4	88.5	92.7	88.5	92.7	95.7	65.8	70.6	74.8	7.09	15.1	24.6	8.05	16.8	26.8
80.8	**110**	2.8	99.9	99.9	100	99.1	99.4	99.5	98.8	99.2	99.4	72.1	76.2	79.5	84.6	89.8	93.4	89.6	93.5	96.1	66.9	71.7	75.5	8.37	16.4	26.1	9.47	18.3	28.4
80.8	**120**	2.8	99.9	99.9	100	99.1	99.4	99.5	98.8	99.3	99.4	72.9	76.9	80.1	85.8	90.8	94.2	90.4	94.2	96.6	68	72.6	76.3	9.33	17.7	27.8	10.6	19.7	30.2
80.8	**130**	2.8	99.9	100	100	99.1	99.4	99.5	98.9	99.3	99.4	73.6	77.5	80.7	86.8	91.5	95	91.1	94.7	97.1	68.8	73.4	77.1	10.1	19.2	29.1	11.4	21.4	31.7
80.8	**140**	2.8	99.9	100	100	99.2	99.4	99.5	98.9	99.3	99.5	74.2	78.1	81.2	87.8	92.4	95.7	91.8	95.3	97.5	69.7	74.2	77.8	11.4	20.5	31	12.9	22.8	33.8
80.8	**150**	2.8	99.9	100	100	99.2	99.5	99.6	99	99.3	99.5	74.7	78.5	81.6	88.5	92.9	96.1	92.3	95.7	97.8	70.3	74.7	78.2	11.9	21.3	32.4	13.5	23.8	35.3
80.8	**160**	2.8	99.9	100	100	99.2	99.5	99.6	99	99.4	99.5	75.3	79	82	89.2	93.6	96.6	92.9	96.1	98.1	71	75.3	78.8	13.1	22.7	33.5	14.8	25.3	36.5
80.8	70	1	99.9	100	100	99.3	99.4	99.5	99	99.3	99.5	73.6	77.9	80.9	86.9	92.3	95.8	91.4	95.3	97.7	68.7	73.9	77.6	8.49	18	27.6	9.63	20.1	30.2
80.8	70	1.2	99.9	100	100	99.1	99.4	99.5	98.9	99.3	99.4	73.2	77.5	80.7	86.5	91.7	95.5	91	95	97.5	68.3	73.4	77.2	8.17	17.1	26.7	9.27	19.1	29.2
80.8	70	1.4	99.9	100	100	99.1	99.4	99.5	98.9	99.3	99.4	72.7	77.1	80.4	85.7	91.2	95	90.4	94.6	97.2	67.7	72.8	76.8	7.74	16.4	26.4	8.78	18.3	28.8
80.8	70	1.6	99.9	99.9	100	99.1	99.4	99.5	98.8	99.3	99.4	72.1	76.6	79.9	84.8	90.4	94.2	89.8	94.1	96.7	67	72.2	76.1	7.19	15.6	25.5	8.16	17.4	27.8
80.8	***70***	***1.8***	***99.9***	***99.9***	***100***	***99.1***	***99.4***	***99.5***	***98.8***	***99.2***	***99.4***	***71.6***	***76***	***79.4***	***83.9***	***89.6***	***93.5***	***89.1***	***93.4***	***96.3***	***66.2***	***71.4***	***75.4***	***6.77***	***15***	***24.1***	***7.68***	***16.8***	***26.4***
80.8	70	2	99.9	99.9	100	99	99.4	99.5	98.7	99.2	99.4	71	75.5	78.9	83.2	88.8	92.9	88.6	92.9	95.9	65.6	70.7	74.8	6.12	14.1	23.2	6.95	15.8	25.3
80.8	70	2.2	99.8	99.9	100	99	99.3	99.5	98.7	99.2	99.3	70.4	74.9	78.4	82.1	88	92	87.8	92.3	95.3	64.7	70	74.1	6.02	13.5	22.9	6.83	15.1	25
80.8	70	2.4	99.8	99.9	100	98.8	99.3	99.4	98.5	99.1	99.3	69.7	74.1	77.9	81.2	86.8	91.3	87	91.5	94.8	63.9	69.1	73.5	5.27	12.7	22.1	5.97	14.1	24.1
80.8	70	2.6	99.8	99.9	100	98.8	99.3	99.4	98.4	99	99.3	68.7	73.4	77.2	79.7	85.7	90.1	85.8	90.7	94	62.8	68.1	72.5	4.84	11.7	20.9	5.49	13.1	22.8
80.8	70	2.8	99.8	99.9	99.9	98.6	99.2	99.4	98.2	99	99.2	67.7	72.5	76.5	78.2	84.4	89.2	84.7	89.6	93.3	61.5	67	71.6	4.19	10.9	19.9	4.75	12.2	21.7
80.8	70	3	99.8	99.9	99.9	98.4	99.2	99.4	97.9	98.9	99.2	66.4	71.5	75.8	76.3	83	88.2	83.1	88.5	92.6	60	65.8	70.8	3.65	10.2	19	4.15	11.4	20.7
80.8	70	3.2	99.6	99.9	99.9	98.3	99.2	99.3	97.7	98.8	99.2	64.9	70.4	75.2	74.1	81.4	87.4	81.3	87.3	92	58.2	64.5	70.1	3.11	9.26	18.2	3.53	10.3	19.8
80.8	70	3.4	99.6	99.9	99.9	97.9	99	99.3	97.3	98.6	99.1	63	69.1	74.5	71.5	79.6	86.5	79	85.8	91.3	56.1	63	69.3	2.47	8.51	17.2	2.8	9.49	18.8
80.8	70	3.6	99.4	99.9	99.9	97.6	98.9	99.3	96.9	98.4	99.1	60.6	67.8	73.9	68.1	77.8	85.5	76	84.2	90.5	53.4	61.5	68.4	2.04	7.55	16.5	2.32	8.44	18
80.8	70	3.8	99.2	99.9	99.9	97	98.7	99.3	96.1	98.2	99	57.6	66.3	73.3	64.1	75.7	84.8	72.3	82.5	89.9	50.2	59.8	67.8	1.61	6.82	15.7	1.83	7.63	17.1

[1]According to EUCAST [390].

Italic values: Highlight rows based on comparable covariate values of $CLCR_{CG}$, body weight and serum albumin concentration.
Colour coding: *Green*: CFR≥90%, *Yellow*: CFR 80-<90%, *Orange*: CFR>50-<80%, *Red*: CFR≤50%; *Grey shaded values*: Extrapolated covariate range not covered by the study population or $CLCR_{CG}$ ≥154 mL/min (=inflection point of $CLCR_{CG}$-CL relationship).
Abbreviations: *CL*: Clearance; *$CLCR_{CG}$*: Creatinine clearance estimated according to Cockcroft and Gault [2]; *I category*: Category 'susceptible at increased exposure' [4]; *MIC*: Minimum inhibitory concentration; *$P_{0.05}$*: 5th percentile; *$P_{0.5}$*: 50th percentile = median; *$P_{0.95}$:* 95th percentile, *q8h*: Every 8 hours; *S category*: Category 'susceptible at normal dosing' [4]; *$T_{>MIC}$:* Time period that total drug concentration exceeds the MIC.

Table S23: (Project IV): Probability of target (98%$T_{>MIC}$) attainment (PTA, %) for different short-term infusion dosing regimens of meropenem for the first day of treatment (modified from [243]). PTA is given for varied values of creatinine clearance and for selected MIC values and is presented as the median ($P_{0.5}$), 5th ($P_{0.05}$) and 95th percentile ($P_{0.95}$) of the 1000 PTA values derived from the 1000 Monte Carlo simulations considering PK parameter uncertainty.

Dosing regimen	CLCR$_{CG}$[1] [mL/min]	MIC [mg/L]																	
		0.004			0.008			0.015			0.03			0.06			0.12		
		$P_{0.05}$	$P_{0.5}$	$P_{0.95}$	$P_{0.05}$	$P_{0.5}$	$P_{0.95}$	$P_{0.05}$	$P_{0.5}$	$P_{0.95}$	$P_{0.05}$	$P_{0.5}$	$P_{0.95}$	$P_{0.05}$	$P_{0.5}$	$P_{0.95}$	$P_{0.05}$	$P_{0.5}$	$P_{0.95}$
SI2$_{12}$ (1000 mg, 30-min i.v. infusion, q12h)	10	100	100	100	100	100	100	100	100	100	100	100	100	100	100	100	100	100	100
	20	100	100	100	100	100	100	100	100	100	100	100	100	100	100	100	99.8	100	100
	30	100	100	100	100	100	100	100	100	100	100	100	100	99.8	100	100	99.4	100	100
	40	100	100	100	100	100	100	99.8	100	100	99.8	100	100	99.4	100	100	98.4	99.8	100
	50	100	100	100	99.8	100	100	99.8	100	100	99.4	100	100	98.6	99.8	100	96.6	99.2	100
	60	99.8	100	100	99.6	100	100	99.4	100	100	98.6	99.8	100	97	99.2	100	93.6	97.6	99.6
	70	99.6	100	100	99.4	100	100	98.6	99.8	100	97.2	99.2	100	94.4	97.8	99.6	89	94.2	98
	80	99.4	100	100	98.8	99.8	100	97.6	99.4	100	95.2	98.2	99.6	90.8	95.4	98.6	82.8	89.2	95
	90	98.8	99.8	100	97.8	99.4	100	96	98.6	99.8	92.4	96.4	99	85.8	92	96.4	74.6	82.9	89.8
	100	98.2	99.6	100	96.4	98.8	100	93.8	97.2	99.4	88.6	93.8	97.6	79.6	86.8	93	64.8	74.8	83.4
	110	97	99	100	94.4	97.6	99.6	90.4	95.2	98.6	83.6	90	95.6	71.6	80.8	89	54	66	76.8
	120	95.6	98.4	99.8	92.2	96.2	99	87.2	92.6	97.4	77.6	85.6	93.4	63.2	74.2	84.6	43.8	57.9	70.4
	130	93.8	97.4	99.6	89	94.4	98.6	82.2	89.6	96.2	71	80.8	90.6	54.8	67.4	80.4	34.4	50	65.4
	140	91.6	96	99.4	86	92.2	98	77.4	86.3	95.2	64.2	76	89	46.6	61.4	77.8	26.8	43.4	62
	150	88.6	94.8	99.2	81.2	89.8	97.6	71.2	82.8	94.6	56.6	71.6	88.4	39	55.8	77	20.8	37.8	60.6
	≥154	88	94.2	99.2	80.4	88.8	97.6	70.2	81.6	94.4	54	69.8	88.2	35.6	53.8	77.2	18.8	36.1	60.2
SI3$_{8}$= standard dosing regimen (1000 mg, 30-min i.v. infusion, q8h)	10	100	100	100	100	100	100	100	100	100	100	100	100	100	100	100	100	100	100
	20	100	100	100	100	100	100	100	100	100	100	100	100	100	100	100	100	100	100
	30	100	100	100	100	100	100	100	100	100	100	100	100	100	100	100	100	100	100
	40	100	100	100	100	100	100	100	100	100	100	100	100	100	100	100	100	100	100
	50	100	100	100	100	100	100	100	100	100	100	100	100	100	100	100	99.8	100	100
	60	100	100	100	100	100	100	100	100	100	100	100	100	99.8	100	100	99.6	100	100
	70	100	100	100	100	100	100	100	100	100	100	100	100	99.8	100	100	99.4	100	100
	80	100	100	100	100	100	100	100	100	100	99.8	100	100	99.6	100	100	98.8	99.8	100
	90	100	100	100	100	100	100	99.8	100	100	99.6	100	100	99.2	99.8	100	97.8	99.4	100
	100	100	100	100	99.8	100	100	99.8	100	100	99.4	100	100	98.6	99.8	100	96.2	98.8	100
	110	100	100	100	99.8	100	100	99.6	100	100	99.2	99.8	100	97.8	99.4	100	94.4	97.6	99.4
	120	99.8	100	100	99.8	100	100	99.4	100	100	98.6	99.6	100	96.6	98.8	100	92	96.2	98.8
	130	99.8	100	100	99.6	100	100	99.2	99.8	100	97.8	99.4	100	95	98	99.8	88.6	94	98
	140	99.8	100	100	99.4	100	100	98.6	99.8	100	97	99	100	93	97.2	99.6	85	91.8	97.6
	150	99.6	100	100	99.2	100	100	98.2	99.6	100	95.8	98.6	100	90.6	96	99.4	80.2	89.4	97.2
	≥154	99.6	100	100	99	99.8	100	97.8	99.6	100	95.2	98.4	100	90	95.4	99.4	78.2	88.2	97.4
SI6$_{8}$ (2000 mg, 30-min i.v. infusion, q8h)	10	100	100	100	100	100	100	100	100	100	100	100	100	100	100	100	100	100	100
	20	100	100	100	100	100	100	100	100	100	100	100	100	100	100	100	100	100	100
	30	100	100	100	100	100	100	100	100	100	100	100	100	100	100	100	100	100	100
	40	100	100	100	100	100	100	100	100	100	100	100	100	100	100	100	100	100	100
	50	100	100	100	100	100	100	100	100	100	100	100	100	100	100	100	100	100	100
	60	100	100	100	100	100	100	100	100	100	100	100	100	100	100	100	99.8	100	100
	70	100	100	100	100	100	100	100	100	100	100	100	100	99.8	100	100	99.8	100	100
	80	100	100	100	100	100	100	100	100	100	100	100	100	99.8	100	100	99.6	100	100
	90	100	100	100	100	100	100	100	100	100	99.8	100	100	99.6	100	100	99.2	99.8	100
	100	100	100	100	100	100	100	99.8	100	100	99.8	100	100	99.4	100	100	98.6	99.8	100
	110	100	100	100	100	100	100	99.8	100	100	99.6	100	100	99	99.8	100	97.8	99.4	100
	120	100	100	100	99.8	100	100	99.8	100	100	99.4	100	100	98.4	99.6	100	96.6	98.8	99.8
	130	100	100	100	99.8	100	100	99.6	100	100	99.2	99.8	100	98	99.4	100	95.2	98	99.6
	140	99.8	100	100	99.8	100	100	99.4	100	100	98.6	99.8	100	97	99.2	100	93.2	97	99.6
	150	99.8	100	100	99.6	100	100	99.2	100	100	98.2	99.6	100	95.4	98.8	100	90.4	96	99.4
	≥154	99.8	100	100	99.6	100	100	99	100	100	97.8	99.6	100	95.2	98.6	100	89.6	95.6	99.4

Dosing regimen	CLCR$_{CG}$[1] [mL/min]	MIC [mg/L]																							
		0.25			0.5			1			2			4			8			16			32		
		$P_{0.05}$	$P_{0.5}$	$P_{0.95}$	$P_{0.05}$	$P_{0.5}$	$P_{0.95}$	$P_{0.05}$	$P_{0.5}$	$P_{0.95}$	$P_{0.05}$	$P_{0.5}$	$P_{0.95}$	$P_{0.05}$	$P_{0.5}$	$P_{0.95}$	$P_{0.05}$	$P_{0.5}$	$P_{0.95}$	$P_{0.05}$	$P_{0.5}$	$P_{0.95}$	$P_{0.05}$	$P_{0.5}$	$P_{0.95}$
SI2$_{12}$ (1000 mg, 30-min i.v. infusion, q12h)	10	99.8	100	100	99.6	100	100	98	100	100	92	99.8	100	73.4	96.8	100	30.6	74.3	98.6	0.79	9.9	47.2	0	0	0
	20	99.4	100	100	98	100	100	93.6	99.4	100	81.6	96.4	100	52.6	81	97	12.6	36.6	66.2	0	1	6.2	0	0	0
	30	98.2	99.8	100	95	99.2	100	86	96.2	99.6	67.4	85.4	96.2	34	55.4	75.4	3.6	13.2	26	0	0	1	0	0	0
	40	96	99.2	100	90	96.6	99.6	76.2	88.2	96.4	50.6	67.3	80.6	16.6	31	43.8	0.6	3.8	10.4	0	0	0.2	0	0	0
	50	91.8	97	99.4	82.2	90.8	96.6	63.2	75.2	85.4	33.2	47	58.6	6.2	15	25.4	0	1	4.4	0	0	0	0	0	0
	60	86.6	92.6	97.2	72.2	81.2	89.6	48.2	59.6	70.2	18.2	29.6	40.8	1.6	7	15	0	0.2	2	0	0	0	0	0	0
	70	78.2	85.6	92.4	59.4	69.2	78.4	31.8	43.8	54.8	7.8	17.8	28.8	0.2	3	8.8	0	0	1	0	0	0	0	0	0
	80	68.2	76.2	84.4	44.6	56	65.6	18.4	30.8	42.6	2.99	10.2	20.2	0	1.2	5.4	0	0	0.6	0	0	0	0	0	0
	90	54.8	66.3	75.6	30.8	43.7	55.2	9.4	20.8	33.6	0.8	5.4	14	0	0.4	3.2	0	0	0.2	0	0	0	0	0	0
	100	42	55.4	66.6	19.4	33	45.8	4.4	13.4	25	0.2	3	9.8	0	0.2	2.01	0	0	0.2	0	0	0	0	0	0
	110	30.4	45.2	58.2	11	24.3	37.6	1.8	8.6	19.6	0	1.6	6.8	0	0	1.2	0	0	0	0	0	0	0	0	0
	120	22	36.6	51.6	6.4	18	32.2	0.8	5.8	15.2	0	0.8	5	0	0	0.8	0	0	0	0	0	0	0	0	0
	130	14.8	29.4	46.6	3.6	13	27.2	0.4	3.8	12	0	0.4	3.6	0	0	0.41	0	0	0	0	0	0	0	0	0
	140	10.6	24.2	42.8	2.2	10	23.8	0.2	2.6	10.2	0	0.2	2.8	0	0	0.4	0	0	0	0	0	0	0	0	0
	150	6.8	19.8	40.4	1.4	7.4	21.4	0	1.6	8.6	0	0.2	2.4	0	0	0.2	0	0	0	0	0	0	0	0	0
	≥154	6.39	18.4	39.6	1.2	7	21.4	0	1.6	8.4	0	0.2	2.2	0	0	0.2	0	0	0	0	0	0	0	0	0
SI3$_{8}$= standard dosing regimen (1000 mg, 30-min i.v. infusion, q8h)	10	100	100	100	100	100	100	100	100	100	99.6	100	100	96.8	100	100	78.2	98	100	16	54.6	93.6	0	0	0.8
	20	100	100	100	100	100	100	99.6	100	100	98.4	100	100	90.6	99	100	59.2	86.2	98.6	4.6	19.4	44.4	0	0	0
	30	100	100	100	99.8	100	100	99	100	100	95.6	99.4	100	81.2	94.2	99.4	39	62.8	81.2	0.6	4.8	13.4	0	0	0
	40	99.8	100	100	99.4	100	100	97.6	99.6	100	90.2	97	99.6	68.8	82.6	93.2	21.6	37.4	51	0	1	4.6	0	0	0
	50	99.6	100	100	98.4	99.8	100	94.6	98.4	99.8	82.8	91.2	97.2	52.4	65.6	77	8.39	18.7	30.2	0	0.2	1.8	0	0	0
	60	98.8	99.8	100	96.8	99.2	100	90	95.6	98.8	73	81.8	89.8	34.8	47.2	57.8	2.2	8.8	18.2	0	0	0.8	0	0	0
	70	98	99.6	100	94.2	97.8	99.6	84.2	90.6	96	59.6	69.2	78.2	19.4	31.8	43.4	0.4	4	11.2	0	0	0.4	0	0	0
	80	96.4	98.8	100	90.2	95	98.4	75.4	83	90	43.8	55.6	66.2	8.19	19.9	32.2	0	1.6	6.8	0	0	0.2	0	0	0
	90	94	97.4	99.4	84.4	90.8	95.6	64	73.6	81.8	29.2	42.8	54.8	3	12.2	23.6	0	0.6	4.2	0	0	0	0	0	0
	100	90	95.2	98.4	77.4	85.2	91.4	51.4	63.2	73.4	16.8	31.6	44.8	1	7	17.2	0	0.2	2.4	0	0	0	0	0	0
	110	85.8	92	96.6	68.8	78.2	86.2	39.4	53	65.2	9.2	22.7	37	0.39	4.1	12.6	0	0	1.6	0	0	0	0	0	0
	120	81	87.6	94	59.6	71.2	81	28.4	44.1	58.2	5.2	16.4	30.8	0	2.4	9.6	0	0	1	0	0	0	0	0	0
	130	74.2	83.4	91.8	50.4	63.6	76.8	19.4	36	52	2.6	11.8	25.8	0	1.4	7.2	0	0	0.6	0	0	0	0	0	0
	140	67.8	78.8	90.4	41	56.8	74.2	14	29.8	49.2	1.4	8.8	23	0	0.8	6.2	0	0	0.6	0	0	0	0	0	0
	150	60	74.4	89.4	32.8	51	73.4	9.99	24.5	46.6	0.8	6.4	20.6	0	0.6	5	0	0	0.4	0	0	0	0	0	0
	≥154	57.4	72	89.6	30.8	48.8	73.6	8.79	23.2	47	0.79	6	20.6	0	0.4	4.6	0	0	0.4	0	0	0	0	0	0
SI6$_{8}$ (2000 mg, 30-min i.v. infusion, q8h)	10	100	100	100	100	100	100	100	100	100	100	100	100	99.6	100	100	96.8	100	100	78.4	98	100	15.4	55.3	93.2
	20	100	100	100	100	100	100	100	100	100	99.8	100	100	98.2	100	100	91	99	100	60.4	86	98.4	4.4	19.2	44.2
	30	100	100	100	100	100	100	99.8	100	100	99	100	100	95.6	99.4	100	81.2	94	99.4	39.4	62.2	81.4	0.6	4.8	13.2
	40	100	100	100	99.8	100	100	99.4	100	100	97.6	99.6	100	90.8	97	99.8	68.2	82.6	93	21.6	37.4	51.2	0	1	5
	50	99.8	100	100	99.6	100	100	98.4	99.8	100	94.8	98.4	99.8	83.2	91.2	97.2	52.6	65.6	77.2	8.59	18.6	30	0	0.2	1.8
	60	99.6	100	100	99	99.8	100	96.6	99.2	100	90.4	95.6	98.8	72.8	81.8	90	34.8	47	58	2.39	8.8	18.2	0	0	0.6
	70	99.2	100	100	98	99.6	100	94	97.6	99.6	84	90.6	95.8	58.8	69.2	77.8	18.4	31.4	43	0.4	3.8	11	0	0	0.4
	80	98.6	99.8	100	96.4	98.8	99.8	90	95	98.4	75.4	82.8	89.8	43.4	55.6	65.6	8.4	20.2	32	0	1.6	6.8	0	0	0.2
	90	97.8	99.4	100	94	97.4	99.4	84.4	90.8	95.8	63.6	73.6	81.8	29	42.6	55	3.4	12	24	0	0.6	4.2	0	0	0
	100	96.2	98.6	99.8	90.4	95	98.4	77.4	85	91.6	51.2	63.4	73.4	17	31.4	45.2	1	7	17.2	0	0.2	2.6	0	0	0
	110	94	97.4	99.4	85.8	91.8	96.6	68.8	78.4	86	39.6	53	65	8.6	22.7	37	0.4	4.2	12.8	0	0	1.6	0	0	0
	120	91.4	95.6	98.6	81	87.8	94	59.6	71	81	28.4	43.6	57.6	5	16.3	30.8	0	2.4	9.2	0	0	1	0	0	0
	130	88.6	93.6	97.8	74.8	83.1	91.2	50.2	63.6	76.6	19.6	35.8	52.2	2.8	11.6	25.8	0	1.4	6.8	0	0	0.8	0	0	0
	140	84	91.4	97.2	67.8	79.2	89.6	41	57	73	14.2	29.6	48.8	1.4	8.4	22.2	0	0.8	5.6	0	0	0.6	0	0	0
	150	79.4	88.6	96.8	60.2	74	89.4	33	50.8	73	9.79	24.4	47	0.8	6.4	21.2	0	0.6	5	0	0	0.4	0	0	0
	≥154	77.6	87.5	97	57.2	72.4	89.4	30.4	49	73.2	8.2	23	46	0.8	5.8	19.6	0	0.4	4.6	0	0	0.4	0	0	0

[1]Body weight and albumin set to median of first study day (i.e. 70 kg and 2.8 g/dL). ***Colour coding***: *Green*: PTA≥90%, *Yellow*: PTA 80-<90%, *Orange*: PTA>50-<80%, *Red*: PTA≤50%; *Grey shaded values*: Extrapolated CLCR$_{CG}$ range not covered by the study population or CLCR$_{CG}$ ≥154 mL/min (=inflection point of CLCR$_{CG}$-CL relationship).

Abbreviations: *CL*: Clearance; *CLCR$_{CG}$*: Creatinine clearance estimated according to Cockcroft and Cockcroft and Gault [2]; *MIC*: Minimum inhibitory concentration; $P_{0.05}$: 5th percentile; $P_{0.5}$: 50th percentile = median; $P_{0.95}$: 95th percentile, *q8h*: Every 8 hours; $T_{>MIC}$: Time period that total drug concentration exceeds the MIC.

Table S24: (Project IV): Probability of target (98%$T_{>MIC}$) attainment (PTA, %) for different prolonged infusion dosing regimens of meropenem for the first day of treatment (modified from [243]). PTA is given for varied values of creatinine clearance and for selected MIC values and is presented as the median ($P_{0.5}$), 5th ($P_{0.05}$) and 95th percentile ($P_{0.95}$) of the 1000 PTA values derived from the 1000 Monte Carlo simulations considering PK parameter uncertainty.

Dosing regimen	$CLCR_{CG}$[1] [mL/min]	MIC [mg/L]																																									
		0.004			0.008			0.015			0.03			0.06			0.12			0.25			0.5			1			2			4			8			16			32		
		$P_{0.05}$	$P_{0.5}$	$P_{0.95}$	$P_{0.05}$	$P_{0.5}$	$P_{0.95}$	$P_{0.05}$	$P_{0.5}$	$P_{0.95}$	$P_{0.05}$	$P_{0.5}$	$P_{0.95}$	$P_{0.05}$	$P_{0.5}$	$P_{0.95}$	$P_{0.05}$	$P_{0.5}$	$P_{0.95}$	$P_{0.05}$	$P_{0.5}$	$P_{0.95}$	$P_{0.05}$	$P_{0.5}$	$P_{0.95}$	$P_{0.05}$	$P_{0.5}$	$P_{0.95}$	$P_{0.05}$	$P_{0.5}$	$P_{0.95}$	$P_{0.05}$	$P_{0.5}$	$P_{0.95}$	$P_{0.05}$	$P_{0.5}$	$P_{0.95}$	$P_{0.05}$	$P_{0.5}$	$P_{0.95}$	$P_{0.05}$	$P_{0.5}$	$P_{0.95}$
$PI2_{12}$ (1000 mg i.v. infusion, 3-h, q12h)	10	100	100	100	100	100	100	100	100	100	100	100	100	100	100	100	100	100	100	100	100	100	99.8	100	100	99.2	100	100	96.4	100	100	83.2	98.8	100	38	79.3	96.8	0	0	0.4	0	0	0
	20	100	100	100	100	100	100	100	100	100	100	100	100	100	100	100	100	100	100	99.8	100	100	99.2	100	100	97.4	99.8	100	89.8	98.6	100	66.2	89.8	99	19.2	46.8	76.4	0	0	0	0	0	0
	30	100	100	100	100	100	100	100	100	100	100	100	100	100	100	100	99.8	100	100	99.4	100	100	98	99.8	100	93.4	98.8	100	80.2	93	98.8	47.4	69.6	86.4	6.8	19.4	35.4	0	0	0	0	0	0
	40	100	100	100	100	100	100	100	100	100	100	100	100	99.8	100	100	99.4	100	100	98.4	99.8	100	95.4	99	100	87	95	99	65.8	80.6	91.2	29	45.6	60.2	1.6	6.4	15	0	0	0	0	0	0
	50	100	100	100	100	100	100	100	100	100	99.8	100	100	99.4	100	100	98.8	99.8	100	96.4	99.2	100	91.2	96.2	99.2	77.4	87	94.4	50.6	63.8	75.2	14.2	26	37	0.2	2	6.8	0	0	0	0	0	0
	60	100	100	100	100	100	100	99.8	100	100	99.6	100	100	99	99.8	100	97.4	99.4	100	93.4	97.2	99.6	84	91.2	96.6	65.8	75.2	84.6	33.6	45.4	56.4	4.8	13.2	23.4	0	0.6	3.2	0	0	0	0	0	0
	70	100	100	100	99.8	100	100	99.6	100	100	99	99.8	100	98	99.4	100	95	98.2	99.8	88.2	94	97.8	75.8	83.4	90.6	50.8	61.6	70.8	18.4	30.4	41.8	1.4	6.6	14.8	0	0.2	1.6	0	0	0	0	0	0
	80	99.8	100	100	99.6	100	100	99.2	100	100	98.2	99.6	100	96.2	98.8	99.8	91.6	96	98.8	81.8	88.6	94.2	64	73.2	81.2	35.6	47.6	58.2	8.39	19.2	31.2	0.2	3	9.41	0	0	0.8	0	0	0	0	0	0
	90	99.6	100	100	99.2	100	100	98.6	99.8	100	97	99	100	94	97.2	99.4	87.6	92.8	97	73.6	81.6	88.6	50.8	62.2	71.6	21.4	35.4	47.6	3.4	11.8	22.6	0	1.4	6	0	0	0.4	0	0	0	0	0	0
	100	99.4	100	100	98.8	99.8	100	97.8	99.4	100	95.4	98.2	99.6	90.2	95	98.4	81.4	87.8	94	63.2	73.2	81.8	38	51.2	62.2	12.4	25.6	38.6	1.4	7	17	0	0.6	4	0	0	0.2	0	0	0	0	0	0
	110	99	99.8	100	98.2	99.6	100	96.4	98.8	99.8	93	96.6	99.2	86.2	91.9	96.6	74	82	89.6	52.4	64.4	74.6	25.8	40.6	54.2	6.6	18	31.4	0.4	4.2	12.4	0	0.2	2.4	0	0	0.2	0	0	0	0	0	0
	120	98.8	99.8	100	97.2	99.2	100	94.8	97.8	99.6	89.8	94.6	98.4	81.6	88	94.6	65.6	75.8	85.6	41.6	55.6	68.2	18	32.4	47.4	3.6	12.4	25.4	0	2.4	9.2	0	0.2	1.8	0	0	0	0	0	0	0	0	0
	130	98	99.4	100	96	98.6	99.8	92.6	96.6	99.4	86.4	92.2	97.6	75.2	83.8	92.2	56.8	69.4	81.4	32.6	47.8	62.8	11.8	25.6	41.6	1.8	9	21.4	0	1.4	6.8	0	0	1.2	0	0	0	0	0	0	0	0	0
	140	97	99.2	100	94.4	98	99.8	90.2	95.4	99	81.8	89.8	96.8	68.4	79.6	90.8	49.2	63.4	79	25.4	41.1	59.4	8.19	20.4	38.2	1	6.4	18.2	0	0.8	5.6	0	0	0.8	0	0	0	0	0	0	0	0	0
	150	96	98.8	100	92.4	97	99.6	86.8	93.6	99	76.6	86.8	96.2	61.2	75	90.6	41	57.4	78.4	19.6	35.4	58.8	5.59	16.4	36.2	0.6	4.8	16.6	0	0.6	5	0	0	0.8	0	0	0	0	0	0	0	0	0
	≥154	95.6	98.6	100	91.8	96.6	99.6	85.6	93	98.8	74.2	85.6	96	58.4	73	90.4	37.4	55.8	78.6	17.2	33.8	58.2	4.6	15.2	35.2	0.4	4.2	16.2	0	0.4	4.61	0	0	0.6	0	0	0	0	0	0	0	0	0
$PI3_{8}$ (1000 mg i.v. infusion, 3-h, q8h)	10	100	100	100	100	100	100	100	100	100	100	100	100	100	100	100	100	100	100	100	100	100	100	100	100	100	100	100	100	100	100	99.2	100	100	82.8	95	99.2	0	0	0.8	0	0	0
	20	100	100	100	100	100	100	100	100	100	100	100	100	100	100	100	100	100	100	100	100	100	100	100	100	100	100	100	99.6	100	100	97	99.8	100	70	89.6	97.4	0	0	0.2	0	0	0
	30	100	100	100	100	100	100	100	100	100	100	100	100	100	100	100	100	100	100	100	100	100	100	100	100	99.8	100	100	98.8	100	100	92.4	98.6	100	53.8	74.8	89.4	0	0	0.2	0	0	0
	40	100	100	100	100	100	100	100	100	100	100	100	100	100	100	100	100	100	100	100	100	100	99.8	100	100	99.4	100	100	96.8	99.6	100	84.8	94.2	99	35.8	53.2	68	0	0	0	0	0	0
	50	100	100	100	100	100	100	100	100	100	100	100	100	100	100	100	100	100	100	100	100	100	99.8	100	100	98.8	99.8	100	94	98.2	99.8	74.4	84.8	93	19.6	32.3	44.2	0	0	0	0	0	0
	60	100	100	100	100	100	100	100	100	100	100	100	100	100	100	100	100	100	100	99.8	100	100	99.4	100	100	97.4	99.4	100	88.8	94.8	98.6	60.8	71.4	80.8	7.6	18	29	0	0	0	0	0	0
	70	100	100	100	100	100	100	100	100	100	100	100	100	100	100	100	100	100	100	99.6	100	100	98.8	99.8	100	94.8	98.2	99.8	82	88.8	94.8	44.2	56	65.6	2.2	9.2	19.2	0	0	0	0	0	0
	80	100	100	100	100	100	100	100	100	100	100	100	100	100	100	100	99.8	100	100	99.4	100	100	97.6	99.4	100	91.2	95.8	98.8	72.2	80.2	87.8	27	41.4	52.4	0.4	4.6	12.6	0	0	0	0	0	0
	90	100	100	100	100	100	100	100	100	100	100	100	100	99.8	100	100	99.8	100	100	98.8	99.8	100	95.8	98.6	99.8	85.6	92.2	96.4	59.6	69.8	79	14.8	28.8	42.6	0	2.2	8.4	0	0	0	0	0	0
	100	100	100	100	100	100	100	100	100	100	100	100	100	99.8	100	100	99.4	100	100	97.8	99.6	100	93.2	97	99.2	79.8	86.8	92.6	45.6	58.9	69.6	6.8	19.2	33.6	0	1	5.6	0	0	0	0	0	0
	110	100	100	100	100	100	100	100	100	100	99.8	100	100	99.8	100	100	99	99.8	100	96.8	99	99.8	89.8	94.8	98	71.2	80.2	87.6	33.2	48	61	3	12.8	26.6	0	0.4	3.4	0	0	0	0	0	0
	120	100	100	100	100	100	100	100	100	100	99.8	100	100	99.6	100	100	98.4	99.6	100	95.2	98	99.6	86	91.6	96.4	63	73	82.8	22.8	38.7	54.4	1.4	8.6	20.8	0	0.2	2.4	0	0	0	0	0	0
	130	100	100	100	100	100	100	100	100	100	99.8	100	100	99.2	100	100	97.8	99.4	100	93	97	99.2	80.6	88	94.2	52	65.6	78	14.6	31.2	47.6	0.4	5.6	16.8	0	0	1.6	0	0	0	0	0	0
	140	100	100	100	100	100	100	99.8	100	100	99.6	100	100	99	99.8	100	96.8	99.2	100	90.8	95.6	98.8	75.2	84.2	93.2	43.6	59.2	75.8	10.4	25.1	43.8	0.2	3.8	14	0	0	1	0	0	0	0	0	0
	150	100	100	100	100	100	100	99.8	100	100	99.6	100	100	98.6	99.8	100	95.6	98.6	100	87.4	93.6	98.8	68.4	80.1	92.4	34.8	52.8	75.2	6.79	20.6	42	0	2.8	12.8	0	0	1	0	0	0	0	0	0
	≥154	100	100	100	100	100	100	99.8	100	100	99.4	100	100	98.4	99.8	100	95	98.4	100	85.6	93	98.8	65.4	78.6	92.6	32.6	51	74.4	5.8	19.2	41.8	0	2.4	12.6	0	0	1	0	0	0	0	0	0
$PI6_{8}$ (2000 mg i.v. infusion, 3-h, q8h)	10	100	100	100	100	100	100	100	100	100	100	100	100	100	100	100	100	100	100	100	100	100	100	100	100	100	100	100	100	100	100	100	100	100	99.2	100	100	82.8	95	99	0	0	0.8
	20	100	100	100	100	100	100	100	100	100	100	100	100	100	100	100	100	100	100	100	100	100	100	100	100	100	100	100	100	100	100	99.6	100	100	97	99.8	100	71	89.4	97.6	0	0	0.2
	30	100	100	100	100	100	100	100	100	100	100	100	100	100	100	100	100	100	100	100	100	100	100	100	100	100	100	100	99.8	100	100	98.8	100	100	92	98.6	100	54	74.6	89.4	0	0	0.2
	40	100	100	100	100	100	100	100	100	100	100	100	100	100	100	100	100	100	100	100	100	100	100	100	100	100	100	100	99.4	100	100	97	99.6	100	84.2	94.2	98.8	35.6	53.4	67.8	0	0	0
	50	100	100	100	100	100	100	100	100	100	100	100	100	100	100	100	100	100	100	100	100	100	100	100	100	99.8	100	100	98.6	99.8	100	93.6	98	99.8	74.4	84.9	93.4	19.2	32.6	44.8	0	0	0
	60	100	100	100	100	100	100	100	100	100	100	100	100	100	100	100	100	100	100	100	100	100	99.8	100	100	99.4	100	100	97.2	99.4	100	88.6	94.6	98.4	60.8	71.4	80.8	7.8	18	29.4	0	0	0
	70	100	100	100	100	100	100	100	100	100	100	100	100	100	100	100	100	100	100	100	100	100	99.6	100	100	98.8	99.8	100	94.8	98.2	99.8	82	88.6	94.8	44.4	55.6	65.2	2.4	9	19.2	0	0	0
	80	100	100	100	100	100	100	100	100	100	100	100	100	100	100	100	100	100	100	99.8	100	100	99.4	100	100	97.4	99.4	100	91.4	95.8	98.8	72.2	80	87.8	27.2	41	52.6	0.59	4.6	12.6	0	0	0
	90	100	100	100	100	100	100	100	100	100	100	100	100	100	100	100	99.8	100	100	99.6	100	100	98.8	99.8	100	96	98.6	99.8	86.6	92	96.4	59.8	69.8	78.6	14.2	29.2	42.6	0	2	8.4	0	0	0
	100	100	100	100	100	100	100	100	100	100	100	100	100	100	100	100	99.8	100	100	99.4	100	100	98	99.4	100	93.2	97	99.2	79.4	86.6	92.4	45.8	58.8	69.4	6.99	19.4	34	0	1	5.2	0	0	0
	110	100	100	100	100	100	100	100	100	100	100	100	100	100	100	100	99.6	100	100	99	99.8	100	96.8	99	100	89.8	94.8	97.8	72	80.2	87.8	33.2	48.2	61	3	13.4	26.2	0	0.4	3.4	0	0	0
	120	100	100	100	100	100	100	100	100	100	100	100	100	99.8	100	100	99.6	100	100	98.4	99.6	100	95.2	98	99.6	86	91.6	96.4	62	73.2	82.2	22.4	39.2	53.4	1.4	8.6	21	0	0.2	2.2	0	0	0
	130	100	100	100	100	100	100	100	100	100	100	100	100	99.8	100	100	99.4	100	100	97.6	99.4	100	93	96.8	99.2	80.8	88.2	94.2	53	65.6	78	14.6	31.2	48.2	0.6	5.6	17.2	0	0	1.8	0	0	0
	140	100	100	100	100	100	100	100	100	100	99.8	100	100	99.6	100	100	99	99.8	100	96.6	99	100	90.2	95.6	98.8	74.4	84.6	92.8	44.2	59	75.6	9.99	25.3	44.8	0.2	4	14.4	0	0	1.2	0	0	0
	150	100	100	100	100	100	100	100	100	100	99.8	100	100	99.4	100	100	98.6	99.8	100	95.4	98.4	100	87	93.8	98.8	68	80.2	92.8	34.8	52.8	73.8	6.4	21	41.2	0	2.8	13	0	0	1	0	0	0
	≥154	100	100	100	100	100	100	100	100	100	99.8	100	100	99.4	100	100	98.4	99.6	100	95	98.4	100	85.8	93.2	98.6	65.4	78.4	92.4	33.4	50.8	74.2	5.6	18.8	42	0	2.4	12.4	0	0	1	0	0	0

[1] Body weight and serum albumin concentration set to median of first study day (i.e. 70 kg and 2.8 g/dL). ***Colour coding***: *Green*: PTA≥90%, *Yellow*: PTA 80-<90%, *Orange*: PTA>50-<80%, *Red*: PTA≤50%; *Grey shaded values*: Extrapolated $CLCR_{CG}$ range not covered by the study population or $CLCR_{CG}$ ≥154 mL/min (=inflection point of $CLCR_{CG}$-CL relationship).

Abbreviations: *CL*: Clearance; *$CLCR_{CG}$*: Creatinine clearance estimated according to Cockcroft and Cockcroft and Gault [2]; Minimum inhibitory concentration; *$P_{0.05}$*: 5th percentile; *$P_{0.5}$*: 50th percentile = median; *$P_{0.95}$*: 95th percentile, *q8h*: Every 8 hours; *$T_{>MIC}$*: Time period that total drug concentration exceeds the MIC.

Table S25: (Project IV): Probability of target attainment (PTA, %) for different continuous infusion dosing regimens of meropenem for the first day of treatment (modified from [243]). PTA is given for varied values of creatinine clearance and for selected MIC values and is presented as the median ($P_{0.5}$), 5th ($P_{0.05}$) and 95th percentile ($P_{0.95}$) of the 1000 PTA values derived from the 1000 Monte Carlo simulations considering PK parameter uncertainty.

[continued on next page]

Dosing regimen; PK/PD target[2]	$CLCR_{CG}$[1] [mL/min]	MIC [mg/L]																																						
		0.004			0.008			0.015			0.03			0.06			0.12			0.25			0.5			1			2			4			8			16			32		
		$P_{0.05}$	$P_{0.5}$	$P_{0.95}$	$P_{0.05}$	$P_{0.5}$	$P_{0.95}$	$P_{0.05}$	$P_{0.5}$	$P_{0.95}$	$P_{0.05}$	$P_{0.5}$	$P_{0.95}$	$P_{0.05}$	$P_{0.5}$	$P_{0.95}$	$P_{0.05}$	$P_{0.5}$	$P_{0.95}$	$P_{0.05}$	$P_{0.5}$	$P_{0.95}$	$P_{0.05}$	$P_{0.5}$	$P_{0.95}$	$P_{0.05}$	$P_{0.5}$	$P_{0.95}$	$P_{0.05}$	$P_{0.5}$	$P_{0.95}$	$P_{0.05}$	$P_{0.5}$	$P_{0.95}$	$P_{0.05}$	$P_{0.5}$	$P_{0.95}$	$P_{0.05}$	$P_{0.5}$	$P_{0.95}$	$P_{0.05}$	$P_{0.5}$	$P_{0.95}$
CI3 (3000 mg, CI, q24h following 500 mg, 30-min loading dose); $98\%T_{>4xMIC}$	10	100	100	100	100	100	100	100	100	100	100	100	100	100	100	100	100	100	100	100	100	100	100	100	100	100	100	100	100	100	100	95.2	99.4	100	0	0.2	1.6	0	0	0	0	0	0
	20	100	100	100	100	100	100	100	100	100	100	100	100	100	100	100	100	100	100	100	100	100	100	100	100	100	100	100	100	100	100	89.4	97.8	100	0	0	0.6	0	0	0	0	0	0
	30	100	100	100	100	100	100	100	100	100	100	100	100	100	100	100	100	100	100	100	100	100	100	100	100	100	100	100	99.8	100	100	79.6	93	98.8	0	0	0.2	0	0	0	0	0	0
	40	100	100	100	100	100	100	100	100	100	100	100	100	100	100	100	100	100	100	100	100	100	100	100	100	100	100	100	99.6	100	100	68.4	82.6	93	0	0	0	0	0	0	0	0	0
	50	100	100	100	100	100	100	100	100	100	100	100	100	100	100	100	100	100	100	100	100	100	100	100	100	100	100	100	99	100	100	54	67.6	79.2	0	0	0	0	0	0	0	0	0
	60	100	100	100	100	100	100	100	100	100	100	100	100	100	100	100	100	100	100	100	100	100	100	100	100	100	100	100	98	99.6	100	38	50.8	62	0	0	0	0	0	0	0	0	0
	70	100	100	100	100	100	100	100	100	100	100	100	100	100	100	100	100	100	100	100	100	100	100	100	100	100	100	100	95.6	98.6	100	22.6	35.4	47.2	0	0	0	0	0	0	0	0	0
	80	100	100	100	100	100	100	100	100	100	100	100	100	100	100	100	100	100	100	100	100	100	100	100	100	100	100	100	92.6	96.8	99.2	11.8	23.5	36	0	0	0	0	0	0	0	0	0
	90	100	100	100	100	100	100	100	100	100	100	100	100	100	100	100	100	100	100	100	100	100	100	100	100	99.8	100	100	88	93.6	97.4	5.39	14.9	27.6	0	0	0	0	0	0	0	0	0
	100	100	100	100	100	100	100	100	100	100	100	100	100	100	100	100	100	100	100	100	100	100	100	100	100	99.8	100	100	82.4	88.8	94	2.2	9.4	20	0	0	0	0	0	0	0	0	0
	110	100	100	100	100	100	100	100	100	100	100	100	100	100	100	100	100	100	100	100	100	100	100	100	100	99.6	100	100	75.2	82.8	89.2	0.8	5.6	15.2	0	0	0	0	0	0	0	0	0
	120	100	100	100	100	100	100	100	100	100	100	100	100	100	100	100	100	100	100	100	100	100	100	100	100	99.4	100	100	66.4	75.8	83.6	0.2	3.4	11.4	0	0	0	0	0	0	0	0	0
	130	100	100	100	100	100	100	100	100	100	100	100	100	100	100	100	100	100	100	100	100	100	100	100	100	99	99.8	100	57.4	68.6	79	0	2	8.6	0	0	0	0	0	0	0	0	0
	140	100	100	100	100	100	100	100	100	100	100	100	100	100	100	100	100	100	100	100	100	100	100	100	100	98.6	99.8	100	48.2	62	76.6	0	1.2	7.41	0	0	0	0	0	0	0	0	0
	150	100	100	100	100	100	100	100	100	100	100	100	100	100	100	100	100	100	100	100	100	100	100	100	100	97.8	99.6	100	39.4	55.8	76.2	0	1	6.2	0	0	0	0	0	0	0	0	0
	≥154	100	100	100	100	100	100	100	100	100	100	100	100	100	100	100	100	100	100	100	100	100	100	100	100	97.6	99.4	100	36.2	53.4	75.8	0	0.8	6	0	0	0	0	0	0	0	0	0
CI (3000 mg, CI, q24h following 500 mg, 30-min loading dose); $98\%T_{>1xMIC}$	10	100	100	100	100	100	100	100	100	100	100	100	100	100	100	100	100	100	100	100	100	100	100	100	100	100	100	100	100	100	100	100	100	100	100	100	100	95.2	99.4	100	0	0.2	1.6
	20	100	100	100	100	100	100	100	100	100	100	100	100	100	100	100	100	100	100	100	100	100	100	100	100	100	100	100	100	100	100	100	100	100	100	100	100	89.4	97.8	100	0	0	0.6
	30	100	100	100	100	100	100	100	100	100	100	100	100	100	100	100	100	100	100	100	100	100	100	100	100	100	100	100	100	100	100	100	100	100	99.8	100	100	79.6	93	98.8	0	0	0.2
	40	100	100	100	100	100	100	100	100	100	100	100	100	100	100	100	100	100	100	100	100	100	100	100	100	100	100	100	100	100	100	100	100	100	99.6	100	100	68.4	82.6	93	0	0	0
	50	100	100	100	100	100	100	100	100	100	100	100	100	100	100	100	100	100	100	100	100	100	100	100	100	100	100	100	100	100	100	100	100	100	99	100	100	54	67.6	79.2	0	0	0
	60	100	100	100	100	100	100	100	100	100	100	100	100	100	100	100	100	100	100	100	100	100	100	100	100	100	100	100	100	100	100	100	100	100	98	99.6	100	38	50.8	62	0	0	0
	70	100	100	100	100	100	100	100	100	100	100	100	100	100	100	100	100	100	100	100	100	100	100	100	100	100	100	100	100	100	100	100	100	100	95.6	98.6	100	22.6	35.4	47.2	0	0	0
	80	100	100	100	100	100	100	100	100	100	100	100	100	100	100	100	100	100	100	100	100	100	100	100	100	100	100	100	100	100	100	100	100	100	92.6	96.8	99.2	11.8	23.5	36	0	0	0
	90	100	100	100	100	100	100	100	100	100	100	100	100	100	100	100	100	100	100	100	100	100	100	100	100	100	100	100	100	100	100	99.8	100	100	88	93.6	97.4	5.39	14.9	27.6	0	0	0
	100	100	100	100	100	100	100	100	100	100	100	100	100	100	100	100	100	100	100	100	100	100	100	100	100	100	100	100	100	100	100	99.8	100	100	82.4	88.8	94	2.2	9.4	20	0	0	0
	110	100	100	100	100	100	100	100	100	100	100	100	100	100	100	100	100	100	100	100	100	100	100	100	100	100	100	100	100	100	100	99.6	100	100	75.2	82.8	89.2	0.8	5.6	15.2	0	0	0
	120	100	100	100	100	100	100	100	100	100	100	100	100	100	100	100	100	100	100	100	100	100	100	100	100	100	100	100	100	100	100	99.4	100	100	66.4	75.8	83.6	0.2	3.4	11.4	0	0	0
	130	100	100	100	100	100	100	100	100	100	100	100	100	100	100	100	100	100	100	100	100	100	100	100	100	100	100	100	100	100	100	99	99.8	100	57.4	68.6	79	0	2	8.6	0	0	0
	140	100	100	100	100	100	100	100	100	100	100	100	100	100	100	100	100	100	100	100	100	100	100	100	100	100	100	100	100	100	100	98.6	99.8	100	48.2	62	76.6	0	1.2	7.41	0	0	0
	150	100	100	100	100	100	100	100	100	100	100	100	100	100	100	100	100	100	100	100	100	100	100	100	100	100	100	100	100	100	100	97.8	99.6	100	39.4	55.8	76.2	0	1	6.2	0	0	0
	≥154	100	100	100	100	100	100	100	100	100	100	100	100	100	100	100	100	100	100	100	100	100	100	100	100	100	100	100	100	100	100	97.6	99.4	100	36.2	53.4	75.8	0	0.8	6	0	0	0

Table S25 [continued]

Dosing regimen; PK/PD target[2]	$CLCR_{CG}$[1] [mL/min]	MIC [mg/L] 0.004			0.008			0.015			0.03			0.06			0.12			0.25			0.5			1			2			4			8			16			32		
		$P_{0.05}$	$P_{0.5}$	$P_{0.95}$	$P_{0.05}$	$P_{0.5}$	$P_{0.95}$	$P_{0.05}$	$P_{0.5}$	$P_{0.95}$	$P_{0.05}$	$P_{0.5}$	$P_{0.95}$	$P_{0.05}$	$P_{0.5}$	$P_{0.95}$	$P_{0.05}$	$P_{0.5}$	$P_{0.95}$	$P_{0.05}$	$P_{0.5}$	$P_{0.95}$	$P_{0.05}$	$P_{0.5}$	$P_{0.95}$	$P_{0.05}$	$P_{0.5}$	$P_{0.95}$	$P_{0.05}$	$P_{0.5}$	$P_{0.95}$	$P_{0.05}$	$P_{0.5}$	$P_{0.95}$	$P_{0.05}$	$P_{0.5}$	$P_{0.95}$	$P_{0.05}$	$P_{0.5}$	$P_{0.95}$	$P_{0.05}$	$P_{0.5}$	$P_{0.95}$
CI6 (6000 mg, CI, q24h following 1000 mg, 30-min loading dose)	10	100	100	100	100	100	100	100	100	100	100	100	100	100	100	100	100	100	100	100	100	100	100	100	100	100	100	100	100	100	100	100	100	100	94.8	99.4	100	0	0	1.8	0	0	0
	20	100	100	100	100	100	100	100	100	100	100	100	100	100	100	100	100	100	100	100	100	100	100	100	100	100	100	100	100	100	100	100	100	100	89.2	97.8	100	0	0	0.4	0	0	0
	30	100	100	100	100	100	100	100	100	100	100	100	100	100	100	100	100	100	100	100	100	100	100	100	100	100	100	100	100	100	100	99.8	100	100	80	93	98.8	0	0	0.2	0	0	0
	40	100	100	100	100	100	100	100	100	100	100	100	100	100	100	100	100	100	100	100	100	100	100	100	100	100	100	100	100	100	100	99.6	100	100	67.8	82.6	93	0	0	0	0	0	0
	50	100	100	100	100	100	100	100	100	100	100	100	100	100	100	100	100	100	100	100	100	100	100	100	100	100	100	100	100	100	100	99	100	100	53.4	67.4	79.2	0	0	0	0	0	0
	60	100	100	100	100	100	100	100	100	100	100	100	100	100	100	100	100	100	100	100	100	100	100	100	100	100	100	100	100	100	100	97.8	99.6	100	38	50.8	62.2	0	0	0	0	0	0
	70	100	100	100	100	100	100	100	100	100	100	100	100	100	100	100	100	100	100	100	100	100	100	100	100	100	100	100	100	100	100	95.6	98.6	99.8	22.8	35.2	47.2	0	0	0	0	0	0
	80	100	100	100	100	100	100	100	100	100	100	100	100	100	100	100	100	100	100	100	100	100	100	100	100	100	100	100	100	100	100	92.8	96.8	99.2	11.8	23.5	35.4	0	0	0	0	0	0
	90	100	100	100	100	100	100	100	100	100	100	100	100	100	100	100	100	100	100	100	100	100	100	100	100	100	100	100	99.8	100	100	88.4	93.6	97.4	5	15.2	27	0	0	0	0	0	0
	100	100	100	100	100	100	100	100	100	100	100	100	100	100	100	100	100	100	100	100	100	100	100	100	100	100	100	100	99.8	100	100	82.2	88.8	94.2	2	9.1	20	0	0	0	0	0	0
	110	100	100	100	100	100	100	100	100	100	100	100	100	100	100	100	100	100	100	100	100	100	100	100	100	100	100	100	99.6	100	100	74.6	82.6	89	0.8	5.6	14.8	0	0	0	0	0	0
	120	100	100	100	100	100	100	100	100	100	100	100	100	100	100	100	100	100	100	100	100	100	100	100	100	100	100	100	99.4	100	100	66.6	75.8	84.2	0.2	3.4	11.4	0	0	0	0	0	0
	130	100	100	100	100	100	100	100	100	100	100	100	100	100	100	100	100	100	100	100	100	100	100	100	100	100	100	100	99	99.8	100	57.4	68.6	79.2	0	2.2	9.2	0	0	0	0	0	0
	140	100	100	100	100	100	100	100	100	100	100	100	100	100	100	100	100	100	100	100	100	100	100	100	100	100	100	100	98.6	99.8	100	48.6	61.6	76.4	0	1.4	7	0	0	0	0	0	0
	150	100	100	100	100	100	100	100	100	100	100	100	100	100	100	100	100	100	100	100	100	100	100	100	100	100	100	100	97.8	99.6	100	39.2	55.8	76.4	0	0.8	6.01	0	0	0	0	0	0
	≥154	100	100	100	100	100	100	100	100	100	100	100	100	100	100	100	100	100	100	100	100	100	100	100	100	100	100	100	97.8	99.4	100	36.2	53.4	76.4	0	0.8	6	0	0	0	0	0	0
CI6 (6000 mg, CI, q24h following 1000 mg, 30-min loading dose)	10	100	100	100	100	100	100	100	100	100	100	100	100	100	100	100	100	100	100	100	100	100	100	100	100	100	100	100	100	100	100	100	100	100	100	100	100	100	100	100	94.8	99.4	100
	20	100	100	100	100	100	100	100	100	100	100	100	100	100	100	100	100	100	100	100	100	100	100	100	100	100	100	100	100	100	100	100	100	100	100	100	100	100	100	100	89.2	97.8	100
	30	100	100	100	100	100	100	100	100	100	100	100	100	100	100	100	100	100	100	100	100	100	100	100	100	100	100	100	100	100	100	100	100	100	100	100	100	99.8	100	100	80	93	98.8
	40	100	100	100	100	100	100	100	100	100	100	100	100	100	100	100	100	100	100	100	100	100	100	100	100	100	100	100	100	100	100	100	100	100	100	100	100	99.6	100	100	67.8	82.6	93
	50	100	100	100	100	100	100	100	100	100	100	100	100	100	100	100	100	100	100	100	100	100	100	100	100	100	100	100	100	100	100	100	100	100	100	100	100	99	100	100	53.4	67.4	79.2
	60	100	100	100	100	100	100	100	100	100	100	100	100	100	100	100	100	100	100	100	100	100	100	100	100	100	100	100	100	100	100	100	100	100	100	100	100	97.8	99.6	100	38	50.8	62.2
	70	100	100	100	100	100	100	100	100	100	100	100	100	100	100	100	100	100	100	100	100	100	100	100	100	100	100	100	100	100	100	100	100	100	100	100	100	95.6	98.6	99.8	22.8	35.2	47.2
	80	100	100	100	100	100	100	100	100	100	100	100	100	100	100	100	100	100	100	100	100	100	100	100	100	100	100	100	100	100	100	100	100	100	100	100	100	92.8	96.8	99.2	11.8	23.5	35.4
	90	100	100	100	100	100	100	100	100	100	100	100	100	100	100	100	100	100	100	100	100	100	100	100	100	100	100	100	100	100	100	100	100	100	99.8	100	100	88.4	93.6	97.4	5	15.2	27
	100	100	100	100	100	100	100	100	100	100	100	100	100	100	100	100	100	100	100	100	100	100	100	100	100	100	100	100	100	100	100	100	100	100	99.8	100	100	82.2	88.8	94.2	2	9.1	20
	110	100	100	100	100	100	100	100	100	100	100	100	100	100	100	100	100	100	100	100	100	100	100	100	100	100	100	100	100	100	100	100	100	100	99.6	100	100	74.6	82.6	89	0.8	5.6	14.8
	120	100	100	100	100	100	100	100	100	100	100	100	100	100	100	100	100	100	100	100	100	100	100	100	100	100	100	100	100	100	100	100	100	100	99.4	100	100	66.6	75.8	84.2	0.2	3.4	11.4
	130	100	100	100	100	100	100	100	100	100	100	100	100	100	100	100	100	100	100	100	100	100	100	100	100	100	100	100	100	100	100	100	100	100	99	99.8	100	57.4	68.6	79.2	0	2.2	9.2
	140	100	100	100	100	100	100	100	100	100	100	100	100	100	100	100	100	100	100	100	100	100	100	100	100	100	100	100	100	100	100	100	100	100	98.6	99.8	100	48.6	61.6	76.4	0	1.4	7
	150	100	100	100	100	100	100	100	100	100	100	100	100	100	100	100	100	100	100	100	100	100	100	100	100	100	100	100	100	100	100	100	100	100	97.8	99.6	100	39.2	55.8	76.4	0	0.8	6.01
	≥154	100	100	100	100	100	100	100	100	100	100	100	100	100	100	100	100	100	100	100	100	100	100	100	100	100	100	100	100	100	100	100	100	100	97.8	99.4	100	36.2	53.4	76.4	0	0.8	6

[1]Body weight and serum albumin concentration set to median of first study day (i.e. 70 kg and 2.8 g/dL); [2]PTA for the target 98%$T_{>4xMIC}$ was derived by shifting the results for the target 98%$T_{>MIC}$ two MIC values to the left.

Colour coding: *Green*: PTA≥90%, *Yellow*: PTA 80-<90%, *Orange*: PTA>50-<80%, *Red*: PTA≤50%; *Grey shaded values*: Extrapolated $CLCR_{CG}$ range not covered by the study population or $CLCR_{CG}$ ≥154 mL/min (=inflection point of $CLCR_{CG}$-CL relationship).

Abbreviations: *CL*: Clearance; *$CLCR_{CG}$*: Creatinine clearance estimated according to Cockcroft and Cockcroft and Gault [2]; *MIC*: Minimum inhibitory concentration; *$P_{0.05}$*: 5th percentile; *$P_{0.5}$*: 50th percentile = median; *$P_{0.95}$*: 95th percentile, *q8h*: Every 8 hours; *$T_{>MIC}$*: Time period that total drug concentration exceeds the MIC; *$T_{>4xMIC}$*: Time period that unbound drug concentration exceeds four times the MIC.

Table S26: (Project IV): Cumulative fraction of response (98%$T_{>MIC}$, CFR, %) for different short-term infusion dosing regimens of meropenem for the first day of treatment (modified from [243]). PTA is given for varied values of creatinine clearance and for selected MIC values and is presented as the median ($P_{0.5}$), 5th ($P_{0.05}$) and 95th percentile ($P_{0.95}$) of the 1000 PTA values derived from the 1000 Monte Carlo simulations considering PK parameter uncertainty.

Dosing regimen	$CLCR_{CG}$[1] [mL/min]	Full MIC distribution[2]															MIC distribution of isolates belonging to the S category[2]						MIC distribution of isolates belonging to the I category[2]					
		Escherichia coli			*Klebsiella pneumonia*			*Enterobacter cloacae*			*Pseudomonas aeruginosa*			*Acinetobacter* spp.			*Pseudomonas aeruginosa*			*Acinetobacter* spp.			*Pseudomonas aeruginosa*			*Acinetobacter* spp.		
		$P_{0.05}$	$P_{0.5}$	$P_{0.95}$	$P_{0.05}$	$P_{0.5}$	$P_{0.95}$	$P_{0.05}$	$P_{0.5}$	$P_{0.95}$	$P_{0.05}$	$P_{0.5}$	$P_{0.95}$	$P_{0.05}$	$P_{0.5}$	$P_{0.95}$	$P_{0.05}$	$P_{0.5}$	$P_{0.95}$	$P_{0.05}$	$P_{0.5}$	$P_{0.95}$	$P_{0.05}$	$P_{0.5}$	$P_{0.95}$	$P_{0.05}$	$P_{0.5}$	$P_{0.95}$
$SI2_{12}$ (1000 mg, 30-min i.v. infusion, q12h)	10	100	100	100	99.7	99.8	99.9	99.6	99.8	99.9	84.8	90.6	94.8	81.5	87.3	93.1	98.6	100	100	97.7	100	100	53.6	86.4	99.4	56.7	88	99.5
	20	100	100	100	99.5	99.7	99.8	99.4	99.6	99.7	80.3	86.4	89.9	76.7	83.2	86.6	96	99.5	100	93.9	99.1	100	34.1	60.5	82.7	37	63.7	85
	30	99.9	100	100	99.2	99.6	99.7	98.9	99.5	99.6	75.3	81.6	85.5	70.8	78.2	82.6	91.8	97.4	99.5	88.1	95.7	99.1	19.9	35.9	52.6	22.1	38.9	56.1
	40	99.7	99.9	100	98.6	99.4	99.5	98.2	99.2	99.4	69.3	76	80.5	63.8	71.5	76.8	86	92.9	97	80.5	89.2	94.8	9.2	18.4	28.4	10.4	20.4	30.8
	50	99.5	99.9	99.9	97.7	99	99.3	97	98.6	99.1	62.4	69.2	74.5	55.7	63.3	69.2	78.2	86	91.4	71	79.9	86.7	3.33	8.52	15.7	3.78	9.53	17.2
	60	98.8	99.7	99.9	96.1	98.2	99.1	95.1	97.5	98.6	55	61.7	67.8	47.5	54.6	61.2	69.2	77.2	84.1	60.7	69.4	77.2	0.86	3.85	8.99	0.975	4.35	9.93
	70	97.7	99.3	99.8	93.6	96.7	98.5	92.2	95.6	97.7	46.6	53.7	60.5	38.8	46.1	53.2	58.8	67.4	75.4	49.7	58.8	67.5	0.107	1.61	5.19	0.122	1.83	5.75
	80	96.3	98.5	99.5	90.2	94.4	97.3	88.4	92.8	96	38.4	45.8	53.1	31	38.2	45.7	48.3	57.6	66.4	39.7	48.9	58.2	0	0.645	3.18	0	0.732	3.53
	90	94.1	97.3	99.1	85.6	91.3	95.3	83.4	89.3	93.5	30.3	38.5	46.5	23.9	31.5	39.4	38.2	48.5	58.3	30.6	40.3	50.2	0	0.215	1.81	0	0.244	2.03
	100	91.2	95.3	98.2	80	86.7	92.3	77.5	84.4	90.2	23.4	31.8	40.3	18.1	25.5	33.5	29.4	40	50.5	23.2	32.6	42.8	0	0.107	1.17	0	0.122	1.3
	110	87.2	92.6	96.8	72.9	81.3	88.8	70.4	78.9	86.4	17.5	25.9	34.9	13.4	20.6	28.8	22.1	32.7	43.9	17.2	26.3	36.8	0	0	0.645	0	0	0.732
	120	83	89.4	95.2	65.5	75.5	85	63.3	73.2	82.6	13.3	21.3	30.8	10.2	16.7	25.1	16.8	26.9	38.8	13	21.5	32.1	0	0	0.43	0	0	0.488
	130	77.6	85.8	93.4	57.9	69.4	81.3	56	67.4	79	9.95	17.5	27.5	7.59	13.6	22.2	12.5	22	34.6	9.72	17.4	28.4	0	0	0.22	0	0	0.25
	140	72.2	82	92.2	50.5	64	79	49.3	62.2	76.7	7.65	14.7	25.2	5.85	11.4	20.3	9.64	18.5	31.7	7.49	14.6	25.9	0	0	0.215	0	0	0.244
	150	65.8	78.3	91.6	43.3	58.9	78.2	42.7	57.4	75.8	5.73	12.3	23.8	4.38	9.49	19	7.22	15.5	30	5.61	12.2	24.3	0	0	0.107	0	0	0.122
	≥154	64.2	76.9	91.4	40.4	57.1	78.3	40.2	55.7	75.8	5.24	11.7	23.5	4.01	9.02	18.8	6.61	14.7	29.7	5.14	11.6	24	0	0	0.107	0	0	0.122
$SI3_8$ = standard dosing regimen (1000 mg, 30-min i.v. infusion, q8h)	10	100	100	100	99.8	99.9	100	99.8	99.9	100	91.2	95.2	98	88.2	94	99.1	100	100	100	99.9	100	100	88.2	99.1	100	89.5	99.2	100
	20	100	100	100	99.8	99.8	99.9	99.7	99.8	99.9	88.8	92.1	94.6	85.4	89.1	92.8	99.7	100	100	99.6	100	100	76.1	93.1	99.4	78.3	94	99.5
	30	100	100	100	99.7	99.8	99.8	99.6	99.7	99.8	86.4	89.4	91.4	83	86	88.2	99.3	99.9	100	98.8	99.9	100	61.7	79.7	91	64.7	81.9	92.3
	40	100	100	100	99.6	99.7	99.8	99.5	99.6	99.7	83.7	86.6	88.7	80.4	83.5	85.5	98.2	99.6	100	97.1	99.2	99.9	47	61.7	73.7	50.4	65	76.7
	50	100	100	100	99.5	99.6	99.7	99.4	99.5	99.6	80.5	83.7	86	77	80.6	83.1	96.5	98.6	99.6	94.5	97.7	99.3	32	43.9	55.3	35.2	47.3	58.7
	60	99.9	100	100	99.2	99.5	99.6	99.1	99.4	99.5	76.9	80.4	83.1	72.9	76.9	80	93.8	96.8	98.6	90.8	94.8	97.5	19.7	29.4	39.5	22.1	32.2	42.3
	70	99.9	99.9	100	99.1	99.4	99.5	98.8	99.3	99.4	72.9	76.9	80.2	68	72.5	76.4	90.3	94	96.6	85.7	90.5	94.2	10.6	18.9	28.5	12	20.9	30.8
	80	99.8	99.9	100	98.8	99.3	99.4	98.3	99	99.3	68.2	72.9	77	62.1	67.5	72.2	85.3	90.1	93.8	79	85	89.9	4.4	11.4	20.5	4.99	12.8	22.3
	90	99.6	99.9	99.9	98.2	99	99.3	97.6	98.6	99.1	63	68.5	73.3	55.8	62.2	67.6	79.2	85.3	90.1	71.3	78.7	84.8	1.61	6.83	14.6	1.83	7.67	16
	100	99.4	99.9	99.9	97.5	98.8	99.1	96.6	98.2	98.8	57.4	63.9	69.5	49.4	56.7	63.1	72.3	79.9	86	63.2	72.2	79.5	0.537	3.85	10.4	0.61	4.35	11.4
	110	99.2	99.7	99.9	96.6	98.2	99	95.5	97.4	98.5	52.1	59.1	65.7	43.6	51.4	58.8	65.6	74.2	81.6	55.9	65.6	74.4	0.21	2.2	7.51	0.238	2.5	8.31
	120	98.8	99.6	99.8	95.4	97.6	98.8	94	96.5	98.1	46.9	54.6	62.2	38.4	46.7	55	59.1	68.7	77.5	49.2	59.6	69.7	0	1.29	5.62	0	1.46	6.24
	130	98.2	99.3	99.8	93.9	96.7	98.6	92.1	95.4	97.7	41.6	50.3	59.2	33.5	42.3	51.7	52.5	63.2	74	42.9	54	65.7	0	0.752	4.15	0	0.853	4.62
	140	97.5	99.1	99.8	92.1	95.9	98.3	90	94.3	97.4	37.1	46.5	57.6	29.5	38.6	50	46.7	58.5	72.1	37.7	49.4	63.6	0	0.43	3.61	0	0.488	4.01
	150	96.7	98.8	99.8	89.9	94.8	98.2	87.5	93	97.1	32.6	43.1	56.5	25.7	35.3	48.7	41.1	54.2	70.8	32.9	45.2	62.1	0	0.322	2.87	0	0.366	3.2
	≥154	96.2	98.7	99.8	89.2	94.3	98.2	86.7	92.3	97.2	31.3	41.8	56.7	24.6	34.2	48.9	39.4	52.6	71	31.5	43.8	62.2	0	0.215	2.66	0	0.244	2.96
$SI6_8$ (2000 mg, 30-min i.v. infusion, q8h)	10	100	100	100	99.9	100	100	99.9	100	100	96.9	98.7	99.1	97	99.7	100	100	100	100	100	100	100	98.3	100	100	98.5	100	100
	20	100	100	100	99.9	100	100	99.9	99.9	100	95.1	97.6	98.7	94.4	98.1	99.7	100	100	100	100	100	100	94.9	99.5	100	95.4	99.6	100
	30	100	100	100	99.9	99.9	99.9	99.8	99.9	99.9	92.8	95.5	97.2	91	94.8	97.5	99.8	100	100	99.7	100	100	88.9	96.9	99.7	90	97.3	99.8
	40	100	100	100	99.8	99.9	99.9	99.7	99.8	99.9	90.3	93	94.7	87.7	91.1	93.4	99.6	100	100	99.3	99.9	100	80.3	90.3	96.7	82	91.4	97.1
	50	100	100	100	99.7	99.8	99.8	99.7	99.8	99.8	87.6	90.2	92.2	84.3	87.5	90	98.9	99.8	100	98.4	99.6	100	69	79.4	87.9	71.3	81.2	89.4
	60	100	100	100	99.6	99.7	99.8	99.5	99.7	99.7	84.6	87.4	89.7	81.1	84.4	87.2	97.9	99.3	99.9	96.8	98.8	99.7	55.2	65.7	75.2	58	68.2	77.5
	70	99.9	100	100	99.4	99.6	99.7	99.3	99.6	99.7	81.3	84.6	87.2	77.7	81.4	84.5	96.3	98.4	99.4	94.5	97.3	99	40.1	51.7	61.7	43	54.4	64.2
	80	99.9	100	100	99.3	99.6	99.6	99.1	99.4	99.6	77.9	81.7	84.7	73.9	78	81.6	93.9	96.7	98.5	91.2	94.8	97.3	27.2	39.2	50.1	29.7	41.8	52.5
	90	99.8	99.9	100	99	99.4	99.6	98.7	99.3	99.5	74	78.4	82.2	69.3	74.2	78.5	90.6	94.4	97	86.6	91.4	94.9	17.1	28.4	40.7	19	30.7	42.9
	100	99.7	99.9	100	98.6	99.3	99.5	98.3	99.1	99.4	69.8	74.9	79.4	64.3	70	75.1	86.5	91.3	94.9	81.1	87.1	91.8	9.59	20.1	32.2	10.7	21.9	34.3
	110	99.6	99.9	99.9	98.2	99	99.4	97.6	98.7	99.2	65.4	71.3	76.5	59	65.7	71.6	81.6	87.6	92.3	75	82.3	88.2	4.81	14.1	25.8	5.4	15.5	27.6
	120	99.4	99.9	99.9	97.5	98.8	99.3	96.8	98.3	99	61	67.5	73.7	53.9	61.3	68.3	76.5	83.6	89.6	68.7	77.2	84.7	2.69	9.87	20.8	3.05	10.9	22.4
	130	99.2	99.8	99.9	97	98.4	99.2	96.1	97.8	98.8	56.7	63.9	71.3	49	57.2	65.5	71.2	79.4	87.2	62.6	72.3	81.7	1.5	6.88	17	1.71	7.62	18.4
	140	98.8	99.7	99.9	96	98.1	99.1	94.8	97.3	98.7	52.1	60.7	69.7	44.3	53.6	63.7	65.6	75.8	85.5	56.6	68.1	79.6	0.752	4.88	14.5	0.853	5.43	15.7
	150	98.4	99.6	99.9	94.5	97.7	99.1	93.1	96.7	98.7	47.6	57.4	69.3	39.8	50.1	63.2	60	71.8	85.2	51	63.7	79.1	0.43	3.72	13.7	0.488	4.14	14.9
	≥154	98.2	99.6	99.9	94.2	97.5	99.1	92.7	96.4	98.7	46	56.4	69.1	38.2	49	63	57.9	70.5	85.1	48.9	62.4	79	0.43	3.3	12.7	0.488	3.69	13.8

[1]Body weight and serum albumin concentration set to median of first study day (i.e. 70 kg and 2.8 g/dL).
[2]According to EUCAST [390].
Colour coding: *Green*: CFR≥90%, *Yellow*: CFR 80-<90%, *Orange*: CFR >50-<80%, *Red*: CFR ≤50%; *Grey shaded values*: Extrapolated creatinine $CLCR_{CG}$ range not covered by the study population or creatinine clearance ≥154 mL/min (=inflection point of $CLCR_{CG}$-CL relationship).
Abbreviations: *CL*: Clearance; *$CLCR_{CG}$*: Creatinine clearance estimated according to Cockcroft and Gault [2]; *MIC*: Minimum inhibitory concentration*; I category*: Category 'susceptible at increased exposure' [4]; *$P_{0.05}$*: 5th percentile; $P_{0.5}$: 50th percentile = median; $P_{0.95}$: 95th percentile, q8h: Every 8 hours; S category: Category 'susceptible at normal dosing' [4]; *$T_{>MIC}$:* Time period that total drug concentration exceeds the MIC.

Table S27: (Project IV): Cumulative fraction of response (98%$T_{>MIC}$, CFR, %) for different prolonged infusion dosing regimens of meropenem for the first day of treatment (modified from [243]). PTA is given for varied values of creatinine clearance and for selected MIC values and is presented as the median ($P_{0.5}$), 5th ($P_{0.05}$) and 95th percentile ($P_{0.95}$) of the 1000 PTA values derived from the 1000 Monte Carlo simulations considering PK parameter uncertainty.

Dosing regimen	$CLCR_{CG}$[1] [mL/min]	Full MIC distribution[2]															MIC distribution of isolates belonging to the S category[2]						MIC distribution of isolates belonging to the I category[2]					
		Escherichia coli			*Klebsiella pneumonia*			*Enterobacter cloacae*			*Pseudomonas aeruginosa*			*Acinetobacter* spp.			*Pseudomonas aeruginosa*			*Acinetobacter* spp.			*Pseudomonas aeruginosa*			*Acinetobacter* spp.		
		$P_{0.05}$	$P_{0.5}$	$P_{0.95}$	$P_{0.05}$	$P_{0.5}$	$P_{0.95}$	$P_{0.05}$	$P_{0.5}$	$P_{0.95}$	$P_{0.05}$	$P_{0.5}$	$P_{0.95}$	$P_{0.05}$	$P_{0.5}$	$P_{0.95}$	$P_{0.05}$	$P_{0.5}$	$P_{0.95}$	$P_{0.05}$	$P_{0.5}$	$P_{0.95}$	$P_{0.05}$	$P_{0.5}$	$P_{0.95}$	$P_{0.05}$	$P_{0.5}$	$P_{0.95}$
$PI2_{12}$ (1000 mg, 3-h i.v. infusion, q12h)	10	100	100	100	99.7	99.8	99.8	99.6	99.8	99.8	86.5	90.3	91.4	83.2	86.3	87.1	99.4	100	100	99	100	100	62.3	89.8	98.5	65.5	91.2	98.8
	20	100	100	100	99.6	99.7	99.8	99.5	99.7	99.8	83.3	87.8	90.2	80	84.4	86.3	98.1	99.8	100	96.9	99.6	100	44.4	69.9	88.5	47.8	73	90.2
	30	100	100	100	99.5	99.6	99.7	99.3	99.6	99.7	79.5	84.2	86.9	75.9	81.2	83.9	95.8	98.9	99.9	93.5	98.1	99.7	28.6	46.4	62.8	31.6	50	66.5
	40	99.9	100	100	99.2	99.5	99.6	98.9	99.4	99.5	74.9	80	83.2	70.4	76.4	80.2	91.9	96.5	98.8	88.1	94.3	97.8	16.3	27.5	39.3	18.3	30.3	42.6
	50	99.8	99.9	100	98.7	99.3	99.5	98.3	99.1	99.4	69.7	75	78.9	64.1	70.2	75	86.7	92.2	95.9	81.1	88	93.1	7.72	14.9	23	8.73	16.6	25.2
	60	99.6	99.9	99.9	98.1	99	99.3	97.5	98.6	99.1	63.6	69.1	74	56.8	63	68.6	79.7	86	91.1	72.4	79.7	86	2.58	7.37	14.1	2.93	8.28	15.5
	70	99.1	99.8	99.9	96.9	98.4	99.1	96	97.8	98.7	56.7	62.8	68.3	48.9	55.7	61.7	71.3	78.6	84.7	62.6	70.8	77.9	0.752	3.64	8.69	0.853	4.1	9.65
	80	98.5	99.6	99.8	95.2	97.6	98.7	93.9	96.6	98	49.3	56	62.3	41.1	48.3	55.1	62.1	70.4	77.6	52.7	61.6	69.9	0.107	1.61	5.43	0.122	1.83	6.05
	90	97.6	99.2	99.8	93	96.1	98.1	91.3	94.7	97.1	41.8	49.4	56.4	33.9	41.5	48.9	52.7	62.1	70.5	43.4	53.1	62.2	0	0.752	3.41	0	0.853	3.81
	100	96.4	98.5	99.5	89.6	94	97.1	87.6	92.2	95.6	34.8	42.9	50.8	27.6	35.4	43.3	43.9	54	63.6	35.4	45.2	55.2	0	0.322	2.24	0	0.366	2.52
	110	94.5	97.4	99.1	85.9	91.2	95.4	83.5	89	93.6	28.3	36.8	45.6	22.1	29.9	38.3	35.7	46.4	57.2	28.3	38.2	48.9	0	0.107	1.38	0	0.122	1.54
	120	92.3	96	98.6	81.7	87.7	93.6	78.9	85.3	91.5	23	31.6	41.2	17.8	25.3	34.2	29	39.8	51.7	22.8	32.3	43.7	0	0.107	0.967	0	0.122	1.1
	130	89.6	94.3	98.1	76.1	84	91.6	73.4	81.5	89.2	18.5	27.2	37.5	14.2	21.5	30.9	23.4	34.3	47.2	18.2	27.6	39.5	0	0	0.645	0	0	0.732
	140	86.4	92.6	97.5	70.2	80.3	90.3	67.7	77.7	87.9	15.2	23.6	35.2	11.6	18.5	28.8	19.2	29.8	44.3	14.9	23.7	36.8	0	0	0.43	0	0	0.488
	150	82.4	90.4	97.3	63.8	76.3	90	61.7	73.8	87.5	12.3	20.6	34.3	9.38	16.1	27.9	15.5	26	43.2	12	20.6	35.7	0	0	0.43	0	0	0.488
	≥154	80.8	89.5	97.1	61.3	74.6	89.8	59.2	72.2	87.4	11.1	19.7	33.9	8.47	15.3	27.5	14	24.8	42.7	10.8	19.6	35.2	0	0	0.322	0	0	0.366
$PI3_8$ (1000 mg, 3-h i.v. infusion, q8h)	10	100	100	100	99.8	99.8	99.8	99.8	99.8	99.8	90.6	91.3	91.6	86.5	87	87.2	100	100	100	100	100	100	91.6	97.7	99.6	92.8	98	99.7
	20	100	100	100	99.8	99.8	99.8	99.7	99.8	99.8	89.7	91	91.5	85.8	86.8	87.1	100	100	100	99.9	100	100	84.5	95.1	98.8	86.4	95.8	99
	30	100	100	100	99.8	99.8	99.8	99.7	99.8	99.8	88.3	90.1	91	84.8	86.2	86.8	99.8	100	100	99.7	100	100	74.5	87.6	95.1	77.3	89.3	95.9
	40	100	100	100	99.7	99.8	99.8	99.6	99.7	99.7	86.5	88.5	89.7	83.3	85.1	86	99.5	100	100	99.1	99.9	100	62.1	75.2	84.7	65.7	78.2	86.9
	50	100	100	100	99.7	99.7	99.8	99.6	99.6	99.7	84.6	86.6	88	81.6	83.6	84.7	99	99.8	100	98.4	99.6	100	49	60.5	70.4	53	64.3	74
	60	100	100	100	99.6	99.6	99.7	99.5	99.6	99.6	82.2	84.5	86.2	79.2	81.7	83.3	98	99.3	99.8	96.8	98.7	99.7	36.2	46.7	56.8	40	50.6	60.6
	70	100	100	100	99.5	99.6	99.6	99.4	99.5	99.6	79.6	82.2	84.3	76.3	79.2	81.5	96.5	98.3	99.4	94.5	97.1	98.8	24.8	34.3	44.1	27.8	37.7	47.5
	80	99.9	100	100	99.4	99.5	99.6	99.2	99.4	99.5	76.7	79.8	82.2	72.7	76.3	79.1	94.3	96.8	98.4	91.2	94.5	97	14.7	24.4	34	16.6	27	36.9
	90	99.9	100	100	99.1	99.4	99.5	98.9	99.3	99.4	73.3	77.1	80.1	68.4	72.9	76.4	91.2	94.6	96.9	86.6	91.2	94.5	7.95	16.5	26.8	9.02	18.4	29.2
	100	99.9	99.9	100	99	99.3	99.4	98.7	99.1	99.3	69.9	74.2	77.8	63.9	69.1	73.4	87.5	91.9	94.9	81.4	87.2	91.4	3.65	10.8	20.6	4.15	12.1	22.7
	110	99.8	99.9	99.9	98.8	99.2	99.4	98.4	98.9	99.2	66.3	71.2	75.4	59.3	65.2	70.3	83.3	88.6	92.6	75.7	82.6	88.1	1.61	7.06	15.9	1.83	7.96	17.5
	120	99.8	99.9	99.9	98.5	99.1	99.3	98	98.7	99.1	62.8	68.1	73.3	55	61.4	67.7	79	85.1	90.5	70.3	78	85.1	0.752	4.71	12.3	0.853	5.32	13.6
	130	99.7	99.9	99.9	98.1	99	99.2	97.4	98.5	99	58.7	65.1	71.1	50.2	57.8	65	74	81.6	88.1	64.3	73.6	81.9	0.215	3.01	9.77	0.244	3.41	10.9
	140	99.5	99.9	99.9	97.8	98.7	99.2	96.8	98.2	98.9	55.4	62.4	69.9	46.6	54.6	63.5	69.8	78.3	86.9	59.7	69.7	80.3	0.107	2.04	7.98	0.122	2.32	8.92
	150	99.5	99.8	99.9	97.3	98.6	99.1	96.1	97.9	98.8	51.5	59.7	69.4	42.6	51.6	62.9	64.9	74.9	86.4	54.6	65.9	79.6	0	1.5	7.35	0	1.71	8.2
	≥154	99.4	99.8	99.9	97.1	98.6	99.1	95.8	97.8	98.8	50	58.8	69.3	41.2	50.6	62.7	63.1	73.9	86.2	52.8	64.7	79.4	0	1.29	7.23	0	1.46	8.07
$PI6_8$ (2000 mg, 3-h i.v. infusion, q8h)	10	100	100	100	99.9	100	100	99.9	100	100	97.2	98.1	98.4	97.7	99.2	99.8	100	100	100	100	100	100	99.6	100	100	99.7	100	100
	20	100	100	100	99.9	100	100	99.9	100	100	96.3	97.7	98.3	96.1	98.5	99.6	100	100	100	100	100	100	98.4	99.9	100	98.6	99.9	100
	30	100	100	100	99.9	99.9	100	99.9	99.9	100	94.8	96.6	97.7	93.6	96.6	98.5	100	100	100	100	100	100	95.7	99.4	100	96.1	99.5	100
	40	100	100	100	99.9	99.9	99.9	99.8	99.9	99.9	92.9	94.9	96.2	90.8	93.7	95.7	99.9	100	100	99.9	100	100	91.1	97.1	99.4	92	97.5	99.5
	50	100	100	100	99.8	99.9	99.9	99.8	99.8	99.9	90.9	92.8	94.3	88	90.6	92.6	99.8	100	100	99.6	100	100	84.7	91.9	96.8	86.1	92.9	97.3
	60	100	100	100	99.8	99.8	99.9	99.7	99.8	99.8	88.8	90.8	92.4	85.5	88	90.1	99.5	99.9	100	99.2	99.9	100	75.7	83.9	90.3	77.7	85.5	91.5
	70	100	100	100	99.7	99.8	99.8	99.6	99.7	99.8	86.7	88.8	90.6	83.3	85.7	88	99.1	99.8	100	98.5	99.6	100	64.6	73.3	81.1	67.3	75.7	83.2
	80	100	100	100	99.6	99.7	99.8	99.5	99.6	99.7	84.3	86.8	88.9	81	83.7	86.2	98.3	99.4	99.9	97.3	98.9	99.7	51.4	62	71.5	54.6	64.8	74.1
	90	100	100	100	99.6	99.7	99.7	99.4	99.6	99.7	81.9	84.8	87.2	78.6	81.6	84.3	97.3	98.8	99.6	95.8	97.9	99.2	38.7	51	61.9	42	54	64.5
	100	100	100	100	99.5	99.6	99.7	99.3	99.5	99.6	79.3	82.6	85.4	75.6	79.2	82.3	95.7	97.7	99	93.3	96.2	98.1	27.8	40.6	53	30.6	43.4	55.6
	110	99.9	100	100	99.4	99.5	99.6	99.2	99.4	99.5	76.7	80.5	83.6	72.6	76.7	80.3	93.7	96.4	98.2	90.6	94.2	96.8	19.2	32.1	44.9	21.4	34.6	47.4
	120	99.9	100	100	99.2	99.4	99.6	98.9	99.3	99.5	74	78.2	82	69.2	74	78.3	91.3	94.7	97.2	87	91.6	95.2	12.7	25	38.4	14.2	27.3	40.8
	130	99.9	99.9	100	99	99.4	99.5	98.7	99.2	99.4	71.2	76	80.6	65.8	71.3	76.6	88.5	92.8	96.2	83.2	88.9	93.6	8.12	19.4	33.9	9.13	21.2	36.1
	140	99.8	99.9	100	98.8	99.3	99.5	98.4	99.1	99.4	68.3	74.1	79.6	62.2	68.9	75.5	85.2	91	95.5	78.9	86.2	92.7	5.46	15.4	30.7	6.17	17	32.9
	150	99.8	99.9	100	98.5	99.2	99.5	98	98.9	99.4	65.2	72	79.2	58.4	66.3	74.9	81.7	88.8	95.3	74.4	83.3	92.3	3.44	12.6	28.2	3.9	13.9	30.2
	≥154	99.8	99.9	100	98.5	99.2	99.5	97.9	98.9	99.4	64.3	71.2	79.1	57.4	65.4	74.9	80.6	88	95.2	73.1	82.3	92.3	3.01	11.2	28.3	3.41	12.4	30.4

[1]Body weight and serum albumin concentration set to median of first study day (i.e. 70 kg and 2.8 g/dL).
[2]According to EUCAST [390].
Colour coding: *Green*: CFR≥90%, *Yellow*: CFR 80-<90%, *Orange*: CFR >50-<80%, *Red*: CFR ≤50%; *Grey shaded values*: Extrapolated creatinine $CLCR_{CG}$ range not covered by the study population or creatinine clearance ≥154 mL/min (=inflection point of $CLCR_{CG}$-CL relationship).
Abbreviations: *CL*: Clearance; *$CLCR_{CG}$*: Creatinine clearance estimated according to Cockcroft and Gault [2]; *MIC*: Minimum inhibitory concentration*; I category*: Category 'susceptible at increased exposure' [4]; *$P_{0.05}$*: 5th percentile; $P_{0.5}$: 50th percentile = median; $P_{0.95}$: 95th percentile, q8h: Every 8 hours; S category: Category 'susceptible at normal dosing' [4]; *$T_{>MIC}$:* Time period that total drug concentration exceeds the MIC.

Table S28: (Project IV): Cumulative fraction of response (CFR, %) for different continuous infusion dosing regimens of meropenem for the first day of treatment (modified from [243]).

PTA is given for varied values of creatinine clearance and for selected MIC values and is presented as the median ($P_{0.5}$), 5th ($P_{0.05}$) and 95th percentile ($P_{0.95}$) of the 1000 PTA values derived from the 1000 Monte Carlo simulations considering PK parameter uncertainty.

Dosing regimen; PK/PD target[3]	$CLCR_{CG}$[1] [mL/min]	Full MIC distribution[2]																MIC distribution of isolates belonging to the S category[2]						MIC distribution of isolates belonging to the I category[2]					
		Escherichia coli			*Klebsiella pneumonia*			*Enterobacter cloacae*			*Pseudomonas aeruginosa*			*Acinetobacter* spp.			*Pseudomonas aeruginosa*			*Acinetobacter* spp.			*Pseudomonas aeruginosa*			*Acinetobacter* spp.		
		$P_{0.05}$	$P_{0.5}$	$P_{0.95}$	$P_{0.05}$	$P_{0.5}$	$P_{0.95}$	$P_{0.05}$	$P_{0.5}$	$P_{0.95}$	$P_{0.05}$	$P_{0.5}$	$P_{0.95}$	$P_{0.05}$	$P_{0.5}$	$P_{0.95}$	$P_{0.05}$	$P_{0.5}$	$P_{0.95}$	$P_{0.05}$	$P_{0.5}$	$P_{0.95}$	$P_{0.05}$	$P_{0.5}$	$P_{0.95}$	$P_{0.05}$	$P_{0.5}$	$P_{0.95}$
CI3 (3000 mg, CI, q24h following 500 mg, 30-min loading dose); 98%$T_{>4xMIC}$	10	100	100	100	99.7	99.7	99.7	99.6	99.6	99.6	85.6	85.9	86	83.3	83.6	83.7	100	100	100	100	100	100	51.1	53.5	54.5	58	60.7	61.6
	20	100	100	100	99.7	99.7	99.7	99.6	99.6	99.6	85.2	85.8	86	83	83.5	83.6	100	100	100	100	100	100	48	52.5	54	54.5	59.6	61.2
	30	100	100	100	99.7	99.7	99.7	99.6	99.6	99.6	84.6	85.5	85.9	82.4	83.2	83.5	100	100	100	100	100	100	42.8	50	53.2	48.5	56.7	60.3
	40	100	100	100	99.6	99.7	99.7	99.6	99.6	99.6	83.8	84.8	85.5	81.8	82.6	83.2	100	100	100	99.9	100	100	36.7	44.4	50	41.7	50.4	56.7
	50	100	100	100	99.6	99.6	99.7	99.5	99.6	99.6	82.8	83.8	84.6	80.9	81.8	82.5	99.9	100	100	99.8	100	100	29	36.3	42.6	32.9	41.2	48.3
	60	100	100	100	99.6	99.6	99.6	99.5	99.5	99.6	81.7	82.7	83.4	79.8	80.8	81.5	99.8	100	100	99.6	99.9	100	20.4	27.3	33.3	23.2	31	37.8
	70	100	100	100	99.5	99.6	99.6	99.5	99.5	99.5	80.4	81.6	82.5	78.6	79.8	80.7	99.5	99.8	100	99	99.7	100	12.1	19	25.4	13.8	21.6	28.8
	80	100	100	100	99.5	99.5	99.6	99.4	99.5	99.5	79.5	80.6	81.6	77.5	78.8	79.9	99.2	99.6	99.9	98.4	99.3	99.8	6.34	12.6	19.3	7.19	14.3	22
	90	100	100	100	99.5	99.5	99.5	99.4	99.5	99.5	78.6	79.8	80.9	76.3	77.8	79.2	98.6	99.3	99.7	97.3	98.6	99.4	2.9	8.01	14.8	3.29	9.08	16.8
	100	100	100	100	99.4	99.5	99.5	99.4	99.4	99.5	77.9	79	80.1	75.1	76.7	78.2	98	98.7	99.3	96.1	97.5	98.7	1.18	5.05	10.7	1.34	5.73	12.2
	110	100	100	100	99.4	99.5	99.5	99.4	99.4	99.4	77.1	78.2	79.4	73.8	75.4	77.1	97.1	98	98.8	94.5	96.2	97.6	0.43	3.01	8.17	0.488	3.41	9.27
	120	100	100	100	99.4	99.4	99.5	99.3	99.4	99.4	76.2	77.4	78.6	72.2	74.1	75.9	96.1	97.2	98.1	92.5	94.7	96.4	0.107	1.83	6.13	0.122	2.07	6.96
	130	100	100	100	99.4	99.4	99.5	99.3	99.3	99.4	75.4	76.6	78	70.6	72.8	75	95	96.4	97.6	90.4	93.1	95.4	0	1.07	4.62	0	1.22	5.24
	140	100	100	100	99.3	99.4	99.4	99.2	99.3	99.4	74.5	76	77.7	68.9	71.6	74.5	93.8	95.6	97.3	88.3	91.6	94.9	0	0.645	3.98	0	0.732	4.52
	150	100	100	100	99.3	99.4	99.4	99.2	99.3	99.4	73.5	75.4	77.6	67.3	70.5	74.3	92.7	94.9	97.3	86.2	90.2	94.8	0	0.537	3.33	0	0.61	3.78
	≥154	100	100	100	99.3	99.4	99.4	99.2	99.3	99.4	73.2	75.1	77.6	66.7	70	74.3	92.3	94.6	97.3	85.4	89.6	94.7	0	0.43	3.22	0	0.488	3.66
CI3 (3000 mg, CI, q24h following 500 mg, 30-min loading dose); 98%$T_{>1xMIC}$	10	100	100	100	100	100	100	100	100	100	98.1	98.4	98.5	99.3	99.8	99.9	100	100	100	100	100	100	100	100	100	100	100	100
	20	100	100	100	100	100	100	100	100	100	97.7	98.3	98.5	98.5	99.6	99.9	100	100	100	100	100	100	100	100	100	100	100	100
	30	100	100	100	99.9	100	100	99.9	100	100	97.1	98	98.4	97.3	99	99.7	100	100	100	100	100	100	99.9	100	100	99.9	100	100
	40	100	100	100	99.9	99.9	100	99.9	99.9	100	96.3	97.3	98	95.8	97.7	99	100	100	100	100	100	100	99.8	100	100	99.8	100	100
	50	100	100	100	99.9	99.9	99.9	99.9	99.9	99.9	95.3	96.2	97	94	95.8	97.2	100	100	100	100	100	100	99.5	100	100	99.6	100	100
	60	100	100	100	99.9	99.9	99.9	99.9	99.9	99.9	94.1	95.1	95.9	91.9	93.6	95	100	100	100	100	100	100	99.1	99.8	100	99.2	99.8	100
	70	100	100	100	99.9	99.9	99.9	99.8	99.9	99.9	92.9	94	94.8	89.9	91.6	93.2	100	100	100	100	100	100	98	99.4	100	98.3	99.5	100
	80	100	100	100	99.9	99.9	99.9	99.8	99.8	99.9	92	93	94	88.4	90	91.7	100	100	100	100	100	100	96.6	98.5	99.6	97.1	98.8	99.7
	90	100	100	100	99.8	99.9	99.9	99.8	99.8	99.8	91.3	92.3	93.3	87.4	88.8	90.6	100	100	100	100	100	100	94.3	97	98.8	95.2	97.5	99
	100	100	100	100	99.8	99.8	99.9	99.8	99.8	99.8	90.7	91.6	92.6	86.8	87.9	89.5	100	100	100	100	100	100	91.7	94.8	97.2	93	95.6	97.7
	110	100	100	100	99.8	99.8	99.8	99.8	99.8	99.8	90.2	91	92	86.3	87.2	88.7	100	100	100	100	100	100	88.3	92	95	90.1	93.3	95.8
	120	100	100	100	99.8	99.8	99.8	99.7	99.8	99.8	89.7	90.5	91.5	85.9	86.7	88	100	100	100	100	100	100	84.1	88.8	92.4	86.5	90.6	93.6
	130	100	100	100	99.8	99.8	99.8	99.7	99.7	99.8	89.1	89.9	91	85.6	86.3	87.5	100	100	100	100	100	100	79.8	85.4	90.3	82.8	87.6	91.8
	140	100	100	100	99.8	99.8	99.8	99.7	99.7	99.8	88.6	89.5	90.8	85.2	85.9	87.3	100	100	100	100	100	100	75.3	82.3	89.2	78.9	85	90.9
	150	100	100	100	99.8	99.8	99.8	99.7	99.7	99.8	88	89.1	90.7	84.9	85.7	87.1	100	100	100	100	100	100	70.8	79.3	89	75	82.5	90.7
	≥154	100	100	100	99.7	99.8	99.8	99.7	99.7	99.8	87.8	89	90.6	84.8	85.6	87.1	100	100	100	100	100	100	69.2	78.1	88.8	73.6	81.4	90.6
CI6 (6000 mg, CI, q24h following 1000 mg, 30-min loading dose) 98%$T_{>4xMIC}$	10	100	100	100	99.8	99.8	99.8	99.8	99.8	99.8	91.3	91.6	91.7	87	87.1	87.4	100	100	100	100	100	100	97.6	99.7	100	98	99.8	100
	20	100	100	100	99.8	99.8	99.8	99.8	99.8	99.8	91	91.5	91.6	86.8	87.1	87.2	100	100	100	100	100	100	95	99	100	95.8	99.1	100
	30	100	100	100	99.8	99.8	99.8	99.8	99.8	99.8	90.5	91.2	91.5	86.4	86.9	87.1	100	100	100	100	100	100	90.6	96.8	99.4	92.1	97.3	99.5
	40	100	100	100	99.8	99.8	99.8	99.7	99.8	99.8	89.7	90.6	91.2	86	86.5	86.9	100	100	100	100	100	100	84.9	91.9	96.8	87.2	93.2	97.3
	50	100	100	100	99.8	99.8	99.8	99.7	99.7	99.8	88.9	89.7	90.4	85.4	86	86.4	100	100	100	100	100	100	77.9	84.9	90.4	81.2	87.3	91.9
	60	100	100	100	99.8	99.8	99.8	99.7	99.7	99.7	87.9	88.8	89.5	84.8	85.4	85.8	100	100	100	100	100	100	70.1	77	82.5	74.5	80.5	85.2
	70	100	100	100	99.7	99.7	99.8	99.7	99.7	99.7	86.9	87.8	88.6	84.2	84.8	85.3	100	100	100	100	100	100	61.9	69.3	75.5	67.2	73.8	79.3
	80	100	100	100	99.7	99.7	99.8	99.6	99.7	99.7	86.1	87.1	87.9	83.6	84.3	84.8	100	100	100	100	100	100	55.3	62.9	69.7	61.2	68.2	74.3
	90	100	100	100	99.7	99.7	99.7	99.6	99.6	99.7	85.4	86.4	87.3	83.1	83.8	84.4	100	100	100	100	100	100	49.8	57.3	64.8	55.8	63	69.9
	100	100	100	100	99.7	99.7	99.7	99.6	99.6	99.6	84.9	85.7	86.7	82.7	83.3	84	100	100	100	100	100	100	45.1	51.9	59.9	50.9	57.7	65.2
	110	100	100	100	99.6	99.7	99.7	99.6	99.6	99.6	84.3	85.1	86	82.2	82.8	83.5	100	100	100	99.9	100	100	40.5	47	54.7	45.8	52.5	60
	120	100	100	100	99.6	99.7	99.7	99.6	99.6	99.6	83.7	84.5	85.5	81.7	82.4	83.1	99.9	100	100	99.9	100	100	35.9	42.3	50.5	40.7	47.5	55.8
	130	100	100	100	99.6	99.6	99.7	99.5	99.6	99.6	83	84	85.1	81.1	81.9	82.8	99.9	100	100	99.8	100	100	30.8	37.9	46.8	35	42.7	51.9
	140	100	100	100	99.6	99.6	99.7	99.5	99.6	99.6	82.4	83.5	84.8	80.5	81.5	82.5	99.8	100	100	99.7	100	100	26.1	33.7	44.3	29.6	38.1	F
	150	100	100	100	99.6	99.6	99.7	99.5	99.5	99.6	81.7	83	84.7	79.9	81.1	82.5	99.7	100	100	99.5	99.9	100	21.1	30.4	43.8	23.9	34.3	48.9
	≥154	100	100	100	99.6	99.6	99.7	99.5	99.5	99.6	81.5	82.9	84.7	79.7	80.9	82.5	99.7	99.9	100	99.5	99.9	100	19.4	29.1	43.8	22.1	32.9	48.9
CI6 (6000 mg, CI, q24h following 1000 mg, 30-min loading dose) 98%$T_{>1xMIC}$	10	100	100	100	100	100	100	100	100	100	99.1	99.1	99.2	100	100	100	100	100	100	100	100	100	100	100	100	100	100	100
	20	100	100	100	100	100	100	100	100	100	99.1	99.1	99.2	100	100	100	100	100	100	100	100	100	100	100	100	100	100	100	100
	30	100	100	100	100	100	100	100	100	100	99	99.1	99.1	99.9	100	100	100	100	100	100	100	100	100	100	100	100	100	100	100
	40	100	100	100	100	100	100	100	100	100	98.9	99	99.1	99.9	100	100	100	100	100	100	100	100	100	100	100	100	100	100	100
	50	100	100	100	100	100	100	100	100	100	98.8	98.9	99	99.8	100	100	100	100	100	100	100	100	100	100	100	100	100	100	100
	60	100	100	100	100	100	100	100	100	100	98.6	98.8	98.9	99.6	99.9	99.9	100	100	100	100	100	100	100	100	100	100	100	100	100
	70	100	100	100	100	100	100	100	100	100	98.3	98.6	98.8	99.3	99.7	99.9	100	100	100	100	100	100	100	100	100	100	100	100	100
	80	100	100	100	100	100	100	100	100	100	98.1	98.4	98.7	99	99.5	99.8	100	100	100	100	100	100	100	100	100	100	100	100	100
	90	100	100	100	100	100	100	100	100	100	97.7	98.1	98.5	98.4	99.1	99.6	100	100	100	100	100	100	99.9	100	100	99.9	100	100
	100	100	100	100	99.9	100	100	99.9	100	100	97.2	97.8	98.2	97.6	98.5	99.2	100	100	100	100	100	100	99.9	100	100	99.9	100	100
	110	100	100	100	99.9	100	100	99.9	99.9	100	96.7	97.3	97.8	96.6	97.7	98.5	100	100	100	100	100	100	99.8	100	100	99.8	100	100
	120	100	100	100	99.9	99.9	100	99.9	99.9	99.9	96.1	96.8	97.5	95.6	96.8	97.9	100	100	100	100	100	100	99.7	100	100	99.8	100	100
	130	100	100	100	99.9	99.9	99.9	99.9	99.9	99.9	95.5	96.3	97.1	94.4	95.9	97.2	100	100	100	100	100	100	99.5	99.9	100	99.6	99.9	100
	140	100	100	100	99.9	99.9	99.9	99.9	99.9	99.9	94.9	95.8	96.9	93.3	95	96.9	100	100	100	100	100	100	99.4	99.9	100	99.5	99.9	100
	150	100	100	100	99.9	99.9	99.9	99.9	99.9	99.9	94.2	95.4	96.9	92.1	94.2	96.9	100	100	100	100	100	100	99	99.8	100	99.1	99.8	100

[1]Body weight and serum albumin concentration fixed to median of first study day (i.e. 70 kg and 2.8 g/dL). [2]According to EUCAST [390]; [3]PTA for the target 98%$T_{>4xMIC}$ was derived by shifting the results for the target 98%$T_{>MIC}$ two MIC values to the left. ***Colour coding***: *Green*: CFR≥90%, *Yellow*: CFR 80-<90%, *Orange*: CFR >50-<80%, *Red*: CFR ≤50%; *Grey shaded values*: Extrapolated creatinine $CLCR_{CG}$ range not covered by the study population or creatinine clearance ≥154 mL/min (=inflection point of $CLCR_{CG}$-CL relationship). ***Abbreviations***: $T_{>4xMIC}$: Time period that total drug concentration exceeds four times the MIC; Further abbreviation see Table S27.

Table S29: (Project IV) Comparison of selected dosing regimens based on PTA[a] analyses (A) considering versus (B) not considering uncertainty in the pharmacokinetic parameters in underlying simulations (modified from [243]).

CLCR$_{CG}$[e] [mL/min]	MIC [mg/L]																																						
	0.004			0.008			0.015			0.03			0.06			0.12			0.25			0.5			1			2			4			8			16		
	SI	PI	CI	SI	PI	CI	SI	PI	CI	SI	PI	CI	SI	PI	CI	SI	PI	CI	SI	PI	CI	SI	PI	CI	SI	PI	CI	SI	PI	CI	SI	PI	CI	SI	PI	CI	SI	PI	CI
A: Dosing regimens selected based on PTA analyses **considering** PK parameter uncertainty[b]																																							
10	SI2$_{12}$	PI2$_{12}$	CI3^{c}	SI2$_{12}$	PI2$_{12}$	CI3^{c}	SI2$_{12}$	PI2$_{12}$	CI3^{c}	SI2$_{12}$	PI2$_{12}$	CI3^{c}	SI2$_{12}$	PI2$_{12}$	CI3^{c}	SI2$_{12}$	PI2$_{12}$	CI3^{c}	SI2$_{12}$	PI2$_{12}$	CI3^{c}	SI2$_{12}$	PI2$_{12}$	CI3^{c}	SI2$_{12}$	PI2$_{12}$	CI3^{c}	SI2$_{12}$	PI2$_{12}$	CI3^{c}	**SI3$_{8}$**	PI3$_{8}$	CI3^{c}	SI6$_{8}$	PI6$_{8}$	CI6^{d}	--	--	-
20	SI2$_{12}$	PI2$_{12}$	CI3^{c}	SI2$_{12}$	PI2$_{12}$	CI3^{c}	SI2$_{12}$	PI2$_{12}$	CI3^{c}	SI2$_{12}$	PI2$_{12}$	CI3^{c}	SI2$_{12}$	PI2$_{12}$	CI3^{c}	SI2$_{12}$	PI2$_{12}$	CI3^{c}	SI2$_{12}$	PI2$_{12}$	CI3^{c}	SI2$_{12}$	PI2$_{12}$	CI3^{c}	SI2$_{12}$	PI2$_{12}$	CI3^{c}	**SI3$_{8}$**	PI3$_{8}$	CI3^{c}	**SI3$_{8}$**	PI3$_{8}$	CI6^{d}	SI6$_{8}$	PI6$_{8}$	--	-	-	-
30	SI2$_{12}$	PI2$_{12}$	CI3^{c}	SI2$_{12}$	PI2$_{12}$	CI3^{c}	SI2$_{12}$	PI2$_{12}$	CI3^{c}	SI2$_{12}$	PI2$_{12}$	CI3^{c}	SI2$_{12}$	PI2$_{12}$	CI3^{c}	SI2$_{12}$	PI2$_{12}$	CI3^{c}	SI2$_{12}$	PI2$_{12}$	CI3^{c}	SI2$_{12}$	PI2$_{12}$	CI3^{c}	**SI3$_{8}$**	PI2$_{12}$	CI3^{c}	**SI3$_{8}$**	PI3$_{8}$	CI3^{c}	SI6$_{8}$	PI3$_{8}$	CI6^{d}	--	PI6$_{8}$	--	-	-	-
40	SI2$_{12}$	PI2$_{12}$	CI3^{c}	SI2$_{12}$	PI2$_{12}$	CI3^{c}	SI2$_{12}$	PI2$_{12}$	CI3^{c}	SI2$_{12}$	PI2$_{12}$	CI3^{c}	SI2$_{12}$	PI2$_{12}$	CI3^{c}	SI2$_{12}$	PI2$_{12}$	CI3^{c}	SI2$_{12}$	PI2$_{12}$	CI3^{c}	SI2$_{12}$	PI2$_{12}$	CI3^{c}	**SI3$_{8}$**	PI3$_{8}$	CI3^{c}	**SI3$_{8}$**	PI3$_{8}$	CI3^{c}	SI6$_{8}$	PI6$_{8}$	CI6^{d}	-	--	-	-	-	-
50	SI2$_{12}$	PI2$_{12}$	CI3^{c}	SI2$_{12}$	PI2$_{12}$	CI3^{c}	SI2$_{12}$	PI2$_{12}$	CI3^{c}	SI2$_{12}$	PI2$_{12}$	CI3^{c}	SI2$_{12}$	PI2$_{12}$	CI3^{c}	SI2$_{12}$	PI2$_{12}$	CI3^{c}	SI2$_{12}$	PI2$_{12}$	CI3^{c}	**SI3$_{8}$**	PI2$_{12}$	CI3^{c}	**SI3$_{8}$**	PI3$_{8}$	CI3^{c}	SI6$_{8}$	PI3$_{8}$	CI3^{c}	--	PI6$_{8}$	CI6^{d}	-	-	-	-	-	-
60	SI2$_{12}$	PI2$_{12}$	CI3^{c}	SI2$_{12}$	PI2$_{12}$	CI3^{c}	SI2$_{12}$	PI2$_{12}$	CI3^{c}	SI2$_{12}$	PI2$_{12}$	CI3^{c}	SI2$_{12}$	PI2$_{12}$	CI3^{c}	SI2$_{12}$	PI2$_{12}$	CI3^{c}	**SI3$_{8}$**	PI2$_{12}$	CI3^{c}	**SI3$_{8}$**	PI3$_{8}$	CI3^{c}	**SI3$_{8}$**	PI3$_{8}$	CI3^{c}	SI6$_{8}$	PI6$_{8}$	CI3^{c}	-	--	CI6^{d}	-	-	-	-	-	-
70	SI2$_{12}$	PI2$_{12}$	CI3^{c}	SI2$_{12}$	PI2$_{12}$	CI3^{c}	SI2$_{12}$	PI2$_{12}$	CI3^{c}	SI2$_{12}$	PI2$_{12}$	CI3^{c}	SI2$_{12}$	PI2$_{12}$	CI3^{c}	**SI3$_{8}$**	PI2$_{12}$	CI3^{c}	**SI3$_{8}$**	PI3$_{8}$	CI3^{c}	**SI3$_{8}$**	PI3$_{8}$	CI3^{c}	SI6$_{8}$	PI3$_{8}$	CI3^{c}	--	PI6$_{8}$	CI3^{c}	-	-	CI6^{d}	-	-	-	-	-	-
80	SI2$_{12}$	PI2$_{12}$	CI3^{c}	SI2$_{12}$	PI2$_{12}$	CI3^{c}	SI2$_{12}$	PI2$_{12}$	CI3^{c}	SI2$_{12}$	PI2$_{12}$	CI3^{c}	SI2$_{12}$	PI2$_{12}$	CI3^{c}	**SI3$_{8}$**	PI2$_{12}$	CI3^{c}	**SI3$_{8}$**	PI3$_{8}$	CI3^{c}	**SI3$_{8}$**	PI3$_{8}$	CI3^{c}	SI6$_{8}$	PI3$_{8}$	CI3^{c}	-	PI6$_{8}$	CI3^{c}	-	-	CI6^{d}	-	-	-	-	-	-
90	SI2$_{12}$	PI2$_{12}$	CI3^{c}	SI2$_{12}$	PI2$_{12}$	CI3^{c}	SI2$_{12}$	PI2$_{12}$	CI3^{c}	SI2$_{12}$	PI2$_{12}$	CI3^{c}	**SI3$_{8}$**	PI2$_{12}$	CI3^{c}	**SI3$_{8}$**	PI3$_{8}$	CI3^{c}	**SI3$_{8}$**	PI3$_{8}$	CI3^{c}	SI6$_{8}$	PI3$_{8}$	CI3^{c}	--	PI6$_{8}$	CI3^{c}	-	--	CI6^{d}	-	-	--	-	-	-	-	-	-
100	SI2$_{12}$	PI2$_{12}$	CI3^{c}	SI2$_{12}$	PI2$_{12}$	CI3^{c}	SI2$_{12}$	PI2$_{12}$	CI3^{c}	**SI3$_{8}$**	PI2$_{12}$	CI3^{c}	**SI3$_{8}$**	PI2$_{12}$	CI3^{c}	**SI3$_{8}$**	PI3$_{8}$	CI3^{c}	**SI3$_{8}$**	PI3$_{8}$	CI3^{c}	SI6$_{8}$	PI3$_{8}$	CI3^{c}	-	PI6$_{8}$	CI3^{c}	-	-	CI6^{d}	-	-	-	-	-	-	-	-	-
110	SI2$_{12}$	PI2$_{12}$	CI3^{c}	SI2$_{12}$	PI2$_{12}$	CI3^{c}	SI2$_{12}$	PI2$_{12}$	CI3^{c}	**SI3$_{8}$**	PI2$_{12}$	CI3^{c}	**SI3$_{8}$**	PI3$_{8}$	CI3^{c}	**SI3$_{8}$**	PI3$_{8}$	CI3^{c}	SI6$_{8}$	PI3$_{8}$	CI3^{c}	--	PI6$_{8}$	CI3^{c}	-	--	CI3^{c}	-	-	CI6^{d}	-	-	-	-	-	-	-	-	-
120	SI2$_{12}$	PI2$_{12}$	CI3^{c}	SI2$_{12}$	PI2$_{12}$	CI3^{c}	**SI3$_{8}$**	PI2$_{12}$	CI3^{c}	**SI3$_{8}$**	PI3$_{8}$	CI3^{c}	**SI3$_{8}$**	PI3$_{8}$	CI3^{c}	**SI3$_{8}$**	PI3$_{8}$	CI3^{c}	SI6$_{8}$	PI3$_{8}$	CI3^{c}	-	PI6$_{8}$	CI3^{c}	-	--	CI3^{c}	-	-	CI6^{d}	-	-	-	-	-	-	-	-	-
130	SI2$_{12}$	PI2$_{12}$	CI3^{c}	**SI3$_{8}$**	PI2$_{12}$	CI3^{c}	**SI3$_{8}$**	PI2$_{12}$	CI3^{c}	**SI3$_{8}$**	PI3$_{8}$	CI3^{c}	**SI3$_{8}$**	PI3$_{8}$	CI3^{c}	SI6$_{8}$	PI3$_{8}$	CI3^{c}	--	PI3$_{8}$	CI3^{c}	-	PI6$_{8}$	CI3^{c}	-	-	CI3^{c}	-	-	CI6^{d}	-	-	-	-	-	-	-	-	-
140	SI2$_{12}$	PI2$_{12}$	CI3^{c}	**SI3$_{8}$**	PI2$_{12}$	CI3^{c}	**SI3$_{8}$**	PI2$_{12}$	CI3^{c}	**SI3$_{8}$**	PI3$_{8}$	CI3^{c}	**SI3$_{8}$**	PI3$_{8}$	CI3^{c}	SI6$_{8}$	PI3$_{8}$	CI3^{c}	-	PI3$_{8}$	CI3^{c}	-	PI6$_{8}$	CI3^{c}	-	-	CI3^{c}	-	-	CI6^{d}	-	-	-	-	-	-	-	-	-
150	**SI3$_{8}$**	PI2$_{12}$	CI3^{c}	**SI3$_{8}$**	PI2$_{12}$	CI3^{c}	**SI3$_{8}$**	PI3$_{8}$	CI3^{c}	**SI3$_{8}$**	PI3$_{8}$	CI3^{c}	**SI3$_{8}$**	PI3$_{8}$	CI3^{c}	SI6$_{8}$	PI3$_{8}$	CI3^{c}	-	PI6$_{8}$	CI3^{c}	-	--	CI3^{c}	-	-	CI3^{c}	-	-	CI6^{d}	-	-	-	-	-	-	-	-	-
≥154	**SI3$_{8}$**	PI2$_{12}$	CI3^{c}	**SI3$_{8}$**	PI2$_{12}$	CI3^{c}	**SI3$_{8}$**	PI3$_{8}$	CI3^{c}	**SI3$_{8}$**	PI3$_{8}$	CI3^{c}	**SI3$_{8}$**	PI3$_{8}$	CI3^{c}	--	PI3$_{8}$	CI3^{c}	-	PI6$_{8}$	CI3^{c}	-	--	CI3^{c}	-	-	CI3^{c}	-	-	CI6^{d}	-	-	-	-	-	-	-	-	-
B: Dosing regimens selected based on PTA analyses **not considering** PK parameter uncertainty[b]																																							
10	SI2$_{12}$	PI2$_{12}$	CI3^{c}	SI2$_{12}$	PI2$_{12}$	CI3^{c}	SI2$_{12}$	PI2$_{12}$	CI3^{c}	SI2$_{12}$	PI2$_{12}$	CI3^{c}	SI2$_{12}$	PI2$_{12}$	CI3^{c}	SI2$_{12}$	PI2$_{12}$	CI3^{c}	SI2$_{12}$	PI2$_{12}$	CI3^{c}	SI2$_{12}$	PI2$_{12}$	CI3^{c}	SI2$_{12}$	PI2$_{12}$	CI3^{c}	SI2$_{12}$	PI2$_{12}$	CI3^{c}	SI2$_{12}$	PI2$_{12}$	CI3^{c}	**SI3$_{8}$**	PI3$_{8}$	CI6^{d}	SI6$_{8}$	PI6$_{8}$	-
20	SI2$_{12}$	PI2$_{12}$	CI3^{c}	SI2$_{12}$	PI2$_{12}$	CI3^{c}	SI2$_{12}$	PI2$_{12}$	CI3^{c}	SI2$_{12}$	PI2$_{12}$	CI3^{c}	SI2$_{12}$	PI2$_{12}$	CI3^{c}	SI2$_{12}$	PI2$_{12}$	CI3^{c}	SI2$_{12}$	PI2$_{12}$	CI3^{c}	SI2$_{12}$	PI2$_{12}$	CI3^{c}	SI2$_{12}$	PI2$_{12}$	CI3^{c}	SI2$_{12}$	PI2$_{12}$	CI3^{c}	**SI3$_{8}$**	PI3$_{8}$	CI3^{c}	SI6$_{8}$	PI6$_{8}$	CI6^{d}	-	-	-
30	SI2$_{12}$	PI2$_{12}$	CI3^{c}	SI2$_{12}$	PI2$_{12}$	CI3^{c}	SI2$_{12}$	PI2$_{12}$	CI3^{c}	SI2$_{12}$	PI2$_{12}$	CI3^{c}	SI2$_{12}$	PI2$_{12}$	CI3^{c}	SI2$_{12}$	PI2$_{12}$	CI3^{c}	SI2$_{12}$	PI2$_{12}$	CI3^{c}	SI2$_{12}$	PI2$_{12}$	CI3^{c}	SI2$_{12}$	PI2$_{12}$	CI3^{c}	**SI3$_{8}$**	PI2$_{12}$	CI3^{c}	**SI3$_{8}$**	PI3$_{8}$	CI3^{c}	SI6$_{8}$	PI6$_{8}$	CI6^{d}	-	-	-
40	SI2$_{12}$	PI2$_{12}$	CI3^{c}	SI2$_{12}$	PI2$_{12}$	CI3^{c}	SI2$_{12}$	PI2$_{12}$	CI3^{c}	SI2$_{12}$	PI2$_{12}$	CI3^{c}	SI2$_{12}$	PI2$_{12}$	CI3^{c}	SI2$_{12}$	PI2$_{12}$	CI3^{c}	SI2$_{12}$	PI2$_{12}$	CI3^{c}	SI2$_{12}$	PI2$_{12}$	CI3^{c}	**SI3$_{8}$**	PI2$_{12}$	CI3^{c}	**SI3$_{8}$**	PI3$_{8}$	CI3^{c}	SI6$_{8}$	PI3$_{8}$	CI6^{d}	-	PI6$_{8}$	-	-	-	-
50	SI2$_{12}$	PI2$_{12}$	CI3^{c}	SI2$_{12}$	PI2$_{12}$	CI3^{c}	SI2$_{12}$	PI2$_{12}$	CI3^{c}	SI2$_{12}$	PI2$_{12}$	CI3^{c}	SI2$_{12}$	PI2$_{12}$	CI3^{c}	SI2$_{12}$	PI2$_{12}$	CI3^{c}	SI2$_{12}$	PI2$_{12}$	CI3^{c}	SI2$_{12}$	PI2$_{12}$	CI3^{c}	**SI3$_{8}$**	PI3$_{8}$	CI3^{c}	**SI3$_{8}$**	PI3$_{8}$	CI3^{c}	SI6$_{8}$	PI6$_{8}$	CI6^{d}	-	-	-	-	-	-
60	SI2$_{12}$	PI2$_{12}$	CI3^{c}	SI2$_{12}$	PI2$_{12}$	CI3^{c}	SI2$_{12}$	PI2$_{12}$	CI3^{c}	SI2$_{12}$	PI2$_{12}$	CI3^{c}	SI2$_{12}$	PI2$_{12}$	CI3^{c}	SI2$_{12}$	PI2$_{12}$	CI3^{c}	SI2$_{12}$	PI2$_{12}$	CI3^{c}	**SI3$_{8}$**	PI2$_{12}$	CI3^{c}	**SI3$_{8}$**	PI3$_{8}$	CI3^{c}	SI6$_{8}$	PI3$_{8}$	CI3^{c}	-	PI6$_{8}$	CI6^{d}	-	-	-	-	-	-
70	SI2$_{12}$	PI2$_{12}$	CI3^{c}	SI2$_{12}$	PI2$_{12}$	CI3^{c}	SI2$_{12}$	PI2$_{12}$	CI3^{c}	SI2$_{12}$	PI2$_{12}$	CI3^{c}	SI2$_{12}$	PI2$_{12}$	CI3^{c}	SI2$_{12}$	PI2$_{12}$	CI3^{c}	**SI3$_{8}$**	PI2$_{12}$	CI3^{c}	**SI3$_{8}$**	PI3$_{8}$	CI3^{c}	**SI3$_{8}$**	PI3$_{8}$	CI3^{c}	SI6$_{8}$	PI6$_{8}$	CI3^{c}	-	-	CI6^{d}	-	-	-	-	-	-
80	SI2$_{12}$	PI2$_{12}$	CI3^{c}	SI2$_{12}$	PI2$_{12}$	CI3^{c}	SI2$_{12}$	PI2$_{12}$	CI3^{c}	SI2$_{12}$	PI2$_{12}$	CI3^{c}	SI2$_{12}$	PI2$_{12}$	CI3^{c}	**SI3$_{8}$**	PI2$_{12}$	CI3^{c}	**SI3$_{8}$**	PI3$_{8}$	CI3^{c}	**SI3$_{8}$**	PI3$_{8}$	CI3^{c}	SI6$_{8}$	PI3$_{8}$	CI3^{c}	-	PI6$_{8}$	CI3^{c}	-	-	CI6^{d}	-	-	-	-	-	-
90	SI2$_{12}$	PI2$_{12}$	CI3^{c}	SI2$_{12}$	PI2$_{12}$	CI3^{c}	SI2$_{12}$	PI2$_{12}$	CI3^{c}	SI2$_{12}$	PI2$_{12}$	CI3^{c}	SI2$_{12}$	PI2$_{12}$	CI3^{c}	**SI3$_{8}$**	PI2$_{12}$	CI3^{c}	**SI3$_{8}$**	PI3$_{8}$	CI3^{c}	**SI3$_{8}$**	PI3$_{8}$	CI3^{c}	SI6$_{8}$	PI3$_{8}$	CI3^{c}	-	PI6$_{8}$	CI3^{c}	-	-	CI6^{d}	-	-	-	-	-	-
100	SI2$_{12}$	PI2$_{12}$	CI3^{c}	SI2$_{12}$	PI2$_{12}$	CI3^{c}	SI2$_{12}$	PI2$_{12}$	CI3^{c}	SI2$_{12}$	PI2$_{12}$	CI3^{c}	**SI3$_{8}$**	PI2$_{12}$	CI3^{c}	**SI3$_{8}$**	PI3$_{8}$	CI3^{c}	**SI3$_{8}$**	PI3$_{8}$	CI3^{c}	SI6$_{8}$	PI3$_{8}$	CI3^{c}	-	PI6$_{8}$	CI3^{c}	-	-	CI6^{d}	-	-	-	-	-	-	-	-	-
110	SI2$_{12}$	PI2$_{12}$	CI3^{c}	SI2$_{12}$	PI2$_{12}$	CI3^{c}	SI2$_{12}$	PI2$_{12}$	CI3^{c}	SI2$_{12}$	PI2$_{12}$	CI3^{c}	**SI3$_{8}$**	PI2$_{12}$	CI3^{c}	**SI3$_{8}$**	PI3$_{8}$	CI3^{c}	**SI3$_{8}$**	PI3$_{8}$	CI3^{c}	SI6$_{8}$	PI3$_{8}$	CI3^{c}	-	PI6$_{8}$	CI3^{c}	-	-	CI6^{d}	-	-	-	-	-	-	-	-	-
120	SI2$_{12}$	PI2$_{12}$	CI3^{c}	SI2$_{12}$	PI2$_{12}$	CI3^{c}	SI2$_{12}$	PI2$_{12}$	CI3^{c}	**SI3$_{8}$**	PI2$_{12}$	CI3^{c}	**SI3$_{8}$**	PI3$_{8}$	CI3^{c}	**SI3$_{8}$**	PI3$_{8}$	CI3^{c}	SI6$_{8}$	PI3$_{8}$	CI3^{c}	-	PI3$_{8}$	CI3^{c}	-	PI6$_{8}$	CI3^{c}	-	-	CI6^{d}	-	-	-	-	-	-	-	-	-
130	SI2$_{12}$	PI2$_{12}$	CI3^{c}	SI2$_{12}$	PI2$_{12}$	CI3^{c}	**SI3$_{8}$**	PI2$_{12}$	CI3^{c}	**SI3$_{8}$**	PI2$_{12}$	CI3^{c}	**SI3$_{8}$**	PI3$_{8}$	CI3^{c}	**SI3$_{8}$**	PI3$_{8}$	CI3^{c}	SI6$_{8}$	PI3$_{8}$	CI3^{c}	-	PI6$_{8}$	CI3^{c}	-	-	CI3^{c}	-	-	CI6^{d}	-	-	-	-	-	-	-	-	-
140	SI2$_{12}$	PI2$_{12}$	CI3^{c}	SI2$_{12}$	PI2$_{12}$	CI3^{c}	**SI3$_{8}$**	PI2$_{12}$	CI3^{c}	**SI3$_{8}$**	PI3$_{8}$	CI3^{c}	**SI3$_{8}$**	PI3$_{8}$	CI3^{c}	**SI3$_{8}$**	PI3$_{8}$	CI3^{c}	SI6$_{8}$	PI3$_{8}$	CI3^{c}	-	PI6$_{8}$	CI3^{c}	-	-	CI3^{c}	-	-	CI6^{d}	-	-	-	-	-	-	-	-	-
150	SI2$_{12}$	PI2$_{12}$	CI3^{c}	**SI3$_{8}$**	PI2$_{12}$	CI3^{c}	**SI3$_{8}$**	PI2$_{12}$	CI3^{c}	**SI3$_{8}$**	PI3$_{8}$	CI3^{c}	**SI3$_{8}$**	PI3$_{8}$	CI3^{c}	SI6$_{8}$	PI3$_{8}$	CI3^{c}	-	PI3$_{8}$	CI3^{c}	-	PI6$_{8}$	CI3^{c}	-	-	CI3^{c}	-	-	CI6^{d}	-	-	-	-	-	-	-	-	-
≥154	SI2$_{12}$	PI2$_{12}$	CI3^{c}	**SI3$_{8}$**	PI2$_{12}$	CI3^{c}	**SI3$_{8}$**	PI2$_{12}$	CI3^{c}	**SI3$_{8}$**	PI3$_{8}$	CI3^{c}	**SI3$_{8}$**	PI3$_{8}$	CI3^{c}	SI6$_{8}$	PI3$_{8}$	CI3^{c}	-	PI3$_{8}$	CI3^{c}	-	PI6$_{8}$	CI3^{c}	-	-	CI3^{c}	-	-	CI6^{d}	-	-	-	-	-	-	-	-	-

[a]For SI and PI the PK/PD target 98%$T_{>MIC}$ was evaluated, for CI 98%$T_{>4xMIC}$. [b]Lowest possible dosing regimen for which the 5[th] percentile of the 1000 Monte Carlo simulations considering PK parameter uncertainty achieved PTA≥90% (A); Lowest possible dosing regimen for which the 50[th] percentile (=median) of the 1000 Monte Carlo simulations considering PK parameter uncertainty (comparable to PTA not considering PK parameter uncertainty) achieved PTA≥90% (B). [c]For first day of treatment: Daily dose of 3412.5 mg incl. loading dose. [d]For first day of treatment: Daily dose of 6875 mg incl. loading dose. [e]Body weight and albumin fixed to median of first study day (i.e. 70 kg and 2.8 g/dL).

Grey shaded areas: Extrapolated covariate range not covered by the study population or $CLCR_{CG}$ ≥154 mL/min (=inflection point of $CLCR_{CG}$-CL relationship). *Blue shaded areas*: Differences between dosing regimens suggested based on PTA analyses considering PK parameter uncertainty (A) and dosing regimens suggested based on PTA analyses not considering PK parameter uncertainty (B). ***Dosing regimens***: *SI2$_{12}$*: 1000 mg, 30-min i.v. infusion, q12h; *SI3$_{8}$*: 1000 mg, 30-min i.v. infusion, q8h (=standard dosing; highlighted in bold); *SI6$_{8}$*: 2000 mg, 30-min i.v. infusion, q8h; *PI2$_{12}$*: 1000 mg, 3-h i.v. infusion, q12h; *PI3$_{8}$*: 1000 mg, 3-h i.v. infusion, q8h; *PI6$_{8}$*: 2000 mg, 3-h i.v. infusion, q8h; *CI3*: 3000 mg, CI, q24h following 500 mg, 30-min loading dose; *CI6*: 6000 mg, CI, q24h following 1000 mg, 30-min loading dose. ***Colour coding***: *light blue*: Daily dose of 2000 mg; *blue*: Daily dose of 3000 mg (3412.5 mg for first day of CI, incl. loading dose); *pink*: Daily dose of 6000 mg (6875 mg for first day of CI, incl. loading dose). ***Abbreviations***: *$CLCR_{CG}$*: Creatinine clearance estimated according to Cockcroft and Gault [2]; *h*: Hours; *MIC*: Minimum inhibitory concentration; *min*: Minutes; *PI*: Prolonged infusion; *PK*: Pharmacokinetics; *PTA*: Probability of target attainment; *SI*: Short-term infusion; *q8h*: Every 8 hours; *q12h*: Every 12 hours; *q24h*: Every 24 hours; *$T_{>MIC}$:* Time period that total drug concentration exceeds the MIC; *$T_{>4xMIC}$:* Time period that total drug concentration exceeds four times the MIC.

7.2 Supplementary figures

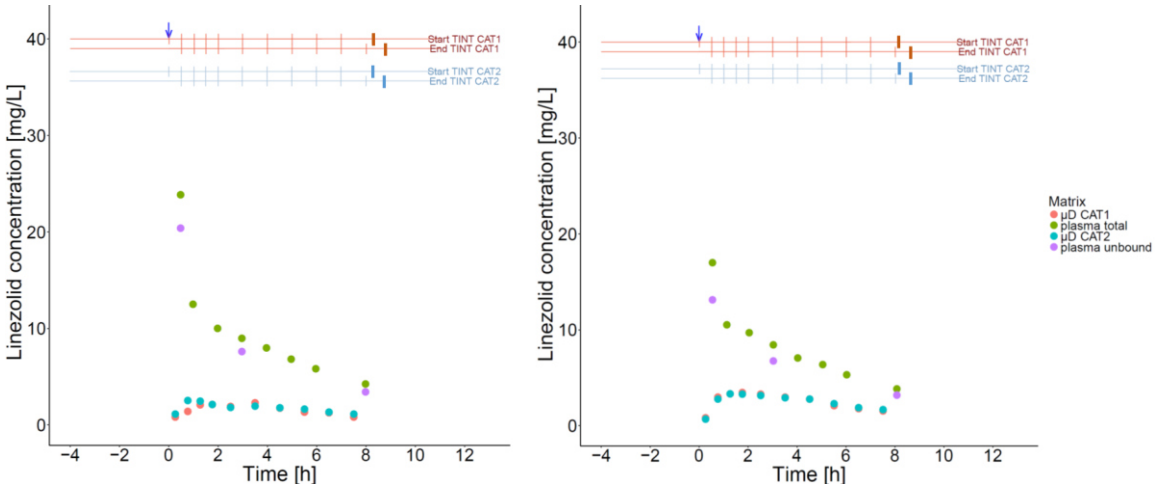

Figure S1: (Project I) Individual graphical evaluation of the micro- and retrodialysis sampling schedule for linezolid, illustrated as an example for two selected patients.
Colour coding and symbols: *Green circles*: Total plasma concentrations; *Purple circles:* Unbound plasma concentrations; *Red circles:* Microdialysate concentrations determined with CAT1, *Blue circles:* Microdialysate concentrations determined with CAT2; *Blue arrow*: Start of linezolid infusion; *Red vertical lines*: Start and end of micro- (thin lines) retrodialysis (bold lines) and collection interval of CAT1; *Blue vertical lines*: Start and end of micro- (thin lines) retrodialysis (bold lines) and collection interval of CAT2.
Abbreviation: *CAT1*: Catheter 1; *CAT2*: Catheter 2; *TINT*: Micro-/Retrodialysis collection interval.

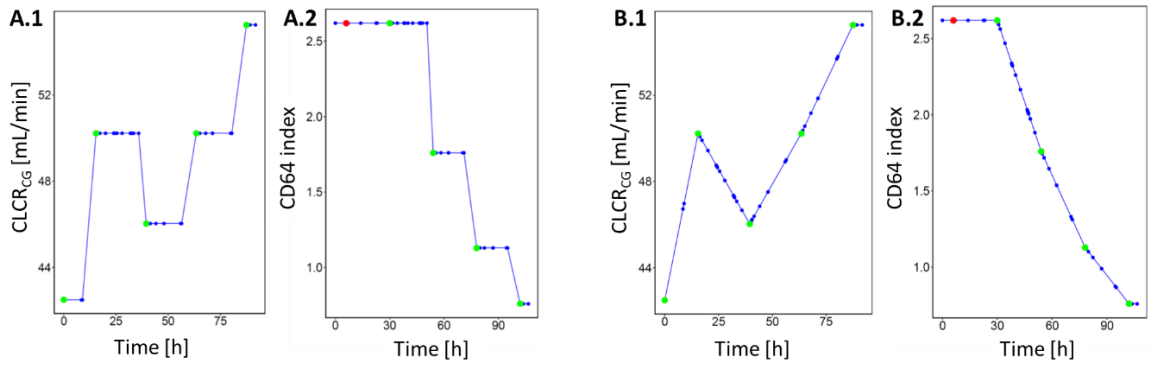

Figure S2: (Project IV) Graphical assessment of the two imputation/interpolation strategies 'stepwise' (A) and 'linear' (B), demonstrated by the example of creatinine clearance (A) and CD64 (B) for one selected individual.
Colour coding: *Green circles*: Observed values; *Red circles*: Imputed values; *Blue circles*: Interpolated values for time points in dataset.
Abbreviations: *CLCR$_{CG}$*: Creatinine clearance estimated according to Cockcroft and Gault [2].

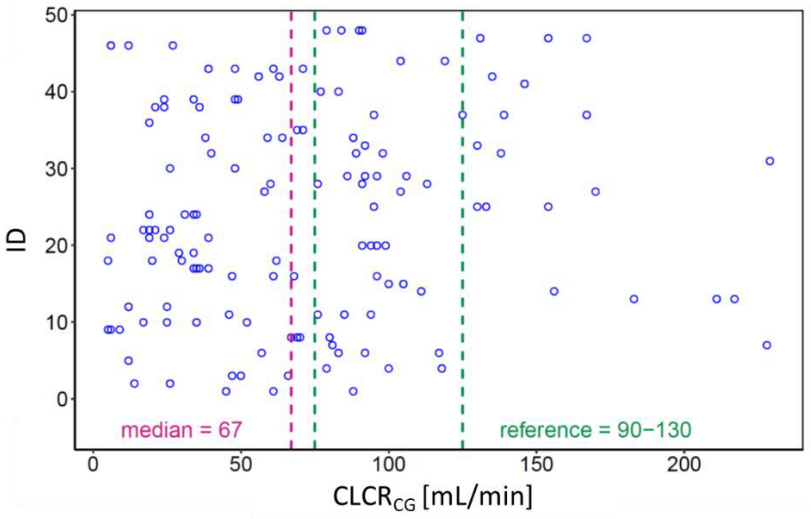

Figure S3: (Project IV) Index plot demonstrated by the example of creatinine clearance.
Blue circles: Observed $CLCR_{CG}$ values; *Pink dashed line*: Median of observed $CLCR_{CG}$ values; *Green dashed lines*: Limit values of reference range.
Abbreviations: *$CLCR_{CG}$*: Creatinine clearance estimated according to Cockcroft and Gault [2]; *ID*: Individual identifier.

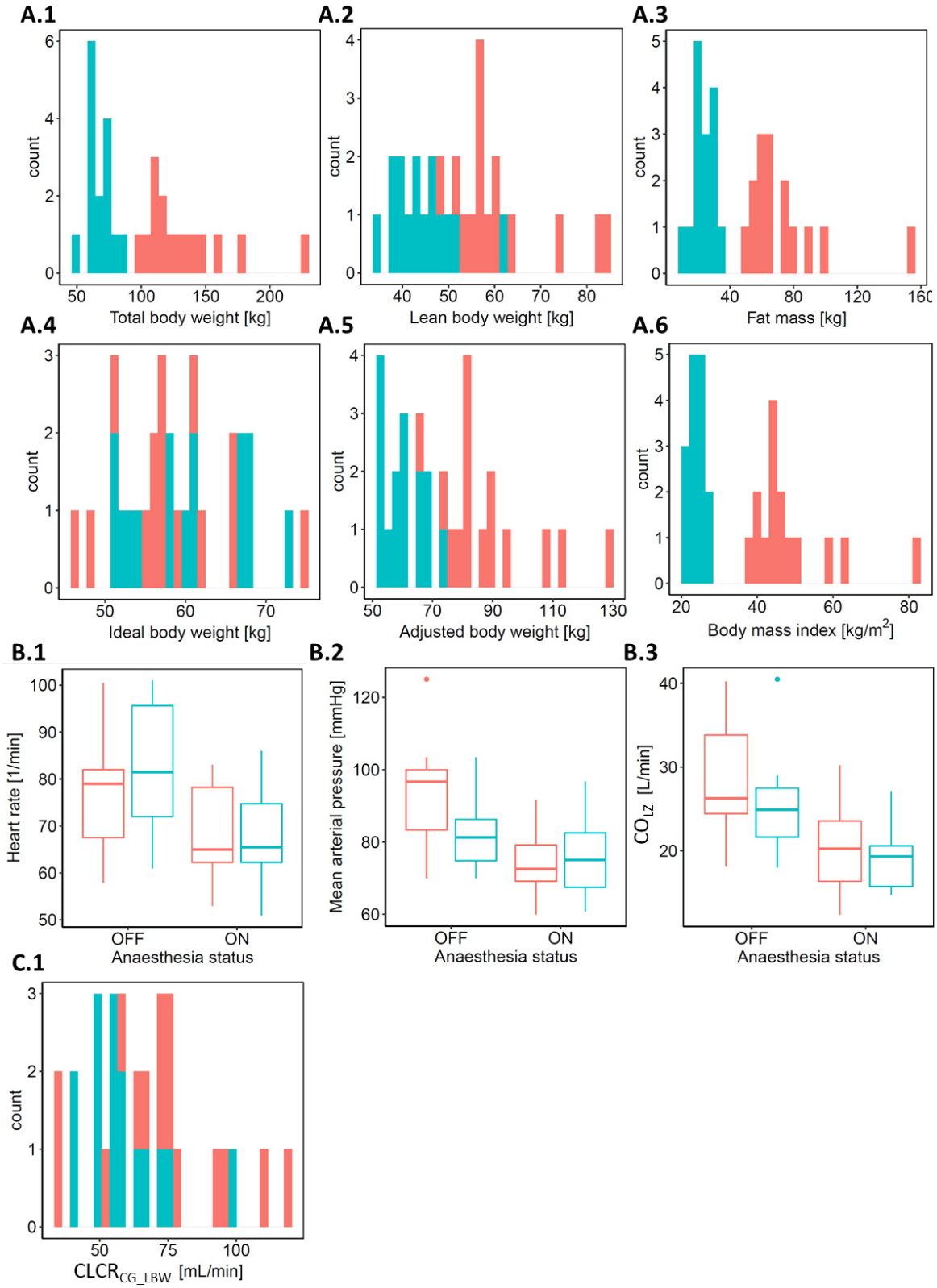

Figure S4: (Project I) Frequency distributions of body size descriptors (A), haemodynamic markers (B) and a renal function marker (C) of obese (red) and nonobese (green) patients.
B: Summary statistics based on individual median observed intra-anaesthetic data and post-anaesthetic data, respectively. ***Colour coding***: *Red*: Obese patients; *Green*: Nonobese patients.
Abbreviations: $CLCR_{CG\_LBW}$: Creatinine clearance estimated according to Cockcroft and Gault [2] using LBW; CO_{LZ}: Cardiac output according to Liljestrand and Zander (unadjusted) [3]; *LBW*: Lean body weight.

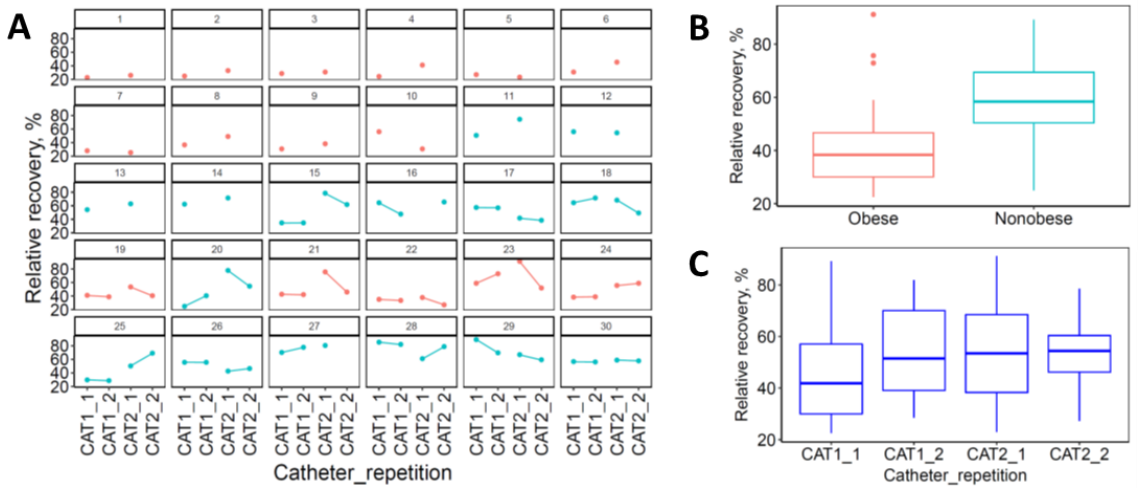

Figure S5: (Project I) Individual relative recovery values for linezolid (A) and boxplots stratified by obesity status (B) and catheter and retrodialysis repetition (C).
Colour coding: *Red*: Obese patients; *Green*: Nonobese patients.
Abbreviations: *CAT1*: Catheter 1; *CAT2*: Catheter 2; *CAT1_1:* Catheter 1, Retrodialysis repetition 1; *CAT1_2*: Catheter 1, Retrodialysis repetition 2; *CAT2_1:* Catheter 2, Retrodialysis repetition 1; *CAT2_2*: Catheter 2, Retrodialysis repetition 2;

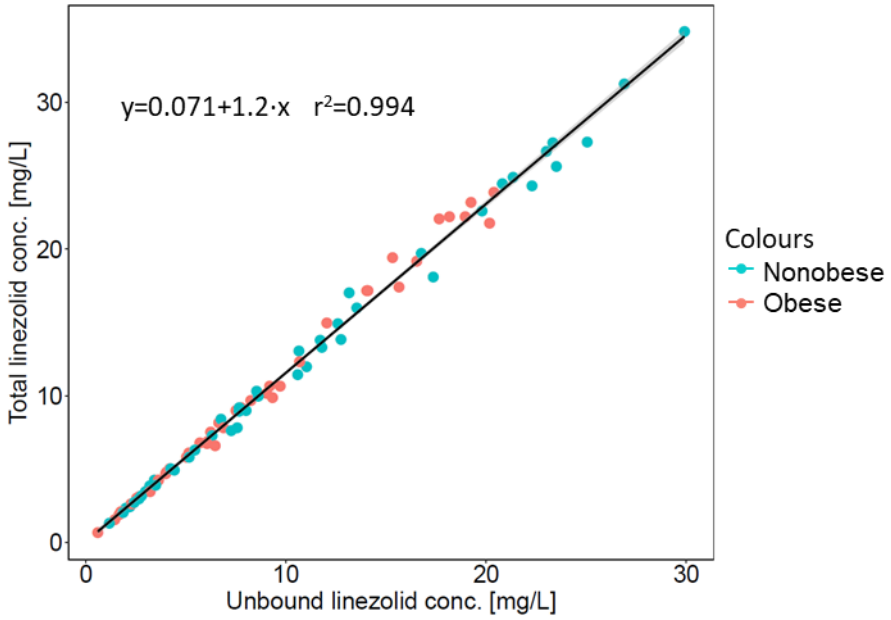

Figure S6: (Project I) Total vs. unbound linezolid plasma concentrations stratified by the obesity status of the patient.
Symbols: *Line*: Linear regression line; *Grey shaded area*: 95% confidence interval around regression line; *Red circles*: Observed plasma linezolid concentration for obese patients; *Green circles*: Observed plasma linezolid concentration for nonobese patients.
Abbreviations: *ISF*: Interstitial space fluid; r^2*:* Coefficient of determination.

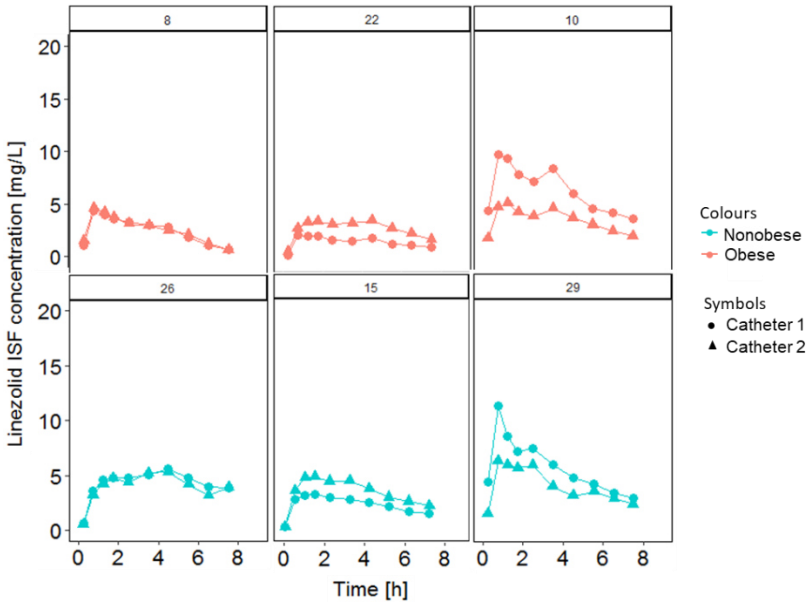

Figure S7: (Project I) Individual linezolid concentration-time profiles in the ISF of the s.c. adipose tissue of selected patients, in which the two catheters result in similar profiles (left column), different profiles (middle column: catheter 1 < catheter 2; right column: catheter 1 > catheter 2). ISF concentrations are displayed at mid time of the respective collection intervals.
Colour coding: *Red*: Obese patients; *Green*: Nonobese patients.
Abbreviations: *ISF*: Interstitial space fluid.

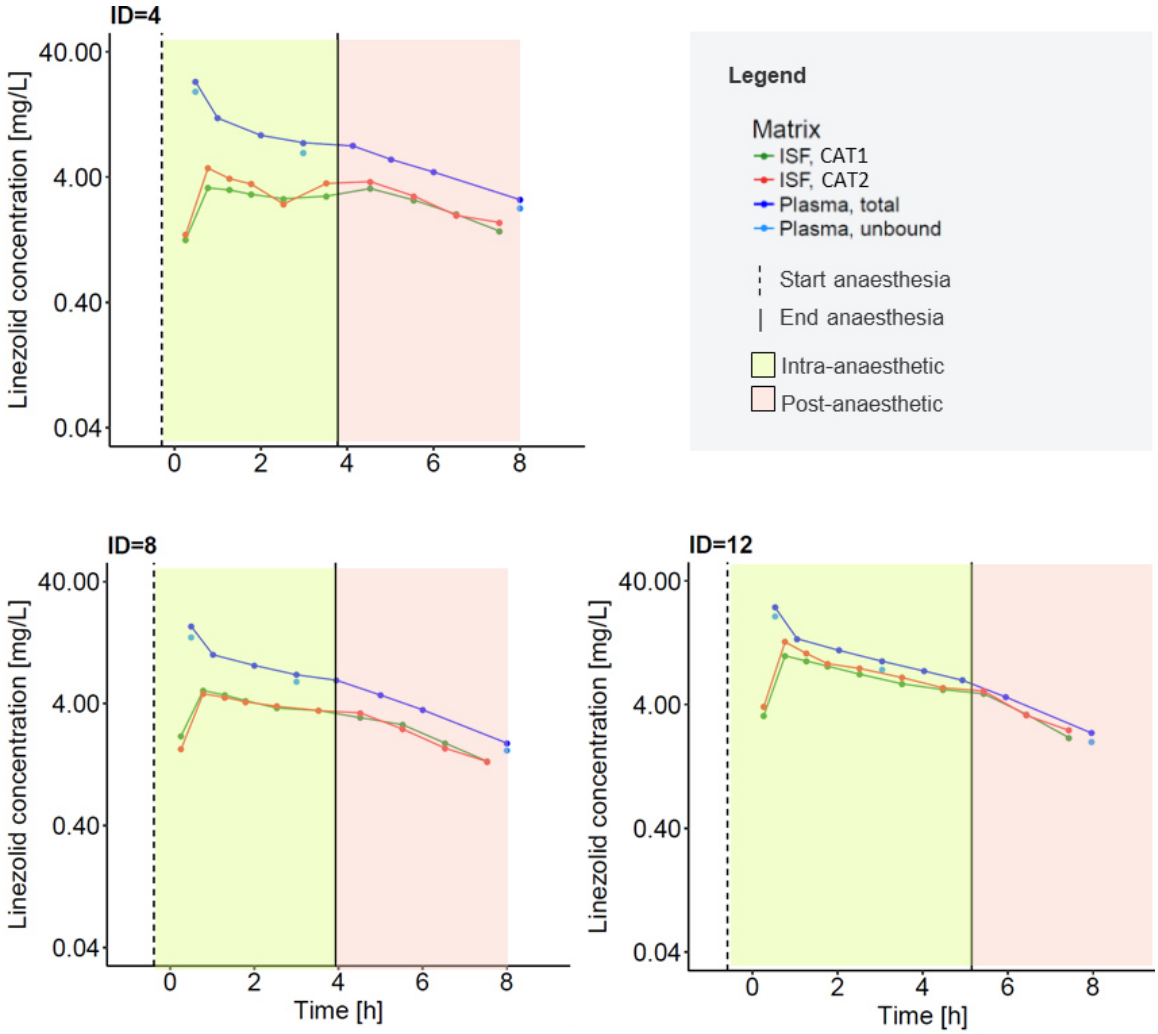

Figure S8: (Project I) Linezolid concentration-time profiles in plasma and ISF of the s.c. adipose tissue for selected patients including the intra- and post-anaesthetic time period.
Colour coding: *Green circles/lines*: ISF concentration determined with CAT1; *Red circles/lines:* ISF concentration determined with CAT2; *Dark blue circles/lines:* Total plasma concentrations; *Light blue circles/lines:* Unbound plasma concentrations; *Green shaded area:* Intra-anaesthetic time period; *Red shaded area:* Post-anaesthetic timer period.
Abbreviations: *CAT1*: Catheter 1; *CAT2*: Catheter 2; *ISF*: Interstitial space fluid.

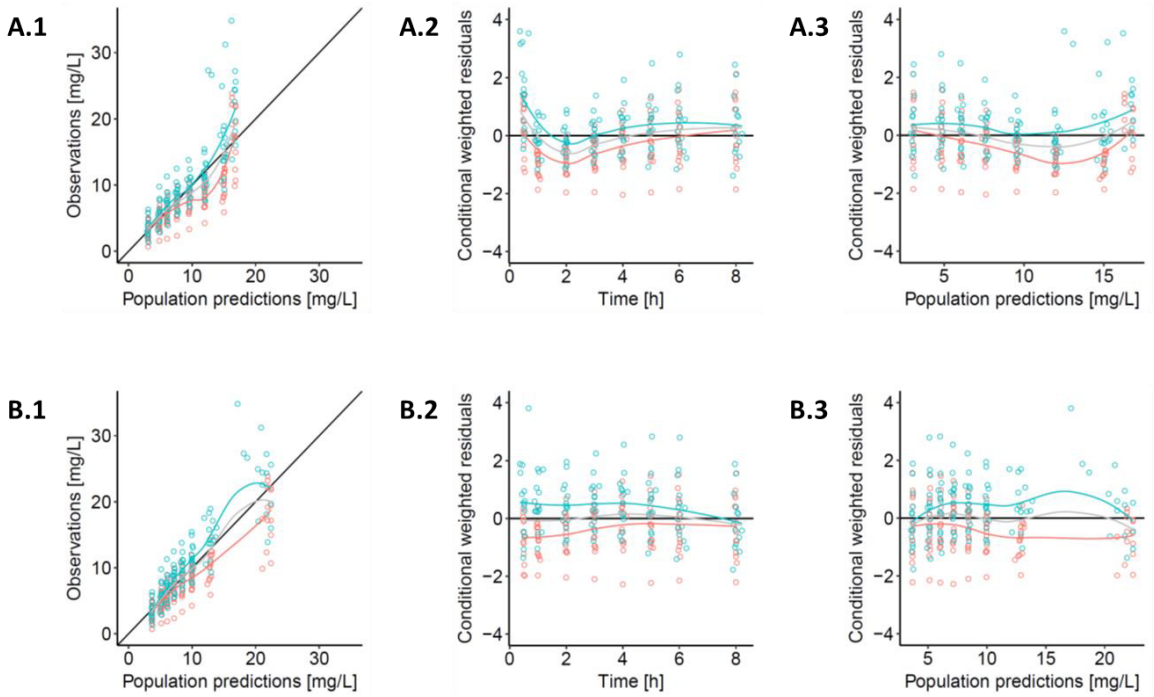

Figure S9: (Project I) Observed vs. population predicted linezolid concentrations (1) and CWRES vs. time (2) and population predicted linezolid concentrations (3) for a one-CMT model (A) and a two-CMT (B) structural model without IIV and with combined RUV, for the total linezolid plasma concentrations.
Lines: *Black lines*: Line of identity (1), reference lines at y=0 (2, 3); *Grey, red and green lines*: Loess smoothers for all patients, obese patients and nonobese patients, respectively [250].
Colour coding: *Red*: Obese; *Green*: nonobese.
Abbreviations: *CMT*: Compartment; *CWRES*: Conditional weighted residuals; *IIV*: Interindividual variability; *RUV*: Residual unexplained variability.

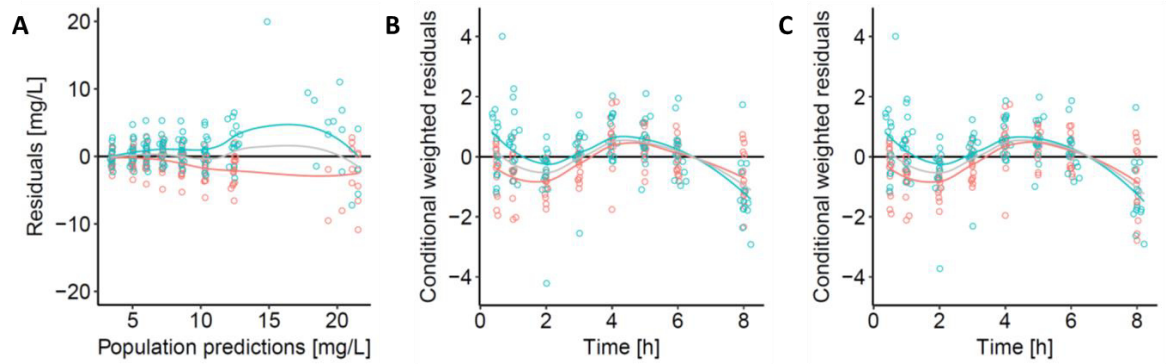

Figure S10: (Project I) Residuals vs. population predicted linezolid concentrations (A) and CWRES over time (B, C) for the two-CMT linezolid model (incl. IIV) with a combined (A, B) and proportional RUV model (C) for total linezolid concentrations.
Lines: *Black lines*: Line of identity; *Grey, red and green lines:* Loess smoothers for all patients, obese patients and nonobese patients, respectively [250].
Colour coding: *Red*: Obese; *Green*: nonobese.
Abbreviations: *CMT*: Compartment; *CWRES*: Conditional weighted residuals; *IIV*: Interindividual variability; *RUV*: Residual unexplained variability.

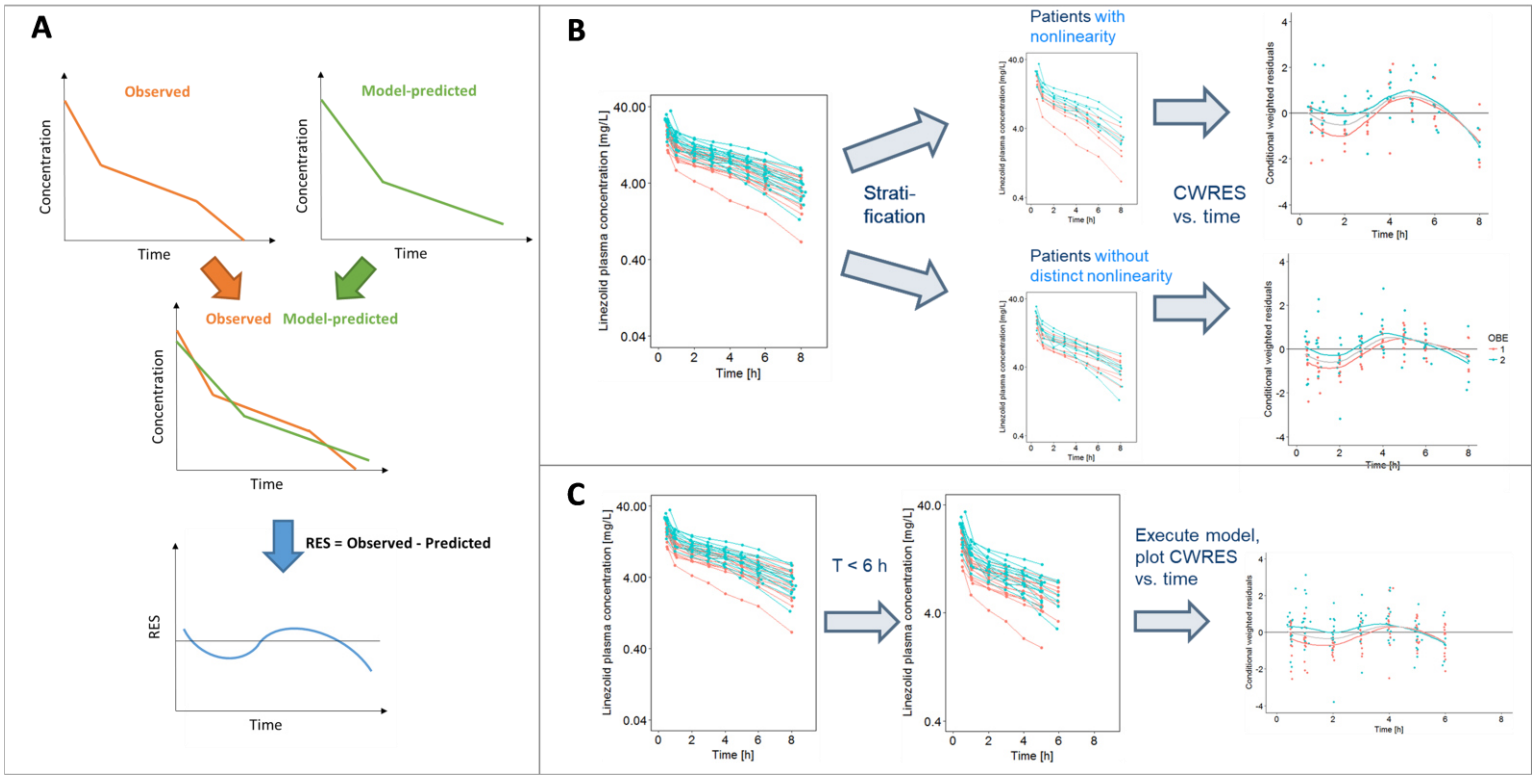

Figure S11: (Project I) Graphical illustration of evaluation of undulating pattern in "CWRES versus time" plot for the linezolid plasma concentrations, to assess whether the pattern is linked to the observed nonlinearity in the linezolid concentration-time profile.

A: Graphical sketch to illustrate how the undulating pattern in the CWRES could be explained by observed nonlinearity in the concentration-time profile (i.e. third steep phase in the terminal phase), which is not captured in the model predicted concentration-time profile by a classical (mammalian) two-CMT model. ***B***: Workflow of first evaluation to assess the above described relation between the pattern and the nonlinearity. The individual linezolid concentration-time profiles were visually stratified by whether the patients showed a clear nonlinearity. The 'CWRES vs. time" plot was stratified accordingly and evaluated. The observed pattern (Loess smoother [250]) was more pronounced for the patient group for which a clear pattern in the CWRES was observed.

C: Workflow of second evaluation to assess the above described relation between the pattern and the nonlinearity. Only the linezolid concentration data which were collected <6 h after start of infusion were subset to exclude the third steep phase in the profile. The model was re-executed and the "CWRES vs. time" plot evaluated. The observed pattern in the CWRES (Loess smoother [250]) was clearly reduced in comparison to the model based on all available linezolid concentration data.

Abbreviations: *CWRES*: Conditional weighted residuals; *RES*: Residuals; *T*: Time.

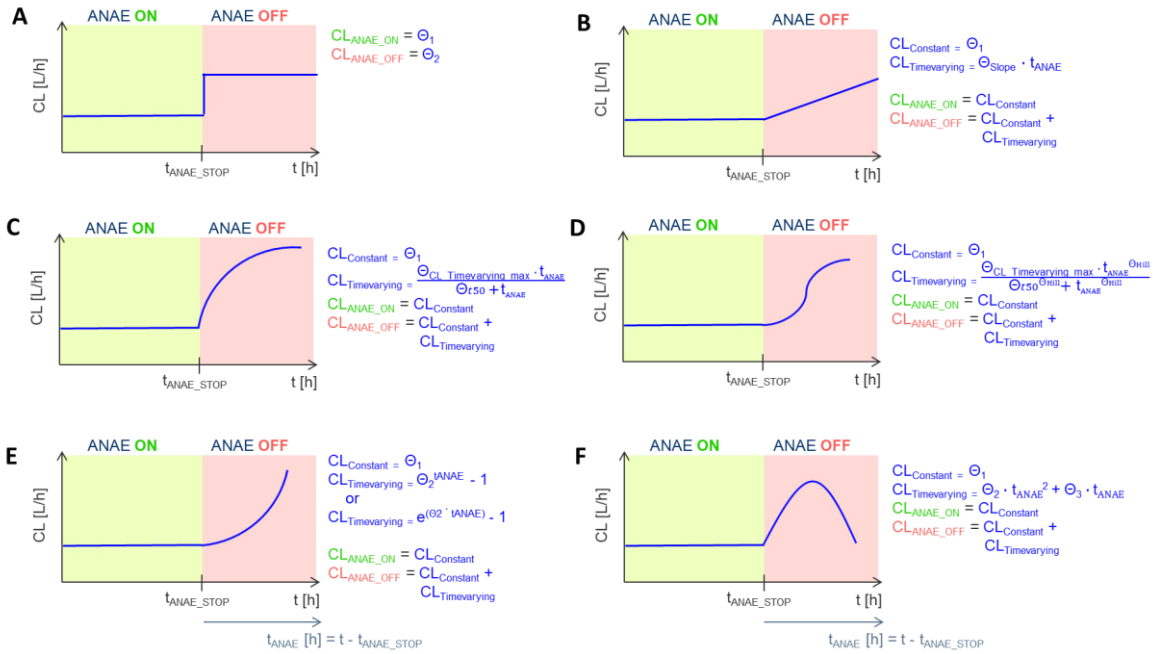

Figure S12 (Project I) Graphical illustration and mathematical equations for the six investigated 'anaesthesia models' (A-F) which describe a change of linezolid clearance at the end of anaesthesia.
Change of linezolid clearance after end of anaesthesia: Stepwise increase (A); Linear increase (B); Increase according to E_{max} model (C); Sigmoidal increase (D); Exponential increase (E); Hyperbolic change (F).
Abbreviations: *ANAE*: Anaesthesia status; *CL*: Clearance; max: Maximum; *t:* Time; t_{50}*:* Time to reach half-maximum of time-varying clearance; t_{ANAE}: Time since anaesthesia start; t_{ANAE_STOP}: Time of anaesthesia end.

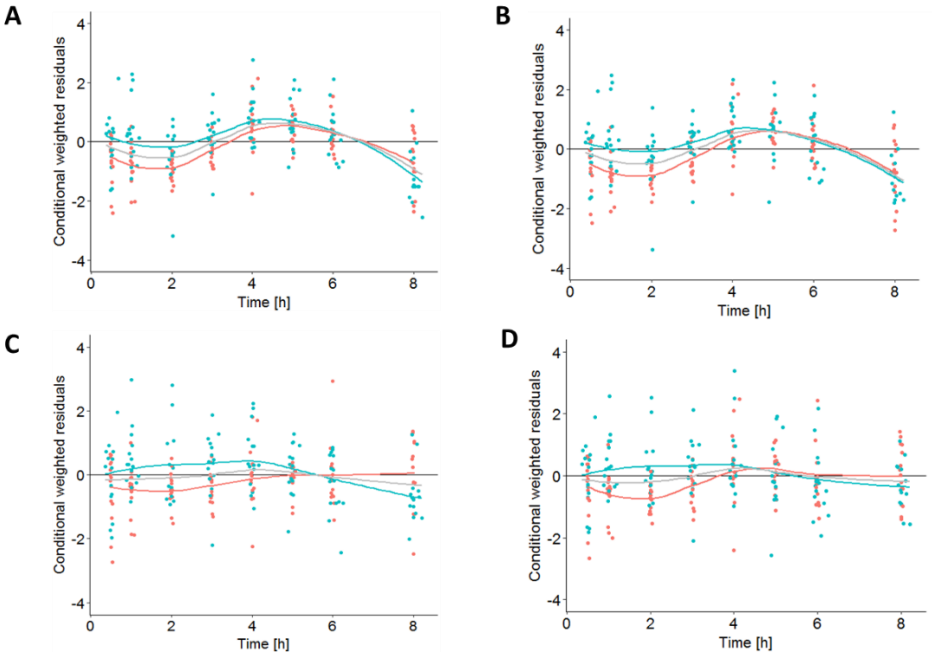

Figure S13: (Project I) CWRES over time for the plasma base models for linezolid with different clearance models.
A: Linear CL; ***B:*** Heart rate as covariate on CL; ***C:*** Time-varying CL according to an E_{max} model after end of anaesthesia; ***D:*** Concentration-dependent parallel linear and nonlinear Michaelis-Menten clearance.
Lines: *Black lines*: Reference lines at y=0; *Grey, red and green lines:* Loess smoothers [250] for all patients, obese patients and nonobese patients, respectively.
Colour coding: *Red*: Obese; *Green*: nonobese.
Abbreviations: *CL*: Clearance; *CWRES*: Conditional weighted residuals.

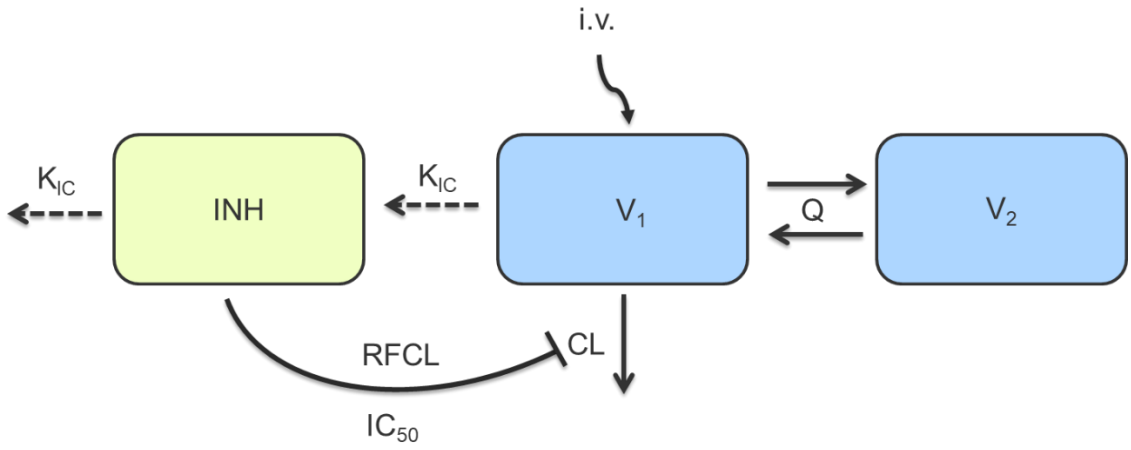

Figure S14: (Project I) Sketch of two-CMT model with an empirical inhibition CMT causing a time- and concentration-dependent CL.
Abbreviations: *CL*: Clearance; *CMT*: Compartment; IC_{50}: Concentration in INH yielding 50% of CL inhibition; *INH*: Inhibition CMT; *i.v.*: Intravenous; K_{IC}: Rate constant for the transfer into INH; *Q*: Intercompartmental clearance; *RFCL*: Remaining fraction of CL at maximum CL inhibition; V_1, V_2: Central and peripheral volume of distribution.

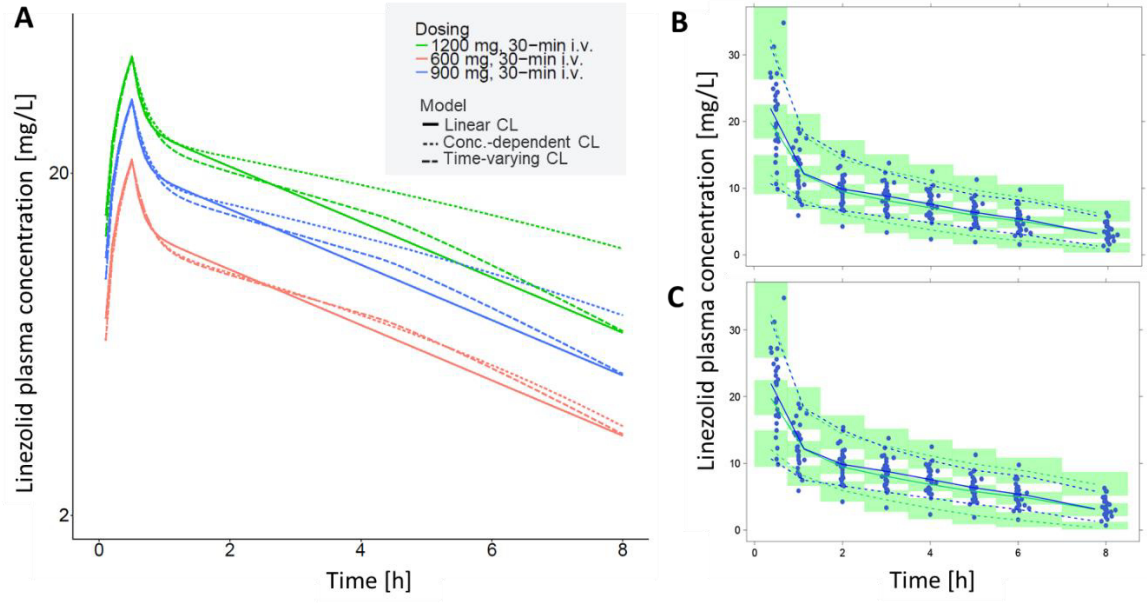

Figure S15: (Project I) Comparison of the two most adequate clearance models in Step 1 with respect to extrapolation of linezolid plasma concentration to higher doses (A) and predictive performance (B, C).
A: Deterministic simulations of linezolid plasma concentrations resulting from a dose of 600 mg (red), 900 mg (blue) and 1200 mg (green) linezolid administered as 30-min i.v. infusion using the NLME model with linear CL (solid line), time-varying increase of CL according to an E_{max} model after end of anaesthesia (dashed line) and concentration-dependent parallel linear and nonlinear Michaelis-Menten clearance (dotted line).
B, C: VPCs (n=1000 simulations) for the NLME model with time-varying increase of CL according to an E_{max} model after end of anaesthesia (B) and concentration-dependent parallel linear and nonlinear Michaelis-Menten clearance (C); Circles: Observed linezolid concentrations; Lines: 5^{th}, 95^{th} percentile (dashed), 50^{th} percentile (solid) of the observed (blue) and simulated (green) data. Green shaded areas: 95% confidence interval around 5^{th}, 50^{th} and 95^{th} percentile of simulated data.
Abbreviations: *CL*: Clearance, *i.v.*: Intravenous; *VPC*: Visual predictive check.

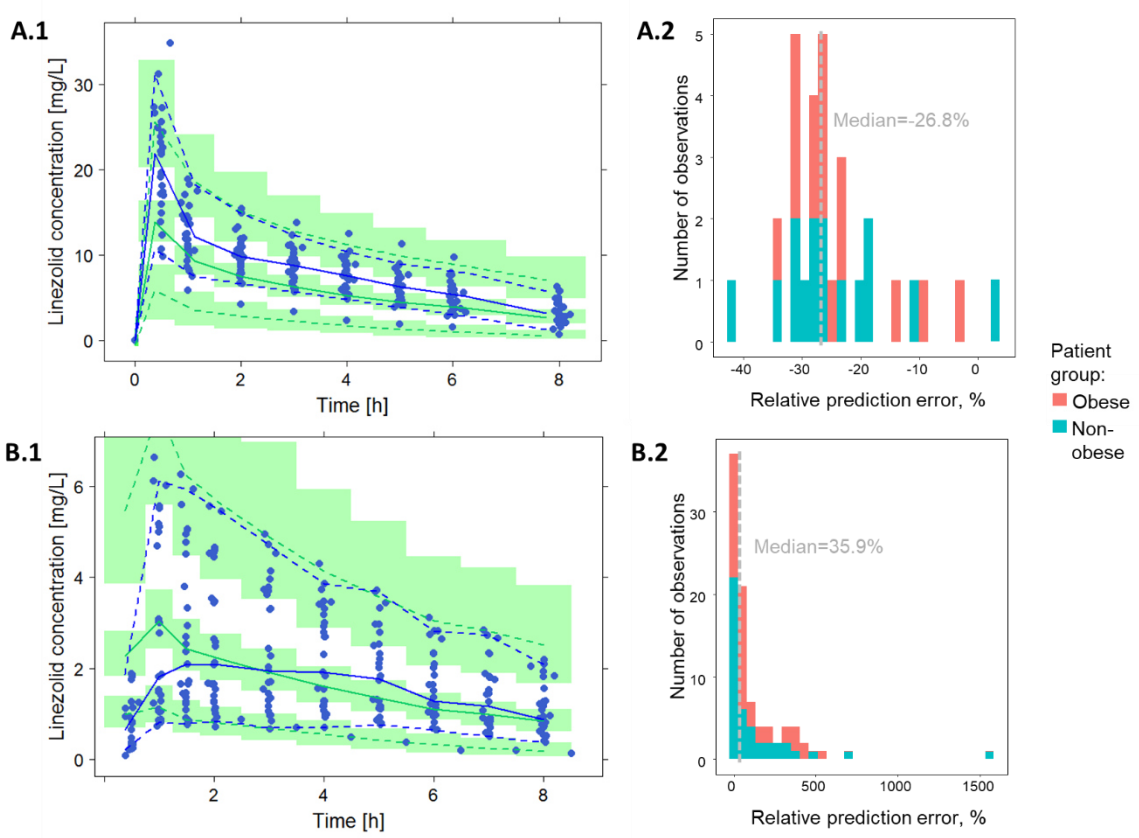

Figure S16: (Project I) Selected results of the external evaluation of a pooled NLME linezolid model [45] for the applicability to predict plasma (A) and microdialysate PK data (B) in the obese and nonobese patient population.
A.1, B.1: VPCs (n=1000 simulations) for plasma (A.1) and microdialysate data of catheter 1 (B.1). Circles: Observed linezolid concentrations; Lines: 5th, 95th percentile (dashed), 50th percentile (solid) of the observed (blue) and simulated (green) data. Green shaded areas: 95% confidence interval around 5th, 50th and 95th percentile of simulated data.
A.2, B.2: Distribution of relative prediction errors (Section 2.3.3.8) for plasma (t=0.5 h after infusion start, A.2) and microdialysate data of catheter 1 (t=0-1.5 h after infusion start, B.2) for obese (red) and nonobese patients (green).
Abbreviations: *NLME*: Nonlinear mixed-effects; *PK*: Pharmacokinetics; *VPC*: Visual predictive check.

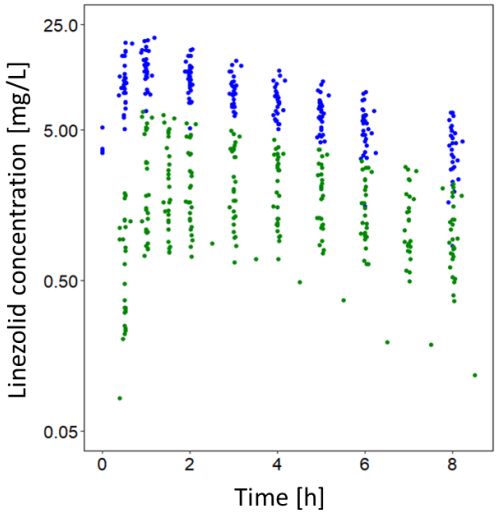

Figure S17: (Project I) Comparison of model predicted linezolid concentrations in the peripheral compartment of plasma base model (blue) with observed microdialysate data (green) on semilogarithmic scale.

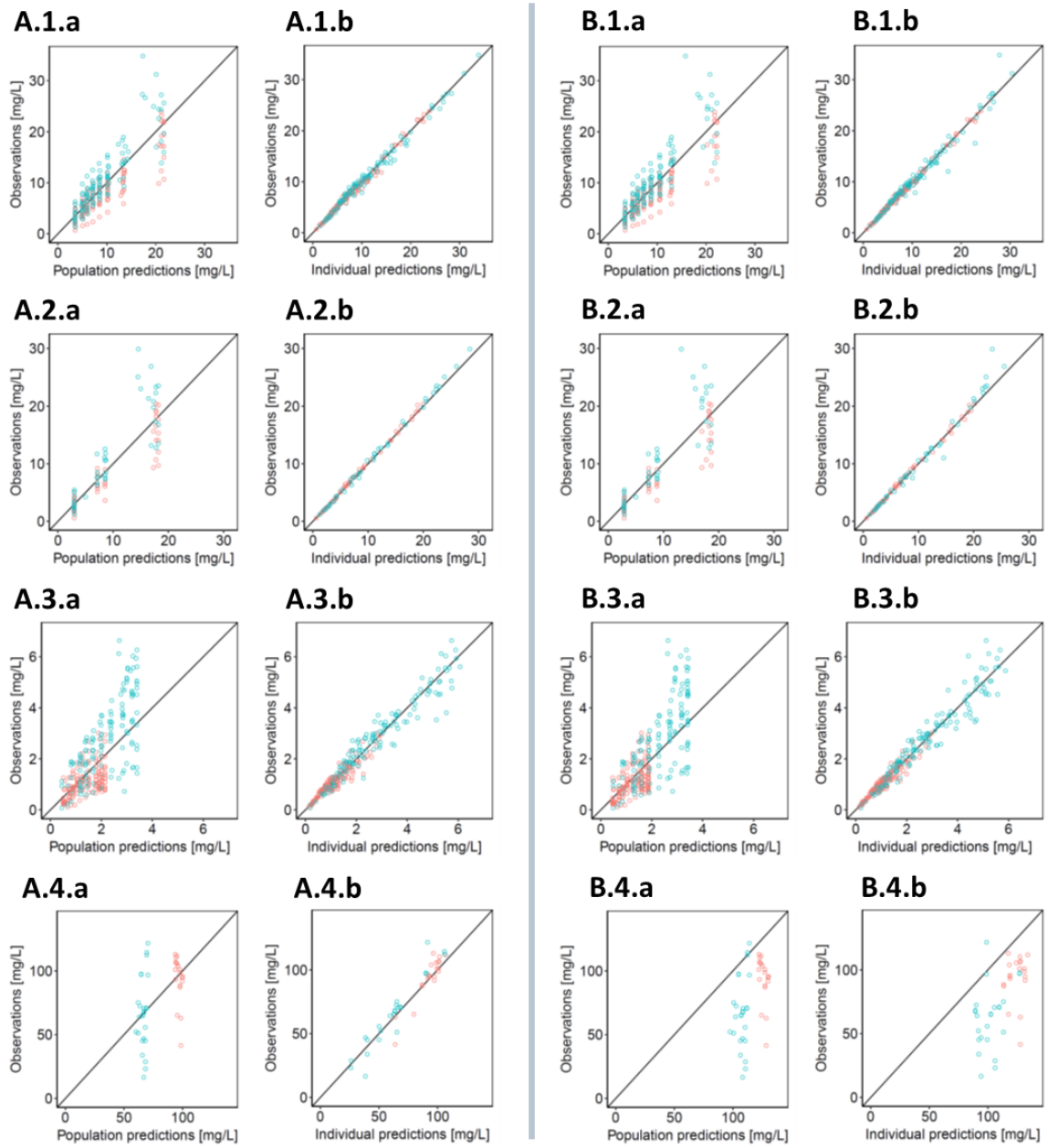

Figure S18: (Project I) Observed vs. population predicted (a) and individual predicted (b) total plasma linezolid concentrations (1), unbound plasma (2), microdialysate of catheter 1 (3) and retrodialysate linezolid concentrations for Model B (A) and Model C (B).

Model B: Assignment of ISF of the s.c. adipose tissue to the already existing peripheral compartment of the plasma base model and estimation of additional tissue scaling factor; *Model C*: Assignment of ISF of the s.c. adipose tissue to a new separate peripheral compartment and estimation of intercompartmental clearance and the volume of distribution of the respective compartment (Figure 3.3). *Black lines*: Line of identity.

Colour coding: *Red*: Obese; *Green*: nonobese.

Abbreviations: *ISF*: Interstitial space fluid.

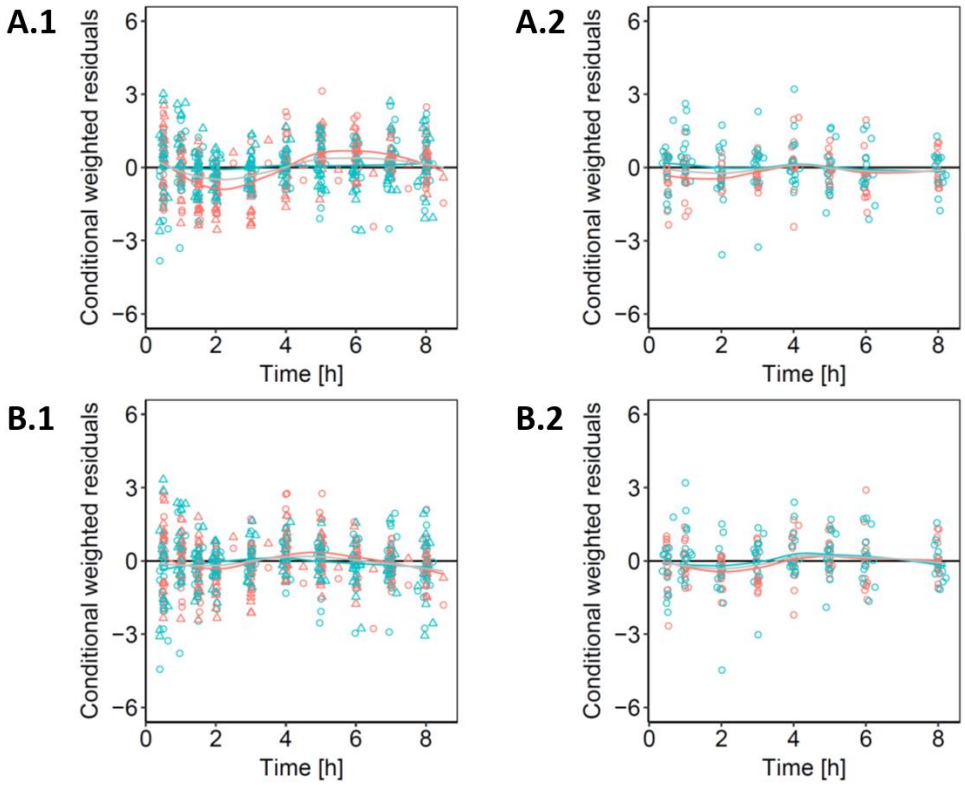

Figure S19: (Project I) Conditional weighted residuals vs. time for linezolid microdialysate (1) and plasma concentrations (2) for the base (A) and final joint NLME model (B).
***Symbols**: Circles*: Conditional weighted residuals of plasma and microdialysate concentrations of catheter 1; *Triangles*: Conditional weighted residuals of microdialysate concentrations of catheter 2.
***Lines:** Black solid line:* Reference lines at y=0; *Grey, red and green lines:* Loess smoothers [250] for all patients, obese patients and nonobese patients, respectively.
***Colour coding:** Red*: Obese; *Green*: nonobese.
***Abbreviations:** NLME*: Nonlinear mixed-effects.

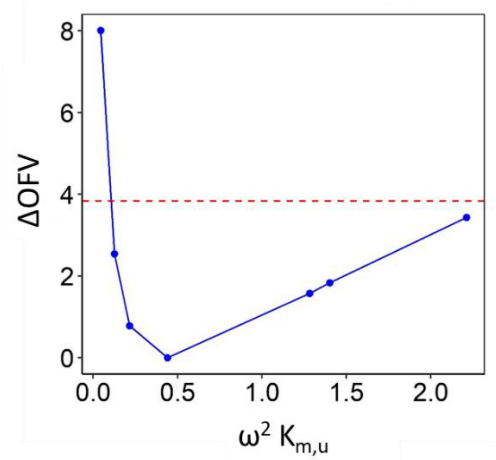

Figure S20: (Project I) Log-likelihood profiling of the interindividual variability parameter of the Michaelis-Menten constant of unbound linezolid (ω^2 $K_{m,u}$) of the final joint NLME model for linezolid.
***Lines:** Blue solid line*: Log-likelihood profile, *Red dashed line*: ΔOFV=+3.84 with respect to the final joint NLME model. X-axis values at the intersection of blue solid line with the red dashed line represent the limits of the 95% confidence interval of ω^2 $K_{m,u}$.
Abbreviations: $K_{m,u}$: Michaelis-Menten constant of unbound linezolid; *OFV*: Objective function value.

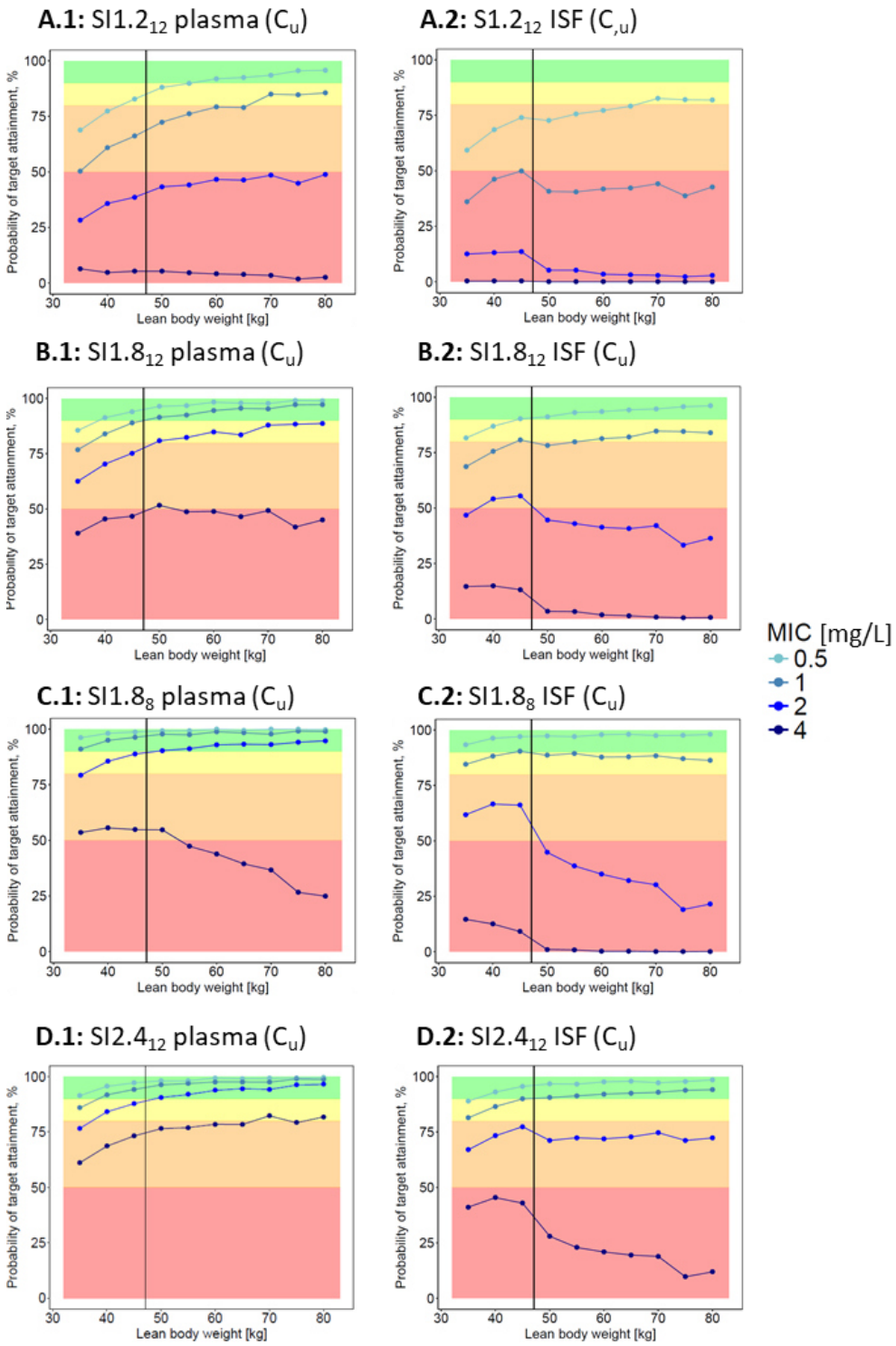

Figure S21: (Project II) Probability of target (95%$fT_{>MIC}$) attainment vs. LBW in plasma (1) and ISF of the s.c. adipose tissue (2) for different short-term infusion regimens (A-D) [continued on next page].

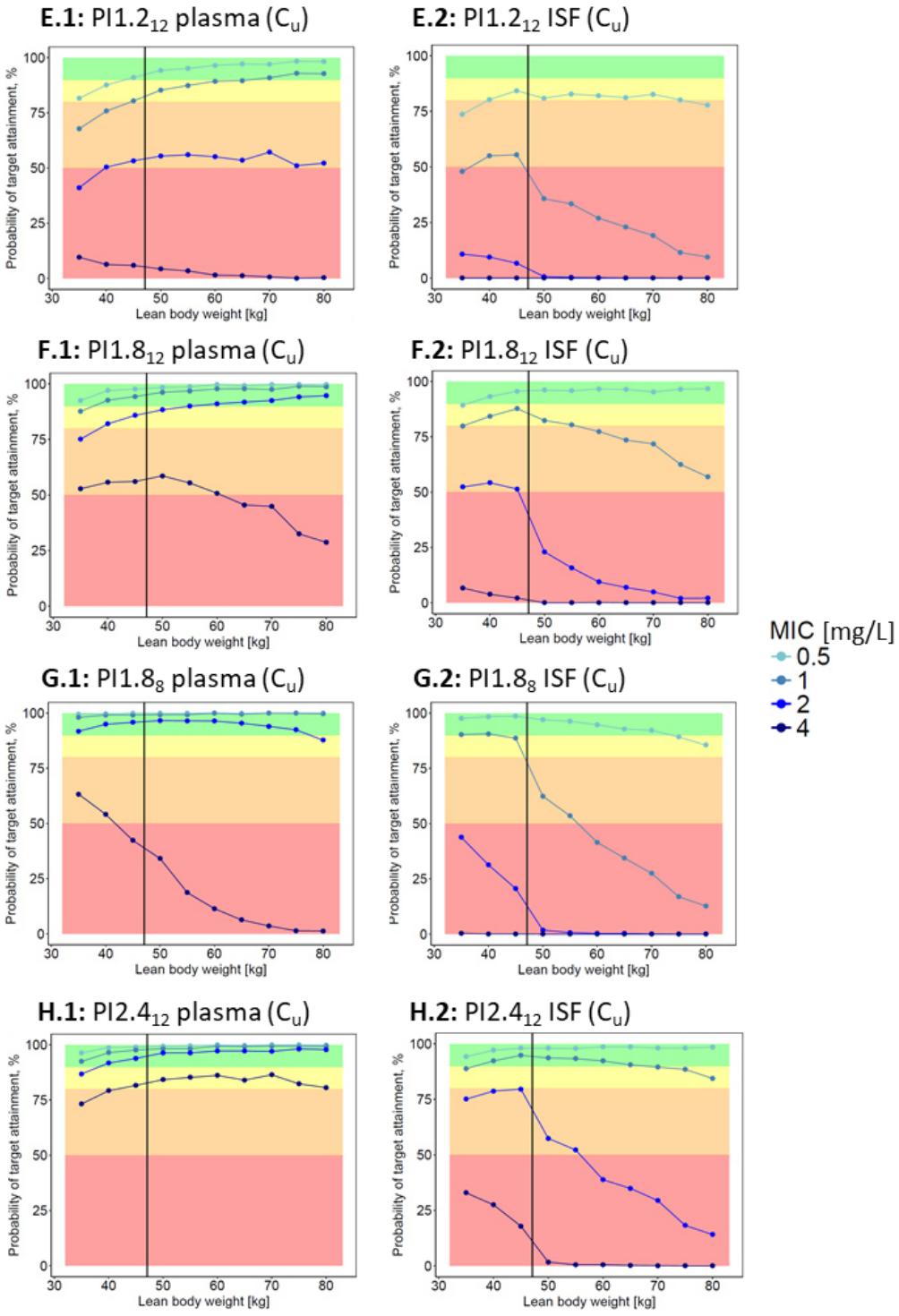

Figure S21 [continued]: (Project II) Probability of target (95%$fT_{>MIC}$) attainment vs. LBW in plasma (1) and ISF of the s.c. adipose tissue (2) for different prolonged infusion regimens (E-H).

All other covariates in the NLME model were set to median values of the patient population (for detailed information on patient characteristics see Table 2.4 B). Deterministic simulations for different linezolid dosing regimens: Appendix Figure S22.

Vertical line: LBW obesity threshold of 47.1 kg (translating into the BMI obesity threshold of 30 kg/m^2 for a 1.65 m tall female patient).

Dosing regimens: *SI1.2$_{12}$*: 600 mg 30-min i.v. infusion, q12h; *SI1.8$_{12}$*: 900 mg 30-min i.v. infusion; *SI1.8$_8$*: 600 mg 30-min i.v. infusion, q8h; *SI2.4$_{12}$*: 1200 mg 30-min i.v. infusion, q12h; *PI1.2$_{12}$*: 600 mg 4-h i.v. infusion, q12h; *PI1.8$_{12}$*: 900 mg 4-h i.v. infusion, q12h; *PI1.8$_8$*: 600 mg 4-h i.v. infusion, q8h; *PI2.4$_{12}$*: 1200 mg 4-h i.v. infusion, q12h.

Abbreviations: *C_U:* Unbound concentration; *ISF*: Interstitial space fluid; *LBW*: Lean body weight; *q8h*: Every 8 h; *q12h*: Every 12 h; *MIC*: Minimum inhibitory concentration. *s.c.* Subcutaneous; *$fT_{>MIC}$:* Time period that unbound drug concentration exceeds the MIC.

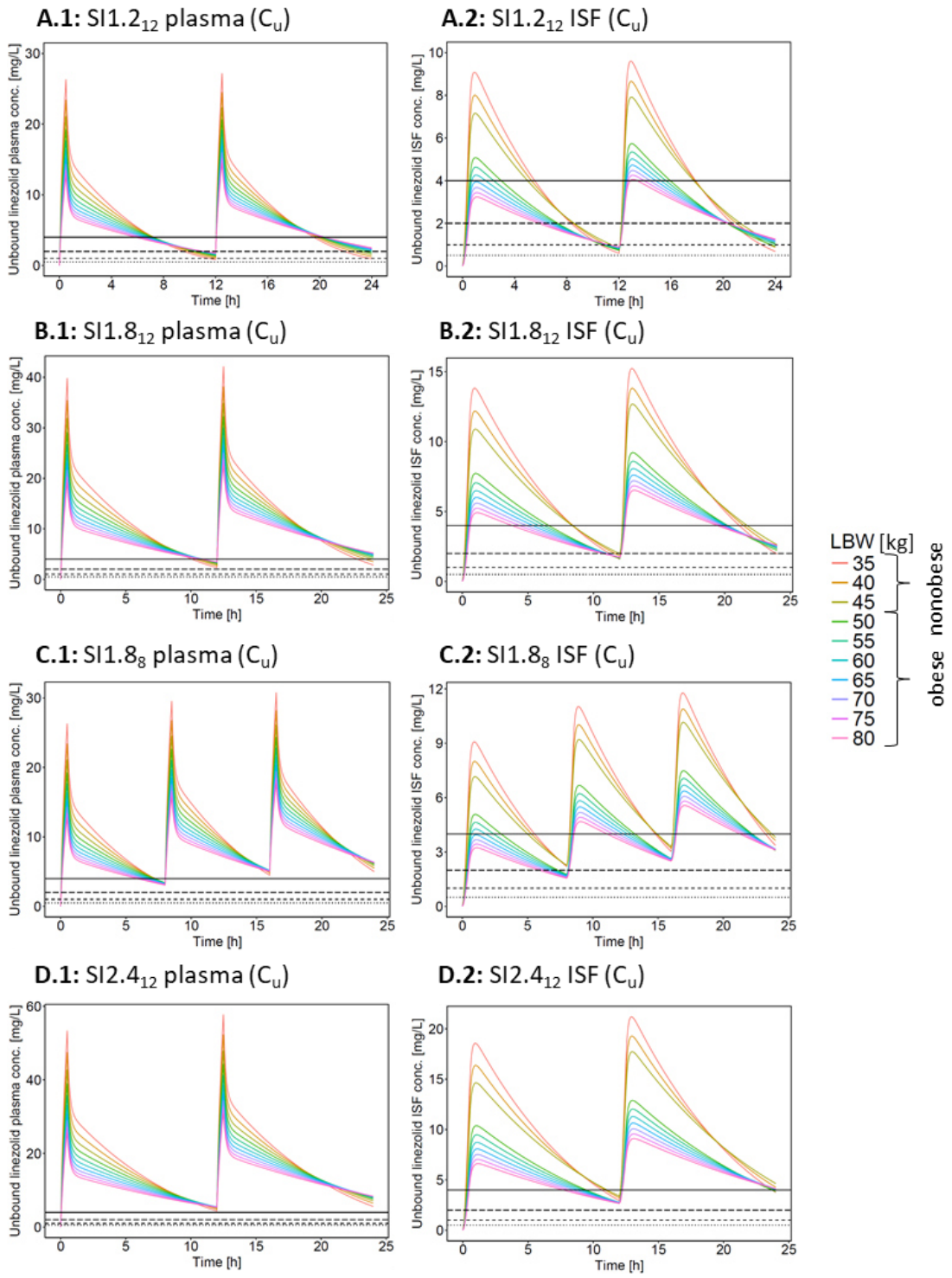

Figure S22: (Project II) Simulated unbound linezolid concentration-time profiles in plasma (1) and ISF of the s.c. adipose tissue (2) for patients with varying LBW, following different short-term infusion regimens (A-D) [continued on next page].

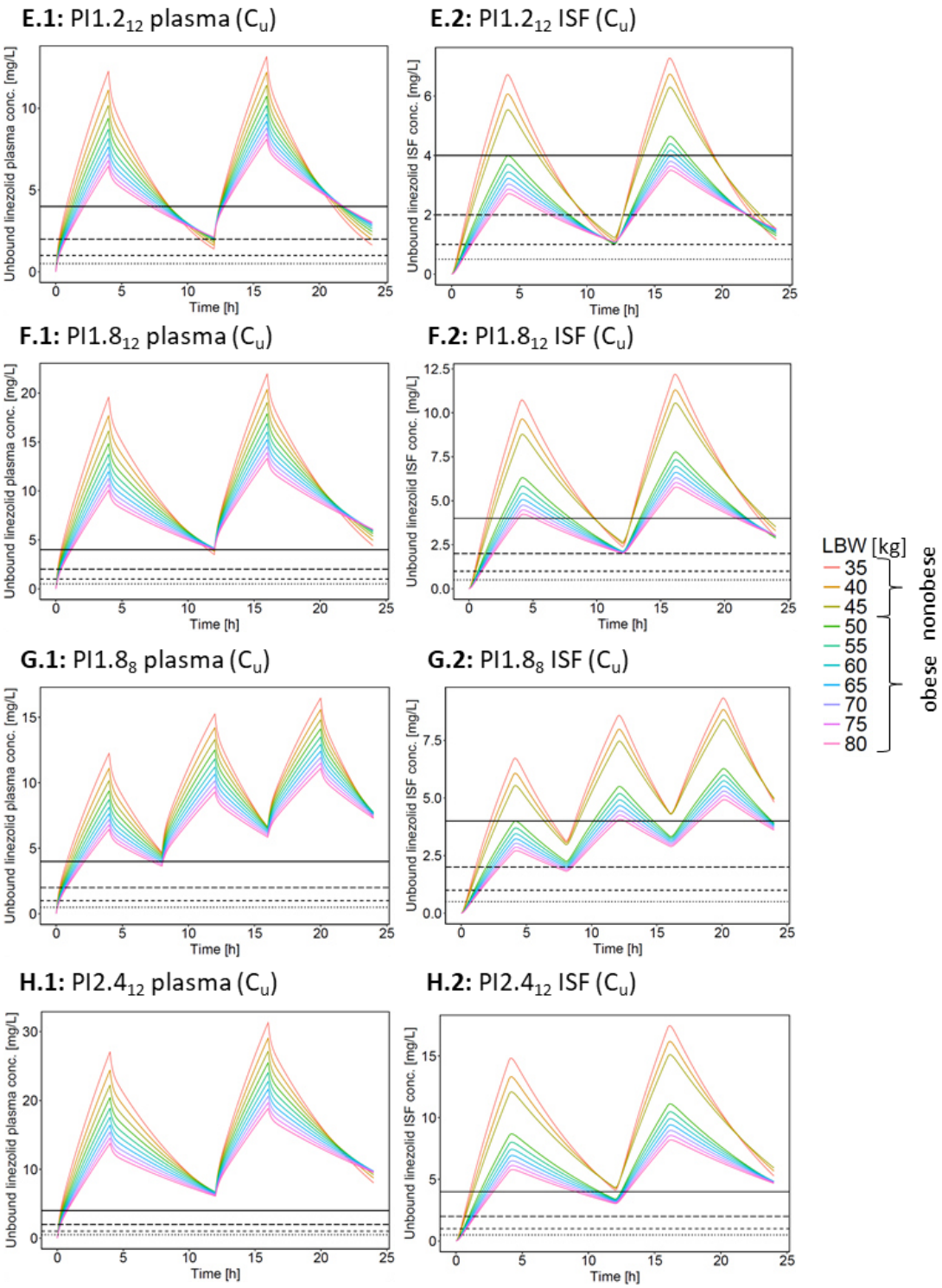

Figure S22 [continued]: (Project II) Simulated unbound linezolid concentration-time profiles in plasma (1) and ISF of the s.c. adipose tissue (2) for patients with varying LBW, following different prolonged infusion regimens (E-H).

All other covariates in the NLME model were set to median values of the patient population (for detailed information on patient characteristics see Table 2.4 B). Note the different y-axis scales in the subfigures.

Horizontal lines: *Solid*: MIC=4 mg/L; *Long dashed*: MIC=2 mg/L; *Short-dashed*: MIC=1 mg/L; *Dotted*=0.5 mg/L.

Dosing regimens: *SI1.2$_{12}$*: 600 mg 30-min i.v. infusion, q12h; *SI1.8$_{12}$*: 900 mg 30-min i.v. infusion, q12h; *SI1.8$_8$*: 600 mg 30-min i.v. infusion, q8h; *SI2.4$_{12}$*: 1200 mg 30-min i.v. infusion, q12h; *PI1.2$_{12}$*: 600 mg 4-h i.v. infusion, q12h; *PI1.8$_{12}$*: 900 mg 4-h i.v. infusion, q12h; *PI1.8$_8$*: 600 mg 4-h i.v. infusion, q8h; *PI2.4$_{12}$*: 1200 mg 4-h i.v. infusion, q12h.

Abbreviations: *C$_U$:* Unbound concentration; *ISF*: Interstitial space fluid; *LBW*: Lean body weight; q8h: Every 8 h; *q12h*: Every 12 h; *MIC*: Minimum inhibitory concentration; *s.c.*: Subcutaneous.

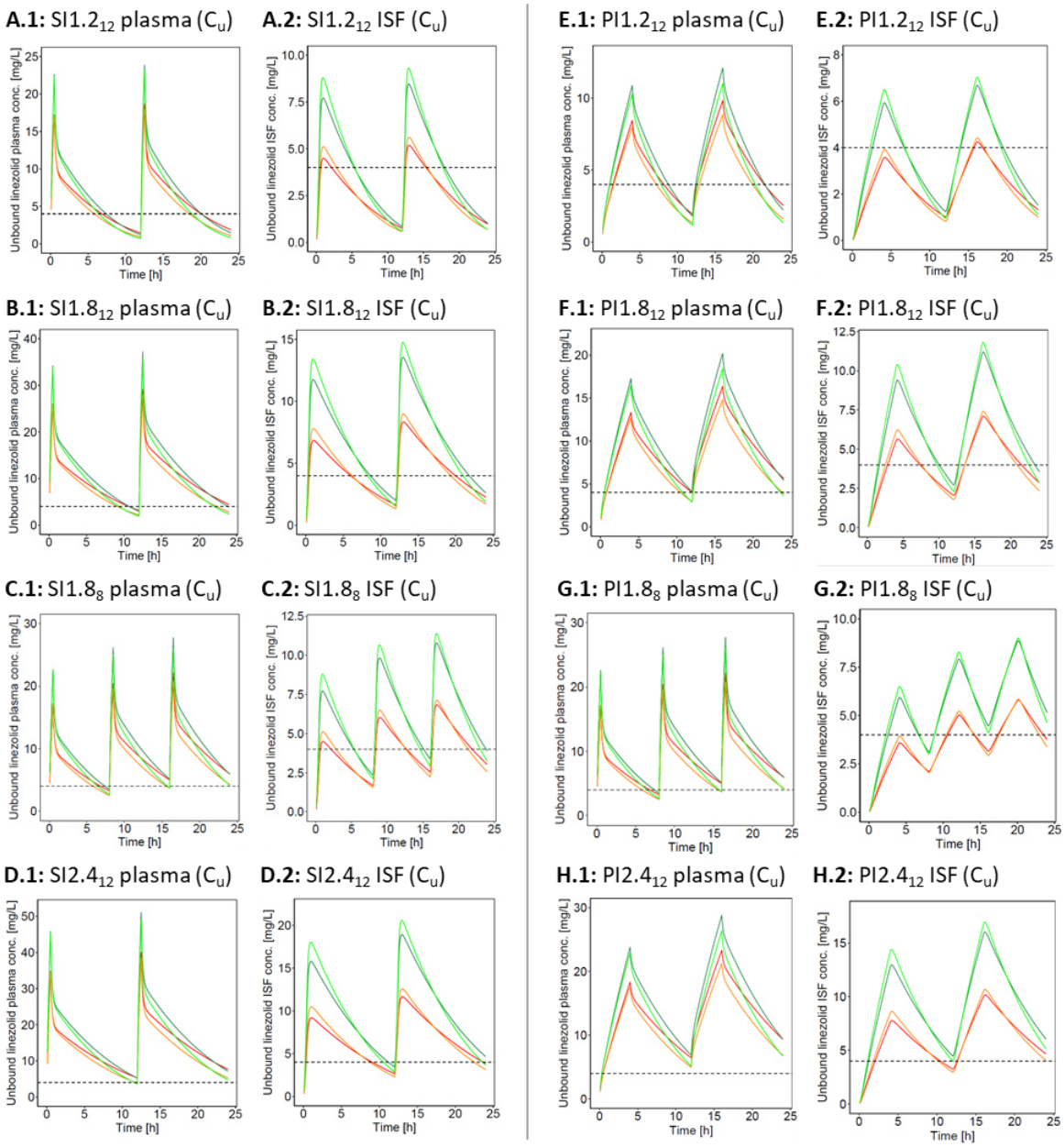

Figure S23: (Project II) Simulated unbound linezolid concentration-time profiles in plasma (1) and ISF of the s.c. adipose tissue (2) for selected typical patients, following different short-term (left panel: A-D) and prolonged infusion regimens (right panel: E-H).

Note the different y-axis scales in the subfigures

Dashed horizontal line: Exemplary MIC value of 4 mg/L.

Dosing regimens: *SI1.2$_{12}$*: 600 mg 30-min i.v. infusion, q12h; *SI1.8$_{12}$*: 900 mg 30-min i.v. infusion, q12h; *SI1.8$_8$*: 600 mg 30-min i.v. infusion, q8h; *SI2.4$_{12}$*: 1200 mg 30-min i.v. infusion, q12h; *PI1.2$_{12}$*: 600 mg 4-h i.v. infusion, q12h; *PI1.8$_{12}$*: 900 mg 4-h i.v. infusion, q12h; *PI1.8$_8$*: 600 mg 4-h i.v. infusion, q8h; *PI2.4$_{12}$*: 1200 mg 4-h i.v. infusion, q12h.

Colour coding: *Red*: Obese and intra-anaesthetic patient; *Dark green:* Nonobese and intra-anaesthetic patient; *Orange*: Obese and post-anaesthetic patient; *Light green:* Nonobese and post-anaesthetic patient (for detailed information on patient characteristics see Table 2.4 A).

Abbreviations: *C$_U$:* Unbound concentration; *ISF*: Interstitial space fluid; *i.v.:* Intravenous; *q8h*: Every 8 h; *q12h*: Every 12 h; *MIC*: Minimum inhibitory concentration.

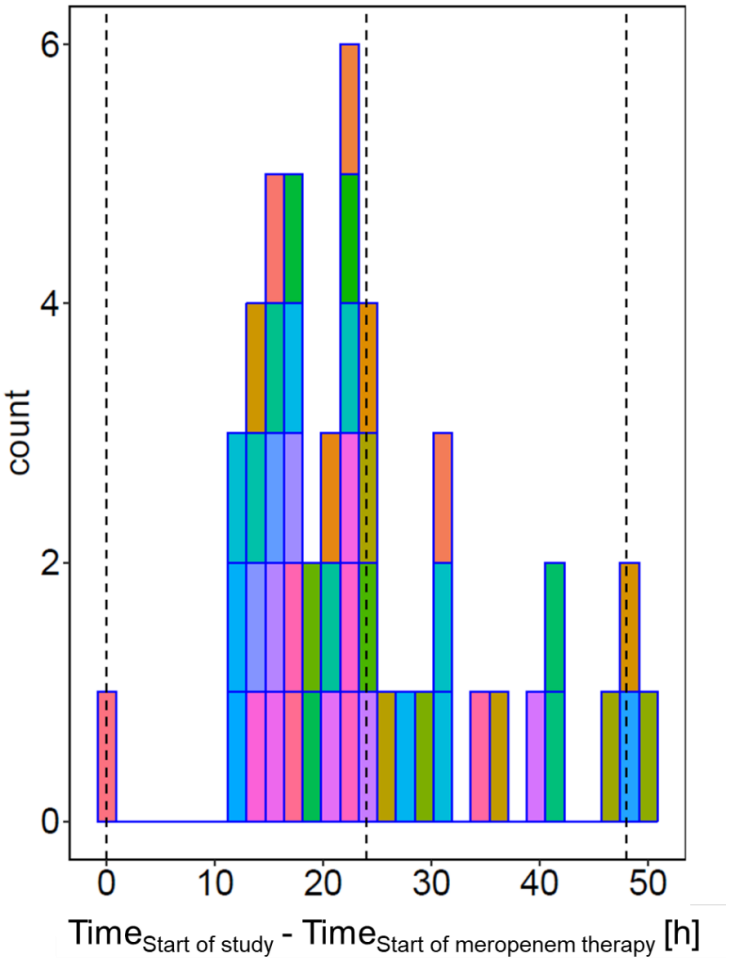

Figure S24: (Project III) Distribution of time of study start relative to time of meropenem therapy. Each colour represents one patient (n=48). The vertical dashed lines indicate 0, 24, 48 h.

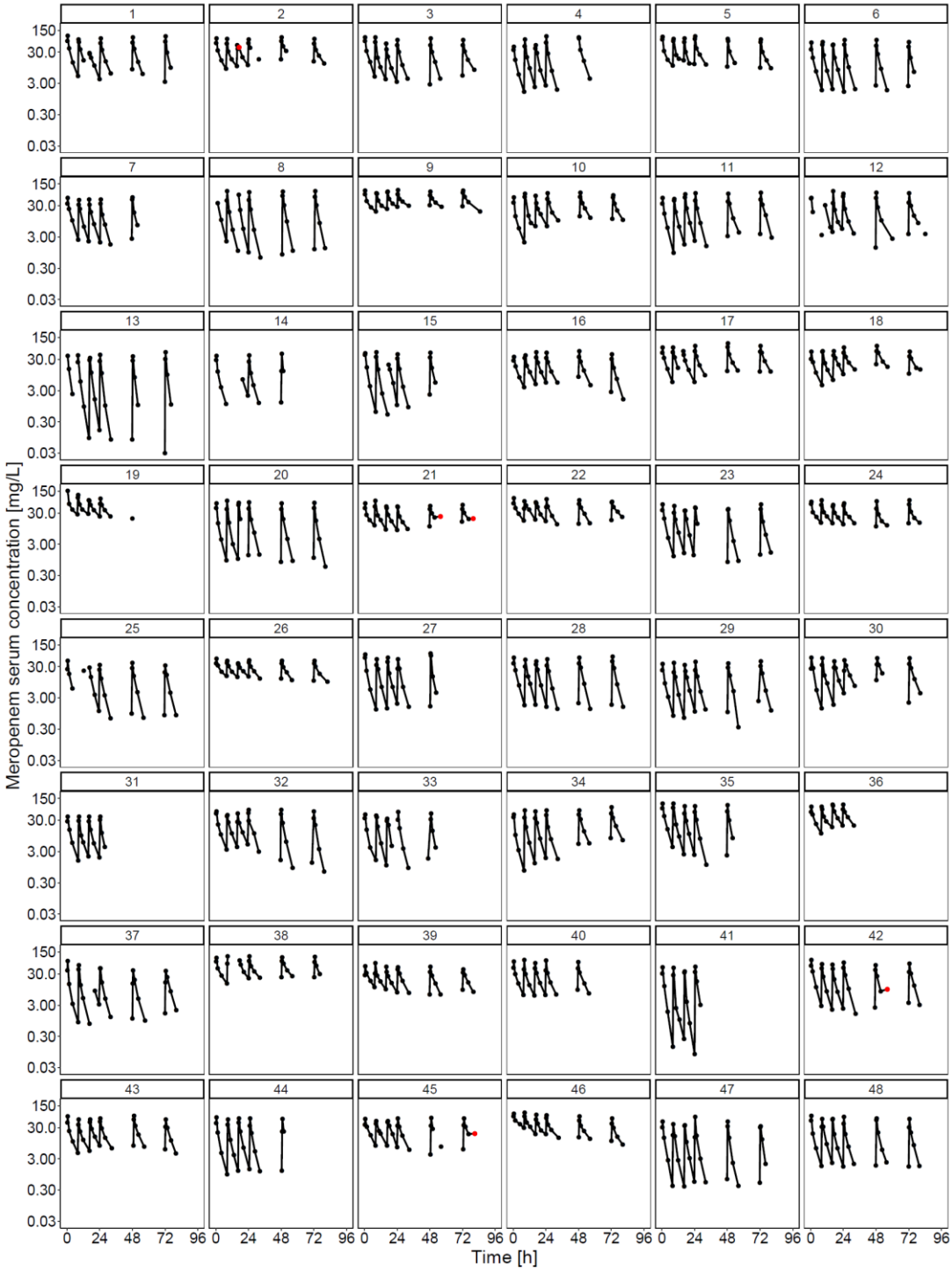

Figure S25: (Project III) Individual meropenem serum concentration-time profiles (modified from [233]).
Number above individual plot: Patient identifier; *Circles*: Measured meropenem concentrations; *Red circles:* Meropenem concentrations excluded from analyses (0.36%, Section 3.3.1.2); *Lines*: Connection of consecutively sampled meropenem concentrations, i.e. gaps represent non-monitored dosing intervals or missing planned meropenem concentration measurements.

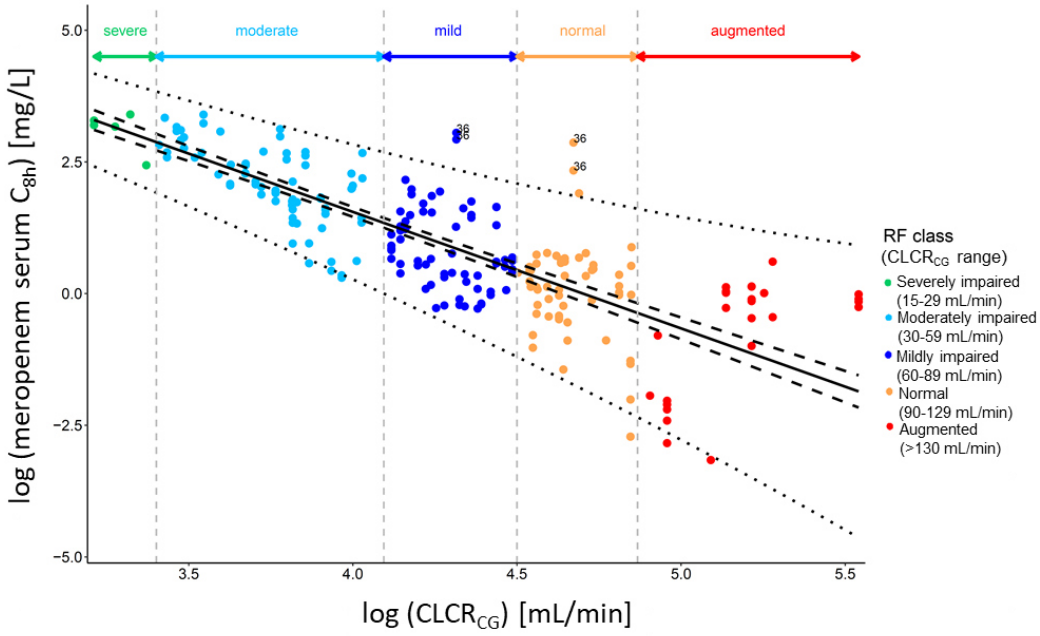

Figure S26: (Project III) Quantified relationship between meropenem serum concentrations and creatinine clearance on logarithmic scale, including confidence and prediction intervals (modified from [233]).
Logarithmised meropenem serum concentrations 8 h after start of infusion (C_{8h}) in non-CRRT patients vs. logarithmised $CLCR_{CG}$ are shown. *Colour of symbols*: Respective renal function (RF) class of a patient at time of determined C_{8h} value; *Dashed vertical lines/horizontal arrows*: Separation of renal function classes; *Data points labelled with 36*: Four C_{8h} values of patient 36; *Black solid line:* Quantified log($CLCR_{CG}$) - log(C_{8h}) relationship (representing log($C_{8h,\,pred}$), excluding data of patient 36); *Black dashed/dotted lines:* 95% confidence interval/95% prediction interval (excluding data of patient 36).
Abbreviations: *$CLCR_{CG}$*: Creatinine clearance estimated according to Cockcroft and Gault [2]; *CRRT*: Continuous renal replacement therapy; *C_{8h}*: Concentration 8 h after start of infusion; RF: Renal function.

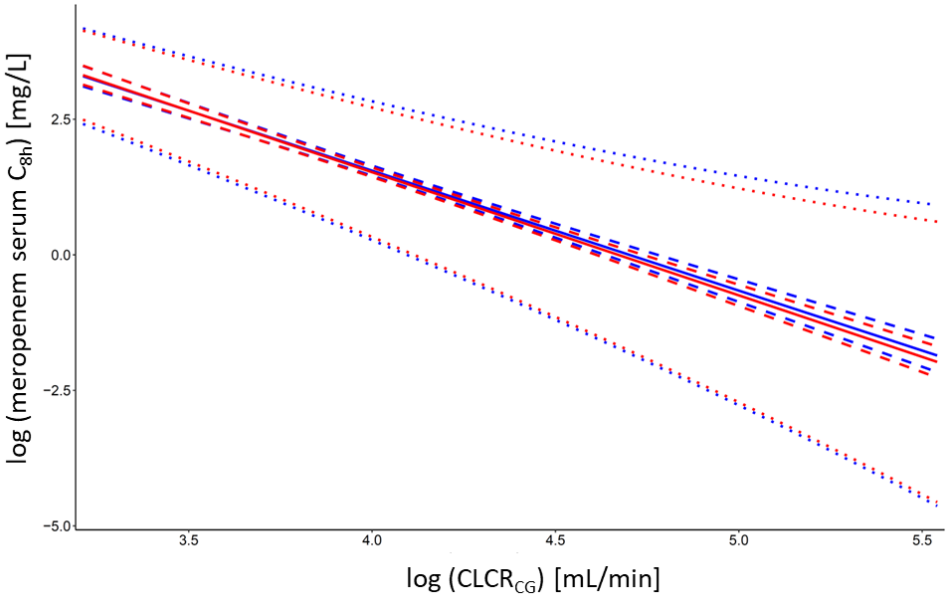

Figure S27: (Project III) Comparison of C_{8h} meropenem predictions including or excluding patient 36 in model parameter estimation (modified from [233]).
Solid/dashed/dotted lines: Quantified log($CLCR_{CG}$) - log(C_{8h}) relationship/95% confidence interval/95% prediction interval; *Red*: Excluding patient 36; *Blue*: Including patient 36.
Abbreviations: *$CLCR_{CG}$*: Creatinine clearance estimated according to Cockcroft-Gault [2]; *C_{8h}*: Concentration 8 h after start of infusion.

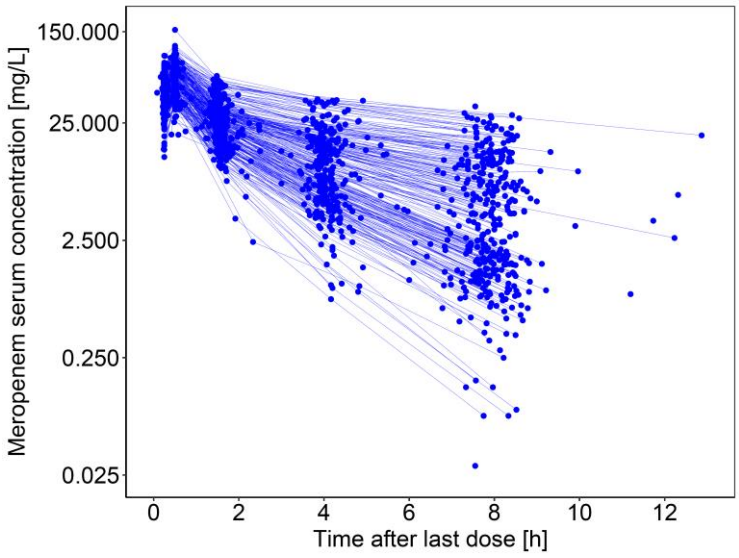

Figure S28: (Project IV) Meropenem serum concentration vs. time after last dose for all patients and all monitored infusions on semilogarithmic scale.

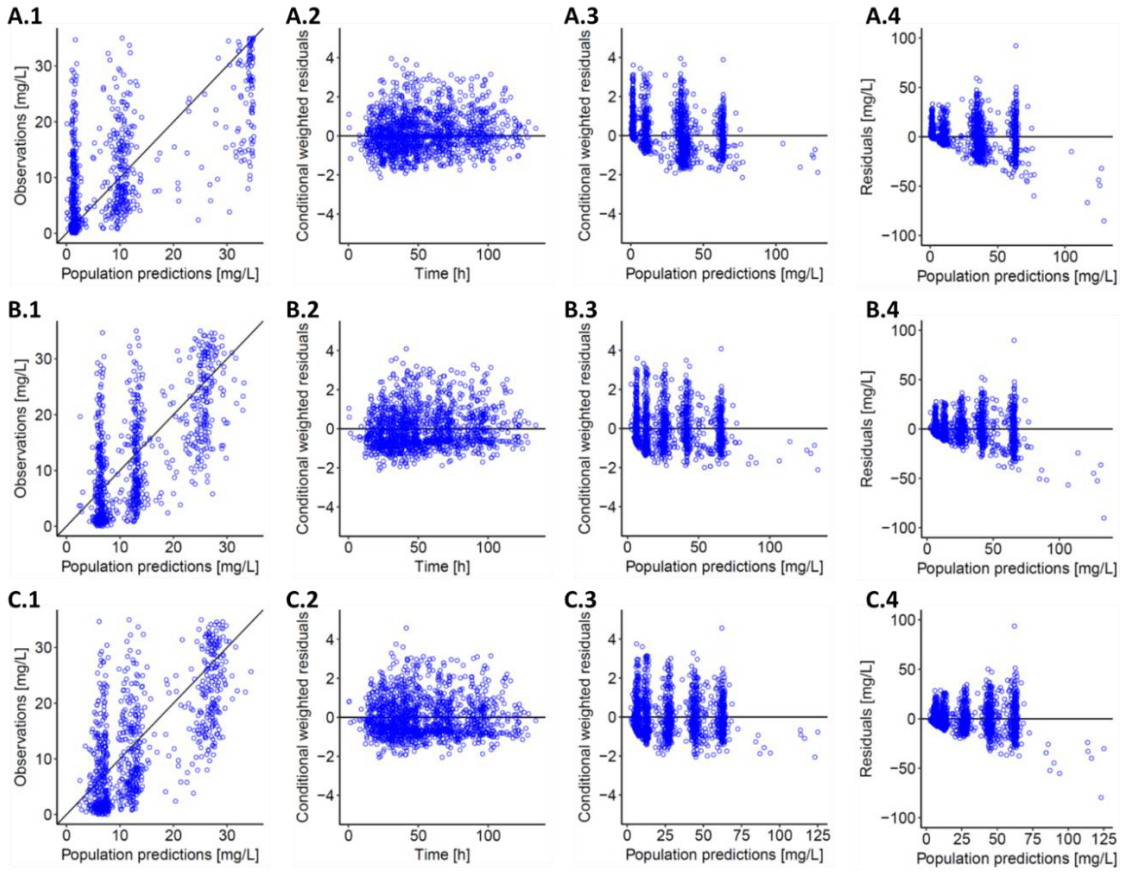

Figure S29: (Project IV) Observed vs. population predicted meropenem concentrations (1), CWRES vs. time (2) and population predicted meropenem concentrations (3) and residuals vs. population predicted meropenem concentrations (4) for a one-CMT model (A), two-CMT (B) and three-CMT (C) structural model without IIV and with combined RUV.

Circles: Observed vs. population predicted meropenem concentrations (1), conditional weighted residuals vs. time (2) and population predicted meropenem concentrations (3).

Lines: Line of identity (1), reference lines at y=0 (2, 3).

Abbreviations: *CMT*: Compartment; *CWRES*: Conditional weighted residuals; *IIV*: Interindividual variability; *RUV*: Residual unexplained variability.

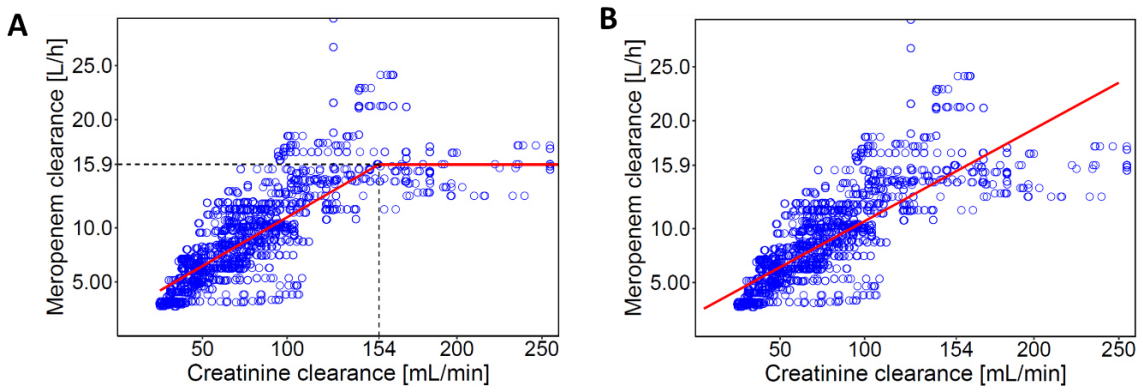

Figure S30: (Project IV): Meropenem clearance vs. creatinine clearance, including a piecewise (A) and linear (B) relationship (modified from [243]).
Blue circles: Individual meropenem clearance (base model); *Red line:* A: Identified piecewise linear relationship between $CLCR_{CG}$ and meropenem clearance of final NLME model, B: Identified linear relationship of the competing model; *Dashed black lines:* Inflection point of $CLCR_{CG}$ (vertical) and maximum meropenem clearance (horizontal).
Abbreviations: *$CLCR_{CG}$*: Creatinine clearance estimated according to Cockcroft and Gault [2].

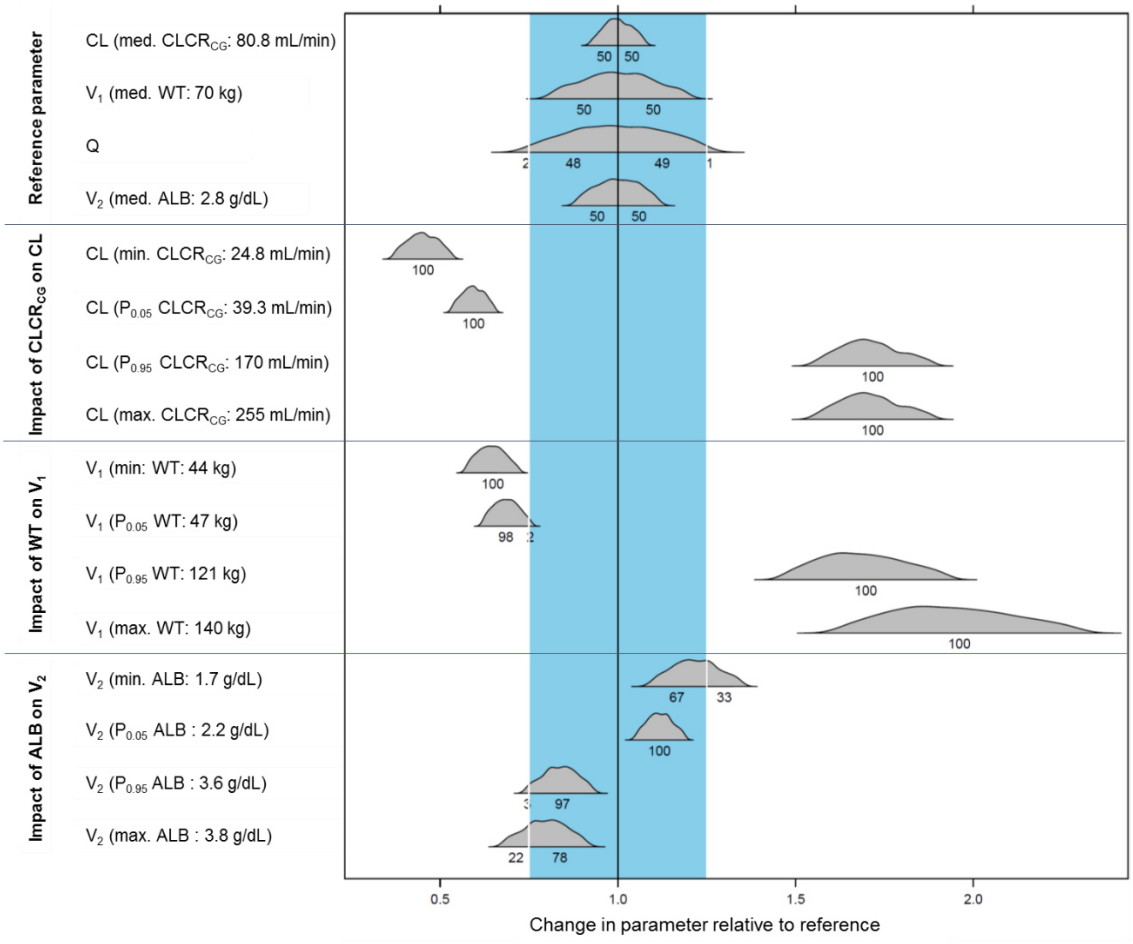

Figure S31: (Project IV) Forrest plot for the final NLME model, illustrating the impact of the covariates on the PK parameters.
Vertical line: Reference (x=1); *Blue shaded area*: ±20% change from reference (x=0.8-1.2); *Grey distribution* (upper panel): Distribution of the PK parameter for the reference covariate value; *Grey distribution* (lower thee panels): Distribution of relative change from the reference PK parameter, for a specific covariate value.
Abbreviations: *ALB*: Serum albumin concentration; *CL*: Clearance; *$CLCR_{CG}$*: Creatinine clearance according to Cockcroft and Gault; *CMT*: Compartment; *max.*: Maximum; *med.*: Median; *min.*: Minimum, *Q:* Intercompartmental clearance between CMT 1 and 2, respectively; *V_1, V_2*: Central and peripheral volume of distribution; *WT*: Total body weight.

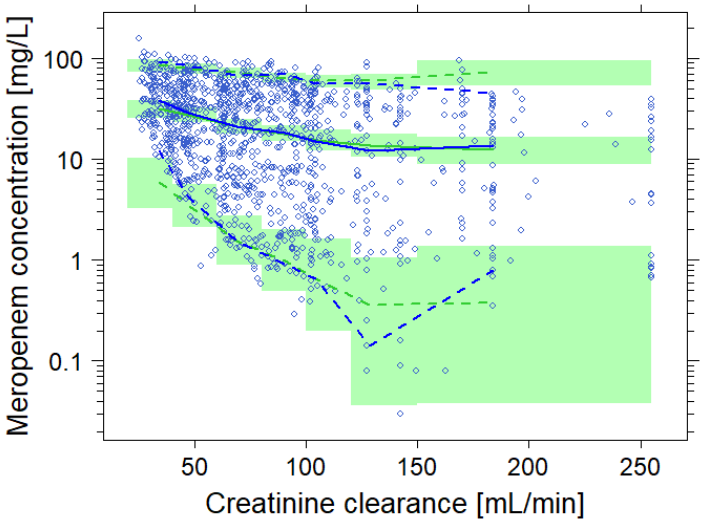

Figure S32: (Project IV) Visual predictive check (n=1000 simulations) for the final NLME model of meropenem in critically ill patients, using $CLCR_{CG}$ as independent variable.
Abbreviations: *$CLCR_{CG}$*: Creatinine clearance according to Cockcroft and Gault

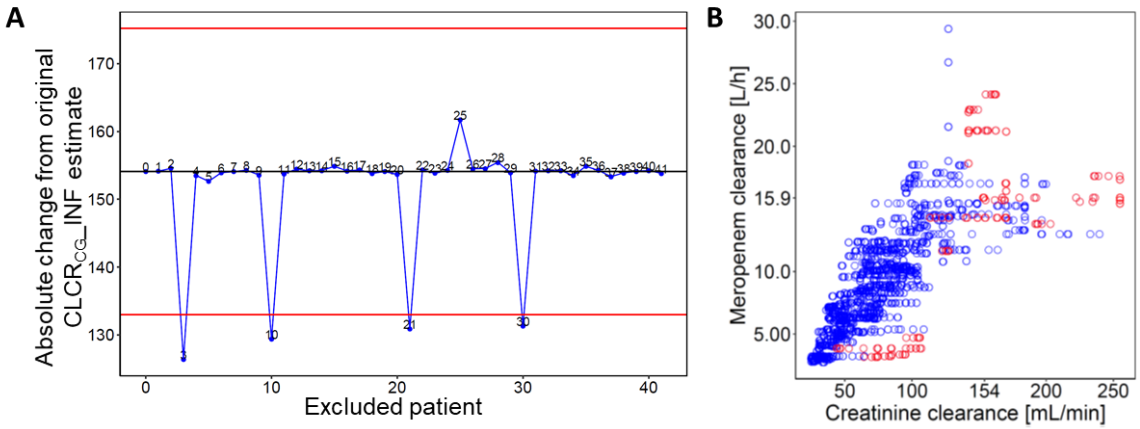

Figure S33: (Project IV) Case deletion diagnostic for the inflection point of $CLCR_{CG}$ (A) and meropenem clearance vs. $CLCR_{CG}$, highlighting the influential individuals detected in A (B).
A: *Blue circles*: $CLCR_{CG}$_INF estimate after exclusion of a specific patient; *Black line*: Original parameter estimate (including all patients); *Red lines*: Limits of 95% confidence interval computed based as parameter estimate (154 mL/min) ± 1.96 · SE (10.6 mL/min). ***B:*** *Red and blue circles*: Individual meropenem clearance (base model) of the influential patients identified in A and the non-influential patient, respectively.
Abbreviations: *$CLCR_{CG}$*: Creatinine clearance according to Cockcroft and Gault; *$CLCR_{CG}$_INF*: $CLCR_{CG}$ value serving as inflection point for meropenem clearance.

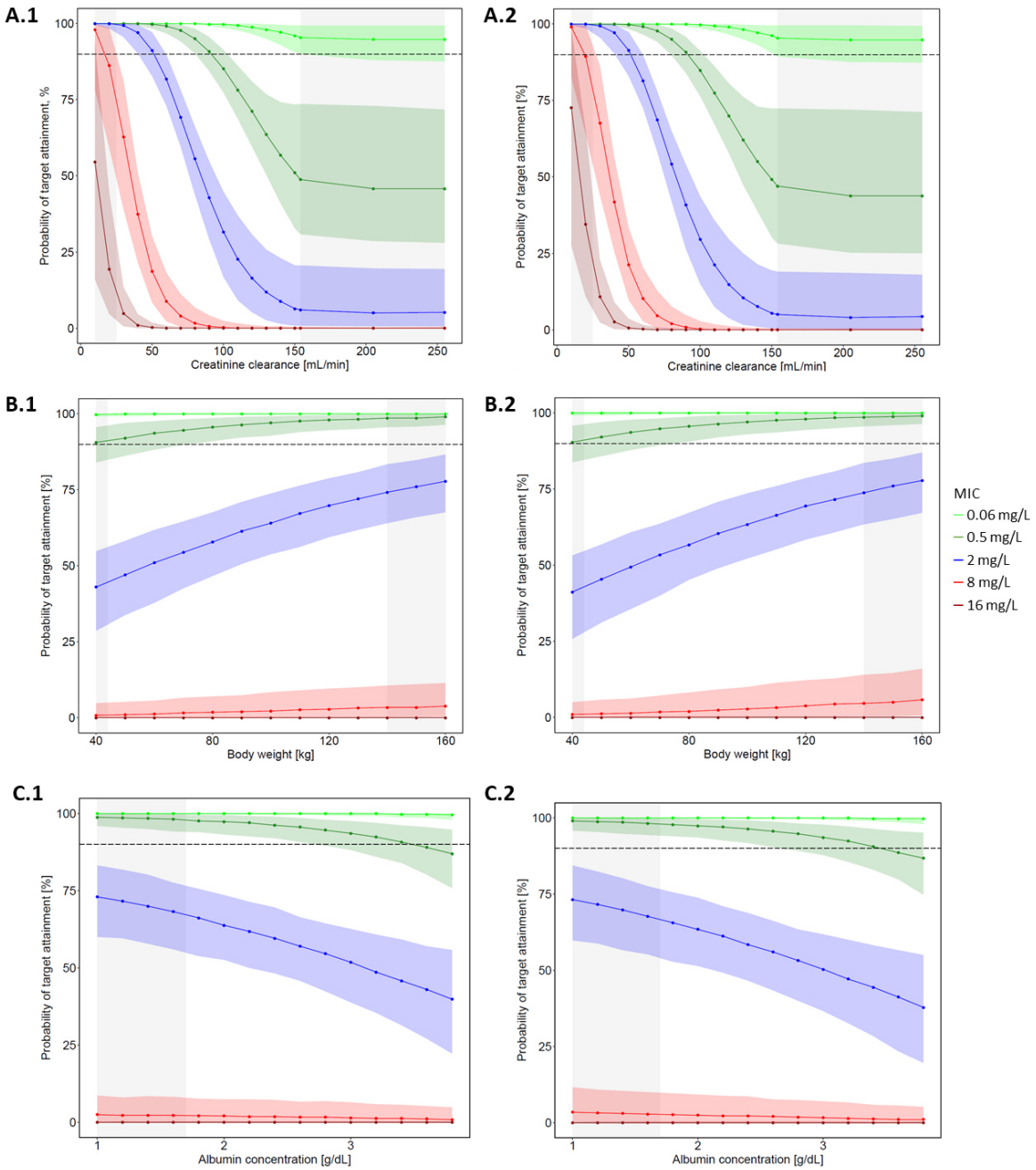

Figure S34: (Project IV) Probability of target (98%$T_{>MIC}$) attainment vs. different covariates given selected MIC values for standard meropenem treatment (1000 mg, 30-min i.v. infusion, q8h) (modified from [243]).
A: Varied $CLCR_{CG}$, body weight and serum albumin concentration set to median of first study day (i.e. 70 kg, 2.8 g/dL); *B:* Varied body weight, $CLCR_{CG}$ and serum albumin concentration set to median of first study day (i.e. 80.8 mL/min, 2.8 g/dL); *C:* Varied serum albumin concentration, $CLCR_{CG}$ and body weight set to median of first study day (i.e. 80.8 mL/min, 70 kg). *Left panel* (A.1, B.1, C.1): Treatment day 1; *Right panel* (A.2, B.2, C.2): Treatment day 4.
Dashed horizontal line: PTA of 90%; *Coloured circles and lines + shaded areas*: Median + 90%CI of 1000 PTA values derived from Monte Carlo simulations considering PK parameter uncertainty; *Grey shaded areas*: Extrapolated covariate range not covered by the study population or $CLCR_{CG}$ ≥154 mL/min (=inflection point of $CLCR_{CG}$ -CL relationship).
Abbreviations: *MIC*: Minimum inhibitory concentration; *CI*: Confidence interval; *CL*: Clearance; *$CLCR_{CG}$*: Creatinine clearance according to Cockcroft and Gault; *PTA*: Probability of target attainment, *q8h*: Every 8 hours; *$T_{>MIC}$:* Time period that total drug concentration exceeds the MIC.

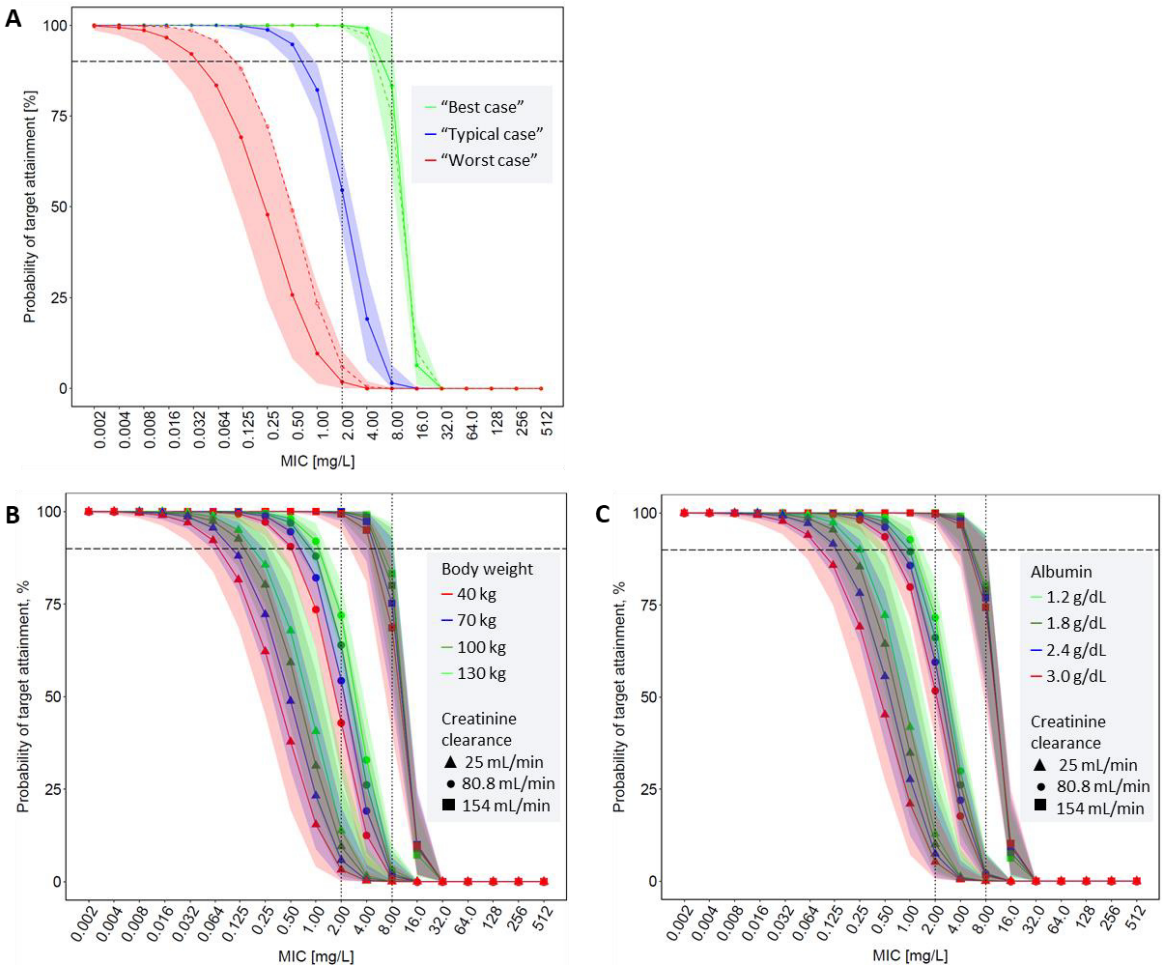

Figure S35: (Project IV) Probability of target ($98\%T_{>MIC}$) attainment vs. MIC for different covariate combinations on the first day of standard meropenem treatment (1000 mg, 30-min i.v. infusion, q8h) (modified from [243]).

A: *Solid line*: Best, typical, worst case based on all three covariates (i.e. Best case: $CLCR_{CG}$ 25 mL/min, body weight 121 kg, serum albumin concentration 2.2 g/dL; Typical case: $CLCR_{CG}$ 80.8 mL/min, body weight 70 kg, serum albumin concentration 2.8 g/dL; Worst case: $CLCR_{CG}$ 154 mL/min, body weight 47 kg, serum albumin concentration 3.6 g/dL); *Dashed line*: Best, typical, worst case based on $CLCR_{CG}$ only (i.e. Best case: $CLCR_{CG}$ 25 mL/min, body weight 70 kg, serum albumin concentration 2.8 g/dL; Typical case: $CLCR_{CG}$ 80.8 mL/min, body weight 70 kg, serum albumin concentration 2.8 g/dL; Worst case: $CLCR_{CG}$ 154 mL/min, body weight 70 kg, serum albumin concentration 2.8 g/dL).

B: Varied body weight, serum albumin concentration set to median of first study day (i.e. 2.8 g/dL), $CLCR_{CG}$ set to minimum, median and inflection point of $CLCR_{CG}$ -CL relationship (i.e. squares: minimum=25 mL/min; circles: median=80.8 mL/min; triangles: inflection point=154 mL/min).

C: Varied serum albumin concentration, body weight set to median of first study day (i.e. 70 kg), $CLCR_{CG}$ set to minimum, median and inflection point of $CLCR_{CG}$ -CL relationship (i.e. squares: minimum=25 mL/min; circles: median=80.8 mL/min; triangles: inflection point=154 mL/min).

Dashed horizontal line: PTA of 90%; ***Coloured circles and solid lines + shaded areas***: Median + 90%CI of 1000 PTA values derived from Monte Carlo simulations considering PK parameter uncertainty. ***Coloured circles and dashed lines***: For comparison: median of PTA simulations (n=1000) including parameter uncertainty for best, typical and worst-case scenario based on $CLCR_{CG}$ only (body weight and serum albumin concentration set to median of first study day).

Abbreviations: *MIC*: Minimum inhibitory concentration; *CI*: Confidence interval; *CL*: Clearance; $CLCR_{CG}$: Creatinine clearance according to Cockcroft and Gault; *PTA*: Probability of target attainment, *q8h*: Every 8 hours; $T_{>MIC}$: Time period that total drug concentration exceeds the MIC.

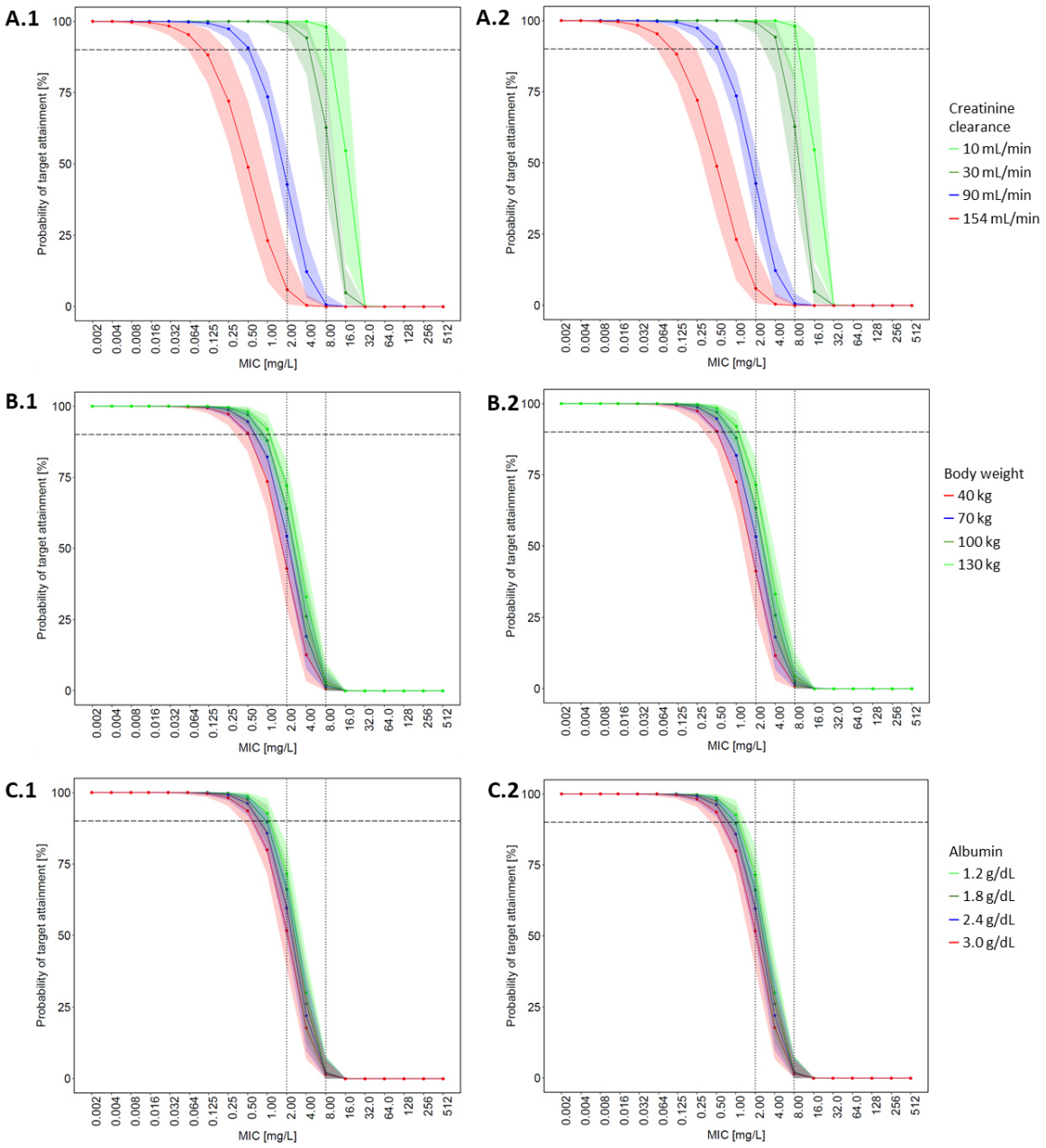

Figure S36: (Project IV) Probability of target (98%$T_{>MIC}$) attainment vs. MIC given selected covariate values for standard meropenem treatment (1000 mg, 30-min i.v. infusion, q8h) (modified from [243]).
A: Varied $CLCR_{CG}$, body weight and serum albumin concentration set to median of first study day (i.e. 70 kg, 2.8 g/dL); *B:* Varied body weight, $CLCR_{CG}$ and serum albumin concentration set to median of first study day (i.e. 80.8 mL/min, 2.8 g/dL); ***C:*** Varied serum albumin concentration, $CLCR_{CG}$ and body weight set to median of first study day (i.e. 80.8 mL/min, 70 kg). *Left panel* (A.1, B.1, C.1): Treatment day 1; *Right panel* (A.2, B.2, C.2): Treatment day 4.
Dashed horizontal line: PTA of 90%; *Dashed vertical line:* Non-species-related EUCAST PK/PD breakpoints for meropenem (S breakpoint: 2 mg/L, R breakpoint: 8 mg/L; [5]); *Coloured dots and lines + shaded areas*: Median + 90%CI of 1000 PTA values derived from Monte Carlo simulations considering PK parameter uncertainty.
Abbreviations: *MIC*: Minimum inhibitory concentration; *CI*: Confidence interval; *$CLCR_{CG}$*: Creatinine clearance according to Cockcroft and Gault; *PTA*: Probability of target attainment, *q8h*: Every 8 hours; *R category*: Category 'resistant' [4]; *R breakpoint*: MIC breakpoint separating I and R category [5]; *S category*: Category 'susceptible at normal dosing' [4]; *S breakpoint*: MIC breakpoint separating S and I category [5]; *$T_{>MIC}$:* Time period that total drug concentration exceeds the MIC.

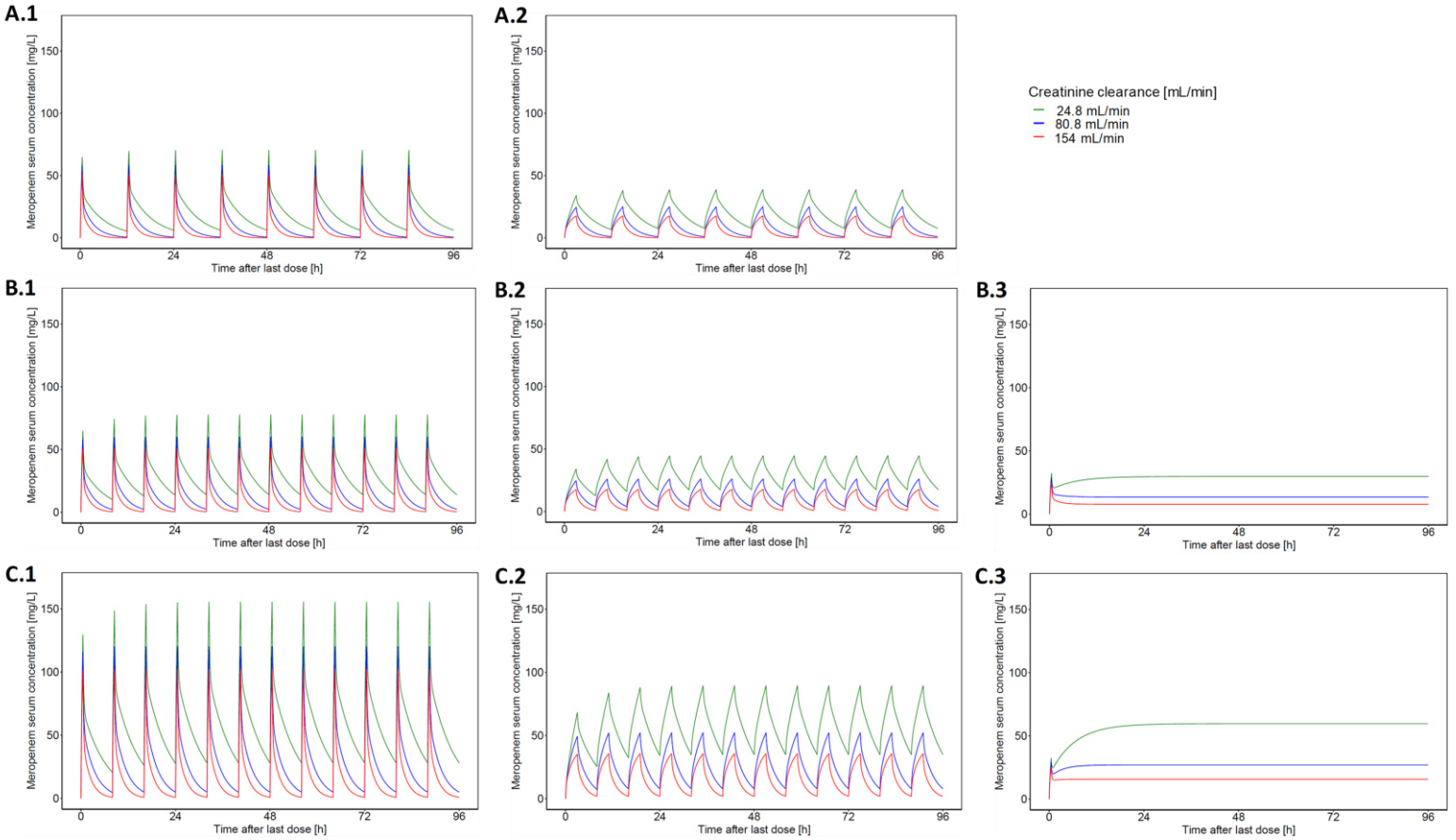

Figure S37: (Project IV) Typical simulated meropenem concentration-time profile for varying $CLCR_{CG}$, following standard and alternative dosing regimens.

Deterministic exposure simulations were performed for short-term (1), prolonged (2) and continuous dosing regimens (3), for daily meropenem dose of 2000 mg (A), 3000 mg (3412.5 mg for first day of CI, incl. loading dose) (B) and 6000 mg (6875 mg for first day of CI, incl. loading dose) (C).

Colour coding indicates $CLCR_{CG}$ value: *green*: 24.8 mL/min (=minimum of first study day), *blue*: 80.8 mL/min (=median of first study day), *red*: 154 mL/min (=inflection point of $CLCR_{CG}$-CL relationship).

Abbreviations: *CL*: Clearance; *$CLCR_{CG}$:* Creatinine clearance estimated according to Cockcroft and Gault [2].

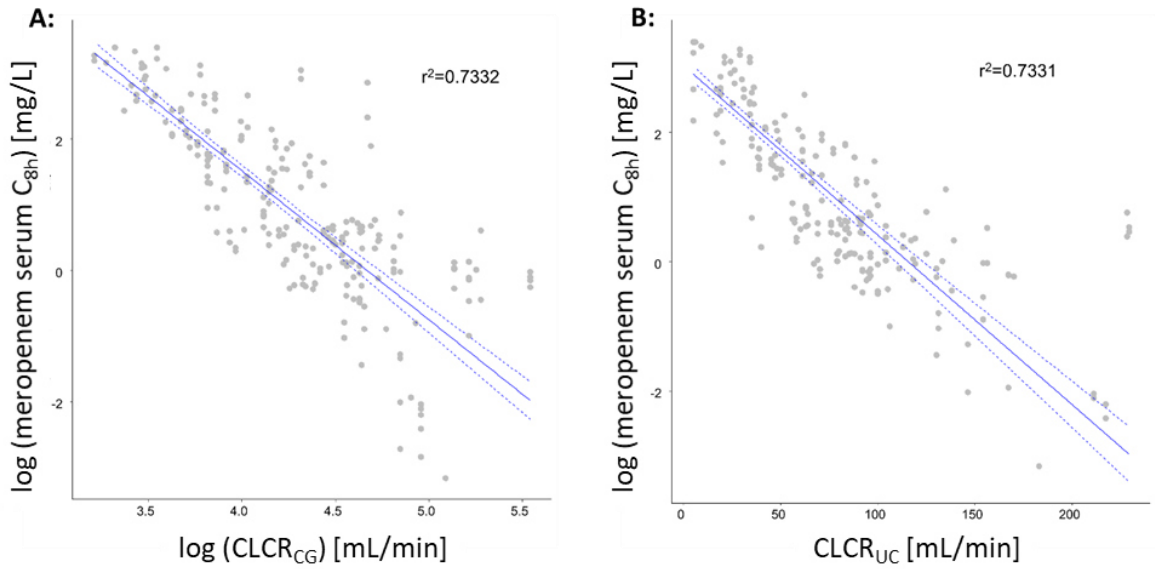

Figure S38: (Project III) Relation between meropenem serum C_{8h} and $CLCR_{CG}$ (A) or $CLCR_{UC}$ (B) (modified from [233]).

Blue solid line: Quantified relationship between renal function marker and meropenem serum C_{8h}. The relationship was quantified using a weighted (1/CLCR) linear least square regression on (A) double logarithmic ($\log(CLCR_{CG})$ and $\log(C_{8h})$) and (B) semilogarithmic scale ($CLCR_{UC}$ and $\log(C_{8h})$) for $CLCR_{CG}$ and $CLCR_{UC}$, respectively; *Blue dotted line*: 95% confidence interval around relationship.

Abbreviations: $CLCR_{CG}$: Creatinine clearance estimated according to Cockcroft and Gault [2]; $CLCR_{UC}$: Creatinine clearance determined using 24-hour urine collection; C_{8h}: Concentration at 8 h after infusion start.

7.3 Supplementary formulae

7.3.1 General statistics

This section summarises general statistical measures to characterise a distribution with respect to the central tendency (Section 7.3.1.1) and the dispersion (Section 7.3.1.2).

7.3.1.1 Measures of central tendency

The following measures of central tendency can be used to describe the typical value of a distribution

Mean		$\bar{x} = \frac{\sum_{i=1}^{n} x_i}{n}$	(Eq. 7.1)
Median	If n is odd:	$\tilde{x} = x_{\frac{n+1}{2}}$	(Eq. 7.2)
	If n is even:	$\tilde{x} = 0.5 \cdot \left(x_{\frac{n}{2}} + x_{\frac{n+1}{2}}\right)$	
Geometric mean		$\bar{x}_{geom} = \sqrt[n]{\prod_{i=1}^{n} x_i}$	(Eq. 7.3)

7.3.1.2 Measures of dispersion

The following measures of dispersion can be used to describe the variability of a distribution:

Variance	$\sigma^2 = \frac{1}{n-1} \cdot \sum_{i=1}^{n} (x_i - \bar{x})^2$	(Eq. 7.4)
Standard deviation	$\sigma = \sqrt{\sigma^2}$	(Eq. 7.5)
Coefficient of variation	$CV, \% = \frac{\sigma}{\bar{x}} \cdot 100$	(Eq. 7.6)
Geometric standard deviation	$\sigma_{geom} = \exp\left(\sqrt{\frac{1}{n} \cdot \sum_{i=1}^{n} \left[ln\left(\frac{x_i}{\bar{x}_{geom}}\right)\right]}\right)$	(Eq. 7.7)
Range	$R = x_{min} - x_{max}$	(Eq. 7.8)

Percentile	If n is odd:	$P = x_{n \cdot p}$	(Eq. 7.9)
	If n is even:	$P = 0.5 \cdot \left(x_{n \cdot p} + x_{n \cdot p+1}\right)$	

For computation of CV in the log-normal domain Eq. 2.6 can be used.

7.3.2 Body size descriptors

A variety of descriptors exist to characterise the body size of a patient. The descriptors are computed based on patient-specific characteristics such as total body weight (WT), body height (HT) or sex.

Body mass index (BMI) [391]		$BMI\left[\frac{kg}{m^2}\right] = \frac{WT[kg]}{(HT[m])^2}$	(Eq. 7.10)
Lean body weight (LBW) [392]	If male:	$LBW_m[kg] = \frac{9270 \cdot WT[kg]}{6680+216 \cdot BMI\left[\frac{kg}{m^2}\right]}$	(Eq. 7.11)
	If female:	$LBW_f[kg] = \frac{9270 \cdot WT\,[kg]}{8780+244 \cdot BMI\left[\frac{kg}{m^2}\right]}$	
Fat mass (FM)		$FM = WT - LBW$	(Eq. 7.12)
Ideal body weight (IBW) [393]	If male:	$IBW_m[kg] = 50 + 0.89 \cdot (HT[cm] - 152.4)$	(Eq. 7.13)
	If female:	$IBW_f[kg] = 45.5 + 0.89 \cdot (HT\,[cm] - 152.4)$	
Adjusted body weight (ABW)		$ABW[kg] = IBW[kg] + 0.4 \cdot (WT[kg] - IBW[kg])$ Equation used if WT>IBW+30%, otherwise IBW used	(Eq. 7.14)

7.3.3 Renal function markers

Creatinine clearance (CLCR) is a marker to describe the renal function of a patient, which can be determined in different ways. CLCR can be measured by urine collection over a defined time interval (Δt) and determination of the urine volume (V_{urine}) as well as the creatinine concentrations in serum (C_{crea_serum}) and urine (C_{crea_urine}). Alternatively, CLCR can be estimated e.g. according to the Cockcroft and Gault equation based on the determinants age, total body weight (WT) and C_{crea_serum}. [2].

Creatinine clearance, urine collection (**$CLCR_{UC}$**)	$$CLCR_{UC}\left[\frac{mL}{min}\right] = \frac{C_{crea\_urine}[mg/dL] \cdot V_{urine}[mL]}{C_{crea\_serum}[mg/dL] \cdot \Delta t[min]}$$	(Eq. 7.15)
Creatinine clearance, Cockcroft and Gault (**$CLCR_{CG}$**) [2]	$$CLCR_{CG}\left[\frac{mL}{min}\right] = \frac{(140 - age[years]) \cdot WT[kg]}{72 \cdot C_{crea_serum}[mg/dL]}$$ $$(\cdot\ 0.85\ if\ female)$$	(Eq. 7.16)

7.3.4 Haemodynamic markers

Different markers exist to describe the haemodynamic of a patient, e.g. heart rate, blood pressure (diastolic blood pressure (DP), systolic blood pressure (SP)), mean arterial pressure (MAP), cardiac output (CO), which can be measured and/or estimated based on different determinants:

MAP	$$MAP\ [mmHg] = \frac{(2 \cdot DP\ [mmHg]) + SP\ [mmHg]}{3}$$	(Eq. 7.17)
CO_{LZ} (Liljestrand and Zander; unadjusted) [3]	$$CO_{LZ}\left[\frac{L}{min}\right] = SV_{Est}\ [L] \cdot HR\ [\frac{1}{min}]$$ $$Stroke\ volume\ [L]\ (SV_{Est}) = \frac{SP\ - DP}{SP + DP}$$	(Eq. 7.18)

7.3.5 Linear interpolation of covariates

Linear interpolation was used in Project IV for longitudinally measured continuous covariates (2.9.2.1 Dataset generation: Handling of missing covariate data: Imputation and interpolation). A graphical illustration is provided in Figure S39 in a generic manner and in Appendix Figure S2 for selected exemplary covariates. The formula for the linear interpolation between two longitudinally measured continuous covariate values is stated as follows (Eq. 7.17):

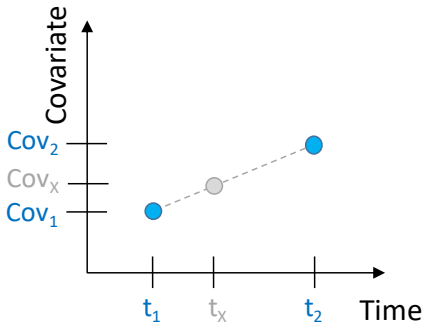

Figure S39: Graphical illustration of linear interpolation of covariates .
Abbreviations: *Cov*: Covariate; *t*: Time.

$$Cov_x = \frac{Cov_2\ -\ Cov_1}{t_2\ -\ t_1} \cdot (t_x\ -\ t_1) + Cov_1 \qquad \text{(Eq. 7.19)}$$

In Eq. 7.17, Cov_1 and Cov_2 represent the measured covariate values at the time points t_1 and t_2, respectively. Cov_x is the linearly interpolated covariate value of interest at a given time t_x, which lies between the two measured covariate values.

7.4 NONMEM® dataset and model script

7.4.1 Project I: NONMEM® dataset

Table S30: (Project I) Subset of NONMEM® dataset for linezolid PK data exemplified for a generic obese patient.

ID	TIME	AMT	RATE	DV	MDV	EVID	CMT	FLAG	CIN	TIN	ANAE	ANSTOP	MAP	OBE	WT	HT	LBW	BMI	SEX	…
1	0	600	1200	.	1	1	1	0	.	.	1	3.82	97.0	1	119	1.65	56.7	43.7	2	…
1	0.02	.	.	.	1	2	3	0	.	0.5	1	3.82	96.3	1	119	1.65	56.7	43.7	2	…
1	0.02	.	.	.	1	2	4	0	.	0.5	1	3.82	96.3	1	119	1.65	56.7	43.7	2	…
1	0.48	.	.	27.1	0	0	1	3	.	.	1	3.82	92.1	1	119	1.65	56.7	43.7	2	…
1	0.48	.	.	23.4	0	0	1	6	.	.	1	3.82	92.1	1	119	1.65	56.7	43.7	2	…
1	0.53	.	.	0.99	0	0	3	1	.	0.5	1	3.82	93.8	1	119	1.65	56.7	43.7	2	…
1	0.53	.	.	1.11	0	0	4	4	.	0.5	1	3.82	93.8	1	119	1.65	56.7	43.7	2	…
1	0.53	.	.	.	1	2	-3	0	.	0.5	1	3.82	93.8	1	119	1.65	56.7	43.7	2	…
1	0.53	.	.	.	1	2	-4	0	.	0.5	1	3.82	93.8	1	119	1.65	56.7	43.7	2	…
1	0.53	.	.	.	1	2	3	0	.	0.52	1	3.82	93.8	1	119	1.65	56.7	43.7	2	…
1	0.53	.	.	.	1	2	4	0	.	0.52	1	3.82	93.8	1	119	1.65	56.7	43.7	2	…
1	0.98	.	.	13.4	0	0	1	3	.	.	1	3.82	77.5	1	119	1.65	56.7	43.7	2	…
1	1.04	.	.	1.88	0	0	3	1	.	0.52	1	3.82	72.3	1	119	1.65	56.7	43.7	2	…
1	1.04	.	.	3.12	0	0	4	4	.	0.52	1	3.82	72.3	1	119	1.65	56.7	43.7	2	…
1	1.04	.	.	.	1	2	-3	0	.	0.52	1	3.82	72.3	1	119	1.65	56.7	43.7	2	…
1	1.04	.	.	.	1	2	-4	0	.	0.52	1	3.82	72.3	1	119	1.65	56.7	43.7	2	…
1	1.04	.	.	.	1	2	3	0	.	0.48	1	3.82	72.3	1	119	1.65	56.7	43.7	2	…
1	1.04	.	.	.	1	2	4	0	.	0.48	1	3.82	72.3	1	119	1.65	56.7	43.7	2	…

Table S30 [continued]

ID	TIME	AMT	RATE	DV	MDV	EVID	CMT	FLAG	CIN	TIN	ANAE	ANSTOP	MAP	OBE	WT	HT	LBW	BMI	SEX	…
1	1.51	.	.	2.25	0	0	3	1	.	0.48	1	3.82	67.0	1	119	1.65	56.7	43.7	2	…
1	1.51	.	.	2.89	0	0	4	4	.	0.48	1	3.82	67.0	1	119	1.65	56.7	43.7	2	…
1	1.51	.	.	.	1	2	-3	0	.	0.48	1	3.82	67.0	1	119	1.65	56.7	43.7	2	…
1	1.51	.	.	.	1	2	-4	0	.	0.48	1	3.82	67.0	1	119	1.65	56.7	43.7	2	…
1	1.51	.	.	.	1	2	3	0	.	0.5	1	3.82	67.0	1	119	1.65	56.7	43.7	2	…
1	1.51	.	.	.	1	2	4	0	.	0.5	1	3.82	67.0	1	119	1.65	56.7	43.7	2	…
1	1.98	.	.	13	0	0	1	3	.	.	1	3.82	66.8	1	119	1.65	56.7	43.7	2	…
1	2.03	.	.	2.61	0	0	3	1	.	0.5	1	3.82	65.1	1	119	1.65	56.7	43.7	2	…
1	2.03	.	.	2.44	0	0	4	4	.	0.5	1	3.82	65.1	1	119	1.65	56.7	43.7	2	…
1	2.03	.	.	.	1	2	-3	0	.	0.5	1	3.82	65.1	1	119	1.65	56.7	43.7	2	…
1	2.03	.	.	.	1	2	-4	0	.	0.5	1	3.82	65.1	1	119	1.65	56.7	43.7	2	…
1	2.03	.	.	.	1	2	3	0	.	0.98	1	3.82	65.1	1	119	1.65	56.7	43.7	2	…
1	2.03	.	.	.	1	2	4	0	.	0.98	1	3.82	65.1	1	119	1.65	56.7	43.7	2	…
1	2.97	.	.	8.71	0	0	1	3	.	.	1	3.82	68.8	1	119	1.65	56.7	43.7	2	…
1	2.97	.	.	7.49	0	0	1	6	.	.	1	3.82	68.8	1	119	1.65	56.7	43.7	2	…
1	3.02	.	.	2.13	0	0	3	1	.	0.98	1	3.82	68.8	1	119	1.65	56.7	43.7	2	…
1	3.02	.	.	2.08	0	0	4	4	.	0.98	1	3.82	68.8	1	119	1.65	56.7	43.7	2	…
1	3.02	.	.	.	1	2	-3	0	.	0.98	1	3.82	68.8	1	119	1.65	56.7	43.7	2	…

Table S30 [continued]

ID	TIME	AMT	RATE	DV	MDV	EVID	CMT	FLAG	CIN	TIN	ANAE	ANSTOP	MAP	OBE	WT	HT	LBW	BMI	SEX	…
1	3.02	.	.	.	1	2	-4	0	.	0.98	1	3.82	69.3	1	119	1.65	56.7	43.7	2	…
1	3.02	.	.	.	1	2	3	0	.	1	1	3.82	69.3	1	119	1.65	56.7	43.7	2	…
1	3.02	.	.	.	1	2	4	0	.	1	1	3.82	69.3	1	119	1.65	56.7	43.7	2	…
1	3.83	.	.	.	1	2	.	8	.	.	1	3.82	69.3	1	119	1.65	56.7	43.7	2	…
1	3.83	.	.	.	1	2	.	8	.	.	1	3.82	69.3	1	119	1.65	56.7	43.7	2	…
1	3.97	.	.	8.79	0	0	1	3	.	.	0	3.82	69.0	1	119	1.65	56.7	43.7	2	…
1	4.01	.	.	2.35	0	0	3	1	.	1	0	3.82	68.4	1	119	1.65	56.7	43.7	2	…
1	4.01	.	.	2.04	0	0	4	4	.	1	0	3.82	68.4	1	119	1.65	56.7	43.7	2	…
1	4.01	.	.	.	1	2	-3	0	.	1	0	3.82	68.4	1	119	1.65	56.7	43.7	2	…
1	4.01	.	.	.	1	2	-4	0	.	1	0	3.82	68.4	1	119	1.65	56.7	43.7	2	…
1	4.01	.	.	.	1	2	3	0	.	1.02	0	3.82	68.4	1	119	1.65	56.7	43.7	2	…
1	4.01	.	.	.	1	2	4	0	.	1.02	0	3.82	68.4	1	119	1.65	56.7	43.7	2	…
1	4.97	.	.	7.31	0	0	1	3	.	.	0	3.82	82.2	1	119	1.65	56.7	43.7	2	…
1	5.02	.	.	2.21	0	0	3	1	.	1.02	0	3.82	82.2	1	119	1.65	56.7	43.7	2	…
1	5.02	.	.	2.00	0	0	4	4	.	1.02	0	3.82	82.2	1	119	1.65	56.7	43.7	2	…
1	5.02	.	.	.	1	2	-3	0	.	1.02	0	3.82	82.2	1	119	1.65	56.7	43.7	2	…
1	5.02	.	.	.	1	2	-4	0	.	1.02	0	3.82	82.2	1	119	1.65	56.7	43.7	2	…
1	5.02	.	.	.	1	2	3	0	.	0.98	0	3.82	82.2	1	119	1.65	56.7	43.7	2	…

Table S30 [continued]

ID	TIME	AMT	RATE	DV	MDV	EVID	CMT	FLAG	CIN	TIN	ANAE	ANSTOP	MAP	OBE	WT	HT	LBW	BMI	SEX	…
1	5.02	.	.	.	1	2	4	0	.	0.98	0	3.82	82.2	1	119	1.65	56.7	43.7	2	…
1	5.97	.	.	6.32	0	0	1	3	.	.	0	3.82	99.8	1	119	1.65	56.7	43.7	2	…
1	6.03	.	.	1.45	0	0	3	1	.	0.98	0	3.82	99.8	1	119	1.65	56.7	43.7	2	…
1	6.03	.	.	1.77	0	0	4	4	.	0.98	0	3.82	99.8	1	119	1.65	56.7	43.7	2	…
1	6.03	.	.	.	1	2	-3	0	.	0.98	0	3.82	99.8	1	119	1.65	56.7	43.7	2	…
1	6.03	.	.	.	1	2	-4	0	.	0.98	0	3.82	99.8	1	119	1.65	56.7	43.7	2	…
1	6.03	.	.	.	1	2	3	0	.	1	0	3.82	99.8	1	119	1.65	56.7	43.7	2	…
1	6.03	.	.	.	1	2	4	0	.	1	0	3.82	99.8	1	119	1.65	56.7	43.7	2	…
1	7	.	.	1.33	0	0	3	1	.	1	0	3.82	97.1	1	119	1.65	56.7	43.7	2	…
1	7	.	.	1.30	0	0	4	4	.	1	0	3.82	97.1	1	119	1.65	56.7	43.7	2	…
1	7	.	.	.	1	2	-3	0	.	1	0	3.82	97.1	1	119	1.65	56.7	43.7	2	…
1	7	.	.	.	1	2	-4	0	.	1	0	3.82	97.1	1	119	1.65	56.7	43.7	2	…
1	7	.	.	.	1	2	3	0	.	1.02	0	3.82	97.1	1	119	1.65	56.7	43.7	2	…
1	7	.	.	.	1	2	4	0	.	1.02	0	3.82	97.1	1	119	1.65	56.7	43.7	2	…
1	7.99	.	.	4.97	0	0	1	3	.	.	0	3.82	102	1	119	1.65	56.7	43.7	2	…
1	7.99	.	.	4.22	0	0	1	6	.	.	0	3.82	102	1	119	1.65	56.7	43.7	2	…
1	8.03	.	.	0.98	0	0	3	1	.	1.02	0	3.82	103	1	119	1.65	56.7	43.7	2	…
1	8.03	.	.	0.87	0	0	4	4	.	1.02	0	3.82	103	1	119	1.65	56.7	43.7	2	…

Table S30 [continued]

ID	TIME	AMT	RATE	DV	MDV	EVID	CMT	FLAG	CIN	TIN	ANAE	ANSTOP	MAP	OBE	WT	HT	LBW	BMI	SEX	…
1	8.03	.	.	.	1	2	-3	0	.	1.02	0	3.82	103	1	119	1.65	56.7	43.7	2	…
1	8.03	.	.	.	1	2	-4	0	.	1.02	0	3.82	103	1	119	1.65	56.7	43.7	2	…
1	8.89	.	.	105	0	0	2	2	154	0.5	0	3.82	103	1	119	1.65	56.7	43.7	2	…
1	8.89	.	.	99.8	0	0	2	5	154	0.5	0	3.82	103	1	119	1.65	56.7	43.7	2	…

Abbreviations: *ID*: Patient identifier; *AMT*: Amount (here: linezolid dose [mg]); *RATE*: Infusion rate (here: [mg/h]); *DV*: Dependent variable (here: linezolid concentration [mg/L]); *MDV*: Missing dependent variable; *EVID*: Event identification (here: 0=observation event, 1=dosing event, 2=turn on/switch off compartment); *CMT*: Compartment (here: 1=Central compartment; 2=Peripheral compartment; 3=Microdialysis compartment of catheter 1; 4=Microdialysis compartment of catheter 2); *FLAG* (here: 0=dose or turn on/switch off CMT, 1=microdialysate observation of catheter 1, 2=Retrodialysis observation of catheter 1, 3=total plasma observation, 4=microdialysate observation of catheter 2, 5=Retrodialysis observation of catheter 1, 6=unbound plasma observation, 8=Covariate event); *CIN*: Retroperfusate concentration (here: linezolid concentration in retroperfusate [mg/L]); *TIN*: Time interval (here: Micro-/retrodialysis collection interval [h]); *ANAE*: Anaesthesia status (here: 0=post-anaesthetic, 1=intra-anaesthetic); *MAP*: Mean arterial pressure (here: [mmHg]); *OBE*: Obesity status (here: 1=Obese, 2=Non-obese), *WT*: Total body weight (here: [kg]), *HT*: Body height (here: [m]), *LBW*: Lean body weight (here: [kg]), *BMI*: Body mass index (here: [kg/m^2]; *SEX* (here: 1=male, 2=female).

7.4.2 Project I: NONMEM® script

```
;; 1. Based on: run256c
;; 2. Description: Final joint NLME model, project 1
;; 3. Label: Final model, all PK data (plasma total&unbound; MD catheter 1&2; RD catheter 1&2)
;; 4. Structural Model: 2 CMT PK model, ISF part of peripheral CMT; 2 MD dummy CMTs
;; 5. Covariate model: OBE on RR, TF; LBW on V1, V2, Q; ANAE on TF, MAP on CLTot
;; 6. Interindividual variability: CL, Km, V1, Q, V2, TF, ANAE_TF
;; 7. Further levels of variability: Intercatheter&Intracatheter variability on RR
;; 8. Residual variability: Separate proportional for PK matrices
;; 9. Estimation: FOCE-I
;; 10. Author: Lisa Ehmann

$PROBLEM    Final joint NLME model
$INPUT      ID TIME AMT RATE DV MDV EVID CMT FLAG CIN TINT ANAE ANSTOP MAP OBE WT HT
LBW BMI SEX (...)
$DATA       KP-MDL01_FinalNONMEMDataset.csv
            IGNORE=@
$SUBROUTINE ADVAN6 TOL=6

;;;;; Model compartments ----------------------------------------------------------------

$MODEL
NCOMP=4
COMP=(CENTRAL)
COMP=(PERIPH)
COMP=(MDCAT1,INITIALOFF)
COMP=(MDCAT2,INITIALOFF)

$PK
IF(NEWIND.LE.1) TANAE=ANSTOP

;;;;; Inter- and intracatheter variabilities ------------------------------------------

; Intercatheter variability in RR (catheter 1)
INTERCV_CAT1=ETA(10) ; if RD or MD catheter 1

; Intercatheter variability in RR (catheter 2)
INTERCV_CAT2=ETA(11) ; if RD or MD catheter 2

; Intracatheter variability in RR (catheter 1)
IF (SAM.EQ.201) THEN ; If catheter 1 (RD1)
INTRACV=ETA(12)
ENDIF
IF (SAM.EQ.202) THEN ; If catheter 1 (RD2)
INTRACV=ETA(13)
ENDIF

; Intracatheter variability in RR (catheter 2)
IF (SAM.EQ.501) THEN ; If catheter 2 (RD1)
INTRACV=ETA(14)
ENDIF
IF (SAM.EQ.502) THEN ; If catheter 2 (RD1)
INTRACV=ETA(15)
ENDIF
```

```
;;;;; PK parameters ---------------------------------------------------------------------

MAP_CLT=THETA(20)

TVCL=THETA(1)
CL=TVCL*EXP(ETA(1))

TVVM=THETA(16)
VM=TVVM*EXP(ETA(7))

TVKM=THETA(17)
KM=TVKM*EXP(ETA(8))

TVV1=THETA(2)*(LBW/51.9)**1
V1=TVV1*EXP(ETA(2))

TVQ2=THETA(3)*(LBW/51.9)**0.75
Q2=TVQ2*EXP(ETA(3))

TVV2=THETA(4)*(LBW/51.9)**1
V2=TVV2*EXP(ETA(4))

TVFU=THETA(5)
FU=TVFU*EXP(ETA(5))

IF(OBE.EQ.1) THEN
TVTF_OFF=THETA(7)
ELSE
TVTF_OFF=THETA(19)
ENDIF

TVANAE_TF=THETA(21)
ANAE_TF=TVANAE_TF*EXP(ETA(16))

IF(ANAE.EQ.1) THEN
TVTF=TVTF_OFF*(1+ANAE_TF)
ENDIF
IF(ANAE.EQ.0) THEN
TVTF=TVTF_OFF
ENDIF

TF=TVTF*EXP(ETA(6))

K10=CL/V1
K12=Q2/V1
K21=Q2/V2

S1=V1
S2=V2
```

```
;;;;; Microdialysis methodology parameter (RR) ----------------------------------------------


IF(OBE.EQ.1) TVRR=THETA(6)
IF(OBE.EQ.2) TVRR=THETA(18)

RR_ID=TVRR*EXP(ETA(9))
RR_ID_CAT1=RR_ID*EXP(INTERCV_CAT1)
RR_ID_CAT2=RR_ID*EXP(INTERCV_CAT2)
RR_ID_CAT1_RD=RR_ID_CAT1*EXP(INTRACV)
RR_ID_CAT2_RD=RR_ID_CAT2*EXP(INTRACV)
RR1=RR_ID_CAT1_RD
RR2=RR_ID_CAT2_RD

IF(FLAG.EQ.2) THEN
CUT1=CIN-(CIN*RR1)
ENDIF

IF(FLAG.EQ.5) THEN
CUT2=CIN-(CIN*RR2)
ENDIF

;;;;; Ordinary differential equations ------------------------------------------------------

$DES
C1=A(1)/V1
CLT=((VM/(KM+C1))+CL)*(1+MAP_CLT*(MAP-75))

DADT(1)=-K12*A(1)+K21*A(2)-C1*CLT                                    ;   Central
CMT
DADT(2)=K12*A(1)-K21*A(2)                                            ;
Peripheral CMT
CISF=(A(2)/V2)*TF
DADT(3)=CISF*RRL                                                     ; MDCAT1
s.c. CMT
DADT(4)=CISF*RRR                                                     ; MDCAT2
s.c. CMT

C2=A(2)/V2

CLL=CL
CLN=VM/(KM+C1)
CLT=CLL+CLN

;;;;; Compute total PK parameters ----------------------------------------------------------

CLL_T=CL*FU
TVCLL_T=TVCL*FU
CLN_T=CLN*FU
CLT_T=CLT*FU
VM_T=VM*FU
TVVM_T=TVVM*FU
KM_T=KM*FU
TVKM_T=TVKM*FU
```

```
V1_T=V1*FU
TVV1_T=TVV1*FU
Q2_T=Q2*FU
TVQ2_T=TVQ2*FU
V2_T=V2*FU
TVV2_T=TVV2*FU
TF_T=TF*FU
TVTF_T=TVTF*FU

;;;;; Residual unexplained variability parameters  ----------------------------------------

$ERROR

IF(FLAG.EQ.3) THEN      ; plasma total
IPRED=(A(1)/V1)/FU
RVA=THETA(8)            ; RUV additive
RVP=THETA(9)            ; RUV proportional
ENDIF

IF(FLAG.EQ.6) THEN      ; plasma unbound
IPRED=(A(1)/V1)
RVA=THETA(10)           ; RUV additive
RVP=THETA(11)           ; RUV proportional
ENDIF

IF(FLAG.EQ.1) THEN      ; MD catheter 1
IPRED=A(3)/TIN
RVA=THETA(12)           ; RUV additive
RVP=THETA(13)           ; RUV proportional
ENDIF

IF(FLAG.EQ.4) THEN      ; MD catheter 2
IPRED=A(4)/TIN
RVA=THETA(12)           ; RUV additive
RVP=THETA(13)           ; RUV proportional
ENDIF

IF(FLAG.EQ.2) THEN      ; RD catheter 1
IPRED=CUT1
RVA=THETA(14)           ; RUV additive
RVP=THETA(15)           ; RUV proportional
ENDIF

IF(FLAG.EQ.5) THEN      ; RD  catheter 2
IPRED=CUT2
RVA=THETA(14)           ; RUV additive
RVP=THETA(15)           ; RUV proportional
ENDIF


W=SQRT(RVA**2+(RVP*IPRED)**2)
Y=IPRED + W* EPS(1)

IRES=DV-IPRED
IWRES=IRES/W
```

```
;;;; Initial estimates ----------------------------------------------------------------

$THETA
 (0,3.47)                          ; CL
 (0,17)                            ; V1
 (0,62.8)                          ; Q2
 (0,33.4)                          ; V2
 (0,0.856,1)                       ; FU
 (0,0.374,1)                       ; RR_OBE
 (0,0.543)                         ; TF_OBE
 (0) FIX                           ; PLTot_RVadd
 (0,0.0469)                        ; PLTot_RVprop
 (0) FIX                           ; PLUnb_RVadd
 (0,0.0452)                        ; PLUnb_RVprop
 (0) FIX                           ; MD_RVadd
 (0,0.124)                         ; MD_RVprop
 (0) FIX                           ; RD_RVadd
 (0.019) FIX                       ; RD_RVprop
 (0,44.1)                          ; VMax
 (0,2.84)                          ; KM
 (0,0.575,1)                       ; RR_NOBE
 (0,0.691,1)                       ; TF_NOBE
 (0.00825)                         ; MAP_CLT
 (-0.137)                          ; ANAE_TF

$OMEGA
 0.337                             ; IIV_CL
 0.162                             ; IIV_V1
 0.193                             ; IIV_Q2
 0.0284                            ; IIV_V2
 0  FIX                            ; IIV_FU
 0.0213                            ; IIV_TF
 0  FIX                            ; IIV_VM
 0.519                             ; IIV_KM
 0  FIX                            ; IIV_RR
$OMEGA  BLOCK(1) 0.066             ; InterCV_RR (catheter 1)
$OMEGA  BLOCK(1) SAME              ; InterCV_RR (catheter w)
$OMEGA  BLOCK(1) 0.0723            ; IntraCV_RR (RD:1, catheter 1)
$OMEGA  BLOCK(1) SAME              ; IntraCV_RR (RD:2, catheter 1)
$OMEGA  BLOCK(1) SAME              ; IntraCV_RR (RD:1, catheter 2)
$OMEGA  BLOCK(1) SAME              ; IntraCV_RR (RD:2, catheter 2)
$OMEGA  0.511                      ; IIV_ANAE_TF

$SIGMA  1  FIX                     ; EPS(1)
```

```
;;;;; Estimation and table output  ----------------------------------------------------------

$ESTIMATION METHOD=1 INTER NSIG=2 SIGL=6 NOABORT MAXEVAL=9999 PRINT=5 MSFO=MSF256f
NOABORT
$COVARIANCE PRINT=E

$TABLE ID OBE FLAG TIME PRED IPRED C2 CISF DV MDV IWRES
       CWRES WRES IRES EVID AMT NOPRINT ONEHEADER FILE=sdtab256f
$TABLE ID OBE FLAG TIME DV CL VM VM_T TVVM_T KM KM_T
       TVKM_T CLL CLL_T CLN CLN_T CLT CLT_T V1 V1_T TVV1_T Q2
       Q2_T TVQ2_T V2 V2_T TVV2_T FU TVRR RR_ID RR_ID_CAT1
       RR_ID_CAT2 RR1 RR2 TF TF_T TVTF_T MAP_CLT ANAE_TF ETA1
       ETA2 ETA3 ETA4 ETA5 ETA6 ETA7 ETA8 ETA9 ETA10 ETA11 ETA12
       ETA13 ETA14 ETA15 ETA16 NOPRINT NOAPPEND ONEHEADER FILE=patab256f
$TABLE ID TIME OBE NOPRINT NOAPPEND ONEHEADER FILE=catab256f
$TABLE ID TIME WT LBW TANAE MAP NOPRINT NOAPPEND ONEHEADER FILE=cotab256f
```

7.4.3 Project IV: NONMEM® script

```
;; 1. Based on: run262
;; 2. Description: Final NLME model, project 4
;; 3. Label: Final model with covariates
;; 4. Structural Model: 2 CMT PK model
;; 5. Covariate model: CLCRCG on CL, WT on V1, ALB on V2
;; 6. Interindividual variability: CL, V1, V2
;; 7. Interoccasion variability: CL
;; 8. Residual variability: Combined
;; 9. Estimation: FOCE-I
;; 10. Author: Lisa Ehmann

$PROBLEM      Final NLME model
$INPUT        ID TIME AMT RATE DV MDV EVID ID OCC SEX AGE WT HT BMI CLCRCG ALB (…)
$DATA         KP-MDL01_FinalNONMEMDataset.csv
              IGNORE=@
$SUBROUTINE   ADVAN6 TOL=6

;;;;; Model compartments -----------------------------------------------------------

$MODEL
NCOMP=2
COMP=(CENTRAL)
COMP=(PERIPH)

$PK

;;;;;  Interoccasion variability ---------------------------------------------

IF (OCC2.EQ.1) THEN
        IOVCL=ETA(5)
ENDIF
IF (OCC2.EQ.2) THEN
        IOVCL=ETA(6)
ENDIF
IF (OCC2.EQ.3) THEN
        IOVCL=ETA(7)
ENDIF
IF (OCC2.EQ.4) THEN
        IOVCL=ETA(8)
ENDIF
IF (OCC2.EQ.5) THEN
        IOVCL=ETA(9)
ENDIF
IF (OCC2.EQ.6) THEN
        IOVCL=ETA(10)
ENDIF
```

```
;;;;; PK parameters ------------------------------------------------------------------------

CLCRCG_INF = THETA(10)                          ; estimated CLCRCG inflection point
CLCRCG_IND = 0                                  ; indicator value
IF(CLCRCG.GE.CLCRCG_INF) CLCRCG_IND = 1

TVCL = (THETA(1)*( 1 + THETA(7)*(CLCRCG - 80.8))*(1-CLCRCG_IND))
     + (THETA(1)*( 1 + THETA(7)*(CLCRCG_INF - 80.8))*CLCRCG_IND)

CL = TVCL*EXP(ETA(1)+IOVCL)

TVV1 = THETA(2)*((WT/70)**THETA(8))
V1 = TVV1*EXP(ETA(2))

TVQ = THETA(3)
Q = TVQ*EXP(ETA(3))

TVV2 = THETA(4)*( 1 + THETA(9) * (ALB - 2.79))
V2 = TVV2*EXP(ETA(4))

K10=CL/V1
K12=Q/V1
K21=Q/V2
S1 = V1
S2 = V2

;;;;; Ordinary differential equations ------------------------------------------------------

$DES
DADT(1)=-K10*A(1)-K12*A(1)+K21*A(2)
DADT(2)=K12*A(1)-K21*A(2)

C2=A(2)/V2

;;;;; Residual unexplained variability parameters  ----------------------------------------

$ERROR
IPRED=A(1)/V1

RVP=THETA(5)
RVA=THETA(6)

W=SQRT(RVA**2+(RVP*IPRED)**2)
Y=IPRED+W*EPS(1)

IRES=DV-IPRED
IWRES=IRES/W
```

```
;;;;; Initial estimates ----------------------------------------------------------------

$THETA
(0, 9.22)                                   ; THETA(1) = CL
(0.001, 9.19)                               ; THETA(2) = V1
(0, 23.2)                                   ; THETA(3) = Q
(0.001, 14.5)                               ; THETA(4) = V2
(0, 0.149)                                  ; THETA(5) = RVProp
(0, 0.261)                                  ; THETA(6) = RVadd
(0, 0.0098)                                 ; THETA(7) = CL_CLCR_2
(0.783)                                     ; THETA(8) = V1_WT_5
(-0.2)                                      ; THETA(9) = V2_ALB_2
(0, 154, 250)                               ; THETA(10) = CLCRCG_INF

$OMEGA
 0.0711                                     ; ETA(1) = IIV on CL
 0.0721                                     ; ETA(2) = IIV on V1
 0 FIX                                      ; ETA(3) = IIV on Q
 0.0317                                     ; ETA(4) = IIV on V2

$OMEGA BLOCK(1)
0.0167                                      ; ETA(5) = IOV on CL (OCC: 1)
$OMEGA BLOCK (1) SAME                       ; ETA(6) = IOV on CL (OCC: 2)
$OMEGA BLOCK (1) SAME                       ; ETA(7) = IOV on CL (OCC: 3)
$OMEGA BLOCK (1) SAME                       ; ETA(8) = IOV on CL (OCC: 4)
$OMEGA BLOCK (1) SAME                       ; ETA(9) = IOV on CL (OCC: 5)
$OMEGA BLOCK (1) SAME                       ; ETA(10) = IOV on CL (OCC: 6)


$SIGMA
 1 FIX  ; EPS(1)

;;;;; Estimation and table output  ------------------------------------------------------

$ESTIMATION METHOD=1 INTER NOABORT MAXEVAL=9999 PRINT=5 MSFO=MSF262e

$COVARIANCE PRINT = E

$TABLE ID TIME TALD DV MDV EVID PRED RES WRES CWRES IPRED C2 IRES IWRES CIWRES
        ONEHEADER NOPRINT FILE=sdtab262e
$TABLE ID TIME OCC DV CL V1 Q V2 ETA1 ETA2 ETA3 ETA4 ETA5 ETA6 ETA7 ETA8 ETA9 ETA10 IOVCL
CLCRCG_INF CLCRCG_IND
        NOAPPEND ONEHEADER NOPRINT FILE=patab262e
```

8

Publications

Original articles

L. Ehmann*, P. Simon*, D. Busse, C. Dorn, W. Huisinga, A. Dietrich, M. Zeitlinger, H. Wrigge, C. Kloft. Risk of target non-attainment in obese compared to non-obese patients in calculated linezolid therapy. Clin. Microbiol. Infect. (2019) [in revision]. (*equal contribution)

L. Ehmann*, M. Zoller*, I.K. Minichmayr, C. Scharf, W. Huisinga, J. Zander[#], C. Kloft[#]. Development of a dosing algorithm for meropenem in critically ill patients based on a population pharmacokinetic/pharmacodynamic analysis. Int. J. Antimicrob. Agents. 54: 309-317 (2019). (*equal contribution, [#]shared senior authorship)
https://doi.org/10.1016/j.ijantimicag.2019.06.016

P. Simon, D. Petroff, C. Dorn, **L. Ehmann**, C. Kloft, C. Prettin, A. Dietrich, M. Zeitlinger, F. Kees, H. Wrigge. Measurement of soft tissue drug concentrations in morbidly obese and nonobese patients – a controlled clinical trial. Contemp. Clin. Trials Commun. 15: 100375 (2019). https://doi.org/10.1016/j.conctc.2019.100375

D. Burau, D. Petroff, P. Simon, **L. Ehmann**, C. Weiser, C. Dorn, A. Kratzer, H. Wrigge, C. Kloft. Drug combinations and impact of experimental conditions on relative recovery in in vitro microdialysis investigations. Eur. J. Pharm. Sci. 127: 252-260 (2019).
https://doi.org/10.1016/j.ejps.2018.10.030

M.G. Vossen, **L. Ehmann**, S. Pferschy, A. Maier-Salamon, M. Haidinger, C. Weiser, J.M. Wenisch, K. Saria, C. Kajahn, S. Jilch, R. Lemmerer, M. Bécède, M. Zeitlinger, C. Kloft, W. Jäger, F. Thalhammer. Elimination of doripenem during dialysis and pharmacokinetic evaluation of post-hemodialytic dosing in intermittent renal replacement therapy. Antimicrob. Agents Chemother. 62: e02430-17 (2018).
https://doi.org/10.1128/AAC.02430-17

L. Ehmann*, M. Zoller*, I.K. Minichmayr, C. Scharf, B. Maier, M.V. Schmitt, N. Hartung, W. Huisinga, M. Vogeser, L. Frey, J. Zander[#], C. Kloft[#]. Role of renal function in risk assessment of target non-attainment after standard dosing of meropenem in critically ill patients: A prospective observational study. Crit. Care. 21: 263 (2017). (*equal contribution, [#]shared senior authorship)
https://doi.org/10.1186/s13054-017-1829-4

Discussed in an editorial of the following issue: M.H. Abdul-Aziz, J. Lipman, J.A. Roberts. Identifying 'at-risk' patients for sub-optimal beta-lactam exposure in critically ill patients with severe infections. Crit. Care. 21: 283 (2017).
https://doi.org/10.1186/s13054-017-1871-2

P. Simon*, D. Busse*, D. Petroff, C. Dorn, **L. Ehmann**, S. Hochstädt, A. Dietrich, M. Zeitlinger, F. Kees, C. Kloft, H. Wrigge. Linezolid soft tissue concentrations in obese patients – a controlled clinical trial. Anesthesiology (2019) [submitted]. (*equal contribution)

Oral presentations

Towards clinical decision support for antibiotic therapy in special patient populations: Leveraging modelling and simulation approaches. Department of Clinical Pharmacology and Pharmaco-epidemiology, Heidelberg University Hospital, Heidelberg, Germany, 19 September 2018.

Towards translational approaches to optimise antibiotic therapy in special patient populations. 6th PharMetrX Symposium, Frankfurt, Germany, 04 May 2017.

Making use of modelling and simulations: Exploring standard meropenem dosing in intensive care patients. Tag der Pharmazie, Berlin, Germany, 01 July 2016.

Conference abstracts

D. Busse, P. Simon, **L. Ehmann**, D. Petroff, C. Dorn, W. Huisinga, R. Michelet, H. Wrigge, C. Kloft. Differences in meropenem pharmacokinetics between obese and non-obese surgery patients are largely explained by body size and estimated creatinine clearance. Annual Meeting of the Deutsche Pharmazeutische Gesellschaft (DPhG), Heidelberg, Germany, 01-04 September 2019.

L. Ilia, R. Michelet, D. Busse, **L. Ehmann**, C. Kloft. Identification and quantification of microdialysis variability using a dynamic *in vitro* microdialysis system and nonlinear mixed-effects modelling. Annual Meeting of the Deutsche Pharmazeutische Gesellschaft (DPhG), Heidelberg, Germany, 01-04 September 2019.

F.A. Weinelt, **L. Ehmann**, R. Michelet, W. Huisinga, J. Zander, M. Zoller, C. Kloft. A joint pharmacokinetic model of piperacillin/tazobactam including mechanistic renal clearance in critically ill patients. 28th Population Approach Group Europe (PAGE), Stockholm, Sweden, 11-14 June 2019.

D. Busse, P. Simon, D. Petroff, **L. Ehmann**, R. Michelet, C. Dorn, W. Huisinga, H. Wrigge, C. Kloft. Analysis of target-site distribution of meropenem in morbidly obese and non-obese patients using nonlinear mixed-effects modelling. 28th Population Approach Group Europe (PAGE), Stockholm, Sweden, 11-14 June 2019.

L. Ilia, R. Michelet, D. Busse, P. Simon, C. Dorn, **L. Ehmann**, C. Kloft. Quantitative comparison of in vitro and in vivo variability of microdialysis experiments using nonlinear mixed-effects modelling on the example of linezolid. 28th Population Approach Group Europe (PAGE), Stockholm, Sweden, 11-14 June 2019.

P. Simon, D. Petroff, R. Werdehausen, **L. Ehmann**, D. Busse, D. Hochstädt, A. Dietrich, C. Kloft, M. Zeitlinger, C. Dorn, F. Kees, S.N. Stehr, H. Wrigge. Modellierung von Linezoliddosierungen anhand von Plasma- und Gewebespiegel normalgewichtiger und adipöser Patienten. 33. Wissenschaftliche Arbeitstage der DGAI, Würzburg, Germany, 15 February 2019.

F.A. Weinelt, **L. Ehmann**, R. Marrek, W. Huisinga, J. Zander, M. Zoller, C. Kloft. Variability of piperacillin serum concentrations in intensive care patients. Annual Meeting of the Deutsche Pharmazeutische Gesellschaft (DPhG), Hamburg, Germany, 02-05 October 2018.

L. Ehmann, M. Zoller, I.K. Minichmayr, M.V. Schmitt, N. Hartung, W. Huisinga, J. Zander, C. Kloft. Development of a tool to identify intensive care patients at risk of meropenem therapy failure. 46th ESCP Symposium on Clinical Pharmacy, Heidelberg, Germany 09-11 October 2017.

L. Ehmann, P. Simon, D. Petroff, I.K. Minichmayr, D. Burau, M. Zeitlinger, C. Dorn, W. Huisinga, H. Wrigge, C. Kloft. Is a pooled population pharmacokinetic model predictive of plasma and microdialysate pharmacokinetics of linezolid in obese and nonobese patients? 26th Population Approach Group Europe (PAGE), Budapest, Hungary, 06-09 June 2017.

F. Kluwe, C. Kirbs, **L. Ehmann**, F. Drescher, P. Matzneller, W. Huisinga, M. Zeitlinger, C. Kloft. Population pharmacokinetics of unbound voriconazole following two different routes of administration during sequence therapy. 26th Population Approach Group Europe (PAGE), Budapest, Hungary, 06-09 June 2017.

L. Ehmann, M. Zoller, I.K. Minichmayr, C. Scharf, M. Vogeser, L. Frey, J. Zander, C. Kloft. Target attainment of standard meropenem dosing in critically ill patients: High impact of renal function. 27th European Congress of Clinical Microbiology and Infectious Diseases (ECCMID), Vienna, Austria, 22-25 April 2017.

F. Kluwe, C. Kirbs, **L. Ehmann**, F. Drescher, J. Weiss, P. Matzneller, M. Zeitlinger, C. Kloft. Target-site pharmacokinetics of voriconazole during sequence therapy. 27th European Congress of Clinical Microbiology and Infectious Diseases (ECCMID), Vienna, Austria, 22-25 April 2017.

L. Ehmann, M. Zoller, I.K. Minichmayr, C. Scharf, L. Frey, M. Vogeser, Huisinga W., J. Zander, C. Kloft. Pharmacokinetics of meropenem in critically ill patients with varying renal function. 25th Population Approach Group Europe (PAGE), Lisbon, Portugal, 07-10 June 2016.

P. Simon, D. Petroff, D. Burau, **L. Ehmann**, C. Nestler, A. Dietrich, A.W. Reske, C. Kloft, M. Zeitlinger, F. Kees, H. Wrigge. Agreement of double measurements when determining soft tissue concentrations of linezolid in normal weight and morbidly obese patients by microdialysis. 8th International Symposium on Microdialysis, Uppsala, Sweden, 25-27 May 2016.

D. Burau, P. Simon, **L. Ehmann**, D. Petroff, H. Wrigge, C. Kloft. Is relative recovery influenced by drug combinations? 8th International Symposium on Microdialysis, Uppsala, Sweden, 25-27 May 2016.

M. Zoller, **L. Ehmann**, C. Scharf, I.K. Minichmayr, M. Vogeser, L. Frey, C. Kloft, J. Zander. Meropenemspiegel in der initialen Therapiephase bei kritisch kranken Patienten. Deutscher Anästhesie Congress (DAC), Leipzig, Germany, 14-16 April 2016.

L. Ehmann, M. Zoller, C. Scharf, I.K. Minichmayr, M. Vogeser, L. Frey, J. Zander, C. Kloft. Pharmacokinetic/pharmacodynamic analysis of meropenem in critically ill patients. 26th European Congress of Clinical Microbiology and Infectious Diseases (ECCMID), Amsterdam, Netherlands, 09-12 April 2016.

L. Ehmann, J. Zander, M. Zoller, C. Scharf, I.K. Minichmayr, C. Kloft. Variability of meropenem serum concentrations in intensive care patients. Annual Meeting of the Deutsche Pharmazeutische Gesellschaft (DPhG), Düsseldorf, Germany, 23-25 September 2015.

9

Curriculum vitae

According to the EU privacy protection prescription (DSGVO) the curriculum vitae has been removed from the electronic version